Distribution
Category
UC-400

ARGONNE NATIONAL LABORATORY
9700 South Cass Avenue, Argonne, Illinois 60439

ANL--87-15

DE89 015624

ANL-87-15

7-GeV ADVANCED PHOTON SOURCE CONCEPTUAL DESIGN REPORT

April 1987

work sponsored by

U.S. DEPARTMENT OF ENERGY
Office of Energy Research

TABLE OF CONTENTS

TABLE OF CONTENTS (Cont'd)

TABLE OF CONTENTS (Cont'd)

TABLE OF CONTENTS (Cont'd)

LIST OF FIGURES

LIST OF TABLES

I.

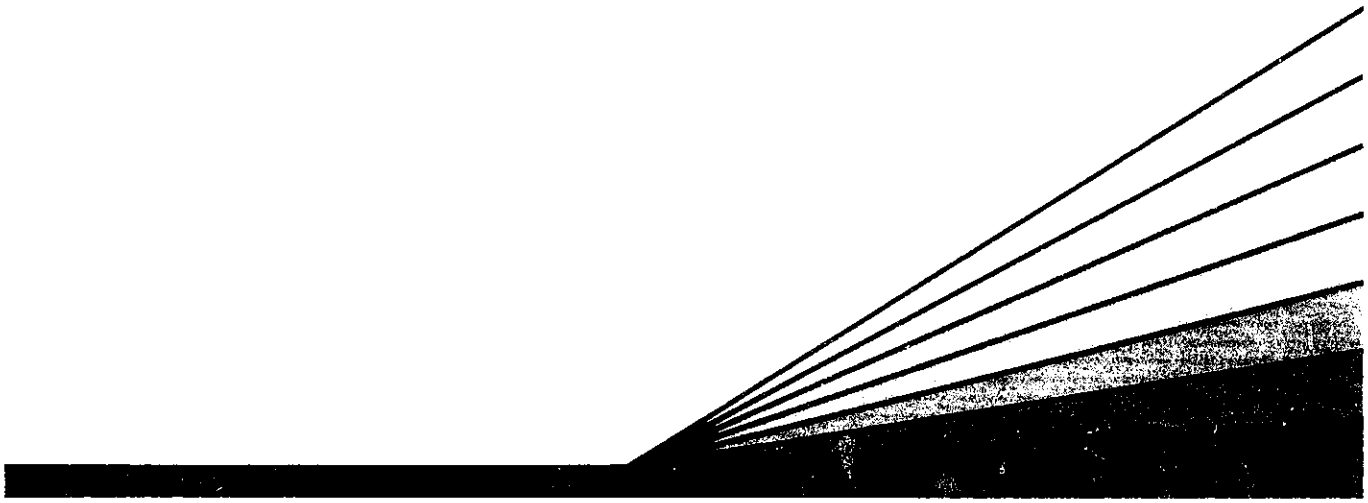

Background & Overview

I. 1. INTRODUCTION

1.1 Background

During the past decade, synchrotron radiation emitted by circulating electron beams has come into wide use as a powerful, versatile source of x-rays for probing the structure of matter and for studying various physical processes. Several synchrotron radiation facilities with different designs and characteristics are now in regular operation throughout the world, with recent additions in this country being the 0.8-GeV and 2.5-GeV rings of NSLS at Brookhaven National Laboratory. However, none of the operating facilities has been designed to use a low-emittance, high-energy stored beam, together with modern undulator devices, to produce a large number of hard x-ray beams of extremely high brilliance.

In October of 1983, an ad hoc committee was convened by the U.S. Department of Energy (DOE), Office of Basic Energy Sciences, with the charter to "solicit and evaluate ideas from synchrotron-radiation providers and users as to the future opportunities and technical needs for synchrotron-radiation based research." The committee had a membership of 17 scientists actively pursuing research using synchrotron radiation and was co-chaired by Peter Eisenberger and Michael L. Knotek. The committee[1] found that current research and development programs in materials science, physics, biology, chemistry, and other fields that use synchrotron radiation could greatly benefit from the availability of two additional facilities in the U.S. The one with the higher priority was a high-energy storage ring capable of providing fundamental undulator radiation in the x-ray region of the spectrum up to 20 keV, with an early 1990's target date for full operation. Such a storage ring requires an electron or positron beam of energy around 6 GeV. The second priority went to a lower-energy ring capable of providing fundamental undulator radiation in the soft x-ray region of the spectrum up to 2.0 keV. Such a ring requires a beam energy around 1.5 GeV. Both machines should be based on insertion devices (undulators and wigglers) and should be capable of accommodating a large number of these insertion devices (IDs).

The recommendation by the Eisenberger-Knotek Committee was later studied and endorsed by the Major Materials Facilities Committee of the National Academy of Sciences, chaired by Frederick Seitz and Dean E. Eastman,[2] and the top priority for the 6-GeV facility was clearly reaffirmed. During the past year, the high priority need for this facility has also been strongly endorsed by the National Research Council (Brinkman) Committee[3] and by two subcommittees of the DOE Energy Research Advisory Board.[4,5]

This document is a proposal to the Department of Energy to construct and operate such a high-energy synchrotron radiation facility at Argonne National Laboratory. As described below, we have now chosen to set the design energy of this facility at 7.0 GeV, with the capability to operate at up to 7.5 GeV.

1.2 Storage Ring Energy

Following the intent that we described in our 1986 Conceptual Design Report,[6] and as recommended by the DOE Design Review Committee in its favorable review of that report, we have given additional consideration to the choice of storage ring energy for this facility. As a starting point, a National Task Group was formed in early 1986 to reconsider user needs for photon energy tunability of undulator beams. The report of that Task Group[7] makes the following two principal recommendations:

- For the initial phase of operation, an undulator should provide fundamental radiation tunable over the range of 7 to 14 keV. In addition, 20-keV radiation should be available in the fundamental of a second undulator or, if possible, by the third harmonic of the first undulator.

- At the mature phase of operation, the minimum gap and the ring energy should allow for the first undulator to be tunable over the interval of 4.7 to 14 keV. A second undulator should deliver 20-keV radiation. Again, although two devices per straight section are considered reasonable, the third harmonic intensities of the first undulator might be large enough in many applications to dispense with the need for a second undulator on the same straight section.

The design of the storage ring to operate nominally at 7.0 GeV, with the capability to achieve energies up to 7.7 GeV, will permit us to meet the above criteria, as will be described in Section II.9. We are planning to configure the storage ring as follows:

- During the initial period of operation, the ring will use a straight section vacuum chamber that permits a minimum ID gap of 1.4 cm.

- The minimum ID gap will be reduced to 1.0 cm during mature operation to enhance both the tunability range and the undulator brilliance.

In this way, we have chosen parameters for mature operation that will provide a good balance among: (1) storage ring energy (and related capital and operating costs); (2) expectations for achievable beam size in the straight sections; and (3) capability to normally meet diverse experimental needs with just one undulator per straight section (which yields simplifications and cost savings). As will be described in Section II.9, in order to meet the above tunability criteria, the dependence of the required storage ring energy upon the minimum undulator gap is substantial, approximately 0.25 GeV per mm. For this reason, we have placed strong emphasis on the goals of minimizing both the vacuum chamber wall thickness (1 mm) and the vacuum chamber straightness deviations in the straight sections, and we have also planned the two-stage operating scenario outlined above.

Since the nominal design energy of this storage ring will be 7.0 GeV, we have named the facility the "7-GeV Advanced Photon Source."

1.3 Project Description

The 7-GeV Advanced Photon Source (APS) design presented here uses a storage ring having a 1060-m circumference with the capability of accommodating 34 IDs and their associated photon beam lines. In addition, 35 photon beams can be provided from bending magnets. The experimental area is large enough to accommodate beam lengths up to 80 m within the experiment hall. Design considerations include arrangements such that long beam lines can be extended through the external wall of the experiment hall with minimal disruption.

The design brilliances of the ID photon beams are much higher than any existing. The design positron beam energy is 7.0 GeV, but the system can be operated at energies as high as 7.7 GeV. Reliability, stability, and flexibility are emphasized in the design. Specifically, the storage ring is designed to accommodate all types of IDs with all tuning conditions desired by the users.

Twelve ID and three bending-magnet beam lines are included in this construction proposal. We anticipate that a comparable number will be ready at commissioning through the efforts of Participating Research Teams (PRTs; see Appendix C). Further ID and bending-magnet beam lines will be added later. Figure I.1.3-1 shows a layout of the proposed 7-GeV Advanced Photon Source.

The design for the APS is the combined effort of a large number of scientists and engineers, many of whom have participated in the design and operation of other user-oriented facilities at Argonne. Examples of such facilities include the 12-GeV Zero Gradient Synchrotron for high energy physics research, the high-current 22-MeV electron linac for chemistry research, the Intense Pulsed Neutron Source for condensed matter research, and the recently completed Argonne Tandem-Linear Accelerator System (ATLAS) for heavy ion, atomic, and nuclear physics research.

Argonne also has a number of scientists now carrying out research that uses synchrotron radiation from sources elsewhere and developing related instrumentation. This group, currently concentrated in the Materials Science Division, constitutes a strong nucleus for the large scientific and user liaison team that will be in place prior to commissioning.

The total area occupied by the facility is about 79 acres. A convenient and attractive site with good geology is available at Argonne. The Laboratory is centrally located in the country and conveniently accessible from O'Hare Airport, one of the largest airports in the United States.

Assuming the initiation of construction in FY 1989, the total cost is estimated to be $384 million, including contingency and escalation. The estimated time required from ground breaking to commissioning is four and a half years.

The European Synchrotron Radiation Facility (ESRF), which is planned for a 1987 construction start in Grenoble, France, uses a 6-GeV storage ring, and its design[8] is

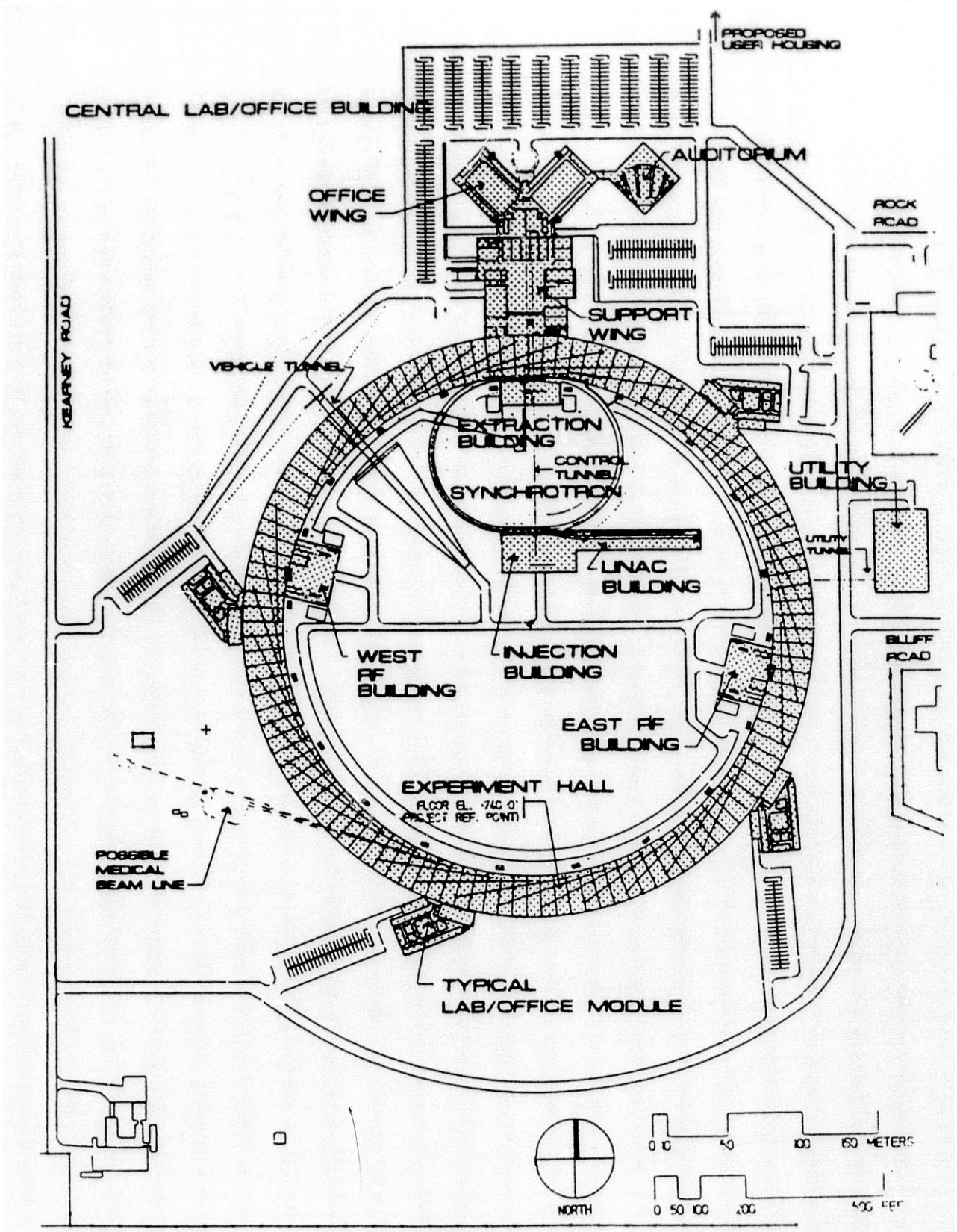

Figure I.1.3-1
Layout of the Advanced Photon Source.

similar in many respects to that of the APS. We have good communication with the ESRF design group, allowing valuable exchanges of design ideas and independent checks of important calculations.

The remainder of this introductory chapter gives further overview information about the project. The other chapters contain in-depth descriptions of the 7-GeV Advanced Photon Source project, including the storage ring and accelerator systems and components, the insertion devices and beam lines, the conventional facilities, estimated costs, schedules, user policies and procedures, and a research and development plan. We have not included a discussion of the scientific/technological justification for the project in this volume. Extensive descriptions of the scientific case appear in Refs. 1 and 2, and there are recent summaries by P. Eisenberger in *Science* magazine[9] and in the report of the Scientific Case Workshop.[10]

2.1 Accelerator System

The original performance specifications for the high-energy synchrotron x-ray source were discussed first by the Eisenberger-Knotek Committee,[1] and then extensively during a scoping meeting held in Ames, Iowa, in October 1984, involving accelerator designers and users of x-rays. The report of the Ames meeting included a short table of desired performance parameters.[11] These specifications were further studied and reconfirmed at several subsequent meetings and workshops, notably at the Machine Workshop on the 6-GeV Synchrotron Radiation Source held at the National Bureau of Standards in March 1985.[12]

As described in Section I-1.2 above, we have now chosen a central design energy of 7.0 GeV for the storage ring. We have also (provisionally) chosen a 40-sector Chasman-Green lattice. The following list compares key parameters of the APS with those chosen at the Ames meeting.

	Ames (1984)	APS (1987)
Beam Energy	6 GeV	7 GeV
Beam Current	≥100 mA	≥ 100 mA
Beam Lifetime	$\tilde{>}$10 h	$\tilde{>}$10 h
Number of Bunches	1-40	1-60
Bunch Duration	10-100 ps	10-100 ps
Horizontal Emittance	$\leq 7\times10^{-9}$ m·rad	$\leq 7\times10^{-9}$ m·rad
Circumference	≈ 800 m	1060 m
Number of Straight Sections	32	40
Straight Section Length (standard)	6 m	6 m
Straight Section Vertical Aperture	8 mm	8 mm
Radiation Sources	Undulators Wigglers, Bending Magnets	Undulators, Wigglers, Bending Magnets
Fundamental Undulator Energy (10-mm ID gap)	20 keV	20 keV (tunable)
Beam Particle	Positron	Positron
Injection Energy	Full Energy	Full Energy

The APS facility is specifically designed to optimize the use of IDs (undulators and wigglers) because of the extremely high brilliance of the radiation produced by these

devices. Therefore, a large number of straight sections are included to accommodate these IDs. Detailed ID considerations yield the conclusion that each straight section should accommodate an ID up to 5.2 m in length. As discussed later in Section II.9.11, it will be possible for special purposes to have a limited number of extra-long straight sections.

Full-energy injection is an important design criterion because it enables the storage ring to run totally dc. With machine components running at fixed tuning conditions, all beam characteristics will remain static, a most desirable condition for experimental use, particularly for a sensitive low-emittance machine. Moreover, with a full-energy injector, it is possible to just "top-up" the beam when its current has degraded after a period of running.

A positron beam is preferred over an electron beam because the former is positively charged and hence will not trap and be detuned by positive ions from the residual gases.

2.2 Experimental Capabilities

Synchrotron radiation research is a dynamic and changing field, and new and important areas of investigation develop rapidly. Vast improvements in experimental techniques are expected. We have aimed for a storage ring design that will be flexible enough to accommodate and exploit emerging scientific concepts and new devices.

The beam emittance and current are adjustable over a wide range, but the specified minimum emittance and maximum current should be simultaneously achieved. The wide ranges of the number and the length of beam bunches in the ring make possible the use of the machine for a wide variety of applications.

The storage ring lattice is designed so that, in principle, the positron beam size and position at each insertion device can be tuned independently to optimize the performance of the device. The experiment floor is provided with crane coverage and has adequate area for photon beams up to about 80 m in length within the experiment hall. Longer beam lines can be accommodated by extending them beyond the outside wall of the experimental area. The experiment floor is vibration-isolated from all other parts of the facility so that the effects of mechanical vibrations on the storage ring and the photon beam components are minimized. Sufficient shielding is provided around the storage ring, especially at the injection point, so that users do not have to be evacuated from the experiment floor during injection or "top-up" of the beam.

Of the 40 straight sections, six will be occupied by accelerator equipment servicing the storage ring. Thus a total of 34 straight sections are available for IDs.

The brilliance and tunability of the radiation from two typical undulators at the APS are shown in Fig. 1.2.2-1. Such beams will have a brilliance greater by about five orders of magnitude than that of any x-ray beam existing today. The brilliances of a

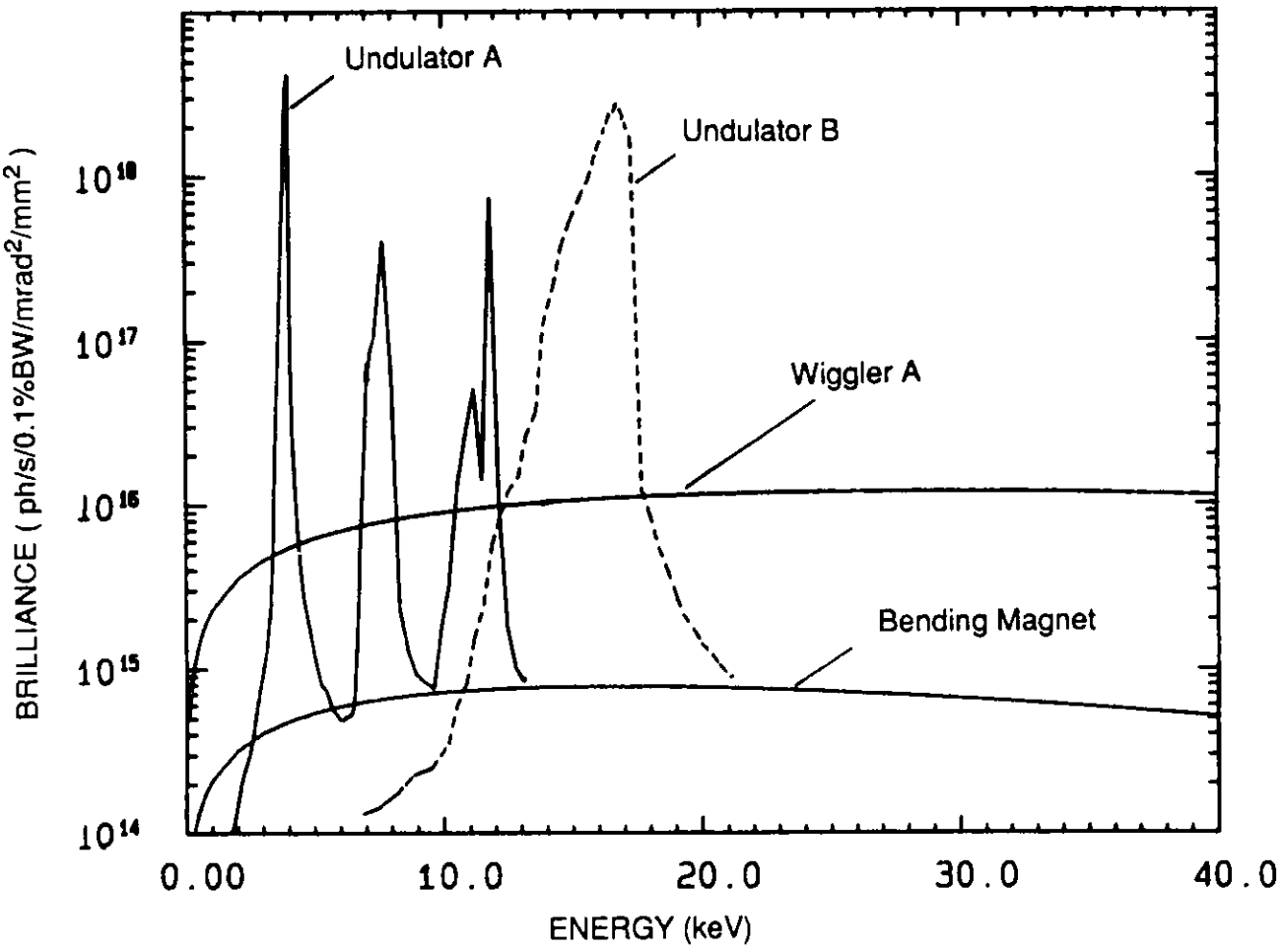

Figure I.2.2-1
High-brilliance characteristics of the hard x-rays from typical insertion devices and the bending-magnet source on the 7-GeV APS. The parameters of the various sources are given in Section II.9.

typical permanent-magnet wiggler and of bending-magnet radiation are also shown in the same graph. The APS bending-magnet beam lines will have unique capabilities above ~20 keV.

3.1 Overview of Accelerator System Design

The storage ring, which has a 1060-m circumference and 40 straight sections (each 6.2 m long), stores a 7-GeV positron beam. To minimize the effects of individual insertion devices on the stored beam emittance, all straight sections have zero dispersion. They are, thus, connected by 9° achromatic bends. Each achromatic bend consists of two dipole magnets separated by a mirror-symmetric section of four quadrupole magnets.

We have chosen to have the beam parameters be identical in each of the straight sections for the nominal tune of the lattice. This is a change from our earlier designs, which used different beam sizes for undulators and for wigglers. To permit sufficient flexibility in adjusting the beam size in the straight sections, three quadrupoles are placed beyond the achromatic-bend dipoles on either end. There are, then, two dipoles and ten quadrupoles between every pair of straight sections. The total ring consists of 40 of these "cells." In addition, to make the dynamic aperture of the ring as large as possible, seven sextupole magnets are strategically interspersed between the quadrupoles. A larger dynamic aperture gives a machine that is more stable and easier to operate.

Altogether, the complement of magnets in the storage ring lattice is as follows:

	Number	Length (m)
Dipole magnets	80	3.06
Quadrupole magnets - three types	80	0.80
	80	0.60
	240	0.50
Sextupole magnets	280	0.24

One cell of the storage ring lattice is shown in Fig. I.3.1-1. This magnet lattice arrangement is a slightly modified version of the well-tested Chasman-Green lattice.

A characteristic of all low-emittance synchrotron radiation source lattices at these high energies is that they are very sensitive to alignment errors. That was the case in our 1986 design of the 6-GeV ring, and similar conclusions were reached by the European Synchrotron Radiation Facility designers from their study of three types of lattices.

In order to alleviate this sensitivity to alignment errors, we have lowered the tune per unit cell from 0.94 to 0.88. This results in a reduction of the sensitivity by a factor of two compared with that for the 1986 design.

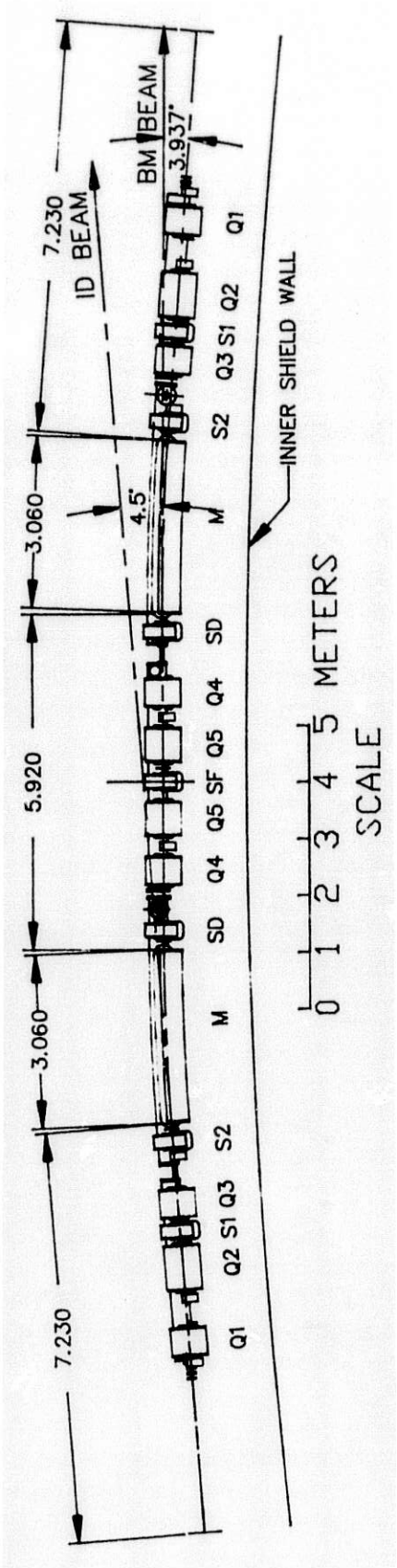

Figure I.3.1-1
One cell of the storage ring magnet lattice.

Further understanding of magnet placement errors has been obtained during the past year. The most harmful effect comes from the displaced orbit in the sextupoles. The displaced orbit is caused by placement errors of the quadrupoles. Using this knowledge, we have designed the orbit corrector system to ensure that the orbit displacements in the sextupoles are minimal.

Further reduction of the sensitivity to misalignment errors is possible by using a "detuned" lattice for the initial tuneup of the storage ring. By allowing the emittance to increase to 11 nm, the tune per cell is reduced to 0.8, producing a lattice that is less sensitive to alignment errors and requires fewer sextupoles.

Another way in which we plan to facilitate the tuneup of the lattice has already been (partially) described. We will first tune the machine with full-size vacuum chambers (4.0-cm vertical aperture) in the straight sections. Then, an initial stage of operation for users will be carried out with a 1.2-cm-aperture vacuum chamber in the straight sections. Finally, when mature operation is achieved, a chamber of 0.8-cm vertical aperture will be installed, allowing a wider energy-tuning range for ID beams.

Six of the 40 straight sections are reserved for injection hardware, rf cavities, positron beam diagnostics, and other equipment. The remaining 34 straight sections can be used to accommodate IDs. Thirty-four photon beams from the IDs can thus emerge through the downstream dipoles. In addition, another 35 bending-magnet-radiation beams emerging from the downstream dipoles can be accommodated. Except for the 69 photon beam ports, the storage ring is enclosed in a narrow concrete tunnel for effective radiation shielding so that experimenters can use the space immediately outside the shielded tunnel.

The ring magnets are of conventional design, modified only in detail to adapt to the specific application. However, a novel and highly effective vacuum system is proposed for the machine. The vacuum system is an important and potentially troublesome component of the storage ring. We have designed the vacuum chamber so that synchrotron radiation will strike only a small number of localized absorbers located far from the stored positron beam. Hence, outgassing by synchrotron radiation is localized, and the small number of local absorbers is easy to vacuum-clean. The newly developed nonevaporable getter (NeG) pumping strips are used throughout to provide high-speed distributed pumping so the desorbed gases from the localized sources are pumped before they ever get to the stored beam. Our research and development program to develop this type of vacuum system is now under way and is yielding encouraging results.

Injection of 7-GeV positrons is from the inner-radius side of the storage ring. High-current (3-A) electron pulses from a 200-MeV linac are made to strike a tungsten target from which 25-mA positron pulses are produced. These positron pulses are accelerated in a second linac to 450 MeV and then injected into a synchrotron. The pulse current at 450 MeV is 15 mA. The synchrotron, which accelerates the positron beam to

7 GeV in 1/3 second, is of relatively conventional design. Each of the linacs and the synchrotron are housed in individual shielded enclosures.

The accelerated positron bunches in the synchrotron are then extracted and injected into any designated numbers of the 1248 available sites (rf buckets) in the storage ring. This way, in every second, a batch of 8 bunches of positrons is injected into the storage ring. It takes only about 4 min to stack up a 100-mA beam in the storage ring. Depending on the number of IDs and on the application, we estimate that a maximum of 300 mA of beam current could be stored under ideal conditions. We anticipate a beam lifetime of $\gtrsim$ 15 h for operation at 100 mA.

A modern computer control system structured around a central network linkage will be employed. The objective is to achieve the greatest flexibility, maximum reliability, feedback to overcome beam position drifts, and the shortest time and maximum ease in converting from one mode of operation to another.

3.2 Overview of Experimental Facilities Design

The photon beams from the IDs located in the 34 straight sections emerge through the beam ports in the vacuum chamber at the downstream ends of the downstream dipoles. The beams travel in vacuum pipes out of the storage ring shielding tunnel into the experiment hall. Each beam is generally manipulated a number of times with various types of optical elements before reaching the sample for the experiment. The beam lines and experiments, some of which may extend more than 80 m in length, occupy the annular floor space around the storage ring, the experimental area, and possibly beyond. To accommodate 80-m beams, the radial width of the experiment hall is about 27 m. It is expected that some extra-long beam lines will extend beyond the outside wall of the experiment hall and will be housed in special extended enclosures. A partial layout of the experiment building showing the photon beams is given in Fig. I.3.2-1.

Generally speaking, a photon beam line consists of four functional sections. The first section is the ID on the storage ring straight section that provides the radiation source. In some cases, the bending magnets deliver the radiation.

The second section, immediately outside the storage ring but still inside the concrete shielding tunnel, is the front-end section. This section contains safety shutters, masks, and other components to define the emerging x-ray beam.

The third section contains hard x-ray optics. In a majority of experiments, this assembly delivers a focused monochromatic beam of x-rays. The section includes crystal and/or mirror optics that are designed to handle the radiation power loads and provide the monochromatization required for the specific investigation.

These monochromatic x-rays are delivered to an experimental station that forms the fourth section. This station contains the sample under investigation and detectors

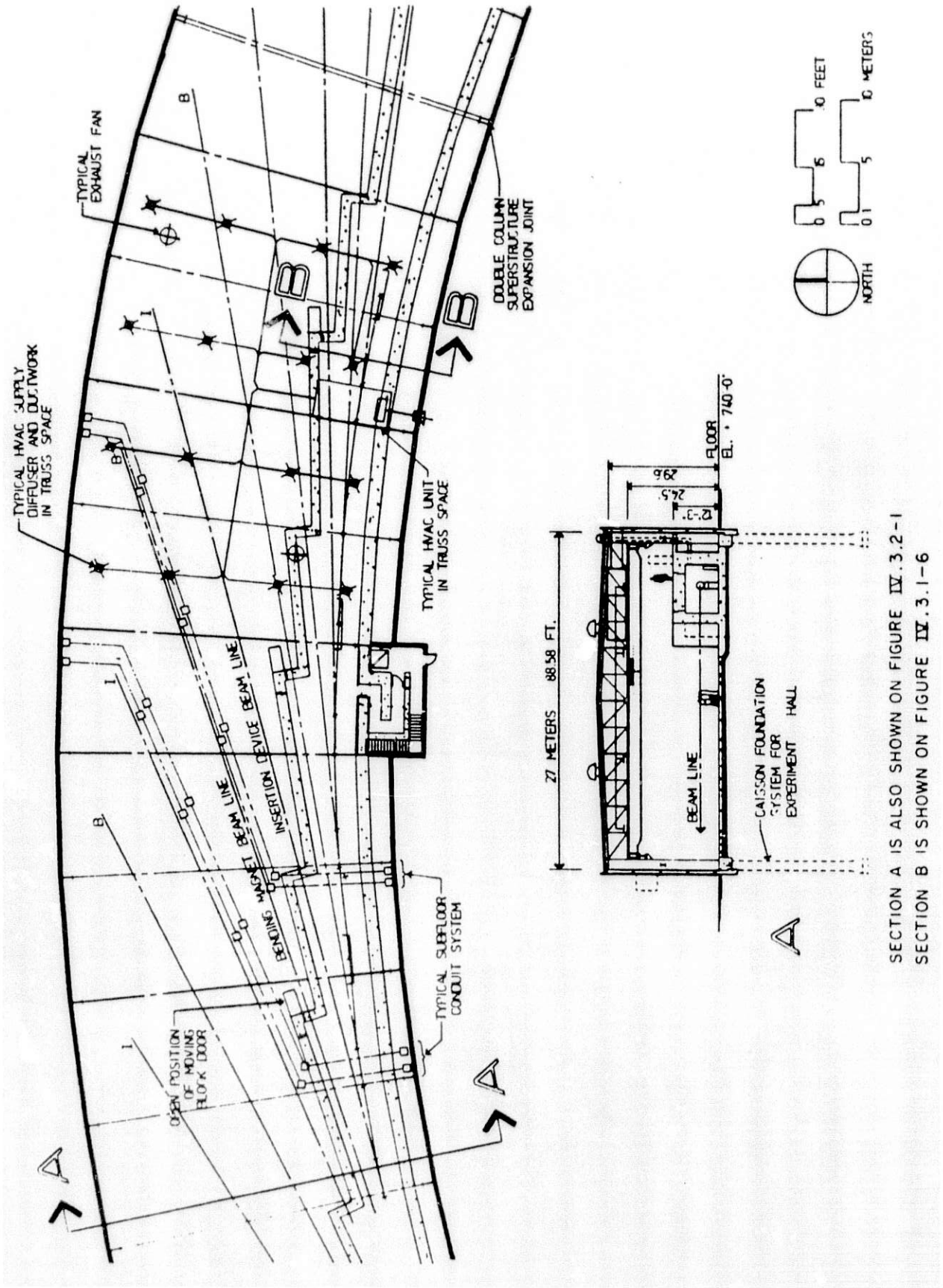

Figure I.3.2-1
Layout of a part of the experiment building.

and/or analyzers to detect and characterize the scattering, imaging, and absorption processes.

Most of the beam lines, including the experimental setups, will be shorter than 80 m and can be housed in the experiment hall. The entire 27-m-wide annular experiment hall is serviced by two 10-ton overhead cranes and by several clusters of offices, laboratories, clean rooms, experiment staging rooms, etc., distributed along the periphery.

The central laboratory/office building is a three-story building with ~180,000 ft^2 total floor area (exclusive of auditorium), located adjacent to the experiment hall. The central laboratory/office building houses the regular operations staff, control room, clean room, staging areas for major component assemblies, computer facilities, auditorium, library, machine shops, and various other services.

Convenient housing for the many outside users of the source will be an important component of the overall facility. Current predictions of user numbers indicate an initial need for a 240-bed complex. It would be highly desirable to have this housing completed approximately one year before the source is user-ready to be available to research groups constructing beam lines prior to commissioning.

We are indeed pleased that the State of Illinois has agreed to help finance such a housing complex. A letter to this effect from Governor James Thompson has been received by the Laboratory; it is reproduced on the next page.

3.3 Special Beam Line Facilities

It is expected that a number of specialized beam line facilities for which funding is not included in the scope of this proposal will be built at the APS.

One example is a special beam line facility for coronary angiography studies. In view of the encouraging results[13] of recent angiography tests at Stanford using synchrotron radiation, further research using a dedicated beam at the APS will be of unique value for developing these techniques and for extending the use of synchrotron radiation into new realms of medical examination and diagnosis.

A proposal[14] for the design, construction, and instrumentation of a Biomedical X-Ray Complex at the APS has recently been submitted to the Office of Health and Environmental Research of DOE. This Complex would include one beam line for basic research in medical imaging, mainly angiography, and two beam lines for protein crystallography.

Another example concerns specialized facilities for classified research. In view of the DOE intent that classified research be carried out at the APS if the need arises, we have considered various means for carrying out such work effectively, with minimal impact on other activities at the APS.

STATE OF ILLINOIS
OFFICE OF THE GOVERNOR
SPRINGFIELD 62706

JAMES R. THOMPSON
GOVERNOR

February 14, 1986

Dr. Alan Schriesheim
Director
Argonne National Laboratory
9700 South Cass Avenue
Argonne, Illinois 60439

Dear Dr. Schriesheim:

I am pleased to inform you of the State's continued commitment to support Argonne and its endeavor to build a major research facility, the 6 GeV X-ray Source. I recognize the importance of this facility to the State and Nation's scientific and technological research communities.

It is my understanding that a 240 bed housing facility will be necessary by June 1990 for use by researchers who will, at that time, be installing their beam lines and other experimental apparatus in preparation for the operation of the 6 GeV X-ray Source in early 1991. The state is interested in providing whatever assistance possible. Obviously, in order to commit bonding available through the Illinois Education Facilities Authority, we would need to have a specific, financially feasible proposal. Assuming Argonne submits such a package, we would be delighted to assist in the provision of housing.

Sincerely,

James R. Thompson
GOVERNOR

If an extensive program of classified research is required, a beam line could be extended southeast some 100 m beyond the wall of the experiment hall into the existing secure area in which Building 316 is located. Smaller-scale classified research would presumably be carried out on beam lines within the APS experiment hall.

3.4 References

1. "Planning Study for Advanced National Synchrotron-Radiation Facilities," P. Eisenberger and M. L. Knotek, Chairmen, Sandia National Laboratory Report (March 1984).

2. "Major Facilities for Materials Research and Related Disciplines," F. Seitz and D. Eastman, Chairmen, National Academy of Sciences, Washington, D.C. (1984).

3. "Physics Throughout the 1990's: An Overview," W. Brinkman, Chairman, NRC Report, National Academy of Sciences, Washington, D.C. (1986).

4. "Review of the National Research Council Report on Major Facilities for Materials Research," F. Stehli, Chairman, Energy Research Advisory Board Subcommittee, DOE (1986).

5. "Review of the National Research Council Report on Physics through the 1990's," B. Ancker-Johnson, Chairperson, Energy Research Advisory Board Subcommittee, DOE (1987).

6. "6-GeV Synchrotron X-Ray Source Conceptual Design Report," Argonne National Laboratory Report, ANL-86-8 (February 1986).

7. "Ring Energy Selections and Extra Long Straight Sections for the Advanced Photon Source: Report and Recommendations by the National Task Group (1987)," G.K. Shenoy (Chairman), G. Brown, Y. Cho, J. Hastings, S. Krinsky, D. Moncton, and P.J. Viccaro, Argonne National Laboratory Report, ANL-87-14 (April 1987).

8. "The Red Book, Draft B," European Synchrotron Radiation Facility (January 1987).

9. P. Eisenberger, Science 231, 687 (1986).

10. "Report on the Workshop on the Scientific Case for a 6-GeV Synchrotron Source," workshop held December 9-11, 1985, at Argonne, Ill., sponsored by U.S. Department of Energy, Office of Basic Energy Sciences, Washington, D.C. (1986).

11. "Report of a Program Review: Synchrotron Radiation Source Research and Development," Ames Laboratory, Iowa State University, Ames, Iowa (October 1984).

12. "Report of Machine Workshop on the 6-GeV Synchrotron Radiation Source," National Bureau of Standards, Gaithersburg, Md. (March 1985).

13. E. Rubenstein, R. Hofstadter, H. D. Zeman, A. C. Thompson, A. C. Otis, G. S. Brown, J. C. Giacomini, H. J. Gordon, R. S. Kernoff, D. C. Harrison, and W. Thomlinson, submitted for publication (1987).

14. E. Westbrook et al., Argonne National Laboratory, unpublished information (January 1987).

II.

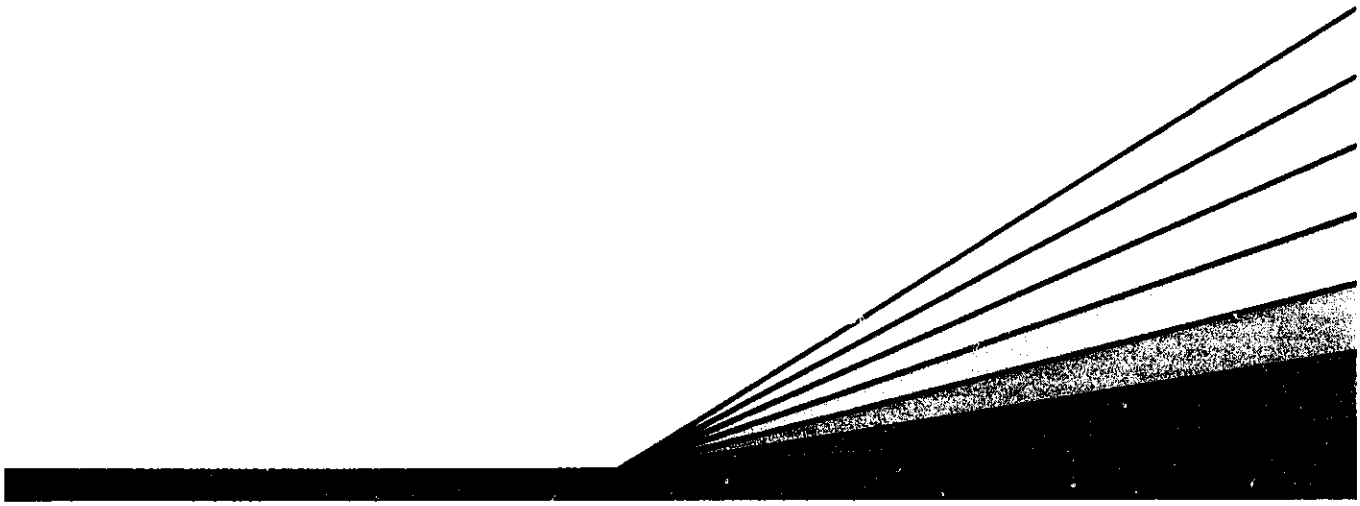

Storage Ring

II. 1. MAGNET LATTICE

1.1 Introduction

The magnetic lattice of the 7-GeV Advanced Photon Source (APS) storage ring is the foundation that determines the character and quality of the emerging photon beams. The parameters of the APS storage ring are derived from the 6-GeV storage ring parameters agreed on by a group of users-at-large and machine designers in a joint meeting held at Ames, Iowa, in October 1984.[1] The basic parameters of the 6-GeV storage ring were reaffirmed in a subsequent meeting held at Gaithersburg, Maryland, in March 1985.[2]

The ring energy of 6 GeV at the Ames meeting was determined by the requirement of producing 20-keV first-harmonic undulator beams. It was pointed out at the meeting that present-day undulator technology, together with its requirement of 8-mm apertures in the storage ring, would give little safety margin in achieving the 20-keV radiation at 6 GeV. Thus, the report recommended the consideration of built-in 7-GeV capability.

Based on these parameters, in February 1986, Argonne personnel produced the "6 GeV Synchrotron X-ray Source Conceptual Design Report."[3] The 1986 design of the storage ring was optimized to operate at 6 GeV, but the design of the hardware included the capability of operating at 7 GeV. During the 6-GeV-ring design phase, it became apparent that with a 6-GeV ring, providing a wide range of photon beam energy to a beam line required several undulators per straight section. It was also found that this requirement could be alleviated if the storage ring energy were higher than 6 GeV. Two possible 7-GeV options were discussed in the 1986 design report.[4] The options were: to operate the 6-GeV ring at 7 GeV, and to design an optimized 7-GeV ring.

In the fall of 1986, after extensive discussions with the user community,[5] the DOE Design Review Committee, and advisory groups, we decided to design an optimized 7-GeV storage ring with the capability of operating at 7.5 GeV as described in Chapter I. The 7.5-GeV capability is to ensure early commencement of experimental programs while the storage ring is being commissioned. A 7-GeV storage ring operating with an insertion device gap of 1 cm satisfies the undulator tuning-range requirement of the hard x-ray experimental program, while a 7.5-GeV storage ring operating with 1.4-cm-gap insertion device also satisfies the requirement by using two appropriately ranged undulators per straight section. Therefore, until such time as the circulating beam orbit in the storage ring is well enough understood to permit us to reduce the undulator gap to 1 cm, the operating energy of the storage ring is expected to be 7.5 GeV.

Figure II.1.1-1 shows the relationship between the energy of the storage ring and the minimum gap required for a 7- to 14-keV undulator. The figure shows that for an undulator gap of 1.4 cm, the storage ring energy should be 7.5 GeV when the device is

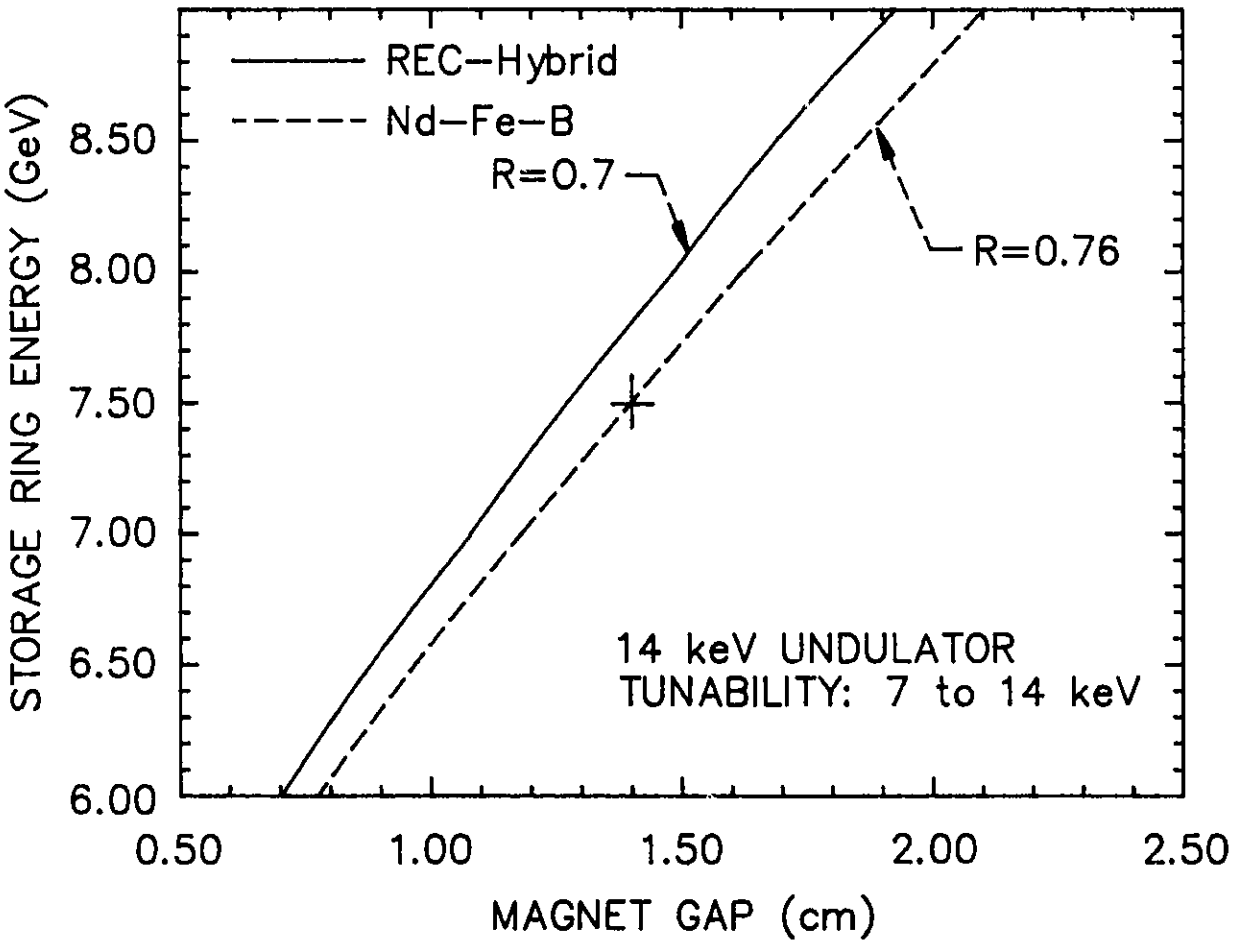

Fig. II.1.1–1

Figure II.1.1-1
Relationship between the energy of the storage ring and the minimum undulator gap required for a 7- to 14-keV undulator. In the figure, R is the ratio of the maximum magnet gap to the undulator period.

made of permanent magnet material Nd-Fe-B. The undulator gap is defined as the magnet gap. The undulator aperture is the vertical aperture of the vacuum chamber in the gap. The vacuum chamber aperture is 2 mm less than the magnet gap.

1.2 Choice of Lattice

The goal of the lattice design effort is to devise a lattice that meets the required basic performance parameters, provides flexibility in tuning and ease of construction and operation, ensures an adequate dynamic aperture for injection, and provides a long storage time. Table II.1.2-1 shows the 7-GeV machine performance parameter goals, along with the Ames meeting parameters of a model 6-GeV ring. The design goal parameters in the table are essentially the same as the Ames parameters, except for the machine energy, circumference, and the number of straight sections. We determined the last two parameters as described in the following discussion.

The lattice choices studied were the Chasman-Green and triple-bend-achromatic (TBA) cell types. The double-bend achromatic or Chasman-Green cell consists of two bending magnets and 10 quadrupoles per unit cell, while a TBA cell consists of three zero-gradient bending magnets and 14 quadrupoles. (For reasons of lattice tunability, the gradient magnet TBA was judged to be less flexible, and no further study of it was performed.)

Increasing the ring energy from 6 GeV to 7 GeV while keeping the 7-nm horizontal emittance of the design requires detailed consideration of lattice types, because the natural emittance of a ring is proportional to the square of the energy and inversely proportional to the third power of the number of bending magnets in the ring.

In order to keep the operating power cost of the radio-frequency (rf) accelerating system of the storage ring at a reasonable level, the bending radius of the dipoles in the ring is increased from 25 m at 6 GeV to 39 m at 7 GeV. The rf power required is proportional to the fourth power of the ring energy and inversely proportional to bending radius. An additional consideration included in the question of energy and bending radius change is the critical energy of the bending-magnet radiation. The critical energy has an important implication for heat removal from accelerator components and beam line optical elements. The critical energy of the 7-GeV ring is about 19 keV, the same as that of the 6-GeV ring. These considerations of power and critical energy are independent of lattice type.

The bending radius change of 14 m results in a circumference increase of less than 100 m. The circumference also depends strongly on the choice of lattice. Therefore, it is worthwhile to discuss and compare the geometries of the two lattice types and the possible trade-offs between various parameters, such as the number of straight sections vs. the number of bending magnets.

Table II.1.2-1

Design Goal Parameters of Storage Rings

	6-GeV Ring[1] (Ames Parameters)	7-GeV Ring (APS)
Beam Energy	6 GeV	7 GeV
Beam Current	>100 mA	>100 mA
Beam Lifetime	>10 h	>10 h
Number of Bunches	1-40	1-60
Bunch Duration	10-100 ps	10-100 ps
Horizontal Emittance	<7 nm	<7 nm
Circumference	~800 m	Open
Number of Straight Sections	32	Open
Machine Aperture (minimum)*	8 mm	8 mm
Straight Section Length	6 m	6 m
Radiation Sources	Bending Magnets, Wigglers, Undulators	Bending Magnets, Wigglers, Undulators
Fundamental Undulator Energy	20 keV	20 keV, Tunable
Beam Particle	Positron	Positron
Injection Energy	6 GeV	7 GeV

*At insertion device.

The TBA lattice, which consists of three bending magnets and 14 quadrupole magnets per unit achromatic cell, has a longer unit cell length due to the number of magnets involved. On the other hand, because there are three dipoles per unit cell, the natural emittance of this lattice is smaller than that of the Chasman-Green type when both types have the same number of cells. An optimization study showed that the cell length is 33.75 m for a 32-cell TBA storage ring with natural emittance in the order of 7 nm or smaller. The resulting circumference of this type lattice is about 1080 m. It must be noted that 1080 m is a minimum circumference, because unlike the Chasman-Green lattice described next, a detailed study of space needed for smaller hardware was not performed.

The Chasman-Green lattice, which consists of two bending magnets and 10 quadrupole magnets per unit achromatic cell, has substantially shorter cell length due to the smaller number of magnets involved. It has a larger natural emittance compared with the TBA lattice for the same number of cells. Therefore, we decided to increase the number of cells in the Chasman-Green lattice to 40 in order to lower its natural emittance. This makes the Chasman-Green lattice a 40-sector machine with a unit cell length of 26.5 m and a circumference of 1060 m, comparable with that of the TBA discussed above. This 1060-m circumference also includes a fine adjustment for inclusion of all necessary hardware.

The above discussions have to do with the ring geometries. In order to decide the lattice type for the APS storage ring, extensive lattice performance investigations have been carried out with both numerical and analytical calculations for the above two lattices. We have then evaluated the results in terms of (1) accelerator physics performance, and (2) constructability and serviceability of the lattice.

Studies performed to date indicate that, as far as accelerator physics is concerned, both lattices provide similar performance within 10-20%. With respect to constructability, the TBA has a disadvantage in extracting the photon beams from the lattice because of the smaller bend angle per dipole. This bend angle makes it difficult to achieve adequate separation between the photon beam and the circulating beam near the photon beam exit port. Furthermore, the 40-sector Chasman-Green lattice has 40 straight sections, compared with 32 in the TBA lattice, allowing for more experiments in the facility.

Taking into account all of these considerations, we have made the following interim decisions: Since there is no distinct advantage in accelerator physics performance of one lattice type over the other, the engineering design of the facility will proceed with the 40-sector Chasman-Green lattice. At the same time, the performance studies of both lattices will be continued until a major review of the choice can be performed with a group of accelerator experts. Should there be a lattice change, the change can be incorporated in the Title I design with little additional effort.

Therefore, this conceptual report is based on the Chasman-Green lattice, and the results of the TBA study are described in Appendix D.

1.3 Description of Lattice

The 7-GeV APS storage ring contains 40 dispersion-free straight sections, 34 of which are available for insertion devices. Four of these sections are reserved for rf cavities, one is used for injection, and one for the beam abort system. The magnet components in a unit cell, 1/40 of the ring, are shown in Fig. II.1.3-1. The centers of two insertion-device straight sections are located at the left and right ends of the figure. Each of these sections contains two sets of triplet quadrupole magnets that can be used

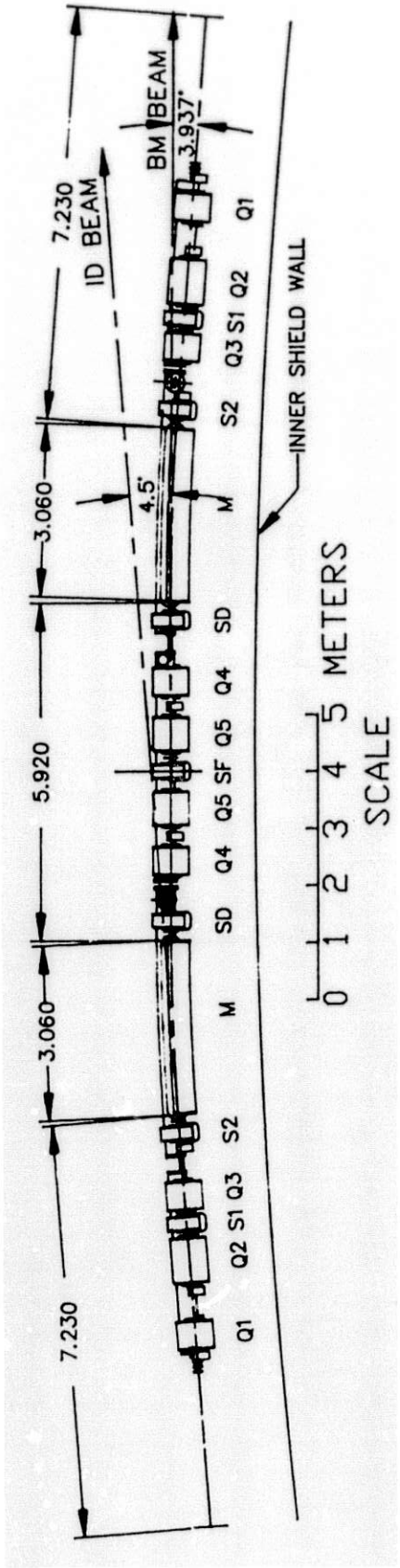

Figure II.1.3-1
Layout of magnets for one cell of the APS storage ring.

to achieve desired lattice functions in the straight sections. The 6.2 m of separation between these triplets can accommodate up to 5.2 m of insertion device.

The achromatic bending system from one dispersion-free section to the next is provided by two 4.5° bending magnets separated by two pairs of doublet quadrupoles. The straight section containing these doublets is called the dispersive straight section.

Fig. II.1.3-2 shows the horizontal and vertical lattice functions, β_x and β_y, for the cell. The dispersion function D is also shown. The cell has reflective symmetry about the center of the dispersive region. The rms beam sizes in the horizontal and vertical planes due to betatron motion are determined by the relations $\sigma_x = \sqrt{\beta_x \epsilon_x}$ and $\sigma_y = \sqrt{\beta_y \epsilon_y}$, where ϵ_x and ϵ_y are the emittances in the two planes. The quantities ϵ_x and ϵ_y are determined by the natural emittance, ϵ_n, and the coupling constant, k, by the relations

$$\epsilon_x = \frac{\epsilon_n}{1+k} \quad ,$$

and

$$\epsilon_y = \frac{k\epsilon_n}{1+k} \quad .$$

The beam size due to the rms energy spread is given by the product of the rms fractional energy spread, σ_E/E, and the dispersion function, D.

The two doublets are adjusted to provide mirror symmetry for the dispersion and β-functions at the midpoint of the cell.

With reflective symmetry at the center of the cell, there are five independent quadrupole adjustments per cell. Since the doublet pair satisfies the achromatic bend condition, the four remaining independent quadrupole adjustments can be used to achieve acceptable values of the beam emittance, the lattice functions in the insertion region, and the phase advance per cell for each plane.

The lattice function values at the midpoints of the insertion straight sections, $\beta_x^* = 13$ m, $\beta_y^* = 10$ m, have been chosen to satisfy the requirements for hard x-rays from high-brightness wigglers and undulators. These values for β_x^* and β_y^* produce better than 94% of the maximum achievable brillance for undulators individually tuned to produce photons with energies above 5 keV. Although the triplets in the insertion straight section can vary β_x^* and β_y^* over a wide range, the chosen values simplify the lattice calculation without compromising the insertion device brilliance. Therefore, all calculations have been carried out with these values.

The horizontal phase advance per cell has been set at $0.88 \times 2\pi$, which produces a natural emittance, ϵ_n, at 7 GeV of 8.0×10^{-9} m. The vertical phase advance per cell has been chosen to avoid coupling and sum resonances produced by the chromaticity-correcting sextupoles (see Section II.1.4). A final adjustment of quadrupoles is made to

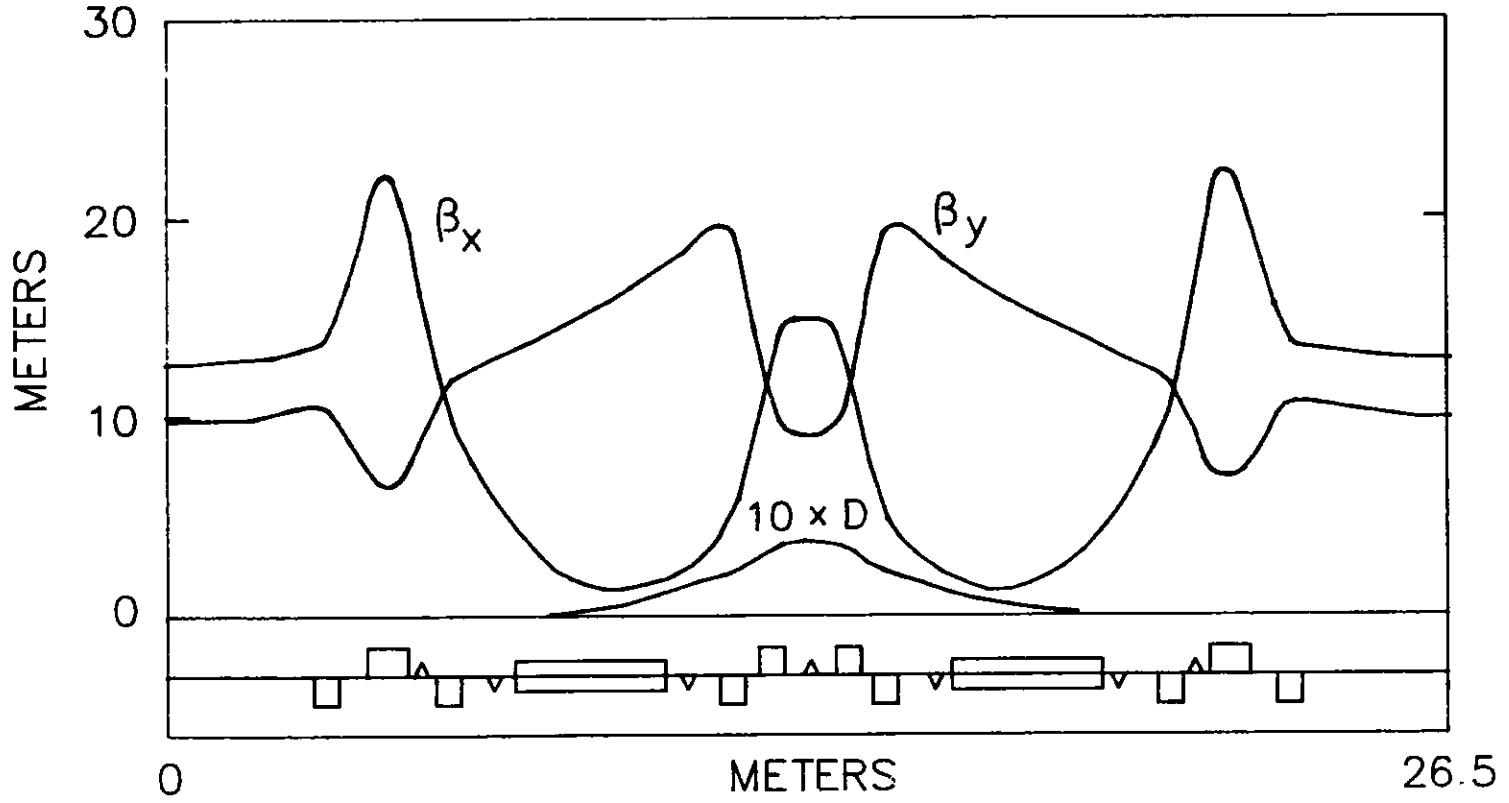

Figure II.1.3-2
Lattice functions, β_x, β_y, and dispersion function, D, for one cell.

ensure that the fractional tune is near 0.25 in both planes. The working point is shown in Fig. II.1.3-3. The cell parameters are given in Table II.1.3-1. The lattice parameters of the storage ring are shown in Table II.1.3-2.

1.4 Dynamic Aperture

1.4.1 Chromaticity Correction

Chromaticity, defined as $\xi = d\nu/(dp/p)$, is the tune shift experienced by individual particles in the machine due to momentum deviation, dp/p. The chromaticities for the lattice described in Section II.1.3 are $\xi_x = -63.7$ and $\xi_y = -26.0$. Chromaticity is corrected by the addition of sextupoles in the dispersive region of the lattice. The momentum deviation of a particle produces an orbit shift in this region equal to the product of the momentum deviation and the dispersion function. This orbit shift in turn introduces a quadrupole field at each sextupole. The tune shift produced in either plane by the sextupole is proportional to the generated quadrupole strength times the β function for that plane.

The three sextupoles (SF, SDs) shown in the dispersive straight section of Fig. II.1.3-1 can be adjusted to simultaneously correct the chromaticities in both planes. The sextupole strengths, $B''\ell/B\rho$, required to correct the chromaticities are $3.92/m^2$ (horizontal focusing) for the center sextupole (SF) and $-4.27/m^2$ (horizontal defocusing) for each of the two side sextupoles (SD).

Since the lattice has a 40-fold symmetry, the first-order intrinsic resonances that can be driven by these sextupoles are

$$3\nu_x = 40\ N\ ,$$

$$\nu_x = 40\ N\ ,$$

$$\nu_x + 2\nu_y = 40\ N\ ,$$

and

$$\nu_x - 2\nu_y = 40\ N\ ,$$

where N is any integer. Since $\nu_x/40 = 0.88$, the dynamic aperture for the lattice described in this report is limited by and can be predicted from the first-order resonances, $3\nu_x = 120$ and $\nu_x = 40$. The dynamic aperture in the presence of nonlinear fields is defined for either plane as the limiting betatron oscillation amplitude that is still stable. It is convenient to express the oscillation amplitudes in terms of beam size. For this purpose we use N_x and N_y, which are, respectively, the horizontal and vertical oscillation amplitudes in units of σ_x and σ_y. The value of σ_x is calculated by using zero

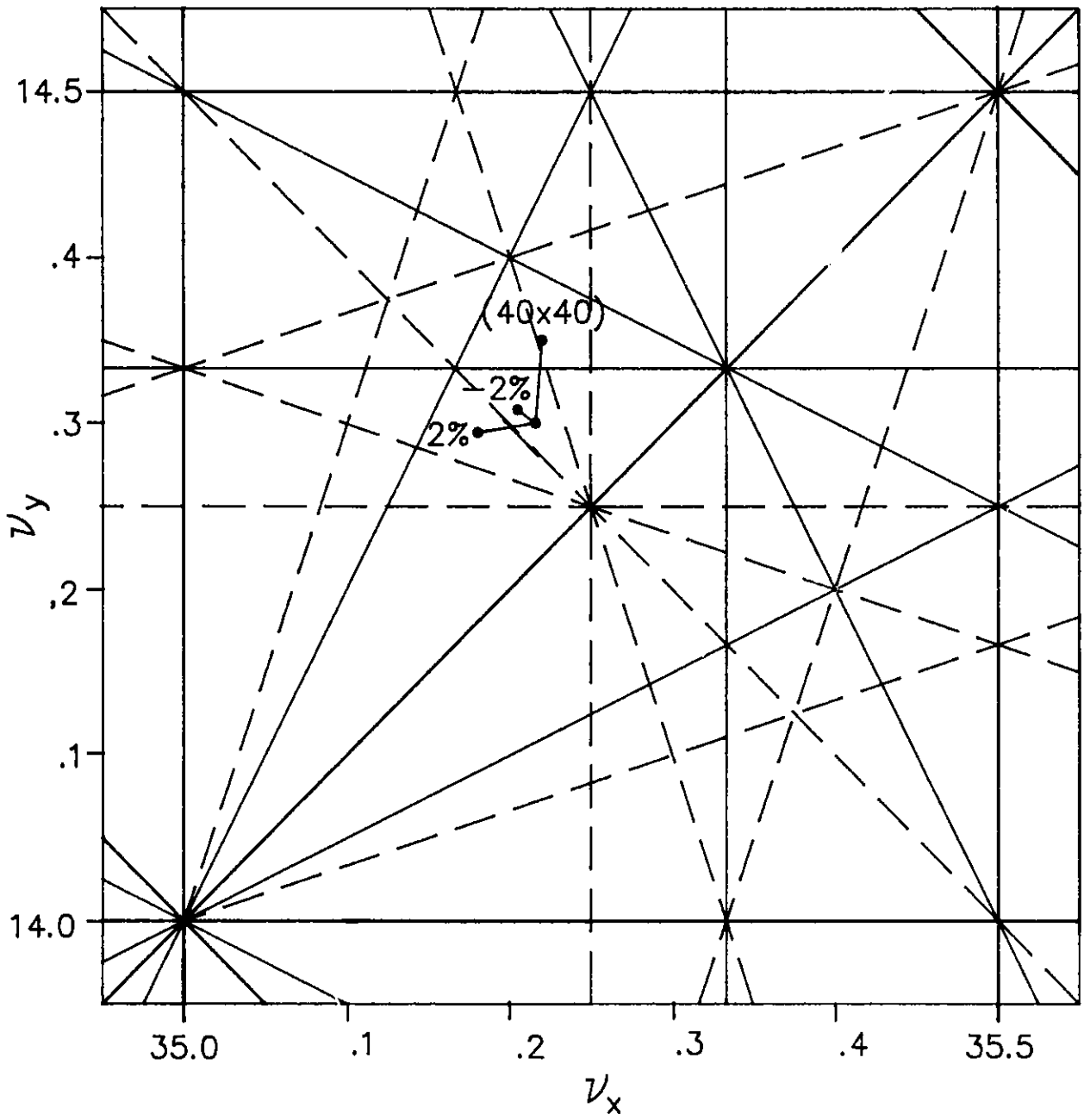

Figure II.1.3-3
Tune diagram showing the working point. Also shown is the tune shift due to momentum changes up to $\Delta p/p = \pm 2\%$ (residual chromaticity) and due to betatron amplitude changes along the coupling line $N_x = N_y$ for $(N_x \times N_y) = (0 \times 0)$ to (40×40).

Table II.1.3-1

Cell Parameters (7 GeV, $B\rho$ = 23.349 T·m)

Element	Length (m)	Magnet Strength B', ρ, B"ℓ/Bρ
L	3.10	
Q1	0.50	-10.8427 T/m
L1	0.66	
Q2	0.80	15.7919 T/m
L21	0.13	
S1	0.24	$1.9023/m^2$
L22	0.13	
Q3	0.50	-10.5850 T/m
L31	0.73	
S2	0.24	$-3.6962/m^2$
L32	0.20	
M	3.06	38.9611 m
L41	0.20	
SD	0.24	$-4.2655/m^2$
L42	0.70	
Q4	0.50	-18.9021 T/m
L5	0.37	
Q5	0.60	18.2479 T/m
L6	0.23	
SF	0.12	$1.9799/m^2$
Reflection Point		

Legend: L = Drift

Q = Quadrupole (B' = field gradient)

M = Bending Magnet (ρ = bend radius)

S = Sextupole ($\frac{B''\ell}{B\rho}$ = integrated normalized sextupole strength)

Table II.1.3-2

Lattice Parameters

Circumference	1060 m
Revolution Time, T_o	3.5358 μs
Energy, E	7 GeV
No. of Insertion Regions	40
Length of Insertion Region	6.2 m
Dipole Length	3.06 m
Dipole Field	0.599 T
Bend Radius, ρ	38.9611 m
Maximum Quadrupole Strength	18.9 T/m
No. of Dipoles	80
No. of Quadrupoles	400
Tunes, ν_x and ν_y	35.22, 14.30
Transition Gamma, γ_T	64.91
Momentum Compaction Factor, α_p	2.374×10^{-4}
Chromaticities, ξ_x, ξ_y	-63.7, -26.0
Chrom. Corr. Sextupoles	3.92, -4.27/m^2
Number of Chromatic Sextupoles	120
Number of Harmonic Sextupoles	160
Maximum Dispersion	0.39 m
Maximum β_x and β_y	22.3, 19.8 m
Natural Emittance, ε_n	8×10^{-9} m
Transverse Damping Time, $\tau_x=\tau_y$	9.08 ms
Synchrotron Damping Time, τ_E	4.54 ms
Bending-Magnet Critical Energy, ε_c	19.5 keV
Energy Loss per Turn, U_o	5.45 MeV
Radio Frequency, f_{rf}	352.96 MHz
Harmonic Number, h	1248
Natural Energy Spread, σ_E/E	0.096%

coupling. The value of σ_y is calculated using full coupling. These are the largest possible σs in each plane. These quantities are given by

$$\sigma_x = \sqrt{\beta_x \varepsilon_n} = 0.32 \text{ mm}$$

and

$$\sigma_y = \sqrt{\beta_y \varepsilon_n / 2} = 0.20 \text{ mm} ,$$

at the center of the insertion region.

Dynamic aperture limits are determined by tracking individual particles around the ring. Particles are considered to be stable if they track for 1000 turns. A number of computer codes have been used for this purpose. These include TR,[6] PATRICIA,[7] MAD,[8] RACETRACK,[9] and PATRIS.[10]

The dynamic aperture for the lattice described in Section II.1.3 with only the chromaticity-correcting sextupoles is shown in Fig. II.1.4-1. The result agrees well with the predicted aperture based on first-order resonance theory. Since the source of these limitations on the dynamic aperture is understood, it can be predicted that tuning harmonic-correcting sextupoles located in the dispersion-free straight sections will allow the dynamic aperture to be increased.[11] The adjustment of the latter sextupoles to both increase the dynamic aperture and reduce the amplitude-dependent tune shifts is the subject of the next section.

The nonlinear tune shift remaining after correction of the chromaticity is small, as is shown in Fig. II.1.4-2. Tracking with ±1.9% momentum error demonstrates that the small residual tune shift has little effect on the dynamic aperture (see Fig. II.1.4-3).

1.4.2 Harmonic Correction

Harmonic-correcting sextupoles are used to enlarge the dynamic aperture and reduce the amplitude-dependent tune shifts that would otherwise occur because of the proximity of the first-order resonance $\nu_x = 40$.[11] Based on first-order perturbation theory, the calculated amplitude-dependent tune shifts are

$$\Delta\nu_x = 2.87\times10^{-4}\, N_x^{\,2} + 0.60\times10^{-4}\, N_y^{\,2}$$

and

$$\Delta\nu_y = 1.20\times10^{-4}\, N_x^{\,2} + 0.39\times10^{-4}\, N_y^{\,2}.$$

The largest contributions come from the $\beta_x^{3/2}$ and $\beta_x^{1/2}\beta_y$ coefficients of the 40th harmonic of the Fourier-expanded Hamiltonian for the equations of motion. These harmonic components can be reduced by the addition of two families of sextupoles in the dispersion-free sections of the lattice. Since the sextupole coefficients of these two harmonic terms are known, it is possible to calculate the harmonic-correction sextupole strengths required to cancel them. Total cancellation of the 40th harmonic components, however, produces a negative amplitude-dependent tune shift. The harmonic-correction sextupoles are optimal at a value that is about 68% of that required for complete

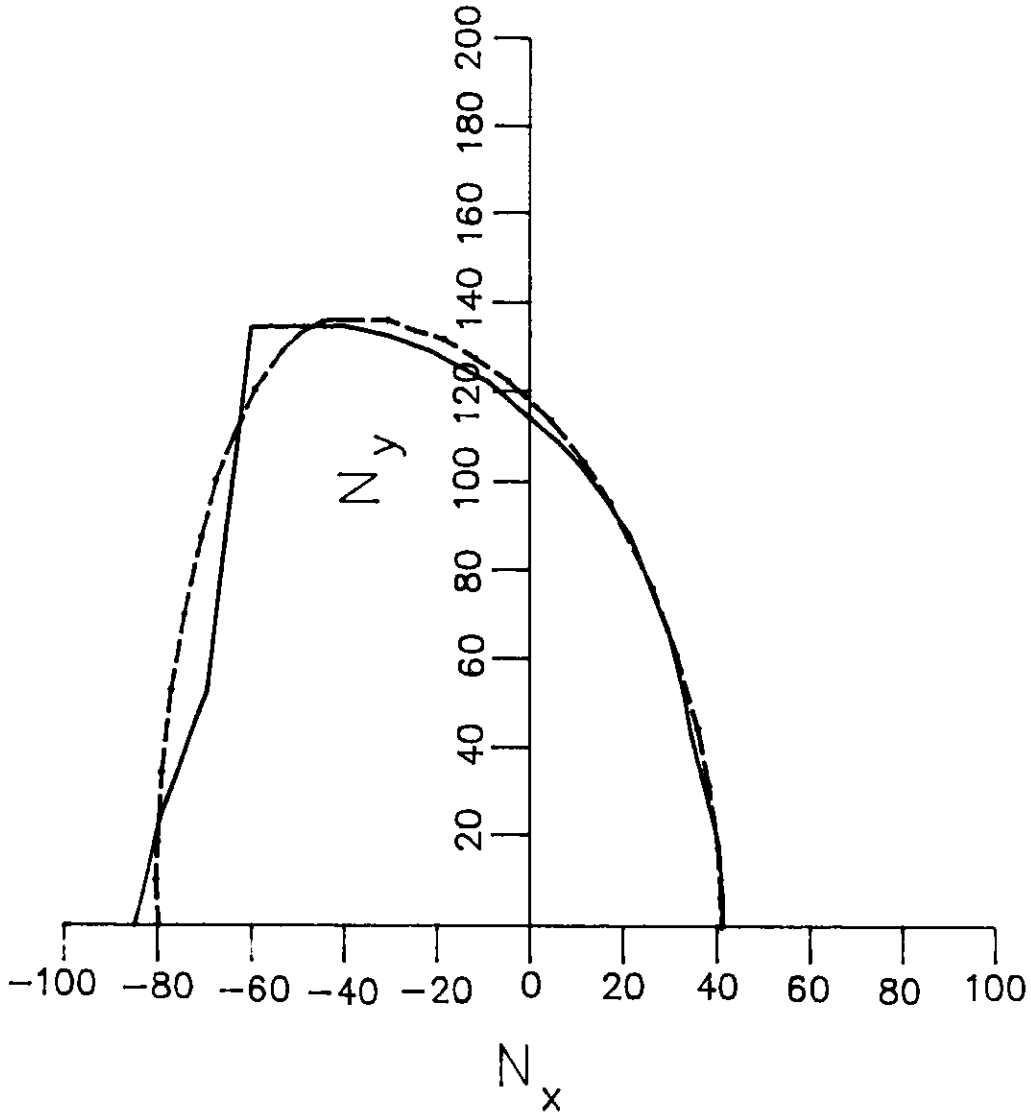

Figure II.1.4-1
Dynamic aperture obtained by tracking (solid curve) and predicted by first-order resonance (dotted curve) with chromaticity-correcting sextupoles only.

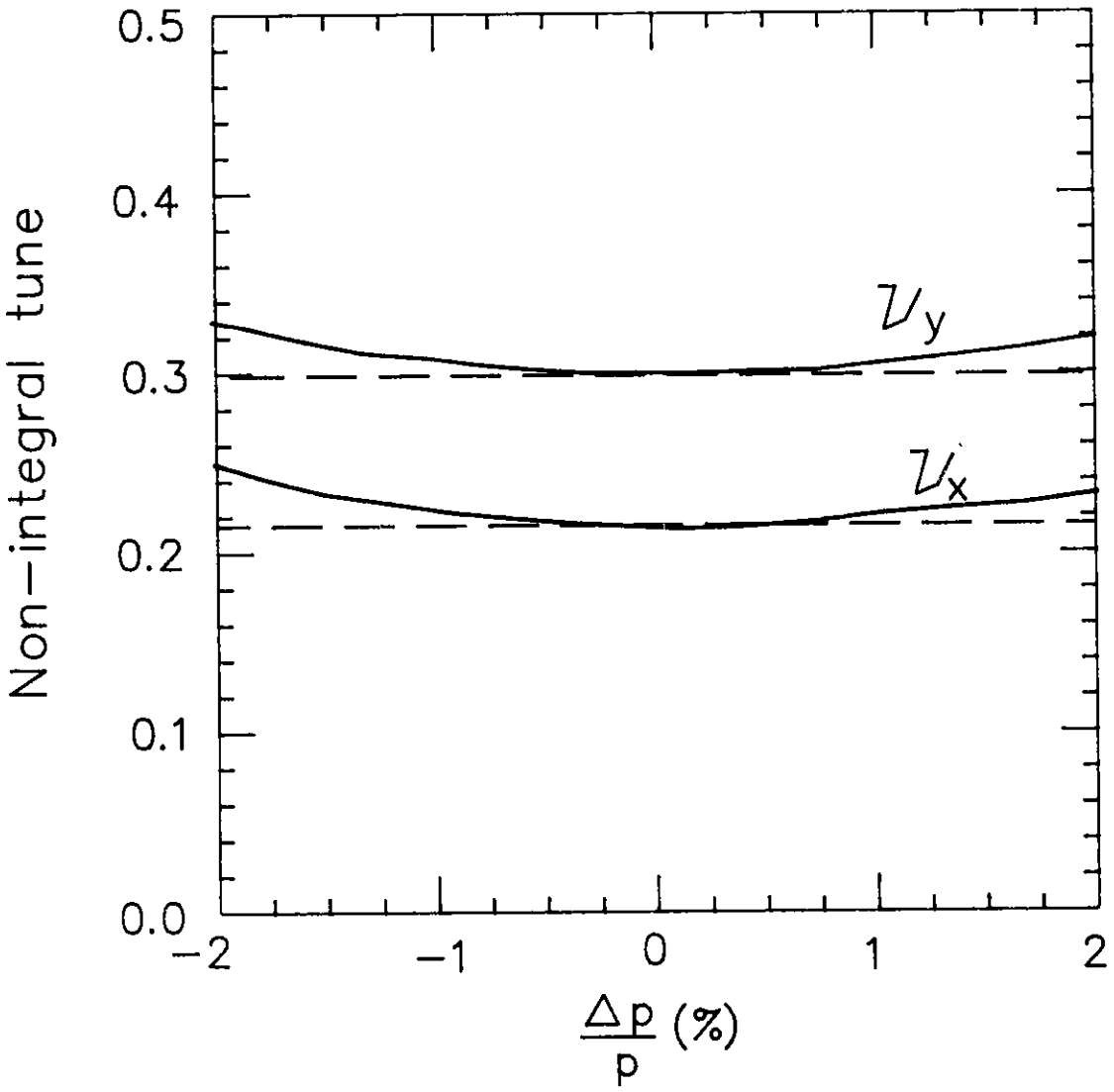

Figure II.1.4-2
Residual tune variations with momentum deviation. Chromaticity-correcting sextupoles only.

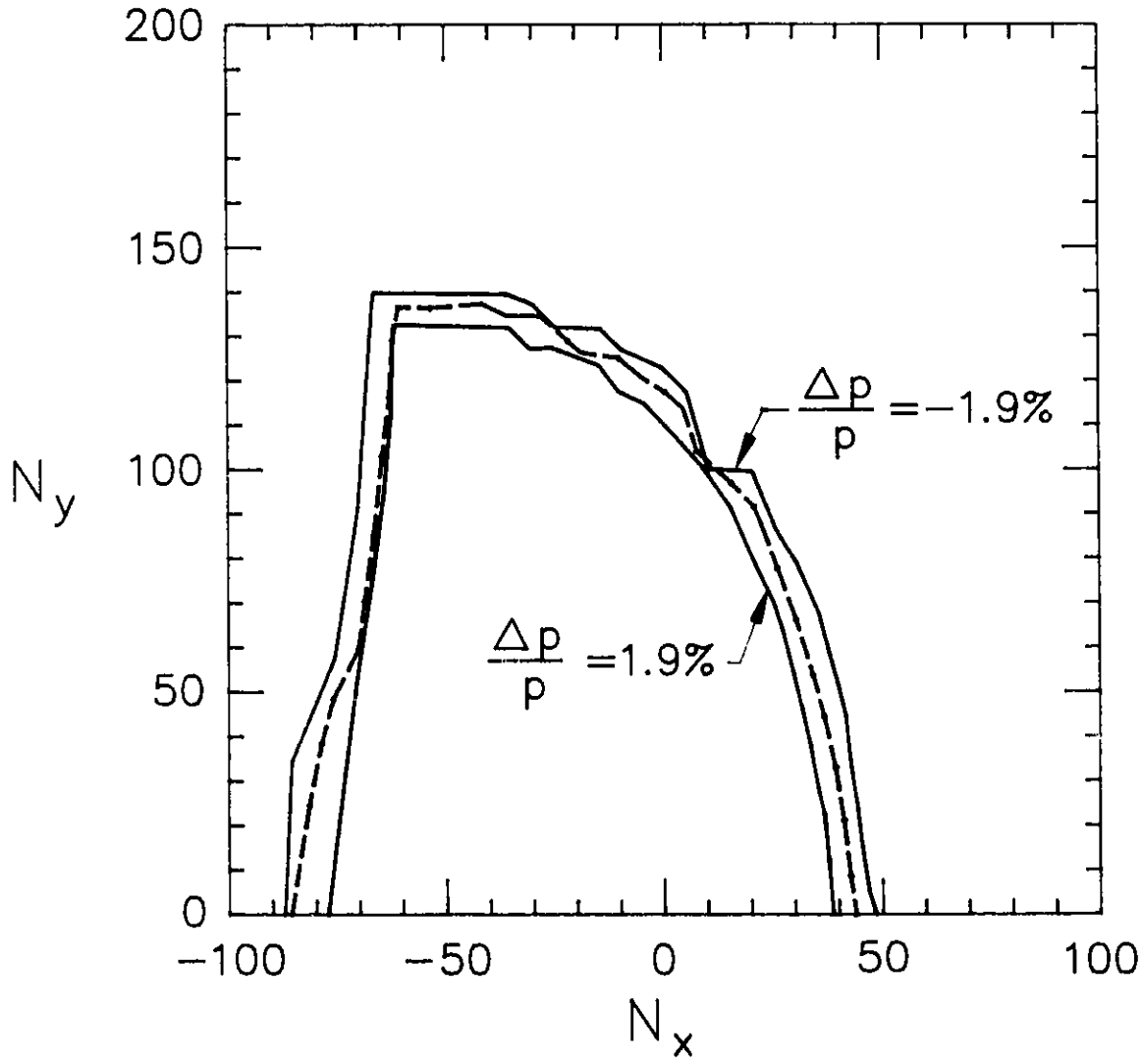

Figure II.1.4-3
Influence of momentum deviation on dynamic aperture. Chromaticity sextupoles only. The dashed curve is the zero-momentum-deviation dynamic aperture.

removal of the harmonic terms. With the sextupoles set to these values, first-order perturbation theory gives

$$\Delta\nu_x = 0.00\ N_x^2 + 0.72\times10^{-5}\ N_y^2$$

and

$$\Delta\nu_y = 1.44\times10^{-5}\ N_x^2 + 0.98\times10^{-5}\ N_y^2\ .$$

The increase in dynamic aperture resulting from the 68% suppression of the harmonic components is shown in Figure II.1.4-4.

The residual chromaticity produced by the four families of sextupoles (chromaticity + harmonic correction) is shown in Fig. II.1.4-5. Comparison with Fig. II.1.4-2 demonstrates that the partial suppression of the harmonic components has led to a very small value of $\Delta\nu_y$ and a change of sign for $\Delta\nu_x$ over the range $\Delta p/p = \pm 2\%$.

The amplitude-dependent tune shifts determined by tracking are shown in Figs. II.1.4-6 and II.1.4-7. These tracking results verify the predictions of the first-order perturbation theory. Together with the increase in dynamic aperture, this reduction of the amplitude-dependent tune shift greatly improves the performance of the lattice, especially with regard to magnet tolerance, as will be discussed in Section II.1.4.3.

1.4.3 Tolerances

Imperfection in magnet construction, fluctuations in magnet power supplies, and misalignment of magnet components during survey and assembly of the machine are unavoidable. State-of-the-art capabilities for construction and alignment are:

- fractional field imperfection $\approx 10^{-4}$
- roll angle misalignment $\approx 10^{-4}$ radians
- transverse misalignment $\approx 10^{-4}$ meters

Depending on the type of magnet, each of these sources of error affects the performance of the storage ring in a different way. This section examines the tolerances to be set for the different kinds of magnets. These tolerances are expressed as a tolerance level (10^{-3} to 10^{-4}) with units as described above.

Individual imperfections or fluctuations in the field of the dipole bending magnets cause horizontal orbit distortion. The magnitude of the distortion caused by any one

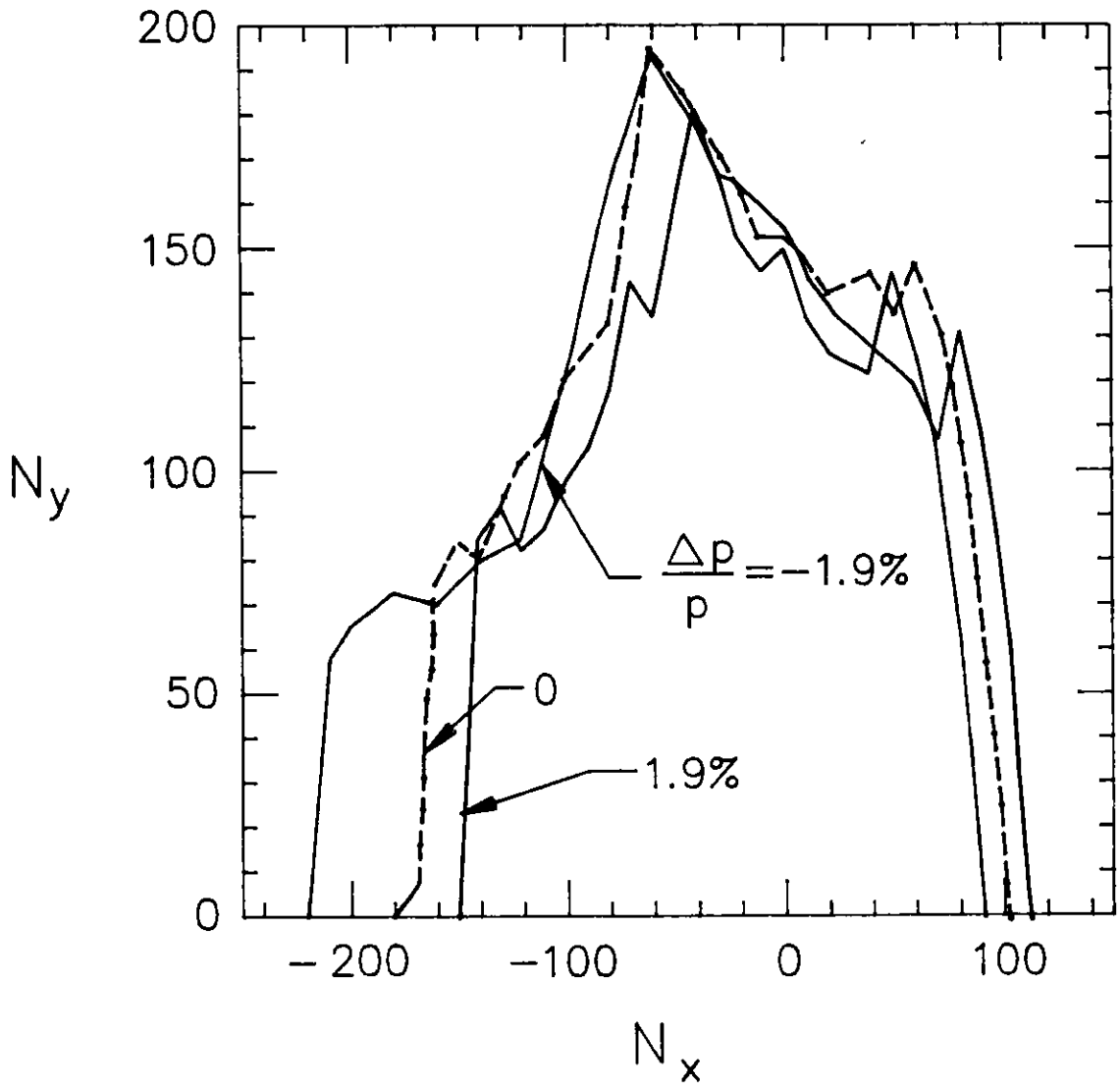

Figure II.1.4-4
Dynamic aperture with chromaticity- and harmonic-correcting sextupoles for $\Delta p/p=0$ and $\pm 1.9\%$. Results are obtained by tracking.

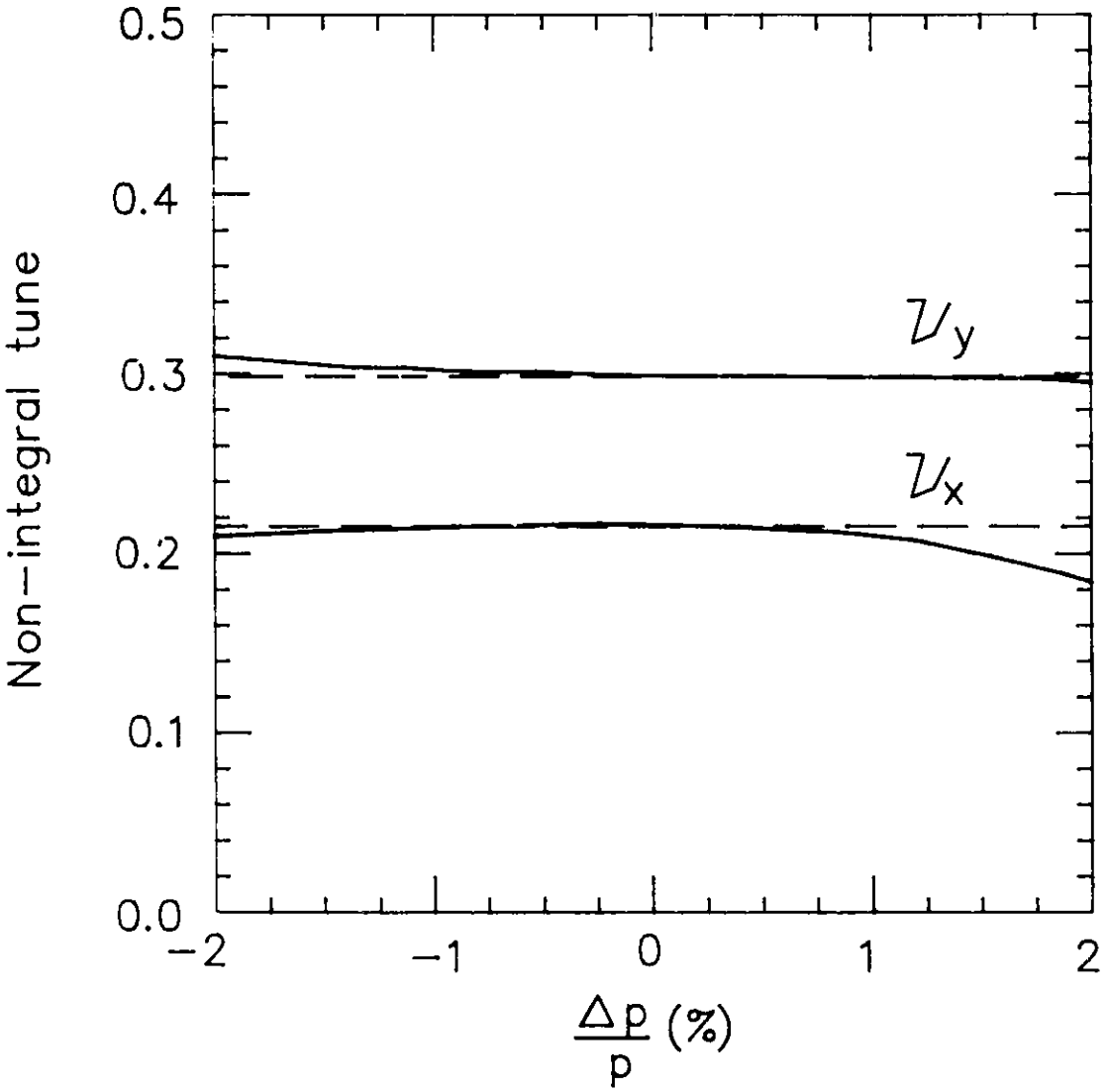

Figure II.1.4-5
Residual tune variation vs. momentum deviation with both chromaticity- and harmonic-correcting sextupoles.

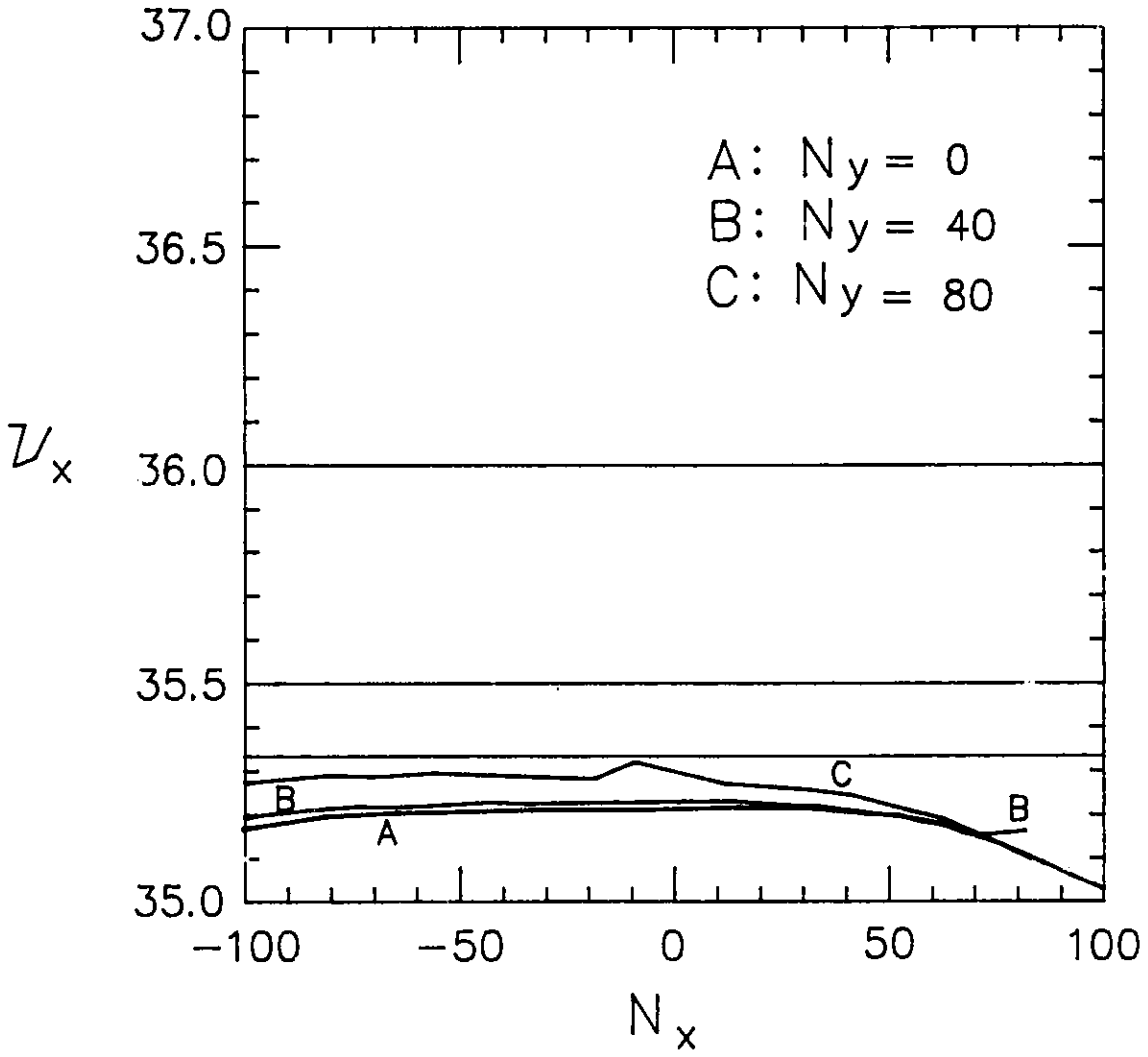

Figure II.1.4-6
Amplitude-dependent tune shifts as a function of N_x for three values of N_y with all sextupoles on. Tunes are obtained from tracking.

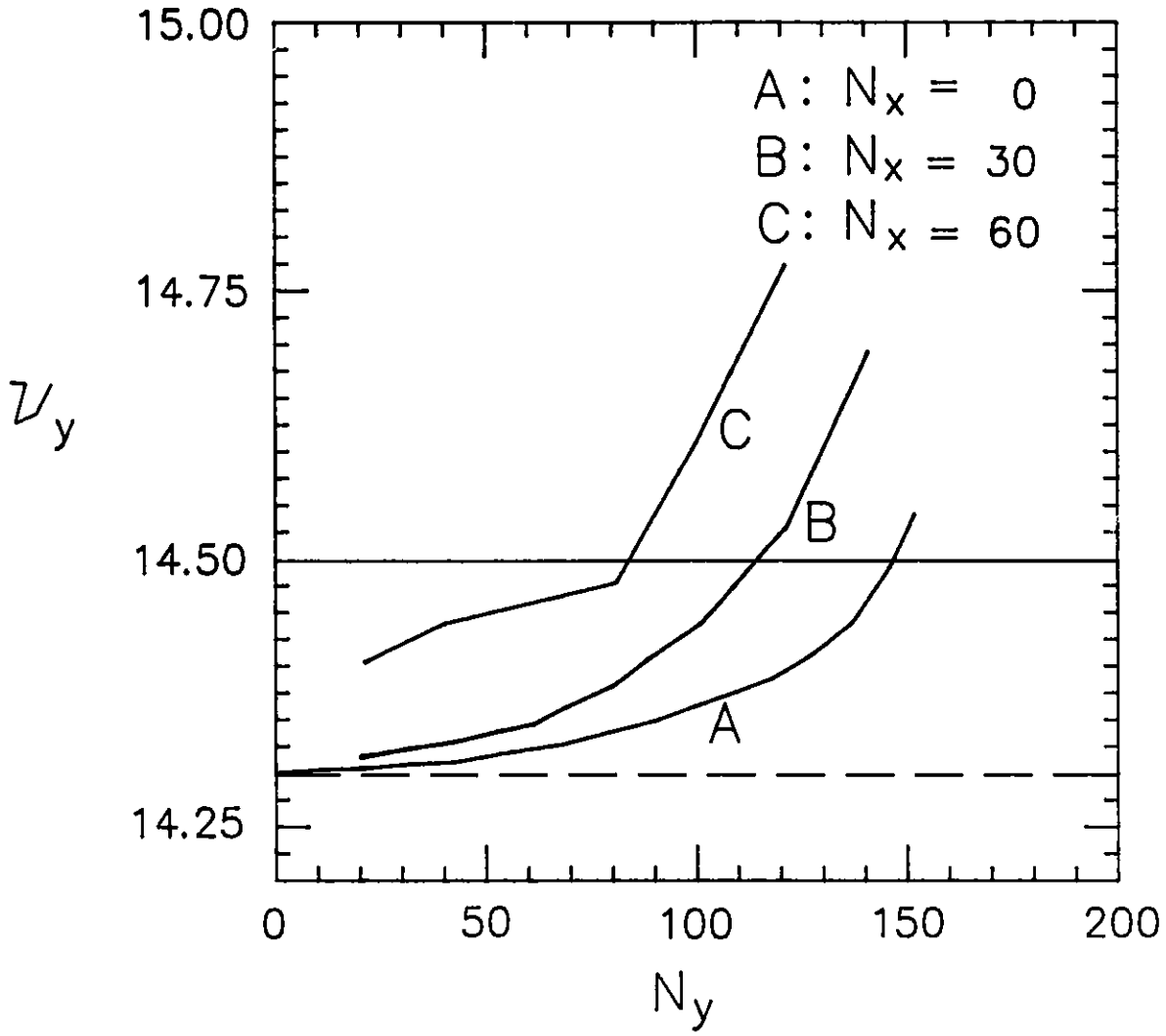

Figure II.1.4-7
Amplitude-dependent tune shifts as a function of N_y for three values of N_x with all sextupoles on. Tunes are obtained from tracking.

dipole magnet imperfection is proportional to the product of the fractional field difference, $\Delta B\ell/B\ell$, multiplied by the lattice function, β_x, in the magnet region. Since β_x is relatively small in the bending magnets, the horizontal orbit distortions are not strongly dependent on $\Delta B\ell/B\ell$. Vertical field misalignment of the dipole magnet produces fractional horizontal field components proportional to the roll angle. Because of the larger value of β_y, the vertical orbit distortions caused by the roll angle are larger than the horizontal distortions.

Figure II.1.4-8(a) shows a plot of the expected rms horizontal and vertical distortions through one lattice period produced by 10^{-3} rms fractional field and roll errors. With tolerances of 10^{-4}, the distortions due to these errors are less than 1 mm.

Quadrupole gradient errors cause tune changes. The sensitivity of the horizontal and vertical tunes to individual quadrupole gradient changes is shown in Table II.1.4-1. The numbers at the bottom of the table are the ratios of the rms tune changes due to the quadrupole fractional gradient errors. Setting a limit of 10^{-4} on the gradient errors limits the tune changes to 10^{-3}.

The most sensitive magnets for generating orbit distortions through misalignment are the quadrupoles. A quadrupole displacement in either plane produces a dipole field proportional to the product of quadrupole gradient times the displacement and causes an orbit distortion in the corresponding plane. The ratio of the rms distortion to the rms placement error is called the amplification factor.

The calculated amplification factors are plotted for one lattice period in Fig. II.1.4-8(b). This figure shows that quadrupole rms placement errors of the order of 0.1 mm are expected to produce rms distortions of up to 8 mm in some quadrupoles. The quadrupole placement tolerances have been set at 0.1 mm.

Sextupole misalignments do not produce significant closed-orbit distortions, but result in tune changes and nonlinear coupling. The expected tune change resulting from an rms sextupole misalignment of 0.1 mm is 0.007. Based on this value, an alignment tolerance of 10^{-4} m is chosen. The magnitude of this tune change is negligible compared with the change coming from closed-orbit distortions produced by quadrupole misalignment. The latter distortion will be reduced by the closed-orbit correction system (see Section II.1.4.5). However, the ultimate improvement of the closed-orbit distortions in the sextupoles will be limited by the sextupole alignment relative to the beam position monitors.

The nonlinear effects on the dynamic aperture due to the closed-orbit distortions in the sextupoles are not easily studied analytically and are treated numerically by using the tracking program RACETRACK.[9] Typically, 10 different machines are generated with Gaussian-distributed random errors defined by the tolerance level given above. The tolerance level has been varied over the range of 10^{-5} to 5×10^{-4}, and at each level the average and rms dynamic apertures are determined for the 10 machines. Figure II.1.4-9

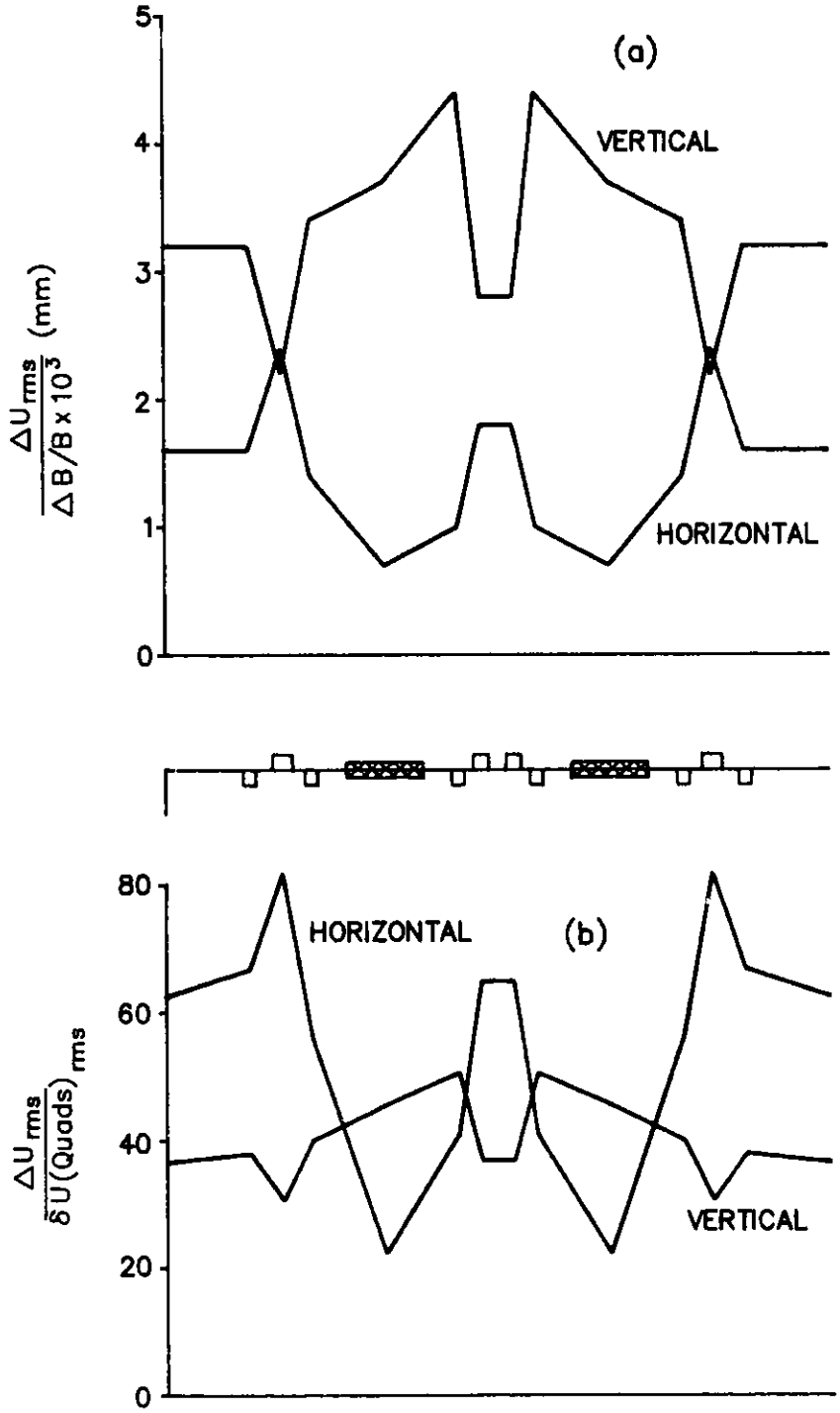

Figure II.1.4-8

ΔU_{rms} for closed-orbit distortions (a) per unit of dipole rms strength error, $\Delta B/B$ (in units of 10^{-3}) and (b) per unit of quadrupole rms alignment error, $\delta U\ (Quads)_{rms}$, where U represents x for horizontal and y for vertical distortions or errors. These ratios are conventionally defined as the closed-orbit amplification factors for dipole and quadrupole errors.

Table II.1.4-1

Horizontal and Vertical Tune Changes Caused by Individual Quadrupole Gradient Errors

	$\frac{\Delta\nu_x}{\Delta B'\ell/B\rho}$	$\frac{\Delta\nu_y}{\Delta B'\ell/B\rho}$	Number of Quads
Q_1	-0.264	0.200	80
Q_2	0.960	-0.300	80
Q_3	-0.191	0.216	80
Q_4	-0.179	0.620	80
Q_5	0.522	-0.380	80
Totals	$\frac{\Delta\nu_{x\ rms}}{(\Delta B'\ell/B\rho)_{rms}} = 10.3$;	$\frac{\Delta\nu_{y\ rms}}{(\Delta B'\ell/B\rho)_{rms}} = 7.5$	

presents the dynamic aperture for a tolerance level of 10^{-4}. This dynamic aperture is more than adequate for efficient injection and operation.

Figure II.1.4-10 shows the dependence of the dynamic aperture ($N_x = N_y$) on the tolerance level. This shows that a finite aperture exists up to a tolerance level of 2×10^{-4}, although not sufficient for routine operation. The effect of closed-orbit correction (described in detail in Section II.1.4.5) is also shown, indicating that this reduction in dynamic aperture can be largely recovered.

This study therefore indicates that the chosen tolerances, which are summarized in Table II.1.4-2, will yield adequate dynamic apertures.

1.4.4 Multipole Imperfections

The influence of systematic and random multipole imperfections on the dynamic aperture is described in this section. The definition of the multipole expansion is given in Section II.4.2. The multipole coefficients common to all magnets of a particular type are the systematic imperfections. Random imperfections are the rms variations of these coefficients between magnets of a given type. The systematic imperfections come from

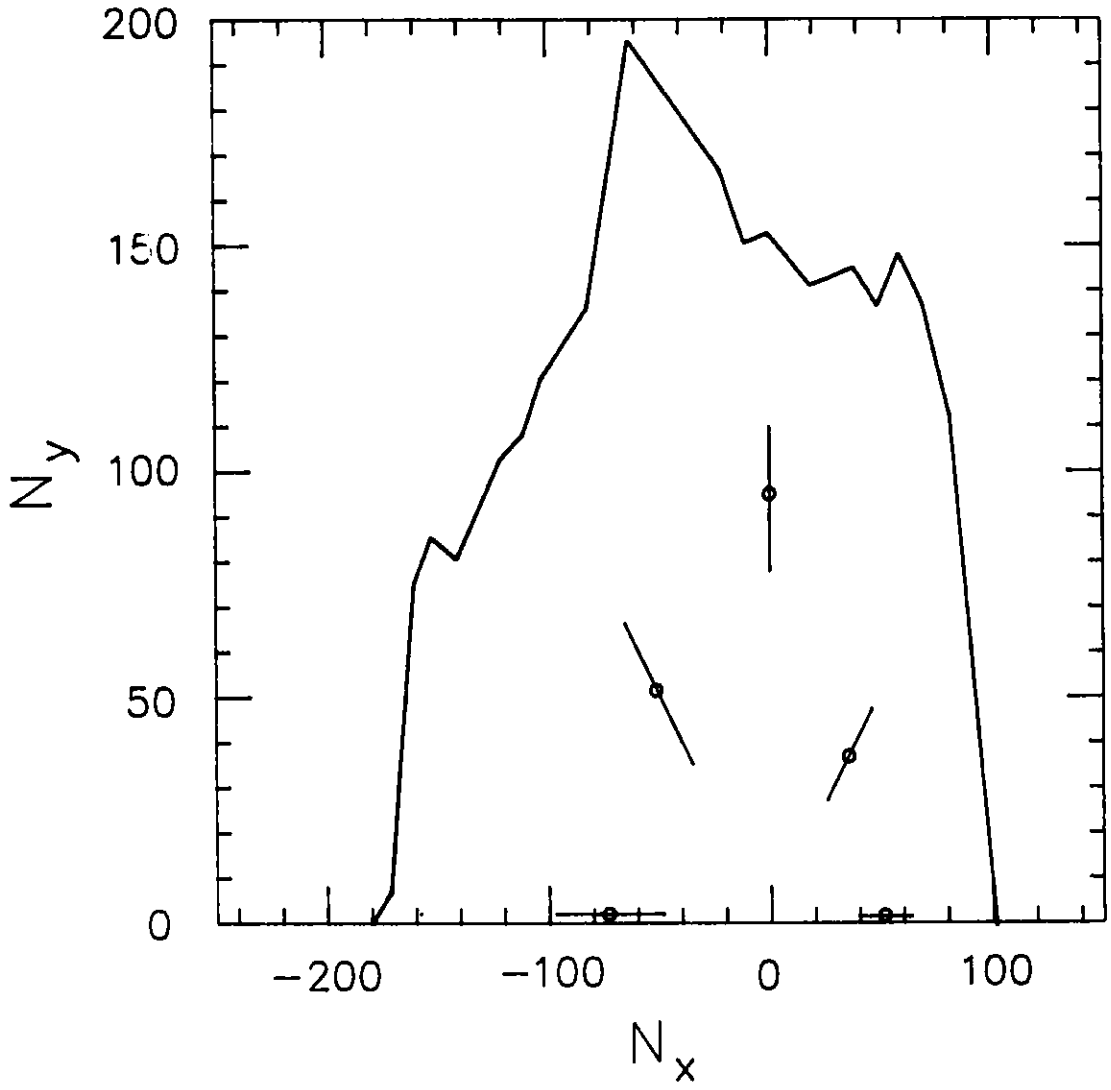

Figure II.1.4-9
Dynamic aperture for a tolerance level of 10^{-4}. The data points are the average dynamic aperture for 10 different machines. The error bars represent the rms spread of the dynamic aperture for the 10 machines. For comparison, the ideal lattice dynamic aperture is plotted as the solid curve.

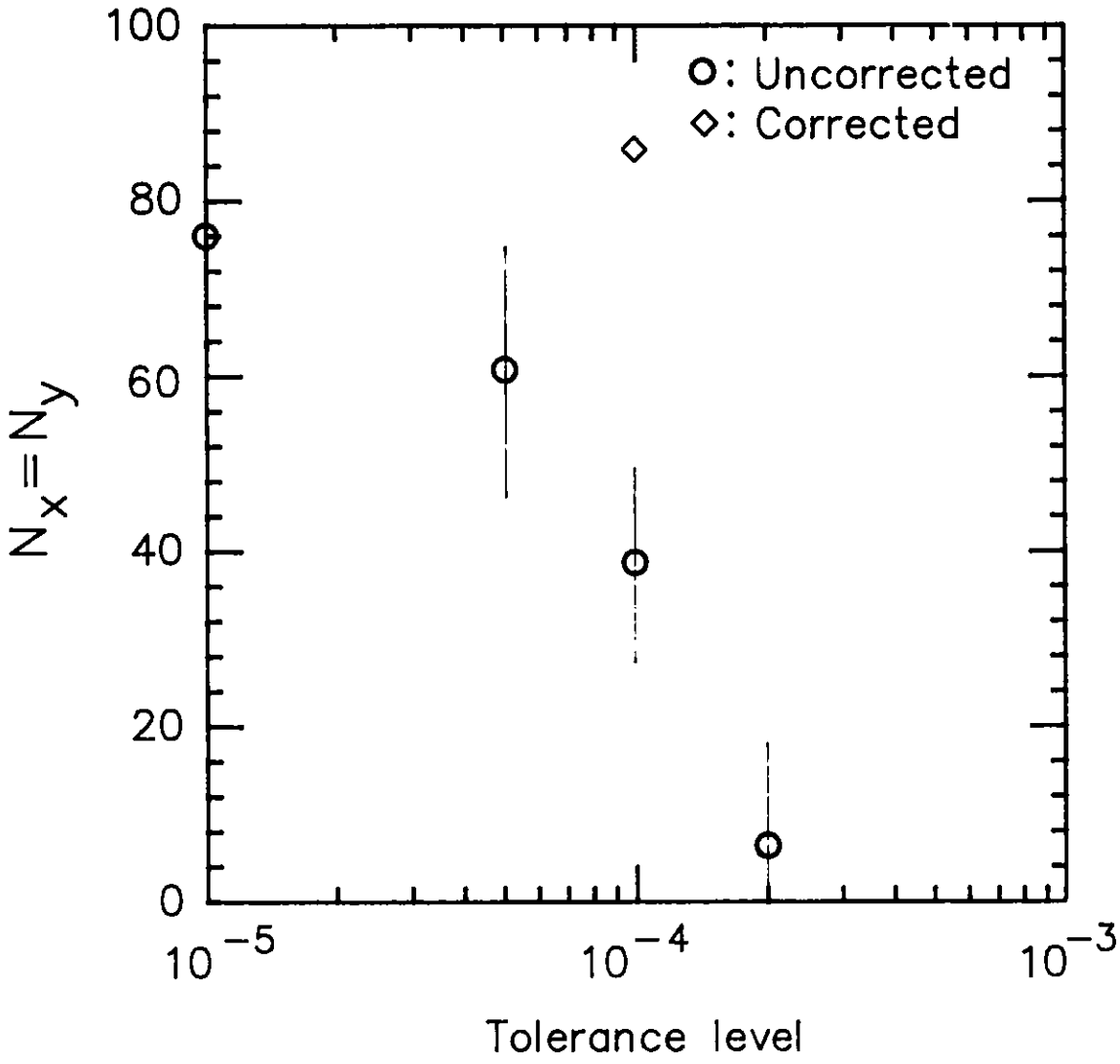

Figure II.1.4-10
The average and rms spread (circles and error bars) of the dynamic aperture $N_x = N_y$ for 10 machines, as a function of the tolerance level. The diamond shows the dynamic aperture for an individual machine resulting from the orbit correction described in Section II.1.4.5.

Table II.1.4-2

Storage Ring Tolerances

Quadrupole Placement	10^{-4} m
Sextupole Placement	10^{-4} m
$\Delta B\ell/B\ell$	10^{-4}
Magnet Roll	10^{-4} rad
$\Delta B'\ell/B'\ell$	10^{-4}
$\Delta B''\ell/B''\ell$	10^{-3}
Correcting-Dipole Current	10^{-3}

magnet design, and the random imperfections come from magnet construction tolerances.

The influence of dipole imperfections has been considered first for a sextupole component. Figure II.1.4-11 shows the reduction of dynamic aperture due to the addition of systematic sextupole coefficients for every dipole magnet equal to $|b_2| = 2.5\times10^{-5}$ cm^{-2}, plus Gaussian-distributed random sextupole coefficients $(b_2)_{rms} = 2.5\times10^{-5}$ cm^{-2}. The reduction in dynamic aperture is about 20% vertically and 15% horizontally and is due almost entirely to the random coefficients. For systematic coefficients alone, a similar dynamic aperture reduction to that of Fig. II.1.4-11 is obtained for a $|b_2| \geq 7.5\times10^{-5}$ cm^{-2}.

The influence of higher-order multipole ($1 < n \leq 9$) imperfections in the dipole magnets was estimated by using the harmonic coefficients calculated by POISSON[12] at a 2-cm radius for the designed dipole magnet at a field of 0.6 T. These multipole components are listed in Table II.1.4-3. Dynamic aperture with systematic multipoles agreed with the aperture without multipoles. By adding a random rms component equal to 100% of the systematic multipoles as shown in Table II.1.4-3, the dynamic aperture was reduced to that shown in Fig. II.1.4-12. The greatest reduction was in the vertical plane, about 15%.

Imperfections in the quadrupole magnets have been parameterized by introducing a dodecapole component, $b_5 = 2.5\times10^{-6}$ cm^{-5}. This error level has insignificant effect on the dynamic aperture for systematic errors, while adding rms random errors at this level results in the reduction of dynamic aperture shown in Fig. II.1.4-13. The largest reduction in aperture is in the horizontal plane, by about 25%.

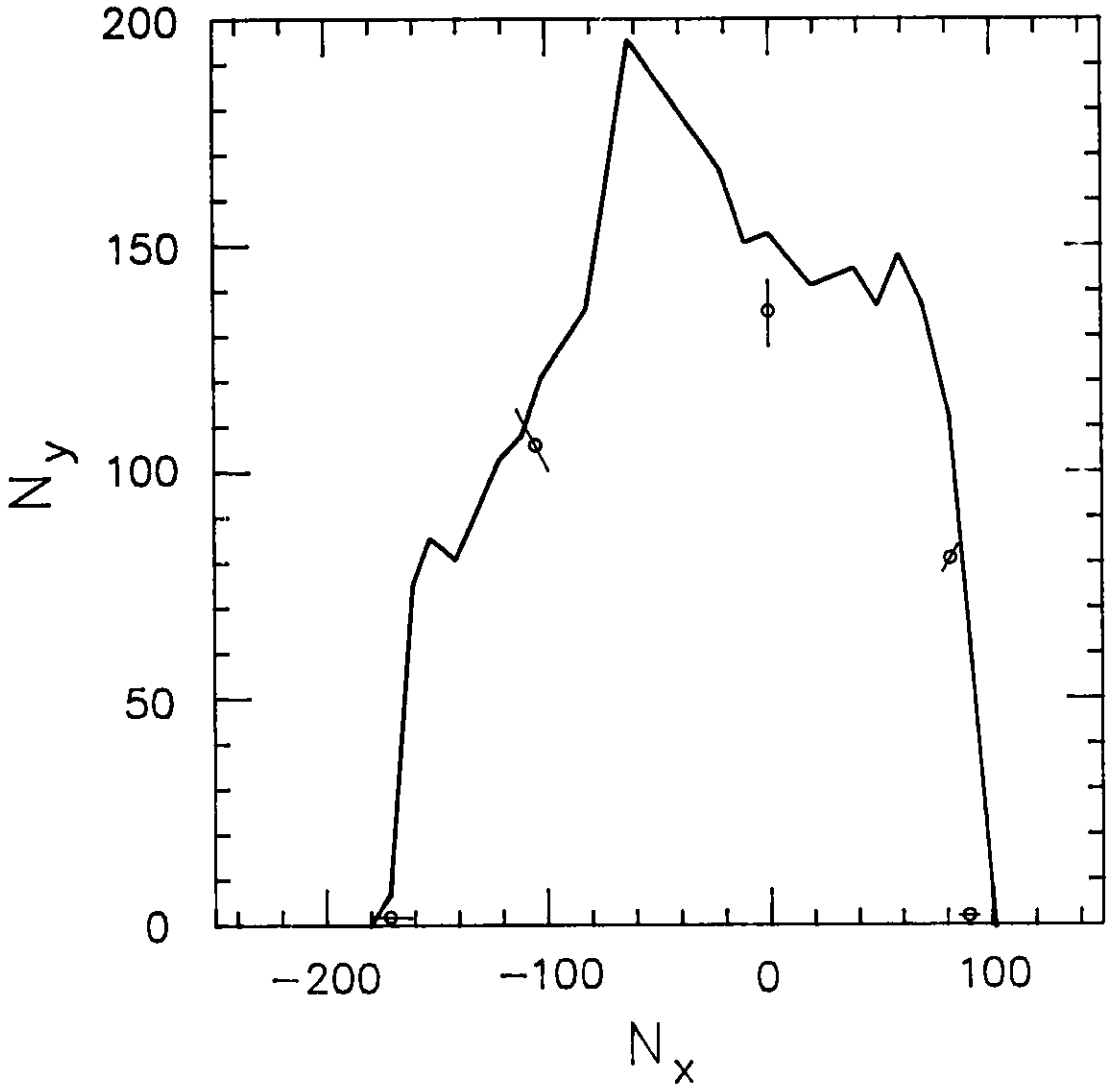

Figure II.1.4-11
Dynamic aperture for systematic and random sextupole components in the dipole, $|b_2| = 2.5\times10^{-5}$ cm^{-2} and $(b_2)_{rms} = 2.5\times10^{-5}$ cm^{-2}.

Table II.1.4-3

Multipole Coefficients for Dipole Magnet at 0.6-T Field

n	$b_n(cm^{-n})$	$a_n(cm^{-n})$
0	1.0	5.67×10^{-7}
1	2.02×10^{-6}	5.0×10^{-7}
2	1.28×10^{-5}	-1.07×10^{-8}
3	9.3×10^{-8}	7.1×10^{-9}
4	5.9×10^{-7}	1.6×10^{-8}
5	4.8×10^{-8}	7.8×10^{-9}
6	-1.2×10^{-7}	1.2×10^{-10}
7	8.5×10^{-9}	8.8×10^{-10}
8	-1.6×10^{-8}	4.3×10^{-10}
9	-1.3×10^{-10}	-3.3×10^{-11}

$$(B_y + iB_x) = B_o \sum_{n=0} (b_n + ia_n)(x + iy)^n$$

Based on these calculations, tolerance levels are set for the following magnets:

- Sextupole component in dipole - b_2 systematic $\leq 7.5\times10^{-5}$ cm^{-2}

  b_2 random $\leq 2.5\times10^{-5}$ cm^{-2}

- Multipole components in dipole - systematic $\leq$ 2 times values given in Table II.1.4-3

  random $\leq$ 1 times values given in Table II.1.4.-3

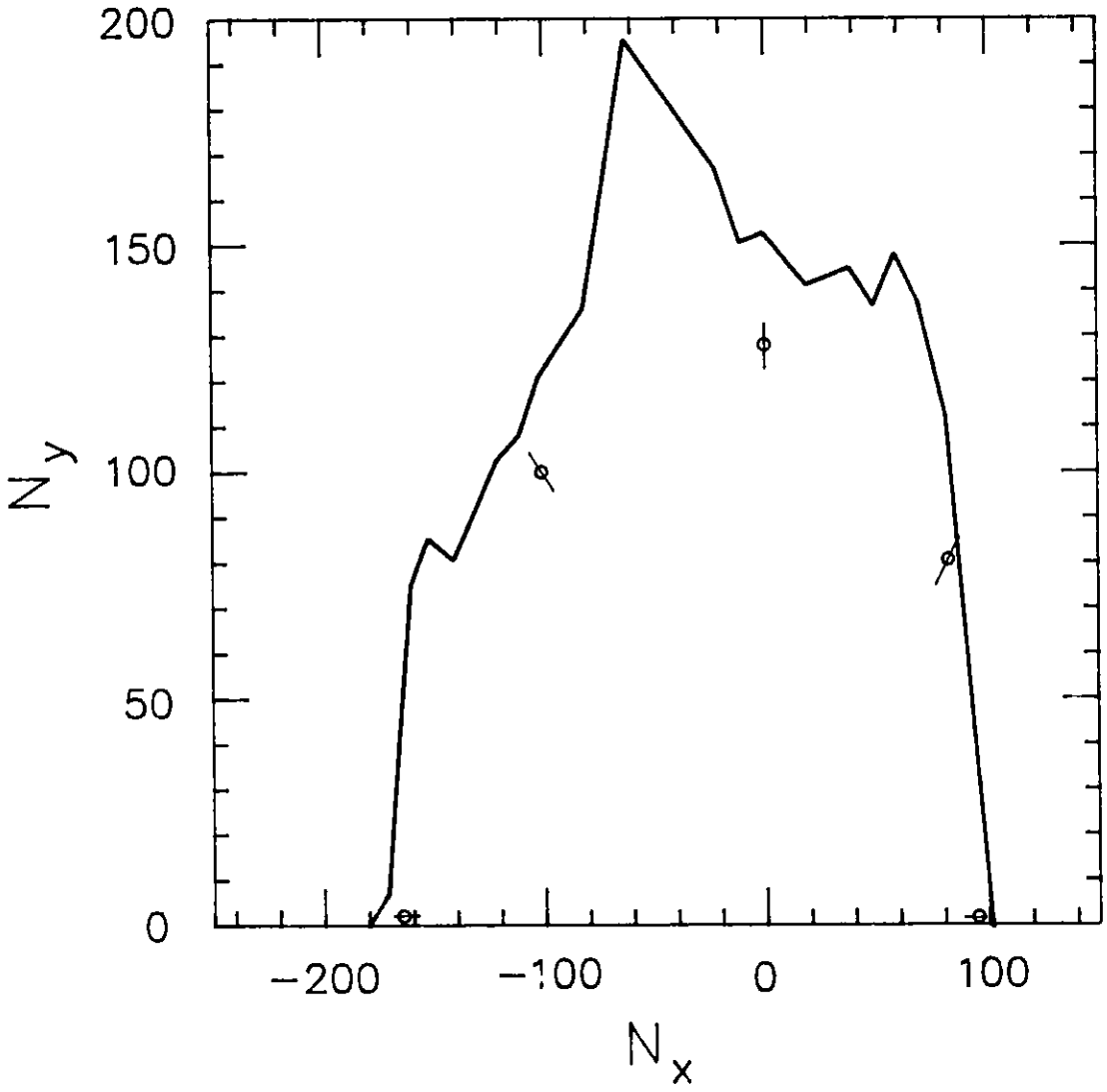

Figure II.1.4-12
Dynamic aperture for systematic and random multipole components in the dipoles, equal to the values listed in Table II.1.4-3.

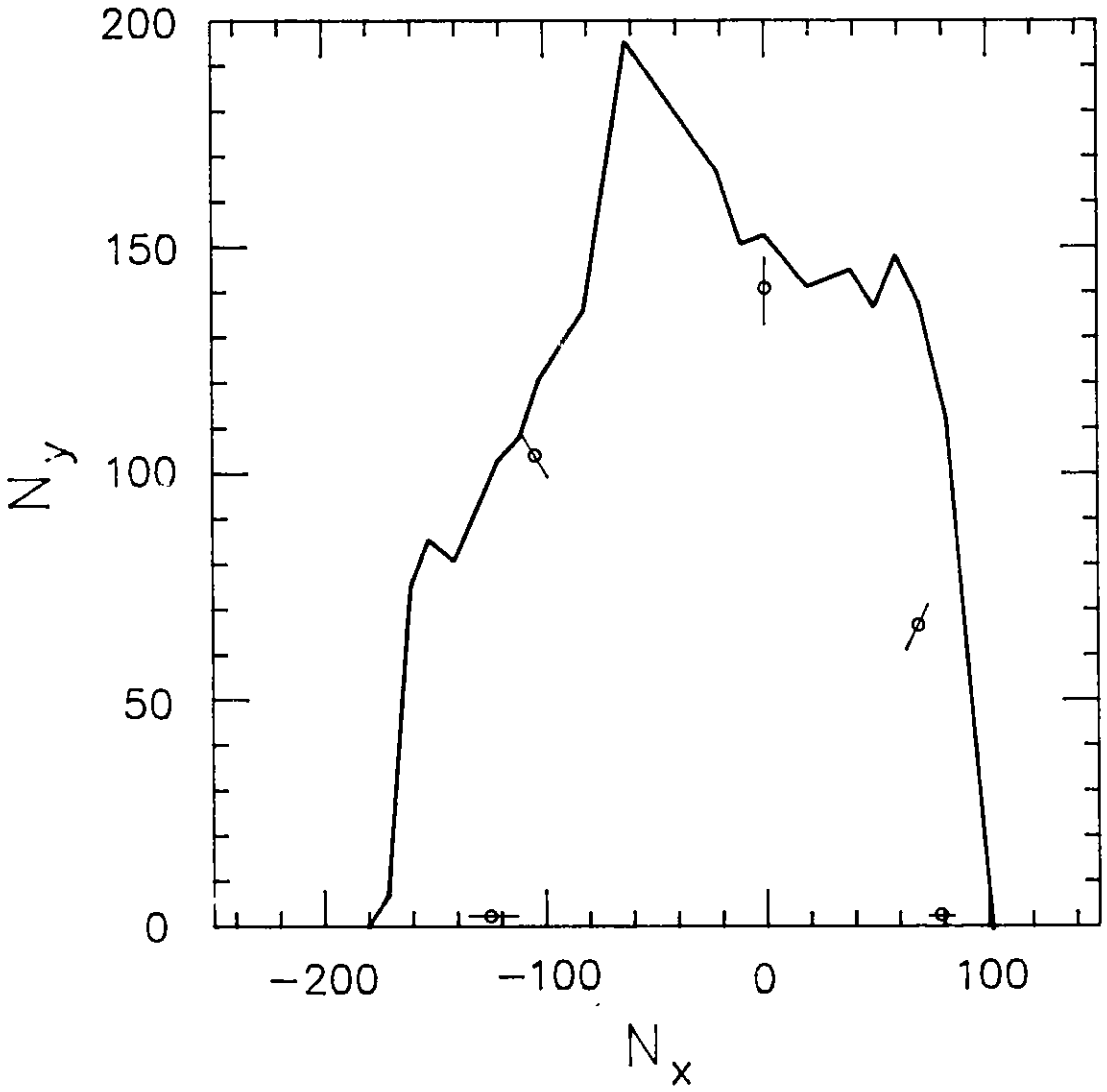

Fig. II.1.4-13
Dynamic aperture for systematic and random dodecapole components in the quadrupoles, $|b_5| = 2.5\times10^{-6}$ cm^{-5} and $(b_5)_{rms} = 2.5\times10^{-6}$ cm^{-5}.

- Dodecapole component in quadrupole - b_5 systematic $\leq 5.0\times10^{-6}$ cm^{-5}

  b_5 random $\leq 2.5\times10^{-6}$ cm^{-5}

These coefficients are comparable with or less than the actual values obtained from PEP magnets.

1.4.5 Closed-Orbit Correction

The reduction in dynamic aperture results mainly from the closed-orbit distortions in the sextupoles. Consequently, beam position monitors for beam steering are provided as close as possible to every sextupole and also at several other locations, as shown in Fig. II.1.4-14. Horizontal and vertical correction magnets (also shown in Fig. II.1.4-14) are placed in the lattice to reduce the closed-orbit distortions at the monitors and therefore in the sextupoles. The correction scheme is simple and uses only four horizontal and four vertical corrector magnets per cell. The remaining correctors are reserved for local steering (see Section II.1.5).

The programs used for orbit correction were RACETRACK,[9] MAD,[8] and PETROS.[13] They indicate that the chosen correction scheme can restore the tune to better than ±0.01 and the emittance to within 2%, for a tolerance level of 10^{-4}. Figure II.1.4-15 (a and b) shows the horizontal and vertical closed-orbit distortions at the monitors before and after correction. The corrected closed orbit is limited by an assumed ±0.1-mm rms monitor positioning accuracy. Figure II.1.4-16 shows the horizontal and vertical corrector strengths for the entire machine. The maximum corrector strength is less than 0.25 mrad for the four machines studied.

The dynamic aperture for the corrected closed orbit is calculated by using tracking in RACETRACK and MAD. These results are presented in Fig. II.1.4-10 and indicate that the dynamic aperture can be fully restored for a tolerance level of 10^{-4} and to better than 70% of the zero-error dynamic aperture, even for levels of 5×10^{-4}.

1.5 Local Steering in the Insertion Regions

Orbit correctors are provided at every straight section containing insertion devices. The positron beam position can be measured to 30 microns. Better position accuracy can be provided by the photon beam. Each photon beam line is equipped with a monitoring and feedback steering system to control the position and direction of the positron beam as it enters the device.

The local orbit steering system is composed of two pairs of magnets for each plane. A pair of magnets in each plane located upstream of the device adjusts both position and angle of the positron beam in the insertion device. The downstream pair of

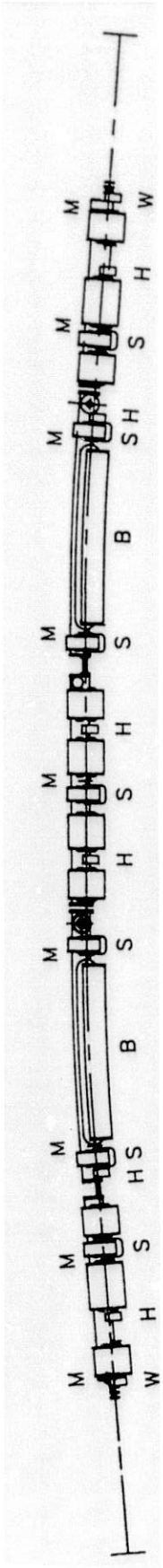

Figure II.1.4-14
Monitors and correction dipole for one cell of the storage ring.

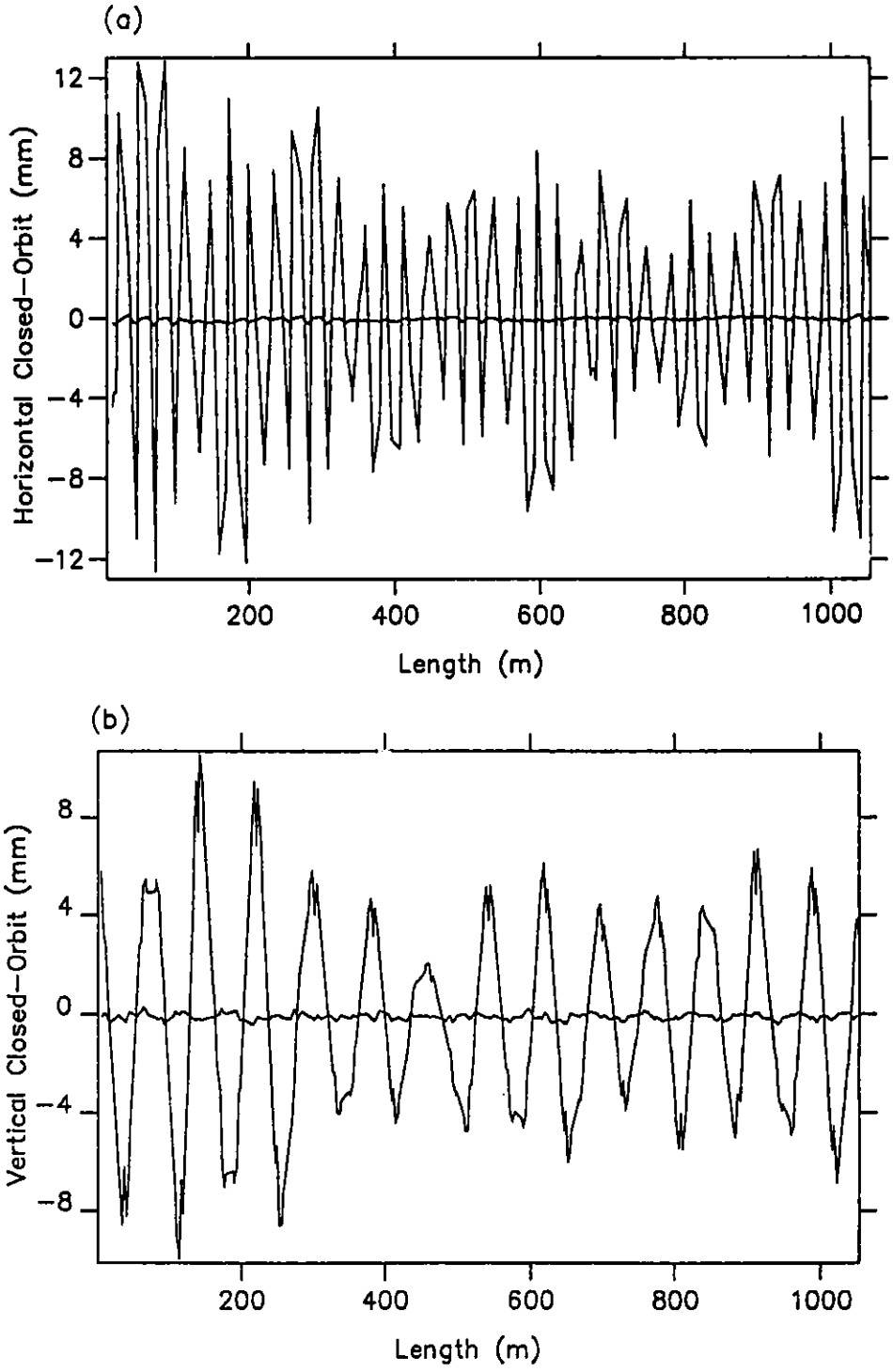

Figure II.1.4-15
Closed-orbit distortions at the monitors for the entire machine, at a 10^{-4} tolerance level, with and without correction: (a) horizontal, (b) vertical.

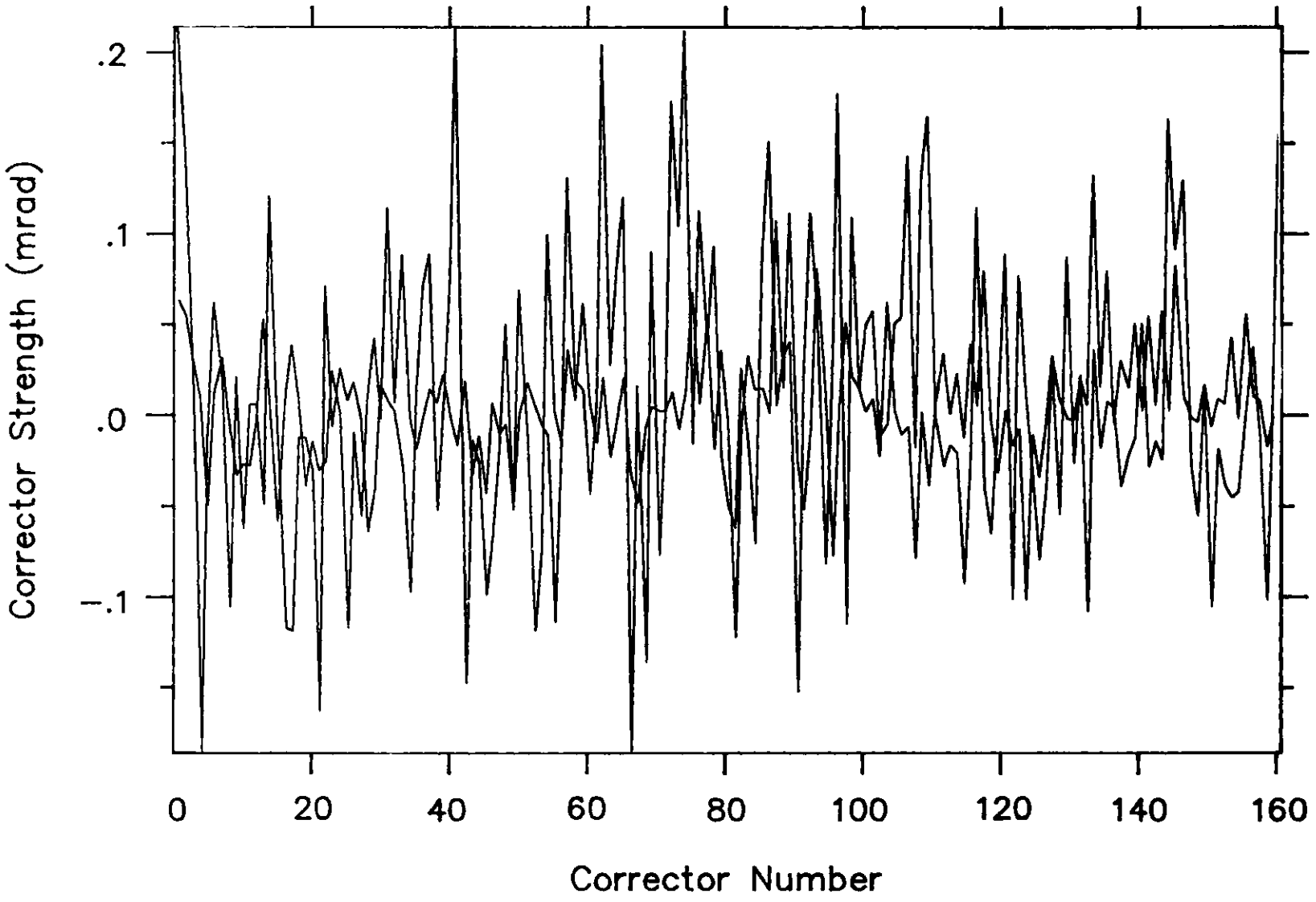

Figure II.1.4-16
Horizontal and vertical correction magnet strength in mrad for the corrections shown in Figure II.1.4-15 (a and b).

magnets in each plane restores the positron beam to the circulating orbit. The distance between the magnets of a pair is 1 m, and maximum integrated field of each magnet is 0.032 T·m. This system produces maximum position and angle changes of 1.4 mm and 1.4 mrad. These local steering magnets are shown in Fig. II.1.4-14.

1.6 Influence of Insertion Devices

The expressions generally used to represent the fields in undulators and wigglers are

$$B_y = B_o \cosh(k_x x) \cosh(k_y y) \cos(kz) ,$$

$$B_x = \frac{k_x}{k_y} B_o \sinh(k_x x) \sinh(k_y y) \cos(kz) ,$$

and

$$B_z = \frac{-k}{k_y} B_o \cosh(k_x x) \sinh(k_y y) \sin(kz) ,$$

where

$$k_x^2 + k_y^2 = k^2 = \left(\frac{2\pi}{\lambda_o}\right)^2 ,$$

λ_o is the period of the insertion device, x and y are the coordinates in the transverse direction, and z is the cooordinate in the longitudinal direction. The nonlinear effects of these fields on the stored beam are discussed below.

With k_x small, the equations of motion about the oscillating equilibrium orbit, averaged over z, are[14]

$$y'' = \frac{-\sinh(2ky)}{4k\rho^2} ,$$

and

$$x'' = 0 ,$$

where ρ is the radius of curvature in the peak field in the insertion devices, B_o.

The vertical linear tune shift caused by a single insertion device of length L is

$$\Delta\nu_y(\text{linear}) = \frac{\beta_y L}{8\pi\rho^2} = \frac{\beta_y L}{8\pi} \frac{B_o^2}{(3.33\ E)^2} ,$$

and

where E is in GeV and β_y is the average vertical lattice function.

At 7 GeV with a field of 0.65 T, L = 5 m and β_y = 10 m, the value is

$$\Delta\nu_y(\text{linear}) = 1.5\times10^{-3} \text{ per ID.}$$

With many such devices around the ring, these tune changes are additive. They can be reduced by adjusting the quadrupoles in the ID section.

In this study, the linear effects of the device are represented by a pseudo-quadrupole matrix with vertical elements equal to those for a vertically focusing quadrupole with a gradient of $B_o/2\rho$ and length L, and the horizontal elements equal to those for a drift space of length L. After introducing the matrix into the insertion region, the quadrupole triplets at both ends of the insertion region are adjusted to match the insertion device into the lattice structure. Since only two quadrupoles are required for the matching, the third quadrupole is adjusted so that the sum of the squares of the tune changes in both planes is a minimum. For the example shown above, the changes in tunes after matching are

$$\Delta\nu_x \text{ (linear)} = \Delta\nu_y \text{ (linear)} = -\ 3\times10^{-4} \text{ per ID.}$$

The quadrupole adjustments are of the order of 2 to 3%.

The nonlinear tune shift is given by

$$\Delta\nu_y \text{ (nonlinear)} = \frac{\beta_y L}{8\pi\rho^2}\left(\frac{\sinh(2ky)}{2ky} - 1\right) \quad .$$

For λ_o = 2.2 cm and y = 4 mm, which is the half-aperture of the vacuum chamber, $\Delta\nu_y$ (nonlinear) is 7×10^{-4}. Therefore, insertion devices have very little effect on the stored beam at 7 GeV. Numerical simulations described below agree with this conclusion.

For tracking purposes, the nonlinear terms of the undulators are lumped at the center. The vertical kick produced by the nonlinear terms is expressed by

$$\Delta y' = \frac{-L}{4k\rho^2}\left[\sinh(2ky) - 2ky\right] \quad .$$

Two tunable undulators designed to cover the photon energy range from 5 to 20 keV were tested. These undulators are listed in Table II.1.6-1.

Table II.1.6-1

Undulator Parameters

Device	λ_o (cm)	No. of Periods	Energy Range (keV)	Gap Range (cm)	Field Range (T)
A	3.3	158	14-3.5	3.25-1.0	0.098-0.81
B	2.2	236	20-14	1.7-1.0	0.165-0.45

Positrons were tracked with up to 10 undulators of type A operating at 0.81 T and up to 14 undulators of type B operating at 0.45 T. This combination of undulators and magnetic fields represents the most extreme case that is expected to be encountered. All dynamic apertures were larger than the ±4 mm physical aperture of the vacuum chamber.

Figure II.1.6-1 is typical of all the tracking runs. For this run, 16 of the type A undulators and 16 of the type B undulators are chosen with fields ranging from minimum to maximum and placed at random in 32 of the insertion straight sections. The resulting vertical dynamic aperture is well outside the physical aperture. Comparison of the physical-aperture-limited results with the corresponding results without insertion devices (Fig. II.1.6-2) shows no real difference. The difference between the aperture (shown as a straight line in both figures) and the aperture-limited vertical oscillation amplitudes is due to the smearing of the vertical amplitudes. This term is used to describe the variations in amplitude of the vertical oscillations caused by coupling with the horizontal oscillations in the sextupoles. Any increase of this smearing due to the presence of the insertion devices would signify a reduction in beam lifetime. The smearing shown in the two figures is almost identical. Therefore, this study indicates that the insertion devices should have no effect on beam lifetime beyond that introduced by the physical aperture itself.

1.7 Adjustment of Horizontal-Vertical Coupling

Twenty skew quadrupoles are used to adjust the horizontal-vertical betatron coupling in order to vary the ratio between the horizontal and vertical emittances. These are located between the upstream Q_4 and Q_5 pair in every other dispersion section. Each skew quadrupole is 15 cm long and capable of a maximum gradient of 2 T/m.

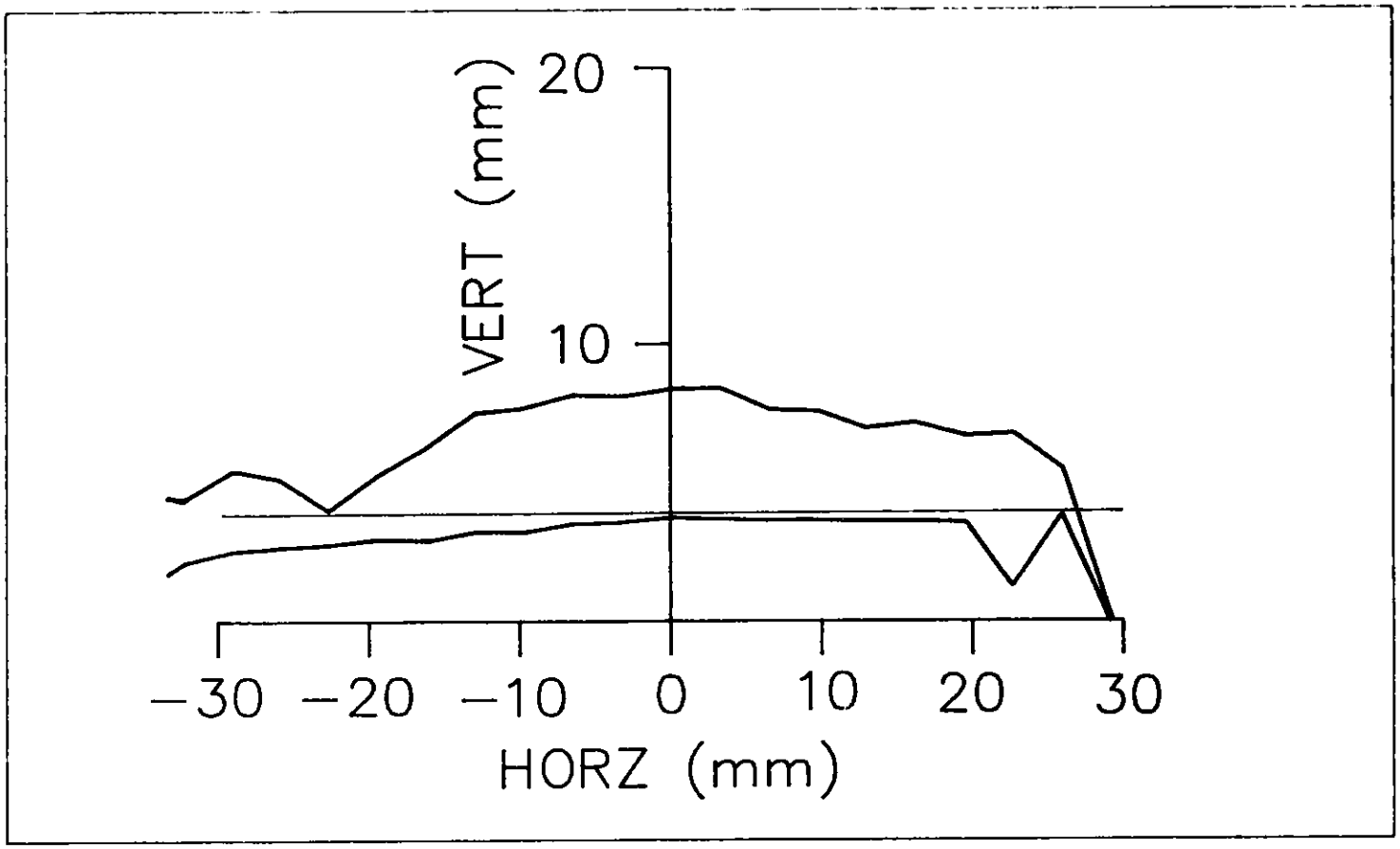

Figure II.1.6-1

The upper curve is the dynamic aperture with 32 insertion devices in the ring. The lower curve shows the limiting initial betatron amplitudes of tracked particles that survived a physical vacuum chamber aperture of ±4 mm, at the 32 insertion devices considered in the upper curve.

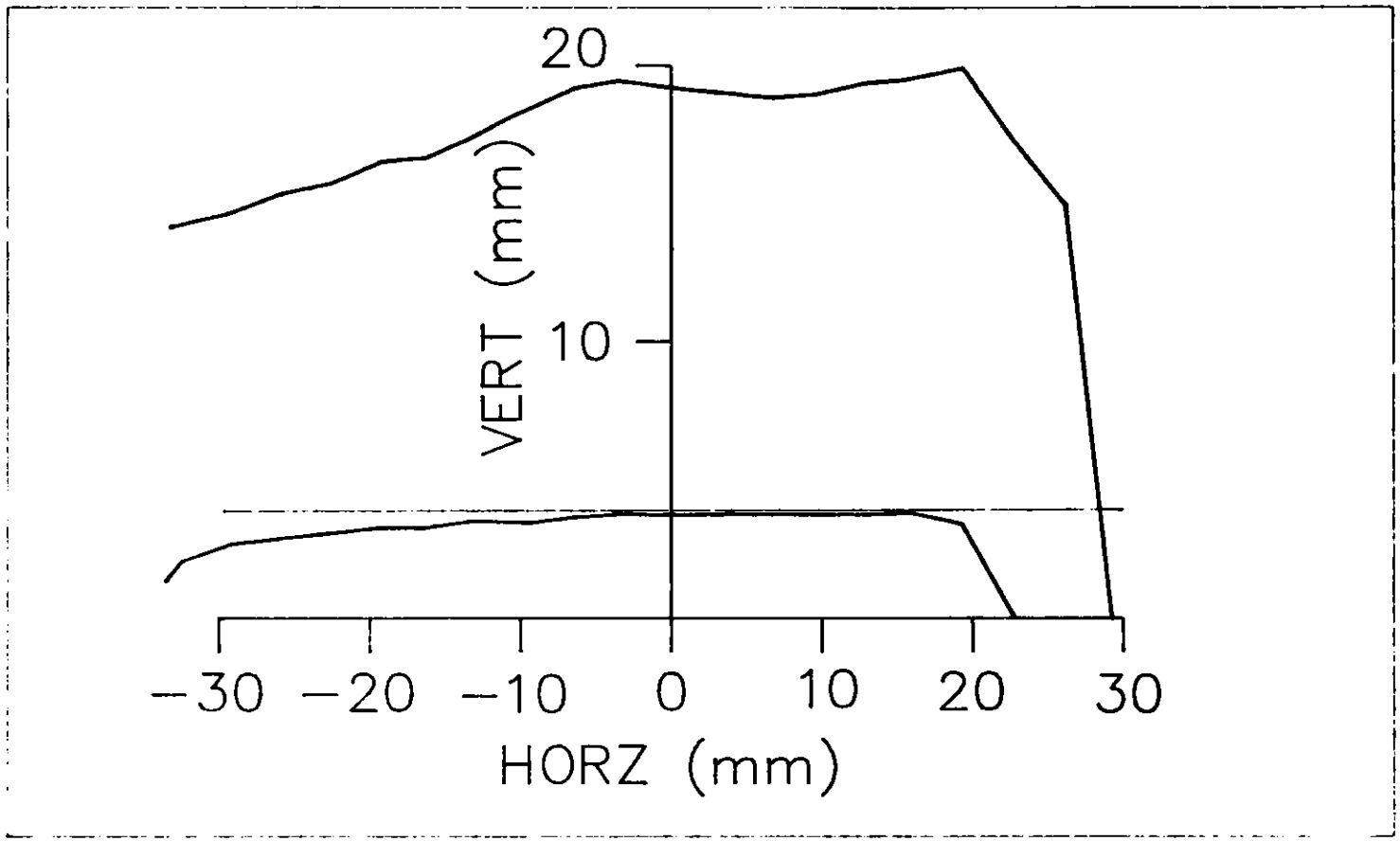

Figure II.1.6-2
The upper and lower curves show the limiting initial betatron amplitudes that survive physical vacuum chamber apertures of ±20 mm and ±4 mm, respectively.

The most effective way to adjust the coupling is to use the harmonic of the skew quadrupole field which excites the nearest linear coupling resonance. For the present tunes of $\nu_x = 35.216$ and $\nu_y = 14.298$, this resonance is $\nu_x - \nu_y = 21$. With 20 symmetrically distributed skew quadrupoles, to create the 21st harmonic we need to excite them in a first-harmonic pattern. To obtain 100% coupling at these tune values, one only needs a gradient of ~ 0.6 T/m, but since tuning for the optimal operating conditions on the completed machine may result in tune values quite different from the design values and since 2 T/m is still a very modest gradient we have chosen this value. This gradient is adequate to yield 100% coupling even if the operating tunes are at the maximum distance of 0.5 away from the 21st-harmonic coupling resonance given above.

At the opposite end, these skew quadrupoles are also necessary to totally decouple the horizontal and the vertical betatron oscillations. Because of imperfections in construction and alignment, error skew quadrupole fields will exist in the storage ring. The skew quadrupole system is needed to compensate for these error fields to obtain total decoupling between the horizontal and the vertical planes.

1.8 Influences of Vibration

In the design of the storage ring, the natural emittance ε is a parameter of prime importance. The natural emittance of this storage ring is 8×10^{-9} m. Any vibrations that lead to distortions in the closed orbit will result in a larger effective emittance.

Vibration criteria for the storage ring, in terms of allowable horizontal and vertical vibration of the pertinent magnets in the lattice, are discussed and defined in this section. Possible excitation sources and a study program that includes vibration measurements, model development and analysis, and vibration isolation are discussed in Section IV.2.5.

1.8.1 Emittance Growth

The total effective emittance is

$$\varepsilon_{eff} = \varepsilon + \Delta\varepsilon$$

where $\Delta\varepsilon$ is the emittance growth due to vibration.

External perturbations associated with mechanical vibration result in closed-orbit deviations that change with time. The vibrations lead to positron and photon beam steering for low frequencies and to an apparent emittance growth for high frequencies. The effect of low-frequency vibrations (below 20 Hz) can be alleviated with feedback systems using steering magnets. Higher frequency vibrations that result in unacceptable emittance growth cannot be corrected in this manner and must be eliminated at their

source or otherwise controlled (see Section IV.2.5). For 10% emittance coupling of the x and y planes, the beam parameters in the ID region are:

$$\sigma_x = 321\ \mu m\ ; \quad \sigma_x' = 24.7\ \mu rad$$

$$\sigma_y = 89\ \mu m\ ; \quad \sigma_y' = 8.9\ \mu rad\ .$$

If the emittance growth is to be limited to 10%, the closed-orbit displacements and angles are:

$$\Delta\sigma_x < 16.1\ \mu m\ ; \quad \Delta\sigma_x' < 1.2\ \mu rad$$

$$\Delta\sigma_y < 4.4\ \mu m\ ; \quad \Delta\sigma_y' < 0.45\ \mu rad\ .$$

These deviations are a small percentage of the nominal beam phase-space dimensions given above.

1.8.2 Vibration Criteria

Establishing criteria for allowable levels and frequencies of vibration of the magnet elements requires development of relationships (magnification factors) between the closed-orbit distortions and magnet vibrations, and the definition of a threshold frequency below which magnet vibrations can be corrected with correction magnets.

Among the basic magnet types (dipole, quadrupole, and sextupole) that make up the storage ring lattice, vibration of quadrupoles has the most significant effect on the closed-orbit distortions and, hence, on the emittance growth. We have considered the effect on emittance growth of: (a) the vibration of a single quadrupole due to local excitation, (b) random (uncorrelated) vibration of all the quadrupoles, and (c) plane-wave vibration of the magnet lattice due to ground motions. The magnification factors, A_x and A_y, of the closed-orbit disturbance corresponding to each of these types of vibration have been calculated and are given in Table II.1.8-1.[15] The results given in this table for excitation of a single quadrupole are for the particular quadrupole giving the highest magnification factor. Since we are most interested in the effective emittance growth in the ID regions, the results given in the table correspond to that region.

Assuming that the maximum allowable emittance growth due to vibration is 10%, these magnification factors yield the maximum allowable vibration amplitudes, which are given in Table II.1.8-2. As noted above, the vibrations at frequencies less than about 20 Hz can be controlled by the correction magnets.

Table II.1.8-1

Magnification Factors A_x and A_y for Closed-Orbit Beam Distortions

Vibration Type	A_x	A_y
Single Quadrupole	7.2	3.4
Random (all quadrupoles)	62	37
Plane Wave* (v in m/s, f in Hz)		
$f < 0.0072\ v$	1.0	1.0
$0.0072\ v < f < 0.015\ v$	1.0	1.0-15.6
$0.015\ v < f < 0.025\ v$	1.0	15.6
$0.025\ v < f < 0.044\ v$	1.0-17.9	15.6
$f > 0.044\ v$	17.9	15.6

*The propagation velocity v of a plane wave in the ground depends on the soil structure of the APS site and is being measured.

1.8.3 Effects of Magnet Supports

The values of the magnification factors of the plane-wave-type vibration listed in Table II.1.8-1 are calculated by assuming that the displacement of the magnet elements is equal to that of the ground. In order to get a more realistic estimate of the magnification factors, one has to take the effects of the magnet support into account.

In each straight section of the storage ring, several quadrupoles and sextupoles are supported on a girder which, in turn, is supported off the floor slab on jacks, as illustrated in Fig. II.4.10-2. The magnet/support assembly represents a dynamic system that can act to either amplify or attenuate vibration motion associated with ground movement. A normal mode method has been used to analyze this system.[16] As an example, we have employed this method to run a numerical simulation using representative values for the parameters characterizing the magnets and support structures. The results are given in Fig. II.1.8-1 as allowable amplitude of ground vibration for an emittance growth of 10%. The results show that at the third (~41 Hz) and fifth (~128 Hz) natural frequencies of the magnet/support system, the inherent dynamic amplification drives the allowable amplitude of ground motion to extremely low values; as a comparison, Fig. II.1.8-2 shows the allowed vibration amplitude when the dynamic characteristics of the supports are neglected.

Table II.1.8-2

Maximum Allowable Vibration Amplitude for an Emittance Growth of 10%*

Vibration Type	$(\delta_m)_{H\|max}$, μm	$(\delta_m)_{V\|max}$, μm
Single Quadrupole	2.2	1.29
Random (all quadrupoles)	0.26	0.12
Plane Wave (v in m/s, f in Hz)		
$f < 0.0072\ v$	16.1	4.4
$0.0072\ v < f < 0.015\ v$	16.1	4.4-0.28
$0.015\ v < f < 0.025\ v$	16.1	0.28
$0.025\ v < f < 0.044\ v$	16.1-0.90	0.28
$f > 0.044\ v$	0.90	0.28

*$(\delta_m)_H$ and $(\delta_m)_V$ are the horizontal and vertical components, respectively, of magnet vibration.

This example serves to illustrate the importance of including the dynamics of the support structure in any vibration analysis. In addition, it should be pointed out that in order to shift the resonant frequencies in Fig. II.1.8-1 when it becomes necessary, a possible way is to change some mechanical parameters of the magnet/support system.

Preliminary measurements of ground vibrations as a function of frequency are shown in Fig. II.1.8-3. The ground vibration amplitudes shown in this figure are substantially less than the allowable amplitudes shown in Figs. II.1.8-1 and II.1.8-2.

1.9 Beam Abort System

In order to remove the stored beam in a safe and controlled manner for normal and abnormal operation, a beam abort system is provided.

The cleanest and most effective beam abort system is high-efficiency single-turn beam extraction. The abort system consists of a fast kicker system, a septum magnet, a beam transport line, and a beam dump. The rise time of the kicker is shorter than the separation time between bunches of about 55 ns and has a flat top of 4 μs so that all beam bunches are extracted in a single turn. The septum magnet is a Lambertson type constructed from permanent magnets and deflects the beam downward.

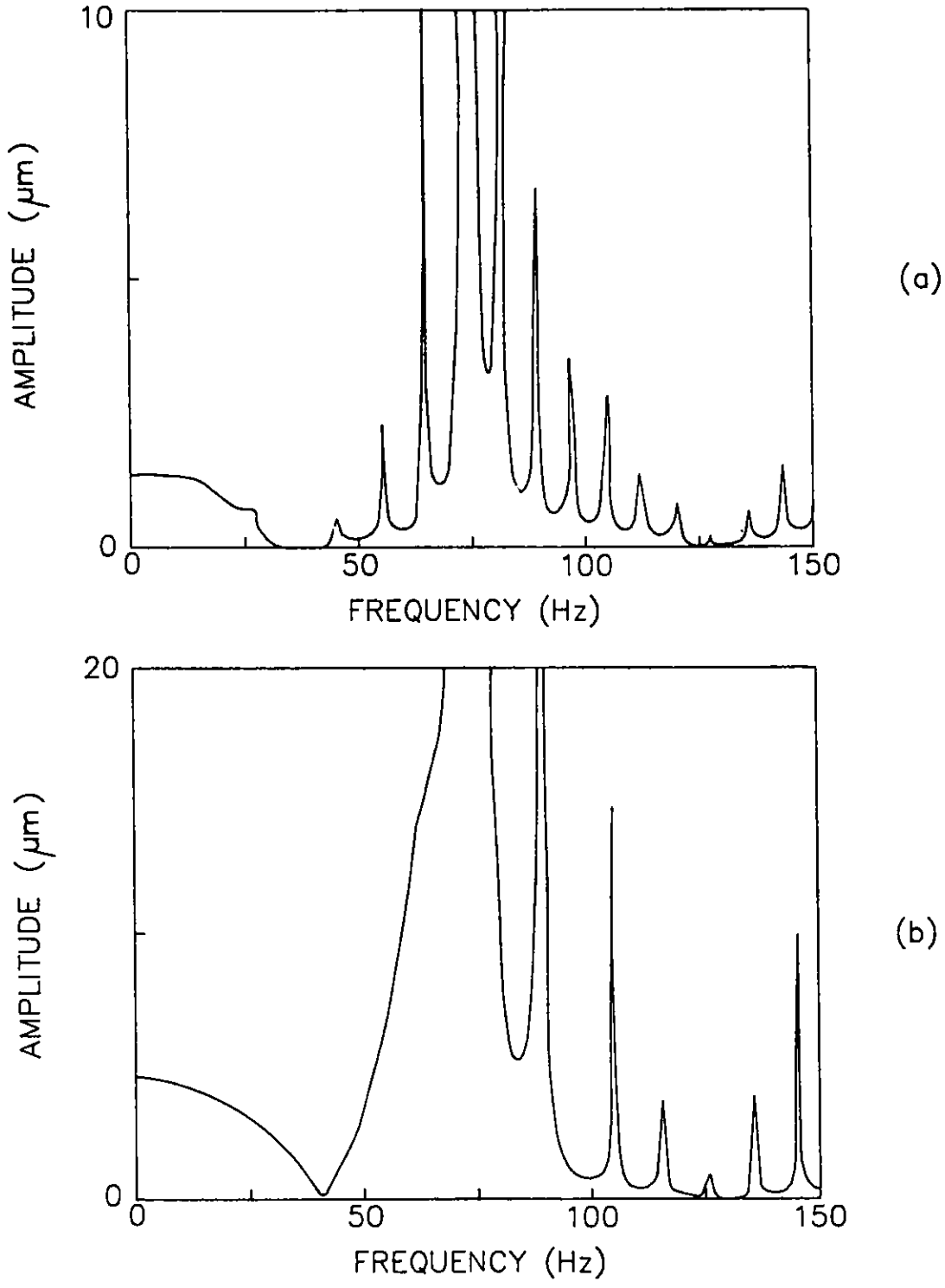

Figure II.1.8-1
Allowable amplitude of ground vibration for 10% growth in emittance when support effects are considered: (a) vertical, (b) horizontal. (Propagation velocity of ground motion is assumed to be 2500 m/s.)

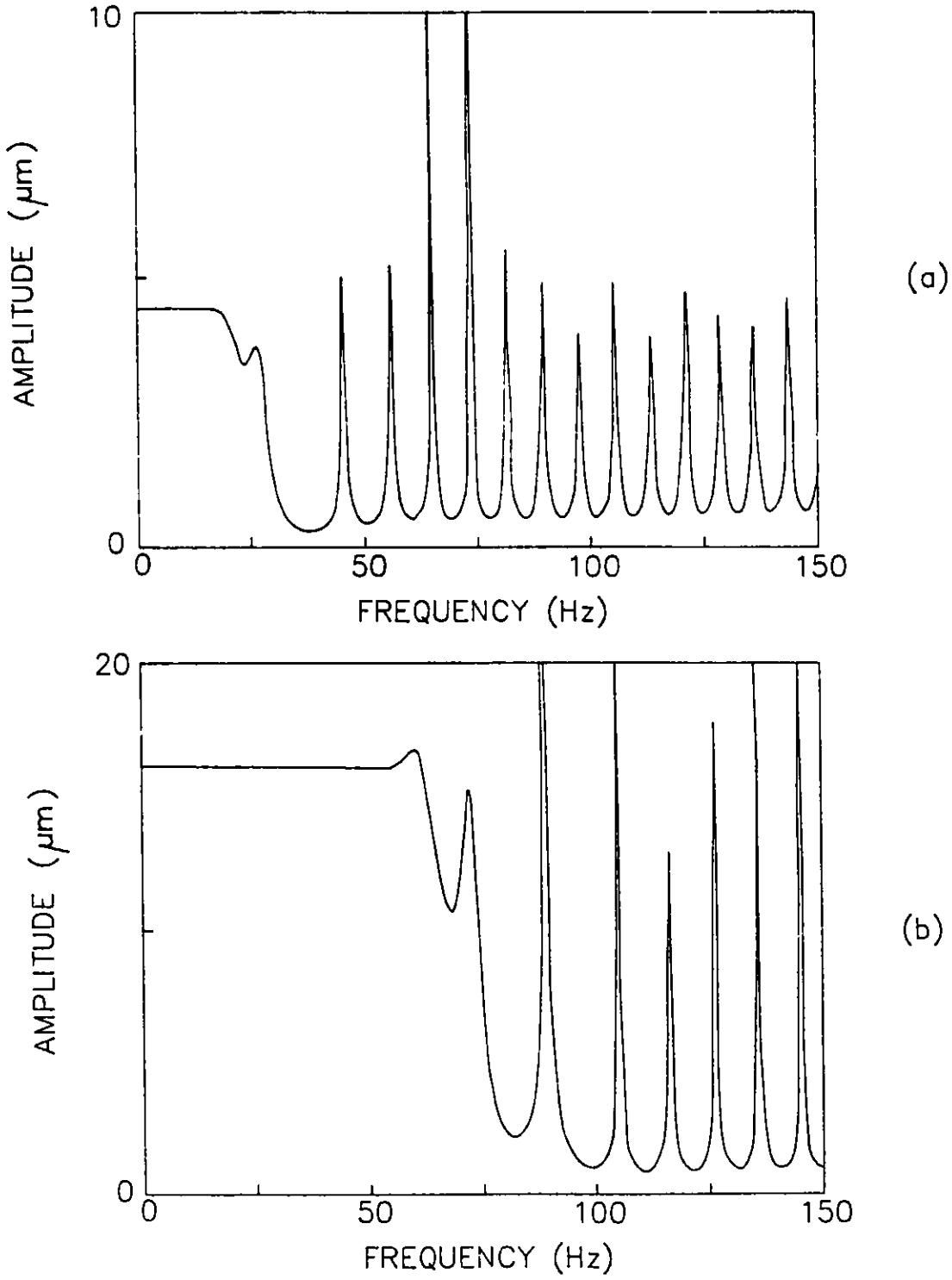

Figure II.1.8-2
Allowable amplitude of ground vibration for 10% growth in emittance when support effects are ignored: (a) vertical, (b) horizontal. (Propagation velocity of ground motion is assumed to be 2500 m/s.)

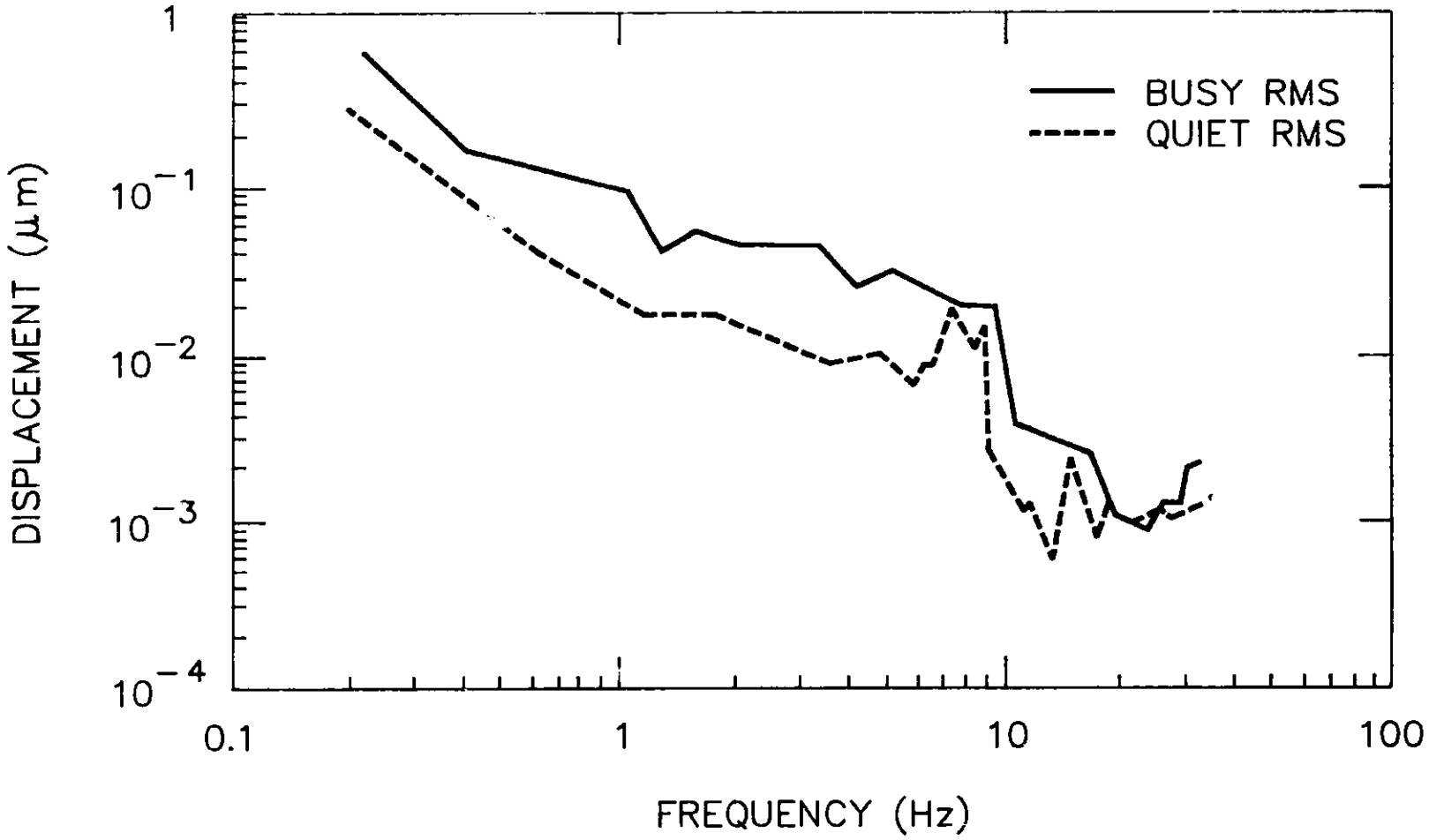

Figure II.1.8-3
Envelope of the peaks of natural rms ground vibrations plotted vs. frequency for a quiet period, December 26, 1985, and a busy period, January 3, 1986.

When the beam is to be aborted, it is first deflected inward 1.14 mrad by a 55-cm kicker K1 as shown in Fig. II.1.9-1. It then traverses through almost a full sector such that at a second kicker K2, it is about 24 mm from the central orbit. K2 deflects the beam outward 1.14 mrad and puts the beam at 19.4 mm, with a slope of 0.7 mrad at the entrance to the septum. The phase advance between K1 and the septum is 290°. Throughout its deflected path, the maximum excursion is 24 mm, as shown in Fig. II.1.9-1. The beam then enters the 3-m-long septum magnet. The septum is 2 mm thick and located 50 σ_x from the central orbit, allowing 4 σ_x for extracted beam clearance, as shown in Fig. II.1.9-2.

The septum magnet bends the beam 5.5° vertically downward. At the first quadrupole downstream of the septum, the beam is 40 cm below and 2 cm to the outside of the central orbit. The beam dump is positioned after this quadrupole, with details shown in Fig. II.1.9-3.

1.10 Injection

Injection into the storage ring is from the inner radius into a long straight section. The injector synchrotron accelerates eight bunches to 7 GeV at a 1-Hz rate. (See Section II.10.1.) These eight bunches are extracted one at a time on the flat top of the synchrotron and injected into designated rf buckets in the ring at a 60-Hz rate. The acceleration cavities of the two machines have equal frequencies and are locked together in phase.

In the storage ring, four bumper magnets are used to locally displace the orbit of the stored beam inward toward a thin-septum magnet. Two of the bumpers are located in the straight section, while the other two are located between Q1 and Q2 (Fig. II.1.10-1). The Q1 provides an additional kick to the beam, requiring the bumpers in the straight section to operate at a higher field. These bumper magnets operate at a 60-Hz repetition rate, but they have rise and fall times of 10.0 μs.

Since the bumped beam stays close to the septum only for a brief time, it is allowed to come within 5 σ_x of the septum. The thin-septum magnet is placed at 50 σ_x from the central orbit. The emittance of 8×10^{-9} m and β_x = 13 m give σ_x = 0.322 mm in the injection region. Therefore, the septum is 16.1 mm and the bumped orbit 14.5 mm from the central orbit.

The injected beam from the synchrotron has a σ_i of 1.3 mm. It leaves the septum magnet at a distance of 2.2 σ_i from the septum. The septum thickness is 2 mm so that the injected beam is 20 σ_x from the bumped orbit. The injection efficiency as a function of the effective aperture of the ring is shown in Fig. II.1.10-2. For an efficiency of more than 95%, the effective aperture must be greater than 28 σ_x. Figure II.1.10-3 shows the relative position and sizes of stored, bumped, and injected beams at the thin septum. The bumper and septum magnets are described in Section II.4.7.

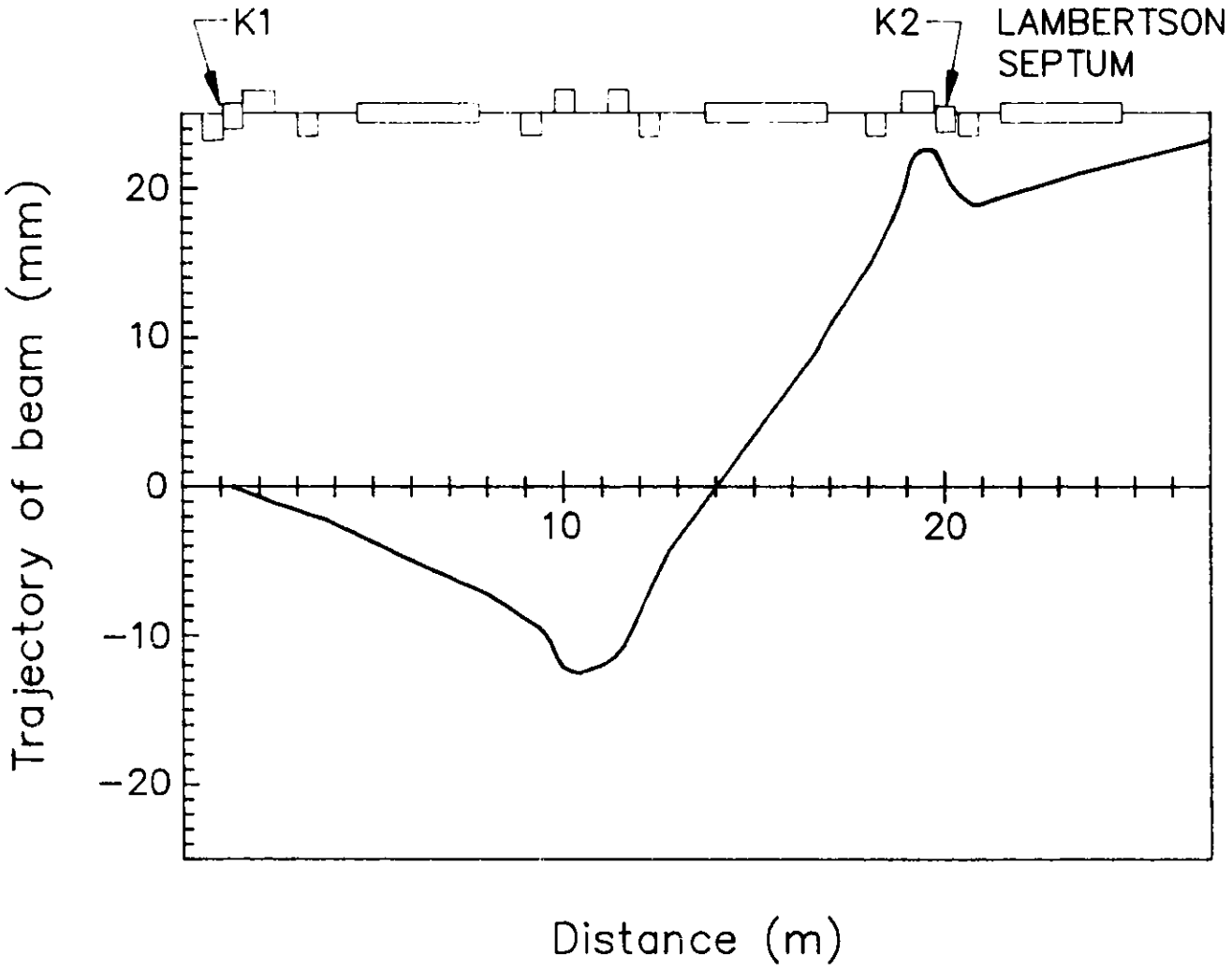

Figure II.1.9-1
Horizontal displacement of beam in abort mode. The septum magnet bends the beam vertically downward (into page).

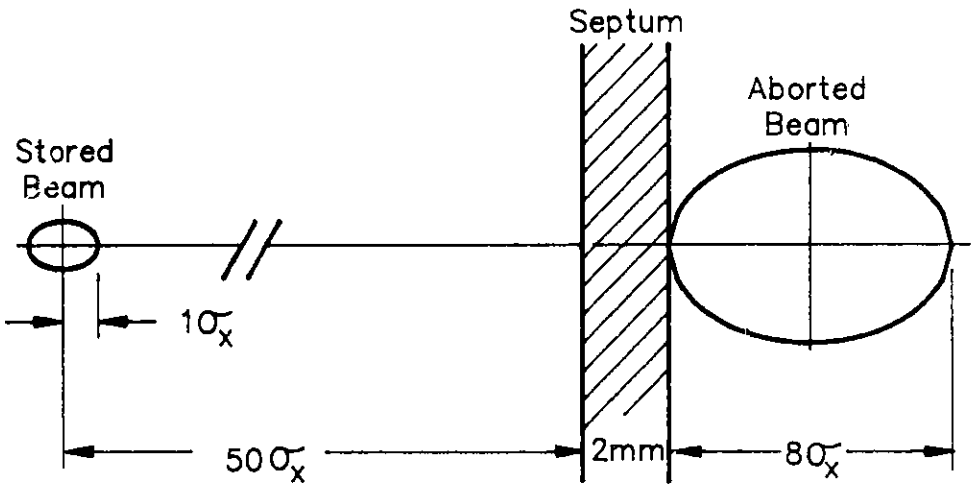

Figure II.1.9-2
Relative positions of the stored and aborted beam with respect to the 2-mm septum in abort system (σ_x = 0.322 mm).

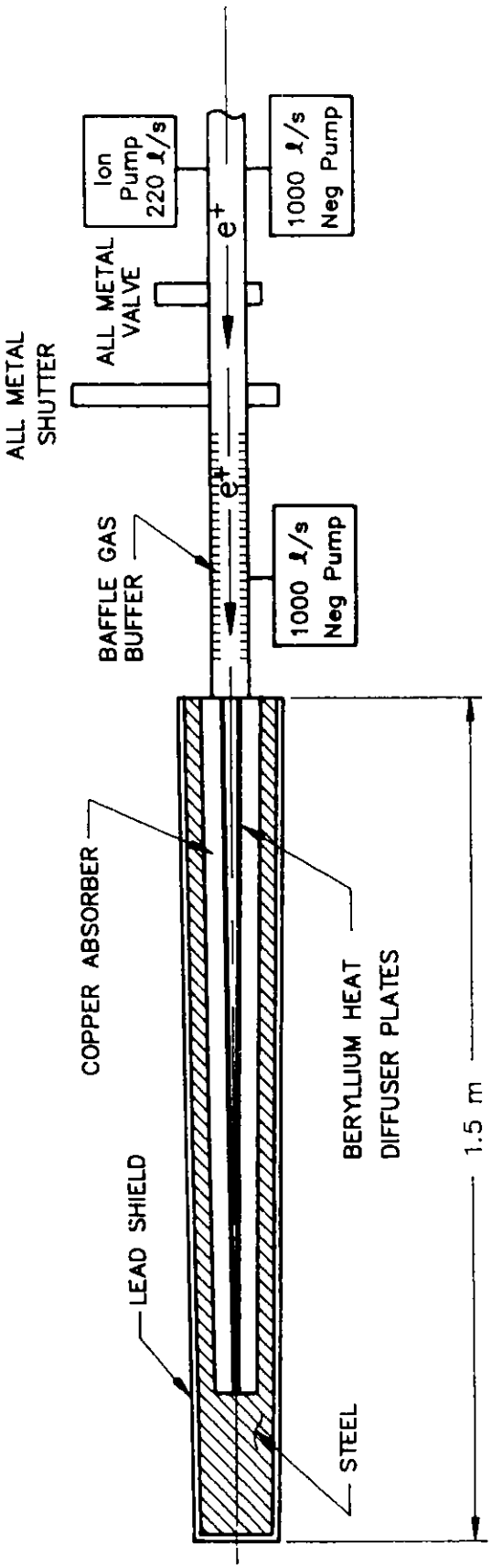

Figure II.1.9-3
Details of the beam dump target.

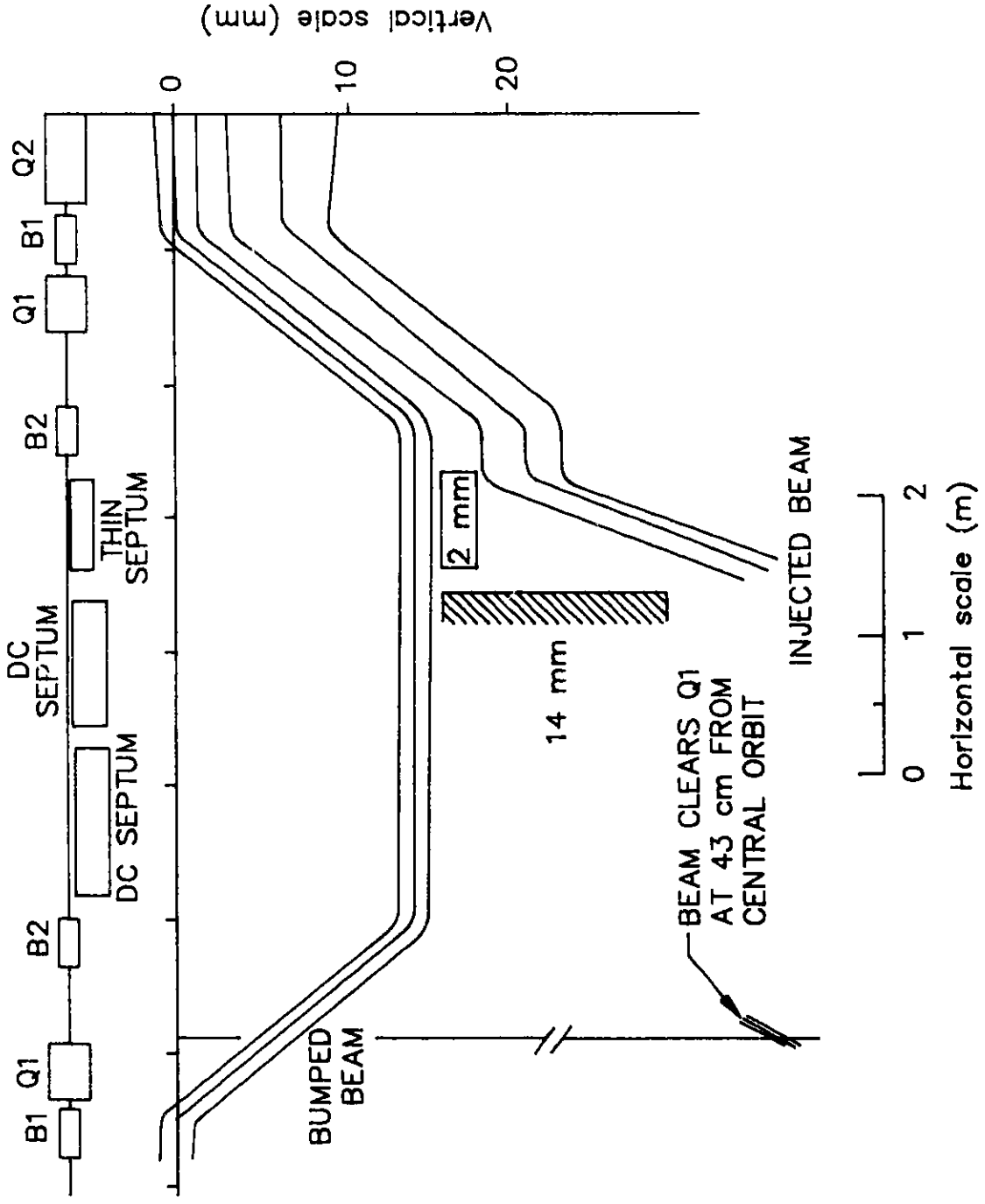

Figure II.1.10-1
Envelope for injected and bumped beam at the injection straight section.

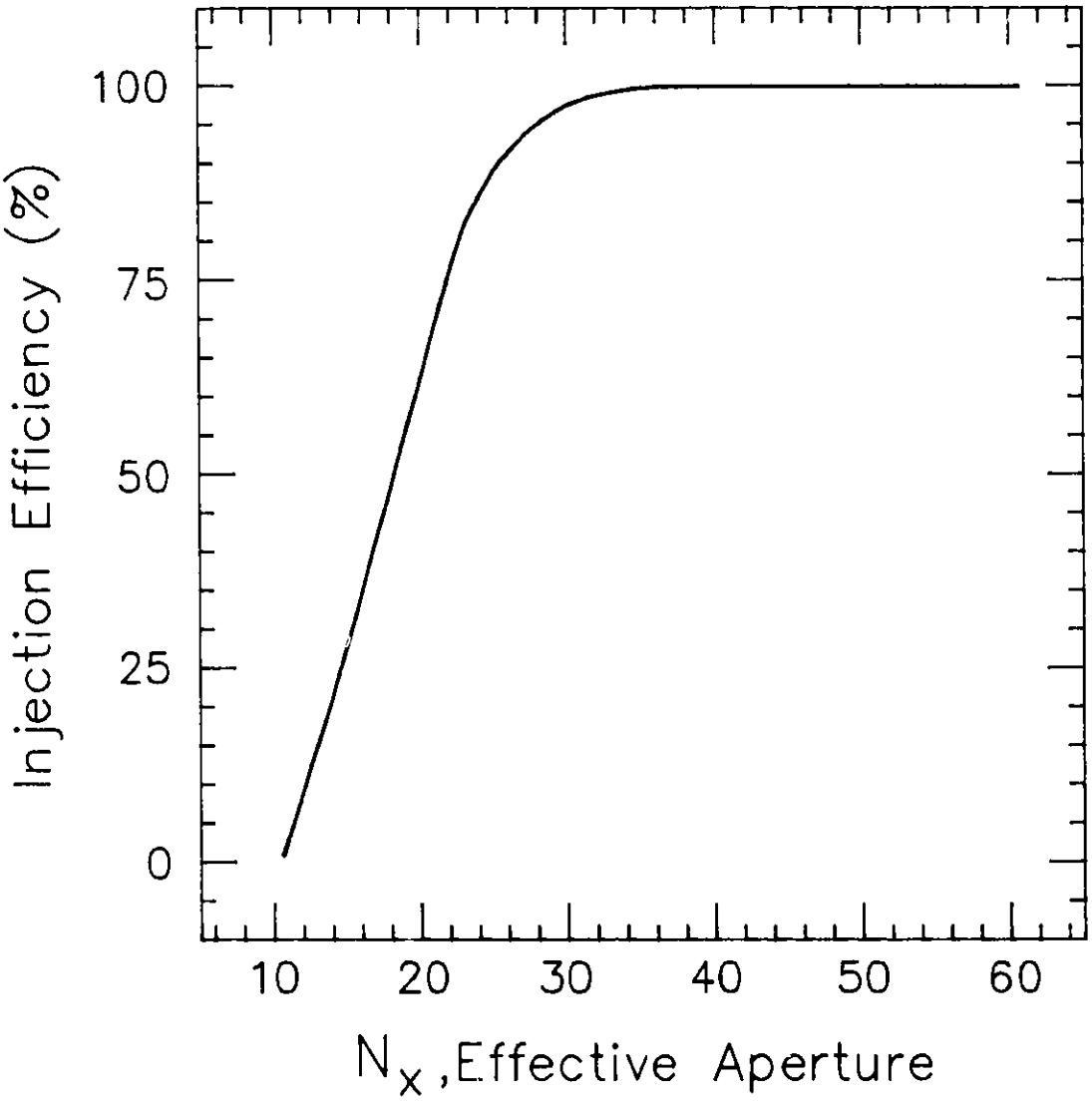

Figure II.1.10-2
Injection efficiency as a function of the effective aperture.

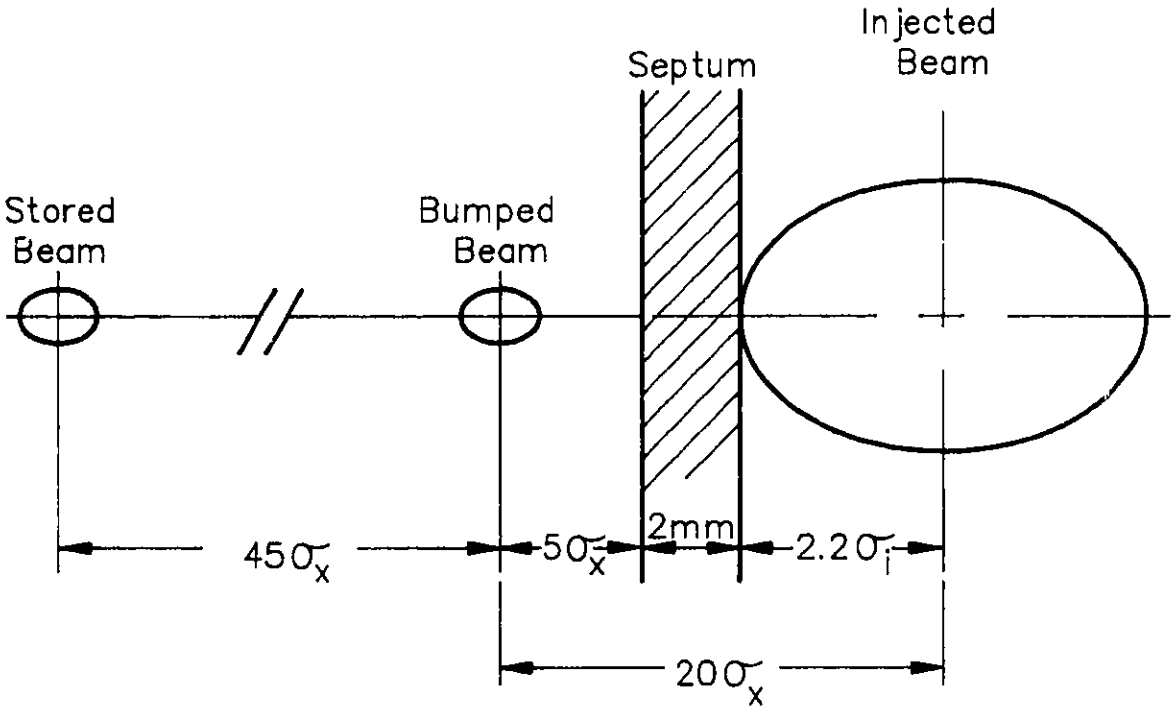

Figure II.1.10-3
The relative positions and sizes of the stored, bumped, and injected beams at the exit of the injection septum.

1.11 Detuned Lattice

For the initial turn-on of the storage ring, the lattice can be tuned to a somewhat higher emittance condition with a reduced phase advance per period. The resulting dynamic aperture given by the chromaticity-correcting sextupoles is large enough so that the harmonic-correcting sextupoles are not required. Operating under these conditions, the storage ring is less sensitive to dipole field and quadrupole placement errors.

The lattice and dispersion functions for the detuned condition are shown in Fig. II.1.11-1. The natural emittance at 7 GeV is 11.0×10^{-9} m. The horizontal and vertical tunes are $\nu_x = 32.22$ (0.805 per period) and $\nu_y = 11.36$, respectively.

The dynamic aperture due to the chromaticity-correcting sextupoles is shown in Fig. II.1.11-2. Because of the larger emittance and β_x in the insertion region, σ_x is about 1.3 times that of the fully tuned machine. In units of mm, the dynamic aperture is about the same as that of the fully tuned machine after enlargement by the harmonic-correcting sextupoles.

Figure II.1.11-2 also shows the average and rms dynamic apertures for 10 machines with uncorrected orbits resulting from a 10^{-4} error level. With full chromaticity correction and without the aid of harmonic-correcting sextupoles, the dynamic aperture of the detuned lattice is comparable, at the same tolerance level, to that of the fully tuned lattice with harmonic-correcting sextupoles. All 10 machines examined for the detuned lattice at a tolerance level of 2×10^{-4} had stable closed-orbit solutions.

Using the procedures described in Section II.1.12, the orbit correctors are adjusted to ensure full injection and beam lifetime capability. The lattice will then be brought to the final low emittance condition by tuning the quadrupoles and adjusting the orbit correction magnets.

1.12 Commissioning Procedures

To expedite commissioning of the accelerator system, special capabilities, concepts, and procedures pertinent to the turn-on process have been incorporated in the design. Such considerations are included in the conceptual design stage because: (a) construction tolerances have major impacts on the commissioning of accelerators; and (b) a majority of these capabilities, though they are low-cost items in the construction phase, may become costly items when they are retrofitted.

The first beam to be injected into the storage ring will be a single bunch of electrons equivalent to a few mA in the ring. The number of electrons needed is about 3×10^{10}. Electrons are used initially to inject a high-current single bunch in order to utilize all diagnostic equipment in the storage ring, keep track of turn-by-turn circulation of the beam in the storage ring, and expedite the injection process.

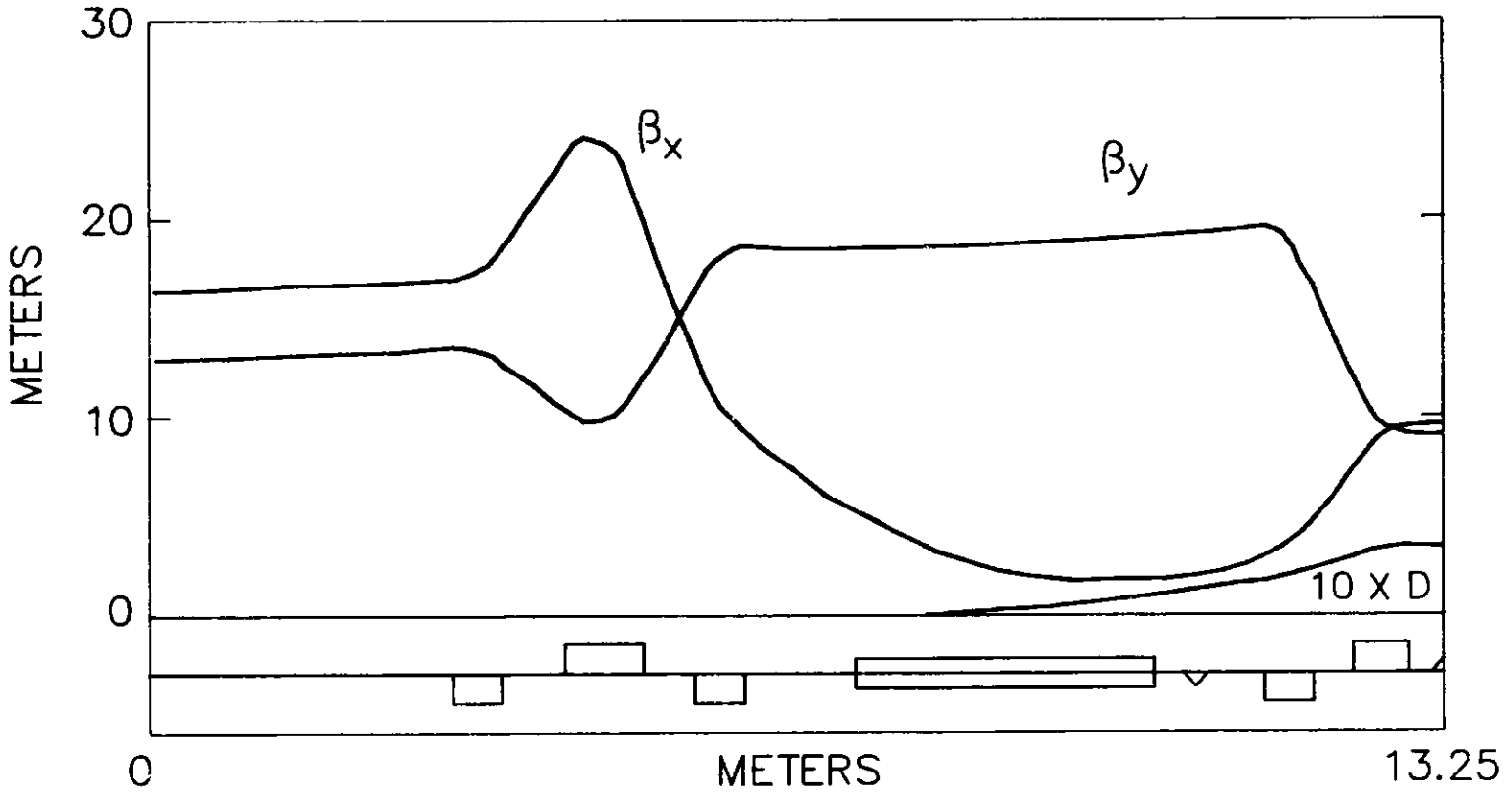

Figure II.1.11-1
Lattice functions β_x, β_y, and D for the detuned lattice.

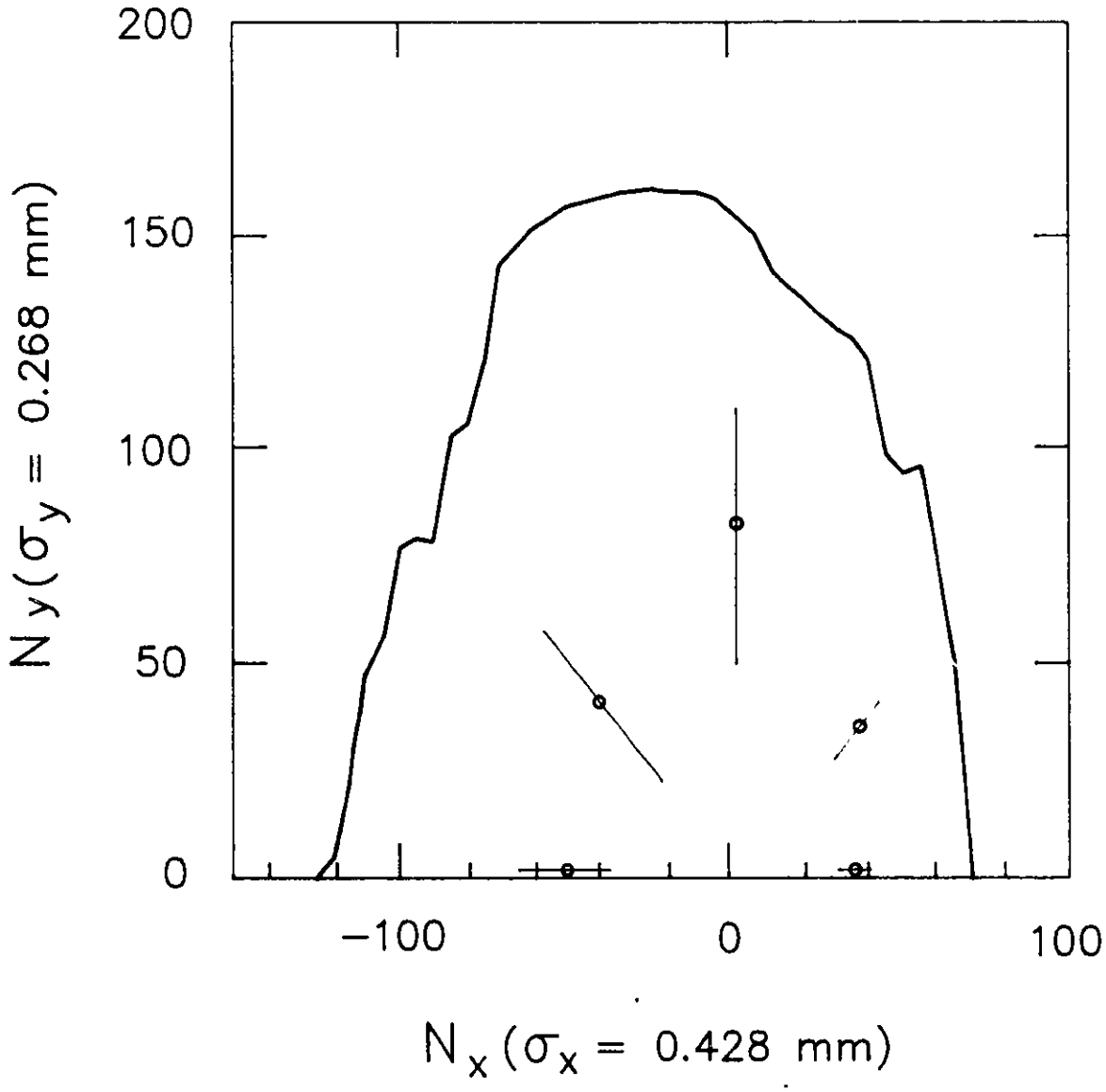

Figure II.1.11-2
Dynamic aperture for the chromaticity-corrected detuned lattice with $\Delta p/p = 0$ (solid curve). The data points and error bars are the average and rms dynamic aperture (for 10 machines) with 10^{-4} tolerance levels. No harmonic-correcting sextupoles are used.

The positron linac and the electron linac described in Section II.10 together are capable of accelerating electrons to 650 MeV with a pulse current of 300 mA and pulse length of 16.5 ns. This single pulse corresponds to 3×10^{10} electrons and a bunch current in the storage ring of 1.6 mA. The injector synchrotron is capable of accelerating a single bunch of 650 MeV electrons from the combined linacs to 7 GeV. To do this, polarity-reversing switches in appropriate power supplies are provided.

The transfer line between the injector sychrotron and the storage ring is equipped with a beam diagnostic system to measure the properties of the synchrotron beam, including the transverse phase spaces, energy, and energy spread during the synchrotron commissioning period. It is planned to know these properties well enough to match into the magnetic field, injection angle, and position at the storage ring.

The next step in the turn-on process is to inject the single bunch into the ring with no coherent betatron oscillation amplitude for the first turn. The purpose of eliminating the coherent oscillation is to avoid confusion between large coherent oscillation due to mismatch and the orbit distortion due to alignment tolerances in the first-turn circulation. To do this, the following three items are considered:

- The synchrotron beam energy and the ring magnetic field should be matched. Measurement of the synchrotron beam energy was already mentioned, and the storage ring magnetic field is monitored in the 81st magnet with an NMR probe. This 81st dipole in the storage ring is discussed in Section II.5.2. Measuring accuracies in $\Delta E/E$ and $\Delta B/B$ of 10^{-3} or better are sufficient for this purpose.

- The injection position should be at the center of the storage ring acceptance. This is achieved by moving the storage ring injection orbit to the incoming beam position in the injection septum magnet. The injection bumpers described in Section II.4 are capable of satisfying the requirement, and a good match between the four bumpers is essential. In-situ wire-orbit measurement can be used to check the bumper matching.

- The injection angle of the incoming beam should be known to the order of 0.5 mrad. This angle is adjusted by the injection septum magnet system.

It should be noted here that, although it has been customary to optimize these variables by independently sweeping each variable, special considerations are included in the design because the storage ring lattice has larger error magnification factors than existing rings.

All of the insertion-device straight sections in the storage ring at the time of start-up are equipped with the large aperture (4 cm × 7 cm) vacuum chambers of the ring, rather than the smaller aperture (8 mm × 5 cm) chambers of the insertion devices.

Commissioning begins with a detuned lattice in order to reduce the sensitivity to errors. All sextupoles are turned off to eliminate the tune shift due to closed-orbit distortion in the sextupoles. In this condition, the quantum lifetime is several seconds, so most of the beam properties can be measured.

With the injection orbit placed in the septum magnet as discussed above, the incoming beam is transported through a sector at a time while optimizing the transmission efficiency and minimizing the orbit deviations using the ring dipole correctors. The diagnostic equipment available for this comprises nine beam position monitors (BPMs) and a scintillator device located in the downstream end of each sector. The scintillator is a destructive monitor that stops the beam, and the BPM is capable of measuring turn-by-turn beam positions. It is important to note that utilization of single-bunch high-intensity electrons makes this process possible.

Once the bunch is transmitted through one turn satisfactorily, the storage ring bumped orbit is moved outside of the septum to permit the second turn to circulate. The second-turn transmission is also done one sector at a time. In this case the scintillator is retracted from the beam, and the BPMs are used to measure beam positions of the first and second turns. The time separation between two turns is about 3.5 μs, and the use of a single bunch makes the turn-by-turn beam position measurements much simpler. The tuning process involves adjustments of dipole correctors to maximize transmission efficiency and to minimize orbit deviations for both turns.

Once a few turns of transmission are established, then the usual procedures of start-up, such as the study of the survival time vs. the quadrupole magnet settings, are carried out to search for a better working point. Once the closed orbit is established, the orbit correction program takes over to correct the orbit. Two important points should be noted: (a) without sextupole magnets energized, the quantum lifetime is sufficiently long to do most of the lattice adjustments, and (b) because all BPMs are placed near the sextupole magnets, it is reasonable to assume that the closed orbit is in the middle of the sextupoles. If this is not the case, the displaced orbit effect should be apparent when each sextupole magnet is energized to compensate for the natural chromaticities of the lattice.

After the properties of the detuned lattice are understood, the low-emittance lattice is implemented in the storage ring. The knowledge gained from the detuned lattice is then used to commission the low-emittance machine.

The use of electrons rather than positrons has the additional advantage of providing rapid beam cleaning of the vacuum chamber. Electron injection rates up to 15 mA/s can be provided, compared with 0.5 mA/s for positron injection.

1.13 References

1. "Report of Synchrotron Radiation Source Research and Development Program Review," Ames Laboratory, Iowa State University, Ames, Iowa (October 1984).

2. "Machine Workshop on the 6-GeV Synchrotron Radiation Source," National Bureau of Standards, Gaithersburg, Md. (March 1985).

3. "6 GeV Synchrotron X-ray Source Conceptual Design Report," ANL Report ANL-86-8 (February 1986).

4. Ref. 3, Appendix C.

5. G. Brown, Y. Cho, J. Hastings, S. Krinsky, D. Moncton, G. K. Shenoy (Chairman), and P. J. Viccaro, "Ring Energy Selection and Extra Long Straight Sections for the Advanced Photon Source: A Report and Recommendations by the National Task Group," ANL Report ANL-87-14 (April 1987).

6. E. Crosbie, unpublished program.

7. H. Wiedemann, SSRL ACD Note 22 (1984).

8. F. Iselin, CERN-LEP-TH/85-15 (1985).

9. A. Wrülich, DESY Report-84-026 (1984).

10. A. Ruggiero, unpublished program.

11. E. Crosbie, "Improvement of the Dynamic Aperture in Chasman-Green Lattice Design Light Source Storage Rings," IEEE Conference Record, 87CH2837-9.

12. POISSON is an improved version of TRIM (A. M. Winslow, J. Computer Phys. 1, 149, 1967) that was developed by K. Halbach et al.

13. K. Steffen and J. Kewisch, "Study of Integer Resonances in Distorted PETRA Optics," DESY PET-76/09 (1976).

14. L. Smith, ESG Technical Note-24 (1986).

15. W. Chou, ANL Report, Light Source Note LS-87 (1987).

16. W. Chou, ANL Report, Light Source Note LS-88 (1987).

2.1 Introduction

A charged particle beam circulating in a metal vacuum chamber induces electromagnetic fields that act back on individual particles in the beam. These wake fields will affect the beam properties and may lead to beam blowup or beam loss and thus could limit the beam current or density. The effect of these fields is expressed below in terms of the effective impedance of various components in the beam pipe as a function of the rms bunch length, σ_ℓ. These impedances are estimated using measurements from other storage rings and calculations for the radio-frequency (rf) cavity. For the beam blowup instabilities, increasing the current per bunch above the threshold value only increases the bunch length. For beam loss instabilities, an attempt to increase the current above the threshold value results in rapid beam loss from the ring.

The beam lifetime is determined by losses of beam due to the following effects:

- The quantum nature of the synchrotron radiation allows positrons in the beam to emit high-energy photons, causing the positrons to lose energy in a random fashion and leading to a diffusion from the stable rf bucket, as well as from the transverse aperture (quantum lifetime, τ_q).

- Collisions of particles within a beam bunch can give rise to exchange of sufficient energy in the transverse plane that particles are lost from the rf bucket or momentum aperture (Touschek lifetime, τ_t).

- Single scattering of beam particles from residual gas molecules can cause beam particles to be lost from the rf bucket (bremsstrahlung lifetime, τ_b) and from the transverse aperture (single elastic scattering lifetime, τ_s).

Effects that do not lead directly to beam loss but to an increase in emittance are multiple Coulomb scattering by residual gas molecules and multiple intrabeam scattering. These effects add to the quantum fluctuations of the beam, which must be counteracted by synchrotron radiation damping. This yields an equilibrium transverse emittance that is dependent on bunch current and greater than the natural emittance.

The parameters on which the above effects depend are numerous and include lattice properties, rf properties, beam current, vacuum pressure and composition, physical apertures, etc. A grand optimization is therefore not easily attained. The method used here is to fix the lattice functions and physical apertures as given in Table II.2.1-1. The rf properties are then chosen to yield adequate lifetime, a beam current of > 100 mA, and sufficient voltage and power for insertion devices. Stability and lifetime then determine the properties of the individual bunches, the current per bunch, and the number of bunches required. The peak rf voltage, with full beam

Table II.2.1-1

Storage Ring Parameters Used for Stability and Lifetime Calculations

Ring Circumference, $C = 2\pi R$	1060 m
Average Radius, R	168.7 m
Revolution Frequency, f_o	0.2828 MHz
Horizontal Tune, ν_x	35.22
Vertical Tune, ν_y	14.30
Average Betatron Function	
Horizontal, $<\beta_x>$	10 m
Vertical, $<\beta_y>$	13 m
Momentum Compaction, α_p	2.374×10^{-4}
Transition Gamma, γ_t	64.9
Beam Energy, E	7 GeV
Horizontal Emittance (10% Coupling), ϵ_x	7.3×10^{-9} m
Vertical Emittance (10% Coupling), ϵ_y	7.3×10^{-10} m
Natural Energy Spread, σ_E/E	0.96×10^{-3}
Minimum rms bunch length	0.58 cm
Bending Magnet Synchrotron Energy Loss, U_o	5.45 MeV/turn
Radio Frequency, f_{rf}	352.96 MHz
Harmonic Number, h	$1248 = 2^5 \cdot 3 \cdot 13$
Peak rf Voltage, $\hat{V}_{rf}$	9.5 MV
Bucket Half Height, $\Delta E_{rf}/E$	2.0%
Synchrotron Frequency, f_s	1.88 kHz
Equivalent Vacuum Chamber Radius, b	30 mm
Minimum Vertical Vacuum Chamber Aperture in Undulator, g	8 mm
Maximum Vertical Betatron Function in Undulator, β_y	11 m
Ring Horizontal Acceptance, $\hat{\epsilon}_x$	32.7×10^{-6}m
Ring Vertical Acceptance, $\hat{\epsilon}_y$	17.1×10^{-6} m
Ring Vertical Acceptance with Undulators, A_y	1.45×10^{-6} m
Vacuum Pressure	1.0 nTorr

intensity, is $\hat{V}_{rf}$ = 9.5 MV, which is obtainable from the present system. In order to ensure adequate lifetime, an rf-bucket height of $\Delta E_{rf}/E = \pm 2.0\%$ or ~21 times the natural (zero current) energy spread is assumed. This yields a long quantum lifetime, even allowing a safety factor of 3 for possible growth in the beam-energy spread. This bucket-height selection determines the synchronous phase angle, ϕ_s, to be

$$\sin \phi_s = \Gamma \leq 0.72$$

and the total average energy loss, U, of the beam to be

$$U = e\hat{V}_{rf}\, \Gamma \leq 6.9 \text{ MeV/turn} .$$

Since the dipoles alone account for an energy loss of U_o = 5.45 MeV/turn, the excess energy available, U_{ex} = 1.45 MeV, to compensate for energy loss in insertion devices, U_{ID}, and for higher-order mode (HOM) losses, U_{HOM}, in the ring is given by

$$U_{ex} = 1.45 \text{ MeV/turn} \geq U_{ID} + U_{HOM}$$

and

$$U_{HOM} = Z_{HOM}\, \bar{I}_B e ,$$

where $\bar{I}_B$ = average beam current (per bunch) and Z_{HOM} = HOM impedance. The HOM losses will limit the number of insertion devices, depending on the average bunch current, as given by

$$U_{ID} = \sum_{i=1}^{N_u} U_i = 1.45 - Z_{HOM}\bar{I}_B e ,$$

where U_i are energy loss per pass for each of the N_u undulators. For this conservative rf design, a total of 12 high field (0.81 T) undulators with U_i = 0.1 MeV/turn are possible. These numbers will allow considerable reserve for the typical operation, which is estimated to be less than half of this total undulator energy loss.

For this voltage and Γ, the bunch length and energy spread of the beam are related by

$$\sigma_\ell = \frac{\alpha_p c}{2\pi f_s} \left(\frac{\sigma_E}{E}\right) = 602 \times \left(\frac{\sigma_E}{E}\right) ,$$

where σ_ℓ is in cm. The zero current bunch length corresponds to σ_ℓ = 0.58 cm.

2.2 Beam Instabilities

2.2.1 Impedance and Loss Parameters

The circulating beam in the storage ring induces electromagnetic fields in the vacuum chamber elements. The induced electromagnetic fields, which are proportional to the impedance seen by the circulating beam, may drive instabilities for the beam. When the growth time of such an instability is longer than the radiation damping time, the beam is stable. As bunch current increases, the growth time becomes shorter; at the threshold current, the growth time and the damping time become equal. Consider now the longitudinal phase space. As current in the bunch increases beyond the threshold value, the bunch will grow in length and energy spread. In effect, this bunch lengthening reduces the bunch current until the new threshold condition is satisfied. However, in the transverse phase space, exceeding the current threshold may result in fast beam loss from the bunch. The threshold current calculated below indicates that there are no single-bunch transverse instability problems below the 10-mA bunch current level.

The impedance will eventually need to be measured for the specific hardware in the ring, but the estimated impedances used here will allow an estimate of threshold currents. To estimate the total impedance, the effective loss parameter for each component in the ring is summed. The effective loss parameter is the average of the real impedance over the power spectrum in the beam and therefore depends on the bunch length, σ_ℓ. We separate the total loss parameters, k_{tot}, into rf cavities, k_{rf}, and vacuum chamber, k_{vc}, components:

$$k_{tot}(\sigma_\ell) = k_{vc}(\sigma_\ell) + k_{rf}(\sigma_\ell) \quad .$$

For the vacuum chamber with bellows, vacuum pump ports, and instrumentation (see Section II.6), the measured loss parameter from PEP is scaled to the storage ring by the ratio of the circumference of the two rings. The measured loss parameter for PEP, in volts per picocoulomb, the unit we will use throughout for the loss parameter, is given by $k_{vc}(\sigma_\ell) = 28[\sigma_\ell(\text{cm})]^{-1.23}$ V/pC.[1] This scaled loss parameter is more than a factor of four larger than that estimated[2] for the bare vacuum chamber designed for this ring, thus accounting for the loss parameters for the additional elements. Scaling the measured PEP vacuum chamber impedance to obtain the storage ring vacuum chamber impedance is valid, despite the presence of the antechamber (see Fig. II.2.2-1), because the transverse-magnetic (TM) modes do not couple between the beam and antechamber below 15 GHz. Computer calculations using SUPERFISH[3] and OSCAR[4] verify this conclusion, as shown in Fig. II.2.2-1, where the magnetic field at the cutoff frequency (first TM mode) is plotted. Since PEP is not designed for synchrotron radiation beams, the effect of 80 beam ports is considered separately. The loss parameter for each beam

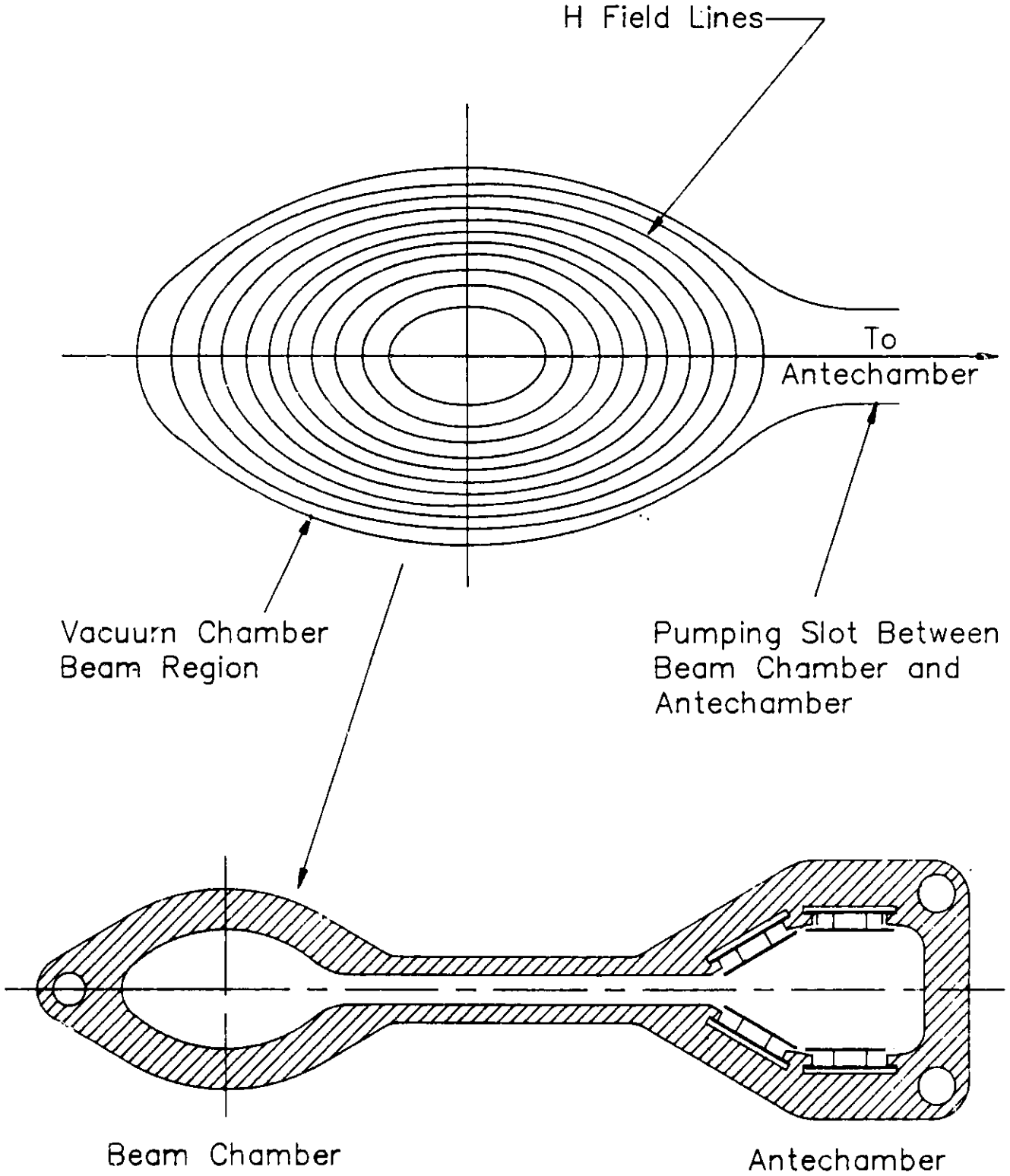

Figure II.2.2-1

SUPERFISH output of the magnetic field lines for the first TM mode of the storage ring beam vacuum chamber. The entire vacuum chamber cross section is shown for reference.

port consists of the loss parameter due to the vacuum chamber discontinuity,[5] $k_d(\sigma_\ell) = 0.08\ [\sigma_\ell(\text{cm})]^{-2}$, and the beam port slot, $k_s(\sigma_\ell) = 0.0055\ [\sigma_\ell(\text{cm})]^{-5}$. The effective vacuum chamber loss parameter is expressed as

$$k_{vc}(\sigma_\ell) = 13.5[\sigma_\ell]^{-1.23} + 6.4[\sigma_\ell]^{-2} + 0.44[\sigma_\ell]^{-5} \quad (V/pC)$$

with σ_ℓ = rms bunch length in cm.

The rf cavity, being a tuned system, has a number of HOMs. The impedance seen by the beam bunch is an effective average over these modes. The loss parameter for the rf cavity is estimated by

$$k_{rf}(\sigma_\ell) = \sum_n k_n(o)\ e^{-\omega_n^2\sigma_\ell^2/c^2} \quad \text{per cavity,}$$

where $k_n(o)$ = calculated loss parameter for mode n and $\omega_n = 2\pi$ times the frequency of mode n. The summation is performed for n = 2,3,4,...,10, thus excluding the first harmonic, which is actively compensated for by the coupling loop feedback. The k_n and ω_n are calculated using the program URMEL[6] and listed in Table II.2.2-1. These parameters are similar to the values for the LEP and ESRP cavities.[7] In order to account for the higher frequency modes, not included in Table II.2.2-1, the total $k_{rf}(\sigma_\ell)$ was increased by 1.7 times the calculated values. This results in a $k_{rf}(\sigma_\ell)$ value within 10% of those measured for the PEP rf cavities.[8] The total loss parameter (vacuum chamber plus 15 rf cavities) is calculated as a function of beam bunch length and is listed in Table II.2.2-2. Figure II.2.2-2 shows the dependence of the loss parameter on σ_ℓ.

The impedance seen by the beam is related to the loss parameter by

$$k_{tot}(\sigma_\ell) = \frac{1}{\pi}\int_o^\infty \text{Re}[Z(\omega)]\cdot\exp[-(\frac{\omega\sigma_\ell}{c})^2]d\omega\ .$$

The impedance $Z(\omega)$ is approximated by a parallel resonant circuit with a quality factor Q = 1 and resonant frequency equal to the cutoff frequency of the vacuum chamber (f_c = 3.82 GHz).[2] The shunt impedance, R_s, is calculated by fitting the loss parameter data with the above integral expression. The longitudinal impedance, $Z_\parallel$, is given by

$$\left|\frac{Z_\parallel}{n}\right| = \frac{R_s}{\frac{f}{(\frac{c}{f_o})}} \quad (\Omega)$$

where n is the mode number (~10^4). Table II.2.2-2 gives the estimated values for R_s and $|Z_\parallel/n|$ as a function of σ_ℓ.

Table II.2.2-1

Fundamental and Higher-Order Modes
for the 353-MHz rf Cavity

Mode No. n	Frequency f_n (MHz)	R_s (MΩ)	10^{-3} Q	Loss Parameter (V/pC)
1	353.0	11.23	49	0.128
2	743.0	0.03	42	0.000
3	925.0	1.25	109	0.017
4	1174	0.33	43	0.014
5	1330	0.03	129	0.001
6	1511	1.09	88	0.029
7	1654	0.07	46	0.004
8	1679	1.06	46	0.060
9	1842	0.33	121	0.006
10	1972	2.98	55	0.165

In order to estimate the bunch length, and therefore the HOM loss in the storage ring, the microwave longitudinal instability model[9] was used. The threshold bunch current, $I_{\|}$, is included in Table II.2.2-2 as a function of bunch length. Below the bunch lengthening threshold current, the bunch shortens slightly as the bunch current is increased due to the potential-well distortion. Above this threshold current, the bunch length increases with current. For an average bunch current of $\bar{I}_B$ = 4.0 mA, a bunch lengthening of three times the zero current bunch length is expected ($\sigma_\ell \approx 1.75$ cm). This also results in a similar increase in the energy spread ($\sigma_E/E \approx 2.9\times10^{-3}$).

The HOM loss can now be estimated for the bunch parameters listed in Table II.2.2-2 using the relation

$$U_{HOM} = eZ_{HOM}\bar{I}_B = \frac{ek_{tot}(\sigma_\ell)\bar{I}_B}{f_o} \quad .$$

The HOM loss at the threshold bunch current is also listed in Table II.2.2-2. For all bunch lengths listed, $U_{HOM} \approx$ 0.2 MeV, leaving an excess energy U_{ID} = 1.25 MeV to compensate for insertion device losses. Increasing the bunch current will result in bunch lengthening and reduced HOM impedance (Z_{HOM}), but the HOM energy loss is

Table II.2.2-2

Impedances and Threshold Current for 7-GeV Storage Ring

	σ_ℓ (cm)					
	0.7	1	1.5	2	3	4
$\frac{\sigma_E}{E}$ (%)	0.116	0.166	0.250	0.333	0.499	0.666
k_{vc} (V/pC)	36.6	20.3	11.1	7.37	4.27	2.85
k_{rf} (V/pC)	7.23	6.65	5.62	4.43	2.37	1.06
k_{total} (V/pC)	43.8	26.9	16.7	11.8	6.58	3.91
R_s (kΩ)	2.06	4.03	8.47	14.2	26.7	38.2
$Z_\parallel/n$ (Ω)	0.15	0.30	0.63	1.1	1.9	2.8
$I_\parallel$ (per bunch) (mA)	1.4	2.0	3.3	4.7	8.3	13.6
U_{HOM} (for $\bar{I}_B = I_\parallel$) (MV)	0.22	0.21	0.20	0.20	0.20	0.19

approximately independent of bunch length. However, increasing the bunch length also means an increase in energy spread and a decrease in the beam lifetime.

In order to ensure that the impedance estimate is reasonable, an attempt was made to measure the loss parameter for a 1-m length of beam chamber, with transition sections.[10] The bench method used a $\tau_\ell \approx 65$ ps signal (corresponding to $\sigma_\ell \approx 2$ cm) on a coaxial wire to measure the energy loss in the beam pipe. Table II.2.2-2 indicates the loss parameter should be approximately $k_{vc}(2\text{ cm}) \approx 0.007$ V/pC (per meter). The measured loss parameter was consistent with zero ($k \leq 0.008$) to within the systematic measurement uncertainty. Although not determining a precise value of k_{vc}, this preliminary measurement supports the claim that the presence of the pumping antechamber yields an insignificant increase in the loss parameter relative to that of an elliptical chamber. Therefore, the use of the scaled PEP value for $k_{vc}(\sigma_\ell)$ is justified.

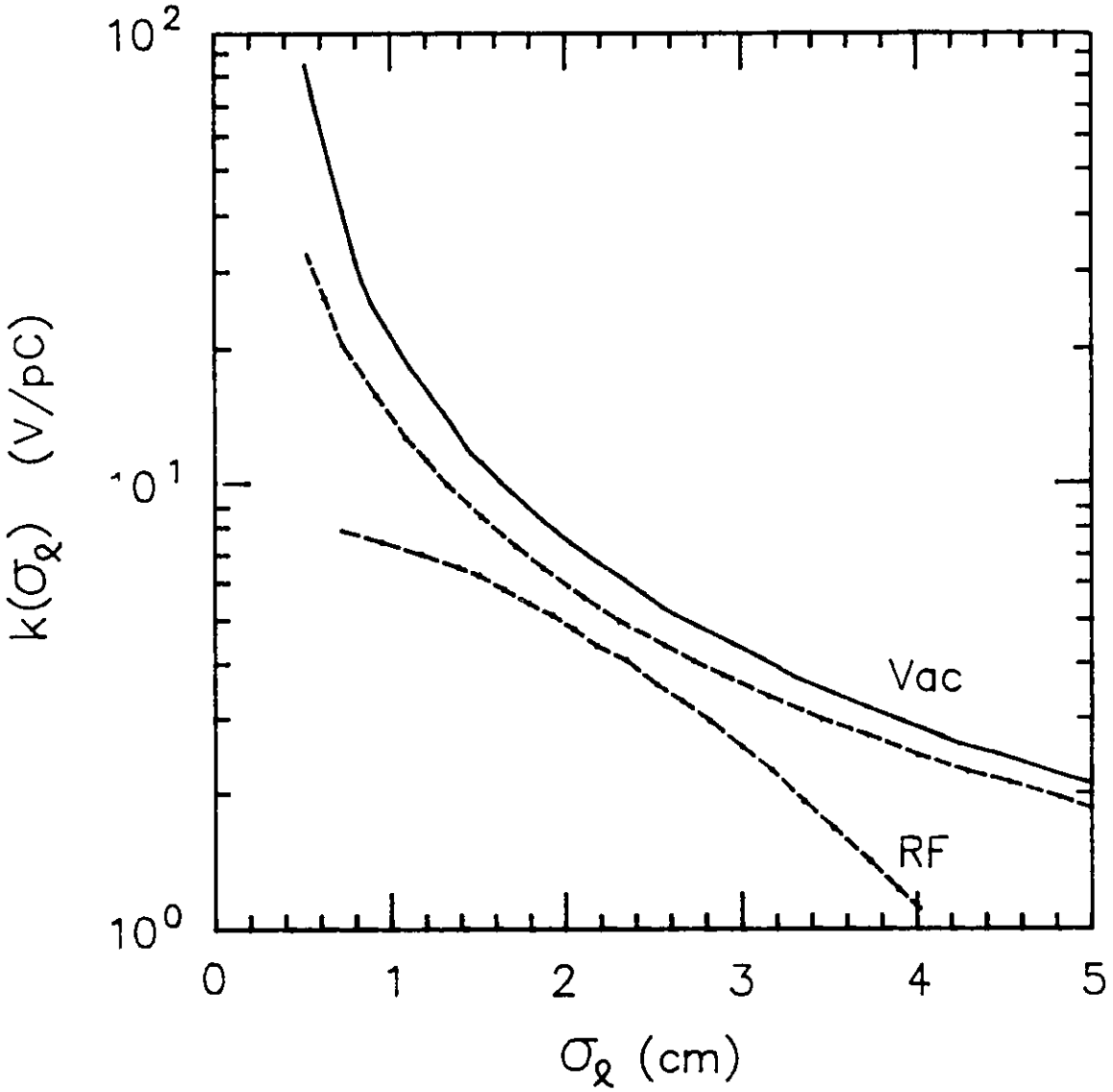

Fig. II.2.2-2
Loss parameter as a function of bunch length. The solid curve shows the total estimated vacuum chamber loss parameter, including transitions and beam ports. The upper dashed curve is the scaled vacuum chamber loss parameter measured at PEP. The lower dashed curve shows the estimated loss parameter for 15 rf cavities.

2.2.2 Impedance Scaling and Bunch Length

The impedance estimates used in Table II.2.2-2 were obtained by using the assumed Q = 1 resonance model for the $Z_{\parallel}(\omega)$ dependence for each bunch length. This method assures agreement between the loss parameter and $Z_{\parallel}(\omega)$. The program ZAP[11] assumes that $|Z_{\parallel}/n|$ is independent of frequency up to the "SPEAR scaling" characteristic frequency $\omega_c = c/b$, where b is the effective beam pipe radius. Above this frequency, the longitudinal impedance is scaled by the empirical "SPEAR scaling." Using this formalism, the estimated impedance is given by the relation

$$\left|\frac{Z_{\parallel}}{n}\right| = A \left(\frac{\sigma_{\ell}}{b}\right)^{1.68} \quad \text{for } \sigma_{\ell} < b \ , \qquad \text{(II.2.2.2-1)}$$

where A is approximately two ohms, which is obtained by fitting impedance values in Table II.2.2-2.

Using this impedance estimate, ZAP can evaluate the bunch length and energy spread as a function of bunch current using the microwave instability model.[9] These results are shown in Figures II.2.2-3 and II.2.2-4. The bunch current estimated using this method is approximately 25% higher than the threshold currents listed in Table II.2.2-2, resulting from a reduction of the estimated impedance for $\sigma_{\ell} < b$ of Eq. II.2.2.2-1.

This reduction in impedance is an empirical estimate of the uncertainty of the impedance at high frequency. The "SPEAR scaling" estimate of bunch lengthening with current is actually larger than the values seen at PEP, PETRA, and CESR.[12] Therefore, the $\bar{I}_B$ = 5 mA estimated here represents a lower value of the current possible in a bunch with σ_{ℓ} = 1.75 cm.

The minimum bunch length for a given bunch current will ultimately be limited by the coherent interaction of the low-frequency synchrotron radiation ($\omega << E_c/\hbar$). This effect can be expressed as a "free space" impedance,[13] described in Section II.2.2.3. The actual impedance of the storage ring must be greater than this value for all σ_{ℓ}. This minimum bunch length for a given bunch current due to this "free space" impedance is also presented in Figure II.2.2-3. This shows that for a bunch length of σ_{ℓ} = 1.75 cm ($\sigma_E/E \leq 2.9 \times 10^{-3}$), the bunch current limit by "free space" impedance is 10 mA, compared to the "SPEAR scaling" value of $\bar{I}_B$ = 5 mA, corresponding to an impedance of $|Z_{\parallel}/n|$ = 0.7 Ω. Therefore, we use the "SPEAR scaling" estimate for $\bar{I}_B$ = 5 mA at σ_{ℓ} = 1.75 cm as a conservative estimate.

Transverse impedance for the vacuum chamber is not easily estimated. However, the cylindrically symmetric vacuum chamber estimate[11] of

$$\left|\frac{Z_{\perp}}{n}\right| = \frac{2}{b}\left|\frac{Z_{\parallel}}{n}\right| \quad \left(\frac{\Omega}{m}\right) \qquad \text{(II.2.2.2-2)}$$

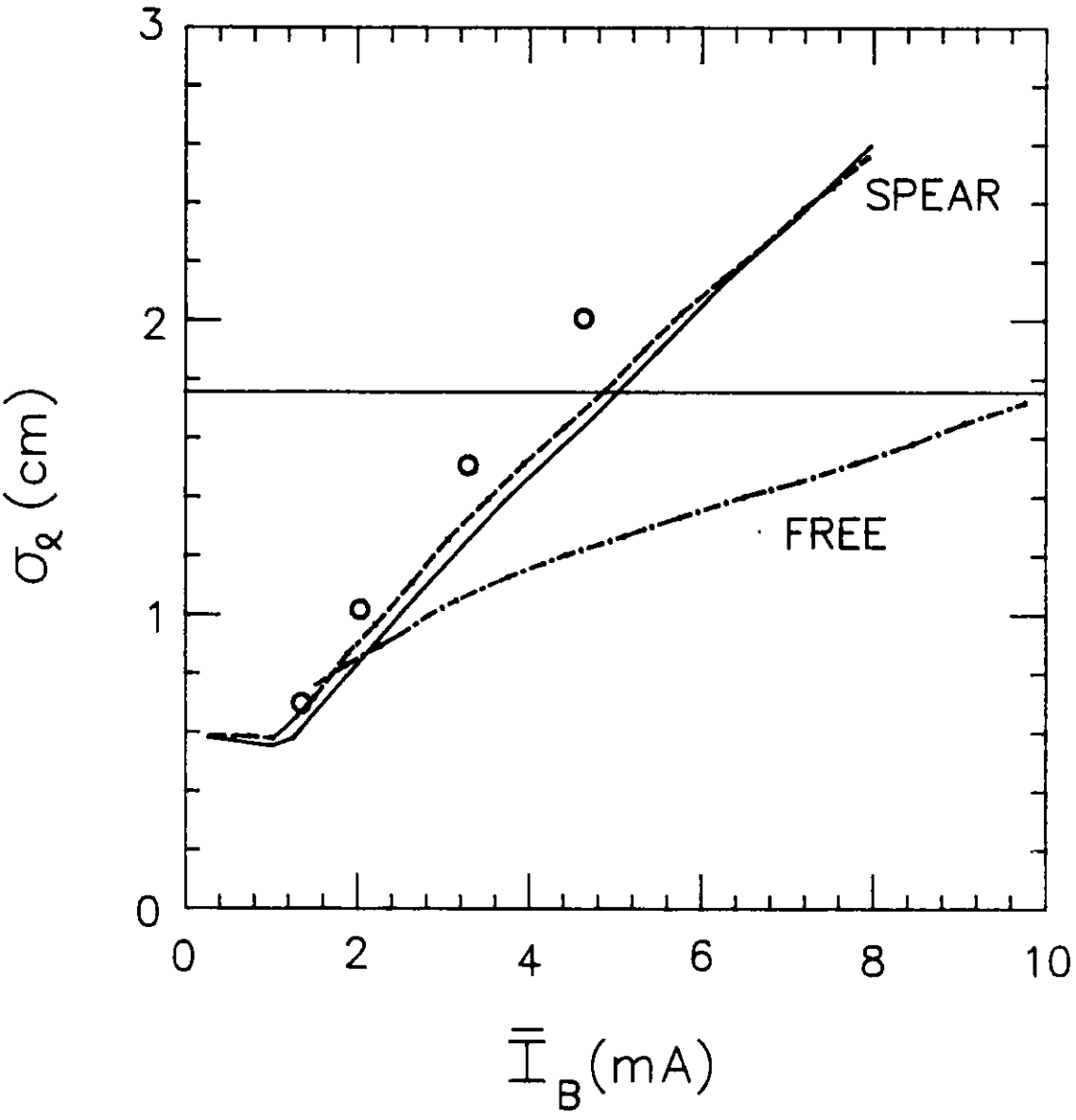

Fig. II.2.2-3

Bunch length as a function of bunch current. The solid and dashed curves show the calculation by ZAP using "SPEAR scaling" with and without the potential well distortion, respectively. The dot-dashed curve presents the minimum bunch length for a given current using the "free space" impedance estimate. The circles are the current values listed in Table II.2.2-2. The horizontal line corresponds to the maximum bunch length (σ_ℓ = 1.75 cm) assumed here, consistent with adequate quantum lifetime.

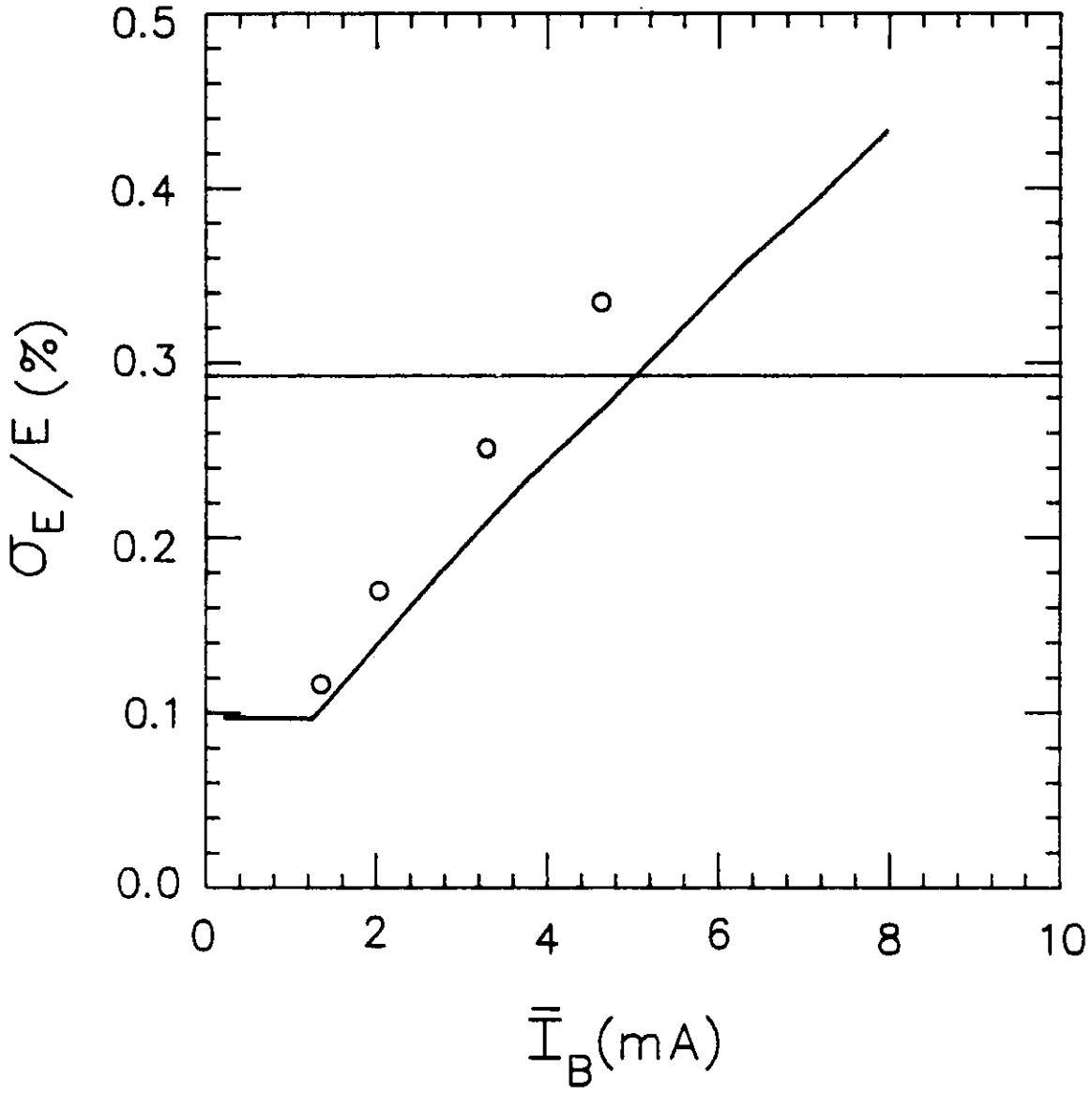

Fig. II.2.2-4
Rms energy spread as a function of bunch current as calculated by ZAP using "SPEAR scaling." The circles are the values presented in Table II.2.2-2. The horizontal line indicates the maximum energy spread ($\sigma_E/E = 2.9\times10^{-3}$) assumed here, consistent with adequate lifetime.

should provide a reasonable estimate and will be used for single bunch fast transverse instability estimates (see Section II.2.2.3).

2.2.3 Single Bunch Instability

A single bunch can be unstable due to internal coherent motion if the coherence wavelength is less than the bunch length. This is true for both longitudinal and transverse motion. The stability limit is represented by the maximum allowable coupling impedances, $|Z_{\parallel}/n|$ and $|Z_{\perp}/n|$, for the longitudinal and transverse motion, respectively, for given beam bunch current and bunch dimensions.

The stability limits are given by the equations[9,11,14]

$$\left|\frac{Z_{\parallel}}{n}\right| \lesssim \frac{\alpha_p E}{Ie} \left(\frac{\Delta p}{p}\right)^2 \qquad \text{(II.2.2.3-1)}$$

and

$$\left|\frac{Z_{\perp}}{n}\right| \lesssim \frac{\alpha_p E \nu_y}{2R\ e\ I}\left|\frac{\Delta p}{p}\right| \ . \qquad \text{(II.2.2.3-2)}$$

These equations come from conventional coasting beam theory. For bunched beam considerations, it is customary to replace the beam current, I, in the above equations by the peak current in the bunch, I_p. The value $(\Delta p/p)$ represents the full width at half-maximum momentum spread.

Equations II.2.2.3-1 and II.2.2.3-2 are valid in the case of the so-called fast instability, where otherwise the bunches are unstable with growth rates larger than the synchrotron frequency. This is the most common and critical limitation of the bunch current.

The relation between the rms energy spread, σ_E/E, or the rms bunch length, σ_ℓ, and $\Delta p/p$ is given by

$$\Delta p/p = 2.355\ \sigma_E/E = 3.92\times10^{-3}\ \sigma_\ell\ (\text{cm}) \ .$$

For Gaussian bunches the average bunch current, $\bar{I}_B$, is related to the peak current by

$$I_p = \frac{\sqrt{2\pi}\ R}{\sigma_\ell}\ \bar{I}_B \ .$$

In terms of the average bunch current, $\bar{I}_B$, and rms bunch length, σ_ℓ, Eqs. II.2.2.3-1 and II.2.2.3-2 give the following coupling impedance limits:

$$\left|\frac{Z_\parallel}{n}\right| \lesssim (0.605\ \Omega)\ \frac{\sigma_\ell^{\,3}}{\bar{I}_B}$$

and

$$\left|\frac{Z_\perp}{n}\right| \lesssim (6.60\ \tfrac{\Omega}{m})\ \frac{\sigma_\ell^{\,2}}{\bar{I}_B}\ ,$$

where σ_ℓ is in cm and $\bar{I}_B$ is in mA. If $\bar{I}_B$ = 5.0 mA and σ_ℓ = 1.75 cm, which corresponds to three times the zero-current bunch length, then the impedances must satisfy

$$\left|\frac{Z_\parallel}{n}\right| \lesssim 0.7\ \Omega$$

and

$$\left|\frac{Z_\perp}{n}\right| \lesssim 5.1\ \Omega/m$$

in order to ensure stability of the individual bunch.

As already mentioned, only wavelengths that are shorter than the bunch length can cause a violent instability within the bunch. This corresponds to frequencies above 20 GHz, a frequency above the cutoff of the vacuum chamber pipe. It is not clear, and it is practically impossible to determine with either calculations or measurements, what the contribution is to the coupling impedance in this frequency range from the various components along the vacuum chamber. The best estimate that can be used is the so-called "free-space" impedance due to the synchrotron radiation itself.

Taking into account the radiation in dipoles and undulators and the absence of radiation in straight sections, the contribution from "free space" is

$$\left|\frac{Z_\parallel}{n}\right| \simeq \frac{220}{n^{2/3}}\ \Omega\ , \qquad \text{(II.2.2.3-3)}$$

which, for this case, is the only contribution that need be taken into account.[13]

For the above case with σ_ℓ = 1.75 cm, the integer mode number n is given approximately by $(2\pi R)/(2\sigma_\ell) = 3.03\times10^4$. Thus,

$$\left|\frac{Z_{\parallel}}{n}\right| \simeq 0.23\ \Omega \quad ,$$

significantly below the estimated threshold value. Figure II.2.2-3 shows the bunch length as a function of current for the "free space" impedance inserted into Eq. II.2.2.3-1. No significant contribution to $Z_{\perp}/n$ is expected from the "free space" impedance.

Using the cylindrically symmetric estimate for the transverse impedance equation, Eq. II.2.2.3-2, the threshold current for transverse fast instability is given by[11]

$$(\bar{I}_B)_{\perp} = \frac{4\ E\ \nu_s \left(\frac{b}{R}\right)^2}{e\left|\frac{Z_{\perp}}{n}\right| <\beta>} \qquad \text{(II.2.2.3-4)}$$

The program ZAP estimates this threshold current without "SPEAR scaling" for $|Z_{\parallel}/n|$. For the bunch length $\sigma_{\ell} = 1.75$ cm, the transverse threshold current is estimated to be $\gtrsim$ 2 times the longitudinal current of 5 mA.

The relationship between the bunch current and the bunch length imposed by these instability threshold equations can be changed by providing a higher harmonic rf system. These threshold equations assume that there is a single rf system of a given frequency which provides a unique relationship among the energy spread, synchrotron frequency, and the bunch length. The addition of a higher harmonic, say third-harmonic, system enables one to vary the bunch length and the synchrotron frequency independently of the energy spread and the rf voltage of the primary system. For this reason, a 1059-MHz cavity system capable of ~2 MV peak voltage is designed. The system can lengthen the bunch length by a factor of 1.7 without increasing the energy spread, thus enabling the bunch current to be increased by a similar factor.

The third-harmonic rf system can also be used to shorten the bunch length, as opposed to the above-mentioned lengthening of the bunch. The "zero" current bunch length of the main rf system is about 39 ps. The third-harmonic system can shorten this length to around 15 ps. The expected bunch current for this case is lower than that of the normal operating current.

2.2.4 Coupled Bunch Instabilities

As the number of bunches, M, increases in the storage ring, a second type of instability must be considered. The higher-order modes (HOMs) in the rf cavities have relatively high quality factors, Q, in the absence of HOM damping, and decay with a time constant $\tau \approx 2Q/\omega$. As the separation between bunches is reduced, the threshold for coupled bunch instabilities, resulting from HOM fields, decreases. The longitudinal instabilities do not generally result in beam loss, but the transverse instabilities may

drive beam loss mechanisms. These instabilities may occur whenever the resonant frequency of the HOM satisfies the relations

$$f^{\parallel}_{HOM} = f_o(p\ M + n + m\ \nu_s) \text{ for longitudinal modes,}$$

and

$$f^{\perp}_{HOM} = f_o(p\ M + n + \nu + m\ \nu_s) \text{ for transverse modes,}$$

where m, n, and p are integers. The threshold currents are obtained when the growth rates of the instabilities are set equal to the radiation damping times.

The programs BBI[15] and ZAP[11] are used for estimating the threshold currents for the m = 1 (dipole) and m = 2 (quadrupole) modes and for M = 13 and 26 bunches. These numbers were deduced from consideration of the harmonic number and the capability for yielding an average current of 100 mA. The longitudinal HOMs are listed in Table II.2.2-1 and the transverse HOMs are taken from a similar rf cavity.[7] In the longitudinal phase space, damped modes are assumed and all 15 cavities are assumed to have the same frequencies for the HOMs. The bunch parameters were taken to be σ_ℓ = 1.75 cm and $(\sigma_E/E) = 2.9\times10^{-3}$. The threshold currents are calculated using growth rates that are scaled from those calculated by ZAP. The growth rate is scaled linearly with current until it is equal to the synchrotron damping rate for each mode. These threshold currents are listed in Table II.2.2-3 for M = 13 and 26 bunches. The smallest current for the coupled bunch mode n for each bunch shape mode m was taken.

The threshold currents listed in Table II.2.2-3 are somewhat higher than the 100 mA for nominal operation, indicating no problem for coupled bunch stability.

2.3 Intrabeam and Gas Scattering

The Coulomb scattering between individual particles within a bunch causes a diffusion of particles to larger transverse phase space. This diffusion rate from intrabeam scattering is counteracted by the transverse synchrotron radiation damping, and the equilibrium emittance increases until the quantum fluctuation plus intrabeam scattering rate equals the damping rate. The increase in the equilibrium emittance is calculated in each plane by the program ZAP, which averages the diffusion rate over the entire lattice. The calculated fractional increase in the emittance for this lattice is given by

$$\frac{\Delta\varepsilon_{x,y}}{\varepsilon_{x,y}} \approx 6.5\times10^{-6}\ \bar{I}_B$$

Table II.2.2-3

Coupled Bunch Threshold Currents

M	σ_ℓ (cm)	Mode, m	$t_\parallel$ (ms)	$\bar{I}_o^\parallel$ (mA)	$t_\perp$ (ms)	$\bar{I}_o^\perp$ (mA)
13	1.75	1	22.6	326	17.8	128
13	1.75	2	94.0	1357	46.6	335
26	1.75	1	14.5	418	19.5	281
26	1.75	2	56.0	1618	49.5	715

$I_o^\parallel$ = total average beam current at longitudinal threshold,

$\bar{I}_o^\perp$ = total average beam current at transverse threshold,

$t_\parallel$ = growth time of longitudinal instability at $\bar{I}_B$ = 5 mA.

$t_\perp$ = growth time of transverse instability at $\bar{I}_B$ = 5 mA.

where $\bar{I}_B$ is the average bunch current in mA. This calculation assumed σ_ℓ = 1.75 cm, but the change is negligibly small even for σ_ℓ = 0.6 cm.

A similar emittance growth will result from multiple Coulomb scattering with the residual gas atoms. The rate of increase in the angular divergence of the beam is given by

$$\frac{d\langle\theta^2\rangle}{dt} = \left(\frac{E_s}{E}\right)^2 \frac{\rho c}{L_R}$$

where $E_s \approx 21.2$ MeV,

E = beam energy,

L_R = radiation length for the residual gas, and

ρ = density of the gas.

The angular divergence growth contributes to an emittance growth

$$Q_m = \frac{d\epsilon_i}{dt} = \frac{<\beta_i> d<\theta^2>}{dt} = \left(\frac{E_s}{E}\right)^2 \frac{<\beta_i>}{L_R} \rho c$$

for i = x or y. Similar to the case for intrabeam scattering, the equilibrium emittance is obtained by setting the sum of the quantum fluctuation and multiple scattering growth rates equal to the synchrotron damping rates:

$$Q_q + Q_m = Q_{damping} = \frac{2\epsilon_i}{\tau_i}$$

where τ_i is the synchrotron damping time. The change in the emittance from the natural emittance is given by

$$\frac{\Delta\epsilon_i}{\epsilon_i} = \frac{\tau_i}{2\epsilon_i} Q_m$$

where i = x or y. For the current lattice, with N_2 gas at pressure P (nTorr), L_R = 38 g/cm^2, and $\rho = 1.496\times10^{-9}$ P (g/m^3), the fractional change in the equilibrium emittance is given by

$$\frac{\Delta\epsilon_i}{\epsilon_i} = 0.747\times10^{-4} \quad P \ .$$

2.4 Beam Lifetime

2.4.1 Quantum Lifetimes

The total decay rate of the beam from the ring is the result of several loss processes considered below. The first effect to be considered is quantum lifetime due to synchrotron radiation loss from the rf bucket or momentum acceptance of the machine. The momentum acceptance due to physical apertures in dispersive sections of the lattice is ± 3.5%. Consequently the maximum momentum error acceptance is determined by the rf-bucket height of ~2.0%. The quantum lifetime is then given by the relationship[16]

$$\tau_q = \frac{\tau_E \, e^{\xi}}{2 \, \xi}$$

where

$$\xi = \frac{1}{2}\left(\frac{\Delta E_{rf}}{\sigma_E}\right)^2 ,$$

τ_E is the longitudinal synchrotron radiation damping time, and ΔE_{rf} is the height of the rf bucket. For $\sigma_E/E = 2.9\times10^{-3}$, the longitudinal quantum lifetime is $\tau_q > 1000$ h, a conservative value for τ_q considering its rapid dependence on σ_E. The quantum lifetime for the transverse aperture limit is obtained by replacing τ_E with τ_x and putting $\xi = 1/2\ N_V^2$, where N_V is the ratio of the dynamic aperture to beam size in the vertical direction. The dynamic aperture from tracking with errors yields $N_V >> 10$, which means a transverse quantum lifetime $\tau_q >> 1000$ h.

2.4.2 Touschek Lifetime

The intrabeam scattering, discussed previously for the transverse emittance blow-up, can also cause an exchange of energy between beam particles in the same bucket. If the energy transfer is great enough, these particles may be scattered outside of the rf bucket or the momentum aperture of the lattice and be lost from the stable beam. The lifetime has been given by Bruck.[17] This formalism can be used by inserting average lattice parameters, but the program ZAP[11] uses this formalism weighted over the actual lattice functions. In addition, ZAP can account for beam loss due to physical momentum aperture, as well as the rf-bucket height. Figure II.2.4-1 shows the lifetime as a function of $\bar{I}_B$ per bunch calculated by ZAP for $\sigma_E/E = 0.96\times10^{-3}$, 1.7×10^{-3}, and 3.3×10^{-3}, corresponding to $\sigma_\ell = 0.58$, 1.0, and 2.0 cm, respectively. Figure II.2.4-1 also shows the Touschek lifetime when the bunch lengthening is calculated by assuming "SPEAR scaling." The effect of increasing bunch current, which tends to reduce the Touschek lifetime, is balanced by the increase in bunch length (decrease in particle density), such that the Touschek lifetime is almost constant ($\tau_t \approx 190$ h) for bunch currents between 2 and 8 mA.

As an additional check, the program BEAMPARAM[18] was used to calculate the Touschek lifetime, which is also shown in Fig. II.2.4-1. This program does not allow for bunch lengthening, but computes the lifetime for $\sigma_\ell = 0.58$ cm and $\sigma_E/E = 0.96\times10^{-3}$. All calculations agree to better than ± 10%.

2.4.3 Bremsstrahlung Lifetime

The positrons in the beam sometimes collide with the atoms in the residual gas, thereby undergoing a deceleration and emission of a photon or photons. If the energy loss is larger than the bucket height, the particle is lost from the rf bucket. The

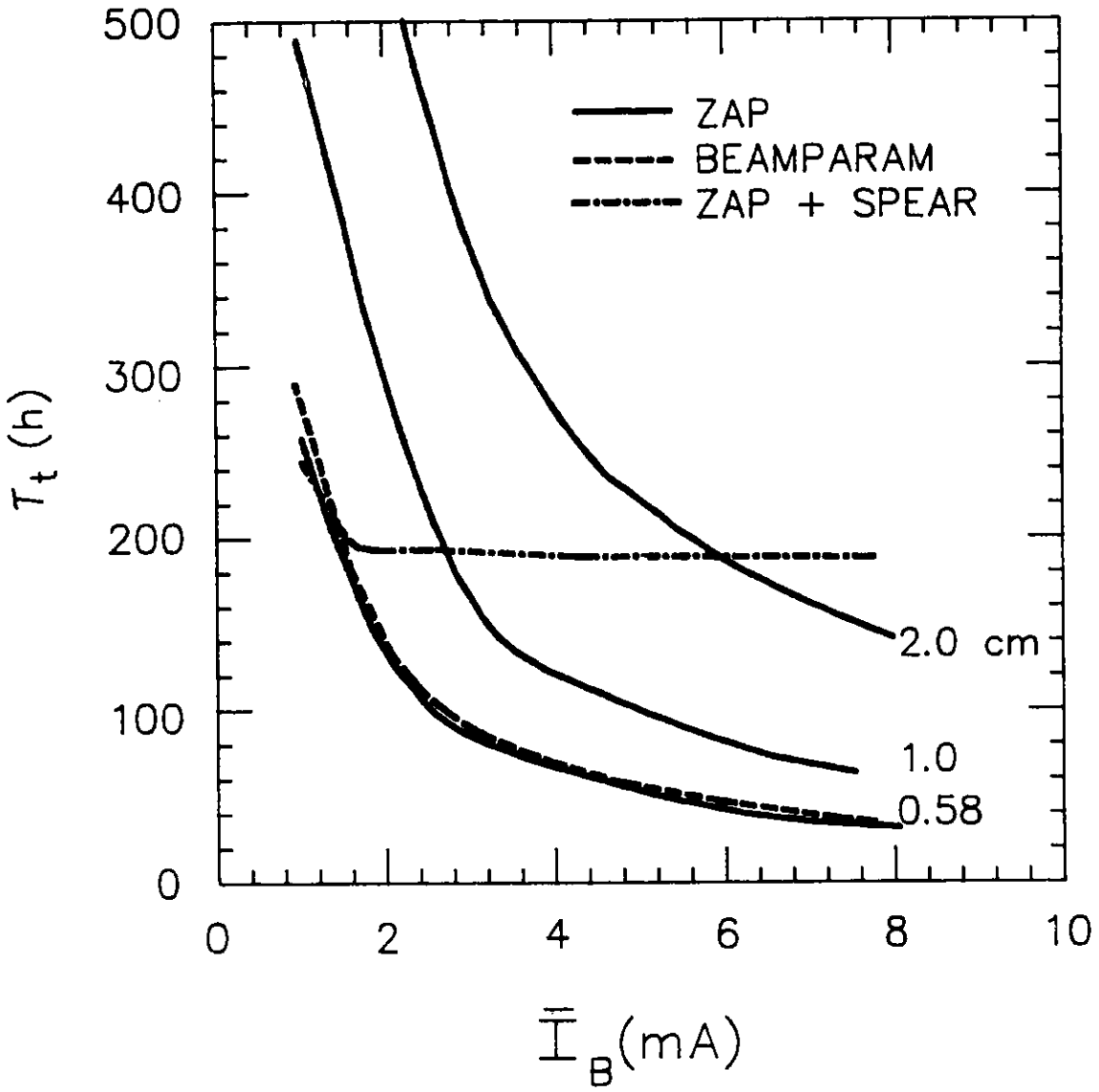

Figure II.2.4-1

Touschek lifetime as a function of the average single bunch current for σ_ℓ = 0.58, 1, and 2 cm. The solid curves are calculated by the program ZAP[11] and the dashed curve by BEAMPARAM.[17] The dot-dashed line is the Touschek lifetime calculated by ZAP, for the bunch lengthening given by the "SPEAR scaling" assumption.

bremsstrahlung cross section that results in beam loss is obtained by integrating the differential cross section from $E_\gamma = \Delta E_{rf}$ to $E_\gamma = E$, and is given by

$$\sigma_b = \frac{4r_e^2}{137} Z(Z + \xi) \left[\frac{4}{3} \ln \left(\frac{E}{\Delta E_{rf}}\right) - \frac{5}{6}\right] \ln \left(183\ Z^{-1/3}\right)$$

where

$$\xi = \frac{\ln (1440\ Z^{-2/3})}{\ln (183\ Z^{-1/3})} ,$$

r_e = classical electron radius, and Z = atomic number of the gas atoms.[19] The rate of beam loss is then given by

$$\frac{1}{\tau_b} = c\ N\ \sigma_b$$

where N is the atomic density of the gas,

$$N = 6.43412 \times 10^{13}\ P \left(\frac{\text{atoms}}{\text{nTorr m}^3}\right)$$

at T = 300 K for a diatomic gas such as H_2, N_2, O_2, etc., and P is the pressure in nTorr. The assumption of Z = 7 (N_2) yields a "worst case" lifetime of

$$\tau_b = \frac{53.3}{P} (h) .$$

For a mixture of gases X and Y, an estimate of the lifetime is obtained by summing the rates for each element at its partial pressure

$$\frac{1}{\tau_b} = \frac{1}{\tau_b(X)} + \frac{1}{\tau_b(Y)} .$$

For a partial pressure mixture of 75% H_2 and 25% CO, we find

$$\tau_b = \frac{187}{P} (h) .$$

Therefore, the bremsstrahlung lifetime at the expected operating pressure of 1 nTorr is 187 hours.

2.4.4 Single Coulomb Scattering

If the positron scatters off the residual gas atoms with a large enough angular deflection to hit the vacuum chamber wall, it is lost. Since the maximum acceptance (A_y) of this ring will be limited by the 8-mm undulator aperture g, the minimum lifetime of the ring will be determined by this value. The cross section for scattering outside this aperture is obtained by integrating the differential cross section from $\phi = \sqrt{Ay/<\beta y>}$ to π, and is given by

$$\sigma_s = \frac{4\pi r_e^2 Z(Z+1)}{\gamma^2} \frac{<\beta_y>}{A_y},$$

where

$$A_y = \frac{(g/2)^2}{\beta_y},$$

β_y = the maximum vertical beta function in the undulator gap, and $<\beta_y>$ = the average β_y for the ring.[19] For Z = 7 (N_2), the "worst case" single scattering lifetime becomes

$$\tau_s = \frac{35.5}{P} \text{ (h)}$$

with P in nTorr.

For the H_2-CO gas composition used above, a more realistic gas scattering lifetime is given by

$$\tau_s = \frac{128}{P} \text{ (h)} \quad .$$

Therefore, the single Coulomb scattering lifetime is 128 hours at the expected operating pressure of 1 nTorr.

2.5 Conclusion

The total lifetime, τ_{total}, of the beam is given by

$$\tau_{total} = \frac{1}{\frac{1}{\tau_t} + \frac{1}{\tau_b} + \frac{1}{\tau_s} + \frac{1}{\tau_q}} \quad .$$

In order to ensure a lifetime of greater than 10 h with the values for τ_b, τ_s, and τ_q derived above, the Touschek lifetime[20] must satisfy $\tau_t \geq 11.5$ h. This lifetime is easily satisfied for the bunch parameters and currents assumed here for 100-mA operation.

Single bunch currents of $\bar{I}_B \approx 5$ mA should be achievable for a bunch lengthening of three times the minimum bunch length. This current was calculated using the "SPEAR scaling" impedance model and is 25% greater than the current obtained using a broadband resonant model that scales with the calculated values of $k(\sigma_\ell)$. However, the "free space" current limit for this bunch length is 10 mA, allowing for increased bunch current capability (without an increased rf voltage) if the ring impedance turns out to be smaller than the presently assumed value. Alternatively, increased bunch lengthening will allow higher single bunch current, while requiring an increased bucket height. The coupled bunch stability is adequate for 100-mA operation.

The higher-harmonic rf system will allow the bunch length to be decoupled from the need of increasing the bucket height. This permits greater flexibility in varying the bunch parameters and current, while ensuring stable bunch operation.

2.6 References

1. P. Wilson, Proc. 1985 U.S. Summer School on High-Energy Particle Accelerators (July 1985).

2. T. Khoe, ANL Report, Light Source Note LS-43 (1985).

3. K. Halbach and R.F. Holsinger, Particle Accelerators 7, 213 (1976).

4. P. Fernandes and R. Parodi, IEEE Trans. Magn. MAG-19, 2421 (1983).

5. T. Khoe, Argonne National Laboratory, unpublished note (1986).

6. T. Weiland, IEEE Trans. Nucl. Sci. NS-30, 2489 (1983).

7. A. Hofman, "Collective Effects in the ESRP," ESRP-IRM-40/84 (1984).

8. J. N. Weaver et al., IEEE Trans. Nucl. Sci. NS-26, 3971 (1979).

9. D. Boussard, "Observation of Microwave Longitudinal Instabilities in the CPS," CERN/Lab II/RF/Int. 75-2 (1975).

10. R. L. Kustom et al., "RF Impedance Studies of a Beam Chamber and Longitudinally Slot - Coupled Vacuum Pumping Antechamber," IEEE Conference Record, 87CH2837-9.

11. M. Zisman et al., ZAP User's Manual, LBL-2/270 (1986); J. Bisognano, et al., IEEE NS-32, 2700 (1985); M. Zisman, IEEE Conference Record, 87CH2837-9.

12. J. Bisognano, "Report of Machine Workshop on the 6-GeV Synchrotron Radiation Source," Gaithersburg, Md. (March 28-30, 1985).

13. A. Faltens and L. J. Laslett, Proc. 1975 ISABELLE Summer Study, III, 486 (1975); A. G. Ruggiero, KEK Report, KEK 80-16 (1981).

14. J. D. Lawson, The Physics of Charged-Particle Beams, pp. 345-383, Clarendon Press, Oxford (1977).

15. M. Gygi-Hanney et al., CERN/LEP-TH/83-2 (1983).

16. M. Sands, SLAC Report, SLAC-121 (1970).

17. H. Bruck, "Circular Particle Accelerators," LANL Report, LA-TR-72-10, translated by R. McElroy Co., Inc. (1972).

18. M. Hanney and E. Keil, CERN-ISR/TH-79-29 (1979).

19. T. Khoe, ANL Report, Light Source Note LS-27 (1985).

20. Touschek lifetime must be expressed as an e^{-1} time in keeping with the definition of the other lifetimes; see S. Kramer, ANL Report, Light Source Note LS-68 (1986).

3.1 Introduction

The rf system must provide adequate voltage and power to compensate for synchrotron radiation from the dipole magnets and the insertion devices, excitation of parasitic modes by the beam, and overvoltage for an adequate beam lifetime. Design limits in the storage ring rf are: (a) 200 kW of rf power per ceramic window and (b) 800-kV accelerating voltage per cavity. The nominal frequency of operation for the storage ring rf system is 353 MHz.

The rf system uses 15 single-cell, spherical cavities. These are the same type of cavities used on the Photon Factory in Tsukuba[1] and the SRS in Daresbury.[2] Three 1-MW klystrons provide the rf power. The power from each klystron drives five cavities. Each group of five cavities is located in a 6-m straight section; these are located in the 9th, 10th, and 29th straight sections after the injection straight section. A third-harmonic cavity, operating at 1059 MHz and 1.8 MV, is located in the 30th straight section after injection. The rf parameters are listed in Table II.3.1-1.

3.2 353-MHz Accelerating Structures

Figure II.3.2-1 shows the cross section and dimensions of the single-cell cavity used for the storage ring. Calculations with the computer program URMEL[3] and estimates made by scaling from the Photon Factory measurements indicate that a single cavity can develop 800 kV with 62 kW of copper loss and with a peak electric field at the copper surface of 5.9 MV/m. The same fabrication technique used for the Photon Factory cavities is used. The cavity is machined in two halves from solid blocks of Oxygen-Free High Conductivity (OFHC) copper, with cooling channels machined into each component. The inner surfaces are machined to a high surface finish and the two halves silver-brazed together. Stainless steel vacuum flanges are fitted to the beam ports.

Each cavity is provided with five 14-cm-diameter ports. One port is used for the coupling loop. The coupling loop, which is post-excited from a WR2300 waveguide, provides for coupling-coefficient adjustments. The post is vacuum-sealed from the air-filled waveguide by a cylindrical ceramic window. The second port is provided with a tuning plunger. The plunger has a 9.5-cm diameter and a 6.0-cm travel. This provides a frequency-tuning range of 1.0 MHz to compensate for beam loading, temperature effects, etc. A third port is used for vacuum pumping. Two 14-cm ports are provided for the beam.

The need for damping the higher-order modes (HOMs) in the cavity to suppress instabilities has been demonstrated on the 2.5-GeV Photon Factory storage ring.[4] Therefore, an antenna and a loop coupler with a band-stop filter for the fundamental

Table II.3.1-1

Radio Frequency Parameters for 7-GeV and 100-mA Operation

Frequency	353 MHz
Harmonic Number	1248
rf Voltage	9.5 MV
rf Voltage per Cavity	633 kV
Number of Single-Cell Cavities	15
Synchrotron Radiation Loss per Turn (bending magnets)	5.45 MeV
Parasitic Voltage Loss	0.20 MV
Voltage for Insertion Devices	1.25 MV
$\sin \phi_s$	0.73
Number of Klystrons	3
Power at 7 GeV and 100 mA	1.27 MW
Installed Power	3.0 MW
With 5.0 mA per Bunch	
Energy Spread, σ_E/E	0.29×10^{-2}
Bunch Length, σ_ℓ	17.5 mm
rf-Bucket Height, $\Delta E_{rf}/E_o$ (with ID and estimated parasitic losses)	2.0% $\simeq 7\ \sigma_E/E$
Synchrotron Frequency	1.88 kHz

frequency are placed in two 5-cm-diameter ports, 90° apart, in order to suppress higher-order modes. A list of the lowest higher-order modes with their undamped shunt impedances and Q values calculated with URMEL is given in Table II.3.2-1. The frequencies agree closely with values scaled from measurements on the 500-MHz cavities at the Photon Factory. Hybrid modes are expected at 482.3, 580.5, 749.6, 796.5, and 871.5 MHz by scaling from measurements made at the Photon Factory. These modes cannot be verified with any of the cavity computer programs, since these programs cannot handle hybrid modes. The antenna- and loop-damping couplers are successful in eliminating the effects of the higher-order longitudinal and transverse modes on the stored beam.

There are, in addition, a few smaller penetrations for pick-up loops and probes to be used for measurement and instrumentation.

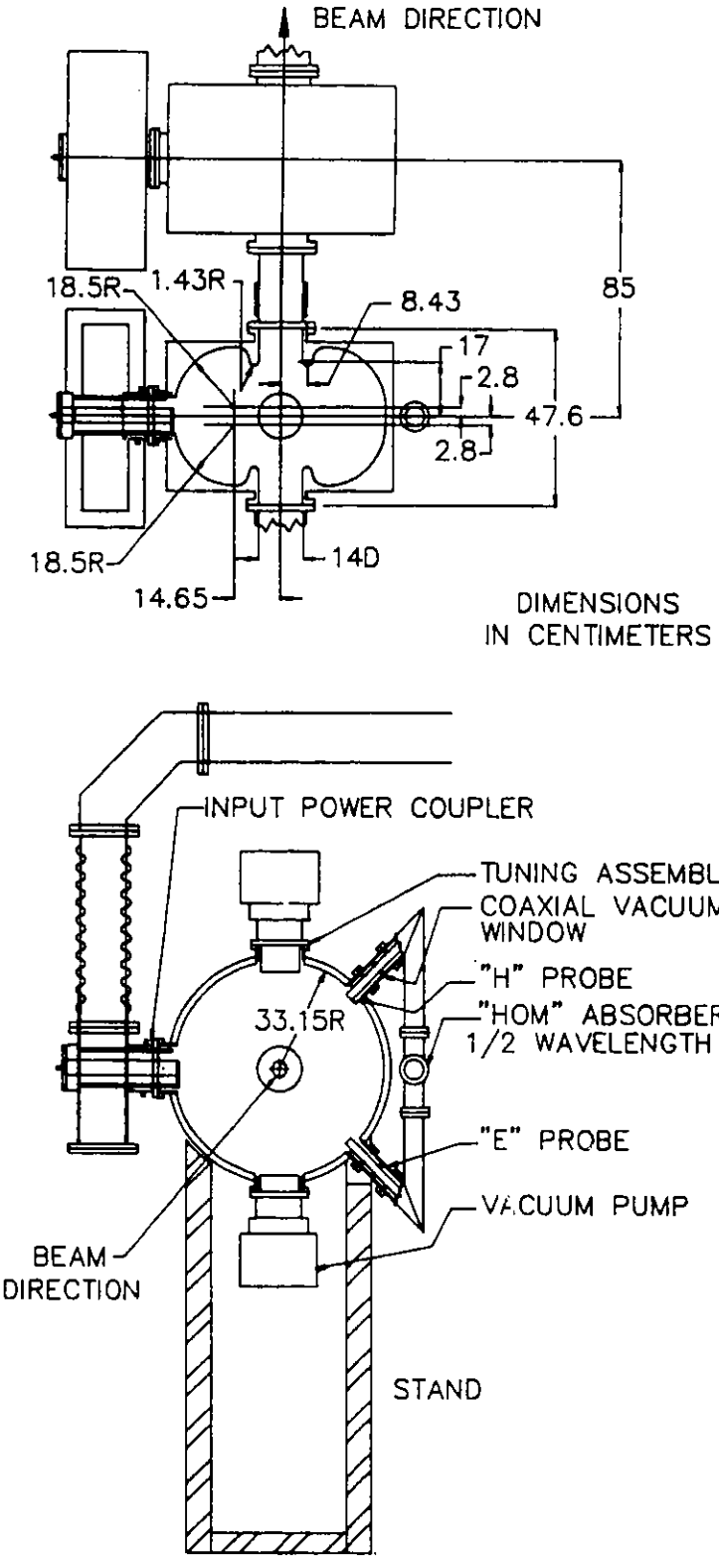

Fig. II.3.2-1
353-MHz rf accelerating structure showing a top view of two cavities and a vertical cross section.

Table II.3.2-1

Shunt Impedances of Some of the Higher-Order Modes of the Single-Cell Spherical Cavity

Frequency MHz	Shunt Impedance (undamped) MΩ	Q (undamped)
353.0	11.23	48,600
743.0	0.03	41,630
925.0	1.25	108,800
1174	0.33	43,450
1330	0.03	129,000
1511	1.09	88,130
1654	0.07	45,770
1679	1.06	46,260
1842	0.33	121,250
1972	2.98	54,850

Each cavity is pumped by a 220-ℓ/s ion pump. Remotely driven beam line valves are provided at each end of the straight section for isolation. One roughing system, including sorption pumps and turbopumps, is provided in each of the two rf power buildings. The base pressure of the cavity reaches 0.75 nTorr.

3.3 Radio Frequency Power System

A 1-MW klystron is used to drive five cavities. A block diagram for the five-cavity arrangement is shown in Fig. II.3.3-1. From the klystron, the power is divided equally to the five cavities. The first division is via a 2/5:3/5 hybrid T plus a second 1/3:2/3 hybrid. Two more 1:1 hybrids provide equal power to each cavity. Table II.3.3-1 lists the operating parameters for the Thomson-CSF TH2089 klystrons. The YK 1350 klystron available from Valvo has similar characteristics, and either tube could be used. A total of three 1-MW klystrons are required for 15 cavities.

The power requirements for several different operating scenarios, including the normal operating condition, are listed in Table II.3.3-2.

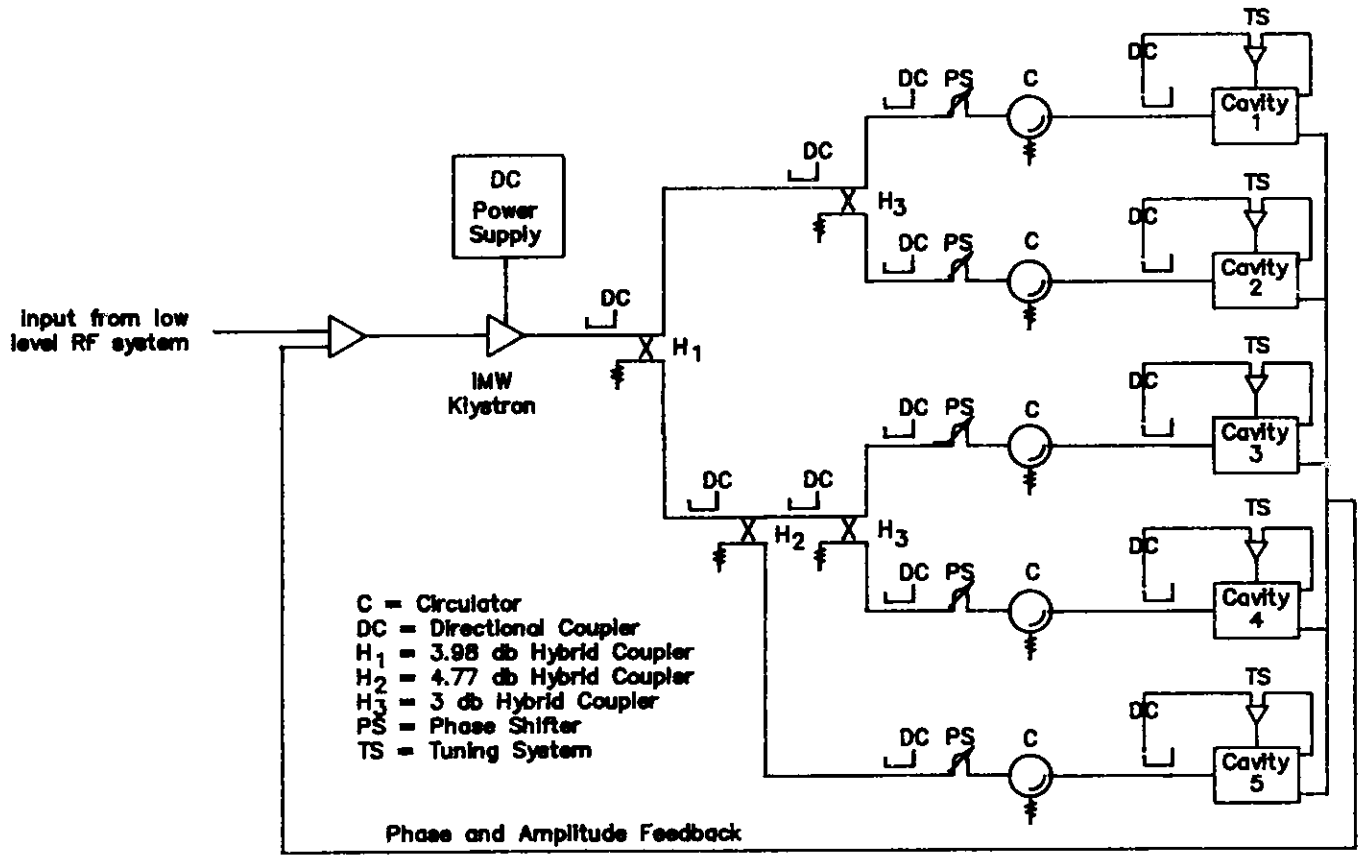

Figure II.3.3-1

Schematic diagram of circuit used to split the power from one 353-MHz, 1-MW klystron and distribute it to five rf cavities.

Table II.3.3-1

Parameters for the Thomson-CSF TH2089 1-MW, 353-MHz Klystron

Operating Frequency	353 MHz
Mechanical Tuning Range with Respect to Center Frequency	± 3 MHz
Continuous Output Power	1.0 MW
Reflected Power, Maximum	16.6 kW
Drive Power, Maximum	200 W
Gain, Minimum	40 dB
Gain, Typical	41 dB
Efficiency	65-70%
Beam Voltage	90 kV
Beam Current	18 A
Length (horizontal position)	4.8 m
Height (horizontal position)	1.85 m
Width	1.0 m
Output Waveguide	WR2300

The load lines for 3-MW input rf power, plotted in Fig. II.3.3-2 for 7.0 GeV and 7.5 GeV, indicate that the rf system will be able to produce voltages and currents well in excess of the nominal operating conditions; 7 GeV and 300 mA is within the system's capabilities, even with 2.2-MeV losses for insertion devices.

The power from the 1-MW klystron is divided five ways. There is a three-port circulator, and a mechanically driven phase-shifter, between the hybrid and the cavity. The harmonic voltages that are generated by the beam are absorbed by the HOM devices on the cavities. The circulator prevents reflected power from reaching the klystron or other branches of the rf system.

The center-to-center spacing of the cavities is 0.8493 m. The waveguide lengths are adjusted to provide the right nominal phase with respect to the beam, and mechanically tunable phase-shifters are used for fine tuning of the cavity phase (≈0.5 to 1.0°).

Table II.3.3-2

Power Required under Different Operating Conditions

	7.0 GeV, 100 mA	7.0 GeV, 300 mA	7.5 GeV, 200 mA
Copper Loss (kW)	582	582	935
Power for Bending Magnet Synchrotron Radiation (kW)	545	1635	1436
Power for Insertion Device Synchrotron Radiation (full complement) (kW)	125	375	286
Power for Parasitic Mode Loss (kW)	20	60	40
Total Power into Storage Ring (kW)	1272	2652	2697
Storage Ring Voltage (MV)	9.5	9.5	12.04

Elevation and plan views of adjacent cavity, waveguide, and klystron systems in an rf power building are shown in Fig. II.3.3-3.

The coupling loop on each cavity is adjustable to change the coupling constant from about 1.0 to 5. Since the circulators and klystron can safely handle large amounts of reflected power, the loop is normally set for optimum operation at the highest expected beam current during the operating period. This implies that the loop is overcoupled for lower currents, which will result in reflected power. The feedback loop that drives the tuning plunger works on only the reactive element of cavity input impedance. The klystrons with circulators can handle the reflected power from overcoupling at power levels below the maximum point in the designated operating cycle.

Klystron beam power is supplied by a 90-kV, 20-A multiphase rectifier with 0.1% ripple and regulation. A modulating anode supply is used to maximize efficiency. The klystron is fully protected by an electronic crowbar and arc detection circuitry.

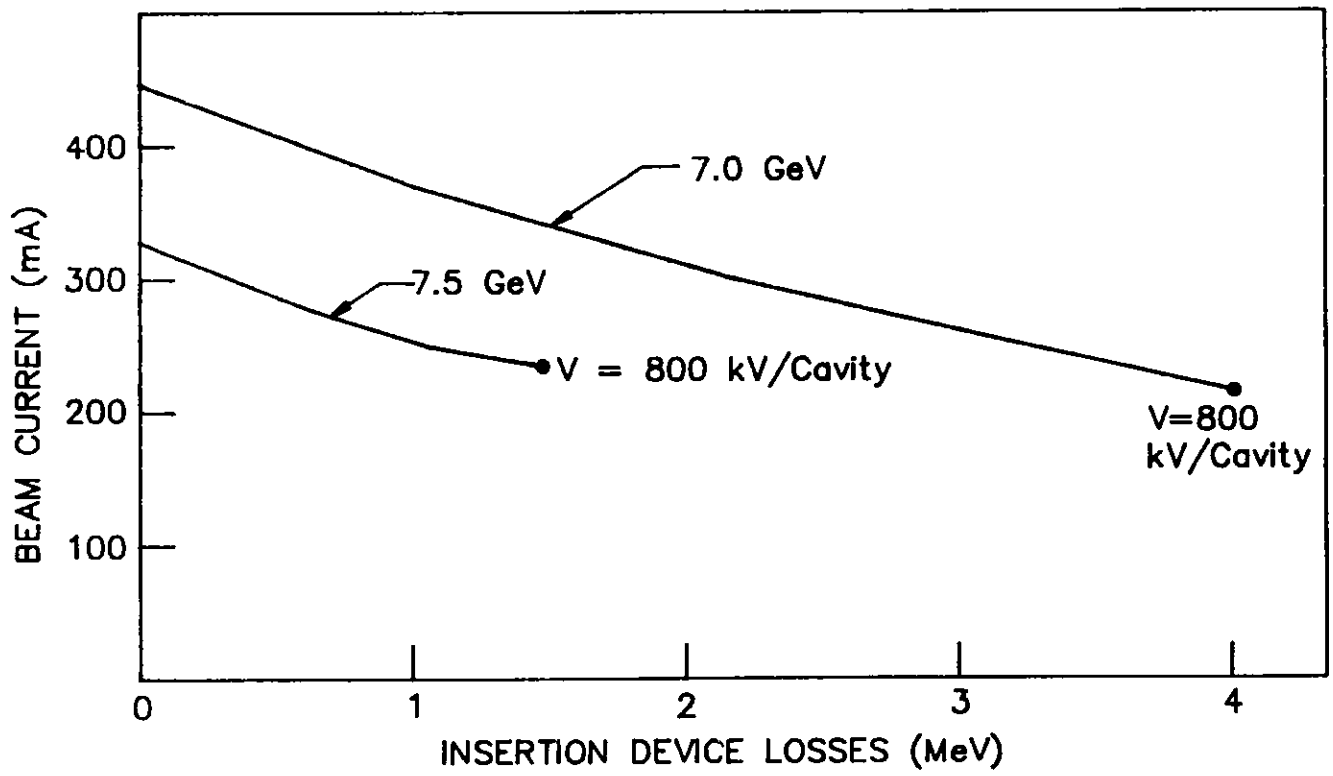

Figure II.3.3-2

Load lines for 7 GeV and 7.5 GeV with 3-MW input rf. The maximum beam current is shown as a function of the insertion device energy loss for 7 and 7.5 GeV operation, with the 3-MW rf system. The end points for each curve represent the maximum design voltage of 800 kV/cavity.

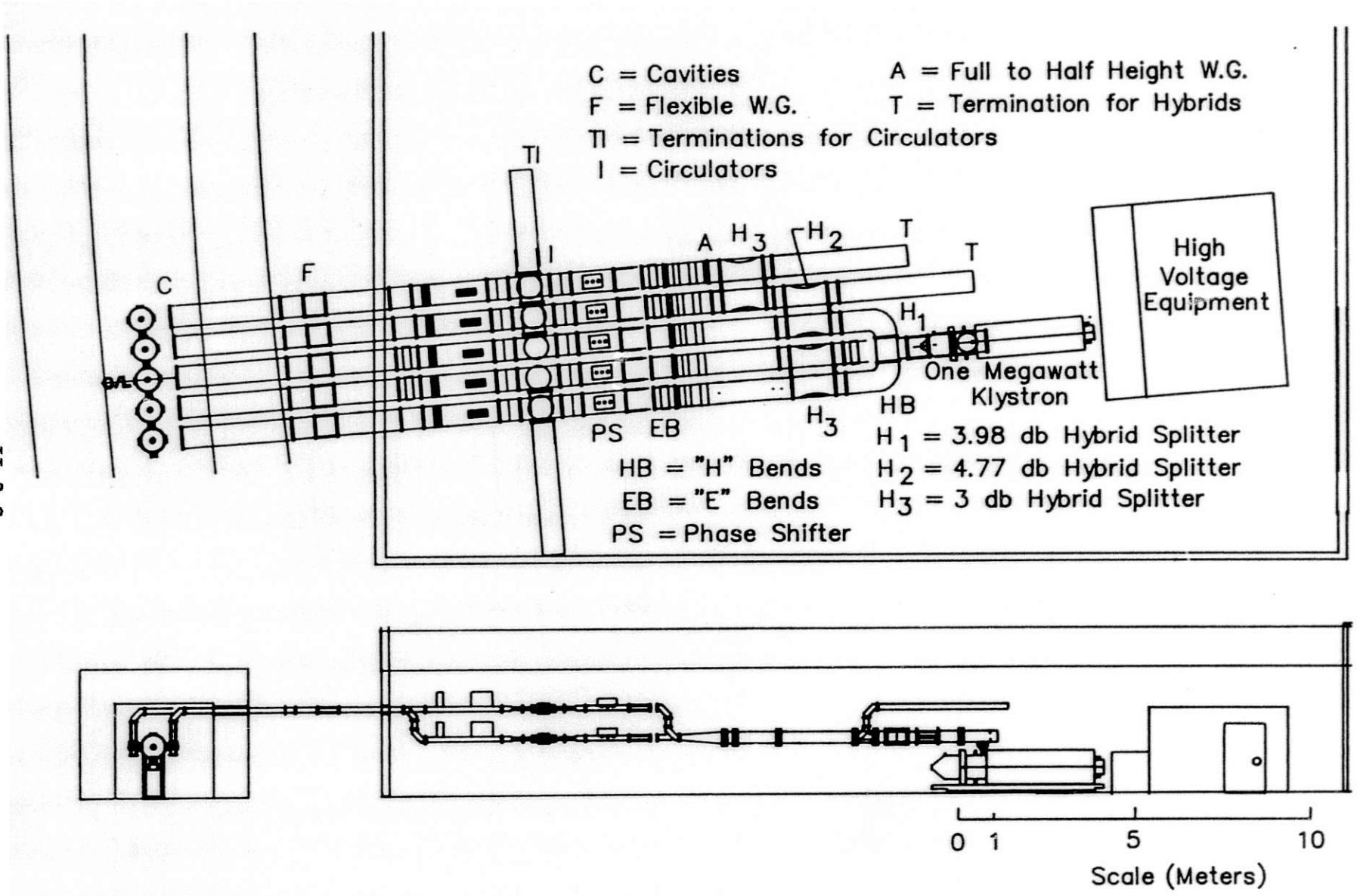

Figure II.3.3-3
Elevation and plan views of adjacent cavity, waveguide, and klystron systems in one of the rf power buildings.

3.4 Beam Loading

The rf power delivered to the beam via the cavities can be much larger than that used to excite the cavity to the required voltage. The highest coupling constant, β, required is about 4.5. The cavity coupling will be adjusted to give a matched condition at the circulating current.

It is necessary to compensate for the reactive component of the beam loading. This is done prior to injection by detuning to comply with the requirement of the Robinson instability criterion.[5] For Robinson stability,

$$[1/(1 + \beta)](Pb/Pc) < 1 \quad .$$

The required amount of detuning from the no-beam resonance condition to the fully loaded condition is

$$\Delta f = -(f_{rf}/2Q_o) \times (Pb/Pc) \times \cot(\text{phase angle})$$

$$= (353\times10^6/2\times40\times10^3) \times (176/39) \times \cot(51.2°) = -16 \text{ kHz} \quad .$$

This detuning coverage can easily be handled by the tuning system, which has a range of 1 MHz. Detuning requires additional power. After beam filling is completed, the cavities are tuned closer to resonance, and the Robinson instability is counteracted with dynamic feedback via the low-level controls. The low-level loops are fast enough for this application.

3.5 1059-MHz Radio Frequency System

A third-harmonic system is included in the design to provide additional Landau damping or bunch lengthening if required for added stability. An axial accelerating voltage of 1.8 MV from a standing-wave biperiodic structure operating in the $\pi/2$ mode is used.

Among the various geometries for cavity structures with high shunt impedance, the most successful are the side-coupled cavity geometry developed at Los Alamos National Laboratory for the LAMPF accelerator[6] and the on-axis coupled structure developed at the Chalk River Laboratories.[7]

Both of these cavities have been studied extensively, and either one could be used for the 1059-MHz rf system. The on-axis coupled structure is used, and is shown in cross section in Fig. II.3.5-1. The inside bore diameter of the iris is 6 cm to allow an unobstructed path for synchrotron radiation.

This geometry has several advantages. Fabrication is simplified because of the coaxial symmetry, and excitation of transverse deflecting modes can be suppressed by

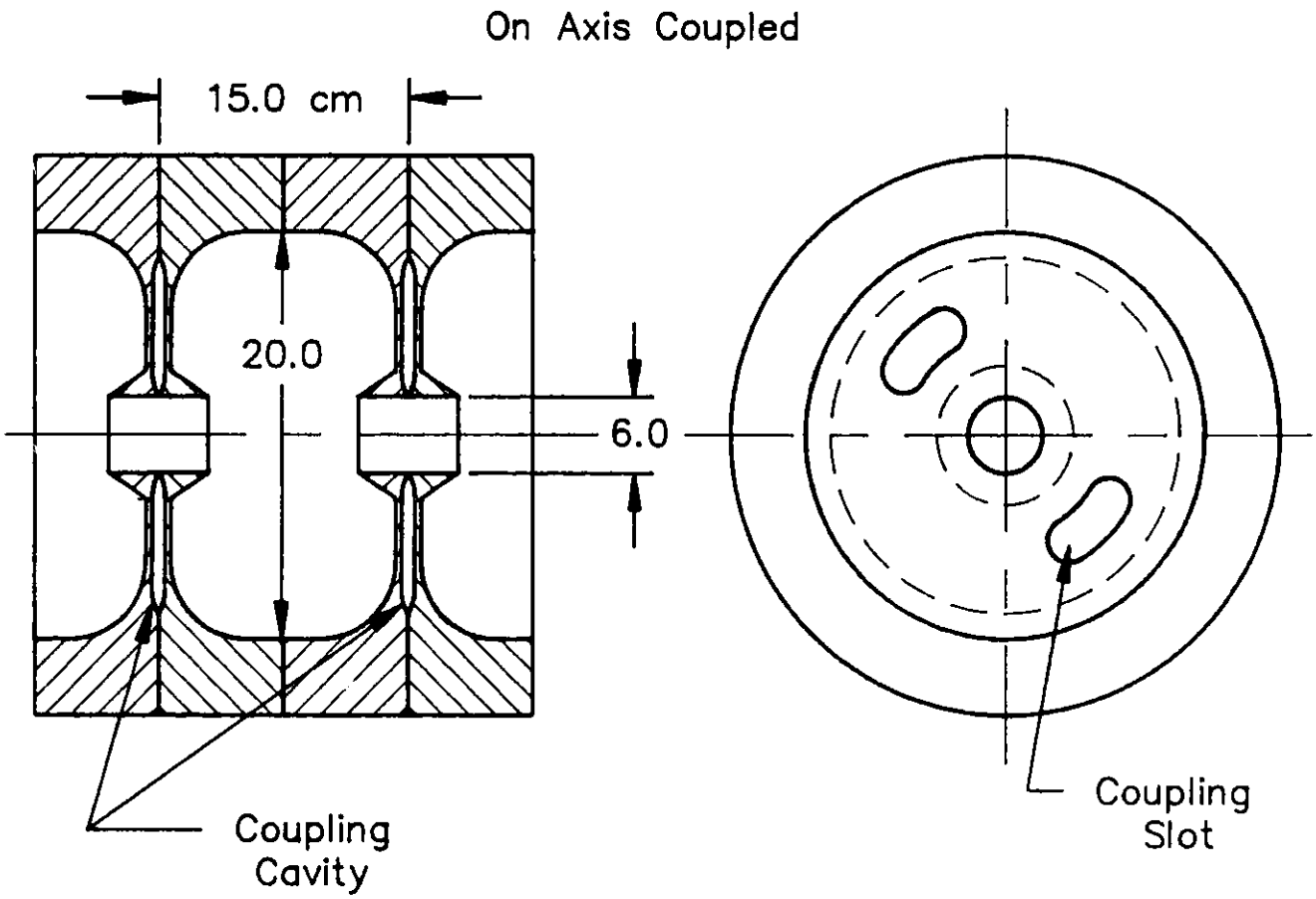

Figure II.3.5-1
1059-MHz on-axis coupled structure.

splitting the resonance frequencies for hybrid HEM_{110}-like modes. This splitting is accomplished by rotating the coupling slots that connect adjacent cavities.[8] For this reason, the Mainz group has successfully used the on-axis coupled geometry for the Mainz microtron (MAMI) system of cascaded microtrons.

The frequency of the cavity is 1.059 GHz with $\beta = 1$, and the effective shunt impedance per unit length (the "bare" shunt impedance per unit length multiplied by the square of the transit time factor) is 41 MΩ/m with a 6-cm diameter aperture. The rf power dissipated in the cavity at the accelerating field of 1.8 MV, is 19 kW/m, and cooling is easily accomplished.

Power is fed into the center of the 2-m-long rf structure through an rf coupler connected by flanges to the two sections. The 10% coupling factor of this type of cavity is quite adequate for this length.

With a bore of 6 cm, three 220-ℓ/s ion pumps (one in each end and one at the center) keep the structure at a pressure below 1 nTorr. The 1.059-GHz cavity is driven from a single klystron. A modified Valvo YK 1250 klystron can be used.

3.6 Low-Level Radio Frequency System and Control

The frequency and phase of the storage ring rf system affect the beam position and energy. The main frequency source is stable and controllable, with phase continuity to several parts in 10^{11}. The low-level rf system utilizes a digital synthesizer to control a phase-locked, voltage-controlled oscillator as the source. The output of this common frequency source is fed via phase-stable cables to each of the klystron amplifiers in the system. The input to each klystron amplifier driver has a computer-controlled rf amplitude modulator and a computer-controlled relative phase shifter. An amplitude comparator compares the sum of the voltages from all cavities and adjusts the rf modulator to maintain the required voltage. The phase of the voltage developed in the cavities is compared with the reference, and the phase of the drive to the klystron is adjusted to maintain the cavity voltage phase within $\pm 1.0^\circ$ (Fig. II.3.3-1).

The klystron power is controlled by a control loop through the modulating anode system, while the klystron drive is maintained in the linear gain region. In this way the klystron efficiency remains optimum.

3.7 References

1. "Photon Factory Activity Report, 1982/83," National Laboratory for High Energy Physics, KEK, Japan (1983).

2. D. M. Dykes and B. Taylor, "Development of a High Power RF System for the Daresbury SRS," IEEE Trans. on Nuclear Science, NS-30, 3475 (August 1983).

3. T. Weiland, "Computer Modeling of Two- and Three-Dimensional Cavities," IEEE Trans. on Nuclear Science, NS-32, 2738 (October 1985).

4. Y. Yamazaki, K. Takata, and S. Tokumoto, "Damping Test of the Higher-Order Modes of the Re-entrant Accelerating Cavity," IEEE Trans. on Nuclear Science, NS-28, 2915 (June 1981).

5. K. W. Robinson, "Stability of Beam in Radio Frequency System," CEAL-1010, p. 8 (February 27, 1964).

6. E. A. Knapp, B. C. Knapp, and J. M. Potter, Rev. Sci. Instr., 39, 979 (1960).

7. S. O. Schriber, E. A. Heighway, and L. W. Funk, Proc. 1972 Proton Linac Conf., LAN Report No. LA-5115, 114 (1972).

8. S. O. Schriber, "Room Temperature Cavities for Accelerating Structures," Proc. Conf. on Future Possibilities for Electron Accelerators, J. S. McCarthy and R. R. Whitney, eds., p. L (January 1979).

4.1 Introduction

The storage ring contains 80 dipoles, 400 quadrupoles, and 280 sextupoles. There are also 678 dipole correctors -- 360 of them are part of the dipole or sextupole magnet assemblies, 240 of them are individual horizontal correctors, and 78 of them provide both vertical and horizontal corrections. The main features of their construction are described in this section. All the magnets are optimized for 7-GeV operation and capable of 7.7-GeV operation. The magnetic field calculations have been done for each of these magnets using the two-dimensional program called POISSON. Conformal transformations[1] of these geometries allowed the linear elements in the calculation to more accurately represent the nonlinear potentials in the gaps. The designs will be verified by building full-scale prototypes and measuring magnetic fields. These prototypes will be used to develop construction techniques.

All magnets allow the synchrotron radiation beam lines to exit the ring from the outside radius. The dipoles, quadrupoles, and sextupoles are assembled from low-carbon (SAE 1010) steel laminations, solid low-carbon steel end plates which are 25 mm thick, and hollow copper conductor which is insulated with fiberglass and vacuum impregnated with epoxy resin. The parameters for these magnets have been determined with the program MADEST[2] and are summarized in Table II.4.1-1.

Each core is held under compression by welded parts on the exterior surfaces or tie rods installed under tension and extending between the end plates. The solid steel end plates transfer the compression to the pole tips, which are located relatively far from the ties near the outside surfaces of the core. These solid plates also facilitate the machining of the contours required to properly control the field shapes at the ends of the poles. They are also easily beveled along the pole edges, allowing the coils to hug the ends of the cores, thereby minimizing the overall lengths of the assembled magnets.

After all magnets have been tested and measured, they are assembled on support structures. These assemblies are initially aligned and then moved as a unit into the ring where a final alignment check is made. To permit this type of installation, the focusing magnets are separated into top and bottom halves. The designs of the horizontal, midplane joints in these units permit them to be reassembled while maintaining the original geometrical alignment of the parts.

4.2 Field Quality

The field quality is expressed in terms of the relative field intensity, $\Delta B/B_0$, for dipole; the relative field gradient, $\Delta G/G_0$, for quadrupole; and the relative field second-gradient, $\Delta K/K_0$, for sextupole. Alternatively, it can be expressed in terms of the multipole coefficients, b_n and a_n. Neglecting the end effects, the two-dimensional field

Table II.4.1-1

Parameters for Storage Ring Magnets

Field Type		Dipole	Quadrupoles			Sextupole
Number Required		80	80	80	240	280
Strength at 7.0 GeV		0.60 T	19.1 T/m			490 T/m^2
Effective Length	(m)	3.06	0.8	0.6	0.5	0.24
Gap Height or Diameter	(mm)	60	80			100
Bending Radius	(m)	38.96				
Total Mass of Magnet	(kg)	5130	1815	1374	1153	580
Coils per Pole		2	1			1
Conductor Height	(mm)	22.0	11.5			7.4
Width	(mm)	12.2	11.5			5.6
Hole Diameter	(mm)	9.0	6.3			3.6
Number of Turns per Pole		32	32			44
Total Inductance	(mH)	51	27	20	17	36
Total Resistance	(mΩ)	38	44	35	30	98
Time Constant	(ms)	1342	614	571	567	367
Peak Current	(A)	452	416			195
Current Density in Coil	(A/mm^2)	1.4	2.6			3.9
Voltage	(V)	17.3	18.5	14.4	12.4	19.0
Power	(kW)	7.8	7.7	6.0	5.2	3.7
Cooling Water Circuits per Magnet		2	4			6
Total Water Flow	(gal/min)	2.4	2.8	3.2	3.4	2.3
Water Pressure Drop	(psi)	100	40			100
Water Temperature Rise	(°C)	12	13	9	7	7

in the transverse plane (rectangular coordinates x,y or polar coordinates r,θ) can be written as

$$B = B_y + iB_x = B_o \sum_{n=0}^{\infty} (b_n + ia_n)(x + iy)^n = B_o \sum_{n=o}^{\infty} (b_n + ia_n)z^n \quad ,$$

where $B \equiv B_y + iB_x$ and $z \equiv x + iy$ are the complex field and position variables. The complex field gradient and second-derivative are given by

$$G \equiv \frac{\partial B}{\partial z} = B_o \sum_{n=1}^{\infty} n(b_n + ia_n)z^{n-1}$$

and

$$K \equiv \frac{1}{2}\frac{\partial^2 B}{\partial z^2} = B_o \sum_{n=2}^{\infty} \frac{n(n-1)}{2} (b_n + ia_n)z^{n-2} \quad .$$

For a dipole magnet, the design field intensity is B_o ($b_o = 1$, $a_o = 0$) and one obtains

$$\frac{\Delta B}{B_o} = \frac{B-B_o}{B_o} = \sum_{n=1}^{\infty} (b_n + ia_n)(x + iy)^n \quad .$$

For a quadrupole magnet, the design field gradient is $G_o \equiv B_o b_1$ ($a_1 = 0$) and one obtains

$$\frac{\Delta G}{G_o} = \sum_{n=2}^{\infty} n\left(\frac{b_n}{b_1} + i\,\frac{a_n}{b_1}\right)(x + iy)^{n-1} \quad .$$

For a sextupole magnet, the design field second-derivative is $K_o \equiv B_o b_2$ ($a_2 = 0$) and one obtains

$$\frac{\Delta K}{K_o} = \sum_{n=3}^{\infty} \frac{n(n-1)}{2} \left(\frac{b_n}{b_2} + i\,\frac{a_n}{b_2}\right)(x + iy)^{n-2} \quad .$$

For skew quadrupole and sextupole magnets, we have $b_1 = 0$, $a_1 = 1$ and $b_2 = 0$, $a_2 = 1$, respectively, and get similar expressions for the relative field gradient and second-gradient.

To measure the multipole coefficients, we need only to measure the θ-harmonics of $\Delta B/B_o$ at radius r_o. The relative field at radius r_o is

$$\frac{\Delta B}{B_o}\left(z = r_o e^{i\theta}\right) = \sum_{n=1}^{\infty} (b_n + ia_n) r_o^{\,n} e^{in\theta} \quad .$$

The n^{th} harmonic coefficient is, therefore, simply $(b_n + ia_n)r_o^{\,n}$ and gives directly the coefficients b_n and a_n.

The calculated two-dimensional relative field deviations and leading multipole coefficients are listed in Table II.4.2-1.

Table II.4.2-1

Field Qualities of Ring Magnets

	Dipole	Quadrupole	Sextupole
Relative Deviation (10^{-4})	$\left(\frac{\Delta B}{B_o}\right)_{\substack{\max \\ \min}} = \begin{matrix} +\ 1.5 \\ -\ 1.0 \end{matrix}$	$\left(\frac{\Delta G}{G_o}\right)_{\substack{\max \\ \min}} = \begin{matrix} +\ 0.5 \\ -\ 2.6 \end{matrix}$	$\left(\frac{\Delta K}{K_o}\right)_{\substack{\max \\ \min}} = \begin{matrix} +\ 14.9 \\ -\ 10.3 \end{matrix}$
	for $\lvert x\rvert \le 30$ mm, $\lvert y\rvert \le 20$ mm	for $r_o \le 25$ mm	for $r_o \le 25$ mm
Multipole Coefficients (10^{-6} cm^{-n})	$b_2 = 12.5$ $b_4 = 0.59$	$b_5 = 0.70$ $b_9 = -0.012$	$b_8 = 1.1$ $b_{14} = 0.00011$

4.3 Dipole Magnets

An end view of the dipole magnet is shown in Fig. II.4.3-1, with dimensions including those of the pole-edge shims. These magnets have 1.5-mm-thick core laminations. The height of the gap between the shims is sufficient to allow the vacuum chamber to be installed from the outside radius. The required vertical gap height is 60 mm, which provides 40 mm for the beam clear space inside the vacuum chamber and on the top and bottom 7 mm for vacuum chamber wall thickness, 1 mm for thermal insulation, and 2 mm for clearance. The thickness of the yoke is sufficient to keep the vertical deflections of the poles to less than 0.025 mm.

The axis of the dipole gap is curved with a radius of 38.96 m, which minimizes the pole width required. The laminations and end plates are assembled as a parallel-ended stack against a curved reference surface along the outside radius (open) side. After stacking, the core is axially compressed, and 12.5-mm-thick steel plates are welded under tension to the end plates and laminations on the top and bottom surfaces. A 9.5-mm-thick steel plate is then drawn up against the inside radius surface of the assembly and welded between the top and bottom plates. These plates form a structure of sufficient strength to limit vertical deflections along the length of the assembly to less than 0.025 mm.

The relative field intensity for the geometry shown has been calculated to be

$$|\Delta B/B_0| \quad \leq 1.5\times10^{-4}$$

within an elliptical aperture of x = ±30 mm, y = ±20 mm. Figure II.4.3-2a shows $\Delta B/B_0$ in the beam aperture. In Fig. II.4.3-2b $\Delta B/B_0$ is plotted along the radial direction within the beam aperture. The leading multipole coefficients are listed in Table II.4.2-1. The normal and skew harmonic coefficients corresponding to random errors due to anticipated manufacturing variations in the coil or conductor placements and pole deflections are much less than these leading terms.

4.4 Quadrupole Magnets

An end view of a quadrupole is shown in Fig. II.4.4-1 with dimensions including those of the pole-edge shims. All quadrupoles in the storage ring have the same design with tapered poles except that there are three different lengths provided: 0.8 m, 0.6 m, and 0.5 m. These magnets are made with 1.5-mm-thick core laminations. The bore diameter is 80 mm, which provides a minimum of 2 mm of clearance between each pole and the vacuum chamber. The vacuum chamber, which contains 2 mm of thermal insulation on the exterior surfaces, is shown in the drawing for reference. Also shown are the photon beam extraction channel and the antechamber, which give the most restrictive requirements on the magnet-joining hardware.

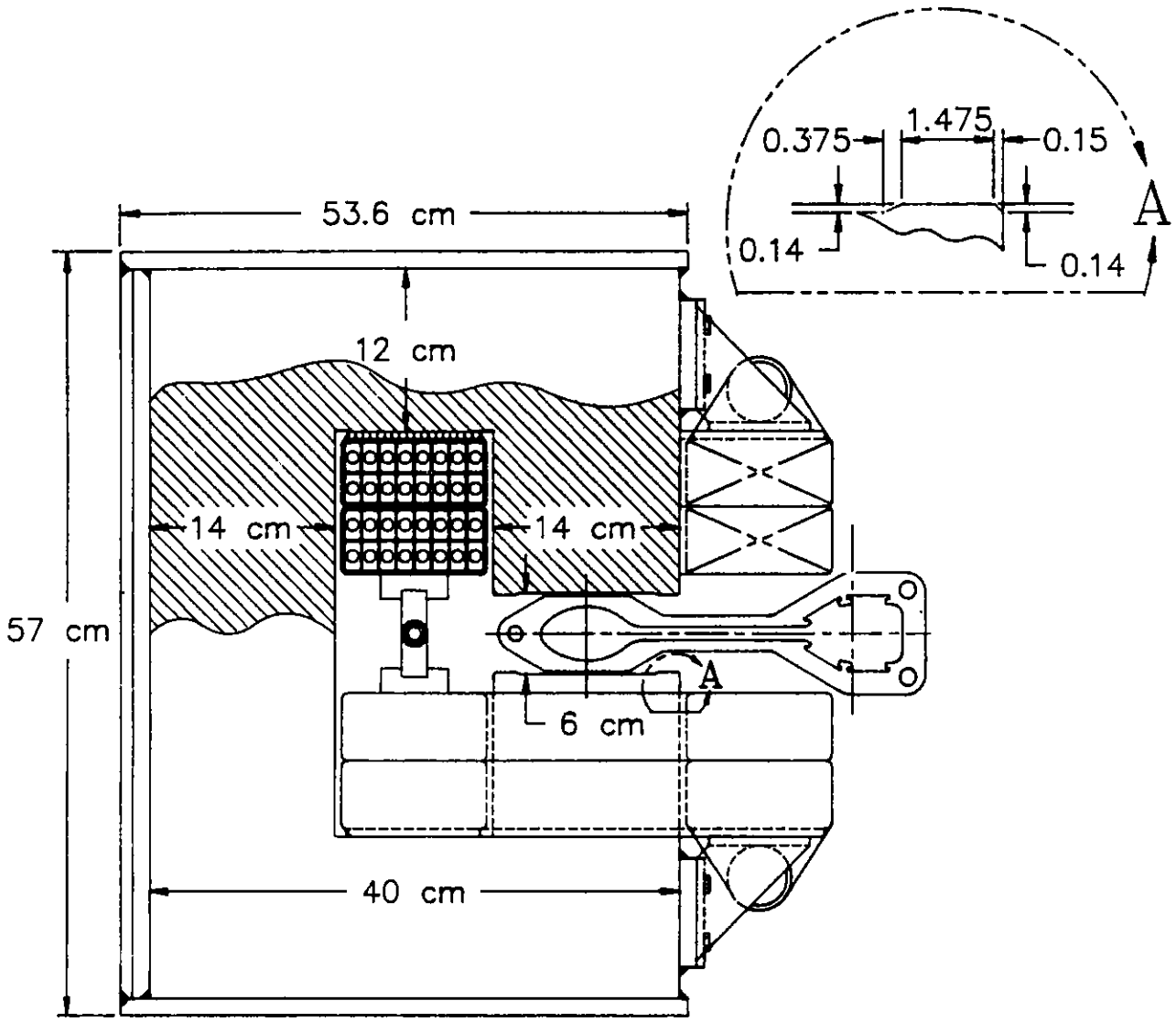

Figure II.4.3-1
End view of the storage ring dipole magnet.

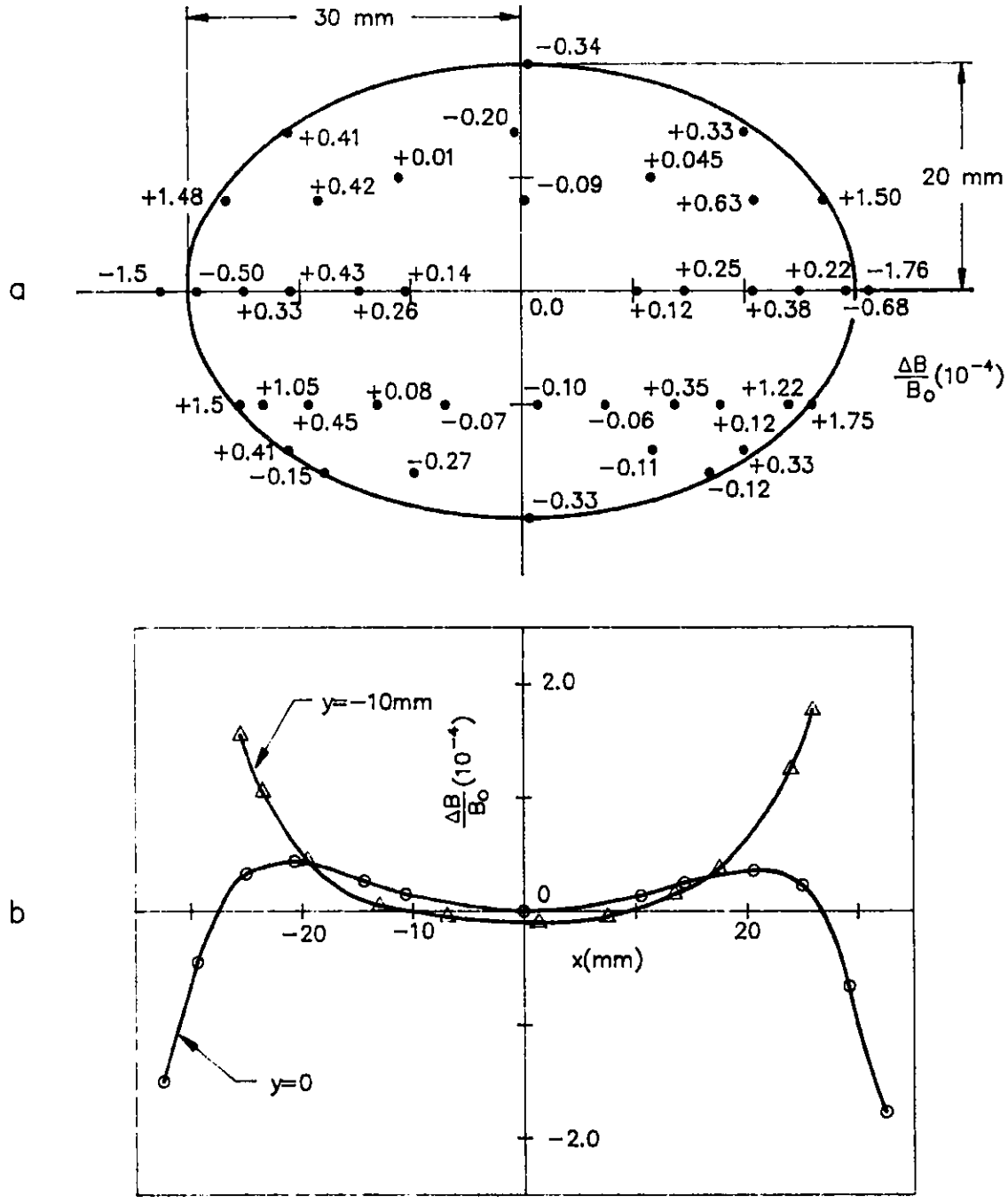

Figure II.4.3-2
The computed field deviation $\Delta B/B_0$ (10^{-4}) of the dipole magnet.

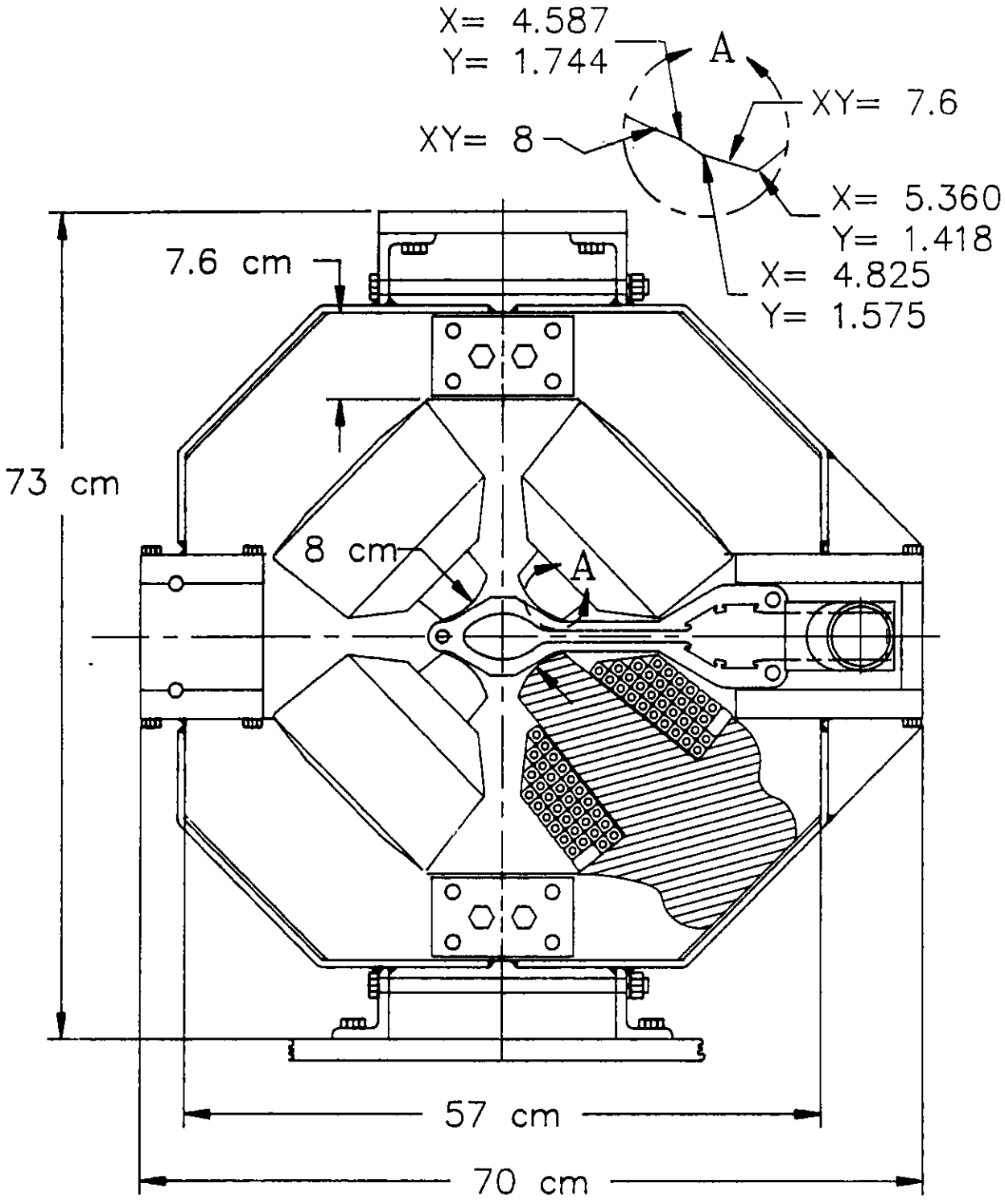

Figure II.4.4-1
End view of the storage ring quadrupole magnets.

The cores of these quadrupoles contain four separate sections, which permits installation of the coils around each pole. The two sections that make up the top and bottom halves, however, are simultaneously assembled as a pair using a fixture containing precision reference surfaces. This fixture supplies a means of securely holding the laminations against the reference surfaces while the stack is compressed and the dowel pins, tie rods, and bars are attached. The required welds in the assembly are applied at this stage.

The top and bottom halves are joined through stainless steel parts that extend across the midplane. On the inside radius side, these parts are solid blocks that are reproducibly located with hardened dowels between bolted flanges welded to the laminations and end plates. On the opposite side, these parts are cylindrical spacers secured between the bolted flanges. These spacers are positioned, for any specific magnet, at several locations along the length and at radii compatible with the vacuum chamber and photon beam channel that must pass through it.

The relative field gradient for the pole-tip-shim geometry shown in Fig. II.4.4-1 has been calculated to be

$$|\Delta G/G_o| \leq 3.0\times10^{-4}$$

inside a radius of 25 mm. The leading multipole coefficients are listed in Table II.4.2-1. The effects of moving all coils 2 mm away from the pole tip and of removing the conductor nearest the pole tip on all poles were determined to be much less than these leading terms.

4.5 Sextupole Magnets

All the sextupoles in the storage ring have the same design with tapered poles. An end view of a sextupole is shown in Fig. II.4.5-1, with dimensions including those for the pole tip. The vacuum chamber is also shown for reference. The bore diameter is 100 mm, which provides clearance between the neck of the vacuum chamber and the two adjacent poles. The outside radius yoke is located to give 2-mm clearance with the antechamber, including 2 mm of thermal insulation. Also shown in the figure is the photon beam vacuum chamber, which approaches the outside edge of the yoke most closely. Because of this chamber, all sextupole magnets have a small relief machined into the outside surface of the yoke, which gives a minimum clearance of about 2 mm with the chamber. For this magnet, the yokes extend across the horizontal midplane. The outside radius yoke, however, is thicker to provide the same reluctance for the flux that passes through it as that for the other five thinner and shorter yokes. This provides the required magnetic symmetry and greatly simplifies the assembly. The core laminations are 0.5 mm thick and allow the magnet to respond to frequencies up to 25 Hz.

To permit the coils to be installed around the poles, the center pole and coil in both the top and bottom halves are inserted as a separate unit. The type of joint

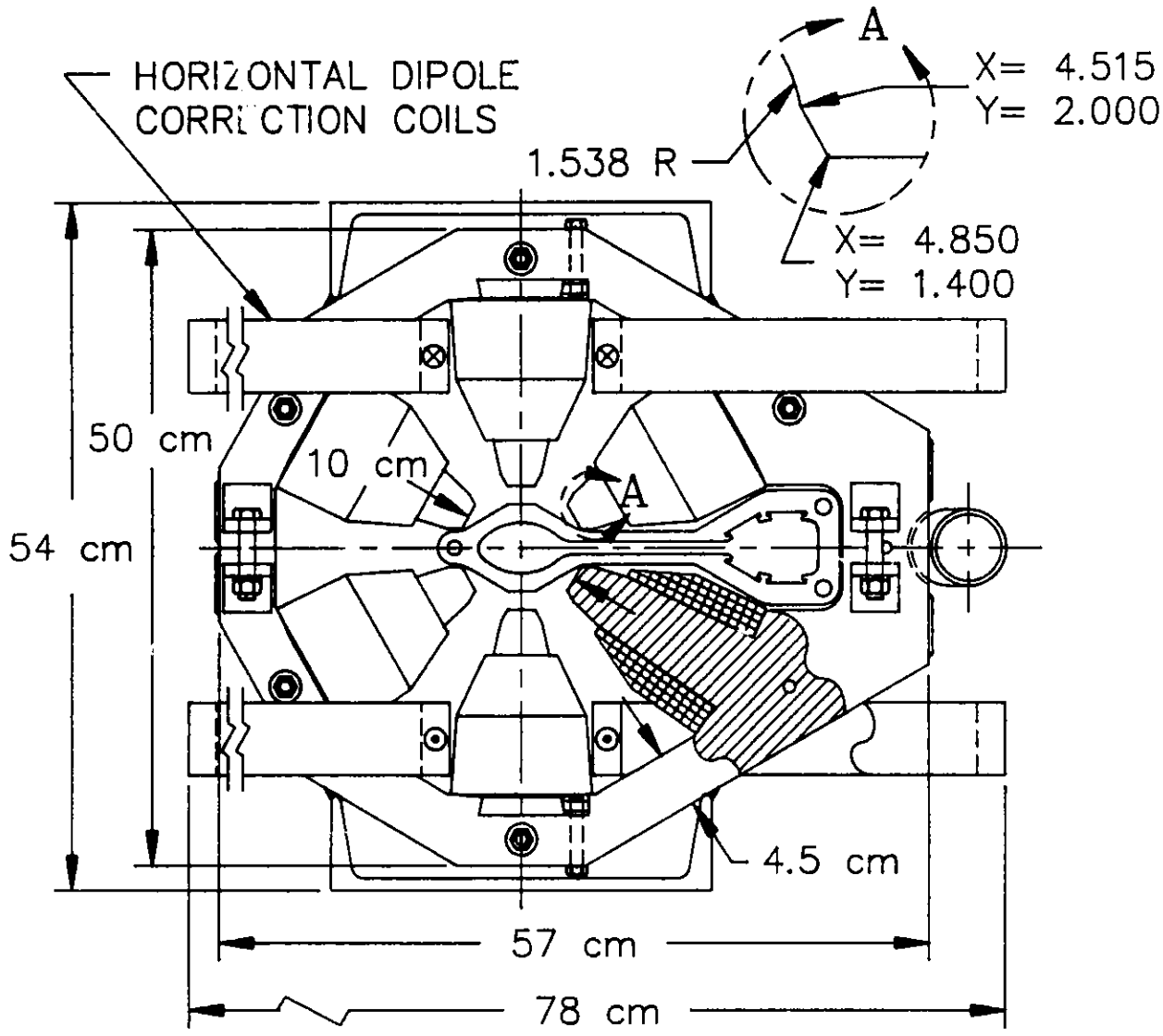

Figure II.4.5-1
End view of the storage ring sextupole magnet.

between the center pole tips and yokes is a modified dovetail. Assembly of the laminations, end plates, and ties for each half of this magnet is done with fixtures similar to those described above for the quadrupoles. The coils are placed over the side poles, and the center pole assembly, complete with its coil, is axially moved into position and held in place with the wedge shown.

The relative field second-derivative for the geometry shown has been calculated to be

$$|\Delta K/K_o| \leq 1.5\times10^{-3}$$

inside a radius of 25 mm. The leading multipole coefficients are listed in Table II.4.2-1.

In addition to the sextupole coils, these magnets contain four coils to produce a horizontal dipole field of magnitude ≤ 0.11 T (± 0.032 T·m) for vertical closed-orbit corrections. Superimposing this dipole field on the sextupole field in the magnet pole iron (hysteresis) causes negligible field errors in the 10-cm magnet aperture. The field at the pole tip, ≤ 0.71 T, is composed of a sextupole contribution ≤ 0.6 T and a dipole contribution ≤ 0.11 T.

4.6 Correction Magnets

Vertical fields for horizontal corrections are provided by auxiliary coils in the main dipole magnets and by separate small magnets. Horizontal fields for vertical corrections are provided by auxiliary coils in the sextupole magnets. In addition, dual-function correction magnets are provided where the vacuum chamber is elliptical. The parameters for these coils and magnets are summarized in Table II.4.6-1 for operation at peak rated currents. The field quality is given at ±20 mm from the magnet axis.

The auxiliary coils in the main dipoles are assembled with the adjacent main coil section before potting. The auxiliary coils in the sextupoles are installed after each half-magnet is assembled.

Small adjustments in the correction fields, except those in the main dipoles, are made at rates of up to 25 Hz with feedback loops. This requires 0.5-mm-thick core laminations for all correction magnets.

The horizontal correction magnet is shown in Fig. II.4.6-1. It has an overall length of 0.14 m. A C-core magnet is used to facilitate placement over the vacuum chamber. The coils are made with hollow copper conductor and insulated with fiberglass and vacuum impregnated with epoxy resin.

The vertical/horizontal correction magnet shown in Fig. II.4.6-2 produces both horizontal and vertical dipole fields with all coils wrapped around the picture-frame yokes. To give about the same field quality for both fields, all coil ends are beveled.

Table II.4.6-1

Parameters of the Correction Dipole Magnets

	Main Dipole Trim Coils	Sextupole Dipole Coils	Horizontal Correction Magnet	Horiz/Vert Correction Magnet
Dipole Field	V	H	V	V/H
Number Required	80	280	240	78
Peak Field at 7.0 GeV (T)	0.04	0.10	0.22	0.14
$\lvert\Delta B/B\rvert$ (%)	0.01	3	0.2	3/2
Physical Length (m)	3.23	0.32	0.14	0.14
Effective Length (m)	3.06	0.28	0.14	0.20
Gap Height (mm)	60	100	80	11.4/13.4
Conductor Height	5.0	5.0	4.3	4.1
Conductor Width	5.0	5.0	4.3	4.1
Conductor Hole Diameter	2.8	2.8	2.4	2.3
Turns/Pole	18	80	84	108/150
Inductance (mH)	16	9	12	3/4
Resistance (mΩ)	243	187	127	95/133
Time Constant (ms)	66	48	94	32/30
Peak Current (A)	49	103	81	122/105
Voltage (dc) (V)	11.9	19.3	10.3	11.6/14.0
Water Flow (gal/min)	0.2	0.6	0.2	0.2
Water Pressure (psi) Drop	100	100	100	100
Water Temp. (°C) Rise	14	15	17	25/32

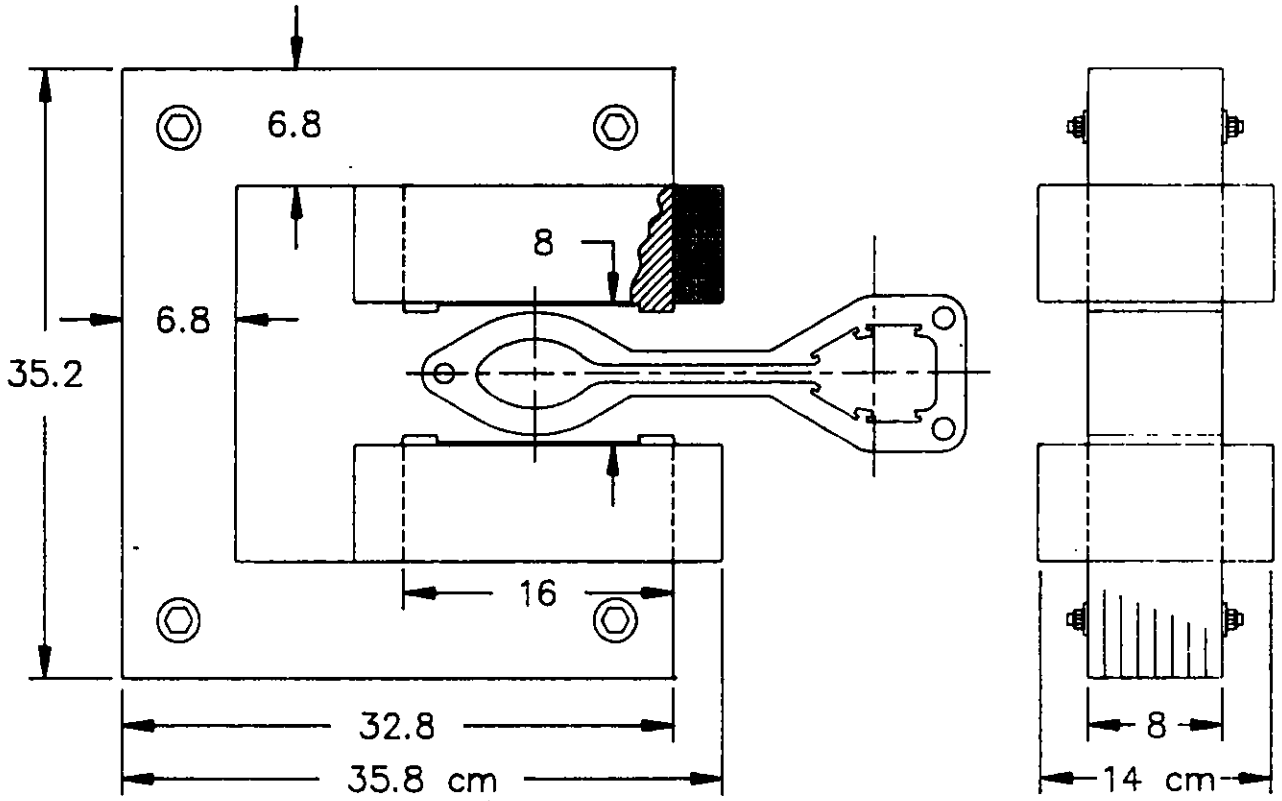

Figure II.4.6-1
Vertical field magnet for horizontal corrections.

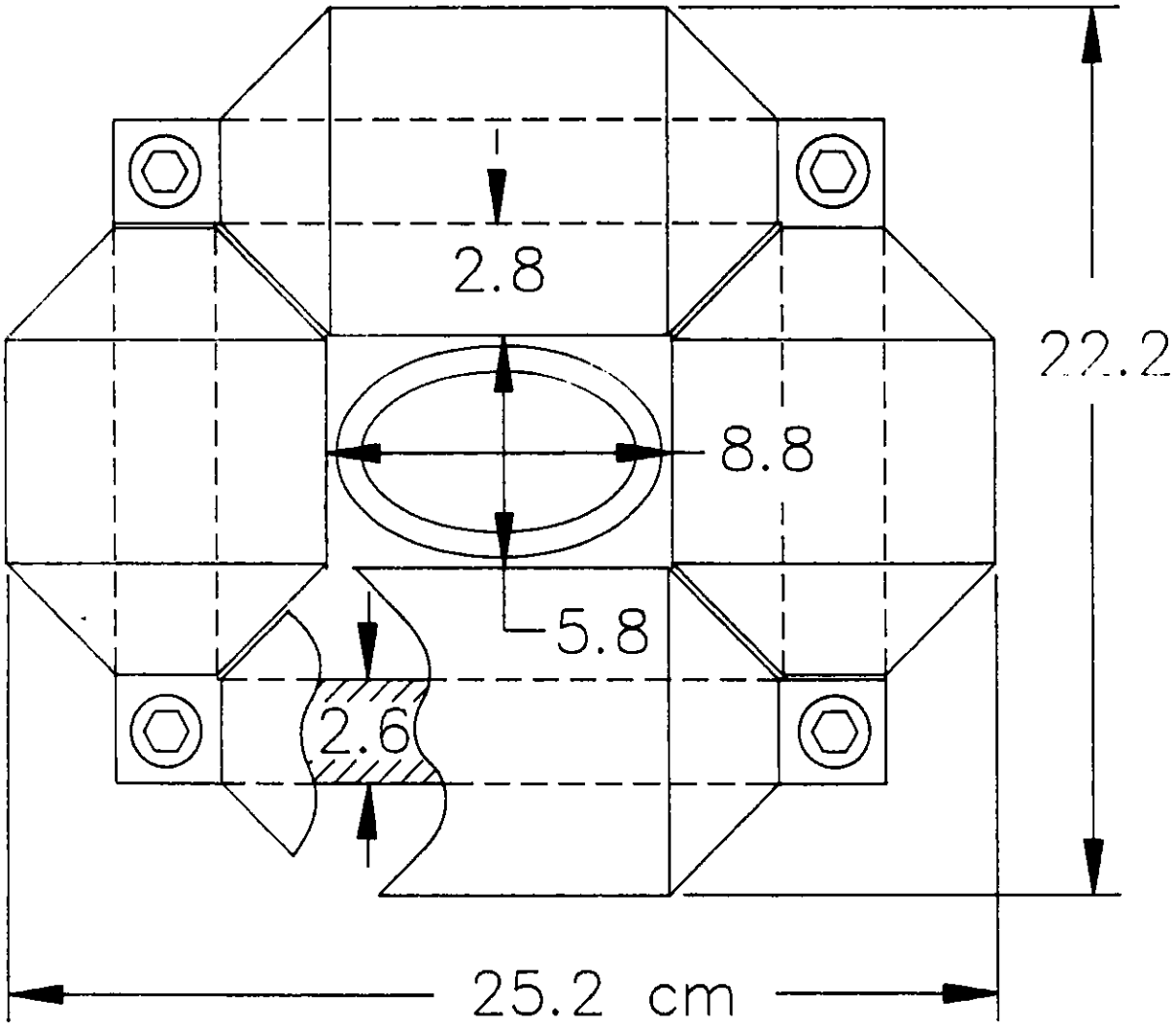

Figure II.4.6-2
Vertical/horizontal correction magnet.

This design is compatible with the elliptical vacuum chamber section at the associated locations in the ring.

4.7 Injection Magnets

4.7.1 Septum Magnets

The septum magnets used for injection into the storage ring consist of a pulsed magnet and two dc magnets. The parameters for these are listed in Table II.4.7-1. The pulsed septum magnet is shown in Fig. II.4.7-1. This magnet is a transformer type with a single-turn secondary winding and a three-turn primary winding. The minimum total thickness of the septum is 2 mm, but it gradually thickens along its length to provide improved mechanical and thermal characteristics. The design of this magnet is similar to the pulsed septum magnet[3] used to extract beam from the IPNS rapid-cycling

Table II.4.7-1

Parameters for Storage Ring Injection Septum Magnets

Type		DC Thick	DC Thin	Pulsed
Minimum Septum Thickness	(mm)	30	14	2
Field at 7 GeV	(T)	1.14	1.14	0.8
Physical Length	(m)	1.25	1.15	0.85
Effective Length	(m)	1.2	1.1	0.8
Gap Height	(mm)	30	25	20
Gap Width	(mm)	40	40	40
Number of Turns		36	12	3
Total Inductance	(mH)	5.2	0.6	0.02
Total Resistance	(mΩ)	98	19	5.4
Peak Supply Current	(A)	740	1860	4286
Peak Power	(kW)	54	66	245
Power	(kW)	54	66	0.28

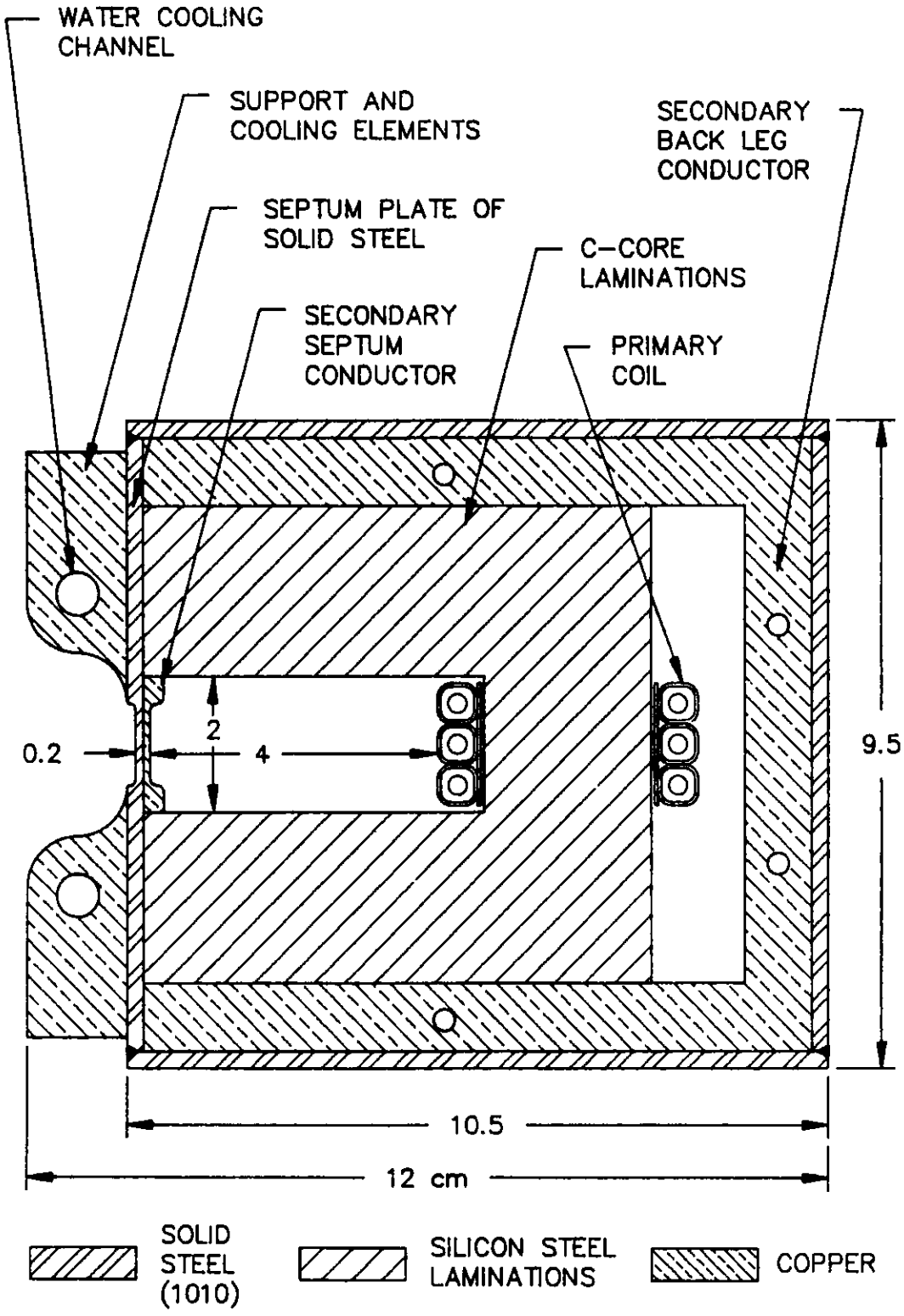

Figure II.4.7-1
Cross section of pulsed septum magnet used for injection into the storage ring.

synchrotron at Argonne. The core is made with 0.15-mm-thick silicon steel laminations that are excited with 1.5-kHz, half-sine-wave pulses at 60 pps for eight pulses every second during the accelerating period of the injector synchrotron. Two dc magnets with different septum widths are used to reduce power consumption. The magnet with the thinner septum is shown in Fig. II.4.7-2. The dc septum magnets have straight axes and multiturn coils made from hollow copper conductor and insulated with fiberglass and vacuum impregnated with epoxy resin.

4.7.2 Storage Ring Injection Bumper

During the injection of each beam bunch from the synchrotron, the circulating beam is moved to a position close to the septum magnet through which the next bunch is injected. This is accomplished by a local orbit bump generated by a set of four bumper magnets. Each magnet has an effective length of 0.4 m, with a peak field of 0.46 T for the B1-type and 0.52 T for the B2-type as shown in Figure II.1.10-1. The system produces eight pulses every second at a 60-Hz rate. A cross section of the bumper magnet is shown in Fig. II.4.7-3. The bumper magnet core is made with 18 C-cores wound from 0.0254-mm-thick, 4-cm-wide grain-oriented silicon steel tape. To assure parallelism of the pole faces and dimensional stability of the air gap, the tape-wound C-cores are machined from uncut cores. The one-turn coil is made from two straight halves, each comprised of a copper conductor 3 mm (W) × 47 mm (H) × 46 cm (L) insulated with mica-tape. After vacuum impregnation, the coil insulation is coated with conducting paint to define the ground plane. This prevents corona formation on the edges of the grounded core laminations. With apertures of 4.54 cm × 6.7 cm and 4.00 cm × 6.7 cm, the 36-cm-long bumper magnets, B1 and B2, have inductances of 0.76 μH and 0.82 μH, respectively. Its ceramic vacuum chamber is aluminized on the inside surface to a thickness of ~10 μm to minimize its impedance to the beam.

4.8 Abort Magnets

The beam abort system includes two fast kicker magnets and a Lambertson septum magnet. Except for initial turn-on, when only a few mA of current are required, the system must be fully operational whenever beam is circulating in the storage ring. To assure this, the pulse-forming network (PFN) for the fast kicker is fully charged. The septum magnet uses permanent magnet material to generate the field and is always ready for use.

4.8.1 Kicker Magnets

Two fast kicker magnets, each 0.55 m long and separated by 18 m, are required. The cross section of each is identical with the injection kicker in Sec. II.10.4.4. The field is 0.0485 T in the gap region (57.5 mm wide and 40.0 mm height), its rise time is 56 ns, the flat-top 4 μs and the fall time 95 ns. The magnet has an inductance of 555 nH per coil.

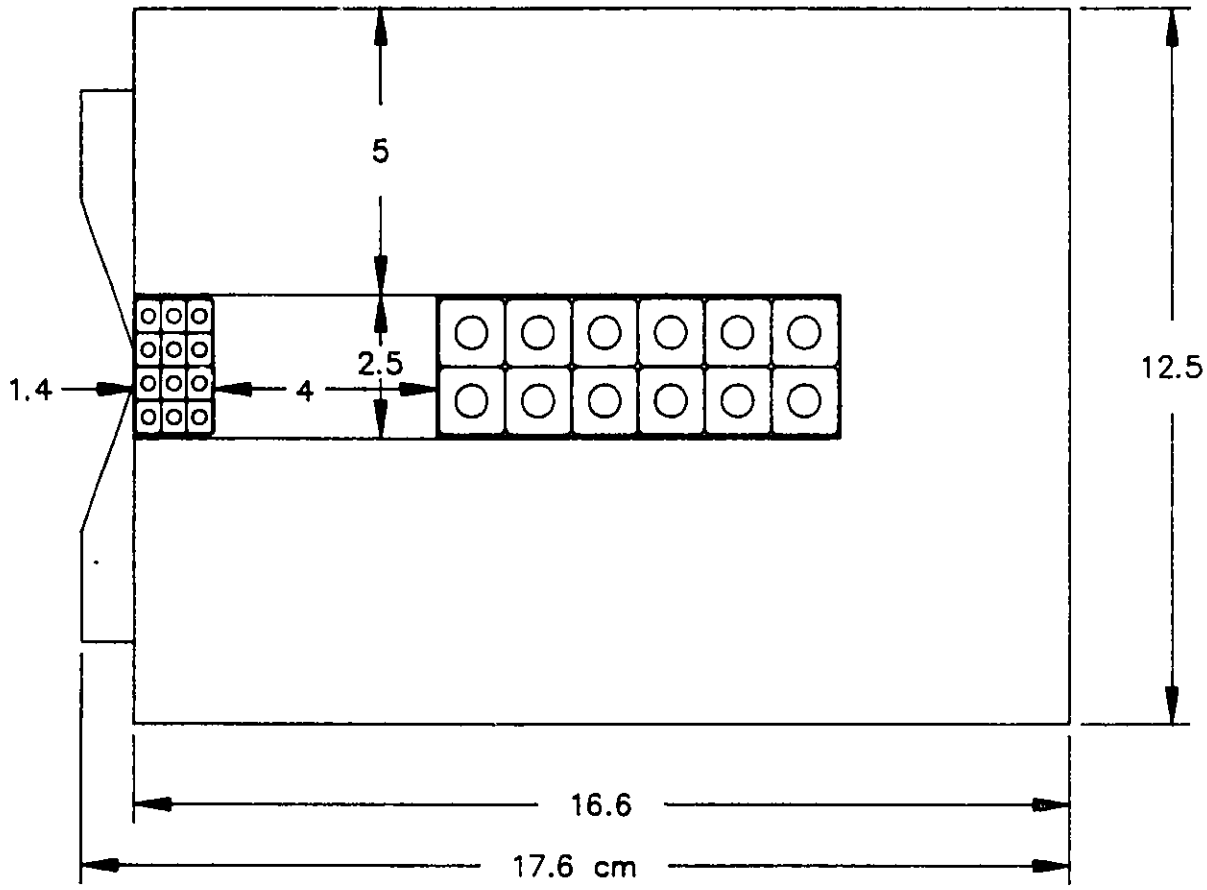

Figure II.4.7-2
Cross section of thin dc septum magnet used for injection into storage ring.

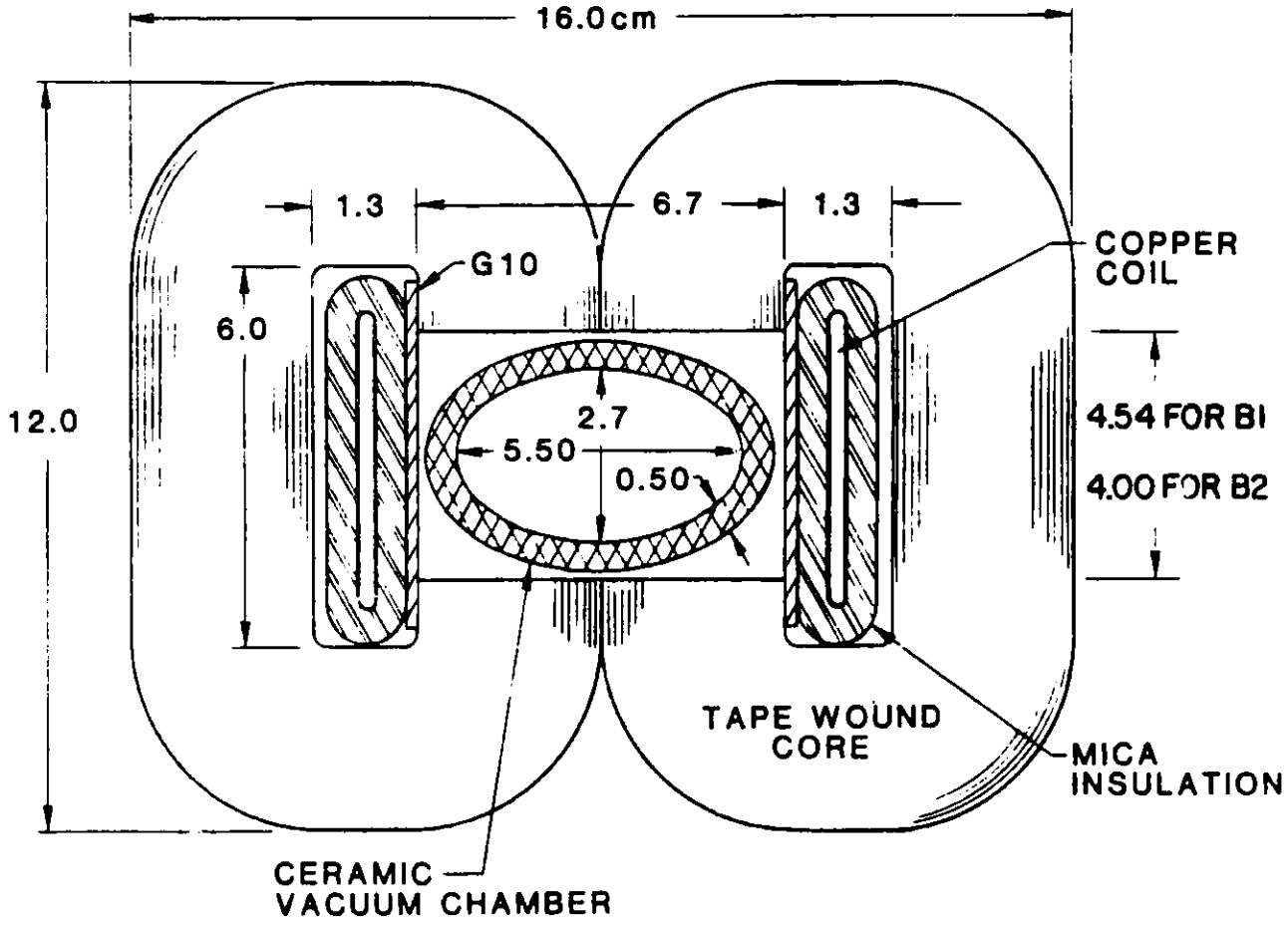

Figure II.4.7-3
Cross section of injection bumper magnet.

4.8.2 Abort Lambertson Septum Magnet

The thin septum magnet, shown in Fig. II.4.8-1, uses Nd-Fe-B permanent magnet blocks to generate the gap field. The field is 0.7 T in the gap region (20 mm wide and 30 mm high), and the minimum thickness of the septum is 2 mm. The effective length of the magnet is 3 m. In order to minimize the magnet dimensions, the gap axis is curved to follow the aborted beam trajectory.

4.9 Magnet-Measuring Facility

Before installation, the magnetic field produced by each magnet is measured over the specified ranges to ensure that the requirements of the field quality are met and to determine the location of the magnetic axes for later alignment. The performance of each magnet is also measured and analyzed with and without the nearest adjacent magnets in the storage ring lattice. The magnet data will be stored for future reference for each magnet during the lifetime of the machine.

The magnet-measuring facility (MMF) is established to provide the required magnet measurements with sufficient accuracy and precision to determine that the fields have the required qualities specified in Sec. II.4.2. Three major and two minor magnet-measuring systems are provided: one major system for dipole magnets and insertion devices, one major one for quadrupole magnets, and one major one for sextupole magnets and two minor systems for correction and all other special magnets. The probes for these measuring stands are search-coil arrays and Hall probes. In addition, an NMR magnetometer system is included in the MMF to provide a calibration standard for the measuring stands. The measurement methods necessary for this MMF have been successfully implemented in existing facilities at Argonne and other laboratories.[4-6]

The measuring stands are semiautomatic systems, in which a computer system reads all switch settings, magnet-exciting currents, probe positions, data values, and their analyses. Before a magnet is removed from the test stand, the results are reviewed to validate the measurements.

4.9.1 Dipoles

The storage ring and synchrotron dipole magnets have positron beam bending angles of 4.5° and 5.3° per dipole, respectively. Because of the bending angles, a pair of planar search coils, instead of a rotating-type search coil, is used for the measurement of the field quality along the beam orbit. One planar coil is used for the vertical and another for the horizontal field components. The planar coils, which are longer than the magnetic field region of the magnet, are curved to follow the beam path through the regions. These coils are moved longitudinally and laterally by a probe-positioning manipulator. The measurements determine the effective lengths of the dipoles and the locations of the magnetic midplanes with accuracies better than 0.1 mm. The multipole coefficients are deduced from sufficient sets of measurements.

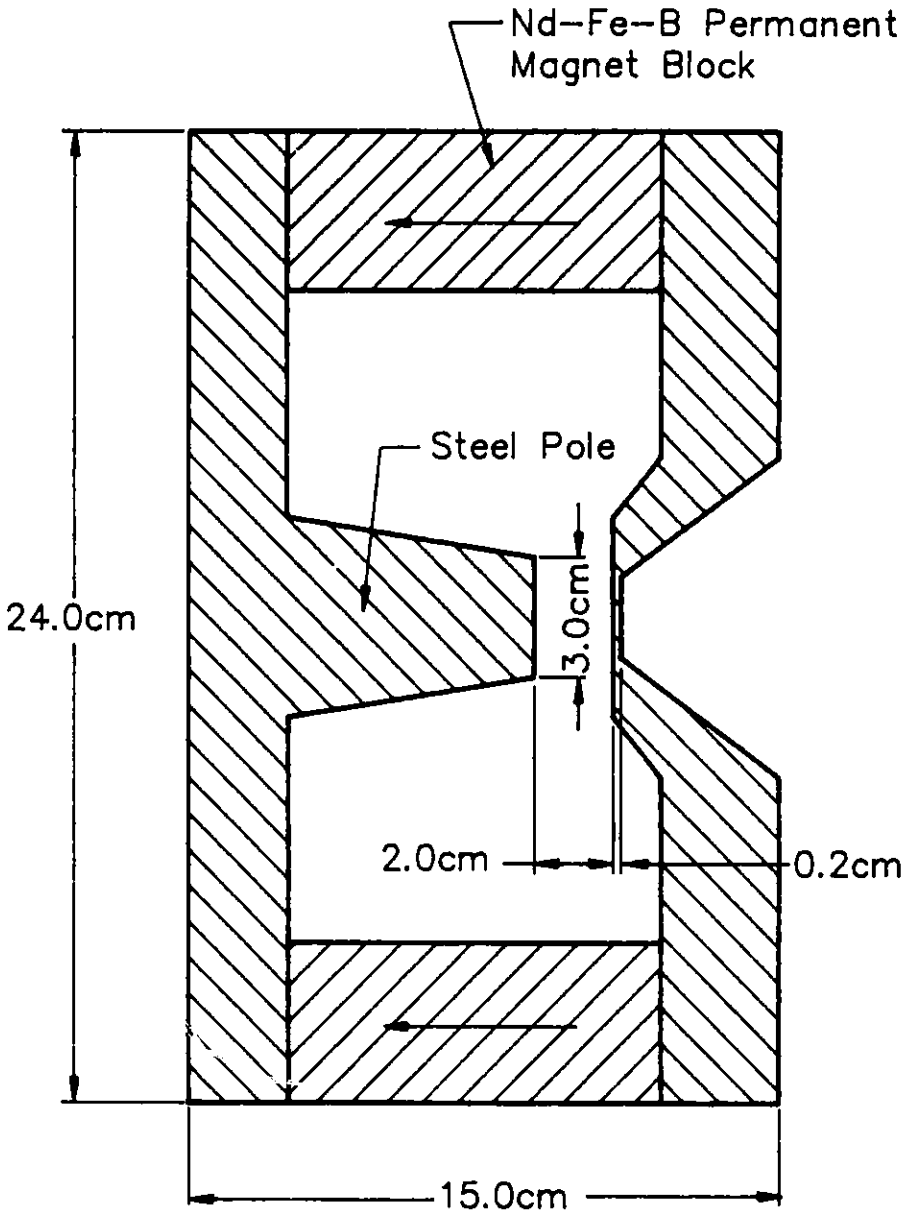

Figure II.4.8-1
Lambertson permanent type septum magnet.

In addition to the integral field measurements of transverse $\Delta B/B_o$ and harmonic coefficients, local field measurements are used to evaluate possible local imperfections in the magnets.

4.9.2 Quadrupoles and Sextupoles

These magnets are straight and relatively short compared to the dipole magnets. Rotating coils of tangential or radial windings measure the field qualities in relatively short times with sufficient accuracy. The coil is rotated at a constant angular velocity. An optical angular encoder attached to the axis of the rotating coil provides triggers to digitize the induced voltage of the coil device. The values of the induced voltage vs. angle are Fourier analyzed to give the harmonic coefficients of the field.

The two-dimensional field can be described in terms of a multipole expansion in Cartesian coordinates

$$B_y + iB_x = B_o \sum_{n=0}^{\infty} (b_n + ia_n)(x + iy)^n \quad ,$$

where b_n and a_n are called the normal and skew multipole coefficients, respectively. The flux linkages of the vertical and horizontal planar coils are related to the above equation to obtain the multipole coefficients.

The flux linkages of the rotating coil probes are related to

$$\vec{B}(r,\theta) = \sum_{n=1}^{\infty} C_n \left(\frac{r}{R}\right)^{n-1} \left[\vec{I}_r \sin n(\theta-\alpha_n) + \vec{I}_\theta \cos n(\theta-\alpha_n)\right] \quad ,$$

where C_n is the magnitude of the $(2n)^{th}$ multipole field at a reference radius R, α_n is the angular orientation of the corresponding multipole, $\vec{I}_r$ is the unit vector in the r direction, and $\vec{I}_\theta$ is the unit vector in the θ direction. Typically, R is the radius of the rotating coil.

The multipole coefficients b_n and a_n are related to C_n by

$$b_n = \frac{C_n}{B_o R^n} \cos(n+1)\alpha_{n+1}$$

and

$$a_n = \frac{-C_n}{B_o R^n} \sin(n+1)\alpha_{n+1} \quad .$$

4.9.3 Insertion Devices

The MMF also measures the magnetic properties of insertion devices. Field measuring probes are mounted on a granite test bed which is flat to better than 0.03 mm over the ID length. The measuring system provides a complete on-axis field profile including field errors. In addition, a single magnetic pole test apparatus measures the three dimensional field profile of any given magnet configuration that is used for the final design of an ID.

4.10 Magnet Supports

4.10.1 Storage Ring Dipole Support

The storage ring dipole, a correction dipole, and two sextupoles are mounted on a common rigid girder about 5 m long as shown in Fig. II.4.10-1. This girder has adequate transverse and torsional stiffness to satisfy deflection and vibration requirements. Three five-ton jacks are mounted on top of a stand that is grouted and bolted to the floor. Between the jack stems and the girder is hardware to provide adjustments for transverse and longitudinal position for precise alignment of the magnet system. The stand and jacks permit adjustments to 0.025 mm. The dipole, correction dipole, and sextupoles are then adjusted using their own supports on top of the girder.

4.10.2 Storage Ring Quadrupole, Sextupole, and Correction Magnet Support

The quadrupole, sextupole, and correction magnets in each dispersive straight section are mounted on a rigid girder 4.0 m long, as shown in Fig. II.4.10-2. This girder has adequate transverse and torsional stiffness to satisfy deflection and vibration requirements. The focusing and correction magnets in the insertion straight sections are similarly mounted on two common rigid girders 3.7 m long.

The individual magnets have their own adjustable supports on the rigid girders so that each magnet is aligned to the common magnetic center of the group within ± 0.1 mm in a staging area. The rigid girders, with their prealigned magnets locked in place, are transported to their positions in the ring and mounted on three vertical five-ton jacks, on stands provided with transverse and longitudinal adjustments. Survey targets on the end magnets allow alignment of the string of magnets to the beam line as a unit, thereby significantly reducing the amount of final alignment in the storage ring tunnel. The magnet supports are designed to be used to hold power bus, control cabling, magnet cooling water piping, and power supplies.

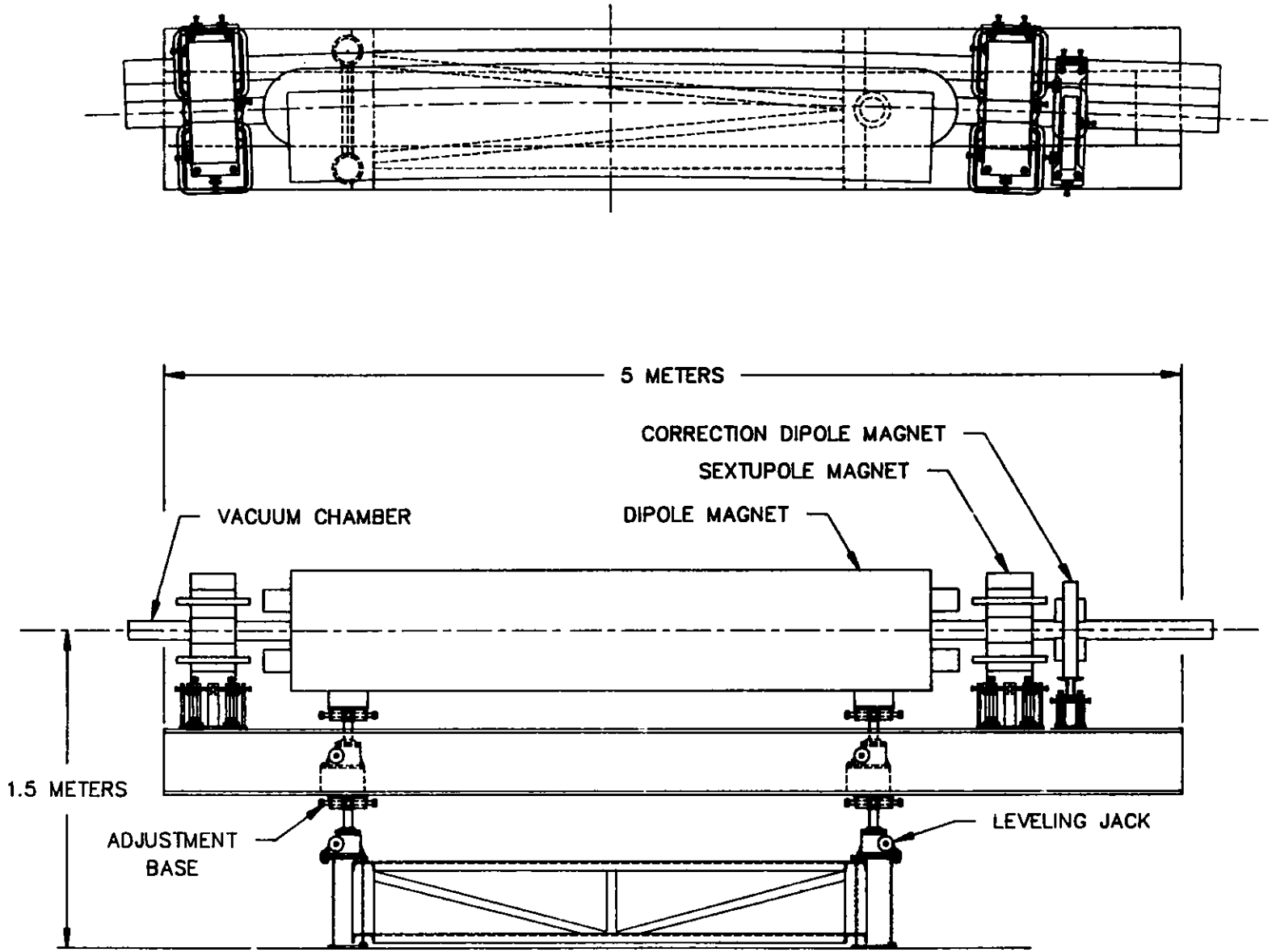

Figure II.4.10-1
Support for the storage ring dipole magnet.

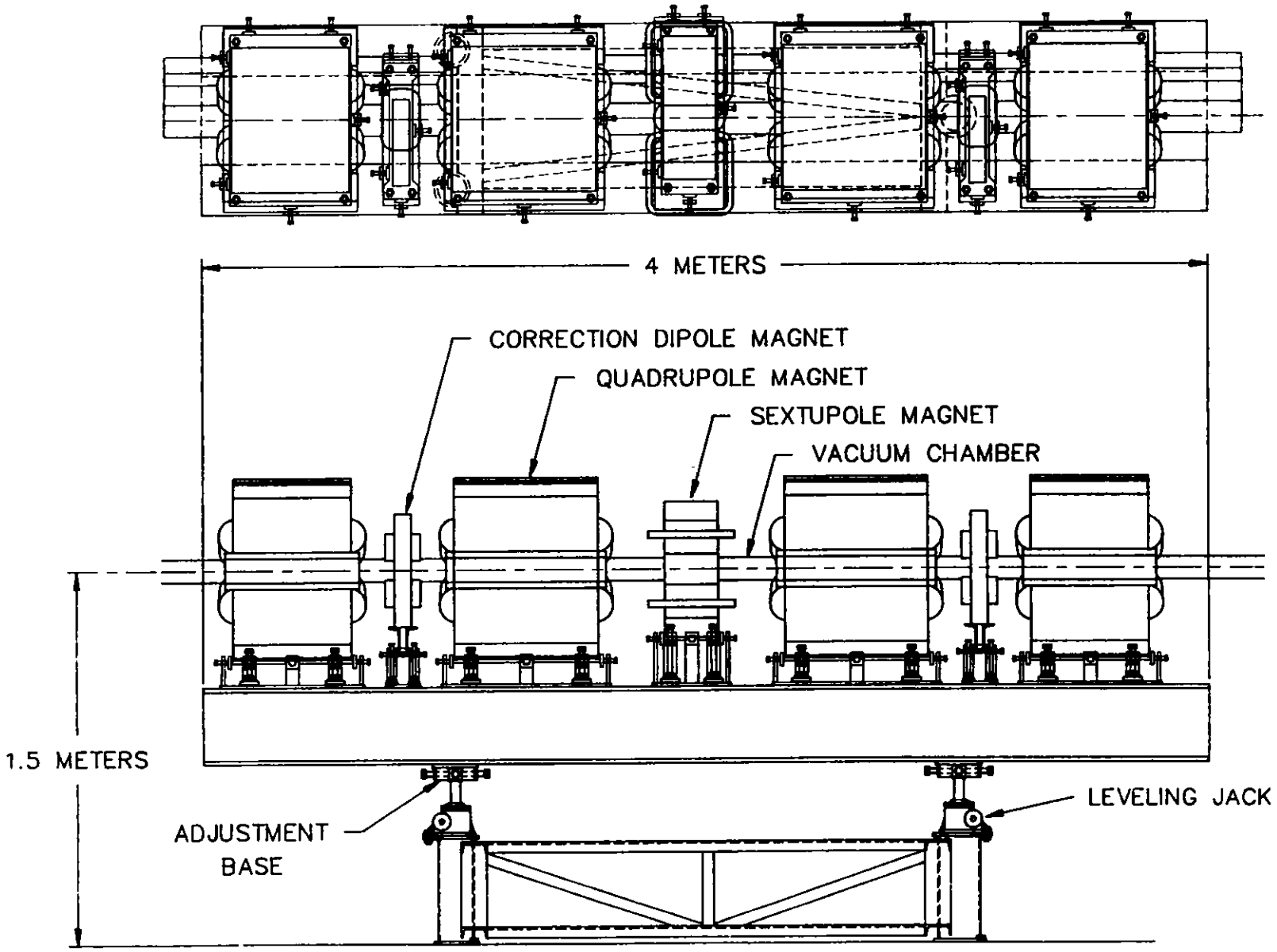

Figure II.4.10-2
Support for the storage ring quadrupoles, sextupoles, and correction dipoles.

4.11 References

1. K. Halbach, "Application of Conformal Mapping to Evaluation and Design of Magnets Containing Iron with Nonlinear B(H) Characteristics," Nucl. Instru. and Meth., 64, 278 (1968).

2. K.M. Thompson, "An Interactive Computer Program for the Design and Costing of Magnets," Proc. 8th International Conf. Magnet Technology, Grenoble, France (1983).

3. M. Foss, K. Thompson, and W. Praeg, "A Transformer Septum Magnet," IEEE Trans. Nucl. Sci., NS-26, 4024 (1979).

4. O. Pagano et al., "A Highly Automated Measuring System for the LEP Magnetic Lenses," J. de Phys., C1-949 (1983).

5. B.C. Brown et al., "Data Acquisition System Design for Production Measurements of Magnets for the Fermilab Anti-Proton Source," IEEE Trans. Nucl. Sci., NS-32, 2050 (1985).

6. K. M. Thompson, Argonne National Laboratory, unpublished information (1981).

5.1 Introduction

A stability of 30 ppm is the design goal for the main bending and focusing magnets (dipoles and quadrupoles), in order to achieve an overall stability of 100 ppm when random field and position errors of the magnets are included. For the correction magnets, the requirements are less stringent; these requirements range from 300 ppm for sextupoles and orbit trim windings in the main dipoles to 400 ppm for dipole correction magnets. All the power supplies have an upper limit of operation corresponding to 7.7 GeV.

The main bending magnets are connected in series and fed from a single 850-kW, 12-phase power supply connected to the 2.4-kV power line. For maximum flexibility in adjusting the lattice functions, all other magnets are energized from individual power supplies, as is done at the Cornell Electron Storage Ring (CESR).[1] For the multipole magnets, the power supplies are unidirectional; for the correction dipoles, they are bipolar. Table II.5.1-1 lists the power supplies, their output ratings, and other performance specifications. Figure II.5.1-1 shows a one-line drawing of the storage ring power supply system. The current stability and reproducibility include effects due to normal power-line fluctuations, load variations, component drifts, and temperature coefficients over the range from 10° to 40°C. The aluminum vacuum chamber of the storage ring, described in Section II.6, is an effective low pass filter.[2] Eddy current shielding attenuates vertical ripple fields above 8 Hz by 6 dB/octave; horizontal ripple fields are attenuated above 25 Hz at the same rate. Because of this filtering effect, the ripple specifications for the magnet power supplies are much less demanding than the stability and reproducibility requirements. An 81st dipole magnet, located outside the storage ring and connected in series with the storage ring magnets, is used to monitor the field with a nuclear magnetic resonance (NMR) probe and permits feedback from the field to the power supply control circuit. There will be 20 three-phase 13.2 kV/460 V, 500 kVA, power distribution transformers spaced uniformly around the periphery of the ring, to provide ac power for the multipole and correction dipole magnets.

The magnetic field attained with a given current depends on the value of the residual field in the core and the eddy currents produced in the core laminations in reaching the given current. Precise repeatability of the residual field is especially critical for the main dipole magnets and for the quadrupole magnets. At the start of every operating period, a reproducible residual field will be attained by cycling all magnets between zero and rated current for several minutes with a fixed current pattern (e.g., an isosceles triangular shape).

Table II.5.1-1

Magnet Power Supplies for the Storage Ring

Magnet Circuit	No. of Units	Rating* I (A)	Rating* V (V)	Rating* P (kW)	ΔI/Imax Stability	ΔI/Imax Reproducibility	ΔI/Imax Current Ripple**	ΔI/Imax Tracking Error	Reference Resolution (bit)
Main Dipole	1	452	1530	692	$\pm 3\times10^{-5}$	$\pm 5\times10^{-5}$	$\pm 4\times10^{-4}$	$\pm 1\times10^{-4}$	17
Trim Dipole	81	49	± 13	0.63	$\pm 3\times10^{-4}$	$\pm 6\times10^{-4}$	$\pm 1\times10^{-2}$	$\pm 7\times10^{-4}$	13
Quad., 0.5 m	240	416	14	5.7					
Quad., 0.6 m	80	416	16	6.7	$\pm 3\times10^{-5}$	$\pm 5\times10^{-5}$	$\pm 2\times10^{-3}$	$\pm 2\times10^{-4}$	17
Quad., 0.8 m	80	416	20	8.4					
Sextupole	280	195	21	4.1	$\pm 3\times10^{-4}$	$\pm 6\times10^{-4}$	$\pm 2\times10^{-3}$	$\pm 7\times10^{-4}$	13
V-Corr.Sex.Dip.	280	103	± 21	2.2					
H-Corr. Dip.	240	81	± 11	0.9	$\pm 3\times10^{-4}$	$\pm 6\times10^{-4}$	$\pm 1\times10^{-2}$	$\pm 7\times10^{-4}$	13
H&V Corr.	78H	122	± 15	1.8					
Dipole	78V	105	± 13	1.4					

*Operating at 7 GeV.

**The aluminum vacuum chamber is an effective low-pass filter.

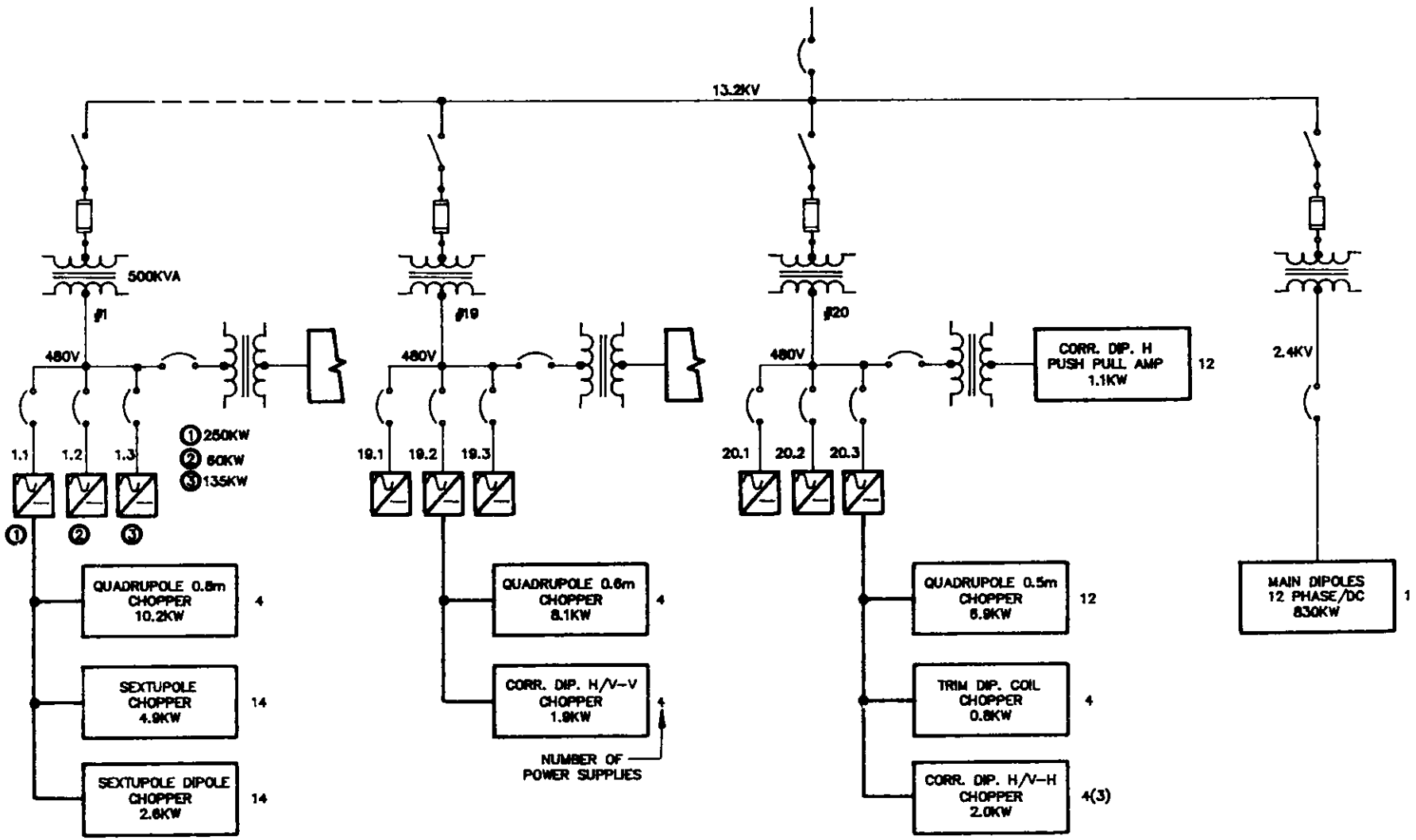

Figure II.5.1-1
One-line diagram of the storage ring magnet power supply system.

5.2 Main Dipole Power Supply

The main dipole magnets are connected in series and energized from a 12-phase dc power supply. Having only one power supply for 81 magnets reduces cost as compared to multiple feedpoints. The voltage to ground of ≤ ±765 V causes current leakage through the cooling water paths. Magnet unbalances caused by these leakage currents are compensated with the dipole trim coils. The magnet cooling water inlet temperature is regulated to be 32° C ± 1.1° C. The corresponding dimensional changes of the dipole (~12 ppm/°C) do not affect ∫Bdl; the changes in gap height are compensated by an equal change in length.

Power supplies offering a true current regulation of 10 ppm with power ratings up to 2 MW are commercially available.[3] Figure II.5.2-1 shows a typical power circuit configuration. The delta- and wye-connected secondaries of the rectifier transformer feed two series-connected silicon-controlled-rectifier (SCR) bridges. The 12-phase raw dc output is filtered by a ground-symmetrical, damped, passive LC-filter[4] to attenuate the fundamental 720-Hz ripple to levels acceptable for the range of the series regulator. A high-frequency (HF) filter to attenuate the common mode voltage ripple is placed between the passive filter and the series regulator. The series regulator consists of parallel-connected power transistors.

A block diagram of the regulator circuit is shown in Fig. II.5.2-2. A fast preregulator attenuates line disturbances before they reach the main filter. The output of the filters is controlled by the tracking regulator, which maintains an average voltage of 9-10 V across the series regulator power transistors. The series regulator controls the final output voltage in accordance with the output of the current regulator, which obtains its feedback from a high-precision current transductor (CT).[5] Communication with the ground potential regulators is via optically isolated amplifiers.

5.3 Quadrupole and Sextupole Power Supplies

A total of 680 unidirectional power supplies, having power ratings from 4.1 to 8.4 kW, are required. Two types of high-frequency, pulse-width-modulated (PWM) power supplies are being considered. The first, a dc-dc converter, uses a solid-state switch to interrupt the magnet current at frequencies above the audio range. It regulates the current by changing the ratio of the ON to OFF time of the switch. Power supplies for magnets with similar voltage ratings are energized from a common dc source, as shown in Fig. II.5.3-1a. A monotonic digital-to-analog converter (DAC) is the reference for the current regulator, which obtains its feedback from a precision CT. Fast changes in the dc bus voltage are corrected by an inner voltage loop controlled by the current loop. As illustrated in Fig. II.5.3-1b, the switch stays closed until the current reaches the value called for by the DAC. The switch then opens, and the magnet current transfers to the diode D across the magnet. The current decays through the diode with the L/R time-constant of the magnet until it falls to the value set by the DAC. This causes closure of the switch, and the above cycle repeats. Figure II.5.3-1c shows the variations of

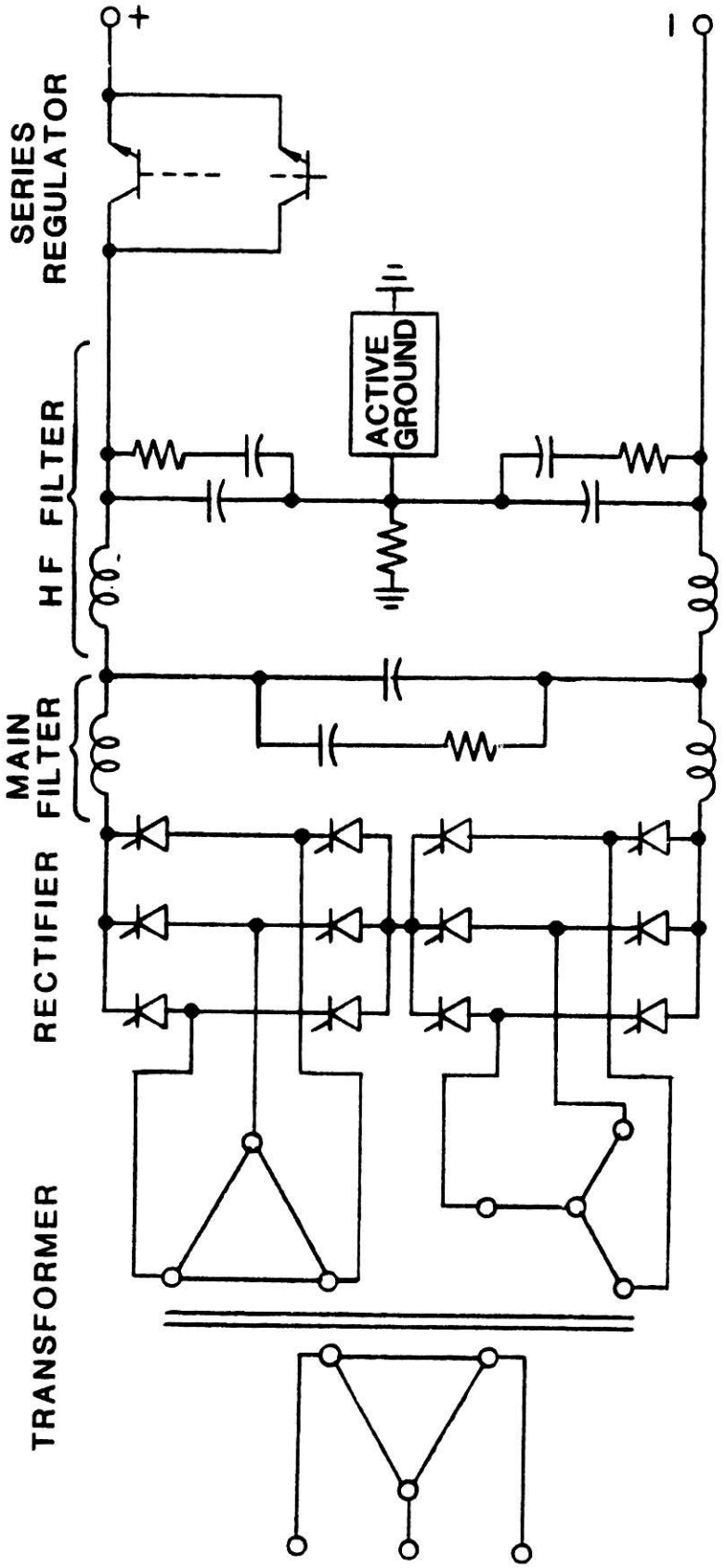

Figure II.5.2-1
Power circuit for dipole power supply.

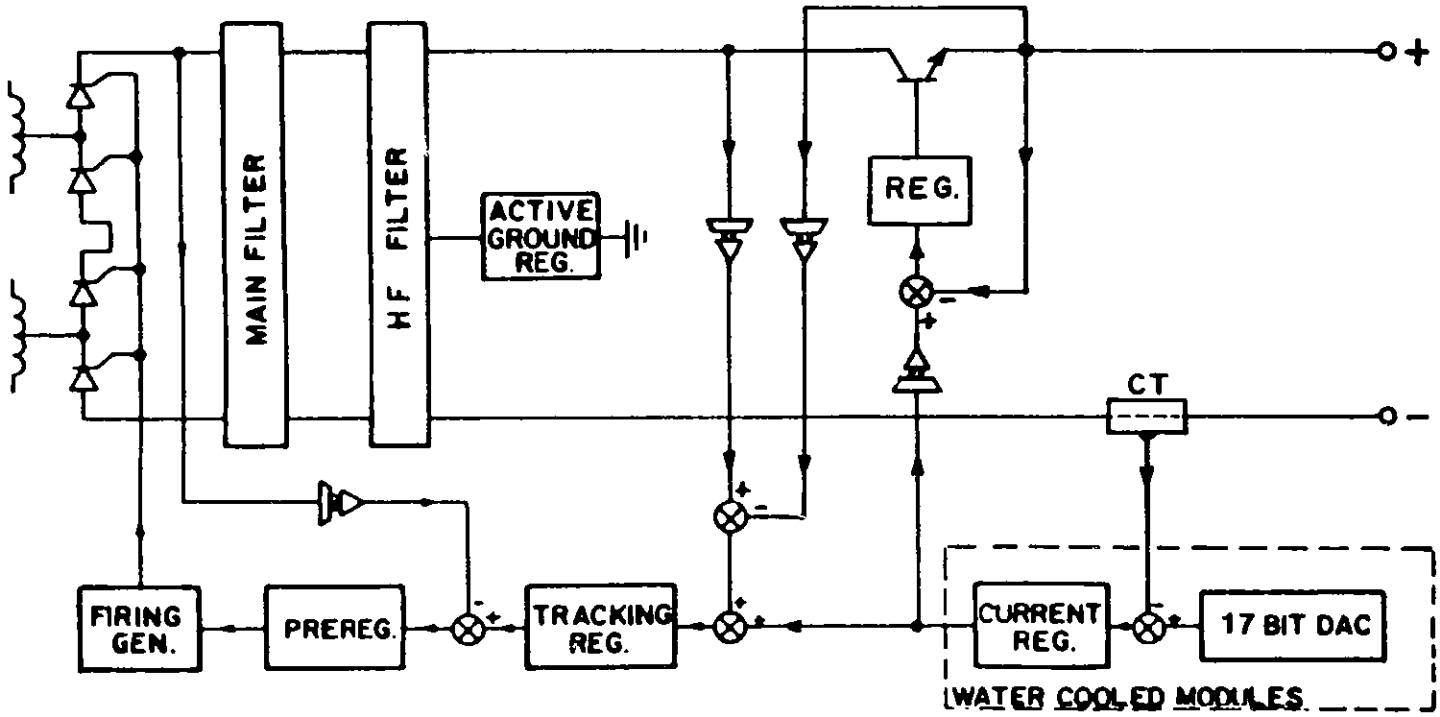

Figure II.5.2-2
Block diagram of regulator for dipole power supply.

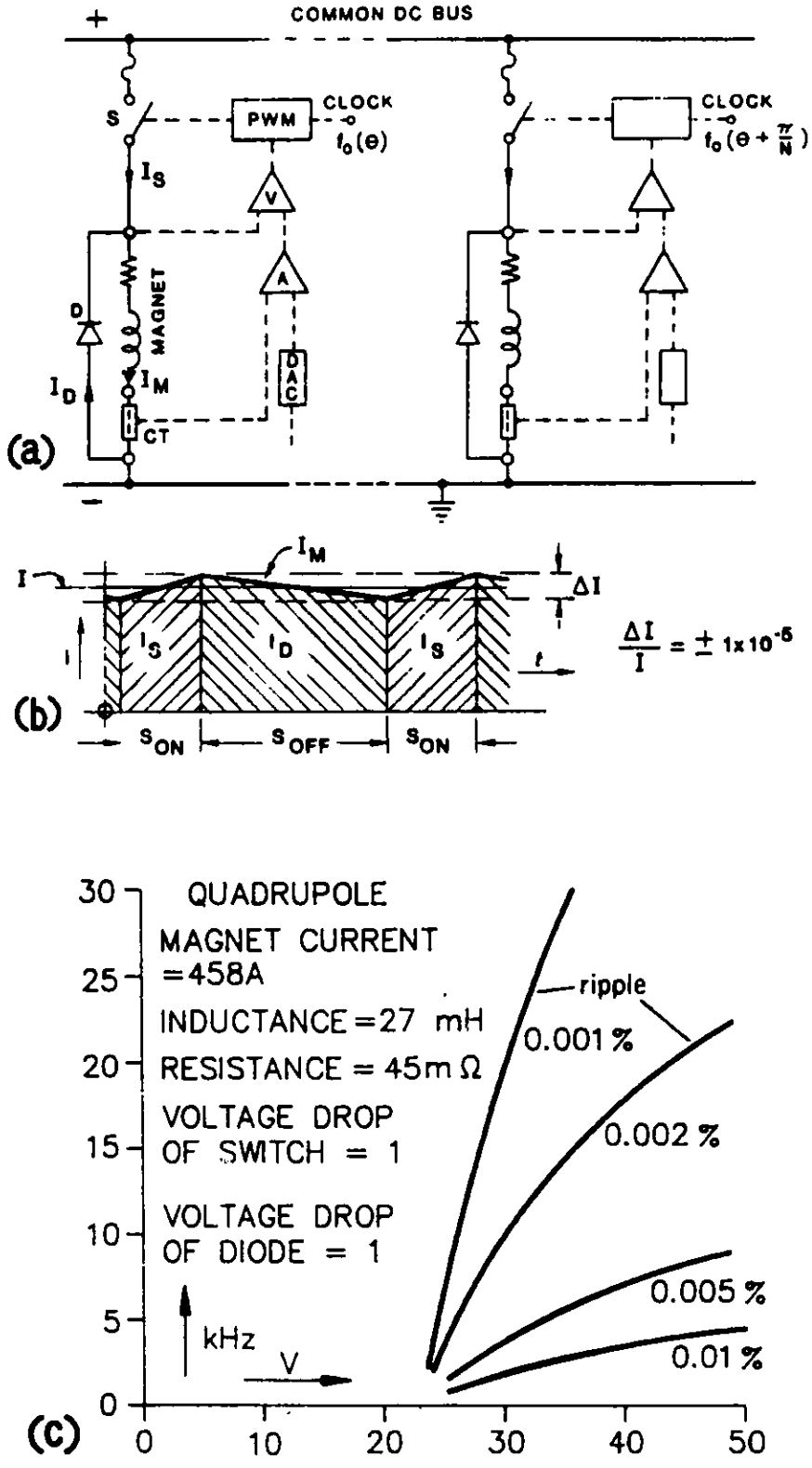

Figure II.5.3-1
Variable-duty-cycle pulse-width-modulated dc power supply.

switching frequency versus dc input voltage for various current ripple parameters.[6] At ~20 kHz, eddy currents in the vacuum chamber attenuate vertical ripple fields by 68 dB and horizontal fields by 58 dB,[2] therefore, no separate ripple filter is required. The pulse load on the line is distributed by arranging the power supplies into smaller groups and by phase-shifting the clock frequency of the PWMs of these groups. This type of system offers great versatility at a low level of complexity and cost. It is inherently capable of operating over a wide current and voltage range, utilizing transistors for low- and thyristors for high-power switches. However, the switch operates at rated magnet current, and the circuit does not permit electrical isolation of the loads.

The second type of PWM high-frequency power supply, a dc-ac-dc converter, uses series-resonant circuits; the spacing between sine waves is controlled. These circuits have the advantage that the switching element does not operate at rated magnet current. A transformer provides electrical isolation and the dc bus voltage can be higher and the switching current correspondingly lower than the magnet current and voltage. As shown in Fig. II.5.3-2, the circuits consist of half- or full-wave bridges driving the primary of an HF transformer. On the transformer secondary is a full-wave rectifier to which the magnet load is connected. Thyristors or transistors may be used as switching elements. These circuits are capable of precise control of large amounts of power over a wide range of load voltages.

For a stability of 30 ppm of full scale, each power supply control loop is placed in an oven in which the temperature is maintained within ±1.0° C. The high-gain, high-stability, low-noise input amplifier of this control loop receives an input signal that is the difference between the reference voltage (magnet current value set with a DAC) and a voltage that is proportional to the magnet current. The cost of the reference voltage and the current measuring device is a major part of the total price of the PWM power supplies. Commercially available high precision zero-flux CTs[5] measure the magnet currents and commercial DACs produce the reference voltages.

5.4 Correction Magnet Power Supplies

A total of 756 power supplies is required for correction coil excitation; they have power ratings of 0.6 kW to 2.2 kW. The need for smooth control of the current through zero requires bipolar supplies. Bipolar converter circuits are used, which operate at frequencies between 20 and 50 kHz and use, as switching elements, power transistors and diodes or reverse conducting thyristors (RCTs).

The principle of the one-quadrant converter of Fig. II.5.3-1 can be applied to two-quadrant operation, as shown in Fig. II.5.4-1. For positive magnet current, Q_1 and Q_2 are turned on. When Q_1 is turned off, the current decays through the still-turned-on Q_2 and D_1. For current control in the negative direction, Q_3, Q_4, and D_2 are used in a similar fashion.[6] Isolation between magnet loads is provided by the circuit of Fig. II.5.4-2. Twenty 50-kW dc power supplies are uniformly spaced around the storage ring periphery for the 280 vertical correction magnets. Each of these power supplies energizes 14 HF

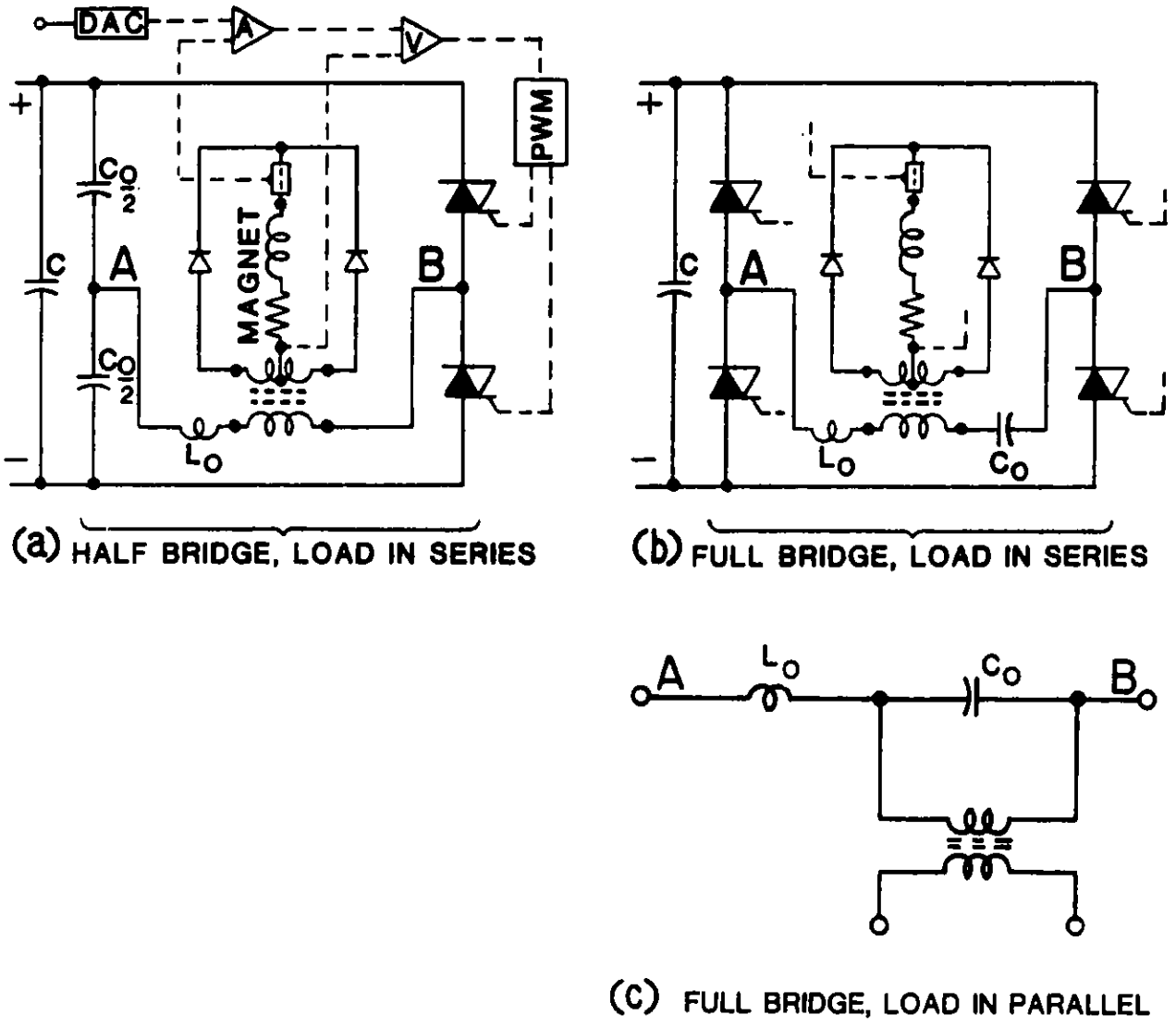

Figure II.5.3-2
Series-resonant PWM dc power supplies.

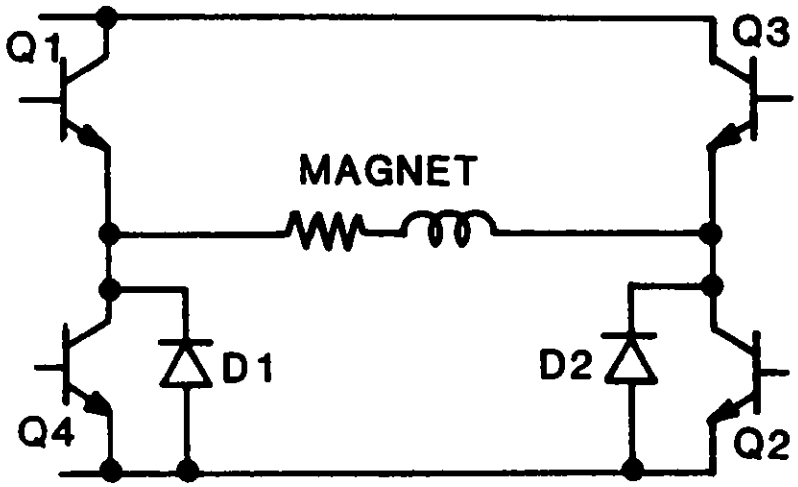

Figure II.5.4-1
Bipolar dc-dc power supply.

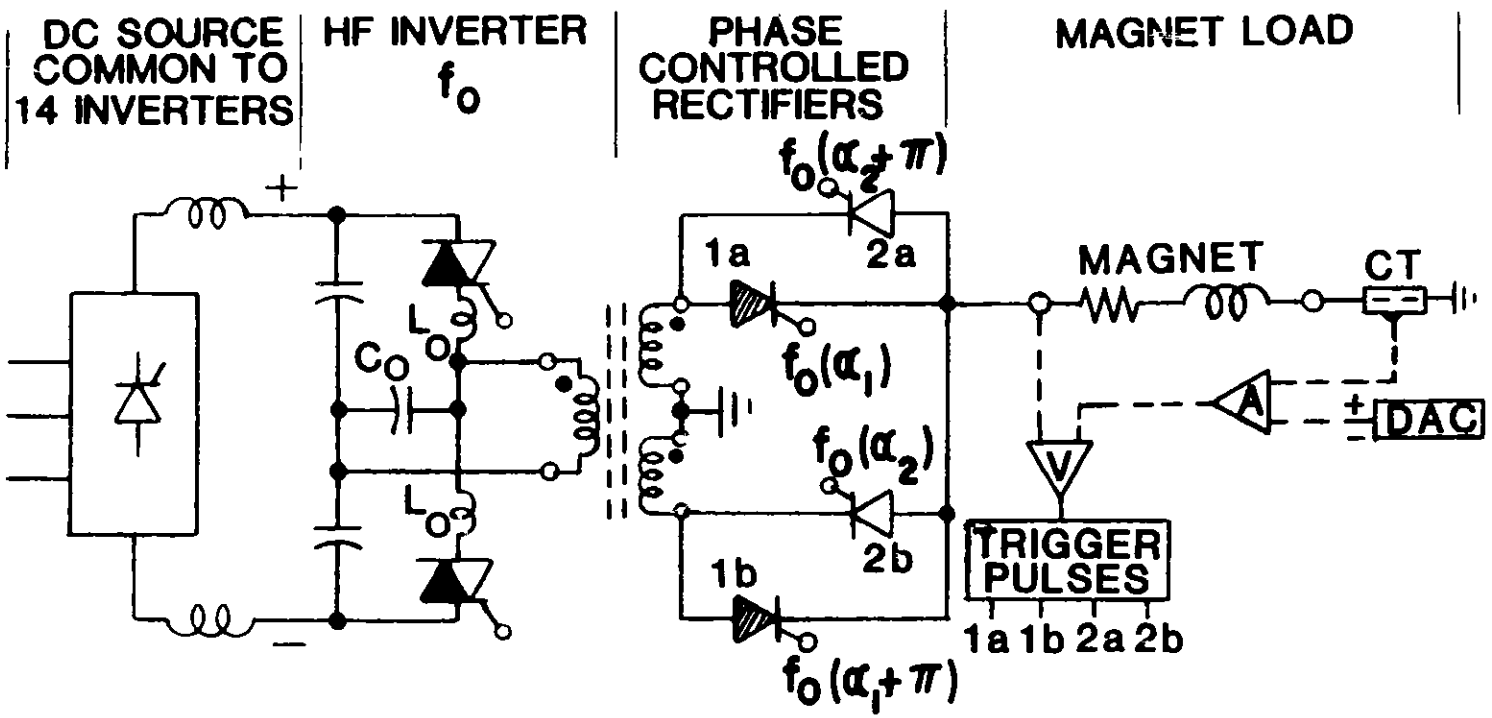

Figure II.5.4-2
Bipolar dc-ac-dc power supply.

inverters. The inverter output transformer is connected to two pairs of phase-controlled full-wave rectifier circuits. These rectifiers control the magnitude and polarity of the magnet current. Both the HF inverters and the phase-controlled rectifiers operate at frequencies above the audio range. The polarity of the magnet current is determined by which pair of rectifiers is selected. The magnitude of the magnet current is controlled by changing the phase delay, α, on the selected rectifier pair. For a positive current, trigger pulses to SCRs, 2b and 2a are blocked, and SCRs 1a and 1b are triggered at phase angles α_1 and $\alpha_1 + \pi$, respectively ($0 \leq \alpha_1 \leq \pi$). The phase angle, α, is measured from the positive zero crossing of the inverter output voltage. The magnet voltage is proportional to $0.5\ (1 + \cos \alpha)$. For a negative magnet current, trigger pulses to SCRs 1a and 1b are blocked, and SCRs 2b and 2a are triggered at phase angles α_2 and $\alpha_2 + \pi$, respectively.

5.5 Electromagnetic Insertion Device Power Supplies

The electromagnetic insertion devices require 600 V, 100 A dc power supplies with an overall regulation of 10^{-4}. They are commercially available.

5.6 Injection Magnet Power Supplies

5.6.1 Septum Magnet Power Supplies

For the pulsed transformer septum magnet, the primary pulse is provided by a capacitor discharge power supply. This supply produces a pulse that is approximately a half-sine-wave with a base width of about 1/3 ms; its peak current is repeatable within ±0.05%. The septum steel is reset by a half-sine-wave pulse of reverse polarity a few milliseconds later.

For the dc septum magnets, commercial dc power supplies, regulated to within ±0.03%, are used.

5.6.2 Storage Ring Injection Bumper Power Supply

When the incoming beam bunch and a specific bucket are in synchronism, the magnetic fields in the 0.4-m-long bumper magnets are energized. A capacitor discharge circuit is used to resonate with the bumper magnets and produce a half-sine-wave current pulse of 20 μs width. The top of the sine wave is within 0.1% of its crest value for 570 ns.

The four bumper magnets are connected in series to form two figure eights, as shown in the power supply circuit of Fig. II.5.6-1. In this circuit, a high-voltage power supply charges two 20.3-μF capacitors to ±6.3 kV ± 0.05% with respect to ground. A deuterium-filled pentode thyratron (English Electric Valve Company type CX 1625) is

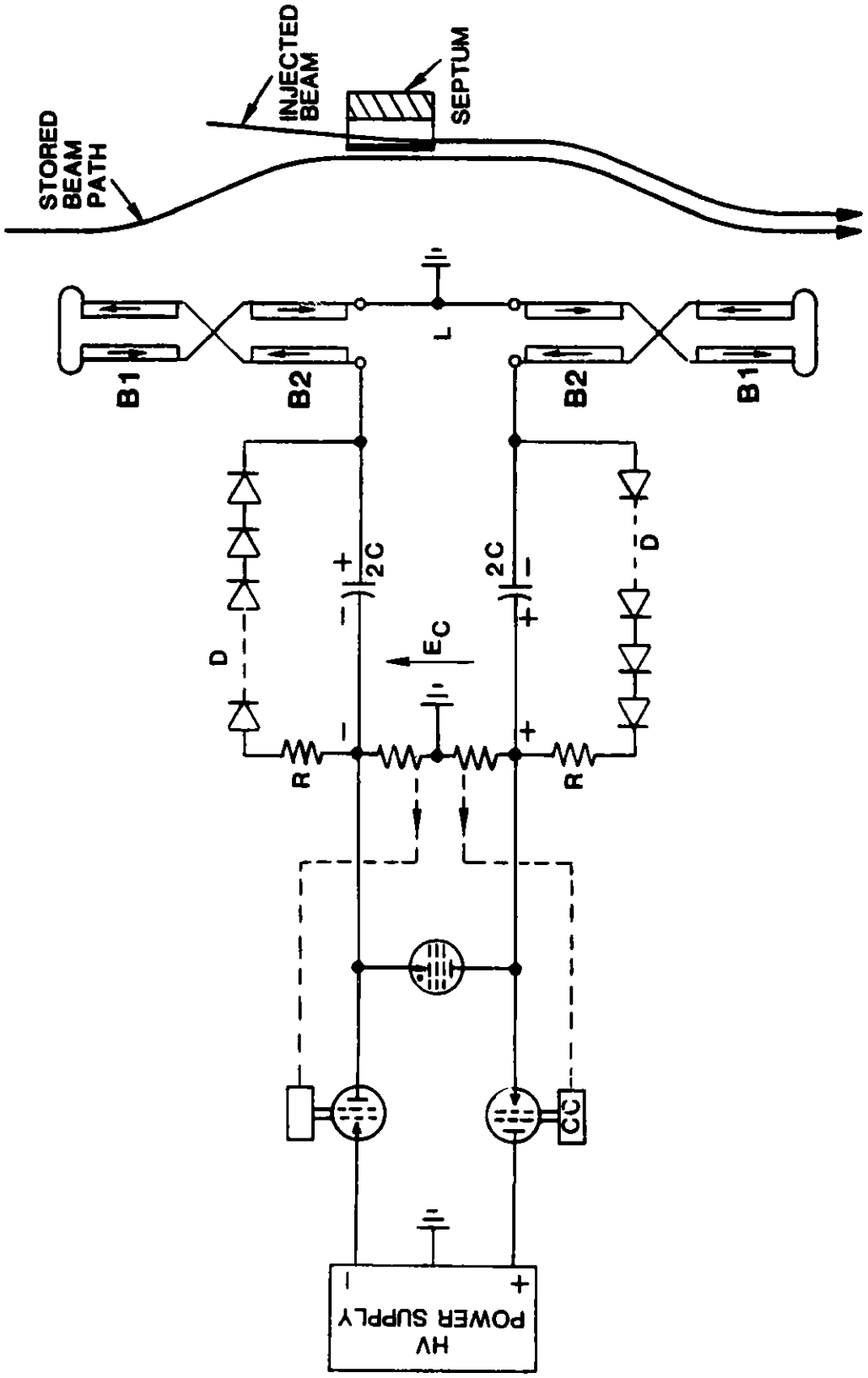

Figure II.5.6-1
Storage ring injector bumper power supply.

triggered 10 μs before bunch injection. The capacitors discharge into the bumper in 10 μs, driving a 1/4-cycle sine-wave current to 16.6 kA. Resistors, R, and diodes, D, in parallel with the capacitors, 2C, limit the voltage and current in the reverse polarity when the bumpers discharge. There is little effect on the crest of the current pulse. At the end of the current pulse, the capacitor voltage is small and discharges to zero through resistors, R. With a 60-Hz repetition rate, the HV power supply charges the capacitors to 12.6 kV ±0.05% within 16 ms via hard-tube series-regulator circuits.

5.7 Storage Ring Abort Kicker Power Supply

For the two fast kicker magnets of Section II.4.8.1 a compact PFN, made from discrete low-Q sections produces a 4-μs flat top. A regulated high-voltage power supply charges and maintains the charge on the PFN. As shown in Fig. II.5.7-1, the PFN discharges through the magnet coils when the thyratron is triggered. The four half-turn coils are connected to terminating networks. The transmission line to the first magnet is shorter than that to the second, which corrects for the time of flight of the beam between the two magnet positions. Table II.5.7-1 gives the system specifications and design requirements.

5.8 Control System and Control Electronics

Since most power supplies must have regulation and control to very high resolution (30 ppm), the critical digital-to-analog (D-A) and analog-to-digital (A-D) conversion devices are incorporated with the regulator circuits within a shielded enclosure close to the magnets. Communication with these regulator units is by means of a multidrop-cable local network. (This local network system is described in Section II.8.2.5, Local MIL-1553 Networks.) These networks operate at a 1-MHz serial bit-rate and are driven from 20 microprocessor clusters located above the ring shield enclosure and spaced uniformly around the ring periphery. The local network slave processor, which controls a multiregulator group, is able to update all current commands according to a downloaded group of settings or by means of a linear, point-slope-derived sequence as update commands are received over the local network.

Local control of the regulator group is by means of a local control console provided for the control system. (See Section II.8.2.4, Microprocessor Clusters.) This local console is able to simulate all local network actions while displaying regulator responses and status. This same system of local control and testing is used in the construction phase to bench-check the regulator systems, with no other control system components required.

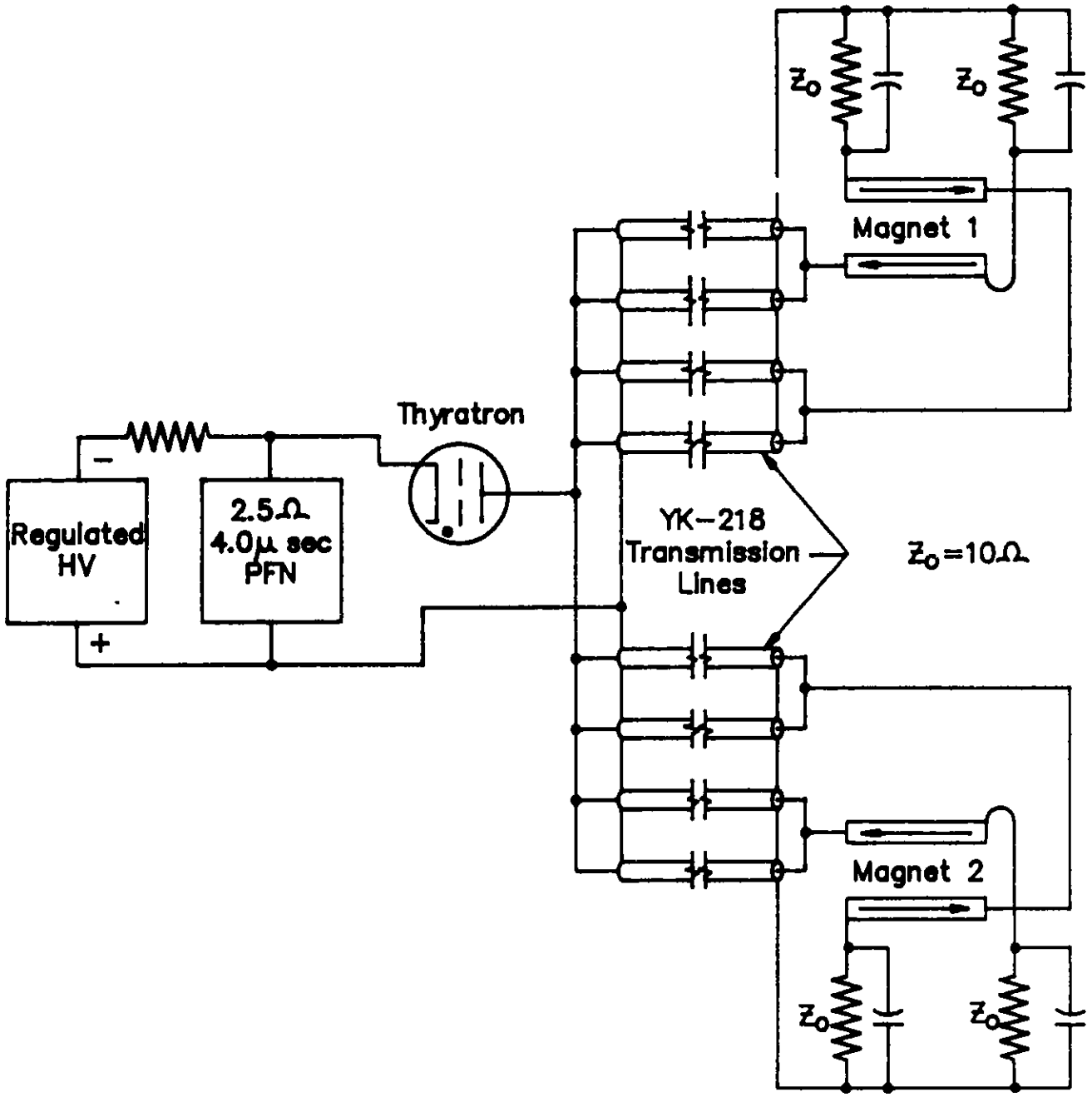

Figure II.5.7-1
Power supply for storage ring abort kicker.

Table II.5.7-1

System Specifications and Design for Abort Kicker Magnets

Rise Time (ns)	56
Flat Top (μs)	4.0
Fall Time (ns)	95
PFN Voltage (kV)	30.9
Transmission Cables	YK-218
Cable Impedance (Ω)	21.0
Time Delay (ns/m)	5.77
Configuration	2 cells
	4 half-turn coils
Peak Field (T)	0.0485
Peak Magnet Current (kA/coil)	1.54
Magnet Inductance (nH/coil)	555
Magnet Gap Dimensions:	
Height (cm)	4
Width (cm)	5.75
Length (cm)	55
Ferrite Type	Ceramic Magnetics Type CMD-5005

5.9 Grounding

A large portion of the problems encountered in power supply applications originate from inappropriate grounding practices which can be explained by the different meanings attributed to the term "ground." For a power-frequency engineer, "ground" is synonymous with "earth"; its function is to provide a low-impedance path for return of power system fault currents to the generator. This low-impedance path serves a safety role by limiting voltage differences during system faults and by allowing sufficient fault currents to assure prompt tripping of the source circuit breakers.

For power electronics and data processing equipment, "ground" is synonymous with "chassis." That is, with the metal enclosure of the equipment, sometimes concentrated into a single metal pad at the bottom of the cabinet, to which all connections to "ground" are routed. The data processing circuitry involves analog or pulse voltage signals of generally less than 15 V, or it involves current loops of a few mA. These signals can be transferred in a balanced, ungrounded circuit or a single-ended circuit with a common reference. Balanced circuits are isolated from ground, but their voltage with respect to ground (common mode) is still significant to the operation and potential susceptibility of the circuits. Single-ended circuits carry signals referred to a common potential, most often that of the equipment's internal chassis, generally called "reference." Thus, in either case, concern is that the referencing system carries signal currents that can become polluted by spurious ground currents, either through common connection points with the earthed system or by common-mode noise coupling.

For electronic circuits, the impedance of the "reference" system includes a substantial inductive component, because of the high frequency of the signal and noise currents. The large existing copper cables, suitable for earthing, are not suitable for referencing. A ground reference grid providing a large number of different path-links for the various noise frequencies will have to be incorporated into the system. For electronic loads, both safety and noise are of concern. Safe operation of an electrical or electronic system depends on the integrity and low impedance of its earthing. Undisturbed operation of the same systems depends on the geometry and intrinsic low impedance of its reference, regardless of the impedance between the reference and the earth.[7]

In addition, to the noise voltages coupled to various equipment by ground currents flowing through a common ground bus, electric and magnetic field coupling between circuits must also be considered.

In summary power supply monitoring and control circuits are designed to:

- Generate as little noise as practicable
- Be affected by noise as little as practicable
- Keep electromagnetic interference to a minimum
- Keep conductive coupling to a minimum
- Keep common impedance coupling to a minimum

At ANL, we have a long and successful history of both conventional and digital computer-based control and monitoring of large, complex power systems. Solutions to problems associated with high and low signal levels in high electromagnetic noise and otherwise hostile environments were found; these include synchrotrons, both conventional

and rapid cycling, bubble chamber magnets, large MHD magnets, and the APEX, FELIX, and ALEX systems.

5.10 References

1. D. L. Hartill and D. H. Rice, "The CESR Magnet Power Supply System," IEEE Transactions on Nuclear Science, NS-26, 4078 (June 1979).

2. W. Praeg, "Frequency Response of Storage Ring Magnets, Eddy Current Shielding of Vacuum Chamber," ANL Report, Light Source Note LS-45 (December 1985).

3. J. McCarthy, D. Wolff, and L. Farkas, "Very High Precision Current Regulated Power Supplies for the Fermilab Antiproton Source," IEEE Transactions on Nuclear Science, NS-32, 3778 (October 1985).

4. W. Praeg, "A High-Current Low-Pass Filter for Magnet Power Supplies," IEEE Transactions on Industrial Electronics & Control Instrumentation, Vol. IECI-17, No. 1, pp. 16-22 (February 1970).

5. HOLEC Industrial Systems, Hengelo, Holland, "A Series Produced Current Transformer with Accuracy of 0.001%."

6. W. Praeg and D. McGhee, "Power Supplies for the Ring Magnets of the Synchrotron X-Ray Source at ANL," IEEE Conference Record. 87CH2837-9.

7. T. Key and F. Martzloff, "A Consensus on Powering and Grounding Sensitive Electronic Equipment," Conference Record of the 1986 IEEE Industry Applications Society Annual Meeting, pp. 1054-1060, Denver, Colo. (Sept. 28-Oct 3, 1986).

6.1 Vacuum Requirements

The storage ring needs a beam-on operating pressure of 1 nTorr or less. This high vacuum is necessary to allow a beam lifetime in the storage ring equal to or greater than 10 h. However, high-intensity synchrotron radiation desorbs gases, which raises the vacuum pressure and reduces beam lifetime. The desorbed gases also limit the beam intensity at start-up. Obtaining the necessary operating pressure in a reasonable period of time requires careful selection of vacuum materials and preconditioning of the chamber walls. The preconditioning is adequate to produce a base pressure of 0.1 nTorr or less in the absence of the circulating beam. Such preconditioning includes chemical or mechanical surface treatments, high-temperature baking, and possibly glow-discharge cleaning. After the beam is injected, photon- and electron-stimulated desorption dominate the gas load, and vacuum materials are chosen to minimize this stimulated desorption, as well as thermal outgassing.

The use of integrated ion pumps is impractical in the storage ring, because only 24% of the ring is occupied with bending magnets. The vacuum system of the storage ring, therefore, will rely on Nonevaporable Getter (NeG) strips as the primary source of distributed pumping in both the bending magnets and straight sections. Lumped NeG modules and/or ion pumps are used at crotch and end flange absorber locations.

6.2 Photon-Induced Desorption

The number of photons of bending-magnet synchrotron radiation per electron-volt per second per milliampere of beam, $d^3N(\varepsilon)/d\varepsilon dt dI$, is given by:[1]

$$\frac{d^3N(\varepsilon)}{d\varepsilon dt dI} = 6.95\times10^{13}\ \frac{\rho}{E^2}\ \int_y^\infty K_{5/3}(x)dx \quad , \tag{II.6-1}$$

where E is the positron energy in GeV,

ε is the photon energy in eV,

$\varepsilon_c = \dfrac{2.2\times10^3 E^3(\text{GeV})}{\rho(\text{m})}$ = the critical energy in eV,

ρ is the bending radius in m,

$y = \dfrac{\varepsilon}{\varepsilon_c}$,

and $K_{5/3}$ is a modified Bessel function of the second kind.

A useful approximation for this integral that is valid for $\varepsilon < \varepsilon_c$ is given by:

$$\frac{d^3N}{d\varepsilon dt di} = 1.51\times10^{14}\ \frac{\rho}{E^2}\ \left(\frac{\varepsilon}{\varepsilon_c}\right)^{-2/3} \quad . \tag{II.6-2}$$

The total number of photons per second per milliampere of stored beam is obtained by integrating Eq. II.6-2 from $\varepsilon = 0$ to ε_c. Above ε_c, the number of photons falls off sharply. In Fig. II.6.2-1 are shown the exact and approximate synchrotron radiation spectra from Eqs. II.6-1 and II.6-2 for PETRA, TRISTAN, the Photon Factory, INS-SOR, and the proposed 7-GeV storage ring.

From Eq. II.6-2, the total photon flux for the storage ring is 1.82×10^{21} photons per second at 7 GeV and 300 mA operation. The distribution of the associated synchrotron radiation power through one sector of the storage ring is shown in Fig. II.6.2-2.[2]

The photon-induced outgassing rate is given by $2n^\circ(\eta\gamma)K$,[3] where $K = 3.11\times10^{-20}$ Torr·ℓ/mol, n° = number of photons per second, and $\eta\gamma = 2\times10^{-7}$ mol/photon after 150 A·h of bombardment. The total photon desorption gas load for the storage ring is therefore 2.26×10^{-5} Torr·ℓ/s. In addition, the thermal outgassing load of the storage ring is 1.51×10^{-5} Torr·ℓ/s, based on a unit outgassing value of 3×10^{-12} Torr·ℓ/(s·cm^2). Therefore, the total gas load is 3.77×10^{-5} Torr·ℓ/s.

The thermal outgassing load is uniformly distributed around the ring and is approximately 1.75×10^{-8} Torr·ℓ/(s·m). The synchrotron-radiation-related gas-load distribution, however, is based on the percentage of photons intercepted by the crotch and end flange absorbers placed downstream of the bending magnet from which the photons originated (see Figs. II.6.2-3 and II.6.2-4). The distribution is shown in Table II.6.2-1.

6.3 Description of Vacuum System

6.3.1 Vacuum Chamber

The cross-sectional view of the vacuum chamber between elements is shown in Fig. II.6.3-1. The chamber consists of two main parts, positron beam aperture and antechamber, which are connected by a photon beam channel with a gap of 10 mm. This gap is wide enough for the extracted photon beams to pass through to the extraction channel, but narrow enough so that the rf leakage is negligible. The outside dimension of the chamber at the beam aperture varies somewhat, depending on its location in the storage ring lattice. The antechamber is shown with the NeG pumping strips in place. The NeG strips are the primary pumping source of the storage ring; they pump unenergized at room temperature (see Sec. II.6.3.3). The antechamber entraps the outgassing that permeates from the absorber locations. The high-speed pumping in the

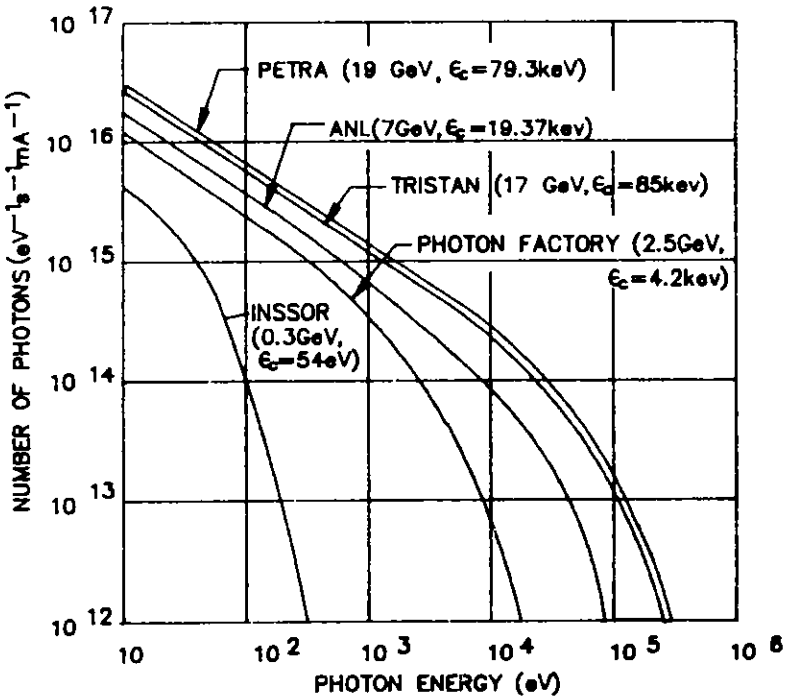

Figure II.6.2-1A
Exact synchrotron radiation spectra of different machines.

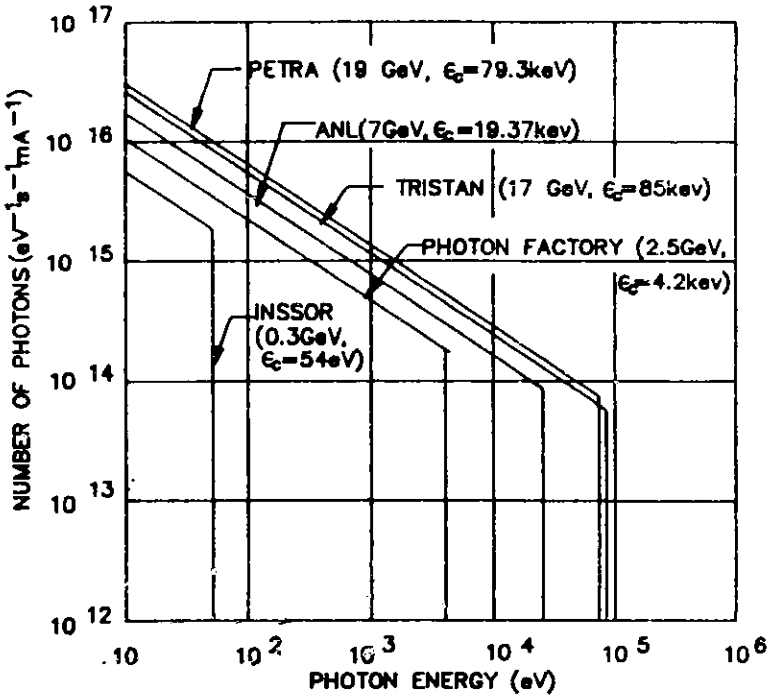

Figure II.6.2-1B
Approximate synchrotron radiation spectra of different machines.

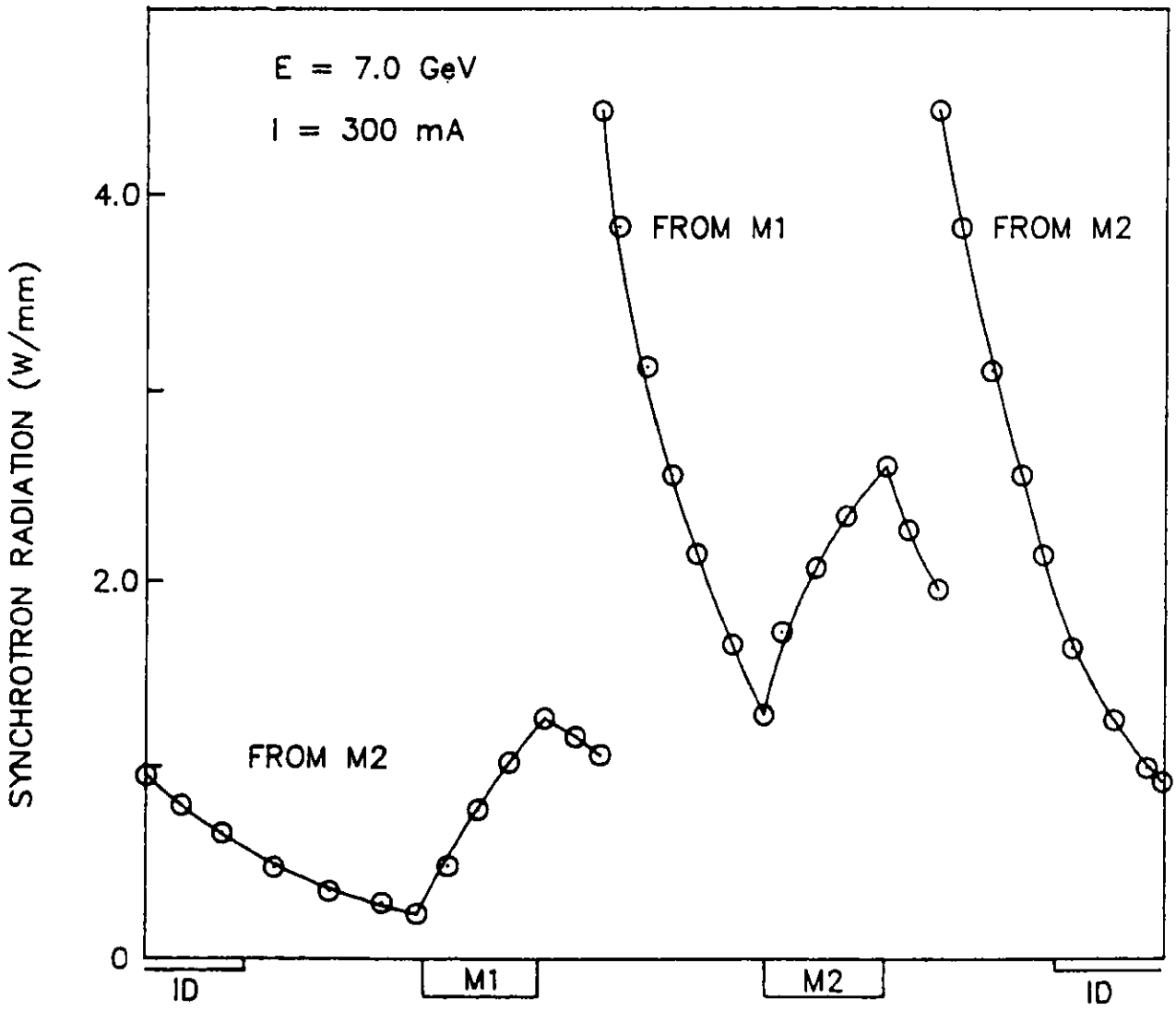

Figure II.6.2-2
Distribution of the bending-magnet radiation on one sector of the vacuum chamber wall without crotches and absorbers. The distance from the storage ring orbit to the wall in the radial direction is 23.8 cm.

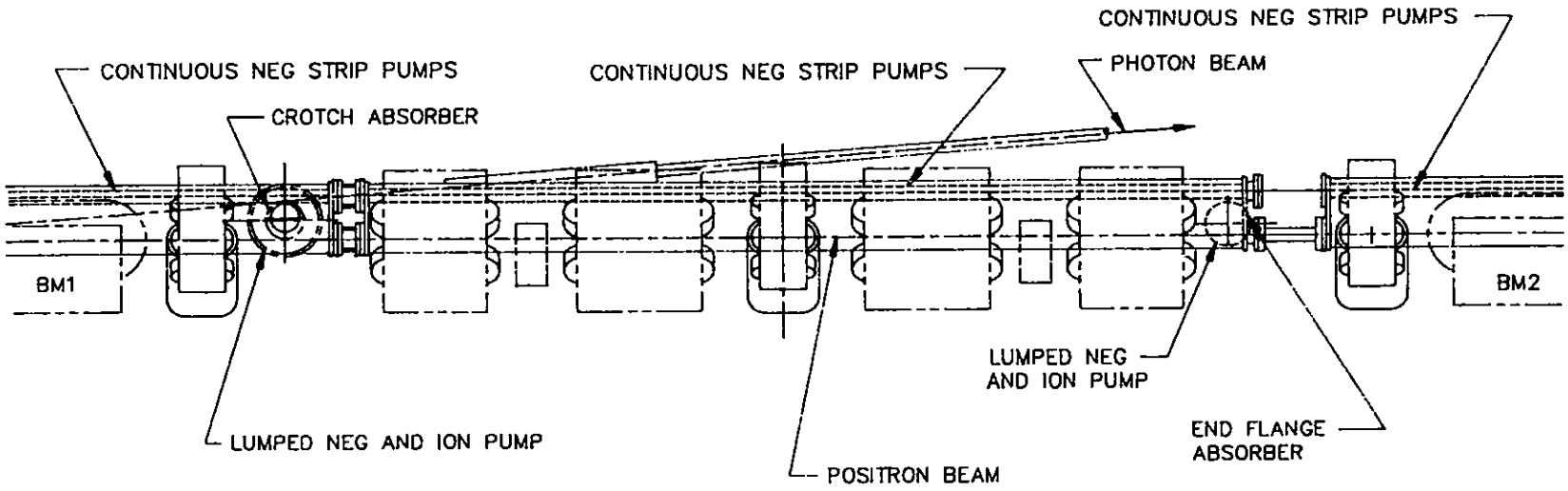

Figure II.6.2-3
Section of cell showing absorbers and pumping.

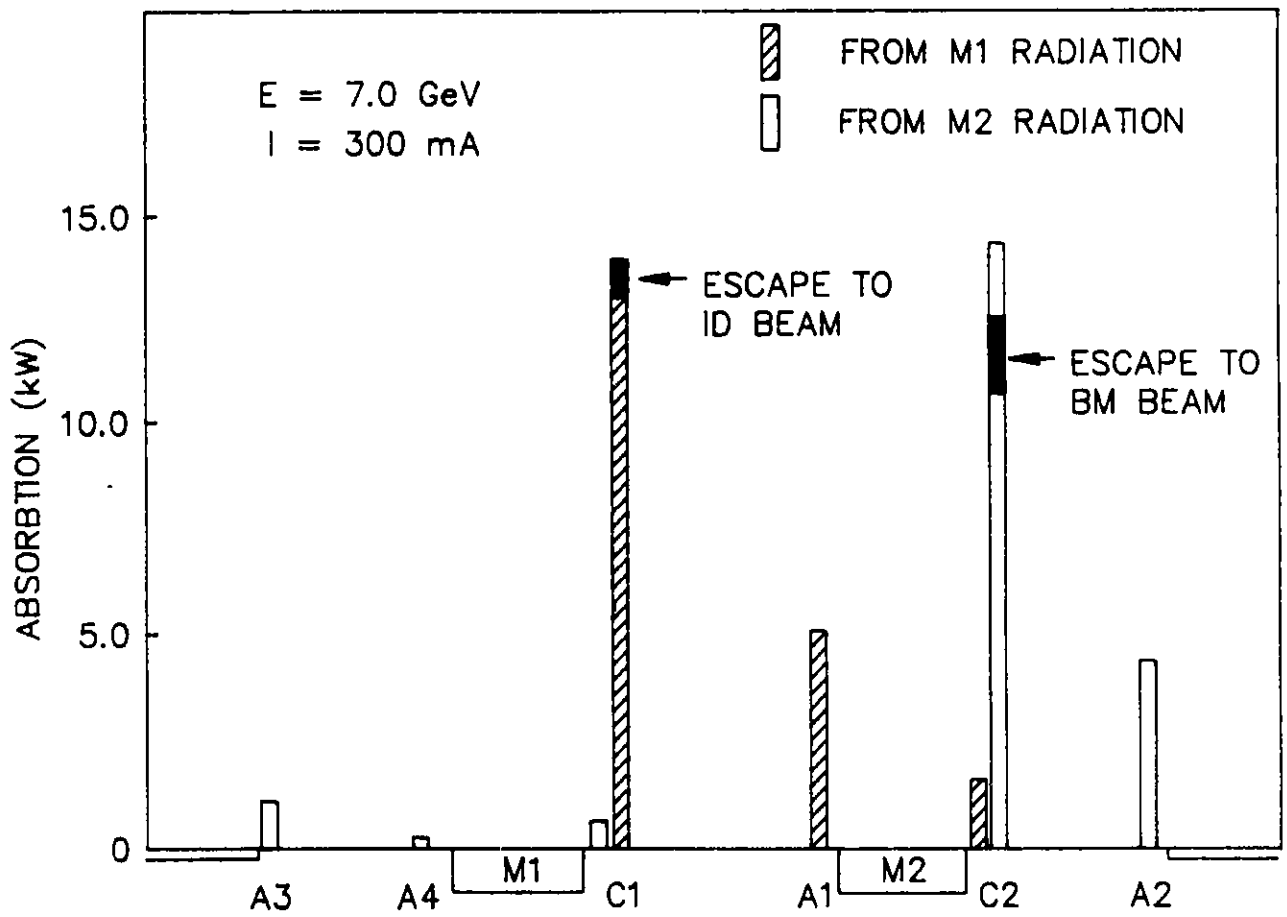

Figure II.6.2-4
Distribution of the power absorbed by the crotches and absorbers, together with their locations.

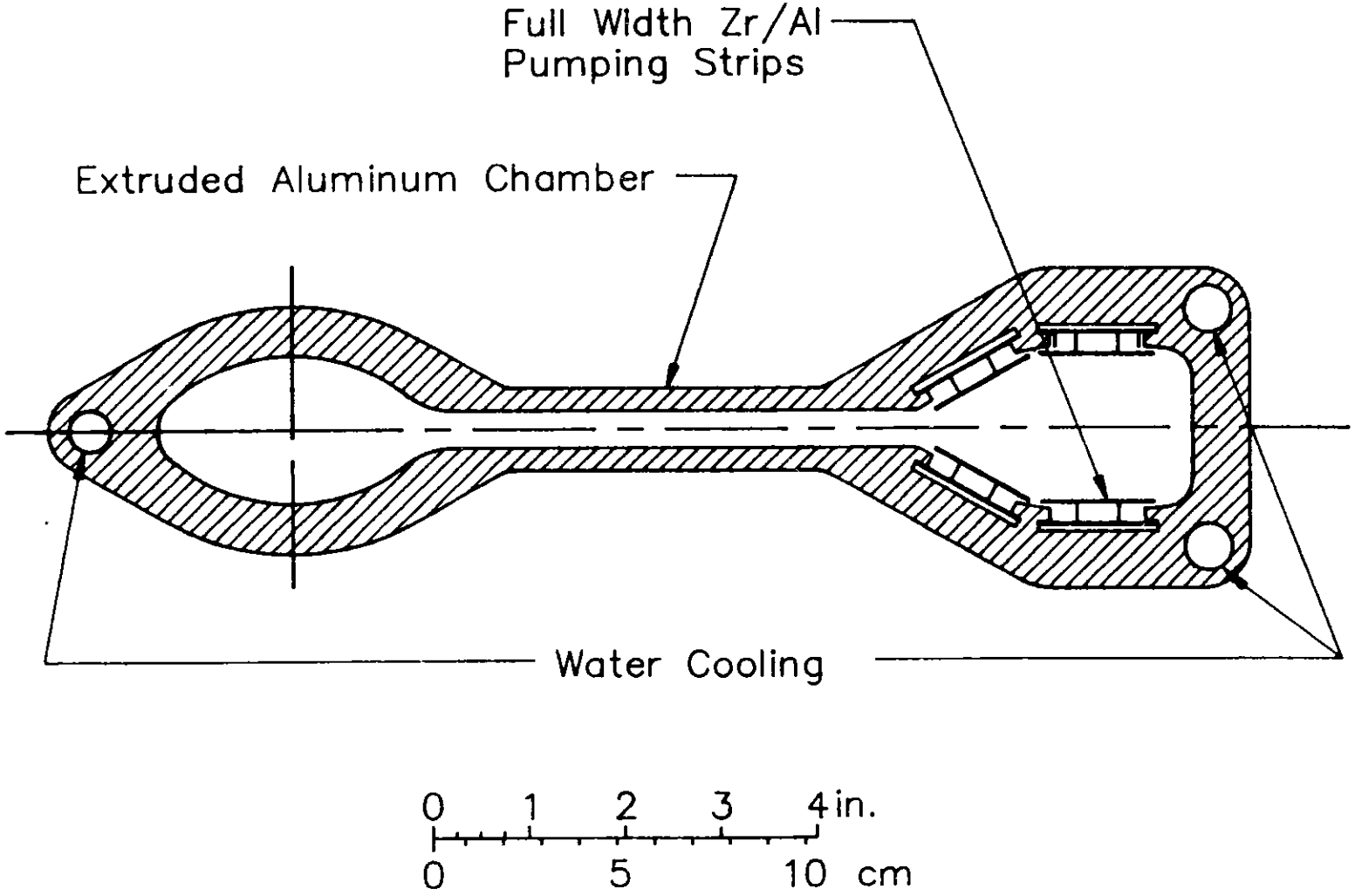

Figure II.6.3-1
Storage ring vacuum chamber cross section.

Table II.6.2-1

Synchrotron-Radiation-Related Gas-Load Distribution/Sector

Absorber	% Intercepted*	Power Absorbed (kW)	Desorption (Torr·ℓ/s) at 10^{-10} Torr
C1	67.5	13.8	1.91×10^{-7}
A1	25	5.1	7.06×10^{-8}
C2	69.5	14.2	1.96×10^{-7}
A2	22	4.5	6.22×10^{-8}
A3 & A4**	5.5	1.1	1.55×10^{-8}
ID Beam	3.0		
BM Beam	7.5		

*Total radiation power from one dipole magnet (100%) at 7 GeV and 300 mA is 20.5 kW.

**Part of this is absorbed by the narrow insertion device (ID) chamber wall.

antechamber assures efficient removal of both photon and thermal desorbed gases. The enlarged cross section of the antechamber improves the conductance of desorbed gases to the pumping surface of the NeG pumps. The chamber is an aluminum extrusion and incorporates the desirable features of the designs of the vacuum chambers for the 1983 ALS by Lawrence Berkeley Laboratory (LBL).[4]

A plan view of a sector is shown in Figure II.6.3-2 with magnet cross sections. The compact placement of machine components clearly indicates the advantage of the antechamber with its distributed NeG pumping strips. The necessity for large numbers of external pumps is eliminated.

6.3.2 Absorbers

Figure II.6.3-3 shows a cross-sectional view of the crotch absorber area with localized pumping of the desorbed gasses. This crotch absorber, similar to the synchrotron radiation exit-line crotch absorber for the CESR ring,[5] is shown just downstream of the dipole magnet in Figure II.6.2-3. It is positioned so as to intercept the greatest percentage of photons without interruption of the experimental beam lines or interference with the positron beam. The crotch absorber features a composite of a beryllium heat diffuser and an axially cooled copper cylinder. The calculated power

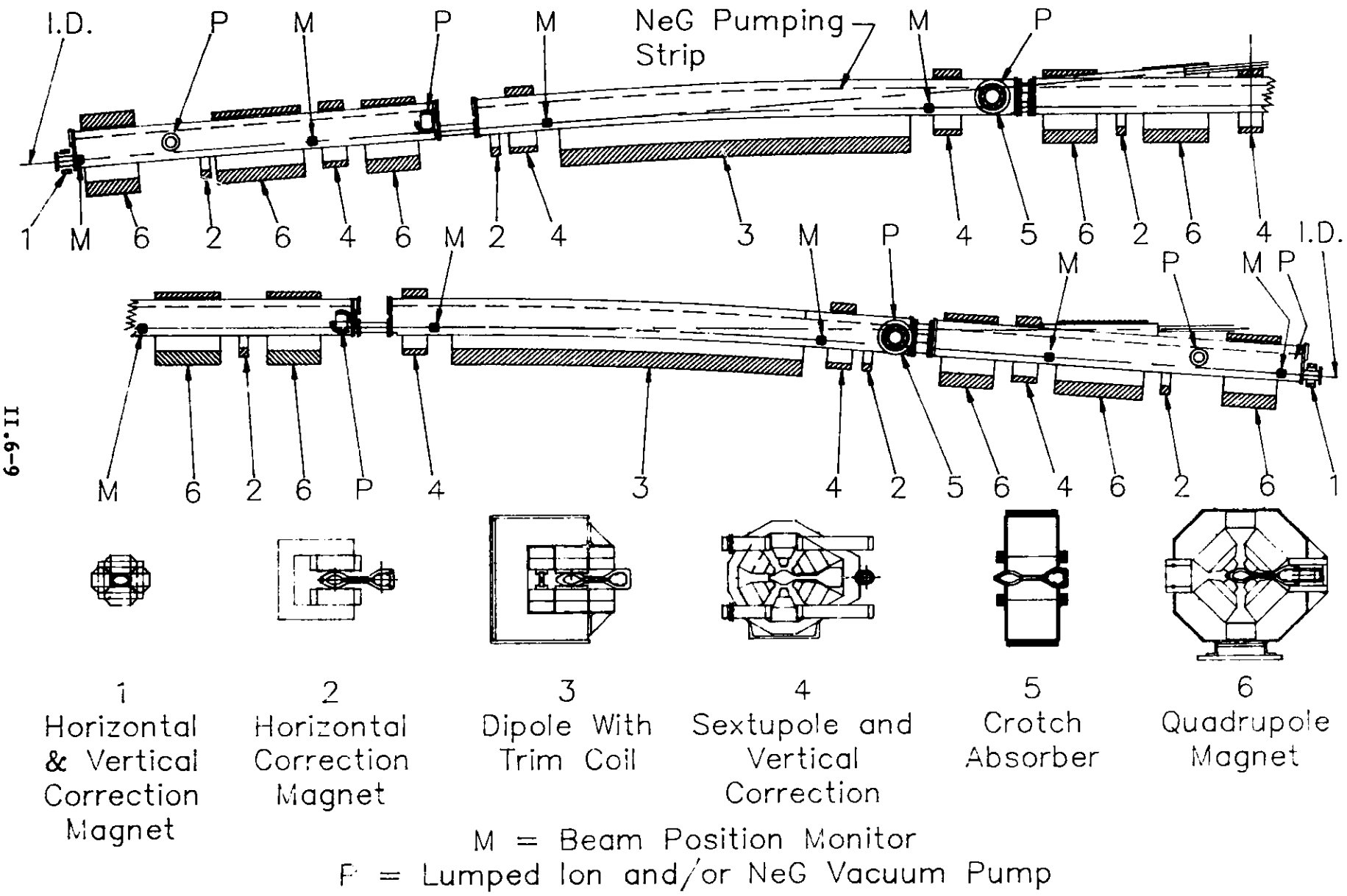

Figure II.6.3-2
Plan view of a sector.

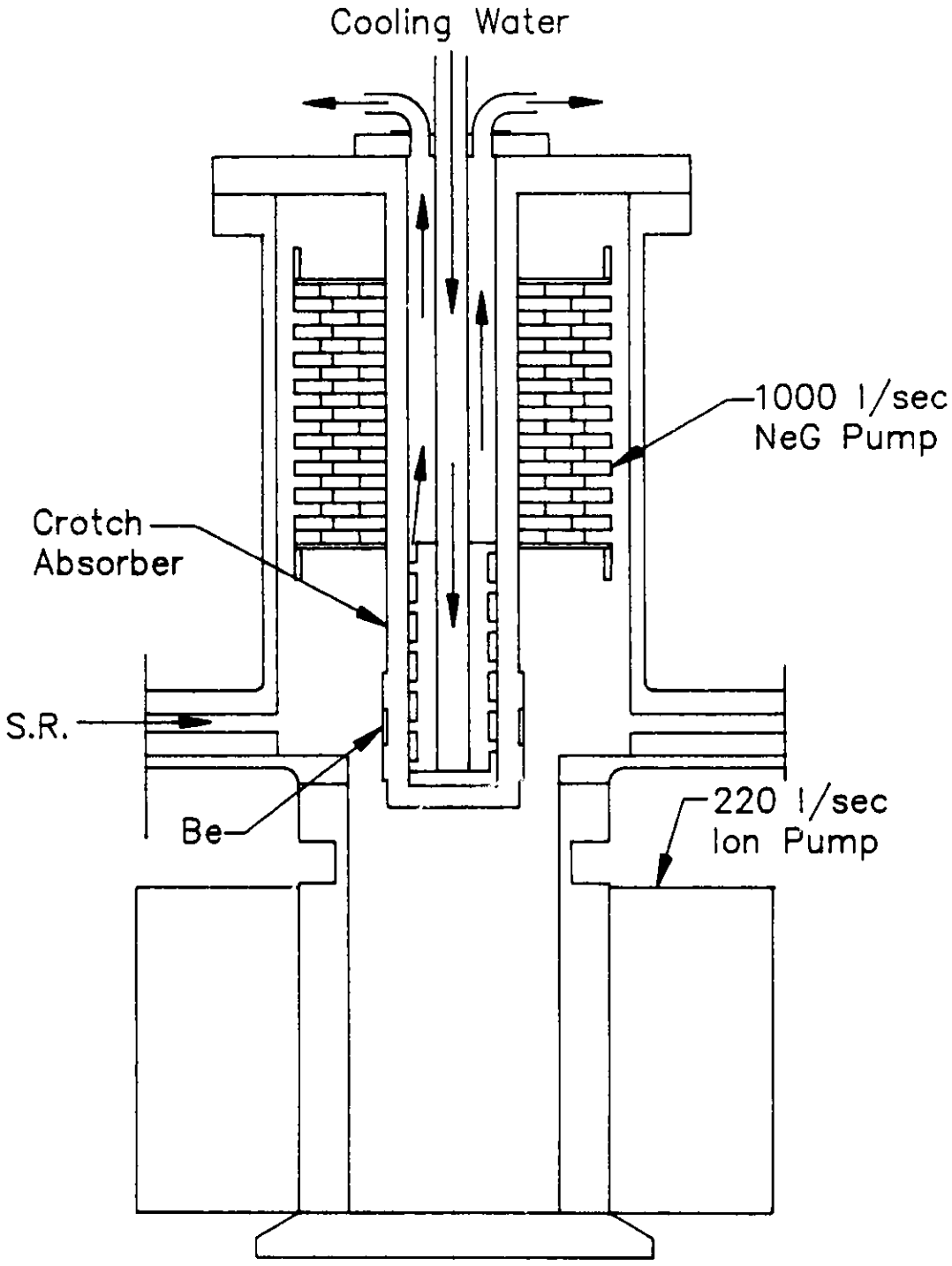

Figure II.6.3-3
Cross section of crotch area showing the synchrotron radiation (S.R.).

density for the storage ring crotches is ≈300 W/mm^2, which is less than the 740 W/mm^2 calculated for the CESR crotch assemblies.

The density of desorbed gas is expected to be highest in the crotch areas. For this reason, higher concentrated pumping speed is provided in these regions. Lumped 220-ℓ/s ion and 1000-ℓ/s NeG pumps are combined here to remove a good portion of the desorbed gases. The remaining gas streaming along the chamber is trapped by the distributed NeG pumping strips in the antechambers.

6.3.3 Nonevaporable Getter Pump

The Nonevaporable Getter[6] is a nonmagnetic strip coated with an alloy of Zr/Al. This alloy forms thermally stable chemical compounds with most of the active gases (O_2, CO, N_2, and CO_2), while the absorption of H_2 is thermally reversible. To become effective as a pump, the strip is activated after pump-down from atmospheric pressure. This procedure consists of heating the getter, which results in diffusion of the saturated surface layer into the bulk of the material. The heating also reduces the H_2 content in the getter whenever the H_2 dissociation pressure of the getter exceeds the H_2 pressure in the vacuum system. After activation, the strength of the gettering action depends on the temperature of the getter and on the amounts and molecular species of the gases that have been pumped. The pumping speeds immediately after activation are high, but they decrease progressively as the getter surfaces saturate. Before saturation, which is dependent on the gas composition, the NeG strip is heated again to restore the pumping speed. The CERN Laboratory has determined experimentally that a few minutes of heating at 400°C is sufficient for this purpose.[7] This operation is referred to as "conditioning" (as distinct from "activation," which is carried out at 700°C for 45 min and is necessary only after exposure to air). Heating of the NeG strips is done only during activation and conditioning. During normal pumping, the strips are not powered and operate at ambient temperature.

After pump-down and activation of the NeG strip, an additional three or four conditionings of the NeG strip will be necessary during beam-on before reaching 150 A·h. However, several hundred conditionings are possible. The total capacity of the NeG is expected to be higher than the lifetime gas load of the storage ring. When the vacuum system is vented, dry N_2 is used instead of air. The N_2 covers the surface and prevents other gases from being absorbed until the NeG strip is activated. With this procedure, ≈30 ventings would result in a pumping-speed reduction of the NeG of only 10%.

The use of NeG as a primary pumping source in the Argonne storage ring is based on experiments carried out at Argonne National Laboratory since 1979; on the in-depth system by CERN; and, in particular, on the actual testing of the CERN studies on electron storage rings at PETRA and DCI. The CERN studies confirmed the feasibility of NeG pumping for the 26-km-circumference ring of LEP. The present experiments at Argonne, using a full-size aluminum test vacuum chamber section with two NeG pumping

strips in the antechamber, confirm thermal desorption pumping results with pumping effectiveness extending to pressures below 0.1 nTorr.

6.3.4 Backup Pumping

The NeG strips do not pump Ar, He, and CH_4; therefore, ion pumps are required. Since high-speed lumped ion and NeG pumps are placed at each absorber, the spacing around the ring is such as to assure adequate pumping of these species for the entire ring. The ion pumps are started after bake-out and just prior to isolation of the turbomolecular pumps as the activated NeG begins to dominate the pumping.

For pump-down from atmospheric pressure, portable oil-free mechanical pumps evacuate the system to ≈50 Torr, after which sorption pumps reduce the pressure to turbomolecular pump starting pressure. Mobile turbomolecular pumping stations are used to further reduce the pressure to NeG and ion pump starting pressure.

6.3.5 Baking and Cooling

The extruded aluminum vacuum chamber contains cooling channels, as shown in Fig. II.6.3-1. Bake-out is achieved by disconnecting the cooling circuit from the main water system and connecting it to mobile water-heating units, which bring the temperature of the chamber up to ≈150°C. Achieving bake-out in this manner results in uniform temperatures with a minimum risk of overheating. The chamber is covered with at least two millimeters of thermal insulation to reduce heat losses. The ion pumps, gauges, valves, bellows, and rf cavities are baked using electrical heating tapes.

6.3.6 System Monitoring

Ionization gauges are distributed along the length of the vacuum chambers. Because the ion pumps are situated in areas of highest desorption rate, their currents are monitored continuously and should provide adequate pressure measurements down to 0.1 nTorr. Gas analyzers, strategically placed around the ring and permanently connected to the central computer control system, are used to monitor the composition of the residual gas. High-pressure gauges are installed in each cell to shut down the NeG power supplies in the event of a vacuum failure during the infrequent activation and conditioning periods.

6.4 Vacuum Chamber Pumping Impedance

A vacuum finite-element-analysis computer program was developed to calculate the pressure profile around the ring.[8,9] A lattice cell of the storage ring is divided into 26 elements for which lengths, volume, conductance, pumping speed, and thermal

Table II.6.4-1

Finite Element Analysis Input Data

#	Element	Length (m)	Volume (ℓ)	Conductance (ℓ/s)	Pump Speed (ℓ/s)	Sync. Rad. Desorp. (Torr·ℓ/s)	Thermal Desorp. (Torr·ℓ/s)
1	Bellows and Valve	0.22	4.800D-01	5.660D+02	0.000D+00	7.020D-06	1.100D-09
2	Trans. Chamber	0.14	3.100D-01	8.930D+02	0.000D+00	4.466D-06	7.000D-10
3	Q1-Q2	1.48	1.032D+01	2.930D+02	5.920D+02	4.727D-05	2.800D-08
4	Q2-Q3	1.48	1.032D+01	2.930D+02	5.920D+02	4.727D-05	2.800D-08
5	Ion Pump	0.22	1.530D+00	1.968D+03	6.000D+01	4.535D-05	4.200D-09
6	Bellows	0.3	6.600D-01	4.140D+02	0.000D+00	9.576D-06	1.500D-09
7	M1-1	1.38	9.620D+00	3.150D+02	5.520D+02	5.850D-05	2.610D-08
8	M1-2	1.38	9.620D+00	3.150D+02	5.520D+02	5.850D-05	2.610D-08
9	M1-3	1.39	9.690D+00	3.120D+02	5.560D+02	5.905D-05	2.630D-08
10	Crotch-1	0.54	3.760D+00	8.020D+02	1.220D+03	2.313D-03	1.020D-08
11	Bellows	0.14	3.100D-01	8.930D+02	0.000D+00	5.946D-06	7.000D-10
12	Q4	0.99	6.900D+00	4.370D+02	3.960D+02	4.206D-05	1.870D-08
13	Q5	0.99	6.900D+00	4.370D+02	3.960D+02	4.206D-05	1.870D-08
14	Q5	0.91	6.340D+00	4.750D+02	3.640D+02	3.863D-05	1.720D-08
15	Q4	0.91	6.340D+00	4.750D+02	3.640D+02	3.863D-05	1.720D-08
16	Ion Pump	0.18	1.250D+00	2.405D+03	2.200D+02	8.578D-05	3.400D-09
17	Bellows	0.31	6.800D-01	4.030D+02	0.000D+00	1.315D-05	1.550D-09
18	M2-1	1.4	9.760D+00	3.080D+02	5.600D+02	4.466D-05	2.650D-08
19	M2-2	1.4	9.760D+00	3.080D+02	5.600D+02	4.466D-05	2.650D-08
20	M2-3	1.405	9.790D+00	3.080D+02	5.620D+02	4.480D-05	2.660D-08
21	Crotch-2	0.375	2.610D+00	1.155D+03	1.220D+03	2.391D-03	7.100D-09
22	Bellows	0.14	3.100D-01	8.930D+02	0.000D+00	4.466D-06	7.000D-10
23	Q3-Q2	1.54	1.073D+01	2.810D+02	6.160D+02	4.918D-05	2.910D-08
24	Q2-Q1	1.54	1.073D+01	2.810D+02	6.160D+02	4.918D-05	2.910D-08
25	Trans. Chamber	0.15	3.300D-01	8.320D+02	7.200D+02	7.503D-04	7.500D-10
26	Bellows and Valve	0.34	7.500D-01	3.690D+02	0.000D+00	1.085D-05	1.700D-09

and photon desorptions were calculated for input to the program. Table II.6.4-1 lists the elements and the various parameters for these elements. The lengths given are not necessarily the lengths of the elements, but they may include some length of chamber protruding from each end.

Figure II.6.4-1 illustrates the expected pressure gradient through each cell as given by the program, based on the input listed in Table II.6.4-1. The curves show typical pressures after 1, 10, and 100 A·h of pump-down. The abundant pumping of the NeG strips in the antechamber sections is clearly evident in the pressures below 0.1 nTorr. This distributed pumping and the reasonably good conductance of the chamber cross section contribute to the achievement of pressures in the low 0.1-nTorr region in the crotch and strip photon absorber sections.[10]

6.5 Experience to Date

An aluminum test vacuum chamber 168 cm long with an internal geometry similar to that of the vacuum chamber has been constructed and used for testing the feasibility of the NeG strip for pumping.[11] Two Zr/V/Fe NeG strips are installed in the test chamber. A pressure of 6.5×10^{-11} Torr has been achieved in this chamber using the pumping techniques described in Section 6.3.3.

A full-size sector (26.5 m in length) of the storage ring is now under construction. It consists of a working vacuum system with diagnostic equipment and full-size models of the magnets. This facility will provide a means of testing fabrication methods, assembly methods, and vacuum performance at full scale. The vacuum chamber extrusions are completed, and the bending-magnet vacuum chambers are being formed to fit the magnet curvature. A welding development program is in progress, and all necessary vacuum hardware has been purchased.

6.6 References

1. J. Kouptsidis and A. G. Mathewson, DESY Report, DESY 76/49 (1976).

2. S. H. Kim, "Distribution of the Bending Magnet Radiation," ANL Report, Light Source Note LS-91 (1987).

3. S. Tazzari, "Synchrotron Radiation Distribution along the Vacuum Chamber," European Synchrotron Radiation Project Report ESRP-IRM-32/84 (1984).

4. "Conceptual Design Report," National Center for Advanced Materials, Vol. 1, Lawrence Berkeley Laboratory Report PUB-5084 (1983).

5. D. M. Mills, D. H. Bilderback, and B. W. Batterman, "Thermal Design of Synchrotron Radiation Exit Ports at CESR," IEEE Trans. Nucl. Sci., NS-26, 3854 (June 1979).

6. B. Ferrario, L. Rosai, and P. della Porta, "Distributed Pumping by Non-Evaporable Getters in Particle Accelerators," IEEE Trans. Nucl. Sci., NS-28, 3333 (June 1981).

7. "LEP Design Report," Vol. II, Chapter 8, CERN-LEP/84-01 (June 1984).

8. J. F. J. Van Den Brand and A. P. Kaan, "Design Study of the Vacuum System for the E.S.R.F.," European Synchrotron Radiation Project Report ESRP-IRM-61/84 (1984).

9. J. Kneuer, unpublished information (1985).

10. R. Wehrle, J. Moenich, S. Kim, and R. Nielsen, "Vacuum System for the Synchrotron X-ray Source at Argonne," IEEE Conference Record 87CH2837-9.

11. R. Nielsen, J. Moenich, and R. Wehrle, "Vacuum Chamber Development for the Synchrotron X-Ray Source at Argonne," IEEE Conference Record 87CH2837-9.

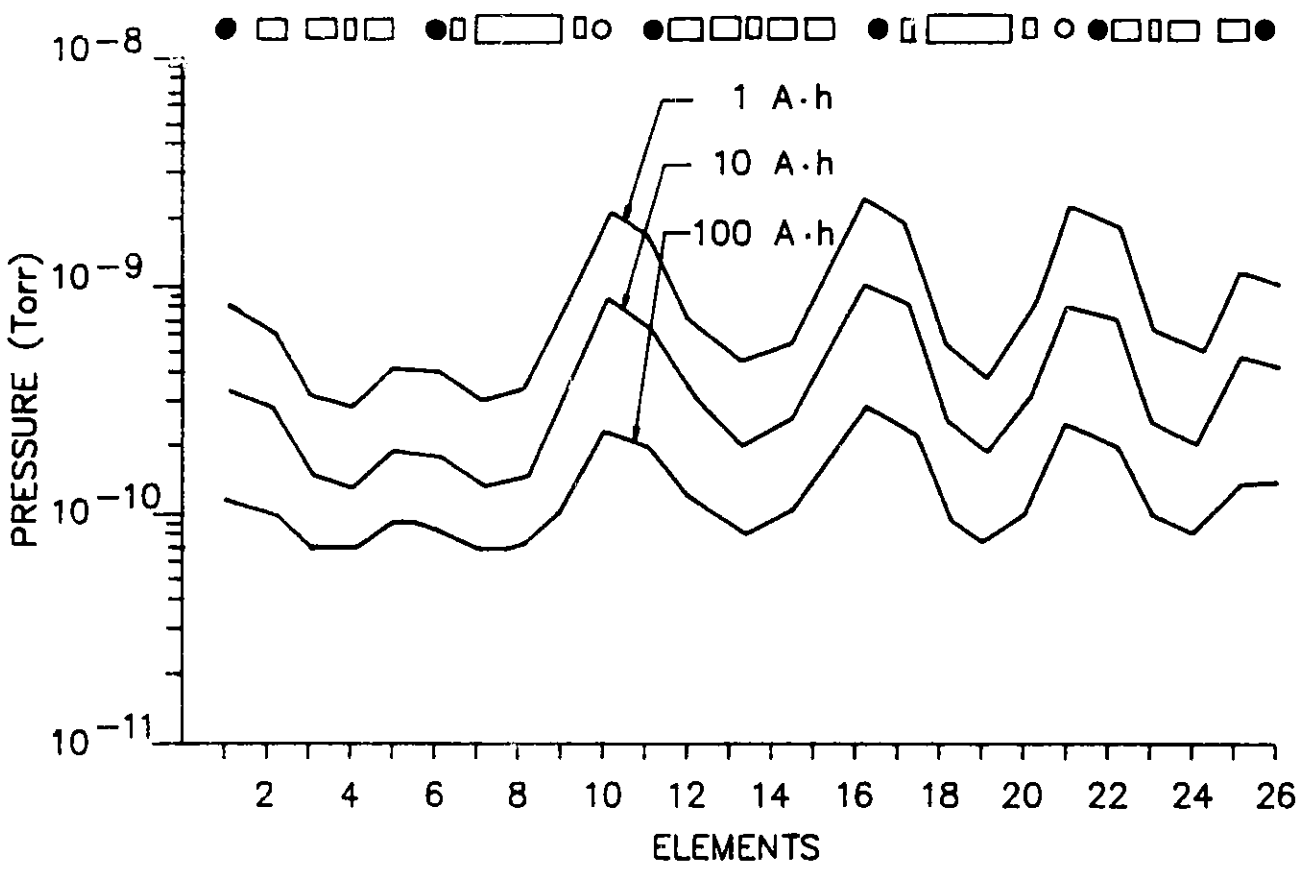

Figure II.6.4-1
Pressure gradient profile.

7.1 Introduction

The APS storage ring requires diagnostic instrumentation to monitor the beam position, profile, current, and beam losses. Table II.7.1-1 shows the types and quantities of the installed instrumentation. The circulating beam trajectory in the storage ring directly determines the external photon beam trajectory. To maintain stability of the photon beam from insertion devices, it has been estimated that, for critical experiments, the path of the positrons through the insertion device must be maintained to ±10 μm in position and less than ±1 μrad in angle.[1] Storage ring beam position monitors (BPMs) are not currently accurate enough to ensure that these requirements are met. Accordingly, photon BPMs are used in the photon beam lines as the signal source for the position correction system in the storage ring. The photon beam feedback system is discussed in Section II.7.7.

7.2 Storage Ring Beam Position Monitors

The main requirement of a beam position measurement system is to provide accurate and repeatable measurements of the circulating beam orbit for input to the control system for closed orbit correction. Not only short-term, but also long-term repeatability is required, to maintain a constant closed orbit for proper storage ring operation and stable photon beam position at the experiments. For the APS storage ring, the BPM system is designed to measure the beam position under normal operating conditions with an accuracy of 30 μm. Methods for maintaining the accuracy and repeatability of the measurements are incorporated.

The beam position is measured at 9 locations in each sector, providing a total of 360 measurements around the storage ring. The BPM locations in a typical sector are shown in Fig. II.6.3-2. Each BPM consists of a set of four button electrodes mounted in the walls of the vacuum chamber. To maintain mechanical stability of the electrodes, the wall thickness of the beam vacuum chamber is maintained at 1.25 cm at the BPM locations. Precision machining of the vacuum chamber ensures that the electrode, mounted to a vacuum feedthrough, is positioned accurately. Each electrode is capacitively coupled to the beam, and by comparing the signal amplitudes from the four electrodes, the position of the center of charge of the circulating beam can be determined. A cross section of the vacuum chamber, showing the location of the four BPM electrodes, is shown in Figure II.7.2-1. The signals from each BPM are transmitted over low-loss, high-frequency cables to processing electronics located outside the storage ring shielding. The cables are routed through conduit, to provide additional shielding from electromagnetic interference.

Each BPM electrode signal is processed independently, to achieve the highest possible accuracy for all signal amplitudes. Independent processing also allows the

Table II.7.1-1

Beam Diagnostic Instrumentation for Storage Ring

Quantity	Monitor Type	Function
2	Current Transformers	Beam Current
360	4-Button Pickups	Beam Position
2	Photon Monitoring Stations Including: Photomultipliers Photodiodes TV Cameras Streak Camera (1)	Intensity, Transverse, and Longitudinal Beam Characteristics
2	RF-Drive Electrodes and Amplifiers	Betatron Tune
2	Stripline Pickups	Longitudinal & Transverse Frequency Components
2	Horizontal and Vertical Pingers	Damping Factor & Beam Transfer Function
80	Loss Monitors	Losses
2	X and Y Beam Scrapers	Injection Halo Trimming, Machine Studies
40	Fluorescent Screens	Injection Position, Profile

system to provide reliable and repeatable signals for continuous closed-orbit correction, as well as the ability to measure the beam position during a single turn. The latter capability is essential for commissioning of the storage ring, although the measurement accuracy in this mode is limited to 200 μm. Each signal is processed by a narrow-band circuit which filters and heterodynes the bunch frequency component to an intermediate frequency of 30 MHz, where the signal is amplified and detected. These signals are sampled by track-and-holds and digitized by 12-bit A-D converters. The BPM computers, located at the control and monitoring system diagnostic nodes, sample, linearize, and correct the signals, they compute the individual beam positions for operator display and closed-orbit correction. Fast signals from selected BPMs are multiplexed into the control room for oscilloscope monitoring.

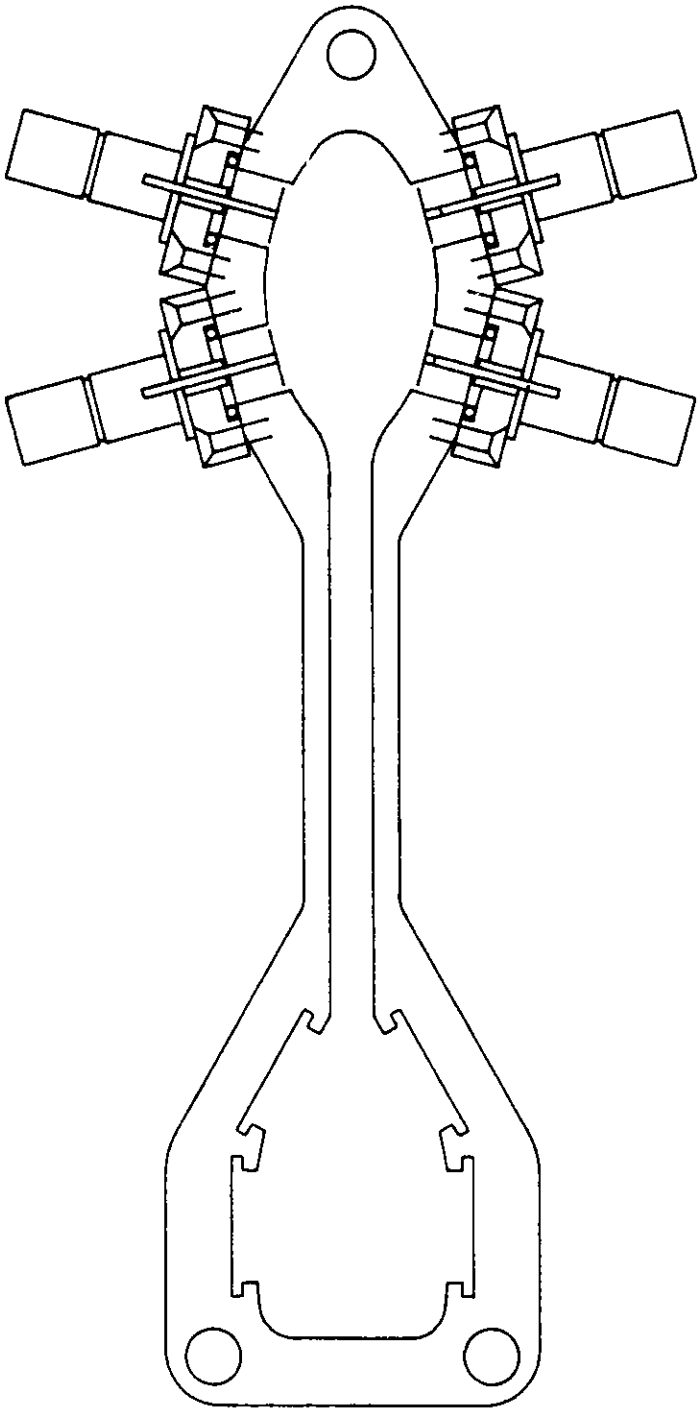

Figure II.7.2-1
Vacuum chamber cross section showing beam position monitor assembly.

To assure the accuracy and repeatability of the signals from the BPM system, each BPM and its electronics is checked thoroughly from installation through operation. After installation of the electrodes in the vacuum chamber, the electrical center and sensitivity of each BPM is measured by transmitting pulses down a wire and measuring the response of the BPM as the wire is moved with precision-positioning stages. The electrical center of each BPM is marked with alignment fiducials on the vacuum chamber. The sensitivity data is recorded in the BPM computer database. During operation, signal averaging techniques are used to improve measurement accuracy. To minimize systematic error effects in the processing electronics, calibration signals are injected and compared by the computer to preset standards. Any deviations are applied as corrections to the succeeding position measurements. In addition, the absolute position of the BPM with respect to the magnetic centers of the adjacent quadrupole and sextupole is calibrated by varying the current in the quadrupole and observing the orbit shift. The beam position at which no measurable beam motion is observed due to the quadrupole current variation is stored by the BPM computer as the center reference for that BPM.

7.3 Current Transformers

The average beam intensity in the storage ring is measured by a dc current transformer based on a design used at many storage rings.[2] Measurement accuracy of better than 0.1% provides fast and accurate measurement of beam lifetime.

The current transformer is mounted on a metallized ceramic vacuum chamber which allows the low frequency beam components to pass through, but blocks the high frequency components and minimizes the impedance seen by the beam. The current transformer is made up of three magnetic cores. A modulator, operating at a low frequency, drives two of the cores in opposite directions into saturation. The circulating beam induces in the cores even harmonics of the core excitation frequency. This induced signal is measured by a sense loop, extracted by a second harmonic synchronous detector, amplified and applied to another loop which cancels the beam-induced flux. This signal, a direct measure of the circulating current, is digitized and processed for display.

7.4 Photon Monitoring Stations

Two photon monitoring stations are provided. One uses photon radiation from a bending magnet and the other from an undulator insertion device. Both stations are equipped with photon beam position monitors and have end stations containing photomultiplier tubes, ion chambers, photodiode arrays and other instrumentation for measuring the circulating beam intensity, and transverse and longitudinal beam characteristics.

The bending magnet station contains two photon beam position monitors. The first is a photoemission type monitor mounted on a high precision movable stage. The

second is an ion chamber located 10 meters downstream from the first. The two measurements provide information on the vertical source position and tangent angle of the positron beam. In addition, a streak camera is contained in the bending magnet end station to measure the length of the particle beam bunches to better than 5 ps. The end station, located outside the ring shield wall, also contains equipment for measurement opf the photon beam intensity.

The insertion device diagnostic beam line contains a low intensity undulator with a $K < 0.5$ and a period of approximately 6 cm. For 7 GeV operation of the storage ring, the first harmonic of the undulator is approximately 7 keV. In order to avoid thermal loading of components, the total power delivered from the undulator is made as small as possible. The lower limit is determined by the amount of stray bending magnet radiation present at the measurement location downstream. The beam line contains four photon position monitors consisting of photoemissive elements mounted on high precision movable stages. The two sets of monitors provide the horizontal and vertical position, size and tangent angle of the positron beam in the undulator region.[3] In addition, a spatial mapping of the first harmonic radiation from the undulator is made using a slit assembly.[4] These measurements are used to calculate the positron beam emittance in the undulator straight section.

7.5 Special Beam Studies Instrumentation

The storage ring is provided with horizontal and vertical high-frequency pickup electrodes, driver electrodes with power amplifiers, and horizontal and vertical pingers. These systems are used for storage ring performance optimization. Measurement of basic beam properties such as the betatron tune, damping factor, and beam transfer functions can be performed. Specialized high-frequency instrumentation, such as spectrum and network analyzers are provided for these measurements.

7.6 Other Beam Diagnostic Instrumentation

Fluorescent screens viewed by TV cameras are provided. These are interceptive beam monitors and are normally located within the vacuum chamber, but outside the circulating beam path. They are remotely inserted to measure the position and profile of the first turn injected into the storage ring.

Ion chamber beam loss monitors are provided throughout the facility at strategic locations, to detect and help locate any excessive beam losses. These monitors, together with the beam position system, are used to initiate a beam abort.

Movable beam scrapers are provided in the storage ring, to trim the injected beam halo and to define the physical aperture.

7.7 Photon Beam Feedback Loop Methodology

The positron beam trajectory through an insertion device or bending magnet controls the photon beam divergence, exit angle, and position. Consequently, photon beam sensors are highly effective monitors of the positron beam orbit errors. In addition, they are essential in beam lines with tight tolerances in the photon beam trajectory. Monitors of this type are presently used in several synchrotron light sources as diagnostic sensors.[5,6,7]

The incorporation of these high-sensitivity photon monitors into the feedback control of the positron beam trajectory occurs after an initial commissioning period, during which time the positron beam monitors are used. The actual schedule, which involves three distinct phases of operation of the ring, is described below.

7.7.1 Phase 1 - Commissioning

During the commissioning phase, when none or very few of the IDs are present, the positron BPMs are used to determine the beam orbit, and correction magnets are used to initially establish a closed orbit and, later, the preferred operating orbit. During this period, the various correction sensitivities are explored and calibrated. Control algorithms are refined to allow orthogonal changes in beam trajectory confined to single ID regions. Accuracy and sensitivity is limited to that of the positron BPMs (about 30 μm).

7.7.2 Phase 2 - Initial Beam Line Operation

During this phase, the needed high-sensitivity photon beam position sensors come into use as the photon beam users who require this sensitivity come on line. The algorithms and control techniques are further refined to work successfully with these higher sensitivities.

7.7.3 Phase 3 - Mature Operation

To provide the means to correct photon beam trajectories for low-frequency vibration and/or long-term drift, a feedback system based on the photon beam is needed. In fact, the small beam size will dictate more stringent control and regulation.[8] To this end, feedback loop control of the photon beam trajectory is incorporated, with four magnets and two photon beam position sensors for each of the two axes (horizontal and vertical). (The closed orbit correction magnets and power supplies with separate control inputs are used for the photon beam correction.) This system is capable of low-amplitude control of the beam trajectory for frequencies up to 20 Hz.

7.8 References

1. K.H. Reich, "Control of Photon Beam Position and Stability," ESRP-IRM-27/84 (March 1984).

2. K. Unser, "A Toroidal DC Current Transformer with High Resolution," IEEE Trans. Nucl. Sci., NS-28, No. 3, 2344 (1981).

3. F.P. Wolf and W. Peatman, "Synchrotron Radiation Diagnostics at Bessy," Nuclear Instruments and Methods in Physics Research, A246, 408 (1986).

4. G. Brown et al., "Operation of PEP in a Low Emittance Mode," IEEE Conference Record 87CH2837-9.

5. R. Hettel, "Beam Steering at the Stanford Synchrotron Radiation Laboratory," IEEE Trans. Nucl. Sci., NS-30, No. 4, 2228 (1983).

6. J. Tischler and P.L. Hartman, "Photo-Electron and Ionization Chamber Position Monitors for CHESS," Nuclear Instruments and Methods, 172, 67 (1980).

7. H. Rarbach, private communication (February 1987).

8. R. Hettel, "Synchrotron Beam Steering," Report of Machine Workshop on the 6-GeV Synchrotron Radiation Source, National Bureau of Standards, Gaithersburg, Md., Appendix D-4 (March 1985).

8.1 Introduction and Philosophy

Several modern accelerator control systems are presently in the process of changing to accommodate expanded or unanticipated accelerator needs and to take advantage of new control system tools now available.[1-6] The APS control system is designed not only to accommodate the known requirements of the present accelerator design, but also to be able to expand in capacity and capability in the future. These are not conflicting requirements; instead, they imply the use of a network of specialized resources to create a distributed, modular control system. Such a methodology adapts to changing needs in several ways:

- It expands in capacity by allowing the addition of units of existing types.
- It expands in capability by the addition of specialized units, such as closed-loop processors or array processors.
- It expands in capability by the substitution of improved versions of existing units.

This methodology is possible and even attractive due to the present trend in computer technology to standardize network protocols and messages, rather than vendor data buses. Peripherals and processors from different vendors can be intermixed to optimize the organization and performance of a distributed computer resource system.

The ability to interconnect with network components of differing characteristics also allows these components to be specialized as to function. The APS control system incorporates processors specialized for computation speed and storage capacity, operator interaction, database maintenance, low-level equipment monitoring, and multiple parallel processor activity. This separation and specialization of function also allows the upgrading or expansion of one or more functional areas without affecting the operation or performance of the remaining areas.

8.2 Control System Components

Figure II.8.2-1 shows schematically the various types of processors and their interconnecting networks. The processor types are listed in decreasing hierarchical order on the right side of the figure and the networks on the left side. Figure II.8.2-2 shows the same elements in geographic relationship to the light source complex and shows how the networks allow the elements to be distributed in optimal ways.

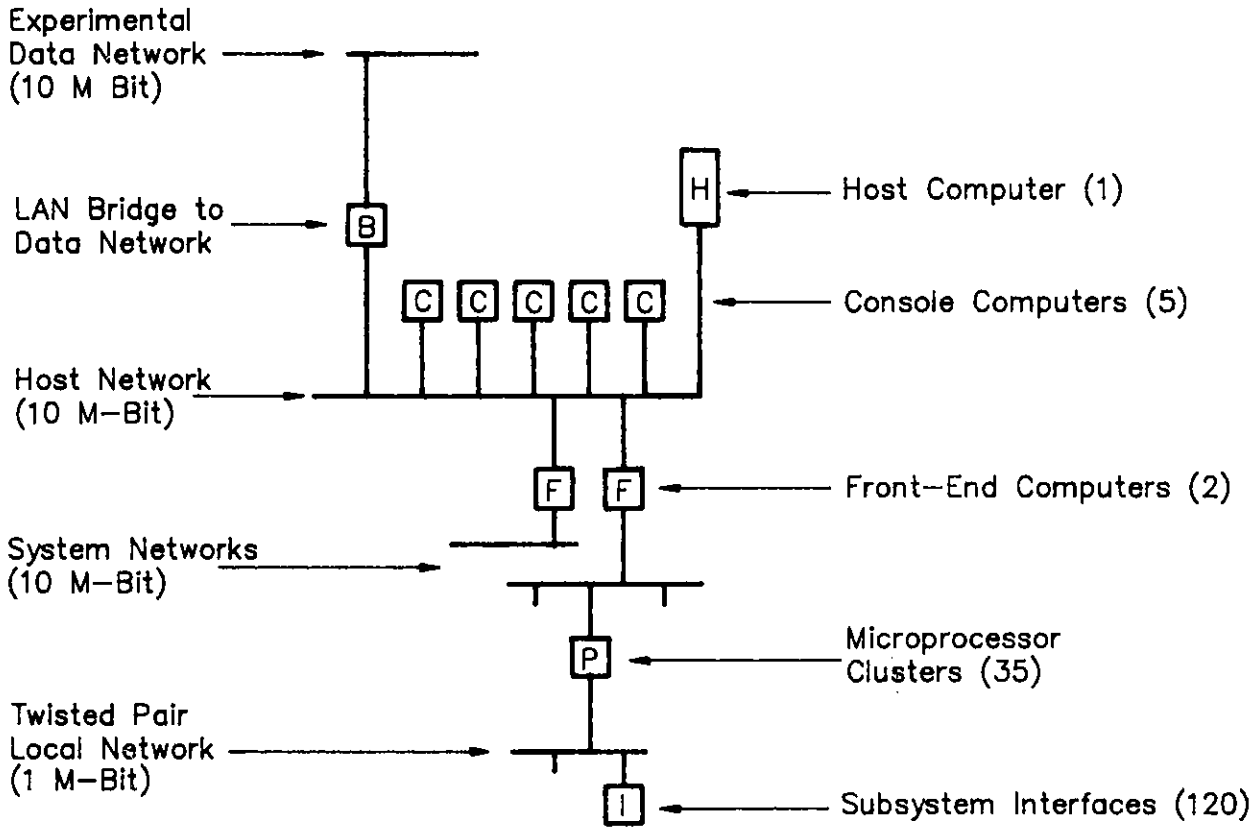

Figure II.8.2-1
Control system processor and network hierarchy.

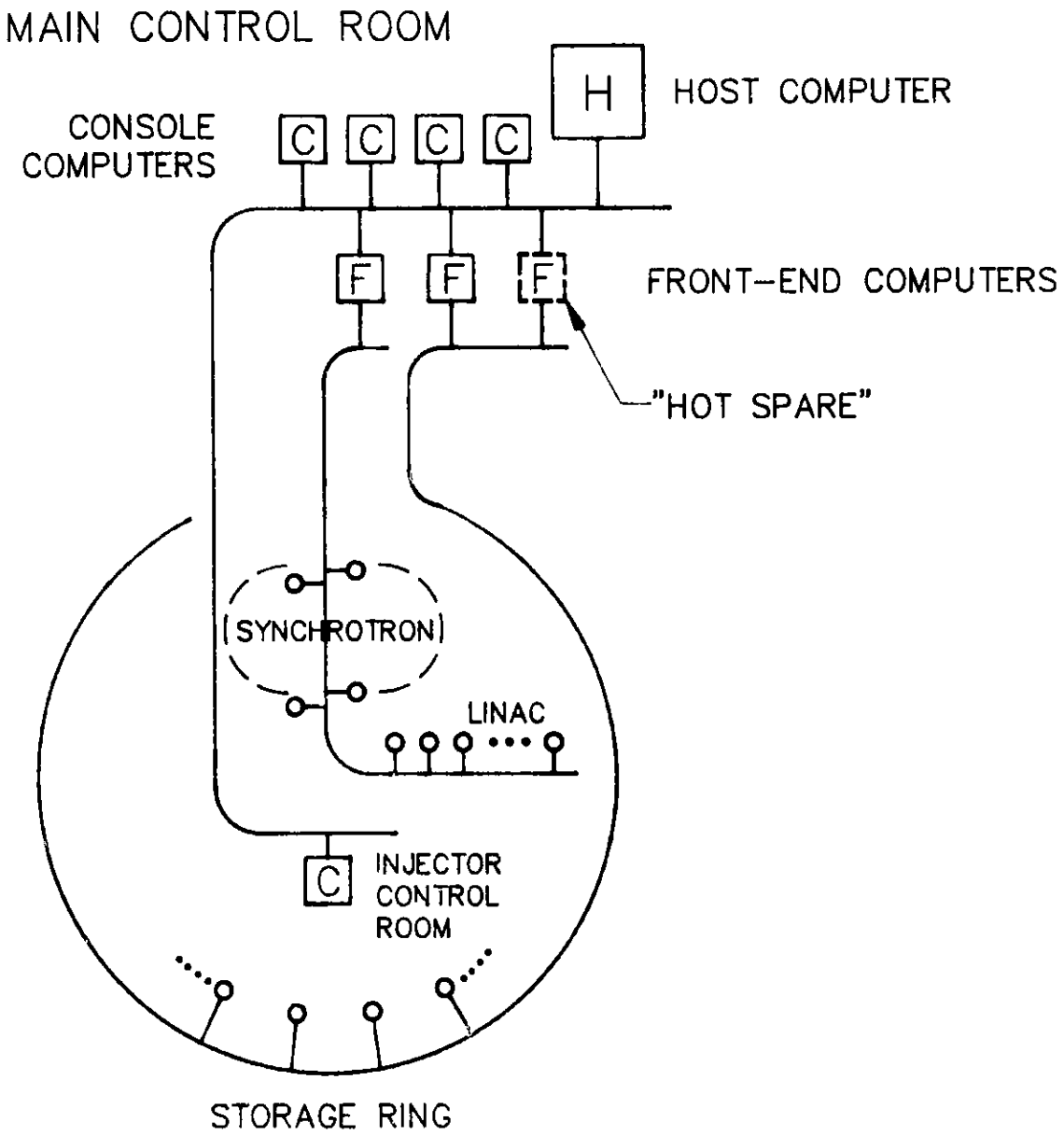

Figure II.8.2-2
Geographic relationship of processors and networks.

8.2.1 Host Computer

The host computer is chosen for its high computation speed, large internal memory capacity, and multiple job stream capability. During the operational phase of the light source, this processor provides database decomposition and downloading, printer and mass storage facilities for other processors in the system, computational services (such as accelerator modeling) for these same processors, and general time-shared services for the control staff involved in software and hardware development. During the development and construction phase, this processor acts as the repository and control point for all software development activities. The capability of the host computer is equivalent to that of a Digital Equipment Corporation (DEC) VAX-8500.

8.2.2 Console Computer

A computer system especially enhanced as an engineering workstation is the primary operator interaction device. Its primary tool is a high-resolution color display system capable of supporting several separate graphic displays simultaneously through the use of "windows." Each window is controlled by separate tasks, all running under a multitasking operating system. A separate microprocessor provides these complex screen services, unloading them from the console computer. Other tasks provide the conventional accelerator interaction tools, such as touch screens and control knobs. Figure II.8.2-3 schematically illustrates the various console features and their tentative arrangement. The console computer also has a virtual memory system, allowing large application programs to be "resident" along with the other tasks and still provide quick response to operator actions.

The console computer capabilities are equivalent to those of a DEC Vaxstation-II/GPX, based on the MicroVAX-II computer. It is estimated to have the computational power of 80 to 90% of a VAX-780. Five identical console systems are provided, with one installed in the injector control area. Both the number and location are, of course, subject to easy adaptation, since they communicate with other processors via a serial network that can reach readily to all areas of the complex. All five console systems have access to all accelerators in the light source complex and, depending on software design, can control any of the various systems. Depending on machine mode (filling, routine storage, autonomous linac and synchrotron operation, initial development, or system maintenance), they are used alone or in conjunction with adjacent console systems.

8.2.3 Front-End Computer

The front-end computers act as interfaces between the host and console computers and the accelerator systems. A separate front-end is provided for each of the major light source components (injector and storage ring), and each maintains a constantly updated database for that component. In this way data needed by the host or

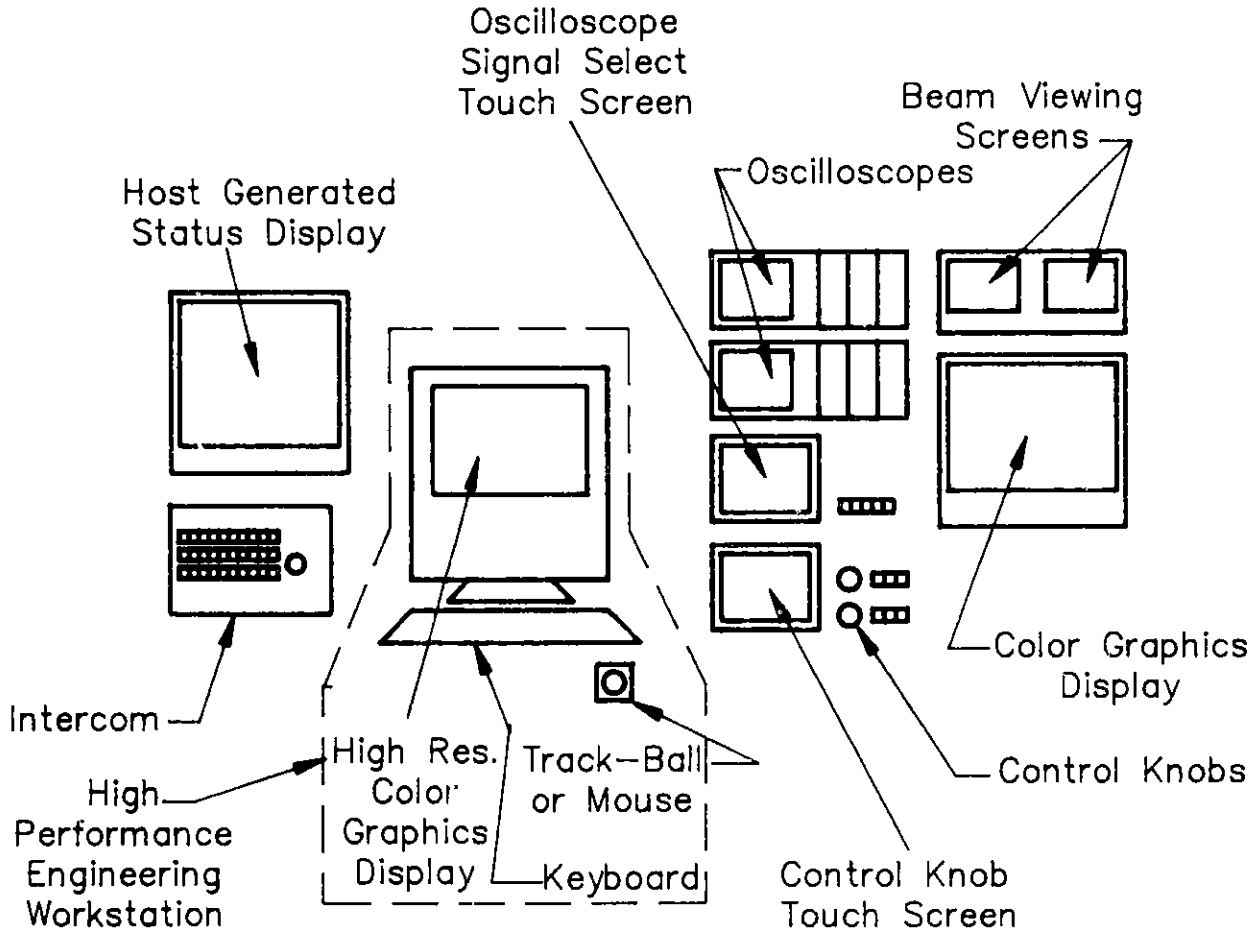

Figure II.8.2-3
Control console features and arrangement (four identical systems provided).

console computers are provided immediately (unless it is a new or time-coordinated data set, in which case an appropriate delay is incurred). (Actually two front-end computers are provided for the storage ring system, as shown in Fig. II.8.2-2; these are described in Section II.8.7, Control System Reliability.) Aside from maintaining a current machine-state database, the primary task of the front-end computer is to take global, multi-parameter data requests from the host and console computers and translate these into one or more data requests for the microprocessor clusters, which do the actual work. Conversely, the data returning from one or several sources are assembled into multi-parameter messages for the host and console computers. Comparison of measured versus nominal operating parameters can also be done in this computer, with error status messages provided over the network or directly via video displays. The capabilities of the front-end computer are equivalent to those of a DEC MicroVAX-II computer. Commonality of parts, operating systems, and software with the console and host computers has a beneficial influence on development and operating costs.

8.2.4 Microprocessor Cluster

The many microprocessor clusters are interconnected with the front-end computers via two system networks, one for the linac and synchrotron, and one for the storage ring. The contents of a typical cluster are illustrated in Fig. II.8.2-4, with the following devices depicted from left to right:

- A network processor, which interprets the network protocol, provides error recovery, and transfers data requests and responses to and from the task processor.

- The task processor, which handles most equipment interface tasks via input-output (I-O) modules or a local network master.

- One or more optional loop processors, which handle high-performance closed-loop functions such as photon beam trajectory control or linac klystron system control.

- A complement of I-O modules, which provide digital-to-analog (D-A), analog-to-digital (A-D), and binary control and monitoring functions.

- An optional local network master, which (through a multidrop network) controls a series of slave crate systems containing additional I-O modules (see Section II.8.2.5).

The task processor design is based on the Motorola 68020 32-bit processor. Additional processors of this type could be added if future needs so dictate. The loop processor choice is based on the needs of the particular control loop. The microprocessor cluster design is based on the Motorola VME crate system because of its advanced

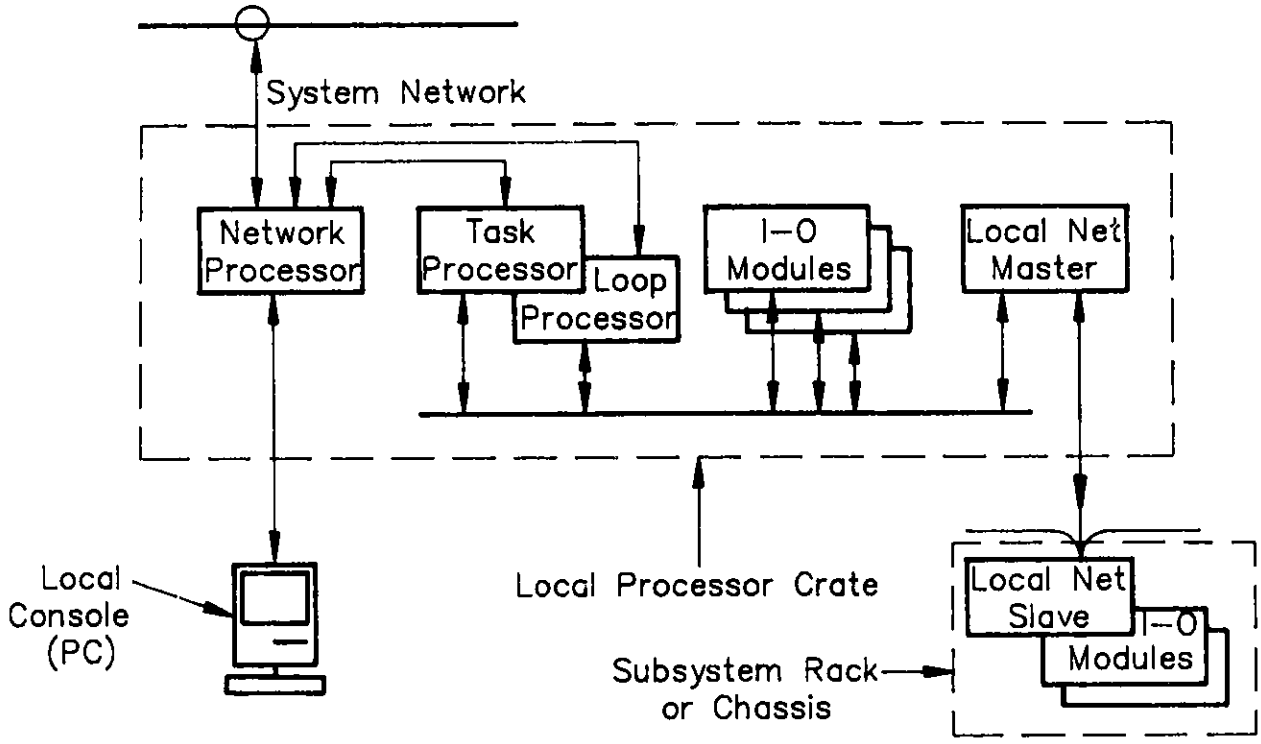

Figure II.8.2-4
Microprocessor cluster components.

processor bus structure, reliable connector system, and multiple vendor support. A local console is implemented through the use of a personal computer connected to the network processor. This console is used in a variety of ways, depending on the software utilized:

- It accesses and uses local I-O modules directly in order to troubleshoot local systems directly.
- It controls the local network master in the same way.
- It reads and writes the task and loop processor memories in order to control, test, and modify their operation.
- Through the network processor, it performs these and other more complex operations by communicating over the system network with other clusters and with the front-end computer.

A local console is provided for about half of the clusters and will have capabilities equivalent to the Apple Macintosh® system. Interference by the local consoles during normal operations is eliminated by front-end computer instructions to the communication processor to discontinue local console service.

8.2.5 Local MIL-1553 Networks

The lowest network level is implemented with the MIL-1553 network protocol. A 1-MHz bit-serial data stream is carried over a multidrop cable to several small crate assemblies located in power supply regulator racks or within diagnostic electronics chassis. These slave crates are used for all applications where high-resolution (14- to 17-bit A-D and D-A) interfacing is needed and where careful control of noise and grounding is required. These applications include virtually all magnet power supplies and most diagnostic systems. A low-performance microprocessor such as the Motorola 6809 is used as a local crate controller and can provide special control intelligence. With a special interface adapter, the local console is used to field- and bench-test this local network and the slave and I-O modules contained in the MIL-1553 crates. Special software loaded into the local console provides sophisticated testing involving a minimum of equipment.

Since these local slave crates control all magnet power supplies, they become the focal point of the coordinated, simultaneous, multimagnet control necessary in storage ring operation. To accomplish this, new magnet settings are downloaded from the host or console computer, through the front-end computer, to the group of several task processors involved. After verifying that all commands have been received accurately, all task processors are commanded to begin issuing current change sequences to the slave crates. Several other scenarios are possible, but the system planned is able to make coordinated changes "simultaneously" to less than 10 μs (see Section II.5.6, Control System and Control Electronics).

8.2.6 Additional Loop Processors

The multiprocessor VME crate system allows the use of additional loop-control digital processors without affecting normal assigned crate functions. A wide range of sophistication is possible, including the use of array processors if necessary. As an example, the photon beam trajectory control system described in Section II.7.7 is handled with a Motorola 68020 having a 68881 floating-point coprocessor. Another possible approach would employ specialized digital signal processing devices, such as the Texas Instruments TMS 320 family, which are designed to process analog signals numerically in real time. Since there is one microprocessor cluster for each pair of insertion device straight sections (a total of 20 around the ring), two such photon beam trajectory control processors share each cluster. The loop gains and polynomial control function parameters are downloaded from the host processor whenever they change as a result of steering, focusing, or other tuning changes.

8.2.7 Host and System Networks

To implement the upper-level, high-performance networks, we employ bus-type, peer-protocol systems. The bus-connected networks permit normal operation with absent, failed, or removed nodes, unlike ring-connected or store-and-forward hubs, which rely on active nodes to relay message streams. A bus network makes small configuration checkouts possible during construction and maintenance periods and allows degraded operation of a system with an inoperable node. A faulty network node can be located and powered down, have replacement modules inserted, be rebooted from the network, and be brought back into service without impairing the use of the network by the remaining network nodes.

A peer-protocol access method extends this philosophy by implementing the access protocol in each node, instead of having a master node that would poll the nodes or otherwise keep track of their normal operation. This Local Area Network (LAN) is the Carrier-Sense, Multiple-Access with Collision Detection (CSMA/CD) protocol, also known as Ethernet. This system has wide industry acceptance due to national standardization and in-service success and reliability.

The use of the CSMA/CD protocol, which resolves simultaneous access attempts with randomly delayed retries, may incur delays when many diagnostic or error messages are produced by the microprocessor clusters as a result of activities that are deliberately or accidentally simultaneous. Since this condition is seen to be likely, an internal protocol layer is implemented that will prioritize these messages in two levels. High-priority error or alarm messages use the normal procedures without delay, while routine front-end-directed responses await specific requests for their transmission.

The host network has a LAN bridge node, which allows communication with the experimental data network (see Fig. II.8.2-1, top). This link serves to provide the experimental area with pertinent operational information and acts as a means for the

beam line personnel to request photon beam steering changes when this becomes possible. The bridge node also prevents excess network traffic by blocking control system traffic from the data network and vice-versa.

8.3 Software

The same separation of function described above with respect to the various processor types and duties is reflected in the software structure and operation. A comprehensive database defines all machine parameters, both real and virtual. This database is edited and maintained in the host computer. It is broken down, encoded, and separated into parts appropriate for use in the various locations and hierarchical levels. These parts are then downloaded to the various processors, where they are used to obtain needed information. Such a database system is in use at SLAC.[7]

8.4 Other Services

8.4.1 Timing System

Two classes of timing coordination are necessary, the first being associated with the need to control beam transfer events and signal sampling in the linac and synchrotron. The second class is associated with the need to control sampling of positron beam position in the storage ring. Both systems use essentially the same methods, but with different clock rates and sources. Depending on the mode of operation, various delay counts are downloaded to the microprocessor clusters and set into clock-delay modules in the VME crates. After a systemwide start pulse is received, the delay modules count a clock source and produce a pulse output after their programmed delay. For event sequencing in the synchrotron, a crystal-derived clock is used that produces real-time triggers. For sampling beam parameters, an rf-based clock is used. The delay calculation takes into account the location of the module and the location of the beam bunch at the time the start pulse is issued. In this way a single bunch is tracked around the machine or all bunches are sampled simultaneously. The timing resolution needed is the interbunch spacing with some margin, since the beam diagnostic electronics is beam-triggered after being armed by the timing pulse. Such a system is in use at SLAC for the same purpose and with similar timing requirements.[8] A system based on a MicroVAX-II has also been described.[9]

8.4.2 Oscilloscope Signal Cross-Bar System

In order to convey the hundreds of high-bandwidth signals to the control console areas and to accommodate the console flexibility described above, a distributed cross-bar connection system is used. The coaxial relay modules are distributed with and controlled by the microprocessor clusters. At the console end the signals are finally switched to the

desired display or instrument. The choice of signal and destination of output are selected by the operator using a touch-screen display.

8.4.3 Beam-View and Access-Control Television

The same distributed cross-bar method used for signal patching is also used for video sources. Again the computer system provides the control. The signals terminate in the console areas and are further gated to selected video displays in the access-control consoles, as well as the operational consoles. In the case of the beam-view video sources, they can be gated to television frame-store memories or to a videocassette recorder for later static or dynamic study, respectively.

8.4.4 Intercom System

A multiline intercommunication system is provided for each major light source component (linac, synchrotron, and storage ring). Eight communication circuits are provided for the local component, plus two tie-lines for each of the other two. Consoles are provided full access to all three components. The door access intercom system is separate and interconnected with the door release system. Access-control console positions are provided in both the main and injector control areas.

8.4.5 Network Access from Offices and Laboratories

Terminal server units are connected to the host network to allow terminal usage with the control system from the office and laboratory areas of the operational staff. This facilitates equipment checkout, status inquiries, and software development to take place on a noninterfering basis. Actual control of the various systems is highly restricted and controlled by the host software required to make such links.

8.5 Relation to the Injection System

The network-connected, modular design of the control system makes possible two important features regarding the injection accelerators:

- Operational independence is provided by the full-feature control console located in the injector control area. As long as the host computer and its network are operational, the injection accelerators can be considered as completely autonomous systems.

- During machine commissioning or subsequent accelerator research with the linac and synchrotron, the full capabilities of the three main control area consoles can be utilized.

8.6. Expert Systems

The APS will be a large, complex machine with many beam lines. The task of commissioning a machine of this size generally involves a sequence of iterative steps. The beam is injected, diagnostic devices are monitored, and then magnet currents are adjusted. These steps are repeated as the beam travels further around the ring and can take a considerable length of time to perform. Because of the time and costs involved in the commissioning, we will investigate the use of artificial intelligence (AI) techniques in the form of an expert system to help tune the beam. The use of expert systems is now being investigated by several accelerator laboratories.[10-12] An expert system is a computer program that can perform a task normally requiring human expertise or experience. Typical characteristics of these systems are their use of "qualitative" processing, flexibility, and ability to handle very complex problems.

8.7 Reliability and Safety

Control system reliability is divided into two broad categories -- software and hardware. With respect to software, there is a growing realization that as software functions and features become more complex, exhaustive pretesting of all operational contingencies becomes impossible. To this end, run-time self-checking of both hardware and software facilities and error recovery procedures are utilized to make the system fail-safe, or at least fail-soft. The penalty paid for this capability is prolonged processing time and additional memory space. For these reasons relatively high-performance processors are used in the cluster, front-end, and console systems.

Reliability of control system hardware is enhanced through the use of proven processors and network concepts. Quick recovery from failures of system components (in some cases without loss of control or the stored beam) is facilitated by the following features:

- A running "hot spare" is provided for the storage ring front-end computer. Connections are made to the host and system networks in parallel with the primary front-end, as shown in Fig. II.8.2-2, and the database of the "hot spare" is periodically updated so that a quick and possibly transparent changeover is achieved. Since the same processor type is used for all front-end and console computers, this extra processor also acts like a ready "cold spare" as well.

- After filling the storage ring, the host computer provides what might be considered nonessential services (printing, archiving, computation assistance, and general time-sharing services), so it is possible to maintain continued operation of the various systems in a degraded mode without the host computer or any of its peripherals.

- Since all five console systems are provided with access to all accelerator systems, normal operation can continue with a console out of service.

For those areas involving both personnel safety and vacuum system protection, hardwired circuits are used; these circuits are monitored by the control system. The access-control console (duplicated for the linac and synchrotron in the injector control area) communicates with the various access door intercoms and door release mechanisms simultaneously in order to ensure proper door operation. Access door switches are monitored by the control system so that interlock chain breaks can be graphically presented to the operator as a troubleshooting aid.

Vacuum system protection is provided by dedicated, hardwired modules that provide interlock logic for valve operation. Remote valve operation through the control system (where possible) is passed through this same permit logic. All valve position and vacuum level data used by these chassis are monitored by the control system, again to help in trouble diagnosis and general vacuum system surveillance.

8.8 References

1. N. Phinney, "Current Status of the SLC Control System," presented at the 1985 Accelerator Controls Workshop, Los Alamos Scientific Laboratory (October 1985).

2. B. Culwick and J. Smith, "Status of the NSLS Controls Upgrade," presented at the 1985 Accelerator Controls Workshop, Los Alamos Scientific Laboratory (October 1985).

3. S. Brown et al., "The LAMPF Controls Upgrade," presented at the 1985 Accelerator Controls Workshop, Los Alamos Scientific Laboratory (October 1985).

4. C. Cork et al., "A Networked Real Time Control System for the Stanford Photon Research Laboratory," IEEE Conference Record 87CH2837-9.

5. M. Lee et al., "Modern Approaches to Accelerator Simulation and Control," IEEE Conference Record 87CH2837-9.

6. A. Abola et al., "Experience in Using Workstation as Hosts in an Accelerator Control Environment," IEEE Conference Record 87CH2832-9.

7. N. Phinney, "Implementation of the SLC Control System Database," presented at the 1985 Accelerator Controls Workshop, Los Alamos Scientific Laboratory (October 1985).

8. K. Thompson and N. Phinney, "Timing System Control Software in the SLC," IEEE Trans. on Nucl. Sci., NS-32, 2123 (1985).

9. J. Potter et al., "Programmable Master Tuner System," IEEE Conference Record 87CH2837-9.

10. S. Clearwater et al., "Prototype Development of a Beam Line Expert System," IEEE Conference Record 87CH2837-9.

11. D. Weygand, "Artificial Intelligence and Accelerator Control," IEEE Conference Record 87CH2837-9.

12. E. Malandain and P. Skarek, "An Expert System for Accelerator Fault Diagnosis," IEEE Conference Record 87CH2837-9.

9.1 Introduction

The primary purpose of the 7-GeV Advanced Photon Source (APS) is to provide insertion device-based radiation sources. Two types of insertion devices (IDs), undulators and wigglers, have been developed to satisfy the requirements of various investigations. These requirements include: (a) the need for pseudo-monochromatic radiation from the first few harmonics of undulators with ultrahigh spectral brilliance or brightness, tunable from about 3 keV to 40 keV, (b) sources a few micrometers in size, (c) radiation with specific polarization characteristics, (d) extremely low divergence radiation, and (e) matching of the radiation characteristics with those of the x-ray optical elements for optimum utilization of such sources. There should be flexibility to install newer devices, such as those producing broad-band undulator radiation and circularly polarized hard x-rays.

Any of the above capabilities can be provided by a proper match between the characteristics of the storage-ring and those of the IDs. Unlike the IDs presently retrofitted on existing storage rings, the undulators and high-brightness wigglers on the APS storage ring are highly optimized in performance, and form an integral part of the design. In addition, the design of the storage ring and the IDs is flexible, in order to accommodate improvements in the use of ID radiation and new applications.

9.2 Nature of Insertion Devices on the APS

The distinction between the two types of IDs, wigglers and undulators, is based on the value of the so-called deflection parameter, K, and the horizontal opening angle of the radiation, θ_H. These are given by

$$K = 0.934 \quad B_o \, \lambda_o$$

and

$$\theta_H = \pm K/\gamma \quad ,$$

where B_o is the peak magnetic field in the device in Tesla, λ_o is the spatial period of the magnetic structure in cm, and γ is the relativistic enhancement of the positron rest energy; γ = 13699 for 7-GeV.

When K is small (<4), the device is called an undulator. The radiation from various periods of an undulator has constructive interference effects which results in a

spectrally-compressed series of narrow peaks at harmonics of the fundamental energy, E_1. This energy is given by

$$E_1(\text{keV}) = \frac{0.95\ E^2\ (\text{GeV}^2)}{\lambda_0(\text{cm})\ (1 + K^2/2)} \quad ,$$

where E is the positron energy. The following are important features of APS undulators:

- The undulators on the APS ring built with available Nd-Fe-B hybrid magnet technology deliver fundamental radiation with energies ranging from a few hundred eV to 22 keV. The typical on-axis, angle-integrated brilliance for the fundamental radiation ranges from 10^{18} to 10^{19} photons/s/0.1%BW/mrad^2/mm^2.

- A fully tunable undulator with a 3.3 cm period on the 7-GeV APS will deliver radiation approximately from 4 to 13 keV in the fundamental and from 12 to 40 keV in the third-harmonic. The energy tunability is achieved by varying the undulator gap from 1.0 cm to about 2.8 cm.

- For applications needing only the high-energy undulator fundamental radiation, a device with a period of 2.3 cm will be tunable from 13 to 20 keV through gap variation.

- The phase space dimensions of the photon source are nearly equal to that of the positron beam for the hard x-rays delivered by the APS undulators, and is minimized to deliver very high brilliance.

- The vacuum chambers for the undulators will permit a minimum gap of either 1.4 cm or 1.0 cm. The former chamber will be used during the initial operation of the APS.

- Because the various applications of the APS undulator radiation impose little demand for harmonics higher than the third,[1] the required magnet design tolerances are well within those achieved for existing devices. The lower limit of 0.5% in field error achievable with present day technology is more than sufficient for the successful operation of the undulators planned for the APS.[2]

When K is large (>10), the device is called a wiggler. The peaks of higher harmonic radiation of a wiggler tend to smooth out, due to the smearing effects of the positron-beam emittance and energy spread. This results in a smooth spectrum, similar to that from a bending magnet (BM). The intensity of the radiation from a wiggler with N periods is approximately equal to an incoherent sum of the intensities from 2N poles. One can also increase or decrease the energy of the photons from a wiggler by a proper

choice of B_0, while maintaining a large value of K. The photon critical energy for the APS operated at 7 GeV is given by

$$\varepsilon_c \text{ (keV)} = 32.59\ B_0 \quad .$$

Several important features of the APS wigglers deserve mentioning:

- They will rarely require magnetic fields produced by superconducting magnets. The field provided either by Nd-Fe-B hybrid magnets or by conventional electromagnets is adequate to obtain large K values and nearly-smooth photon energy spectra.

- Because of the relatively large value of γ, the value of θ_H for the APS wigglers is approximately ±1 mrad. Hence, the APS wigglers deliver very high-brightness hard x-rays, compared with those on low-energy storage rings.

- The availability of 6-m straight sections is suitable for long-period wigglers designed to provide radiation of low critical energy. These devices (with K ~10) operate with $\beta \approx 10$ m, and provide a low divergence photon beam. These high-brightness wigglers are unique to the present machine and are essential for many research programs.

- In many investigations, there is a need for radiation with linear polarization along the vertical axis. A design for a high-brightness wiggler with a hybrid magnet configuration which generates such polarization is presented in Ref. 3.

- For wigglers with a Nd-Fe-B hybrid configuration and $\lambda_0 = 8$ cm, the magnet gap, G, needed to produce a 1.2-T peak field is 2.1 cm. A design for a rigid vacuum chamber with a vertical aperture of 1.4 cm, appropriate for this wiggler, is presented in Section II.9.4.3.

The IDs with $4 < K < 10$ produce energy spectra with features that are intermediate between those of undulators and wigglers.

More details on all the above aspects of the various APS IDs are presented in Refs. 3, 4, 5, and 6. Design studies for two tunable undulators and a wiggler-undulator are presented in Sections II.9.4, II.9.5, and II.9.6. A detailed study of the interaction of IDs with the storage ring is presented in Section II.1.6. The measuring facility for IDs is discussed in Section II.4.9.

9.3 Tunability of Radiation and Choice of Storage Ring Energy

For the APS, the original user requirement[7] for an undulator with a 20-keV fundamental photon energy can be met at a storage ring energy of 6 GeV and the

proposed ring aperture.[8] However, as additional capabilities of the undulator sources were investigated,[9] it became evident that, at 6 GeV, the tunability of undulators with fundamental energies above 10 keV is rather limited. As a result, as many as five undulators would be needed in a single straight section to span the photon energy interval of 5 to 20 keV. The expense and complication of having so many undulators in a given straight section, with the capability of switching from one device to another was an incentive to look for alternate ways to increase the tunability of a single device. As was pointed out,[9,10] the tunability range of an undulator is a complex function of the minimum storage ring aperture and the positron energy.

For hybrid magnets based on Nd-Fe-B magnet blocks and vanadium permendur pole tips, B_o is given by

$$B_o = 0.95 \times 3.44 \exp [- R (5.08 - 1.54 R)] \quad ,$$

where $R = G/\lambda_o$ and G is the undulator gap in cm. In the above equation, the factor 0.95 represents the "filling factor" of the high-permeability blocks in the undulator assembly. This equation is valid only in the interval $0.07 \leq R \leq 0.7$ and only approximately represents the peak field for $0.7 < R \leq 1$. For $R > 0.7$, however, the value of K for small period devices becomes small and results in a small photon flux. Hence, we have taken the ratio R = 0.85 as a conservative and "safe" upper limit for the devices discussed below.

Within all the above constraints, the tunability of an undulator on the APS can be analyzed using the above equations. The analysis is presented in detail in Ref. 10. In Fig. II.9.3-1, the relationship between the storage-ring energy and the gap is shown, which relates to the recommendations of the National Task Group given in Chapter I. The design energy of 7 GeV and the capability to operate the storage ring as high as 7.7 GeV will adequately provide for the required tunability of undulator radiation. The following points are noted:

- During the initial period of operation, the vacuum chamber will permit a minimum ID gap of 1.4 cm.
- The minimum gap will be reduced to 1.0 cm after mature operation is attained. This will increase both the tunability range and the photon brilliance.
- The undulators designed for the initial operation period will deliver their full performance during the mature operation.

The first undulator (A), with a period of 3.3 cm, fulfills all the above operational criteria based on the recommendations of the National Task Group. The characteristics are presented in Figs. II.9.3-2 and II.9.3-3, in which are plotted the tunability of this

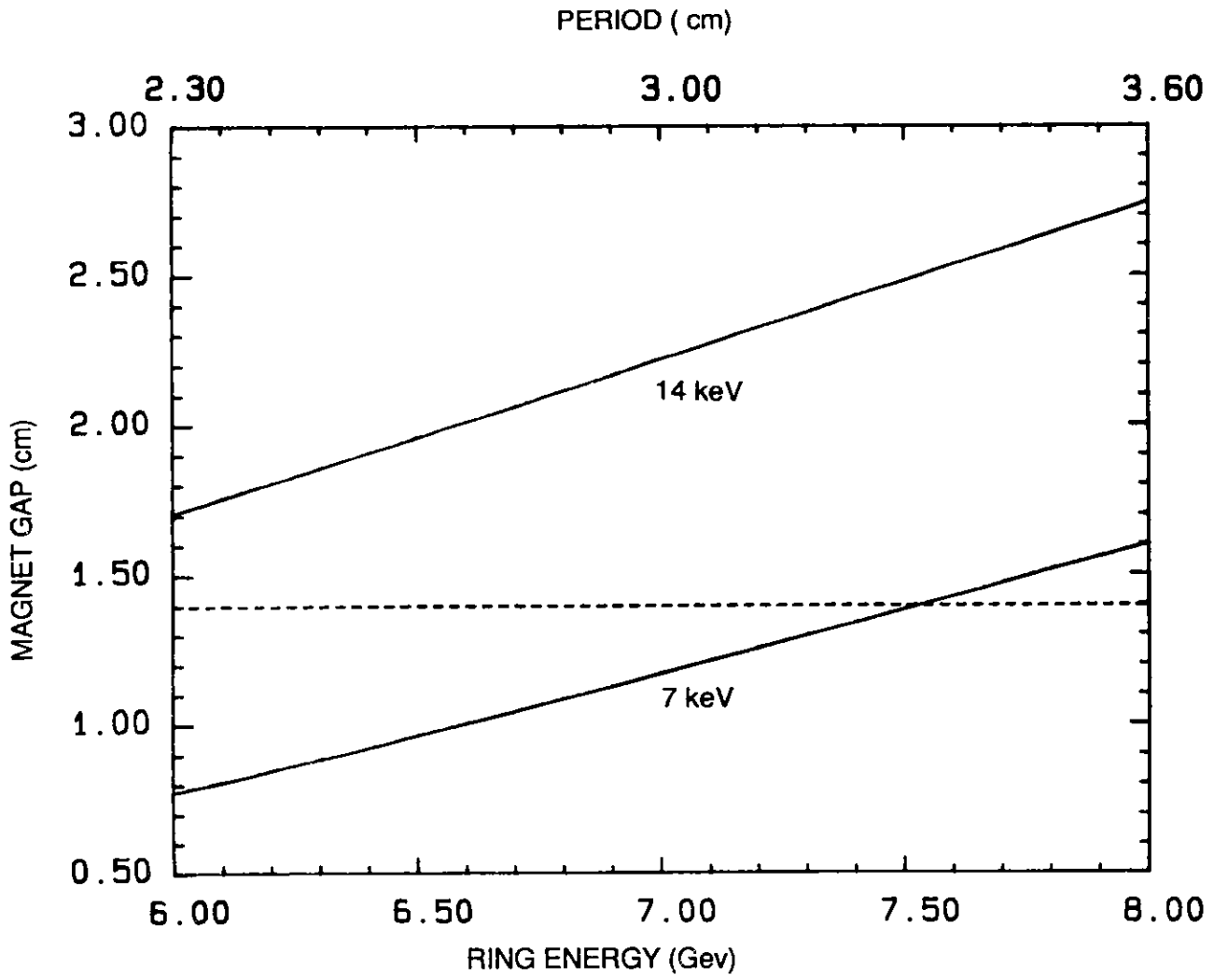

Figure II.9.3-1

The magnet gaps required for an undulator to produce fundamental radiation between 7 and 14 keV as a function of storage ring energy. The period of the device at each ring energy is also shown in the figure. The horizontal line corresponds to the initial APS operation at a minimum gap of approximately 1.4 cm.

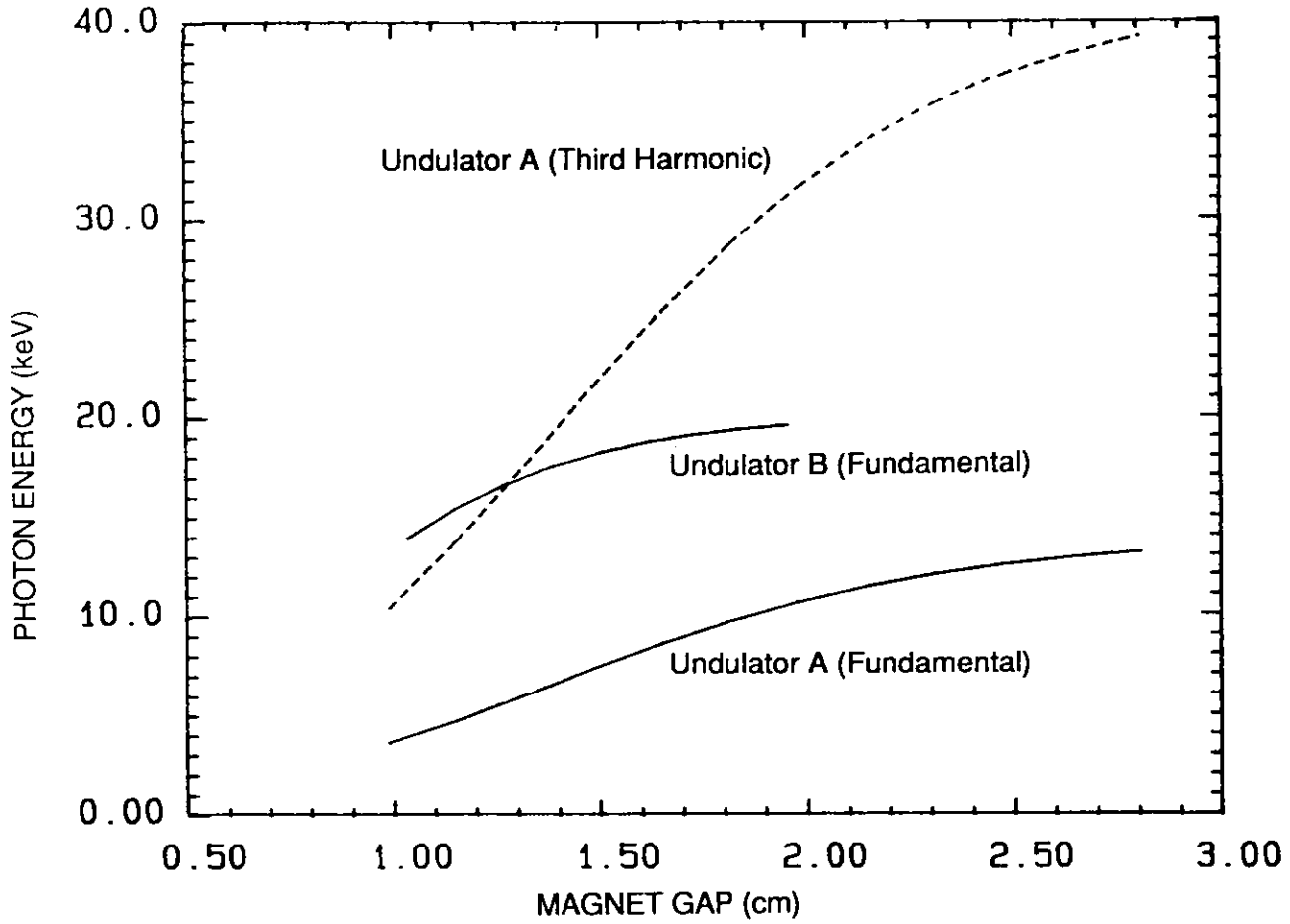

Figure II.9.3-2
Tunability of fundamental undulator radiation of devices A and B as a function of magnet gap for the 7-GeV APS. The tunability of the third-harmonic of device A is shown by the dotted line.

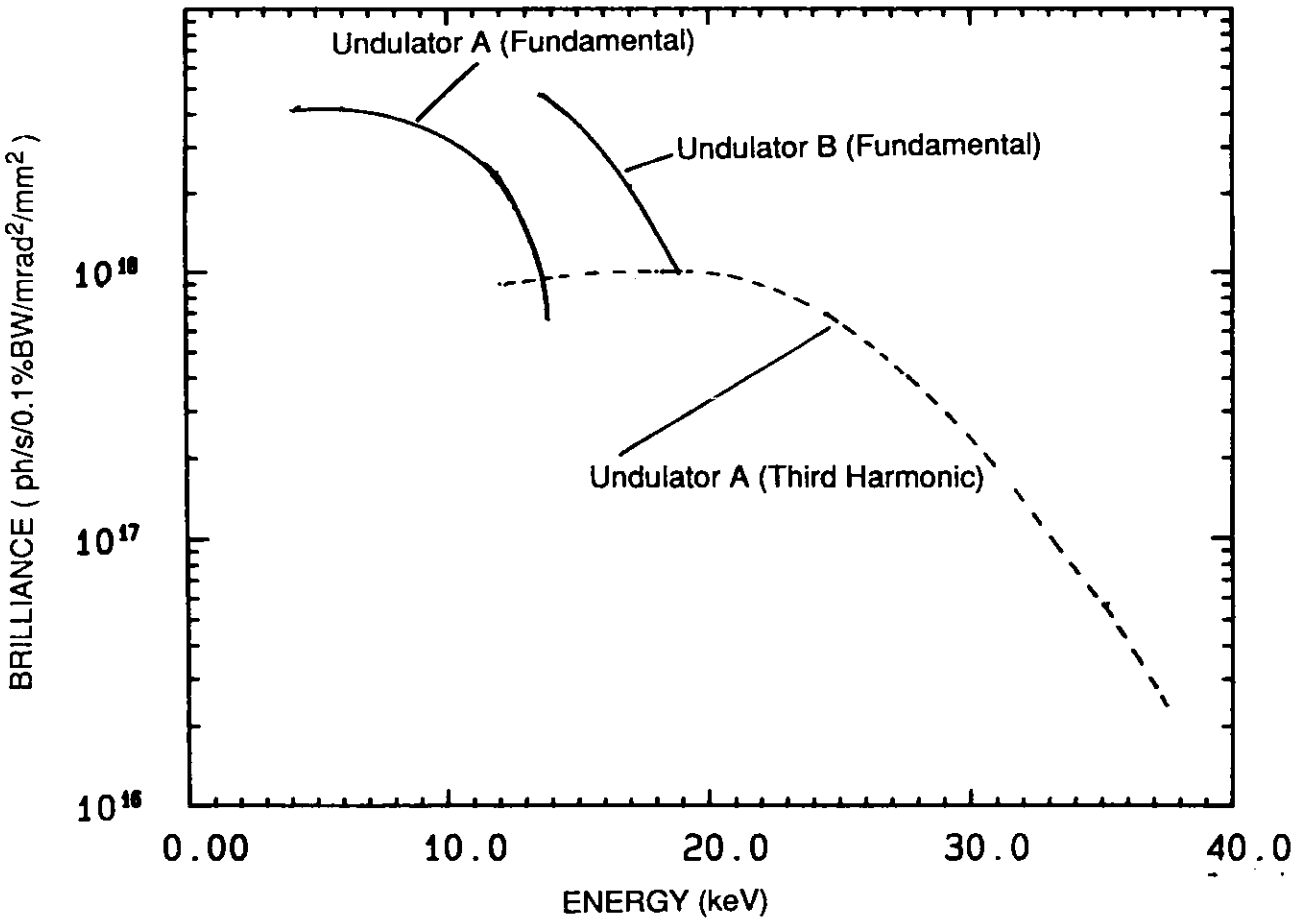

Fig. II.9.3-3
The angle-integrated on-axis brilliance of fundamental and third-harmonic radiation from undulator A and the brilliance of fundamental radiation from undulator B at various photon energies for the 7-GeV APS with 100 mA stored current.

device in terms of the brilliance from the fundamental and the third harmonic as a function of the photon energy.

A second undulator (B), with a period of 2.3 cm, also satisfies the recommendations by the National Task Group. Its tunability and the brilliance characteristics are also shown in Figs. II.9.3-2 and II.9.3-3. The parameters of both undulators A and B during the initial operation at 7.5 GeV and the mature operation at 7.0 GeV are given in Table II.9.3-1.

9.4 Tunable Undulator A

9.4.1 Introduction

One of the undulators (A), as seen above, satisfies the user criteria of providing first-harmonic tunability over the energy range from 7 to 14 keV during the early operation, and from 3.5 to 13.0 keV during mature operation. This criteria for the tunability is set because of the needs of a host of scientific experiments. This section presents a preliminary design study of such an undulator.

Table II.9.3-1

The Tunability Parameters of Two Undulators on the APS Which Satisfy the Recommendations of the National Task Group

		Fundamental Energy Range					
Undulator	Period (cm)	E_{min} (keV)	Gap_{min} (cm)	K_{max}	E_{max} (keV)	Gap_{max} (cm)	K_{min}
Initial Operation (7.5 GeV):							
A	3.3	7.0	1.4	1.6	14.5	2.8	0.4
B	2.3	19.0	1.4	0.6	21.5	1.9	0.3
Mature Operation (7.0 GeV):							
A	3.3	3.5	1.0	2.5	13.0	2.8	0.4
B	2.3	13.0	1.0	1.1	19.5	2.0	0.3

9.4.2 Preliminary Design Parameters[11]

The transverse undulator, A, has a hybrid magnet configuration in which the magnetic field strength and distribution depend on the geometry of the pole tips. The field quality is much less dependent on the magnetic and geometric quality of permanent magnets. For this hybrid geometry, the magnetic material is Nd-Fe-B. The design of this device is based on a preliminary optimization of the magnetic structure with vanadium permendur pole tips. In this procedure, various geometrical parameters of the structure are iteratively optimized through a two-dimensional field computation (yz plane). The resulting parameters are presented in Table II.9.4-1. Three-dimensional effects are estimated in order to obtain a pole width and a magnet width which provides the required field homogeneity.

Table II.9.4-1

Optimized Parameters of a Nd-Fe-B Hybrid Undulator A

Undulator Period, λ_o (cm)	3.3
Magnet Gap Range, G (cm)	1.0 - 2.8
Pole Width in x Direction (cm)	5.0
Pole Height in y Direction (cm)	3.5
Pole Thickness in z Direction (cm)	0.62
Magnet Width in x Direction (cm)	6.6
Magnet Height in y Direction (cm)	4.2
Magnet Thickness in z Direction (cm)	1.03
Pole-Tip Overhang in y Direction (cm)	0.08 to 0.1
Peak Field Range on Axis, B_o (T)	0.78 to 0.21
Peak Field Increase (%) at 0.1 cm off Axis in y Direction	2.0
Maximum Length Available for Undulator (m)	5.2
Maximum Undulator Periods, N	158

Figure II.9.4-1 shows the optimized two-dimensional magnetic flux lines of a quarter period of the 3.3-cm undulator at a gap of 1.4 cm. The shapes of the vanadium permendur pole-tip and the Nd-Fe-B permanent magnet shown in the inset in Fig. II.9.4-1 were optimized to have sinusoidal field variation along the undulator axis, to avoid flux saturation at the corners of the pole-tip, and to avoid demagnetization of the permanent magnet. This optimization reduces the peak field by only 2% from the maximum expected value of 0.5 T.

The field variation along a quarter period of the undulator at its minimum gap of 1.4 cm is shown in Fig. II.9.4-2. At points y = ±1 mm from the undulator axis, the field increase is 2% for various gap values.

The widths of the pole-tips and the permanent magnet blocks are determined from harmonic analysis. The pole-tip width of 5.0 cm is wide enough that the undulator field configuration can be considered as two-dimensional.

The following dimensional tolerances are estimated from a two-dimensional field analysis:

Thickness tolerance	0.05 mm (± 2 mil)
Height tolerance	0.25 mm (±10 mil)
Width tolerance	0.25 mm (±10 mil)

The undulator assemblies have magnetic field end-correctors.

The angle-integrated on-axis brilliance of the fundamental radiation from this undulator A at different gaps is shown in Fig. II.9.4-3.

It should be pointed out that the Argonne team has collaborated with a Cornell group on the design of a 3.2-cm period Nd-Fe-B undulator to be operated on Cornell High Energy Synchrotron Source (CHESS) and this 2.4-m long device is now being built.[12] This is a prototype of the APS undulators and is expected to be commissioned in early 1988.

9.4.3 Insertion Device Vacuum Chamber Mounts

Rigid vacuum chambers are installed in the straight sections of the storage ring for IDs. During initial operation, the chambers will have a minimum magnet gap of 1.4 cm, and during mature operation, 1.0 cm. In addition, a similar vacuum chamber with 1.4-cm gap has been designed. The following discussion is limited to the 1.0-cm gap vacuum chamber.

This vacuum chamber has two sections; the beam chamber and the pumping antechamber, as shown in Fig. II.9.4-4. A Zr/Al NeG pumping strip is mounted in the

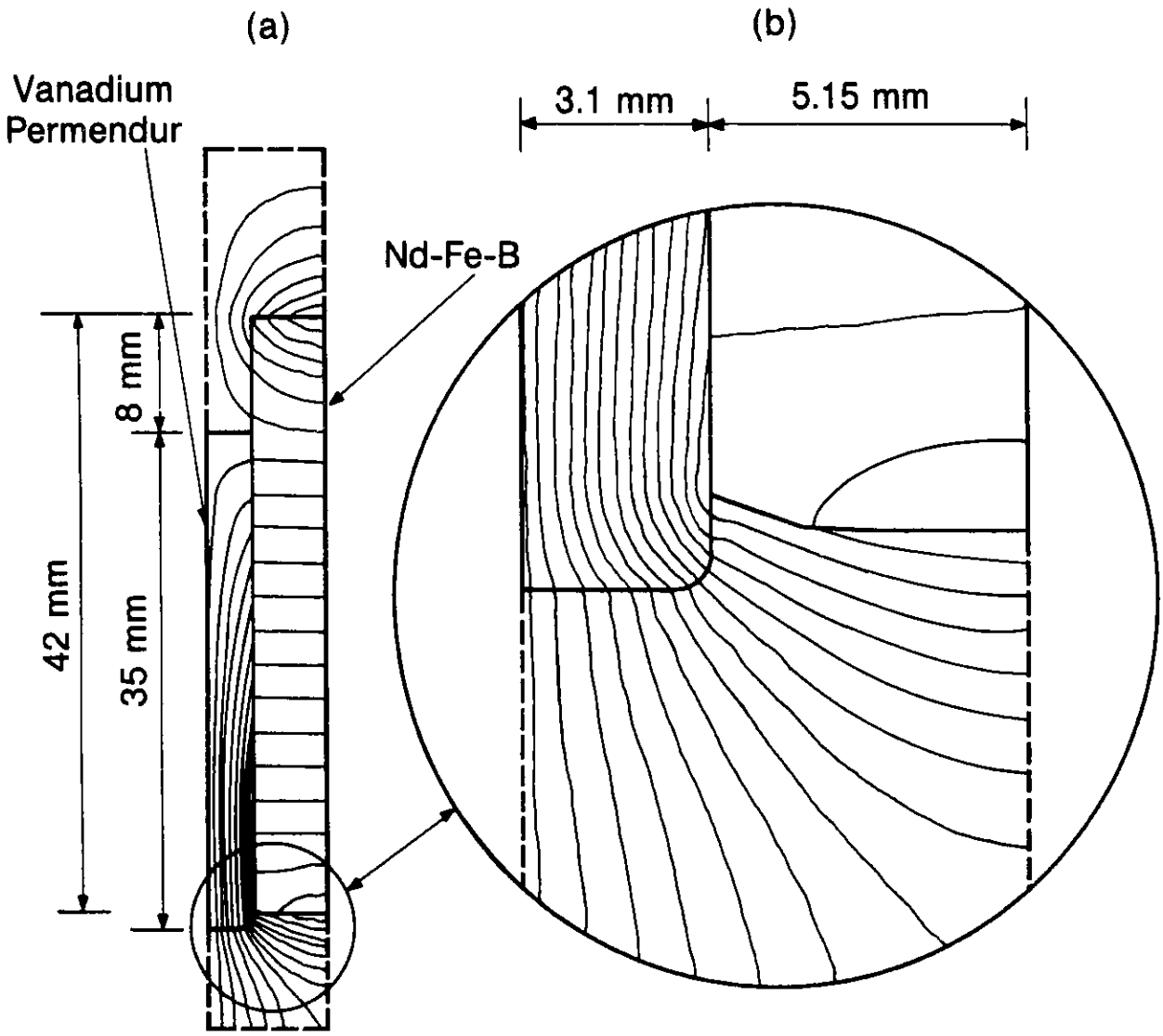

Figure II.9.4-1
Magnetic flux profile of a quarter period of undulator A showing the dimensions of the pole and permanent magnet pieces. The inset shows the detail of the pole and permanent magnet shaping used to avoid saturation and demagnetization.

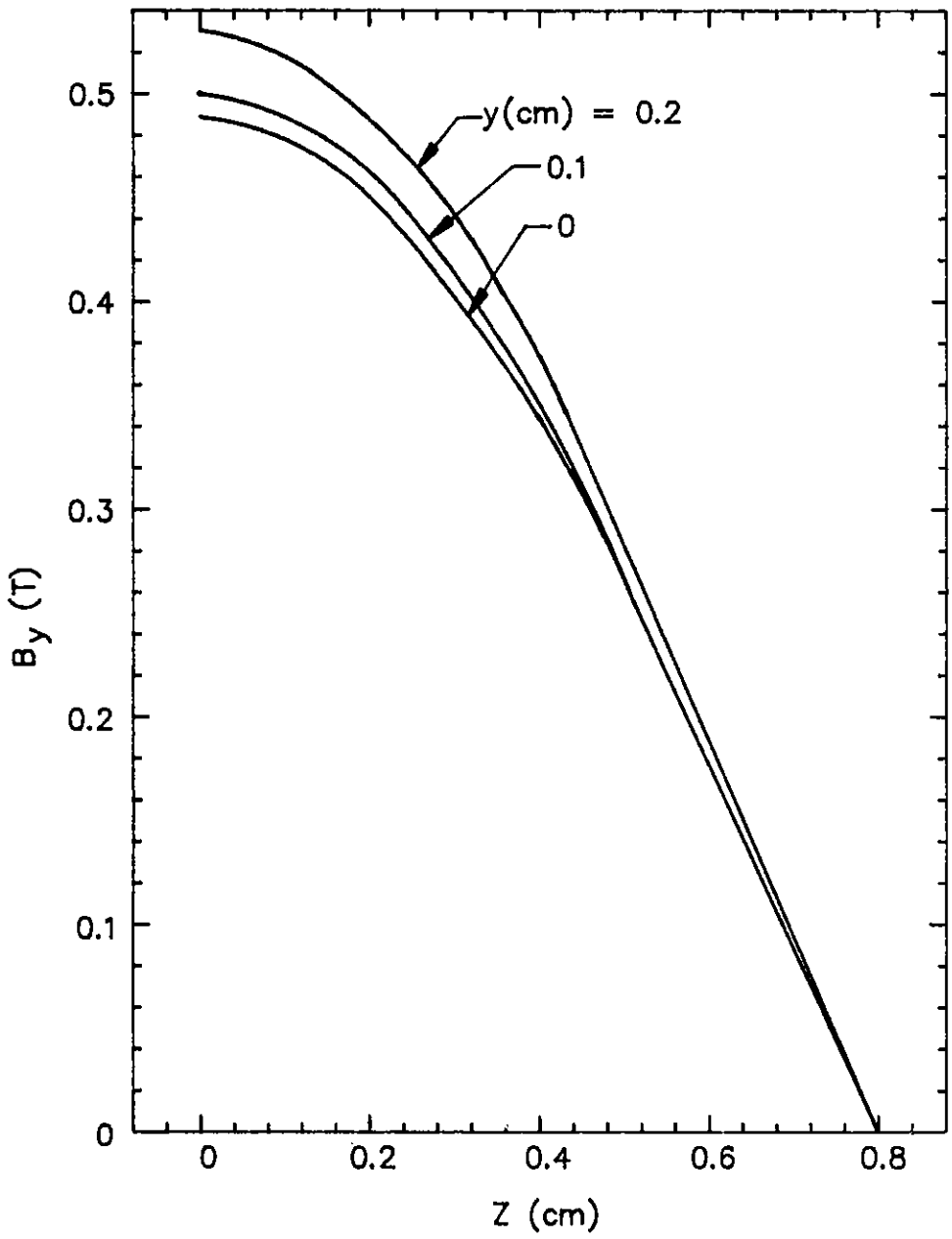

Figure II.9.4-2
Magnetic field variation along the undulator axis (z) over a half-period of undulator A at a gap of 1.4 cm. The y values are distances above and below the mid-plane.

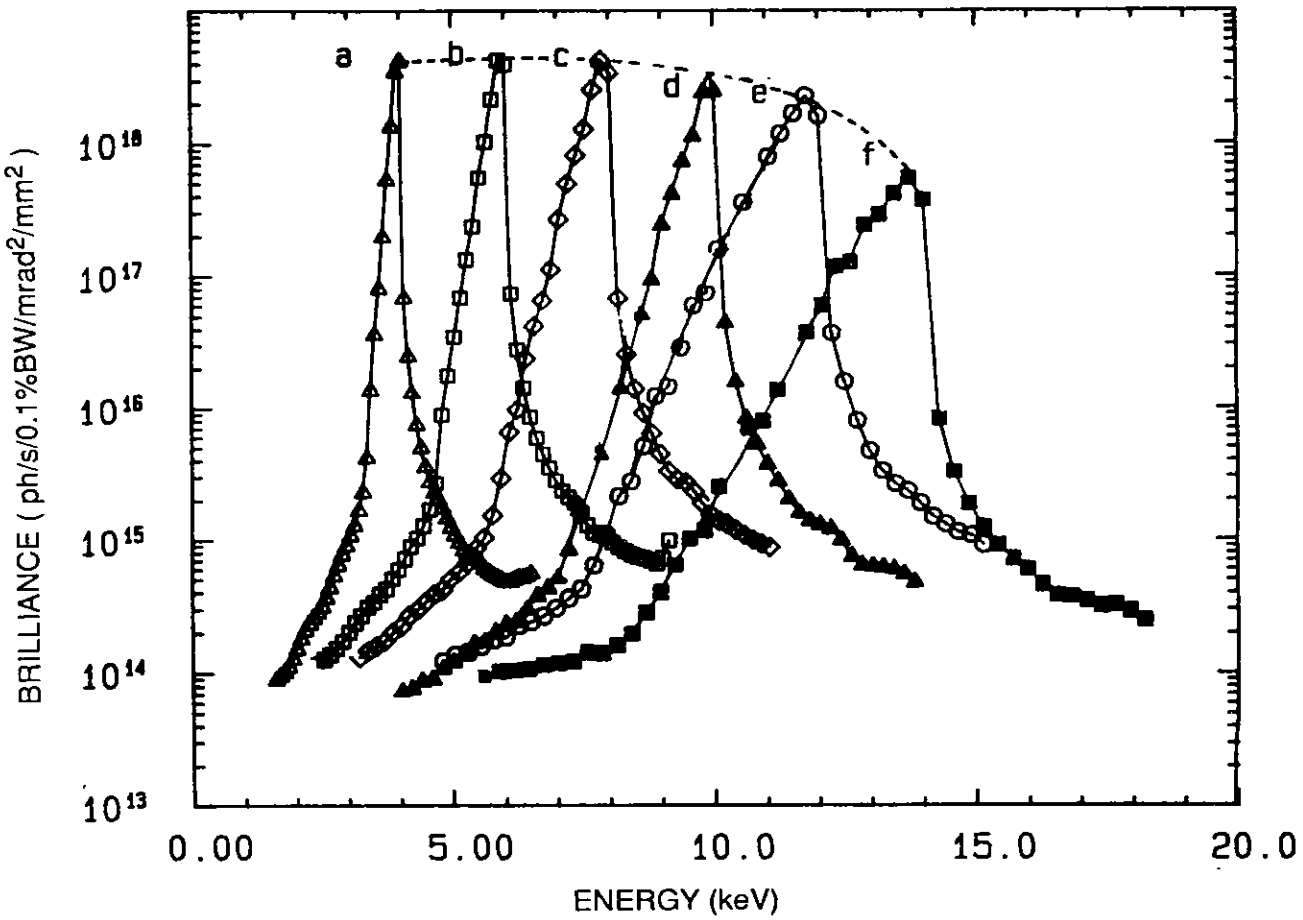

Figure II.9.4-3

The angle-integrated brilliance of the fundamental radiation from the undulator A on the APS with 100 mA at 7 GeV. The fundamental peaks at various photon energies are obtained at magnet gap settings of a) 11.2 mm, b) 13.9 mm, c) 16.5 mm, d) 19.7 mm, e) 24.7 mm, and f) 30.1 mm. These calculations include the phase space dimensions of the positron beam.

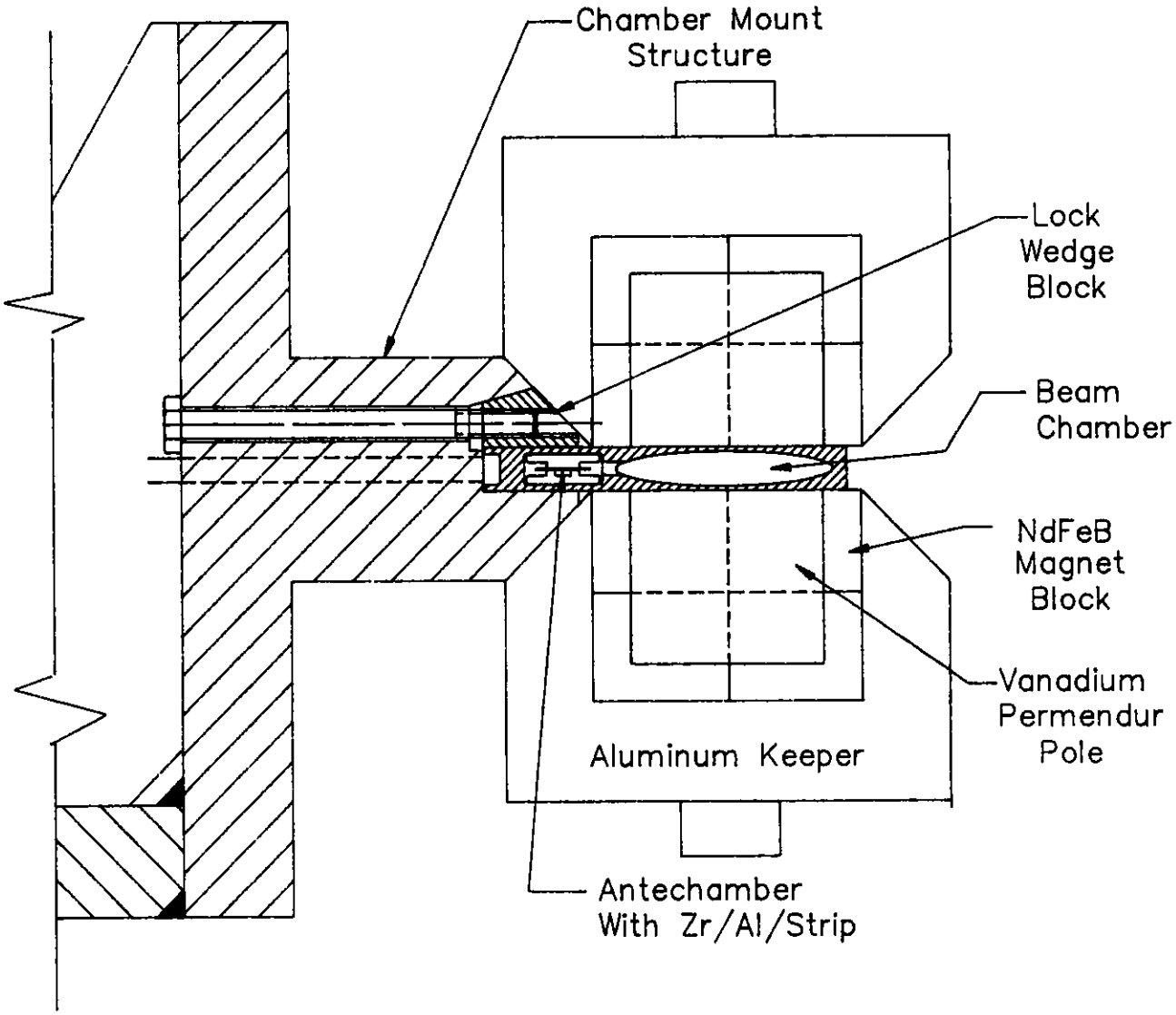

Figure II.9.4-4
A cross section of the ID vacuum chamber and its support. Part of the undulator A assembly is also shown.

antechamber. The entire aluminum vacuum chamber is extruded using standard techniques. The beam chamber and antechamber are connected by a series of slots (1.0 cm long x 0.4 cm high), which are milled in the wall separating the two chambers in the extruded piece. Each slot has a conductance of approximately 1.6 ℓ/s. The initial effective pumping speeds of the vacuum chamber at room temperature for CO and H_2 are 50 and 150 ℓ/s per meter of ID length respectively, assuming the slots to be 0.5 cm apart. Several 6-m-long samples of Al vacuum chamber have been extruded and are being tested for both their mechanical integrity and vacuum performance.

As has been mentioned, the mechanical precision of the gap determined by the height of the undulator vacuum chamber and the alignment of the beam chamber axis along the positron trajectory are both crucial for optimum performance of the insertion device. Hence, careful mounting of the vacuum chamber is essential. The mounting assembly is designed to hold the chamber true to better than ±2 mils over its 6-m length.

The top and bottom halves of the undulator magnet assembly are mounted on backing beams having the capability of changing the gap. The mounting assembly is rigid enough to hold the undulator halves with less than ±2 mils of gap deflection. The gap variation is remotely controlled.

9.5 Tunable Undulator B

9.5.1 Introduction

One of the requirements of the present APS design is to deliver approximately 20-keV of photon energy in the fundamental harmonic radiation of an undulator. This design goal was set because a host of scientific experiments need high-energy (14 to 20 keV), high-brilliance radiation. These experiments range from absorption spectroscopy of the Mo K-edge for understanding the structure of proteins and catalysts to ultra-high-energy-resolution inelastic scattering from collective excitations, such as phonons and charge density waves. This photon energy range is provided by the undulator B with a period of 2.3 cm discussed in Section II.9-3. This section presents a preliminary design study of this undulator.

9.5.2 Preliminary Design Parameters

As pointed out earlier, this device provides photons, in the fundamental harmonic, in the energy range of about 18 to 20 keV during initial operation of the storage ring. The tunability is considerably increased during mature operation (see Table II.9.3-1). For the Nd-Fe-B hybrid configuration, the two-dimensional field optimization discussed in Section II.9.4.3 is carried out for gap values ranging from 1.0 to 1.9 cm. The results of this iterative analysis are given in Table II.9.5-1.

Table II.9.5-1

Optimized Parameters of Nd-Fe-B Hybrid Undulator B

Undulator Period, λ_o	2.3
Magnet Gap Range, G (cm)	1.0-1.9
Pole Width in x Direction (cm)	0.4
Pole Height in y Direction (cm)	2.4
Pole Thickness in z Direction (cm)	0.42
Magnet Width in x Direction (cm)	5.2
Magnet Width in y Direction (cm)	3.0
Magnet Thickness in z Direction (cm)	0.73
Pole-Tip Overhang in y Direction (cm)	0.07
Peak Field Range on Axis, B_o (T)	0.47-0.13
Peak Field Increase (%) at 0.1 cm off Axis in y Direction	2.0
Maximum Length Available for Undulator (m)	5.2
Maximum Undulator Periods, N	226

The angle-integrated on-axis brilliance of the fundamental radiation from undulator B at different gap settings is shown in Fig. II.9.5-1. The vacuum chamber discussed in Section II.9.4.3 is also suitable for this device.

9.6 Segmented Undulator

Long undulators with a large number of periods are built to enhance the brilliance. Indeed, for an idealized single-particle (zero-emittance) beam, one expects the brilliance to depend quadratically on N, the number of periods. This expectation has encouraged the design of long undulators with many periods, requiring close-tolerance engineering designs as described above.

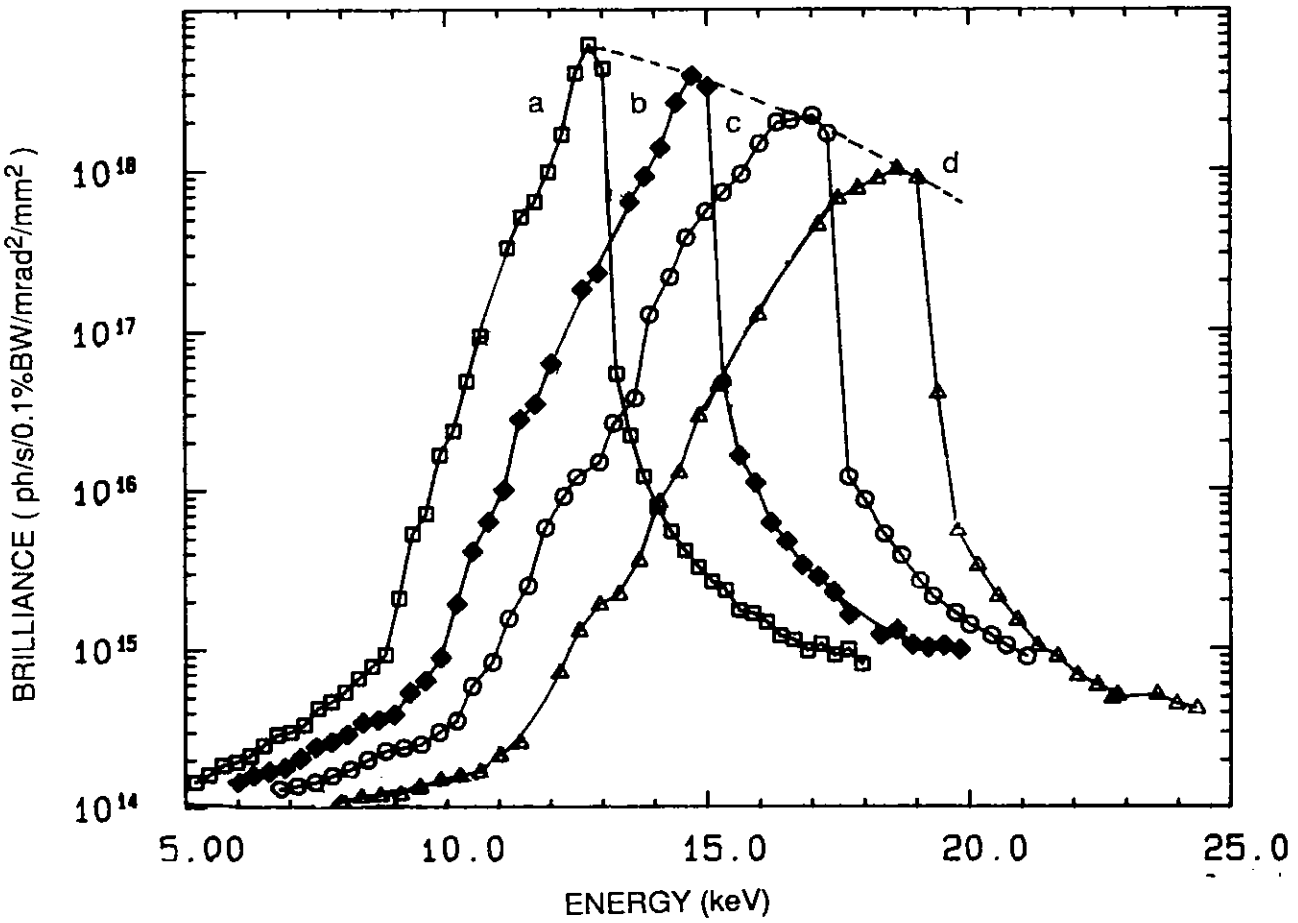

Figure II.9.5-1

The angle-integrated brilliance of the fundamental radiation from the undulator B for the APS at 7 GeV and 100 mA. The fundamental peaks at various photon energies are obtained at magnet gap settings of a) 10 mm, b) 11.5 mm, c) 13.5 mm, d) 17.5 mm. These calculations include the phase space dimensions of the positron beam.

A full Monte Carlo type calculation using a finite emittance shows that the brilliance from an undulator is proportional to N^{α} where $1 \leq \alpha \leq 2$. For the APS undulators, $\alpha=1.2$.[13]

The above fact leads us to simplify the engineering design of the APS undulators by segmenting them and mounting the segments together. In the space available for the ID of about 5.2 m along the straight section, one can design, for example, 2 separate undulators with the same period and equal length. The generic undulator A, with a period of 3.3 cm and 77 periods, will be 2.54 m long. Two such undulators, with additional space for end correctors, can easily be accommodated in a straight section.

The segmentation of a long undulator into two shorter devices reduces the brilliance by only about 13% and, at the same time, provides the following advantages:

- The mechanical design of the ID vacuum chamber is simplified, making it easier to achieve the required tolerances.
- Magnetic measurements on the segmented undulator are considerably easier.
- The CHESS undulator design mentioned above becomes an exact prototype of these segmented undulators.
- Individual segments of the undulator can be separately tested for performance.
- The effects of random errors (see Section II.9.7) are smaller for a segmented undulator.
- The power load on the first optical element can be adjusted for its best performance, by selecting the number of segments. This provides needed flexibility in the optics design.

In view of the above considerations, the option of using segmented undulators will be investigated in greater detail.

9.7 Effects of Random Errors on the Undulator Spectrum

Random mechanical and magnetic field errors affect the radiation spectra from high performance undulators. Construction techniques and tolerances can result in random magnetic field errors of about 0.5 to 2.0% in the peak magnetic field along the axis of the device. The actual size of the error determines the reduction in intensity of the various harmonics from a given undulator. This reduction is greater for radiation from higher harmonics. In the case of the APS undulators, only radiation from, at most, the third harmonic will be used.

The effects of random errors can be estimated, using the model developed by Kincaid.[14] We have determined the influence of random errors on undulators A and B, discussed in Sections II.9.4.2 and II.9.5.2, respectively. Both devices are assumed to be compensated and treated in the large error limit discussed in Ref. 14. The normalized intensity of the fundamental and third harmonic radiation is estimated numerically as a function of the magnetic field error, $\Delta B_o/B_o$. The results are shown in Fig. II.9.7-1. Note that the influence of the field error is greater on the undulator with a shorter period. A field error of 0.5% reduces the intensity of the fundamental radiation from undulators A and B by about 17% and 38%, respectively. A similar error reduces the intensity of the third-harmonic radiation from undulator A by about 30%. The loss of intensity in third-harmonic radiation from the short-period undulator B is even larger. Fortunately, there is no compelling reason to use third-harmonic radiation from short-period undulators, since they have small K values. We conclude that both APS undulators, A and B, will provide the desired radiation from 4 to 40 keV with acceptable loss in intensity, provided the random field errors are kept below 0.5%. Such tolerance figures have already been achieved for devices operating on existing synchrotrons and free-electron laser devices.

Note that the above analysis is based on a single-particle (zero-emittance) trajectory in an undulator. While the inclusion of the finite positron beam emittance is essential for a more complete analysis, the present analysis provides an upper limit on the intensity loss.

9.8 Wigglers

9.8.1 Introduction

As has been pointed out, the prerequisite for wigglers is a large K-value, which will result in a continuous and wide energy spectrum. This is achieved by having either large B_o and/or large λ_o. The critical energy of the spectrum can be made either large or small by proper choice of the peak magnetic field. In Table II.9.8-1, parameters for two typical APS wigglers are given. Wiggler A has high critical energy, while wiggler B is typical of the low critical energy devices. Both kinds of devices have applications in many areas of science. Wiggler A can be assembled with permanent magnets in a hybrid configuration, while wiggler B is best constructed from electromagnets.

In Fig. II.9.8-1, the energy spectra of wigglers A and B are shown. It is noted that wiggler A can provide very high brilliance even at 100 keV. The critical energy of wiggler B is half that of the APS bending magnet radiation (ε_c = 19 keV).

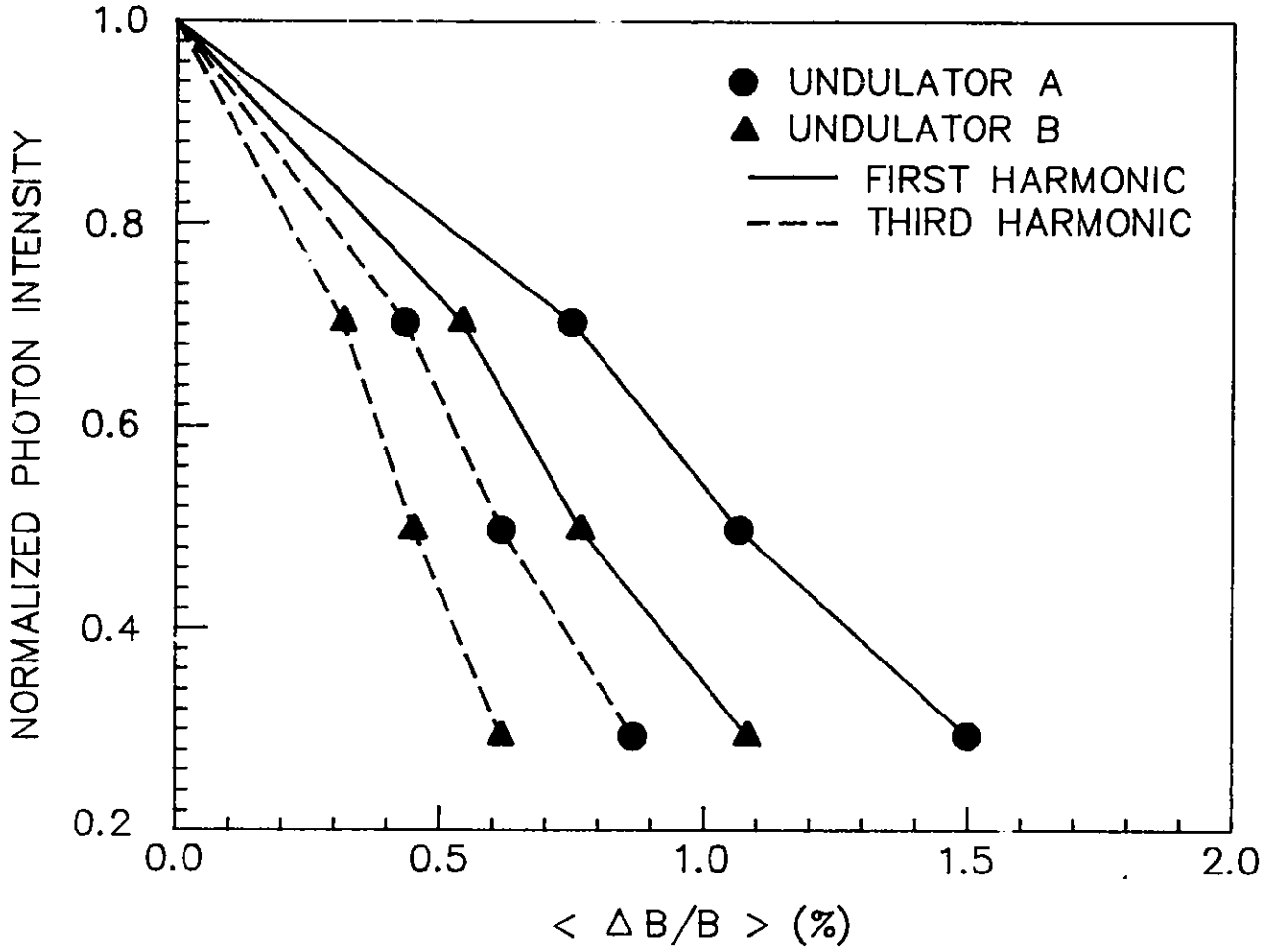

Figure II.9.7-1
The normalized photon intensity of the first and third harmonics of undulators A and B as functions of random magnetic field errors, using Kincaid's model.[14] The K-value is 1 for each device.

Table II.9.8-1

Parameters for Wigglers A and B

Parameters	Wiggler A	Wiggler B
Peak Field on Axis, B_o (T)	1.0	0.3
Gap, G (cm)	3.7	2.5
Period, λ_o (cm)	15.0	25.0
Bending radius, ρ (m)	23.3	78.0
K	14	7
Number of Periods, N	10	20
Length, L (m)	1.5	5.0
Critical Energy, ε_c (keV)	32.6	9.8
Structure	Nd-Fe-B Hybrid	Electromagnet
Flux at ε_c 10^{14} (ph/s/0.1%BW/mrad)	2.2	4.5

9.8.2 Design Parameters of an Undulator-Wiggler

It is very useful to have an ID that provides a wide variability in K from 1 to 9, which can serve both as an undulator and a wiggler. Such a device has many interesting applications, as it permits different kinds of investigations to be carried out on a beam line without restructuring the ID. To demonstrate this capability in the case of the APS, a design is presented for a device with an 8-cm period.

At gaps larger than 4 cm, the device has undulator characteristics, with K varying between 1 and 2.5. The minimum gap necessary for the device to be a wiggler is about 1.7 cm. With the Nd-Fe-B hybrid configuration, we achieve a K value of about 9 at this gap. The results of iterative two-dimensional field optimization, discussed in Section II.9.4.2, are presented in Table II.9.8-2.

The angle-integrated on-axis brilliance as a function of photon energy for this device is shown in Fig. II.9.8-2 for three different values of K. The first-harmonic

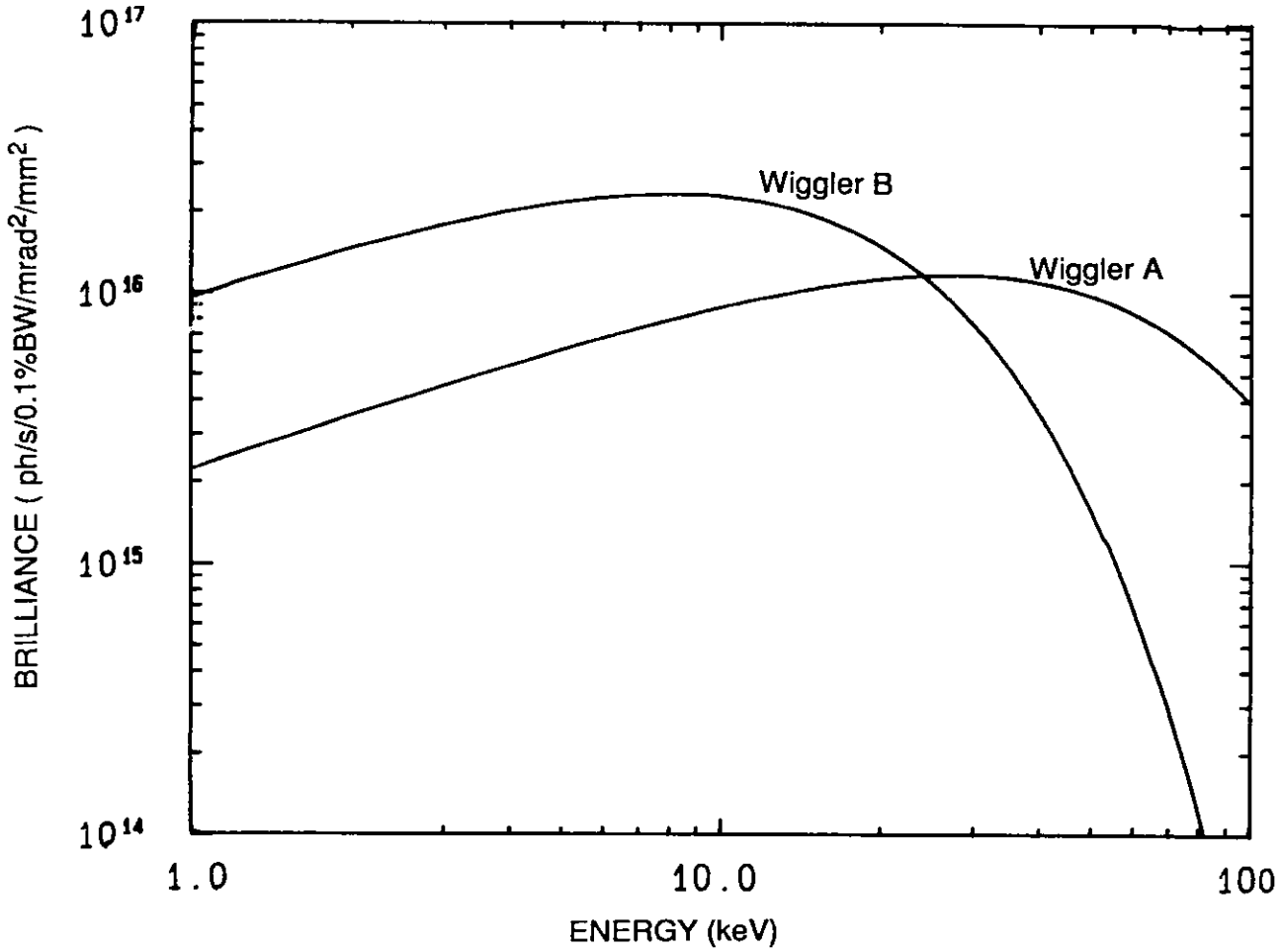

Figure II.9.8-1
The on-axis brilliance of wigglers A and B versus photon energy for the APS at 7 GeV and 100 mA.

Table II.9.8-2

Parameters of Nd-Fe-B Hybrid Undulator-Wiggler

Undulator period, λ_o (cm)	8.0
Magnet Gap, G (cm)	1.5 to 5.8
Pole Width in x Direction (cm)	11.5
Pole Height in y Direction (cm)	'.25
Pole Thickness in z Direction (cm)	2.0
Magnet Width in x Direction (cm)	13.5
Magnet Height in y Direction (cm)	4.5
Magnet Thickness in z Direction (cm)	6.0
Pole-Tip Overhang in y Direction (cm)	0.25
Peak Field on Axis, B_o (T)	1.2 to 0.15
Peak K on Axis	9 to 1
Maximum Length Available for ID (m)	5.2
Maximum Number of Periods, N	62

energy peaks for the two undulator cases are located at approximately 1.6 and 3.0 keV. A vacuum chamber with a minimum magnet gap of 1.4 cm can be used for this device.

9.9 Photon Source Dimensions

The spectral brilliance, the quantity which is maximized in the design, is the spectral intensity emitted per unit phase-space volume of the radiation field. Hence, it is essential to minimize the phase-space volume of the radiation. In the hard x-ray range, the phase-space volume of the photon field is totally determined by the positron phase-space volume. In terms of the beta functions, β_x and β_y, horizontal and vertical, the rms Gaussian widths and divergences of the positron beam are given by

$$\sigma_i = \sqrt{\varepsilon_i \beta_i} \; ; \quad \sigma_i' = \sqrt{\varepsilon_i / \beta_i} \; ; \quad i = x, y,$$

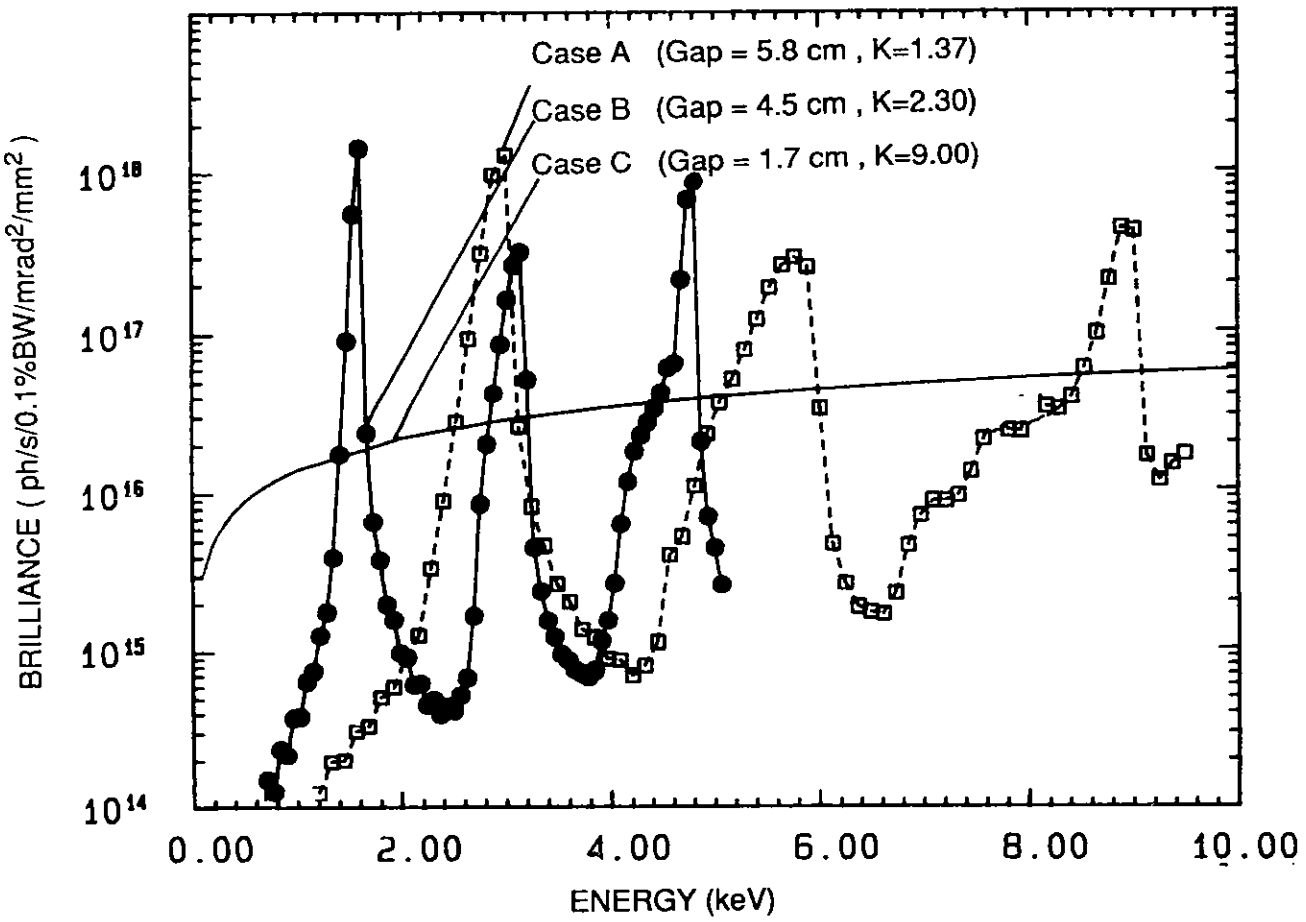

Figure II.9.8-2

The angle-integrated on-axis spectral brilliance versus photon energy for the undulator-wiggler at the three different gap values indicated. The K-values are also shown. The simulation includes the finite emittance of the source.

where $\varepsilon_x = 7 \times 10^{-9}$ m and $\varepsilon_y = 7 \times 10^{-10}$ m are the horizontal and vertical emittances. The phase-space volume is given by $S = 4\pi\sigma_x\sigma_y\sigma_x'\sigma_y'$ and is governed only by the storage ring emittance.[6,15]

The source size however, can be altered by changing the values of the beta functions at the source point. The two sets of quadrupole triplet on either side of an insertion region can be used to vary β_x and β_y for that region over a large range, without changing the values in the other insertion regions. In the undulator straight sections, small values of the beta functions will produce broad energy peaks and higher intensity in the higher harmonics. Such a spectral distribution is useful for certain applications, such as anomalous scattering. On the other hand, many investigations demand small angular divergence of the undulator beam and sharper peaks in the energy spectrum. For these cases, it is appropriate to use larger beta function values. It should be pointed out that, because of the small vertical emittance, the vertical angular divergence is usually small. Hence, it is adequate to increase only the value of β_x, to achieve small-divergence photon beams.

In Table II.9.9-1, some typical values of the beta functions that are possible at various parts of the APS lattice source points are given, along with the resulting source dimensions.

9.10 Special Devices

Many new devices are being planned, which will support special needs of the user community. These devices include a "broad-band" undulator which delivers a nearly-flat

Table II.9.9-1

The Values of Beta Function in the Different Parts of the Lattice and the Dimensions of Different Sources

Source	β_x (m)	β_y (m)	σ_x (μm)	σ_y (μm)	σ_x' (μrad)	σ_y' (μrad)
Bending Magnet	1.8	17.0	114	111	63	7
Undulator 1	13.0	10.0	308	85	24	9
Undulator 2	20.0	5.0	382	60	19	12
Wiggler	13.0	10.0	308	85	24	9

spectral distribution. This device is of considerable value in various spectroscopies and in anomalous dispersive investigations. A preliminary design of a "broad-band" undulator has been developed.[16]

It is possible to control the polarization of hard x-rays with an "asymmetric" wiggler. In such a wiggler,[17] the positrons experience an asymmetric magnetic field distribution and the radiation retains a high degree of circular polarization. This device will be used in the study of circular dichromism, spin polarized x-ray photoelectron spectroscopy (XPS), magnetic Compton scattering, etc.

The wigglers provide radiation with linear polarization in the orbital plane (x-direction). There are numerous experiments that demand that this polarization axis be perpendicular to the orbital plane (y-direction). This can be achieved by a permanent magnet wiggler with field lines in the x-direction. A "vertical" wiggler suitable for this purpose has been designed using available permanent magnet technology.[3]

9.11 Extra-Long Straight Sections

The straight sections in the APS lattice are 6.2 m long and can accommodate a maximum ID length of 5.2 m. There will sometimes be a need for extra-long straight sections, to accommodate unusually long IDs or IDs in tandem in the same straight section.

To determine the need for such extra-long straight sections, and to establish their length, the issue was addressed by the National Task Group mentioned earlier. In their report,[4] the group pointed to the adequacy of 6-m-long straight sections to carry out currently proposed scientific research. The committee suggested that some longer straight sections be included in the lattice design, to increase the flexibility to carry out experiments, in the future that have not yet been conceived.

The suggested length of the extra-long straight section is between 8 and 12 m. The committee emphasized that the inclusion of the extra-long straight sections should not be at the cost of ring performance, and that the number of these extra-long straight sections should be dictated by the symmetry requirements of the lattice.

In the APS design, the above recommendation is met. The extra-long straight sections are provided by removing a quadrupole magnet from each end of a 6.2-m straight section. This produces an 8.5-m extra-long straight section. The removal of the quadrupole magnets is not expected to disturb the storage ring performance, although the values of the beta functions in this straight section may not be easily altered.

9.12 References

1. "Report of a Workshop on the Scientific Case for a 6 GeV Synchrotron Source," edited by J. B. Cohen and K. O. Hodgson, Argonne National Laboratory, December 9-11, 1985. U. S. Department of Energy, Office of Basic Energy Sciences.

2. K. Halbach and E. Hoyer, "Workshop on Insertion Devices for a 6-GeV Synchrotron Source," Argonne National Laboratory (December 11, 1985).

3. "Conceptual Design of Proposed Beam Lines for the 6-GeV Light Source," ANL Report, Light Source Note, LS-51 (March 1986).

4. G. Brown, Y. Cho, J. Hastings, S. Krinsky, D. Moncton, G. K. Shenoy (Chairman), and P. J. Viccaro, "Ring Energy Selection and Extra-Long Straight Sections for the Advanced Photon Source: A Report and Recommendations by the National Task Group," Argonne National Laboratory Report ANL-87-14 (April 1987).

5. G. K. Shenoy and P.J. Viccaro, "An Overview of the Characteristics of the 6-GeV Synchrotron Radiation: A Preliminary Guide for Users," ANL Report ANL-85-69 (October 1985).

6. "Characteristics of the Insertion Devices for the 6-GeV Synchrotron Source", ANL Report, Light Source Note LS-52 (March 1986).

7. Report of a Program Review, Synchrotron Radiation Source Research and Development, Ames Laboratory, Iowa State University, Ames, Iowa (October 1984).

8. "6-GeV Synchrotron X-Ray Source: Conceptual Design Report," ANL Report ANL-86-8 (February 1986).

9. Ref. 8, Appendix C, "Options For 7-GeV Operation."

10. P. J. Viccaro and G. K. Shenoy, "Undulator Tunability and Ring Energy," ANL Report, Light Source Note LS-73 (1986), IEEE Conference Record 87CH2837-9.

11. S. H. Kim, P. J. Viccaro, and G. K. Shenoy, "Spectral Character of Optimized Undulator Insertion Devices for the Synchrotron X-ray Source at Argonne," IEEE Conference Record 87CH2837-9.

12. G. K. Shenoy, P. J. Viccaro, and S. Kim, "Nd-Fe-B Undulator Design for CESR," ANL Report, Light Source Note LS-72 (1986).

13. G. K. Shenoy and P. J. Viccaro, Argonne National Laboratory, unpublished information (April 1987).

14. B. M. Kincaid, "Random Errors in Undulators and Their Effects on the Radiation Spectrum," J. Opt. Soc. Amer., B2, 1294 (1985).

15. Kwang-Je Kim, "Brightness, Coherence, and Propagation Characteristics of Sychrotron Radiation," Nucl. Instrum. Methods, A246, 71 (1986); S. Kim, "Dependence of Brilliance on Beta Functions," ANL Report, Light Source Note, LS-62 (May 1986); Y. Cho, "Optimization of Beta Functions through IDs," ANL Report, Light Source Note, LS-53 (February 1986).

16. G. K. Shenoy and P. J. Viccaro, Argonne National Laboratory, unpublished information (April 1987).

17. J. Goulan, P. Elleaume, and D. Roux, "The Special Multipole Wiggler Beam Design Producing Circularly Polarized Synchrotron Radiation," to be published in Nucl. Inst. and Meth.

10.1 Introduction — Injection Process

Injection of positrons into the 7-GeV storage ring is accomplished via a 200-MeV electron linac, a tungsten positron production target, a 450-MeV positron linac, and a 450-MeV to 7-GeV 1-Hz injector synchrotron. The injector synchrotron has two separate rf accelerating systems. The first, a low-frequency system, is used to capture and accelerate eight positron bunches from the linac to 2.73 GeV. At this energy, the bunch lengths are sufficiently small to fit the higher frequency rf buckets. When these two systems are used, there is no need for a separate positron accumulator and damping ring.

Eight 3-A electron pulses, each 16.5 ns in duration, are accelerated in the 200-MeV linac at a nominal 60-Hz rate. These electrons are focused to a 3-mm-diameter spot at the 7-mm-thick tungsten positron-production target. The target yields 0.0083 (positrons/incident electron) within a solid-angle acceptance of 0.15 steradian and an energy range of 8 ± 1.5 MeV. Hence, each positron pulse from the target has a current of 25 mA and a 95th percentile emittance of 330 × 330 $(\text{mm}\cdot\text{mrad})^2$. The positron pulses from the target are focused by a high-field pulsed solenoid before injection into the positron linac for acceleration to 450 MeV. If a 60% transmission efficiency is assumed, the positron bunch current at 450 MeV is 15 mA. The energy spread is ±2.5 MeV. Including a dilution factor of 1.12, the 95th percentile emittance is 6.6 × 6.6 $(\text{mm}\cdot\text{mrad})^2$. This corresponds to an rms emittance of 1.1 × 1.1 $(\text{mm}\cdot\text{mrad})^2$. The final e^+/e^- ratio is 0.005.

At injection, during the 1/6-s flat bottom of the synchrotron cycle, the lower frequency system (system I, f = 39.218 MHz, h = 48) is turned on at 60 kV. The 16.5-ns pulses of positrons are injected into every sixth 25.5-ns bucket of the rf system using a septum magnet and an injection kicker. The injection kicker operates at 60 Hz with rise and fall times of 100 ns. With eight pulses injected, each containing 15 mA of positrons, the injector synchrotron receives 1.24×10^{10} positrons each cycle.

The longitudinal phase space area for an incoming positron bunch is about 0.082 eV·s/bunch; the rf system, with a cavity voltage of 60 kV at the constant-injection field, provides a stationary bucket area of 0.20 eV·s/bucket. The bucket area is made larger than the bunch area in order to minimize the beam loss during bunch-to-bucket transfer of the beam from the linac to the synchrotron. Because of the synchrotron motion, the bunch area is expected to grow to fit the bucket area. After eight pulses are injected, the rf voltage is increased to 250 kV in a few synchrotron oscillation periods to prepare for the acceleration. Consideration of the β functions and incoming beam emittance leads to the conclusion that there are no aperture restrictions. About 5% of the total beam is assumed to be lost in the injection and capture processes. As the magnetic field of the synchrotron increases and the positrons are accelerated at a

constant rate of 19.65 GeV/s (24.0 keV per turn), the bunch length is damped by radiation and acceleration. At 2.73 GeV, the bunch length is about 2 ns.

The 2-ns bunch length at 2.73 GeV is small enough to fit inside the bucket of the higher frequency (352.964 MHz, h = 432) rf system, designated system II. The positrons are then accelerated to 7 GeV using system II with system I turned off. The total acceleration time is 1/3 s. Our experience indicates that the acceleration and frequency-changing process is at least 90% efficient.

After reaching 7 GeV, the eight positron bunches are extracted individually at a 60-Hz rate on a 1/6-s flat top using a single fast-extraction kicker, a pulsed septum, and extraction magnets. The exact firing time of the kicker magnet is controlled so that each pulse can be injected into any desired bucket in the storage ring. The process of injection into the storage ring is 95% efficient.

The time required for one injector synchrotron cycle is 1 s. In each synchrotron cycle, 1.0×10^{10} positrons are injected into the storage ring. The total time required for an initial fill of the ring to 2.2×10^{12} positrons (100 mA) is 3.7 min. The total efficiency from injection to the positron linac to injection into the storage ring is 49%.

10.2 Linac

10.2.1 Introduction

The general design of the linacs and their beam parameters are set by the requirements of the system and the acceptance of the injector synchrotron (Fig. II.10.2-1). The first section is a 200-MeV high-current electron linac whose 16.5-ns beam of 3.0 A impinges on a converter target to generate the positrons. The positrons thus generated are focused through a pulsed solenoidal magnetic field and then accelerated by the second section of the linac, called the positron linac, to 450 MeV for injection into the synchrotron. The option of injecting 300 mA of electrons with energies up to 650 MeV by withdrawing the positron target is available.

A large energy spread due to transient beam loading will result in a large beam spot at the positron target. For that reason the section immediately after the tapered buncher is a biperiodic standing-wave structure with a 20-MeV/m accelerating field.[1]

The traveling-wave disc-loaded accelerating sections are of the SLAC type with constant gradient, operating in the $2\pi/3$ mode. With an input power of 20 MW, each generates a 16.6-MeV/m accelerating field. This structure is very efficient in both energy gain and stored energy ($\approx$10 joules). The chosen 3-m length is a compromise between rf efficiency and manufacturing ease.

The 4-m-long region between the two linacs contains a spectrometer magnet, a focusing quadrupole triplet for the 200-MeV electrons, and the positron converter. The

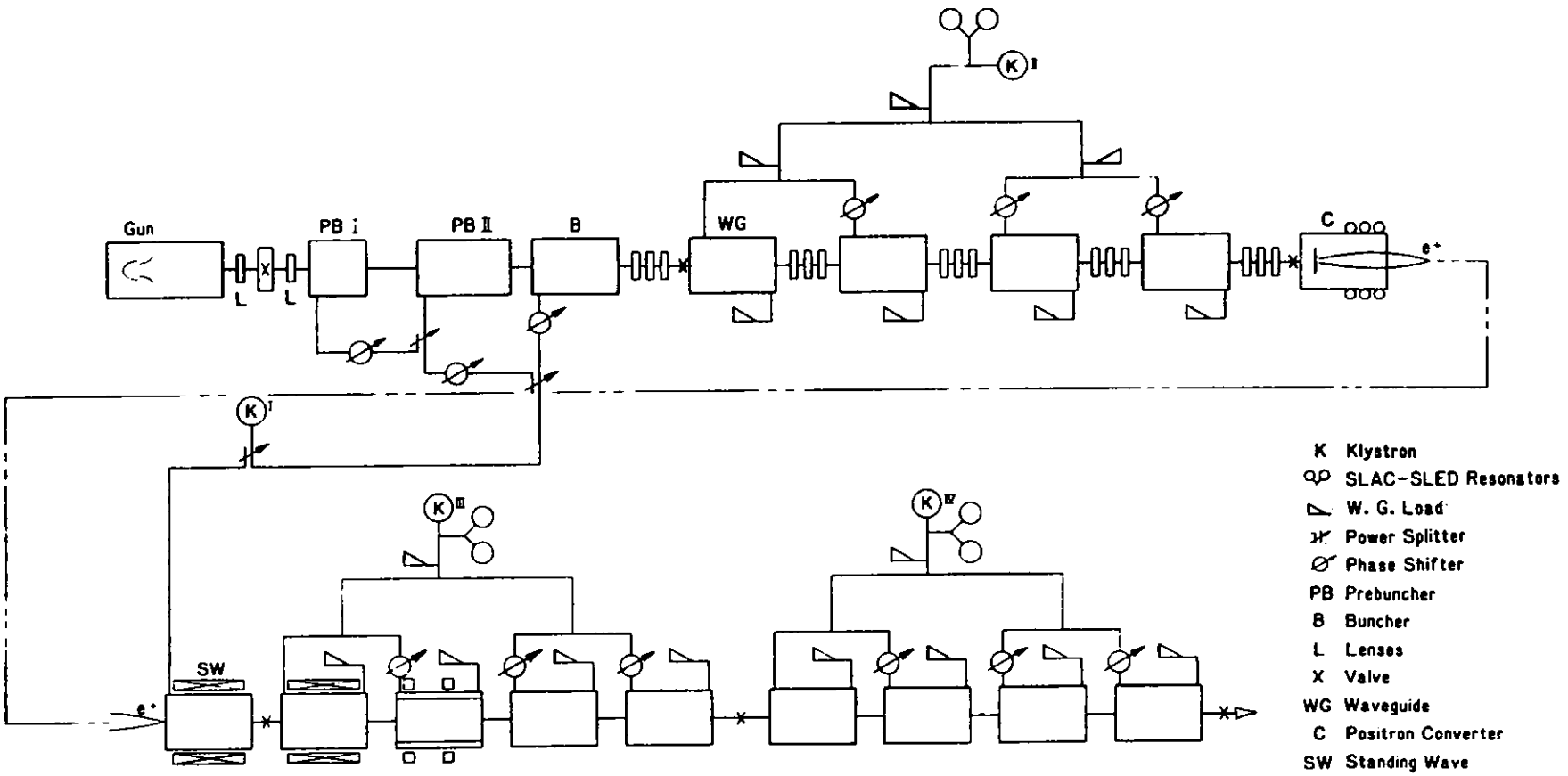

Figure II.10.2-1
Schematic diagram of the electron and positron linacs showing the rf power distribution.

converter itself will absorb about 20% of the electron power. The resulting radiation levels are high enough to require local shielding.

The positron accelerating sections are of the constant-gradient, traveling-wave type, exactly like the electron sections. To avoid arcing due to radiation, the first positron-accelerating section operates at a low field of ~7 MV/m and the following two sections operate at ~11.3 MV/m. The remaining four sections operate at 16.7 MV/m. If arcing requires that the first section operate at an even lower field, there is enough rf power available for the rest of the sections to compensate. Care has been taken to keep the positron beam diameter smaller than 13 mm by using a focusing system similar to those at DESY and LEP. This ensures that the positron beam is injected into the synchrotron with minimal loss. Linac parameters are listed in Table II.10.2-1.

10.2.2 Linac Injection System

The output of the electron linac injection system is a 50-MeV beam of 3.0-A current and 16.5-ns pulse length at 60 Hz, with an emittance of 3.0π mm·mrad and an energy spread of no more than ±5%. The present L-band linac at Argonne[2] accelerates 20 A of electrons in 20-ns pulses with 75% efficiency. Essentially the same system is used here. It consists of a triode electron gun with a thermionic cathode similar to the one used at SLAC for the SLC.[3] It injects a beam pulse of ~5.0 A (the gun is capable of 10 A) and 16.5-ns duration at 135 keV, $\beta = 0.6$. A set of two thin lenses focuses the electrons into a reentrant cavity, which acts as the first prebuncher and operates at the fundamental frequency of 3 GHz. After a drift distance of 60 cm, the electrons are further prebunched in a traveling-wave prebuncher, which is one wavelength long at $\beta = 0.6$. They are then injected into the tapered (from $\beta = 0.6$ to $\beta = 1.0$) bunching section powered by ~5 MW of 3-GHz rf power to produce a tightly bunched electron beam for matched injection into the standing-wave section. This section has a high 20-MV/m accelerating field for low transient beam loading. The power and phase of all the injector components are adjustable through power splitters and phase shifters. The complete injector system, after the gun and including the standing-wave section, is in an axial magnetic field of ~0.1 T provided by a continuous Helmholtz coil system. Provisions are made so that the optimum magnetic profile is established and no external magnetic field penetrates the cathode of the electron gun. A separate 35-MW, non-SLED klystron is used for rf power with appropriate power division between the injector and the first accelerating section of the positron linac.

10.2.3 Linac Accelerating Sections

The linac accelerating sections consist of disc-loaded waveguides operating in the $2\pi/3$ traveling-wave mode with constant field gradient, except for the injection section, which is a biperiodic standing-wave structure operating in the $\pi/2$ mode. There are three traveling-wave sections in the electron linac and 10 in the positron linac.

Table II.10.2-1

Nominal Linac Parameters

General	
Frequency	2.8 GHz
Klystron Power	35 MW
No. of Klystrons	4
No. of Sections/Traveling Wave	13
No. of Sections/Standing Wave	1
Repetition Rate	60 Hz
Beam Pulse Width	16.5 ns
No. of Pulses	8
Electron Linac	
No. of Sections (incl. buncher)	5
Input Current	5.0 A
Input Energy	135 keV
Output Current	3.0 A
Output Energy	200 MeV
Output Emittance	1.2 mm·mrad
Active Length	13 m
Converter	
Type	Tungsten
Thickness	7 mm
Conversion Efficiency e^+/e^- at Converter (for 200-MeV e^-)	0.0083
Positron Linac	
Input Current	25 mA
No. of Traveling-Wave Sections	10
Output Energy	450 MeV
Input Energy (mean)	8 MeV
Resolved Output Current	15 mA
Emittance (95th percentile)	6.6 mm·mrad
Energy Spread, $\Delta E/E$ (95th percentile)	±0.01
Active Length	30 m
Transmission Efficiency	60%
Overall e^+/e^- Efficiency	0.005

Section lengths of 3 m for both electrons and positrons are a compromise between the minimum number of klystrons required and the brazing of long structures. The design of the accelerating sections is similar to the SLAC design.[4] The basic performance criterion is an energy gain of 50 MeV per section, with 25-MW input power and a field gradient of 16.6 MV/m. The first accelerating section of the injector operates at a 20-MV/m accelerating field for low transient beam loading. The first three positron-accelerating sections operate at low accelerating fields of 7 MV/m to 11 MV/m to avoid arcing due to radiation and the presence of electrons from the positron target.

With an attenuation of 0.57 Np per section and 25 MW of input power, 13.0 MW of rf power is dissipated in the section and the rest in the terminating load. Each accelerating section has a separate cooling system that controls its temperature to ±0.2°C, which corresponds to a frequency shift of ±0.5 MHz.

Each section consists of 86 elementary cells, including the two end couplers, with the iris diameter varying smoothly from 2.622 cm to 1.924 cm. The characteristics of the accelerating sections are listed in Table II.10.2-2.

10.2.4 Linac Klystron and Modulators

Since both linacs are working in the transient mode with a very short pulse of 16.5 ns, we use the SLAC-SLED system.[5] Power is stored in the front part for the rf pulse for about 3 ns in two high-Q cavities before a 180° phase reversal at the klystron input causes the energy in the storage cavities to be emptied into the accelerating structures. This increases the real power by a factor of three. These results have been duplicated at Laboratoire de l'Accelerateur Lineaire, Orsay, on a prototype of the SLED system using a 20-MW klystron and working into a resistive load.[6]

Table II.10.2-2

Characteristics of the Accelerating Sections

Frequency	2.856 GHz
Accelerating Mode	$2\pi/3$
No. of cells	86
Range of Iris Diameter	2.622 cm to 1.924 cm
Filling Time	0.83×10^{-6} s
Energy Gain per Section (with 20 MW input)	50 MeV
Group Velocity v_g/c	0.0122
Shunt Impedance	53 MΩ/m
Attenuation τ	0.57 Np
Length	3 m

The rf power sources are 35-MW klystrons, such as the Thomson-CSF.TH2094.[7] Three klystron modulator assemblies using the SLAC-SLED system are required to power the accelerating sections of the electron and positron linacs.

One additional klystron modulator assembly without SLED is used to power the injector and the first accelerating section of the positron linac. Most of the rf power of this klystron is directed to the injector through a power splitter and phase shifter.

The modulators are of the standard pulse-forming network line type with a tetrode charging switch in the input to regulate the input charge accurately. Modulators of this type, with peak powers of 75 MW to 80 MW (280 kV and 290 A) at 60 Hz and without extremely stringent requirements in pulse flatness, do not require extensive engineering and development.

10.2.5 Linac Radio-Frequency Distribution

The output of the SLED resonant cavities (~100 MW) exceeds the arcing threshold of a transmission waveguide pressurized with SF_6; for that reason, the cavities and the transmission waveguide are under vacuum.

Copper rectangular waveguide (WR 284) is used for low rf losses. The estimated rf losses per accelerating section, including those of rf flanges, are ~0.4 db; hence, no water cooling is required.

The output from each SLED cavity is divided and then subdivided into equal parts with magic T's as required (see Fig. II.10.2-1). The phase of the rf power fed to the waveguides is controlled by high-power mechanical phase shifters.

10.2.6 Linac Low-Level Radio-Frequency and Phase Control

The 3-GHz output of an ultrastable master oscillator is amplified to the 20-kW peak power level by a small booster klystron. A rigid coaxial line distributes this signal to the four klystrons through an electronic phase-control circuit.

The phase adjustment of the accelerator is initially made by maximizing the energy of both linacs and at the same time minimizing the energy spread. From then on, the phases of the accelerating and bunching sections are compared to a reference cavity in the injector, and the relative phase difference is kept constant by the control computer. A system measuring the phase difference between two cavities with an accuracy of $\pm 1^\circ$ has been tested at Argonne and is incorporated into the system. The fixed energy, pulse width, and duty cycle for both electrons and positrons make the phase-control system of the linac relatively simple.

10.2.7 Positron Production

For maximum utilization of the geometrical acceptance of the positron-accelerating sections, the 200-MeV electron beam impinging on the positron-conversion target is focused tightly to a spot size of no more than 3 mm in diameter. The chromatic effects of the focusing system, together with the energy spread of the electron beam, would limit achieving a 3-mm-diameter spot size if the energy spread were too large. For this reason, the incoming electron energy spread is limited to ±5%.

Following the DESY design,[8] the positrons are produced in a water-cooled retractable tungsten target, two radiation lengths (7 mm) thick.

Positrons emerging from the target have the typical energy distribution predicted by bremsstrahlung followed by pair-production mechanisms. The energy distribution is inversely proportional to the positron energy; thus, there are more lower energy than higher energy positrons. The energy acceptance of the positron linac is set to accept the positron energy of 8 ± 1.5 MeV. Solid-angle acceptance of the system is defined by a pulsed solenoid placed immediately downstream of the target and by matching into the positron-accelerating waveguide with the solenoid, which has a field strength of 1.5 T. The aperture of the solenoid is equivalent to the acceptance solid angle of 0.15 steradians; thus, the positrons from production angles up to 220 mrad in each transverse plane are captured in the acceptance aperture.

The accepted positron emittance is then ϵ = 330 mm·mrad (220 mrad × 1.5 mm) in each transverse plane, where the beam size of 1.5-mm radius is used. The positron yield per incident electron of 200 MeV accepted by the system is 0.0083. This yield is equivalent to injection of 25-mA positron pulse current into the positron linac. The positron linac loss factor is assumed to be 40% in the first two accelerating sections. The final positron-to-incident-electron ratio is e^+/e^- = 0.005,[8] which results in a 15-mA positron current at 450 MeV.

The 450-MeV positron beam has a 95th percentile emittance of 6.6 mm·mrad (rms emittance of 1.1 mm·mrad) in each transverse plane and an energy spread of $\Delta E/E$ = ±0.006. An emittance dilution of 12% is assumed.

10.2.8 Linac Focusing

The electron beam leaving the gun is focused by two short solenoid lenses. From there on, and all along the injector, the beam is radially focused by an axial magnetic field produced by a Helmholtz coil system of 0.1-T field and appropriate profile.

Downstream from the Helmholtz coil system, the beam is focused by three quadrupole triplets placed between accelerating sections to give the required beam spot on the positron target with a corresponding emittance of 6 mm·mrad (at 200 MeV) for 95% of the electrons.

After the target and the short pulsed solenoid (~1.5 T), the positrons are focused by a solenoid with a 0.4-T magnetic field, which is wound around the first two positron-accelerating sections. There is a limiting aperture of 1.5 cm at the entrance of the first positron-accelerating section.

Subsequent focusing is similar to that at LEP[6] and consists of a matching section of quadrupoles followed by a FODO system. The spacing of the quadrupoles increases with energy.

10.2.9 Vacuum

The only critical item in the vacuum system is the pumping of the 3-m-long traveling-wave accelerating structure. To achieve a satisfactory vacuum in the accelerating structure ($<5\times10^{-7}$ Torr), the Cu structure is enclosed in a stainless steel cylindrical envelope and the pumping is through 4-mm-diameter holes in the outer wall of the cavities. Two 100-ℓ/s ion pumps keep the pressure in the accelerating sections below 5×10^{-7} Torr with rf power on.

Turbomolecular pumps and metal-to-metal valves are installed between vacuum sections, which also correspond to klystron sections.

The positron conversion target system has its own vacuum system. The electron gun also has its own vacuum pump to maintain the pressure below 1×10^{-8} Torr for long cathode life.

10.3 Injector Synchrotron

10.3.1 Introduction

The 366.92-m circumference of the injector synchrotron is 432/1248 times the circumference of the storage ring. With the rf systems of the ring and the synchrotron phase locked at the same frequency (352.96 MHz), this ratio of harmonics provides flexibility for the extraction and injection of the eight equally spaced positron bunches in the synchrotron into any buckets in the ring during each synchrotron cycle.

The lattice is a FODO arrangement to produce a small natural emittance. There are four dispersion-free, empty-magnet, half cells on opposite sides of the synchrotron giving a racetrack shape. Injection is on one side and extraction on the other side. A low-frequency rf cavity is located immediately downstream of the injection kicker. Two of the high-frequency rf cavities are located in the next two downstream sections. There are also two high-frequency rf cavities in two straight sections downstream of the extraction region. Figure II.10.3-1 shows the physical layout of the injector synchrotron.

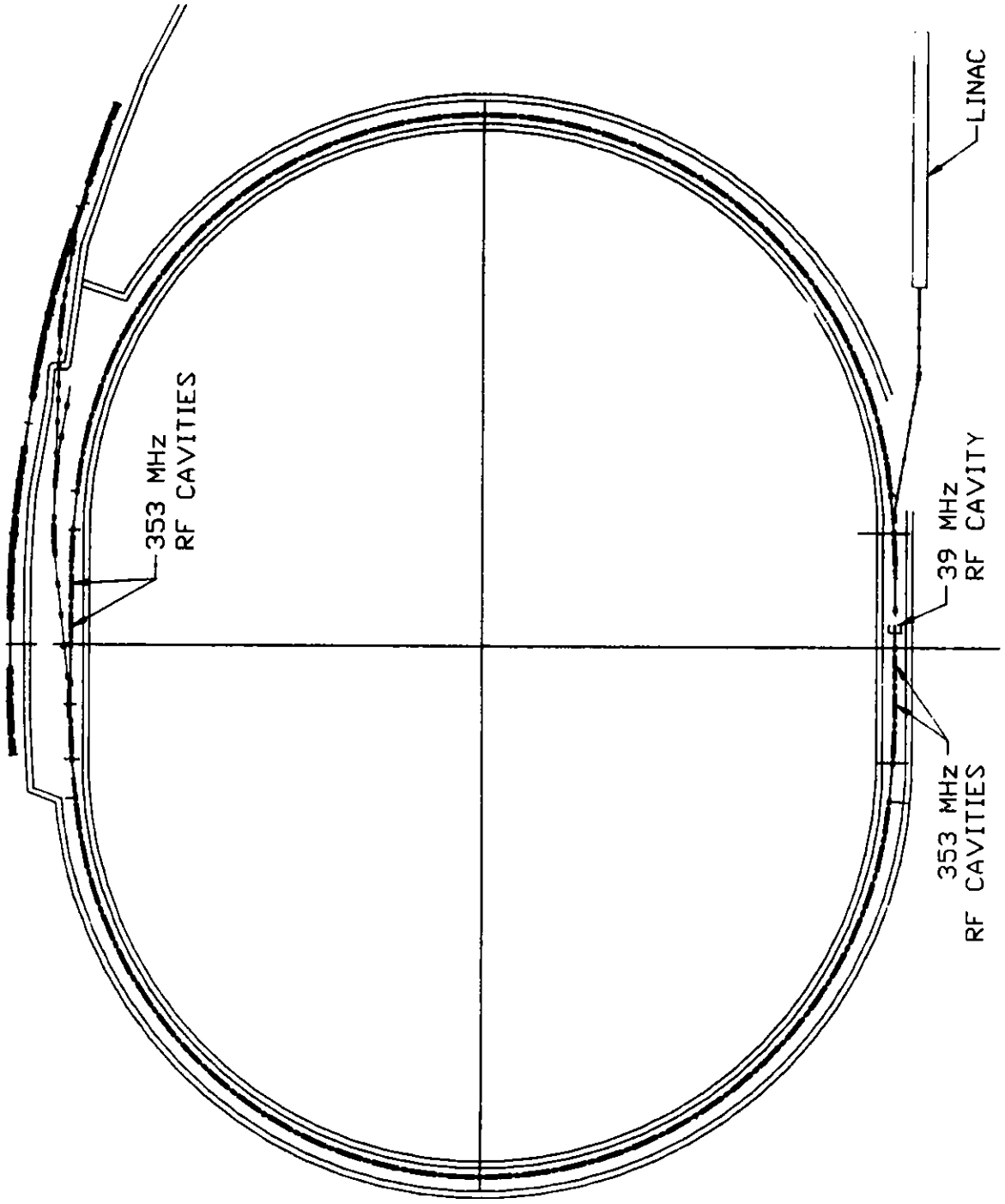

Figure II.10.3-1
Physical layout of the injector synchrotron.

10.3.2 Injector Synchrotron Lattice

The injector synchrotron has 40 FODO cells with phase advance of about 105° and 86° in the horizontal and vertical planes, respectively. Figure II.10.3-2 shows the lattice functions for a normal cell. There are 32 normal cells in the lattice. Dispersion is suppressed by removing a bending magnet from a normal cell, followed by a full empty cell as shown in Fig. II.10.3-3. A unique phase advance in both planes is chosen to remove dispersion with this magnet arrangement. The lattice functions for one quarter of the synchrotron are shown in Fig. II-10.3-4.

For the normal cell values shown in Table II.10.3-1, the horizontal and vertical tunes are, respectively, 11.71 and 9.76. The natural emittance at 7 GeV is 1.3×10^{-7} m. There are four 3.98-m-long dispersion-free straight sections in each super period as shown in Figs. II.10.3-3 and II.10.3-4.

The natural chromaticities of the lattice are $\xi_x = -15.23$ and $\xi_y = -13.01$. To correct the chromaticities, 34 focusing and 34 defocusing sextupoles, each 0.2 m long, are placed near focusing and defocusing quadrupoles. The sextupole strengths required, in units of $B''\ell/B\rho$, are $0.549/m^2$ for the focusing and $-1.083/m^2$ for defocusing sextupoles. The locations of these sextupoles in a normal cell and lattice functions are shown in Fig. II.10.3-2.

The parameter list for the injector synchrotron is shown in Table 10.3-2.

10.3.3 Injector Synchrotron Performance

The lattice for the injector synchrotron is a conventional separate-function strong-focusing system. Sixty-eight sextupoles provided in the lattice control the chromaticities, and the lattice has a large dynamic aperture according to the calculations performed using the tracking code PATRICIA.[9]

The lattice is equipped with 40 horizontal and 40 vertical orbit correctors to correct the closed-orbit displacement due to the quadrupole magnet placement tolerances. The rms tolerance is 0.1 mm, which is the same as that of the storage ring. Since the magnification factor of this tolerance is 14 in each plane, the expected rms orbit distortion is about 1.4 mm without corrections, and the corrected value should be about 0.1 mm.

The most important consideration regarding the aperture of the synchrotron has to do with the injection aperture. The incoming beam rms emittance of 1.1×10^{-6} m and the maximum β function at the synchrotron quadrupoles of 16 m give the rms beam size of 4.2 mm at the quadrupoles. The vertical half-height of the vacuum chamber in the quadrupole is 18.5 mm, which is 4.4 times the rms beam size in the vertical plane. In the bending magnets, the vacuum chamber height is also 37 mm, and the vertical β function is less than 16 m. Since the horizontal chamber dimension is large compared to the vertical dimension, no further discussion is needed for consideration of the aperture.

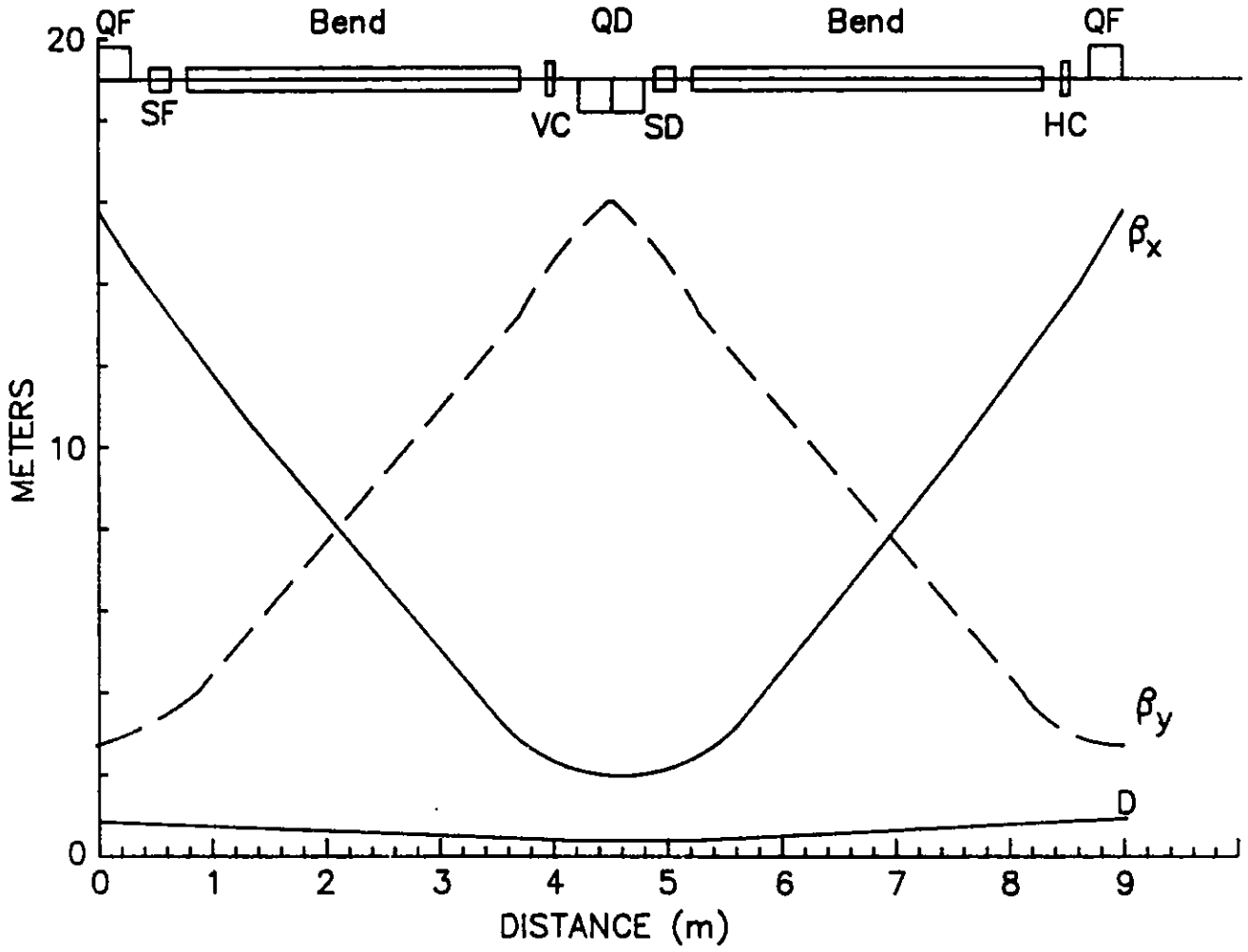

Figure II.10.3-2
Normal cell lattice functions.

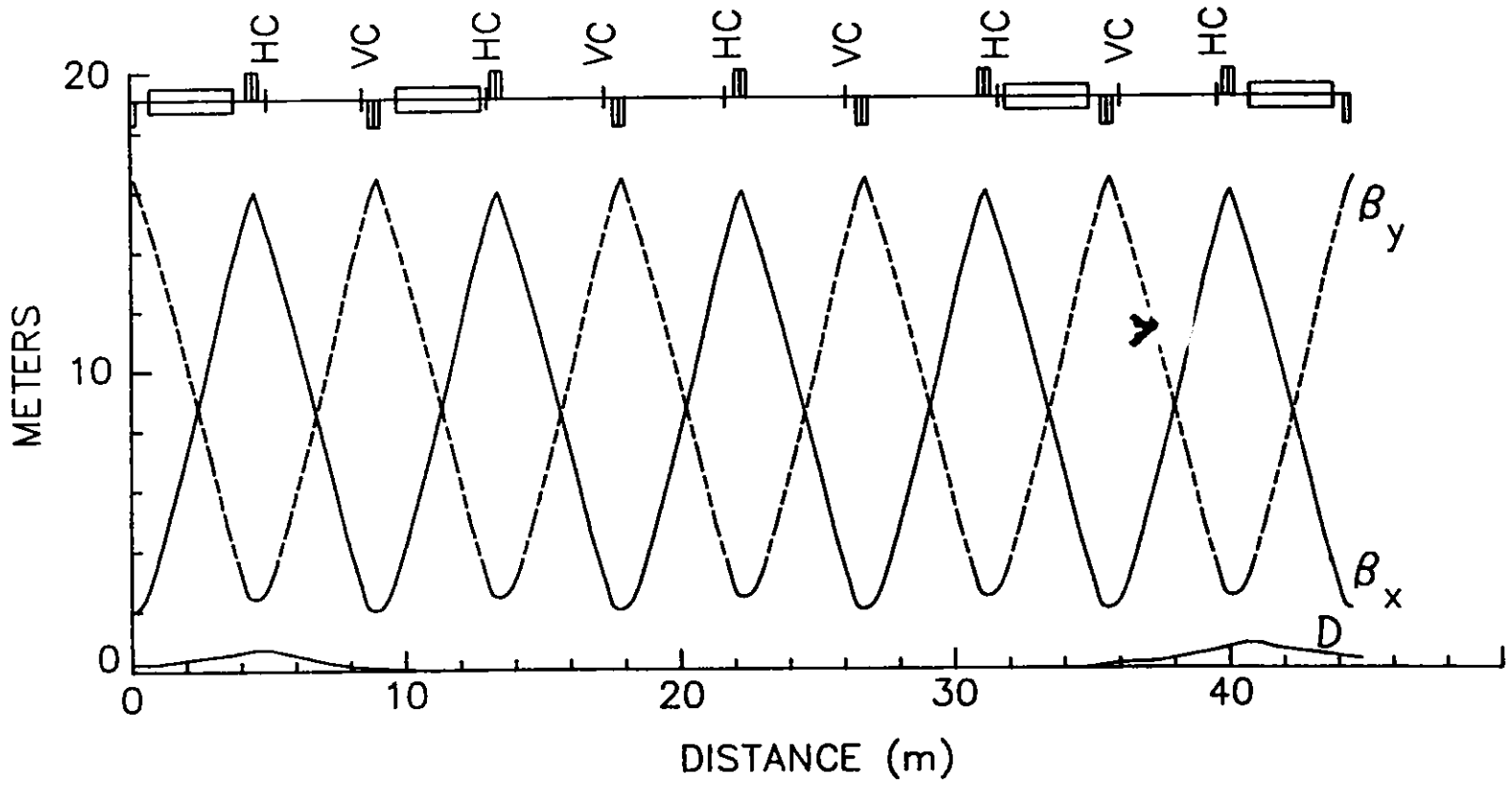

Figure II.10.3-3
Lattice functions through the dispersion suppressor and dispersion free cells.

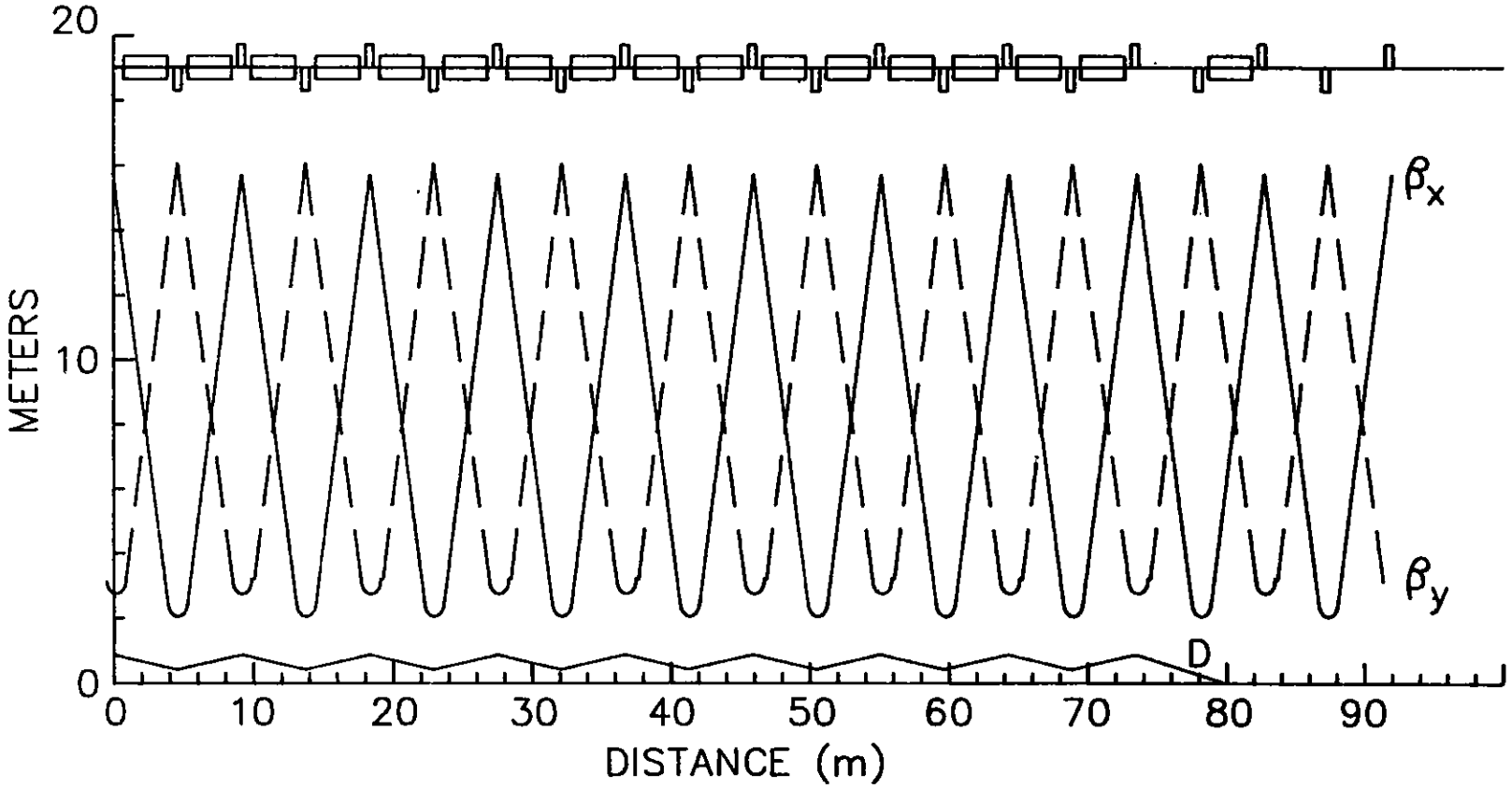

Figure II.10.3-4
Injector synchrotron lattice for one-fourth of the machine. The lattice is symmetrical about either end.

Table II.10.3-1

Injector Synchrotron Normal Cell
Length 9.1731 m ($B\rho$ = 23.3494 T·m)

Element		Length (m)	B, B', or B" (7 GeV) (T, T/m, or T/m^2)
Quadrupole	QD	0.6	-12.5220
Drift	D_1	0.1217	
Sextupole	SD	0.2	-126.390
Drift	D_1	0.1217	
Magnet	B	3.1	0.6960
Drift	D	0.4433	
Quadrupole	QF	0.6	13.9359
Drift	D_1	0.1217	
Sextupole	SF	0.2	64.044
Drift	D_1	0.1217	
Magnet	B	3.1	0.6960
Drift	D	0.4433	

The beam current in the synchrotron injected from the linac is about 1.7 mA in eight bunches or about 0.2 mA per bunch. This current is substantially lower than that of the storage ring. Thus, it is expected that the synchrotron current is far below any instability threshold current.

At injection, special care is taken to contain the longitudinal phase space area of the incoming linac macropulse in the bucket of the 39.22-MHz rf system. The macropulse has a longitudinal phase space area of 0.08 eV·s, while the waiting bucket has 0.2 eV·s. The linac macropulse is 16.5 ns long, while the bucket length is 25.5 ns. These considerations of the phase space areas and the durations of the pulse and the bucket assure a good capture efficiency. The bucket area of 0.2 eV·s is chosen to minimize dilution of the phase space of the injected pulse due to synchrotron oscillation. After capture, the longitudinal phase space of the positron bunch is about 0.13 eV·s.

The transition point of switching from the 48-harmonic system to the 432-harmonic rf system at 2.73 GeV was chosen from the bunch-length damping consideration. At this energy, the bunch length is about 2 ns, which is short enough to fit into the 353-MHz rf system's bucket length of 2.8 ns. This transfer of particle bunches from a lower frequency rf system to a higher frequency system is normal operation for the positron damping ring PIA.[10]

Table II.10.3-2

Injector Synchrotron Parameters

Circumference, m	366.923
Revolution Time, μs	1.224
Injection Energy, GeV	0.45
Nominal Energy, GeV	7.0
Maximum Energy, GeV	7.7
Repetition Time, s	1
Acceleration Time, s	0.33
No. of Super Periods	2
No. of Cells	40
No. of Bending Magnets	68
Magnetic Field at: Injection T	0.0447
Extraction T	0.6960
Tunes ν_x/ν_y	11.713/9.760
Transition Gamma	10.112
Betatron Damping Time at 7 GeV, ms	2.7
Natural Emittance at 7 GeV, m	1.321×10^{-7}
Energy Loss per Turn at 7 GeV, MeV/turn	6.33
Synchrotron Damping Time at 7 GeV, ms	1.35
Bunch Length, σ_ℓ, at 7 GeV, ps	61
Energy Spread, σ_E/E, 7 GeV	1×10^{-3}
Average Beam Current (in 8 buckets), mA	1.6
Energy Gain per Turn, keV	24.0
RF Parameters	
System I: 0.45 to 2.73 GeV	
f, MHz	39.218
h	48
V, kV	250
f_s at 2.73 GeV, kHz	1.81
System II: 2.73 to 7 GeV	
f, MHz	352.962
h	432
V at 7 GeV, MV	11.8
f_s at 7 GeV, kHz	25.34

10.3.4 Injector Synchrotron Magnets, Supports, and Power Supplies

10.3.4.1 Injector Synchrotron Magnets

The major ring magnets for the injector synchrotron consist of 68 dipoles, 80 quadrupoles, and 68 sextupoles. End views of these magnets are shown in Figs. II.10.3-5, II.10.3-6, and II.10.3-7, respectively. These figures show some dimensions and the major components of the assembled units. Also shown is the ring vacuum chamber positioned inside of each magnet. Each magnet is made in two sections, permitting the coils to be installed around each pole and also allowing the magnets to be assembled around the ring vacuum chamber.

The calculated two-dimensional relative field deviations and leading coefficients at 7.0 GeV, according to the definition in Section II.4.2, are listed in Table II.10.3-3. These values at the injection energy of 0.45 GeV are within similar magnitudes.

Table II.10.3-3

Field Qualities of Injector Synchrotron Magnets

	Dipole	Quadrupole	Sextupole*
Relative Deviation (10^{-4})	$\left(\frac{\Delta B}{B}\right)_{o\ \max}^{\min} = {}^{+\ 0.71}_{-\ 1.5}$	$\left(\frac{\Delta G}{G}\right)_{o\ \max}^{\min} = {}^{+\ 2.5}_{-\ 7.0}$	$\left(\frac{\Delta K}{K}\right)_{o\ \max}^{\min} \leq 30$
	for $\lvert x\rvert \leq 25$ mm, $\lvert y\rvert \leq 17.5$ mm	for $r_o \leq 17.5$ mm	for $r_o \leq 17.5$ mm
Multipole Coefficients (10^{-6} cm^{-n})	$b_2 = 17.5$, $b_4 = 3.6$	$b_3 = 3.2$, $b_5 = -3.56$, $b_9 = -0.26$	

*Estimated.

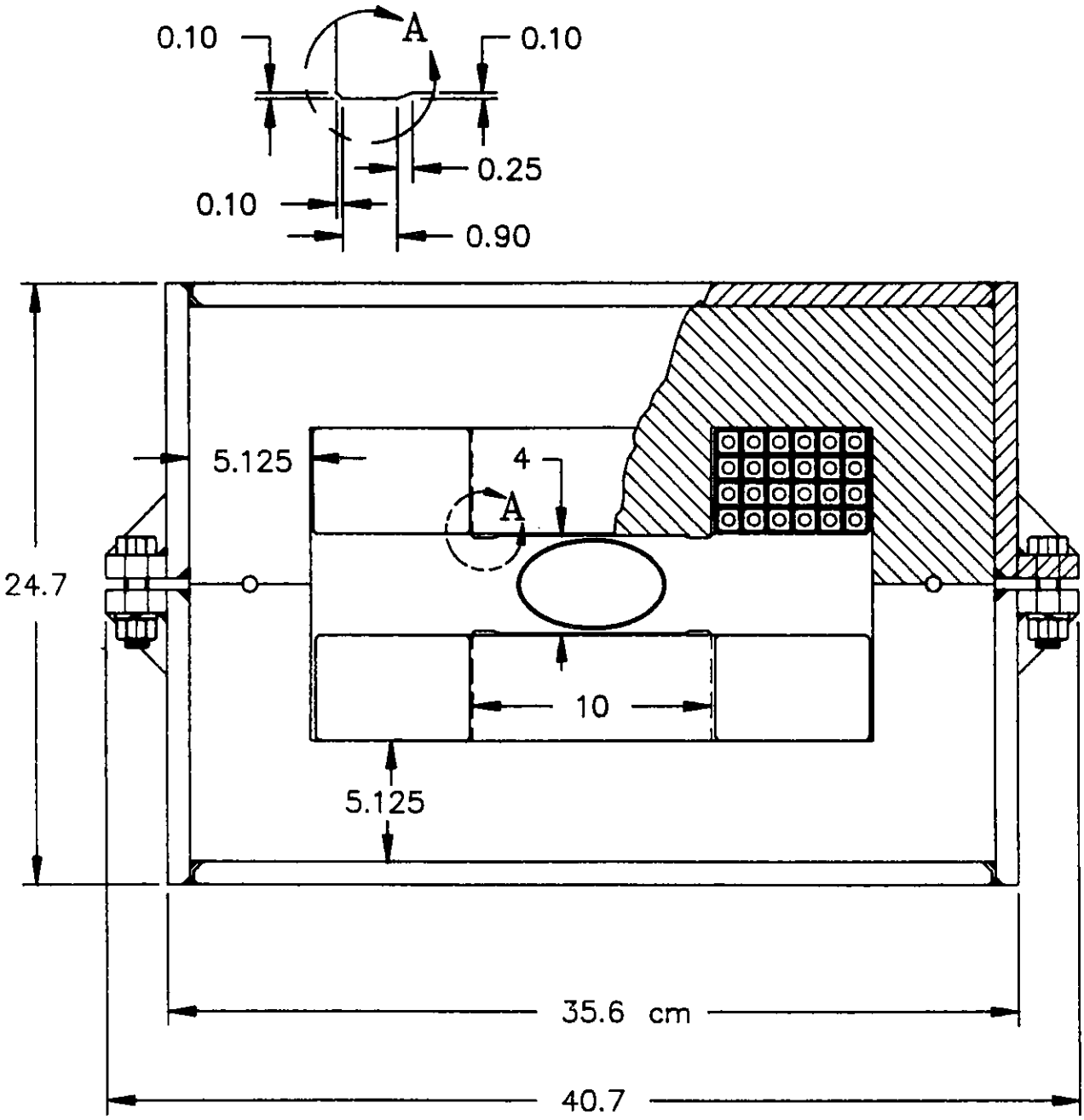

Figure II.10.3-5
End view of the injector synchrotron dipole magnet.

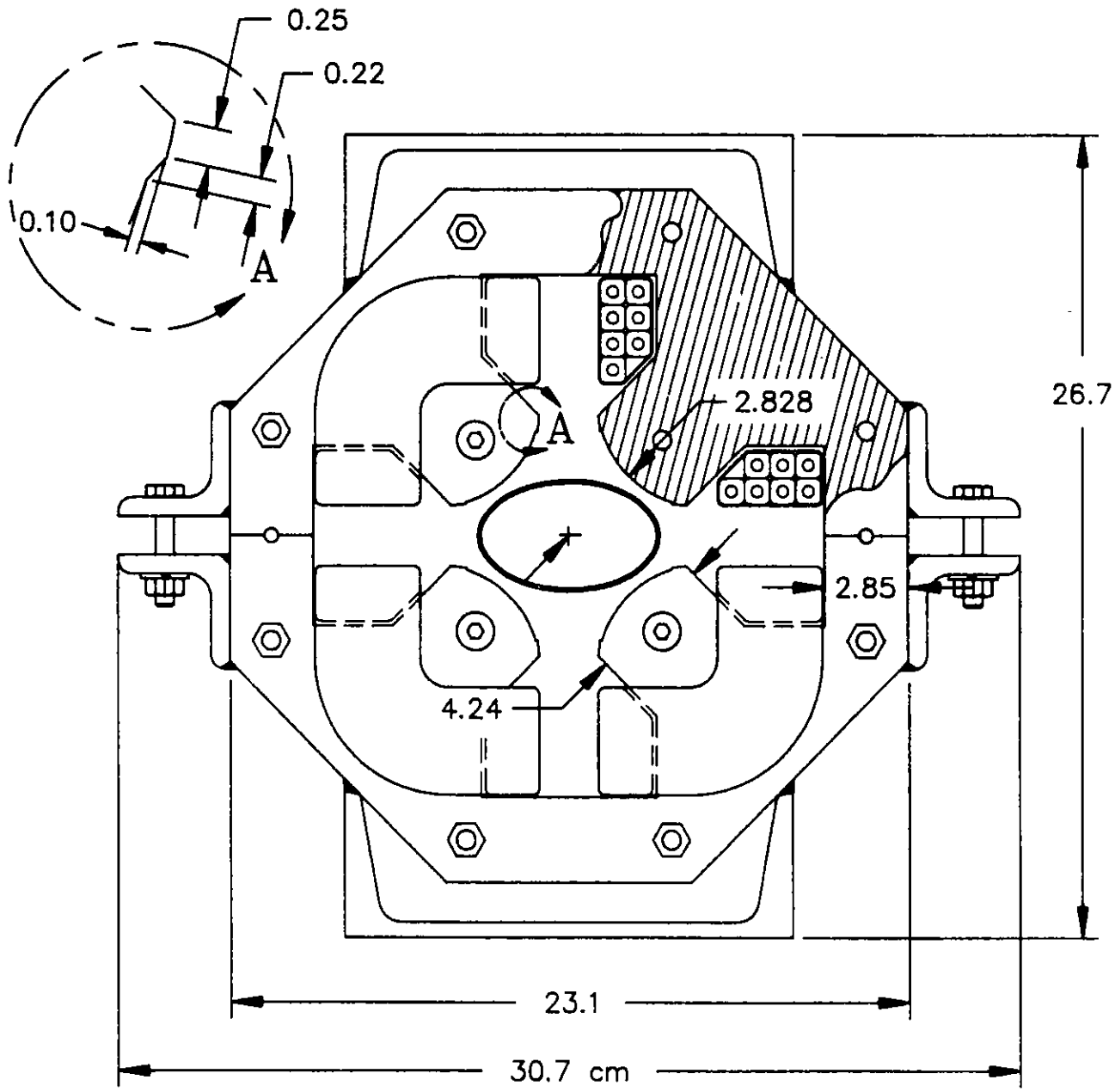

Figure II.10.3-6
End view of the injector synchrotron quadrupole magnet.

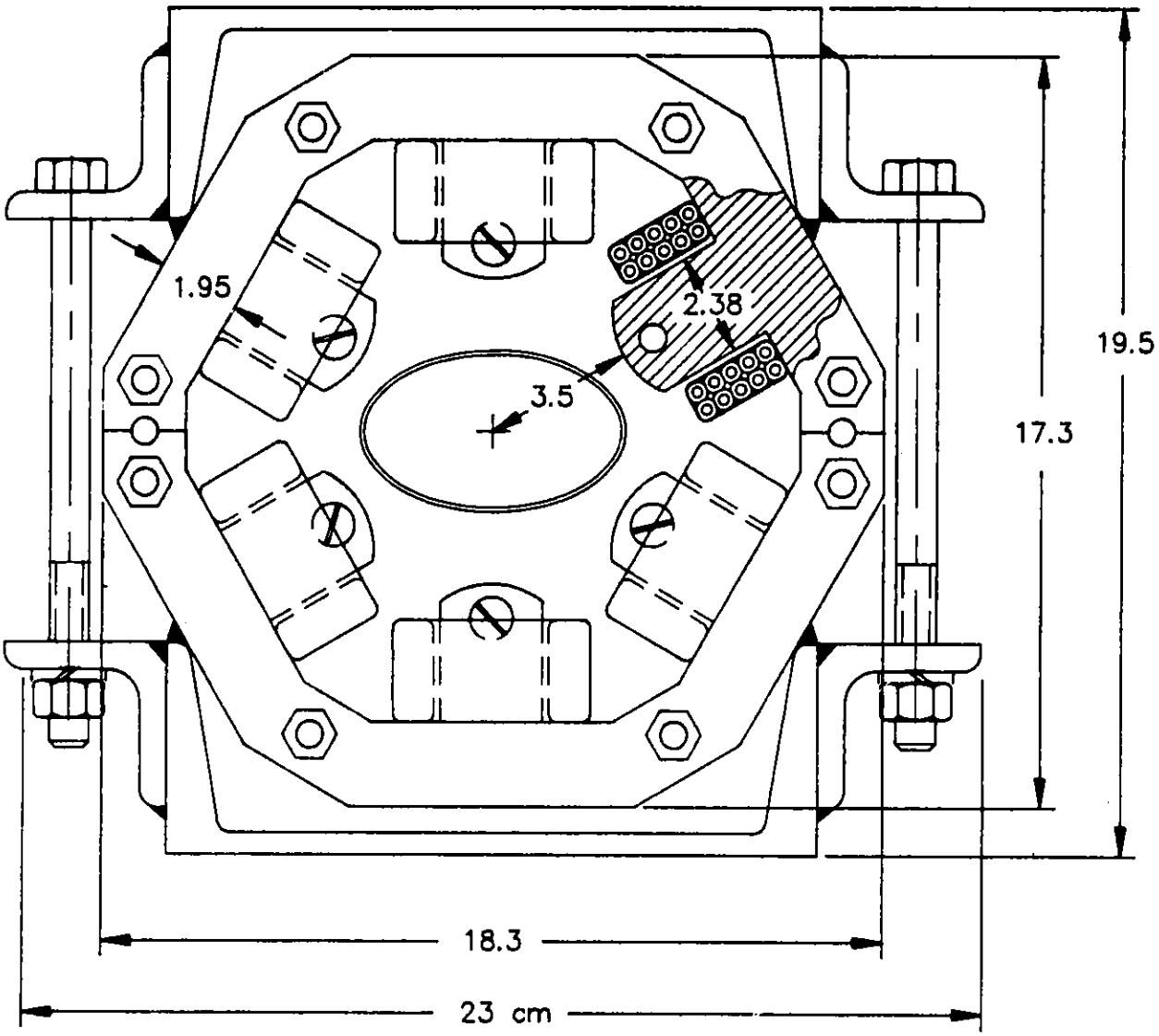

Figure II.10.3-7
End view of the injector synchrotron sextupole magnet.

The cores of these magnets are assembled from 1.5-mm-thick, low carbon steel (1010) laminations stacked between stainless steel end plates. The thicknesses of these end plates are 2.5 cm for the dipole, 1.0 cm for the quadrupole, and 0.6 cm for the sextupole magnet. The cores are held under compression by tie rods and secondary assembly components welded to the end plates and to each lamination. Each magnet has one coil per pole made from hollow copper conductor insulated with fiberglass that is vacuum impregnated with epoxy resin.

The 40 horizontal and 40 vertical correction dipole magnets included in the injector ring provide integrated field values ≤ 0.018 T·m. A separate design is used for each type of correction to minimize the power and maximize the field quality. An end view of the horizontal corrector is shown in Fig. II.10.3-8.

The parameters for the injector ring magnets are listed in Table II.10.3-4. All the magnets are optimized for 7.0 GeV and are capable of 7.7-GeV operation.

10.3.4.2 Injector Synchrotron Magnet Supports

10.3.4.2.1 Dipole Support

The injector dipoles are rigid, welded structures with sufficient stiffness to be supported directly on three vertical 2-ton jacks. The jacks are mounted on a stand that can be adjusted transversely and longitudinally by means of screws at the base, in much the same way that the storage ring magnet supports are adjusted (see Fig. II.4.10-1).

10.3.4.2.2 Quadrupole, Sextupole, and Correction Magnet Support

The quadrupole, sextupole, and correction magnets between the injector dipole magnets are mounted on a common rigid beam. The individual magnets are aligned to their common magnetic center by means of simple adjustable supports on the common beam. The girder is mounted on three vertical 2-ton jacks on a stand and adjusted to align the magnets as a unit, in the same manner as the larger strings of magnets are aligned in the storage ring (see Fig. II.4.10-2).

10.3.4.3 Injector Synchrotron Ring Magnet Power Supplies

The ring magnets of the injector synchrotron are pulsed as shown, for example, in Fig. II.10.3-9(a) for the dipole magnets. After a 1/6-s injection time, the current rises in 1/3 s to a flat top that is maintained for 1/6 s. Thereafter, the current decays to the injection level in 1/3 s, resulting in a pulse repetition time of 1 s. The real-time tracking error between the quadrupoles and dipoles is within $\pm 5 \times 10^{-4}$. With the relatively slow rate of rise and the 1.5-mm core laminations, eddy current effects in the magnet iron are negligible. A general synchrotron current shape is shown in Fig. II.10.3-9(b).

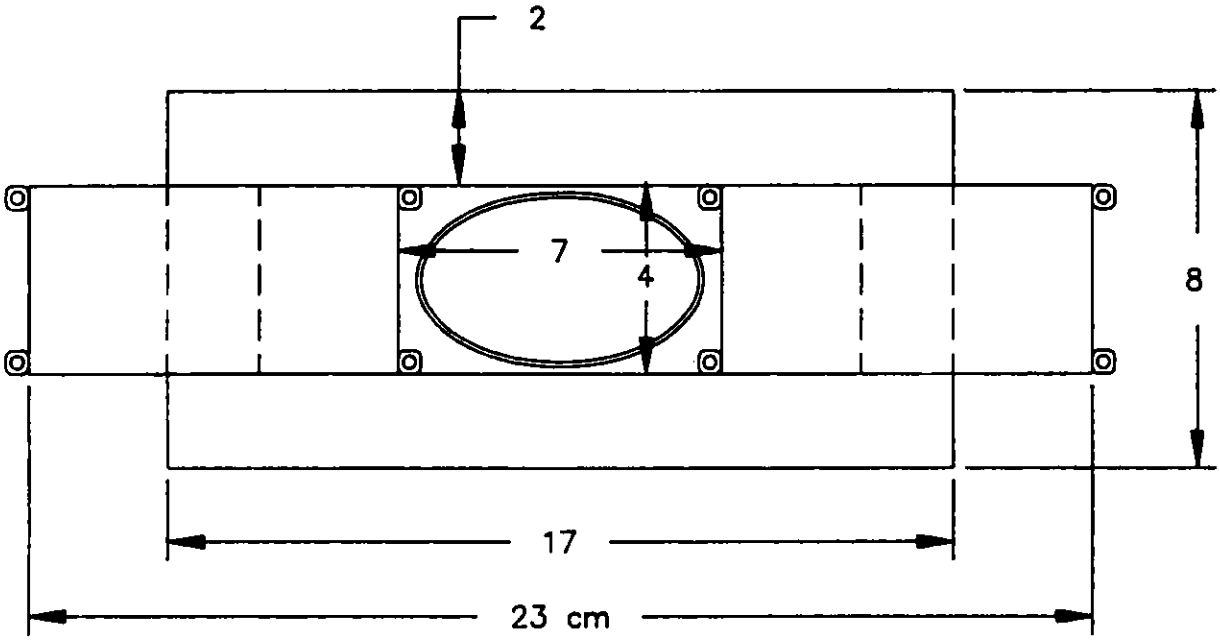

Figure II.10.3-8
Injector synchrotron horizontal correction dipole magnet.

Table II.10.3-4

Parameters for Injector Synchrotron Magnets

Parameter		Magnet				
		Dipole	Quadrupole	Sextupole	Correction H	Correction V
Number Required		68	80	68	40	40
Strength at 7.0 GeV		0.696 T	13.9 T/m(max)	130 T/m^2(max)	0.15 T	0.12 T
Effective Length	(m)	3.1	0.6	0.2	0.12	0.15
Gap Height or Diameter	(mm)	40	56.56	70	40	70
Total Mass of Magnet	(kg)	1650	180	30	7	12
Coils per Pole		1	1	1	1	1
Conductor Height	(mm)	9.0	7.2	4.1	2.0	2.0
Width	(mm)	9.0	7.2	4.1	2.0	2.0
Hole Diameter	(mm)	5.0	3.9	2.4	edge-cooled	
Number of Turns per Pole		24	7	10	252	448
Total Inductance	(mH)	30	0.9	0.8	47	106
Total Resistance	(mΩ)	98	18	50	1378	2422
Time Constant	(ms)	306	50	16	34	44
Supply Current Max	(A)	470	645	80	±19	±15
Min	(A)	30	42	9	-	-
rms	(A)	299	410	51	19	15
Current Density in Coil	(A/mm^2)	2.6	4.9	2.2	4.2	3.2
Voltage at Injection	(V)	2.9	0.8	0.2	-	-
Voltage at Flat Top	(V)	46.1	11.6	4.0	±26	±36
Peak Voltage	(V)	85.7	13.2	4.2	±26	±36
Power	(kW)	8.8	3.0	0.1	0.5	0.5
Cooling Circuits per Magnet		4	4	1	4	4
Total Water Flow	(gpm)	2.1	2.5	0.4	0.2	0.2
Water Pressure Drop	(psi)	100	50	50	50	50
Water Temp. Rise	(°C)	16	4	3	10	10

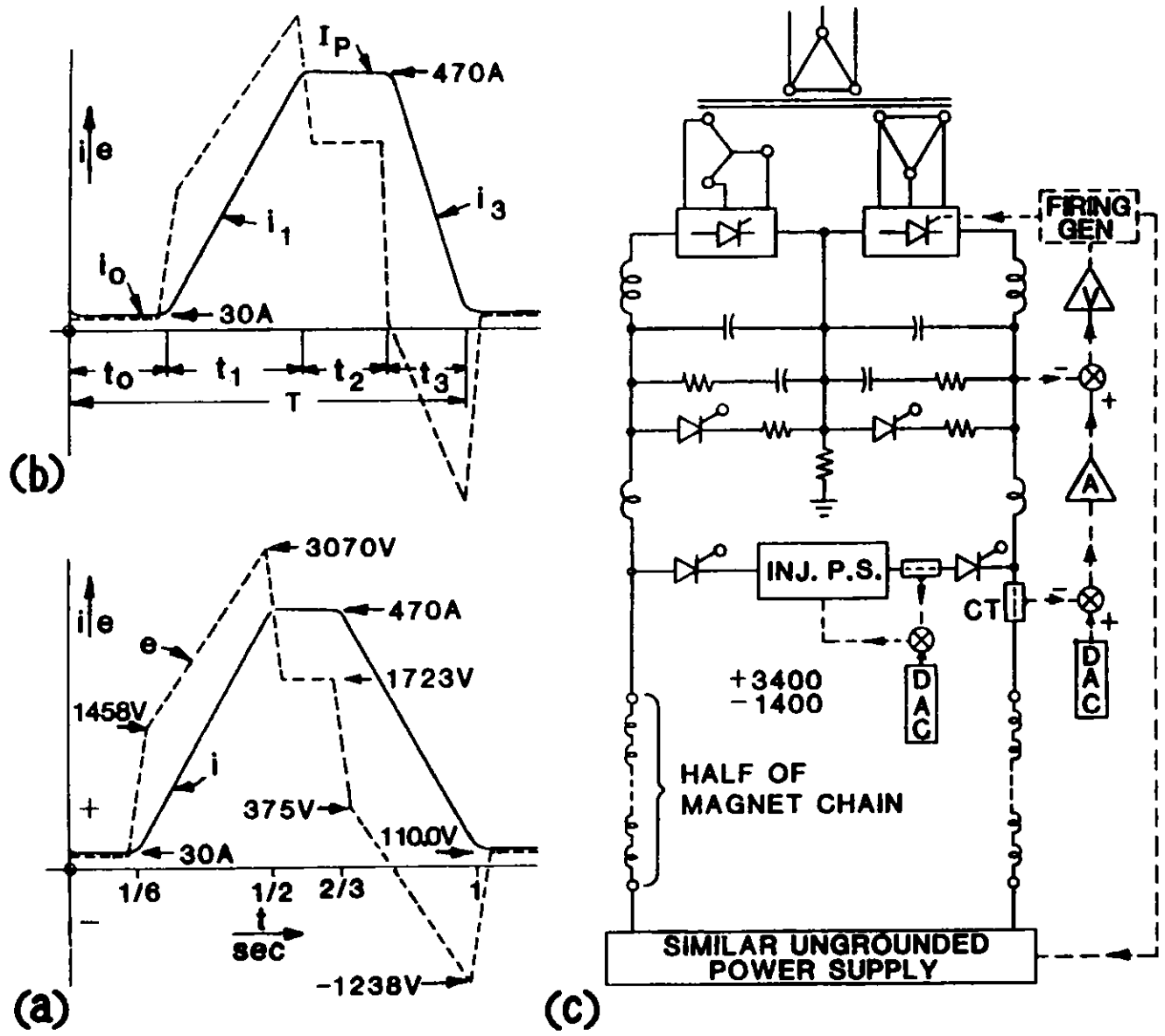

Figure II.10.3-9

Current and voltage shapes and block diagram of the dipole ring magnet power supply for the injector synchrotron.

A repeatable residual field will be attained after a long shutdown by pulsing the magnets at rated current for several minutes before the beam is injected. Table II.10.3-5 lists the power supplies for the ring magnet system and indicates their output characteristics and performance data. The current stability and reproducibility include the effects due to load variations, component drifts, and temperature coefficients over the range of 10°C to 40°C, as well as line fluctuations. The current tracking error applies to the nominal acceleration ramp of 20 GeV/s. All the power supplies have an upper limit of 7.7-GeV operation.

10.3.4.3.1 Dipole Power Supply

Two identical 12-phase power supplies are used to energize the chain of 68 dipoles from feed points 180° apart. Figure II.10.3-9 shows current and voltage shapes of one power supply for two operating conditions, together with a block diagram. In Fig. II.10.3-9(a), the current pulse is symmetrical, with injection and extraction times of nominally 1/6 s. These times can be increased, without changing the pulse repetition rate, by shortening the current decay time. As illustrated by Fig. II.10.3-9(b), this can be done over a wide range by changing the power supply output voltage by means of rectifier phase control. The delta- and wye-connected secondaries of the rectifier transformers feed two series-connected Si-controlled rectifier (SCR) bridges. The desired voltage and current shapes are produced by rectifier phase control of the 12-phase system, with a regulator comprising current and voltage feedback loops. The 12-phase rectified output is filtered by a passive damped LC filter. A 15-bit DAC is programmed by the control computer for the required current shape. The DAC is the reference for the current regulator, which obtains its feedback from a high-precision, low-drift, zero-flux current transductor. Fast correction for line transients is provided by an inner, relatively low gain, voltage loop controlled by the high-gain current loop. The injection current is only 6.4% of maximum current. At this current level, the current stability, ripple, and reproducibility are slightly degraded. Therefore, a separate 150-V, 50-A dc power supply, regulated to 0.01%, is used during injection. At the start of acceleration, the main power supply output voltage of 1458 V back-biases the SCRs in series with the injection power supply, thereby disconnecting it from the circuit. After flat top, when the current has decayed to close to the injection level (i.e., 34 A), the trigger pulses to the power supply SCRs are set for zero output voltage, and the crowbar SCRs, in parallel with the power supply filters, are turned on to discharge the filter capacitors. This causes the magnet current to decay exponentially, reaching the injection level of 30 A after ~23 ms. The injection current is maintained by turning on the SCRs in series with the injection power supply. During standby, the injection power supply operates into a light-load resistor in parallel with a low-inductance capacitor, both operating at the injection voltage of 110 V. Actual injection of eight 60-Hz pulses takes 133 ms.

Table II.10.3-5

Magnet Power Supplies for Injector Synchrotron

Magnet	Number of Units	I_{max} (A)	V_{max} (V)	P_{max} (kW)	P_{rated} (kW)	ΔI/Imax			Ref. Resol. (bit)
						Reproducibility	Current Ripple	Tracking Error	
Dipoles	2	470	+3070 -1238	1443	489	$\pm 1\times10^{-4}$	$\pm 2\times10^{-4}$	$\pm 5\times10^{-4}$	15
Quadrupoles	2	545	+ 576 - 32	372	200	$\pm 1\times10^{-4}$	$\pm 2\times10^{-4}$	$\pm 5\times10^{-4}$	15
Sextupoles	2	80	+ 151	13	8	$\pm 2\times10^{-4}$	$\pm 3\times10^{-4}$	$\pm 5\times10^{-4}$	14
H Corr. Mag.	40	±19	± 29	0.55	±0.5	$\pm 1\times10^{-3}$	$\pm 1\times10^{-3}$	$\pm 4\times10^{-3}$	12
V Corr. Mag.	40	±15	± 40	0.60	±0.5				

Only one regulator circuit is used for the two main power supplies. This regulator controls two sets of identical 12-phase SCR firing pulses that are transmitted to the two power supplies via optical links.

Only one of the two identical injection power supplies is current controlled, as shown in Fig. II.10.3-9; the other operates at a constant voltage of 110 V.

10.3.4.3.2 Quadrupole Power Supply

The two 12-phase power supplies provided have the features shown in Table II.10.3-5. One will energize 40 focusing magnets, the other 40 defocusing magnets. Except for the power rating, the power supply circuit is similar to the one shown for the dipole power supply. It should be noted that a magnet time constant of only 57 ms would permit pulsing of the circuit without power supply inversion. In this case, the crowbar SCRs are replaced with a diode because the power supply voltage is not reversed. At the end of flat top, after the beam has been extracted, the main power supply output voltages are reduced to zero. The quadrupoles discharge exponentially. The magnet current of 585 A decays to its injection level of 44 A in a time interval of 0.147 s.

10.3.4.3.3 Sextupole Power Supply

Two identical power supplies are used to energize the two strings of sextupoles, as shown in Fig. II.10.3-10. Since regulation requirements are not very stringent (see Table II.10.3-5), no separate power supply will be provided for the injection period. The DAC-programmed regulator controls, by means of rectifier phase control, the power supply output. Any arbitrary current shape is possible between zero and maximum current. The power supply peak voltage rating is such that the normalized rate of current change can be up to three times faster than that required for the dipole magnets.

10.3.4.3.4 Correction Magnet Power Supply

A total of 80 independently controlled ≤500-W power supplies are provided. The need for smooth control of the current through zero dictates the use of bipolar linear amplifiers with push-pull output stages. Such amplifiers are commercially available.

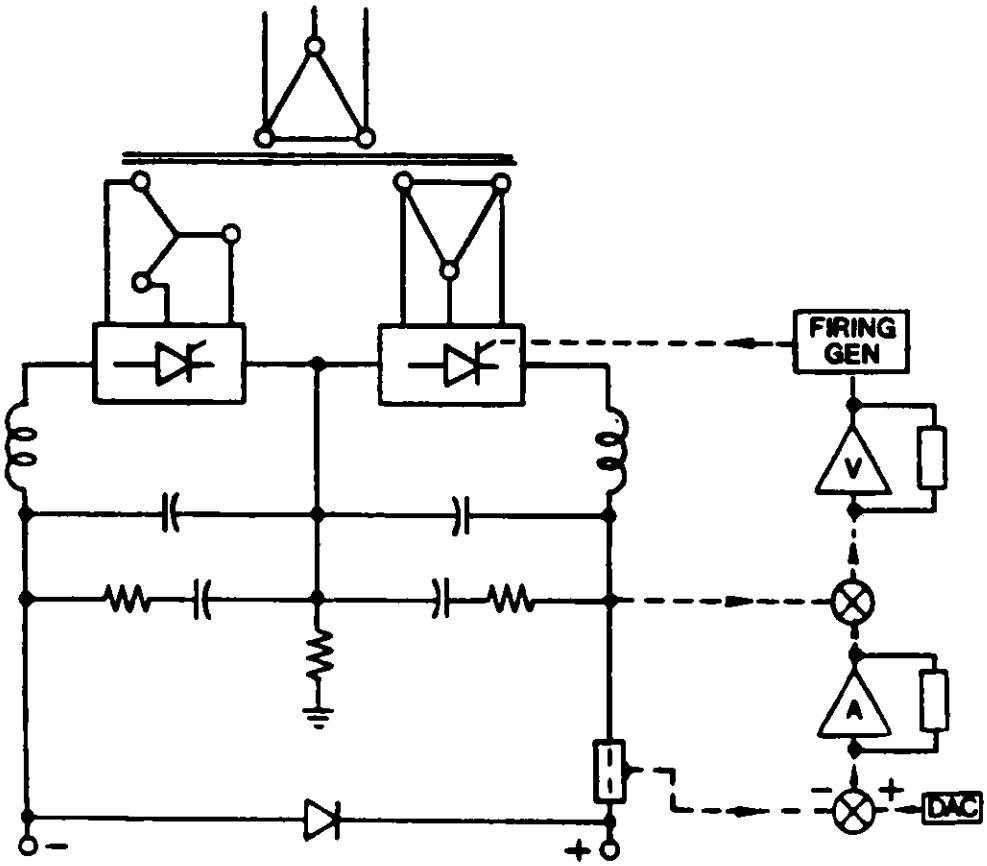

Figure II.10.3-10
Current and voltage shapes and block diagram of the sextupole power supply for the injector synchrotron.

10.3.5 Vacuum System

10.3.5.1 Vacuum Chamber

The chambers for the injector synchrotron are made from 1-mm-thick 304 stainless steel tubes formed to an elliptical shape with inside major and minor axes of 6 cm and 3.7 cm, respectively. This results in a thin metallic chamber without corrugations, which is smooth inside, allows maximum beam space in the magnets, and withstands atmospheric pressure.

Sections of the chambers are bent to fit the magnet curvature. Flanges, position monitors, bellows, etc., are attached by conventional welding techniques and leak tested.

10.3.5.2 Pumping

Ion pumps are used as the primary pumping source to maintain an average pressure of 10 nTorr in the 367-m circumference ring. The elliptical chamber is conductance limited. With a conservative outgassing rate of 1×10^{-11} Torr $\cdot$ ℓ/s/cm^2, 25-ℓ/s pumps spaced ~9.1 m apart are used to maintain the desired pressure. The ion pumps are equipped with heaters for bake-out. Preconditioning of the chambers includes chemical cleaning, bake-out and, if necessary, glow discharge cleaning.

For pump-down from atmospheric pressure, portable oil-free mechanical pumps evacuate the system to ~50 Torr after which sorption pumps reduce the pressure to the turbomolecular pump starting pressure. Mobile turbomolecular pumping stations are used to further reduce the pressure to the ion pump starting pressure.

10.3.5.3 System Monitoring

Ion pumps are uniformly distributed around the ring. Monitoring their current provides adequate pressure measurement. Ionization gauges are also distributed uniformly around the ring. Ring isolation valves eliminate the need for venting the entire ring to the atmosphere should repair in any one segment be necessary. Small isolation valves within each segment permit the mounting of gas analyzers or other monitoring equipment.

10.3.6 Injector Synchrotron Radio Frequency System

10.3.6.1 Introduction

The injector synchrotron rf voltage is provided by two systems operating at different frequencies. Between injection and 2.73 GeV, the frequency is 39.22 MHz. This is the 48th harmonic of the revolution frequency. Injection is into stationary buckets with the peak voltage at 60 kV, which is increased to 250 kV over several synchrotron oscillation periods. The phase-stable angle at 2.73 GeV is 144°. Between 2.73 GeV and extraction at 7 GeV, the 353-MHz system takes over. This is the 432nd harmonic of the revolution frequency. The 353-MHz cavities are deliberately detuned during the operation of the low-frequency system. The rf voltage starts at 2 MV at 2.73 GeV and increases to match the synchrotron radiation losses. At extraction, the maximum rf voltage is 11.8 MV, and the synchrotron radiation loss per turn is 6.33 MeV. The energy gain per turn is negligible compared to the synchrotron radiation loss.

The cavity for the 39.22-MHz system is a capacitively-loaded, coaxial design, and the four cavities for the 353-MHz system are each seven-cell, iris-loaded designs. The 39.22-MHz amplifier delivers 35 kW from a grounded-grid triode amplifier, of which 26.1 kW is needed for the Cu loss at 250 kV. The 353-MHz system is driven by a single 1-MW klystron identical to the ones used for the storage ring. The rf power from the klystron is divided equally among the four cavities. The Cu loss for each seven-cell cavity is about 116.6 kW at a peak accelerating field of 3 MV per cavity.

10.3.6.2 39.22-MHz Cavity

A cross-sectional view of the 39.22-MHz cavity is shown in Fig. II.10.3-11. It is a capacitively-loaded coaxial cavity with a circular tuning plate on the high voltage end. The cavity is excited by a current loop located at the shorted end. The cavity material is Cu-plated stainless steel to provide rugged construction and the ability to bake-out. The Cu plating is 30 μm to 50 μm (0.001 in. to 0.002 in.) thick, and the skin depth is 10 μm. The cavity is fabricated by rolling, welding, and machining the stainless steel plates. The inner surfaces are highly polished and then plated.

A tuning range from 38.7 MHz to 39.74 MHz is provided by a motor-gear drive system that drives the tuning plate back and forth through a bellows arrangement so that the effective gap can be changed between 7.1 cm and 7.5 cm. Cavity dimensions are listed in Table II.10.3-6, and performance characteristics are listed in Table II.10.3-7.

Several ports are provided for field measurements with small probes and loops. Provisions are made for damping antennas and loops for suppression of higher order modes if they become troublesome.

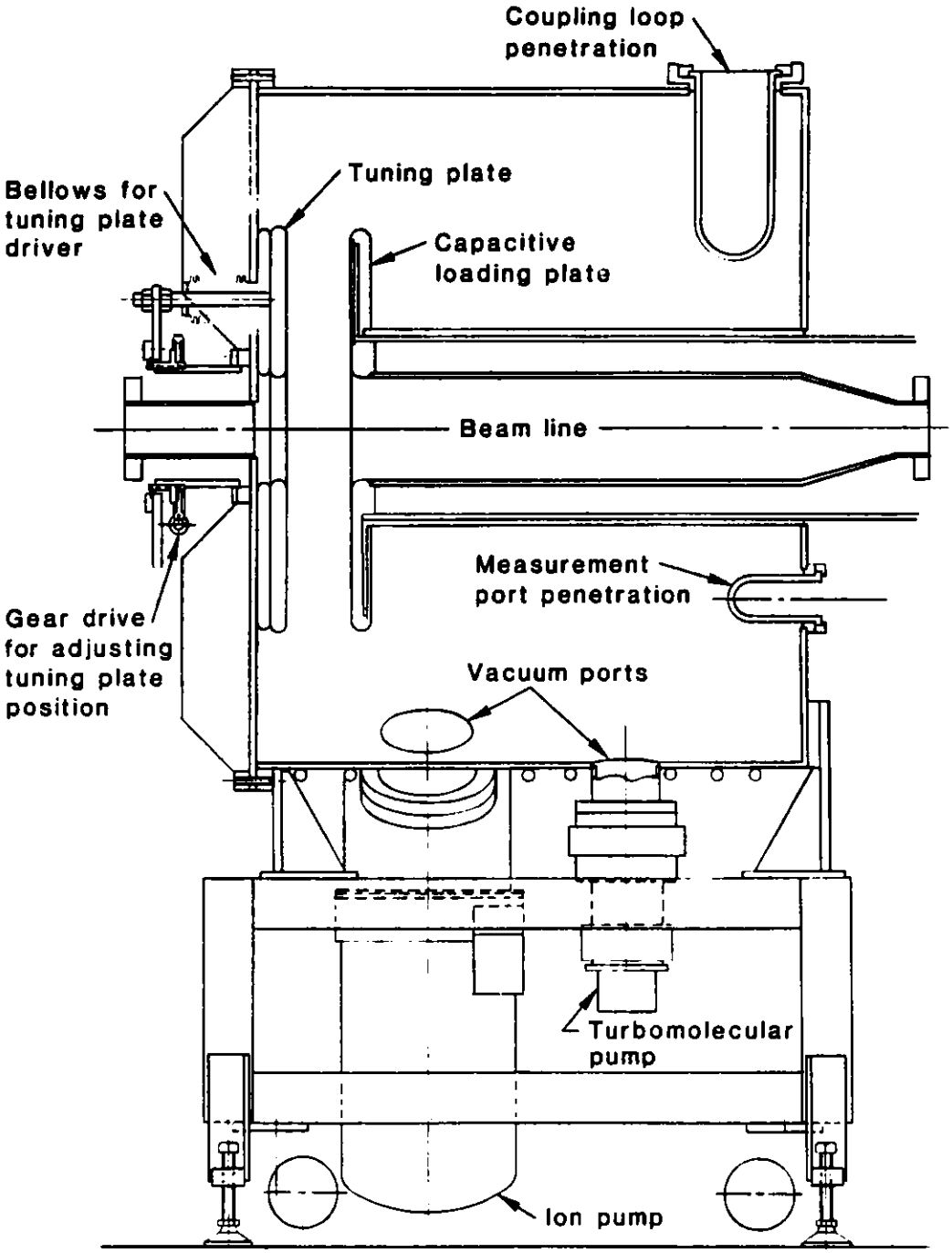

Figure II.10.3-11
39.22-MHz accelerating cavity.

Table II.10.3-6

Dimensions of the 39.22-MHz Cavity (m)

Length of Outer Shell (inside wall to inside wall)	1.028
Radius of Outer Shell (center line to inside of outer wall)	0.5
Length of Inner Conductor (inside face of shorted end of cavity to inside face capacitive-loading plate)	0.928
Thickness of Capacitive-Loading Plate	0.03
Radius of Inner Conductor (center line to outside surface)	0.145
Diameter of Beam Tube	0.077
Outer Radius of Capacitive-Loading Plate	0.30
Outer Radius of Tuning Plate	0.27
Gap between Capacitive-Loading Plate and Tuning Plate	0.071-0.075

Table II.10.3-7

Performance Characteristics of the 39.22-MHz Cavity

Operating Frequency	38.7-39.74 MHz
$\int E_z \cos(kz/\beta)dz$	250 kV
Cavity Power @ 250 kV	26.1 kW
Cavity Q	25,900
Shunt Impedance	5.68 MΩ
Peak Electric Field on Surface @ 250 kV (39.74 MHz)	5.94 MV/m

Vacuum pumping is achieved through a slotted port. A 360-ℓ/s turbomolecular pump and a 400-ℓ/s ion pump are used.

10.3.6.3 39.22-MHz Radio Frequency Amplifier

The rf power for the 39.22-MHz system is provided by a triode amplifier operated in the grounded-grid configuration. The rf amplifier is available from commercial

sources. The cavity is driven by a 50-Ω rigid transmission line (3-1/8-in. dia.), with the length between the cavity and amplifier adjusted to a multiple of λ/2.

10.3.6.4 353-MHz Radio Frequency Cavity

The cavities for the 353-MHz injector synchrotron rf system are essentially copies of the LEP/PEP[11,12] five-cell, λ/2 resonant cavities except for the addition of two extra cells. They have a 10.0-cm diameter beam hole with a reentrant nose. The cell length is λ/2 (42.49 cm). The radius from the center line to the inside of the outer shell is 30.2 cm. The cells are magnetically coupled with two off-axis slots. The seven-cell structure is loop-excited in the center cell using a post-coupler from the WR2300 waveguide. Tuners are provided in the two cells adjacent to the center cell. Vacuum separation between the waveguide and the seven-cell cavity is provided by a cylindrical ceramic window surrounding the waveguide post. The cavity body is made from forged disks and forged seamless cylinders of Cu. These are machined to close tolerances and electron-beam welded.

A list of parameters for the seven-cell cavity is given in Table II.10.3-8. The four 353-MHz cavities are divided into two groups and placed symmetrically on opposite sides of the synchrotron.

Table II.10.3-8

Parameters for the Seven-Cell, λ/2, 353-MHz Cavity

Bore-Hole Diameter	10.0 cm
Cell Length (center line to center line)	42.49 cm
Cell Length (inside of cell, wall to wall)	38.9 cm
Cell Radius	30.2 cm
Number of Cells	7
Active Length of Cavity	2.97 m
Total Length of Cavity	3.17 m
Shunt Impedance	26.1 MΩ/m
Average Accelerating Voltage	1.01 MV/m
rf Power @ 3.0 MV/cavity	116.6 kW

10.3.6.5 353-MHz Radio Frequency Power System

The 353-MHz system for the injector synchrotron is essentially the same as the 353-MHz rf system for the storage ring. The same kind of klystron is used, but optimized to achieve a maximum efficiency of 65-70% at 500 kW instead of 1 MW. A circulator is provided to protect the klystron. Phase shifters are used to adjust the phase to the cavities.

10.4 Transport and Injection into Injector Synchrotron

10.4.1 Transport Line from Linac

The transport line between the linac and injector synchrotron is shown in Fig. II.10.4-1. The 29-m transfer line is made up of two segments. The downstream section, which includes the injection septum in the synchrotron and a 10° bending magnet in the transfer line, is a 360°-phase advance achromatic cell to match the dispersion function in the synchrotron. The upstream section has five quadrupole magnets near the linac for the phase-space matching between two accelerators. Figure II.10.4-2 shows the transfer line β and dispersion functions. The magnet elements needed for this transfer line are shown in Table II.10.4-1.

10.4.2 Injection Geometry and Procedure

The injection geometry is shown in Fig. II.10.4-3. Since the injection procedure planned is to transfer a macropulse of the linac to a waiting rf bucket of the synchrotron in accordance with the linac repetition rate, the geometry is designed for on-axis injection by means of a kicker and a septum magnet. The septum magnet is located in the empty half cell of the dispersion suppressor cell, and the kicker is located about half a cell after the septum. A kicker strength of $\int B d\ell = 0.0077$ T·m is required. The injection trajectory and its associated beam envelopes are shown in Fig. II.10.4-4.

For each cycle of the injector synchrotron, eight positron pulses, each of which is 16.5 ns long, are injected one at a time into every sixth bucket of the 39.22-MHz rf system while the synchrotron field is at the flat bottom. At this time the waiting bucket length is 25.5 ns, and therefore the bucket can accommodate the 16.5-ns pulse easily. The flat-bottom duration is 1/6 s, and the eight-pulse linac duration is 0.133 s. Therefore, there is sufficient time to accomplish the injection. The kicker, which is designed to accommodate the required time durations, is described in Sec. II.10.4.4.

10.4.3 Injection Septum Magnet

The septum magnet is a pulsed device of a design similar to that used for injection into the storage ring. It operates at a peak field of 0.49 T at 60 pulses per second. The

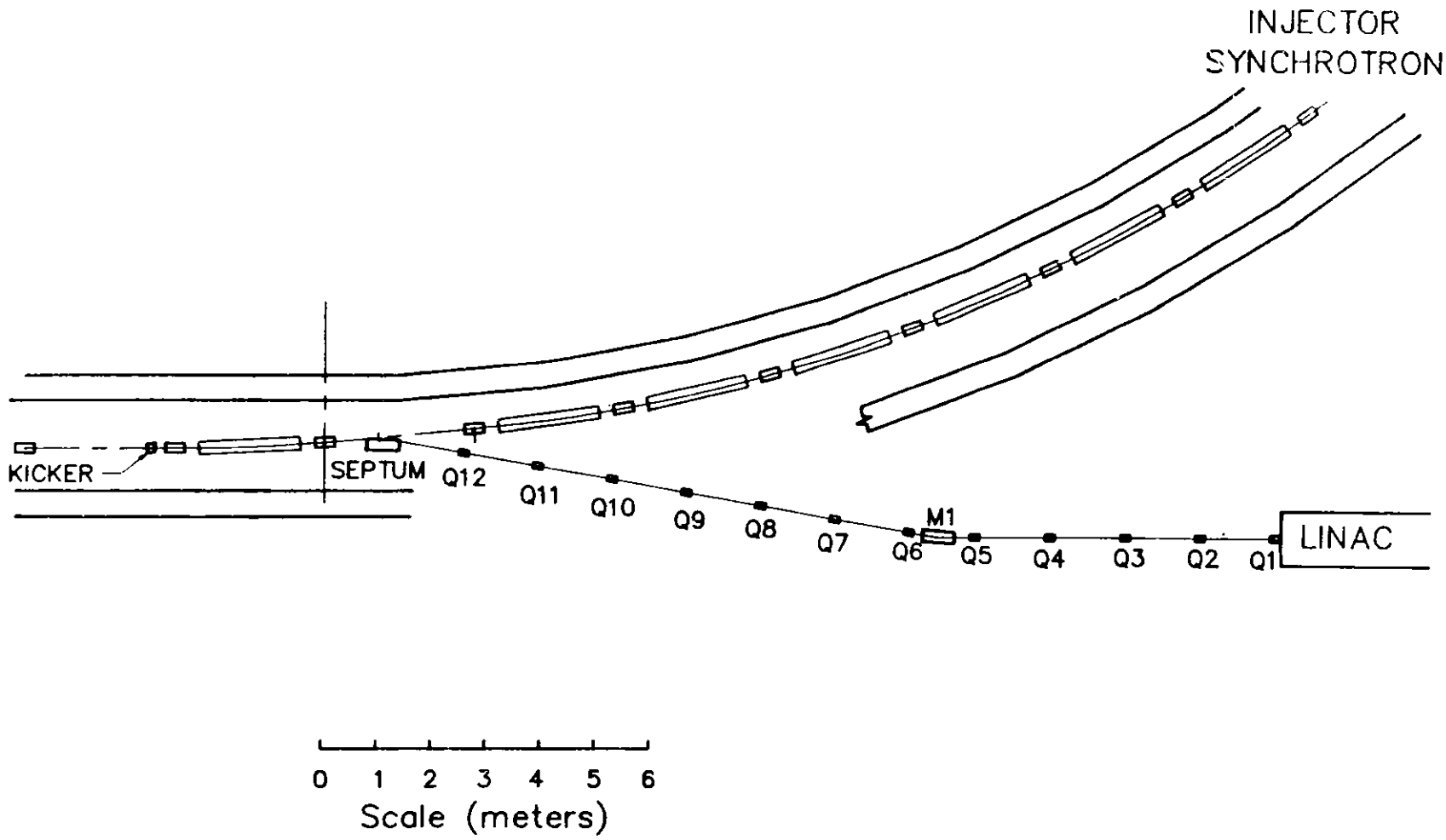

Figure II.10.4-1
Layout for the linac-to-injector-synchrotron transfer line.

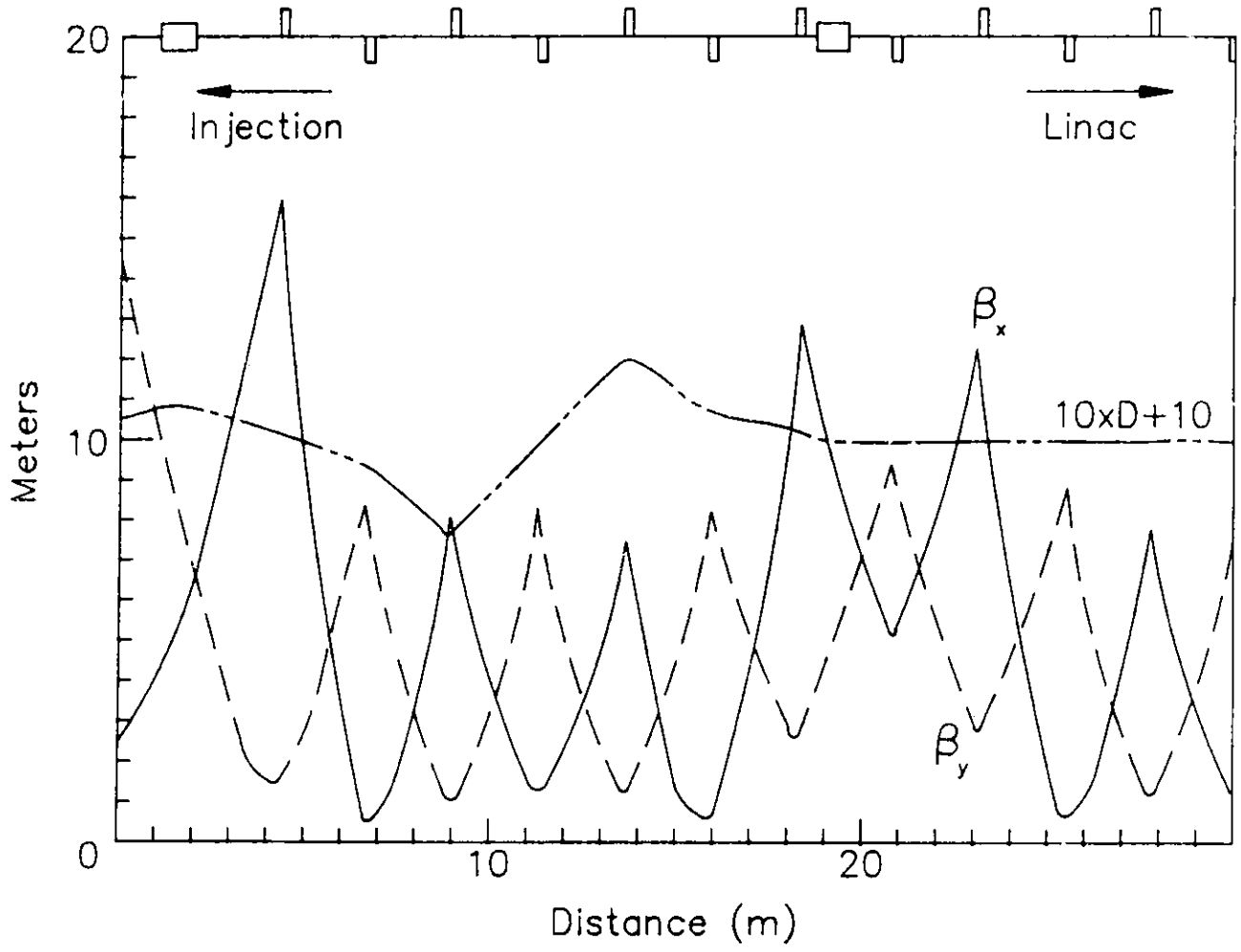

Figure II.10.4-2
β and dispersion functions for linac to synchrotron transfer line.

Table II.10.4-1

Parameters for Magnets in Transport Line between Linac and Synchrotron

		Dipole	Quadrupoles
Number Required		1	12
Field Strength at 450 MeV		0.27 T	3.8 T/m max.
Effective Length	(m)	1.0	0.3
Gap Height or Diameter	(mm)	40	70
Total Mass	(kg)	290	125
Coils per Pole		1	1
Conductor Height	(mm)	6.0	2.0
Width	(mm)	6.0	2.0
Hole Diameter	(mm)	3.3	edge-cooled
Coil Turns per Pole		40	288
Coil Current	(A)	110	7
Current Density in Conductor	(A/mm^2)	2.0	1.5
Voltage	(V)	14.2	28.9
Power	(kW)	1.6	0.2
Cooling Water Circuits per Magnet		2	4
Total Water Flow	(gal/min)	0.4	0.05
Water Pressure Drop	(psi)	100	100
Water Temperature Rise	(°C)	18	15

minimum thickness of the septum is 2 mm, but this increases along the length to improve the mechanical and thermal properties. Table II.10.5-2 lists the parameters of this magnet, together with those of the extraction septum magnets.

10.4.4 Injection Kicker Magnet

The injection kicker has a peak field of 0.031 T and a length of 25 cm. The pulse duration is ~145 ns, with a flat top of ~29 ns, to accommodate the 16.5-ns long linac macropulse.

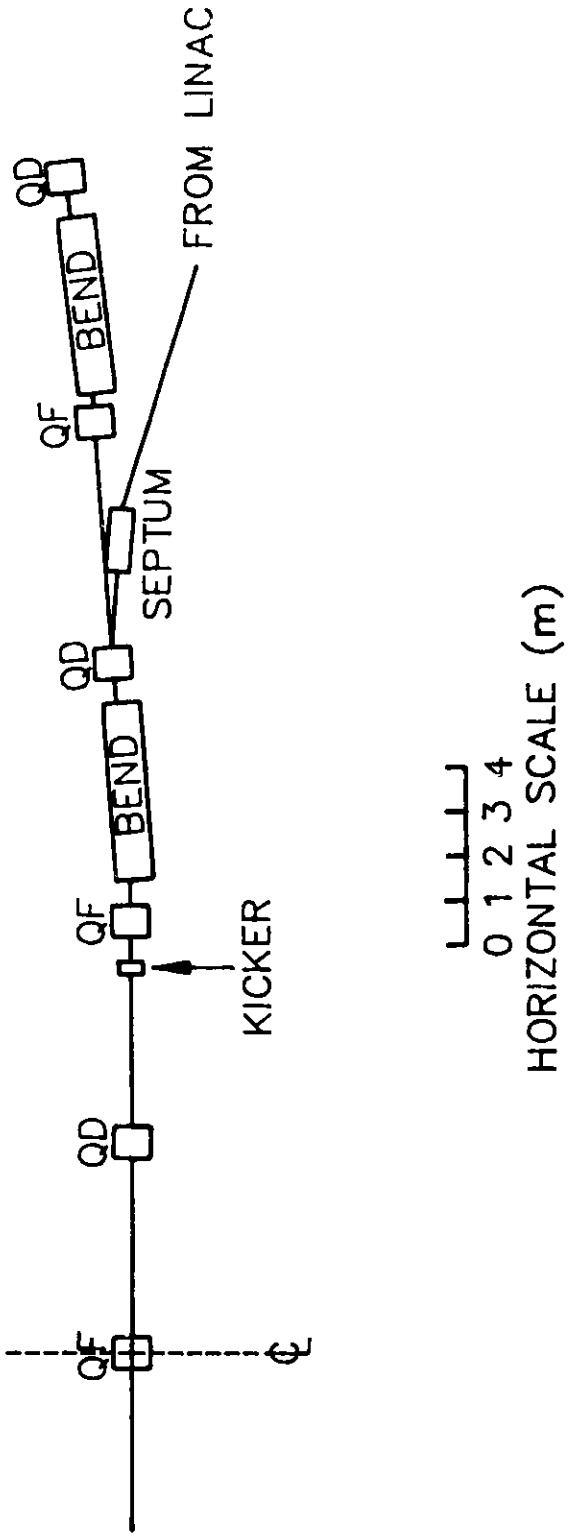
FROM LINAC
QD
BEND
QF
SEPTUM
QD
BEND
QF
KICKER
QD
QF
℄
0 1 2 3 4
HORIZONTAL SCALE (m)

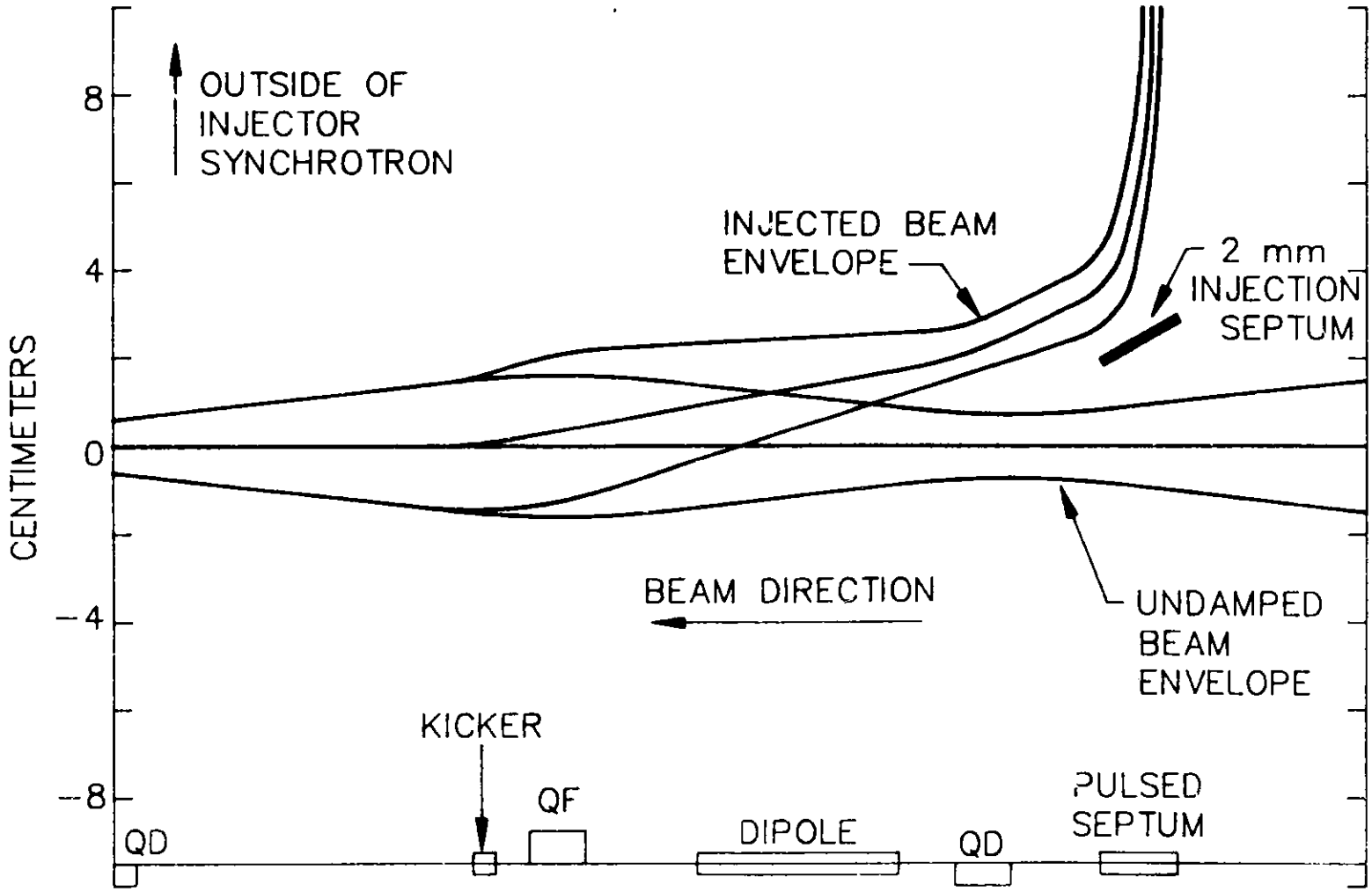

Figure II.10.4-4

Beam trajectory and 4-σ envelope for the injected and undamped beams in the injection region of the injector synchrotron. The 2-mm injection septum is 21 mm from the unperturbed orbit.

A single-turn ferrite core magnet with a picture-frame design is used, as shown in Fig. II.10.4-5. The inside of the ceramic vacuum chamber is aluminized to minimize impedance to the beam. The power supply uses a thyratron-gated PFN made up of 5.4 m of commercially available 14-Ω coaxial cable. The power supply and magnet are shown schematically in Fig. II.10.4-6. The design requirements and system specifications are given in Table II.10.5-1.

10.5 Extraction from Synchrotron and Transport to Storage Ring

10.5.1 Extraction Procedure and Geometry

At the 7-GeV flat top, the bunches are extracted one at a time at a 60-Hz rate for injection into the designated rf buckets in the storage ring. The extraction trajectory and its associated beam envelopes are shown in Fig. II.10.5-1. The bunch to be extracted is initially kicked 2.35 mrad outward by a three-section kicker with a total $\int B d\ell$ = 0.055 T·m. The kicked beam enters the septum magnet 27 mm from the central orbit. The pulsed magnet has a 2-mm-thick septum. The extracted beam clears the outside of the septum by 3 σ.

After this pulsed septum magnet, there are two dc septum magnets providing a total bend of 6.5°. The extracted beam clears the downstream quadrupole by 11 cm.

10.5.2 Kicker Magnet

The fast kicker consists of three identical 0.6-m cells. The cross section is identical with the injection kicker magnet of Section II.10.4.4 and is shown in Fig. II.10.4-5. As shown in Fig. II.10.5-2, a PFN discharges through the magnet coils into terminating loads when the thyratron is triggered. Six parallel cables from the PFN and six half-turn coils connected to separate terminating loads make up the load. The design requirements and system specifications are given in Table II.10.5-1.

10.5.3 Septum Magnet

The extraction septum magnets consist of a pulsed septum operated at a 60-Hz pulse rate, followed by two dc septa. These magnets are the same as those used for injection into the storage ring (see Section II.4.7-1). The parameters for these magnets are listed in Table II.10.5-2.

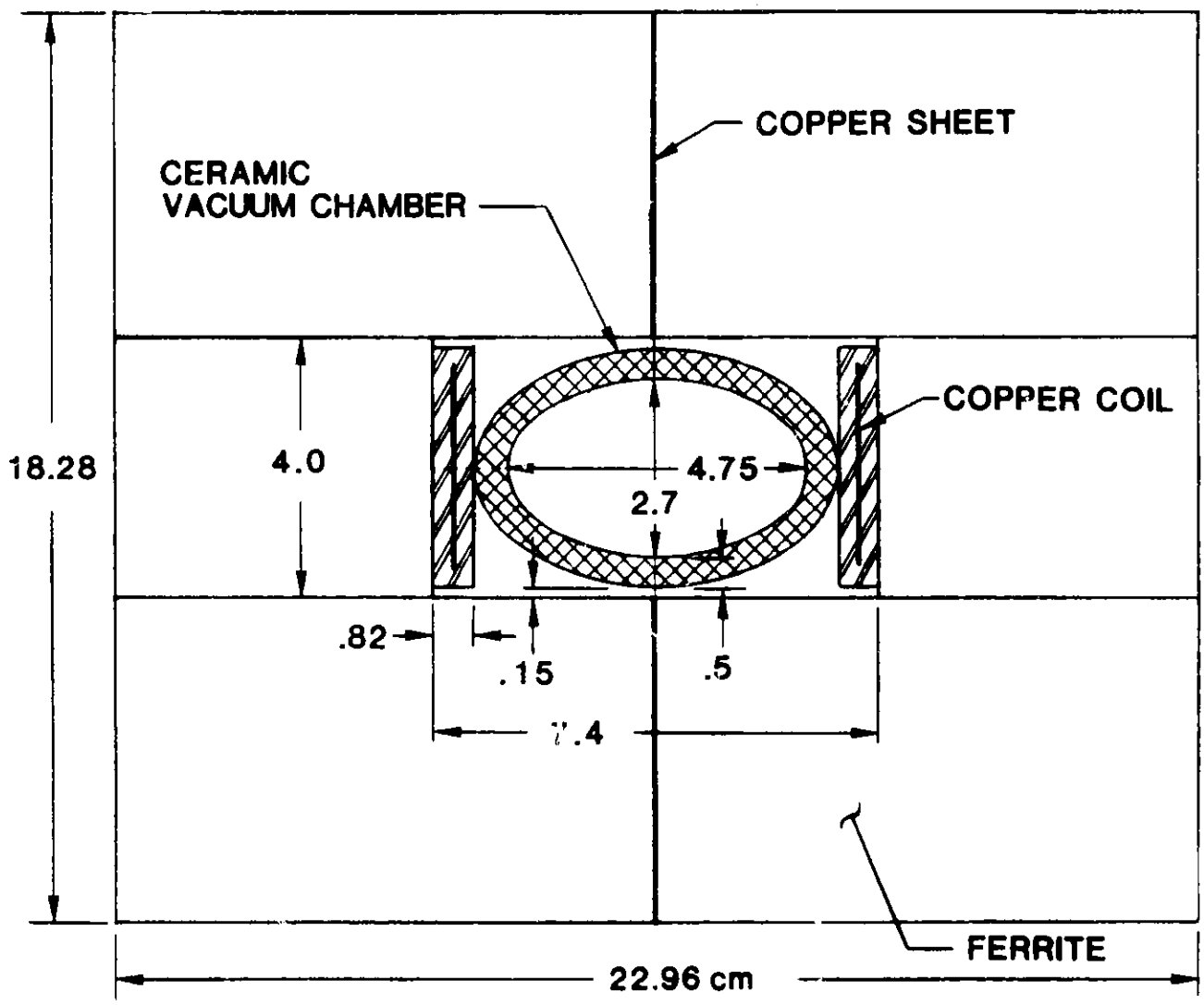

Figure II.10.4-5
Cross section of kicker magnets.

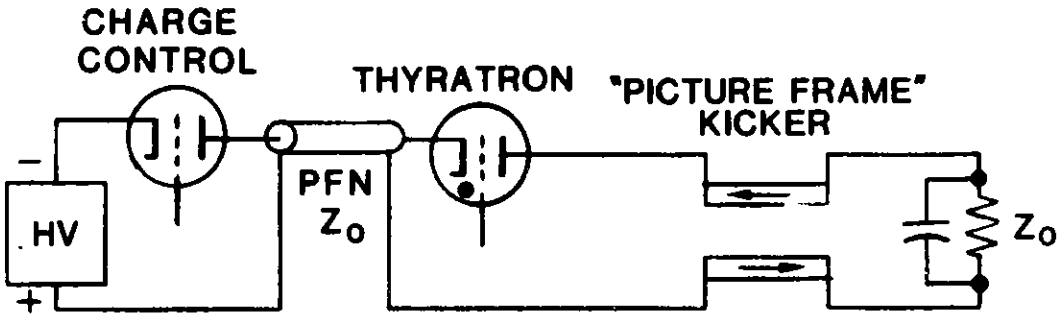

Figure II.10.4-6
Schematic diagram for power supply and injection kicker.

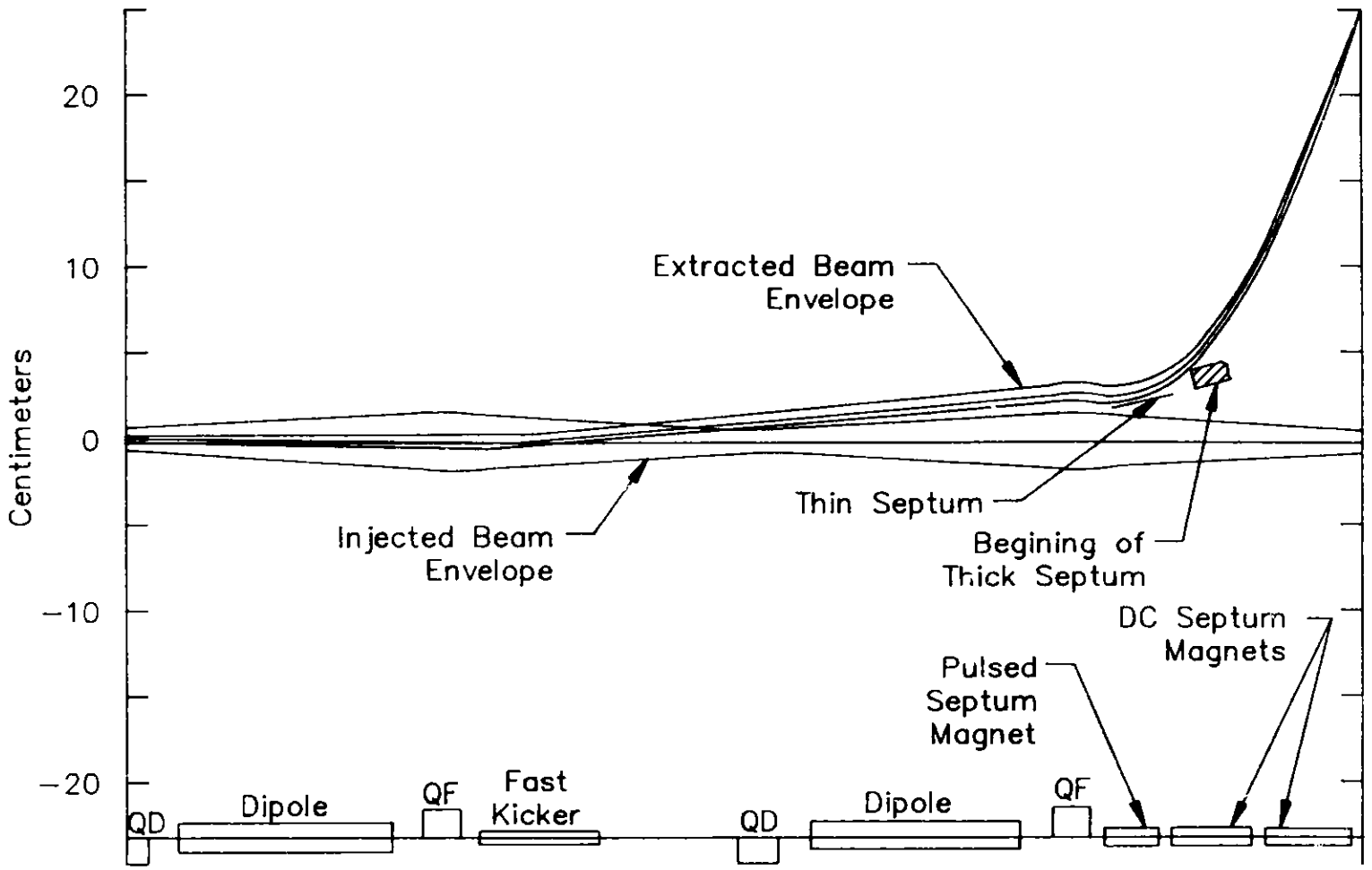

Figure II.10.5-1
Position and 3-σ envelope for extracted beam. The 4-σ envelope for the injected beam is also shown.

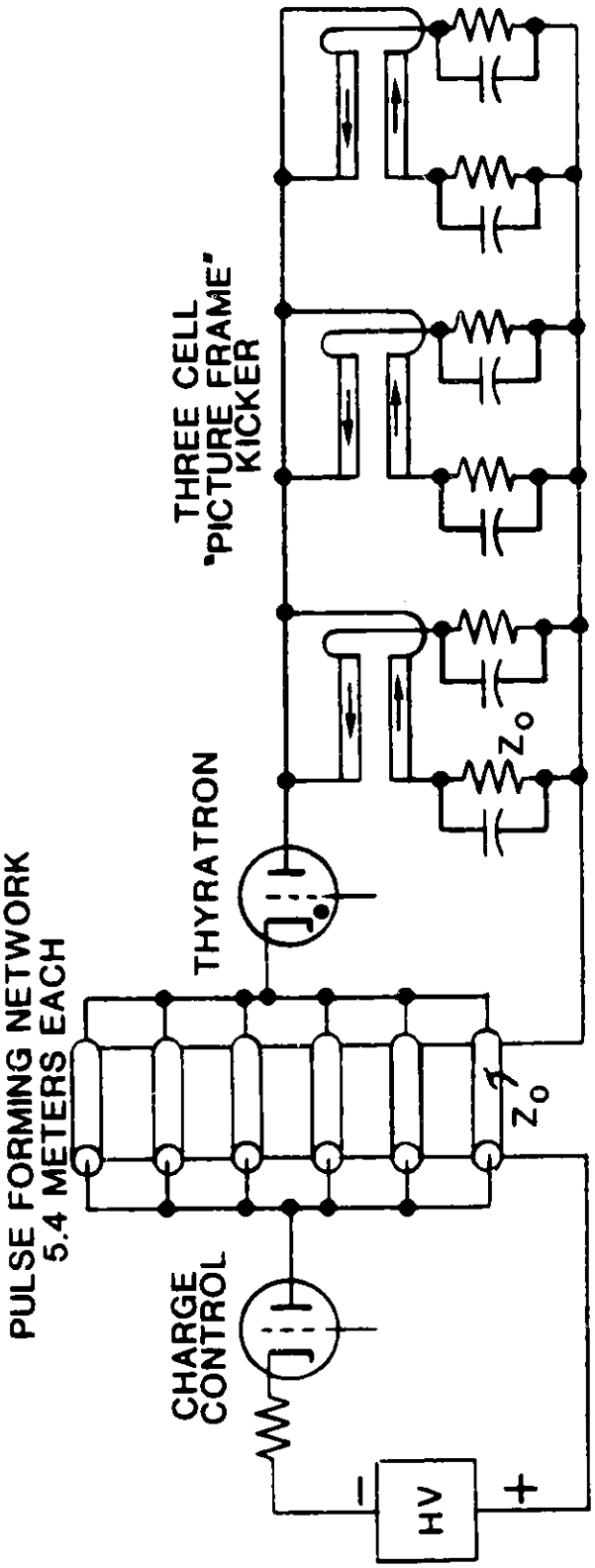

Figure II.10.5-2
Power supply for extraction kicker.

Table II.10.5-1

Design and System Specifications
for Synchrotron Injection and Extraction Kickers

		Injection	Extraction
Rise Time	(ns)	43.2	43.2
Flat Top	(ns)	28.7	28.7
Fall Time	(ns)	72	72
PFN Voltage	(kV)	34.1	39.7
PFN Charge Current	(mA)	5.58	39.1
PFN Cables	(m)	5.4	6×5.4 in parallel
Cable Type		YR-10914	YR-10914
Cable Impedance	(ohms)	14	14
Configuration		1 cell 1 coil	3 cells, 6 coils
Peak Field	(T)	0.0383	0.0445
Peak Magnet Current	(kA/coil)	1.219	1.417
Magnet Inductance	(nH/coil)	402	605
Charge Power Dissip. (60 Hz CW)	(W)	85.4	696
Load Power Dissip. per coil (60 Hz CW)	(W)	85.4	116
Field Dimensions:			
Gap Height	(cm)	4	4
Gap Width	(cm)	5.75	5.75
Length	(m/cell)	0.2	0.6
Ferrite Type		Ceramic Magnetics type CMD-5005	

Table II.10.5-2

Parameters for Injector Synchrotron Septa

Type		Injection	Extraction		
		AC Pulsed	AC Pulsed	DC Thin	DC Thick
Min. Septum Thickness	(mm)	2	2	14	30
Peak Field	(T)	0.49	0.8	0.9	0.9
Physical length	(m)	0.85	0.85	1.15	1.25
Effective Length	(m)	0.8	0.8	1.1	1.2
Gap Height	(mm)	30	20	25	30
Gap Width	(mm)	40	40	40	40
Number of Turns		4	3	12	36
Total Inductance	(mH)	0.021	0.02	0.6	5.2
Total Resistance	(mΩ)	6.7	5.4	19	98
Peak Supply Current	(A)	2954	4286	1510	600
Peak Power	(kW)	138	245	43	36
Power	(kW)	0.157	0.28	43	36

10.5.4 Transport to Storage Ring

The transfer line between the synchrotron and the storage ring is essentially made of three parts. To match the beam optics at both ends of the line, the extraction hardware of the synchrotron and the injection hardware of the storage ring are included in the design optics as shown in Fig. II.10.5-3. The first part of the transfer line is then a 360° phase advance achromatic cell that includes the initial bend of 6.5° from the extraction hardware and an opposite bend of 8.3°. This achromatic cell eliminates the dispersion created by the extraction hardware.

The dispersion-free second part contains eight quadrupoles for matching the β functions from the synchrotron to those of the storage ring.

The third part, which consists of an 8.2° bend and the storage ring injection magnets, is a 180° achromatic cell that matches the dispersion function in the ring.

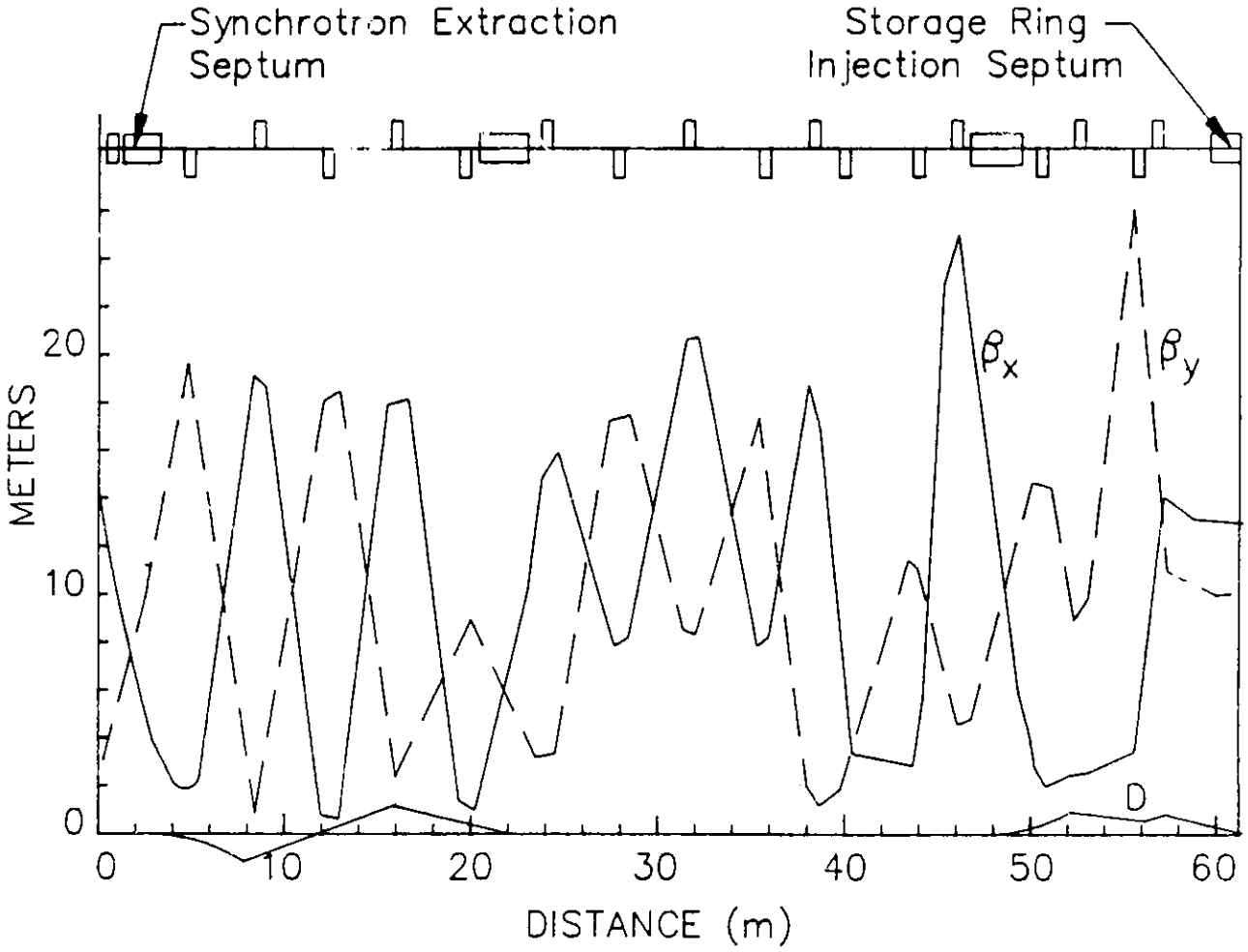

Figure II.10.5-3
β and dispersion functions for synchrotron-to-storage-ring transfer line.

The total length of the transfer line is about 54 m, and the physical layout is shown in Fig. II.10.5-4. The magnet parameters of the line are described in Table II.10.5-3.

10.5.5 Beam Diagnostics Line

Figure II.10.5-4 includes the schematic for the beam-diagnostics transfer line, which consists of two bending magnets and two quadrupoles. The total length of the beam diagnostics line is about 10 m. The magnets used are the same as those in the transport line from the synchrotron. This line is used to measure synchrotron beam properties.

10.6 Beam Diagnostic Instrumentation for Injector System

The beam diagnostic instrumentation discussed here is described in more detail in Section II.7. Table II.10.6-1 shows the types and quantities of the diagnostics installed in the injector system.

The beam position in the synchrotron is measured by buttons identical with the ones in the storage ring. The monitors are able to measure 0.1 mm, with a total circulating current of 1.6 mA. The processing is also identical. Wall current monitors are used to measure the beam position as well as the intensity in the linac and beam transport lines. Processing is similar to that of the button monitors. Signals from the monitors are available in the main control room for viewing on oscilloscopes.

The circulating beam intensity in the synchrotron is measured by current transformers located around metallized ceramic vacuum chambers. Two bending-magnet synchrotron-radiation-monitoring stations are installed for monitoring the transverse and longitudinal characteristics of the beam. The stations are instrumented with photomultipliers, photodiodes, and television cameras. The synchrotron has electrodes and driver amplifiers for measuring betatron tunes. Movable horizontal and vertical beam scrapers are provided. Fluorescent screens and secondary emission grids are installed to measure the position and profile of the beam when needed. These monitors, as well as movable wire scanners, are used in the linear accelerators and beam transport lines.

Ion chamber loss monitors are provided at strategic locations throughout the injector system.

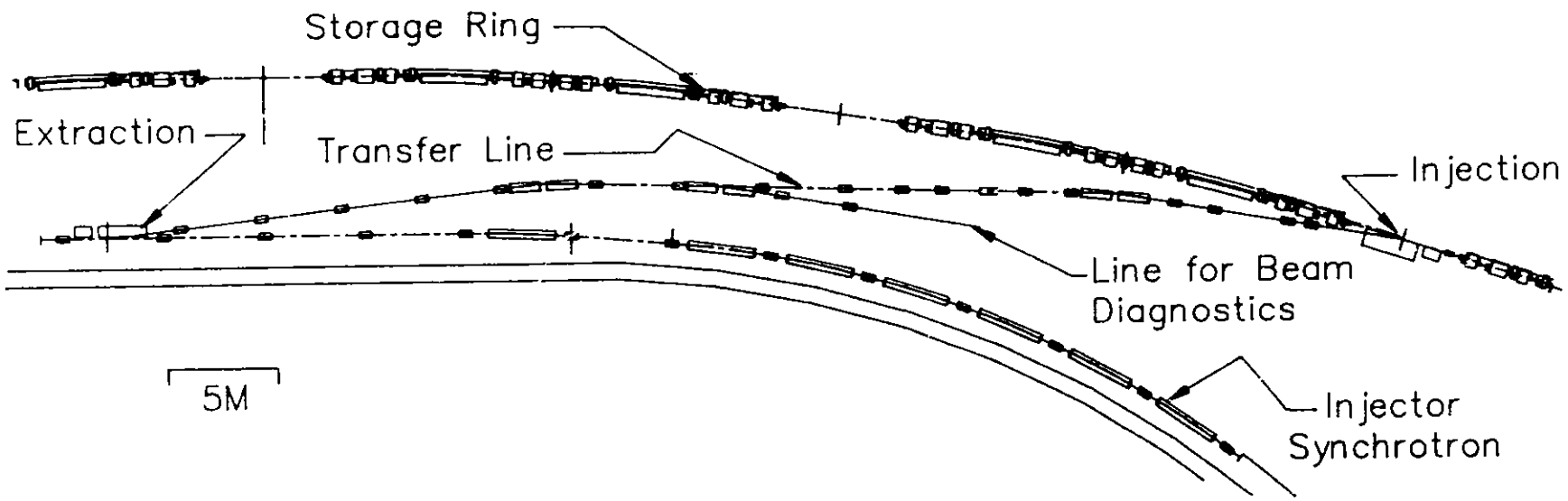

Figure II.10.5-4
Layout of injector-synchrotron-to-storage-ring transfer line.

Table II.10.5-3

Parameters for Magnets in Transport Line to
Storage Ring and Beam Diagnostics Line

		Dipole	Quadrupole
Number Required		6	19
Field Strength @ 7 GeV		1.24 T	20 T/m
Effective Length	(m)	1.36	0.6
Gap Height or Diameter	(mm)	20	50
Total Mass	(kg)	720	760
Coils per Pole		1	1
Conductor Height	(mm)	9.0	6.0
Width	(mm)	9.0	6.0
Hole Diameter	(mm)	5.0	3.3
Turns per Pole		32	96
Supply Current	(A)	318	53
Current Density in Coil	(A/mm^2)	2.9	1.0
Voltage	(V)	19	20
Power	(kW)	6.0	1.1
Cooling Water Circuits/Magnet		4	4
Total Water Flow	(gal/min)	2.7	0.4
Water Pressure Drop	(psi)	100	100
Water Temp. Rise	(°C)	9	15

10.7 Injector Control System

The injector accelerators use the same control system components as those used for the storage ring, and a comprehensive description is found in Section II.8 (Control System). The features pertinent to the injector systems are as follows:

- Microprocessor-based clusters are used to interface with the injector systems, with one cluster provided for each klystron system in the linac, one for each of the two rf systems of the synchrotron, and seven additional clusters provided

Table II.10.6-1

Beam Diagnostic Instrumentation for Injector System

	Quantity	Monitor Type	Function
Electron Linac	2	Current Transformers	Intensity
	8	Wall Current	Position, Intensity
	8	Fluorescent Screens	Position, Profile
	8	Loss Monitors	Losses
Positron Linac	2	Current Transformers	Intensity
	8	Wall Current	Intensity, Position
	8	Fluorescent Screens	Position, Profile
	10	Loss Monitors	Losses
Linac-Synchrotron Transfer Line	2	Current Transformers	Intensity
	4	Wall Current	Intensity, Position
	3	Fluorescent Screens	Position, Profile
	4	Wire Scanners	Position, Profile
	6	Loss Monitors	Losses
Injector Synchrotron	1	Current Transformer	Intensity
	80	4-Button Pickups	Position, Intensity
	1	Photon Monitors	Intensity; Transverse and Longitudinal Beam Characteristics
	2	RF Electrodes and Driver	Betatron Tune, Damping Factor
	40	Loss Monitors	Losses
	8	Fluorescent Screens	Injection Position, Profile
	2	X and Y Beam Scrapers	Injection Halo, Beam Studies
Synchrotron-Storage Ring Transfer Line and Beam Diagnostics	3	Current Transformers	Intensity
	4	Wall Current	Position, Intensity
	6	Fluorescent Screens	Position, Profile
	4	Wire Scanners	Position, Profile
	6	Loss Monitors	Losses

for the injection and extraction lines and the diagnostic, power supply, and vacuum systems (see Section II.8.2.4).

- One front-end computer and network is provided to serve both the linac and synchrotron. These computers maintain a current machine-state data base for use by the host and console computers as well as for formatting and distributing control and monitoring data for the microprocessor clusters (see Section II.8.2.3).

- A separate full-function control console system is provided in the injector control area in the synchrotron injection building. Aside from its ability to access all three accelerator systems, this console also has access to the signal cross-bar and video sources of the linac and synchrotron (see Section II.8.2.2).

- The linac and the synchrotron can be operated autonomously once filling of the storage ring is completed. Control can be from the linac control area or from the central control area, where additional consoles are available (see Section II.8.5.)

- The linac and the synchrotron can be operated autonomously once filling of the storage ring is completed. Control can be from the injector control area or from the central control area, where additional consoles are available (see Section II.8.5).

10.8 References

1. D. T. Tran, "A Low-Cost RF Structure for Electron and Proton Linac," IEEE Trans. Nucl. Sci., NS-24, 1774 (1977).

2. W. Gallagher et al., "A High-Current Electron Linac," IEEE Trans. Nucl. Sci., NS-18, 584 (1971).

3. R. Kooutz et al., "SLAC Collider Injector," IEEE Trans. Nucl. Sci., NS-28, 2213 (1981).

4. R. B. Neal, The Stanford Two-Mile Accelerator (Stanford University Press, 1968), pp. 95-162.

5. Z. D. Farkas et al., "Microwave Developments at SLAC," IEEE Trans. Nucl. Sci., NS-24, 1827 (1977).

6. "LEP Design Report," Vol. I, CERN-LEP/84-01, p. 11 (June 1984).

7. G. Faillon, "New Klystron Technology," IEEE Trans. Nucl. Sci., NS-32, 2945 (1985).

8. G. Stange, "An Inexpensive Positron Converter," IEEE Trans. Nucl. Sci., NS-26, 4146 (1979).

9. H. Wiedemann, "Users Guide for PATRICIA Version 84.9," SSRL ACD-Note 22 (November 1984).

10. A. Febel and G. Hemmie, "Status and Performance of PIA," Proc. Eleventh Intl. Conf. on High Energy Accelerators, Geneva, Switzerland, July 7-11, 1980, p. 43.

11. "LEP Design Report," Vol. II, CERN-LEP/84-01 (June 1984).

12. M. A. Allen et al., "RF System for the PEP Storage Ring," IEEE Trans. Nucl. Sci., NS-24, 229 (June 1977).

III.

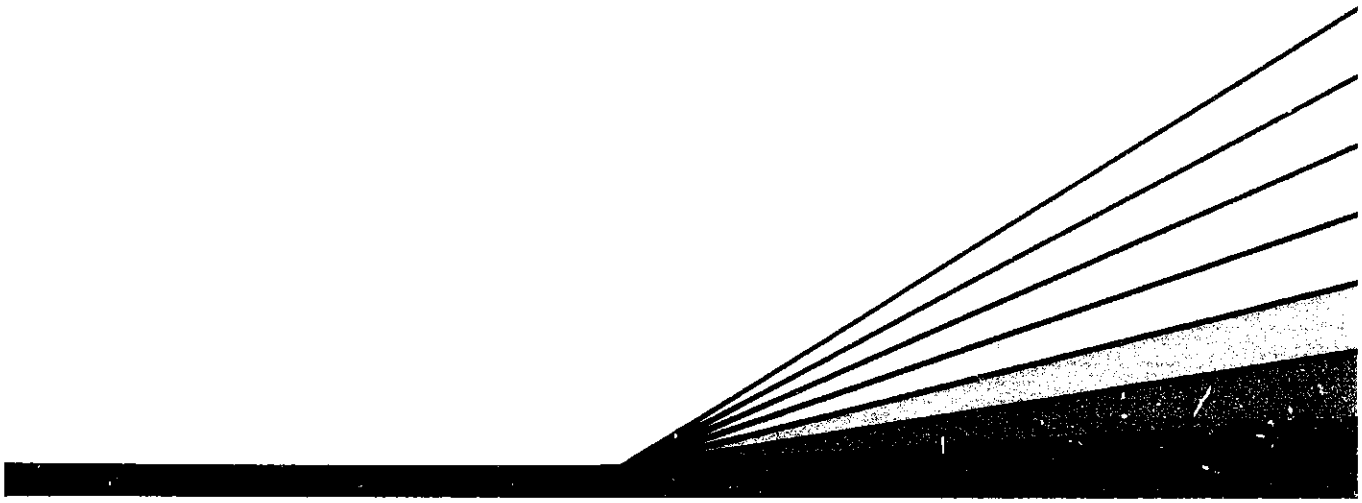

Experimental Facilities

III. 1. GENERAL LAYOUT

1.1 Introduction

The 7-GeV APS design includes provisions for supporting a large number of beam lines and experimental stations to meet the demands of a wide variety of users. The storage ring has 35 ports delivering bending-magnet (BM) radiation and 34 straight-section ports delivering insertion-device (ID) radiation. The photon beam lines are coupled to these ports.

In the present plan an initial complement of 15 beam lines[1] is included as part of the APS construction project. Of these, five are general-purpose "quick-response" beam lines available on relatively short notice to users who need to address technical or scientific problems quickly. All 15 beam lines are to be ready during the initial operational period of the APS. Another 15 PRT beam lines may also be ready for use at that time. Policies and procedures concerning the design, construction, and use of APS beam lines are described in Appendix C.

One of the key issues in beam line design concerns the ability to handle unprecedented power densities and power gradients from the IDs. Feasible approaches to this problem have been implemented at existing synchrotron beam lines. The present design for cooling the first optical element borrows advanced methods and technologies from other areas, such as fission and fusion.

The process of preparing conceptual designs for a number of sample beam lines, including components and optics (see Section III.3), has given us considerable insight and confidence in handling radiation from the high-brilliance storage ring. We will continue to modify these designs to keep pace with technical innovations as they occur.

A closely related issue concerns the length of the beam lines. A length of 80 m has been selected so that the power from the ID source, which has a highly nonuniform density, is spread over a large area on the first optical element. Initial finite-element analysis of a Si premonochromator cooled with liquid Ga shows that, with careful engineering, it can be located 30 m to 60 m from the source without undergoing unacceptably large distortions. However, some applications (e.g., high-resolution topography) require much longer beam lines that extend out of the experimental hall.

The sample beam line designs presented in Section III.3 make use of liquid Ga cooling. Through further research and development (discussed in Appendix B) on thermal loading of optical elements, it is hoped that the first optical elements can be designed so as to cause no loss in the photon beam brightness.

1.2 Disposition of Beam Lines and Experimental Stations

A tentative plan for disposition of beam lines is presented here in order to project the magnitude of this facility. The beam lines are closely related to the nature of the IDs. Enough flexibility is built into the present design to accommodate anticipated changes in device distribution, including the introduction of new types of devices discussed in Section II.9.10.

The BM and wiggler ports can accommodate more than one beam line by employing beam splitters or beam dividers. One example of a split beam line is given in Ref. 1. However, for this discussion, we assume that there is only one beam line per port. Hence, there are 35 BM and 34 ID beam lines (a total of 69), including the above-mentioned initial facility complement of 15. The use of multiple beam lines on the BMs and wigglers permits considerable future expansion, to a maximum of about 100 beam lines. In Fig. III.1.2-1 (see also Fig. IV.2.1-1), a sketch of a part of the storage ring and various types of beam lines is presented. It should be pointed out that, at any straight section, one would normally have undulators or wigglers of the type discussed in Section II.9. In addition, one can insert special radiation devices with the required characteristics. This provides a major capability to alter the nature of the ID radiation at any beam line so as to cater to a larger number of users. It will also become essential to construct tandem experimental stations at some of the expensive ID beam lines so that several kinds of investigations that require radiation with similar characteristics can be carried out on a single beam line.

Every beam line consists of two major parts:

- The front-end comprises all the hardware to handle the radiation emerging downstream from the crotch absorbers. The design of the front-end is largely generic. The BM beam line front-end is somewhat simpler than that of the ID.

- The back-end comprises the first optical element, the remaining optics, the beam transport, and the experimental station. The design of the back-end is tailored to meet the requirements of each investigation.

The details of the APS front-end and the first optical element are discussed in Sections III.2.4 and III.2.5, respectively. The back-ends for sample beam lines are discussed in detail in Ref. 1. Considerable preconstruction research and development is planned to serve as a basis for the design of the facility beam lines. The experience gained and the new technologies developed in this process can be transferred to other users building additional beam lines. In this way the facility can provide strong user support during every phase of beam line design and construction.

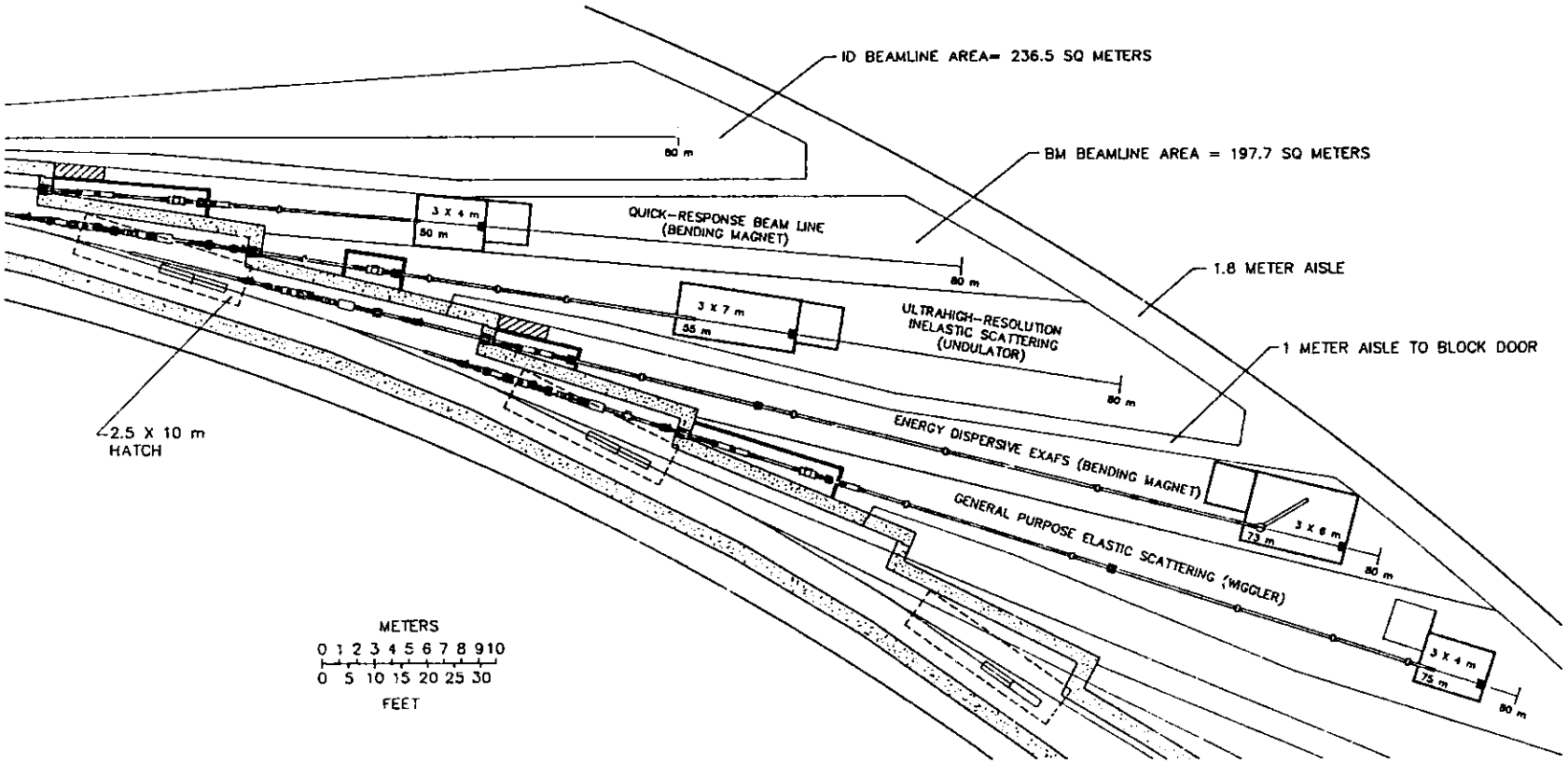

Figure III.1.2-1

Layout of the beam lines in a part of the storage ring experimental hall. These beam lines are defined for a selected set of investigations and use undulator, wiggler, and BM sources.

2.1 Introduction

In this section, an initial design of the front-end of a beam line is presented. The general concepts are applicable to both ID and BM beam lines. Two major considerations underlie this design: (a) the need to handle unprecedented power density and (b) the need to protect the expensive components of the storage ring and the beam line in case of vacuum failure. In seeking solutions to the problems of power dissipation and heat transfer from mechanical and optical components, we have used the expertise of engineers who have handled similar problems in fission and fusion technology. Three-dimensional computer simulations of these problems have been performed, and preliminary results on temperature distributions and thermomechanical stresses and strains have been obtained. One outcome of such a study is the development of a liquid-Ga-based cooling system suitable for optical components.[2]

2.2 Radiation Power

A detailed discussion of the angular dependence of the radiation power from the various sources is presented in Refs. 3 and 4. In the front-end design, the crucial number is the peak power density, W_{xy}, normal to a surface at a specified distance, D, from the source. The value of W_{xy} can be as high as 300 W/mm^2 at D = 30 m for undulators. The total power from IDs ranges from 1 kW to 10 kW. Many measures are implemented in the front-end to reduce this power to a manageable value. Apertures and masks handle a much greater power load than optical elements. In cases where the power density on an optical element is such that the element is rendered inefficient, even after various power-reduction and heat-transfer measures are applied, the optical element will have to be moved farther away from the source. This effectively increases the beam line length.

2.3 Reduction of Power Densities

Because of the large power densities involved, front-end components such as masks or shutters are not placed at normal incidence to the beam, regardless of how efficiently they are cooled, except in the case of BM beam lines.

Soft radiation is removed by using specially constructed water-cooled masks. These masks are at least 15 m away from the source, and their surfaces are slanted to subtend a small angle with respect to the direction of the photon beam and xz plane. This spreads the beam over a larger area of the water-cooled masks and reduces the power density considerably.

Another effective way of reducing the power is by absorbing low-energy photons in a set of very thin absorbers of pyrolytic graphite or Be-Ag alloys. This technique has

worked well at existing facilities and is employed in almost all beam lines of the APS facility, except in cases where soft x-rays are to be extracted.

When the purpose of the beam line is to deliver high-energy photons (>20 KeV), one also uses notch (or band-pass) filters based on the K- or L-absorption properties of atoms. This again reduces the power on the first optical element.

2.4 Front-End Layout

In Fig. III.2.4-1, a preliminary layout of the various components of a generic front-end for an ID beam line is presented. The important components are fixed masks, movable masks, slow and fast valves, an injection or safety shutter, a vacuum delay line, and photon position monitors. In addition, there are lead collars at various critical points along the beam transport that act as collimators to block all optical paths except the beam tube aperture. The functions of these components are given below:

- **Fixed Masks.** The fixed mask is the first component in the photon beam path and limits the horizontal and vertical excursion of the radiation. This mask has water-cooled Cu plates at grazing incidence to the incoming radiation. These masks can handle the full load of the radiation power. The fixed mask is aligned during the beam line survey and installation. A similar mask is mounted at the downstream end of the front-end.

- **Movable Masks.** The movable masks are located following the fixed mask; when closed, they completely intercept the photon beam. The movable masks are water cooled, and the radiation is incident on them at grazing angles. The design is similar to that built for the X-17 superconducting wiggler beam line at NSLS. The movable masks are interlocked to the storage ring vacuum safety system. These masks must be closed prior to closing the vacuum isolation valve or the injection stop.

- **Slow Isolation Valve.** The slow valve is pneumatic, has an all-metal seal, and is remotely operated. Its function is to isolate the front-end from the storage ring vacuum.

- **Fast Isolation Valve.** The fast valve has the usual function of maintaining the vacuum integrity of the storage ring during vacuum catastrophes resulting from beam line hardware failures. The vacuum-detection gauges along the beam transport line trigger the fast valve, which closes in about 10 ms to 20 ms. The fast valve is interlocked with the storage ring rf power and the positron beam abort systems so that the positron beam is dumped before the fast valve closes. A vacuum delay line is provided following the fast valve to provide a delay in the propagation.

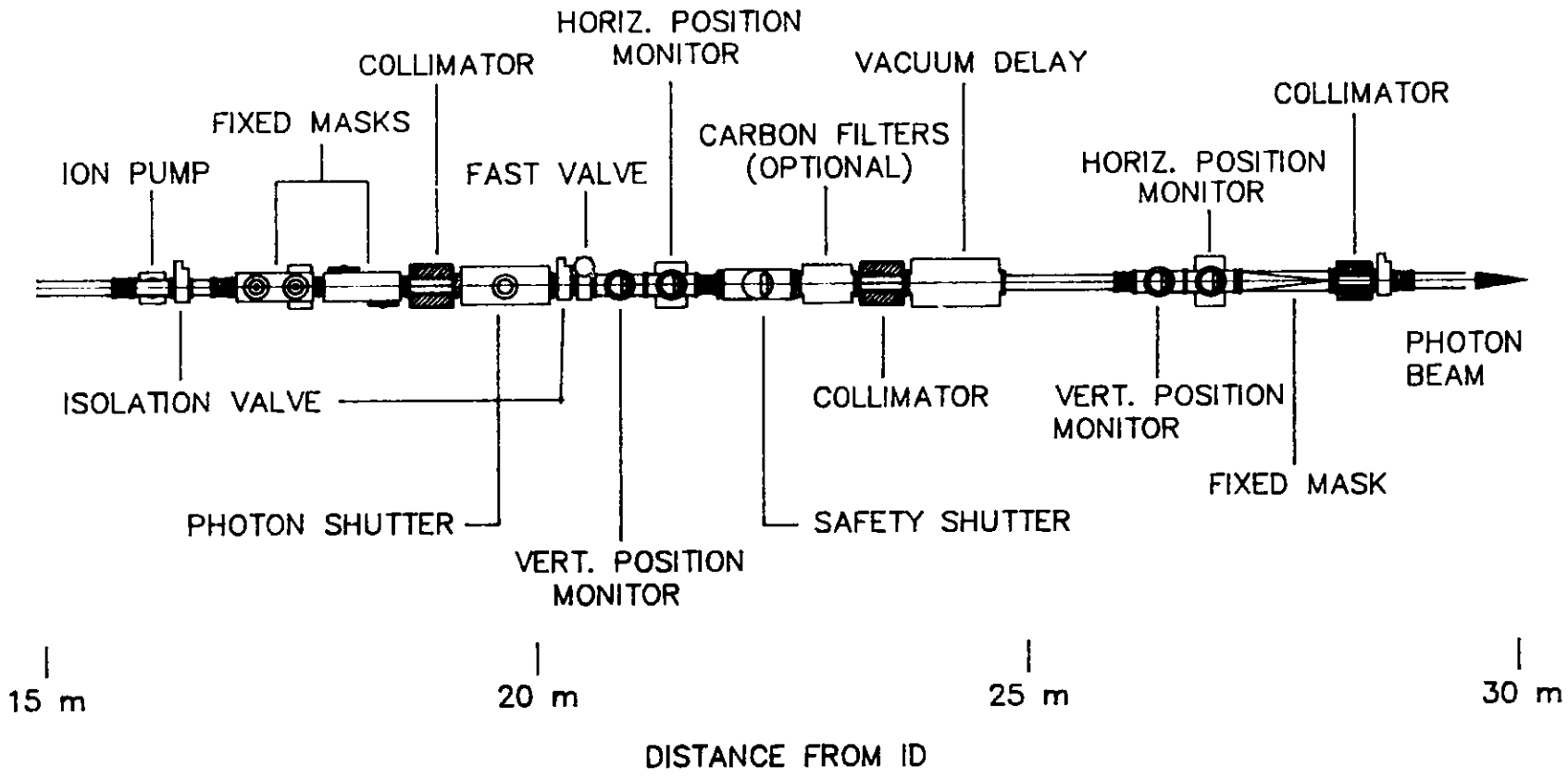

Figure III.2.4-1
Layout of the various components of a generic front-end for an ID source.

- **Injection Stop.** The injection stop (or safety shutter) is made of "Hevimet" alloy and remains closed during positron beam injection. It blocks off any high-energy bremsstrahlung produced during the injection process.

- **Exit Valve.** A second high-vacuum valve, with an all-metal seal, is installed at the exit of the front-end and is similar to the slow isolation valve.

- **Be Window.** A water-cooled Be window, as has been designed for the NSLS X-17 wiggler line, is the last component of the front-end and is located outside the storage ring tunnel in the experimental hall.

- **Photon Position Monitors.** The two sets of vertical and horizontal photon position monitors are separated by roughly 5 m. These monitors provide user information on the photon beam relative position to better than 10 μm. A feedback system based on these monitors will maintain the required positron trajectory. The two sets of photon beam position monitors measure changes in the photon beam position at both locations and are used to control the beam exit angle and source point. Such a control system is essential in many experiments involving ID radiation, in which the position of the photon beam has to be precisely maintained on small samples located 50 m to 80 m away from the source.

The front-end of the BM beam lines is very similar to that of the ID beam lines. The masks, however, need not be at grazing incidence with respect to the radiation, and only the vertical photon beam position monitors are used. The beam emerges from behind the concrete shielding at about 29 m from the ID source point and at about 26 m from the BM source point. These distances are determined by the storage ring geometry. Hence, the entire front-end is accommodated behind the shield wall of the storage ring (see Fig. III.2.4-1).

The first optical element remains outside the shield wall, but will need separate shielding as described below. Access to the first optical element will be interlocked with the movable masks and injection stop, which will be closed when the optical element is accessed for servicing.

2.5 First Optical Component

The material of choice for the first optical component is usually a single crystal of Si cut so that the (111) planes can be used to diffract the photon beam. These crystals are available in large sizes, and their high thermal conductivity and low coefficient of thermal expansion make them well suited for this application. Equally important is their relatively high electrical conductivity, which makes them much less sensitive to radiation damage.

In many beam line configurations, the maximum photon flux available at the experimental sample is determined by the maximum amount of heat that can be absorbed by the first optical component without causing serious distortions of its surface or changes in its internal structure (i.e., changes in the crystal-lattice spacing). In addition, the photon beam intensity changes dramatically over the beam footprint on the first optical element. This variation in intensity results in a corresponding change in the surface temperature. A variation of 10°C across the beam footprint will cause a noticeable loss in the source brightness.

We have done a set of finite-element analysis calculations in three dimensions in order to determine the temperature distributions and thermal stresses in a single crystal of Si exposed to heat loads of 2 kW to 20 kW. The results were used to calculate the distortion of the surface of the crystal and the change in crystal d-spacing across the footprint of the beam. Different geometric arrangements for cooling channels in the crystal and different cooling fluids (e.g., water, oil, liquid Na, and liquid Ga) were included in the second stage of the finite-element analysis. The best heat transfer and smallest surface distortions were obtained when the cooling fluid was allowed to flow through channels in the crystal. The two best fluids for operation at or above ambient temperatures were found to be water and liquid Ga. In all the situations analyzed, variations in temperature across the face of the crystal and consequent aberrations in the optics were at least a factor of two less when liquid Ga was used instead of water. In many cases, liquid Ga was 3 to 10 times better than water.

The very efficient cooling and low vapor pressure of liquid Ga (less than 10^{-12} Torr at 100°C) make it a very attractive cooling fluid for synchrotron applications. A small electromagnetic induction pump for liquid Ga has been designed, built, and tested. A schematic of this pump is shown in Fig. III.2.5-1. A pumping volume of 100 cm^2/s was achieved with a static head pressure of 8 psi. This resulted in an effective heat transfer of 2.2 kW of power.[2] A prototype Ga pump useful for APS applications is being fabricated; it will provide a larger flow rate and heat load handling (up to 10 kW).

The above finite-element analysis of Ga-cooled optics subjected to the APS-ID power loads shows that the first optical element can be located at a distance of 30 m to 60 m from the source point, with the minimum allowable distance determined by the ID power and the nature of the application. This minimum distance will necessitate beam line lengths ranging from 40 m to 80 m.

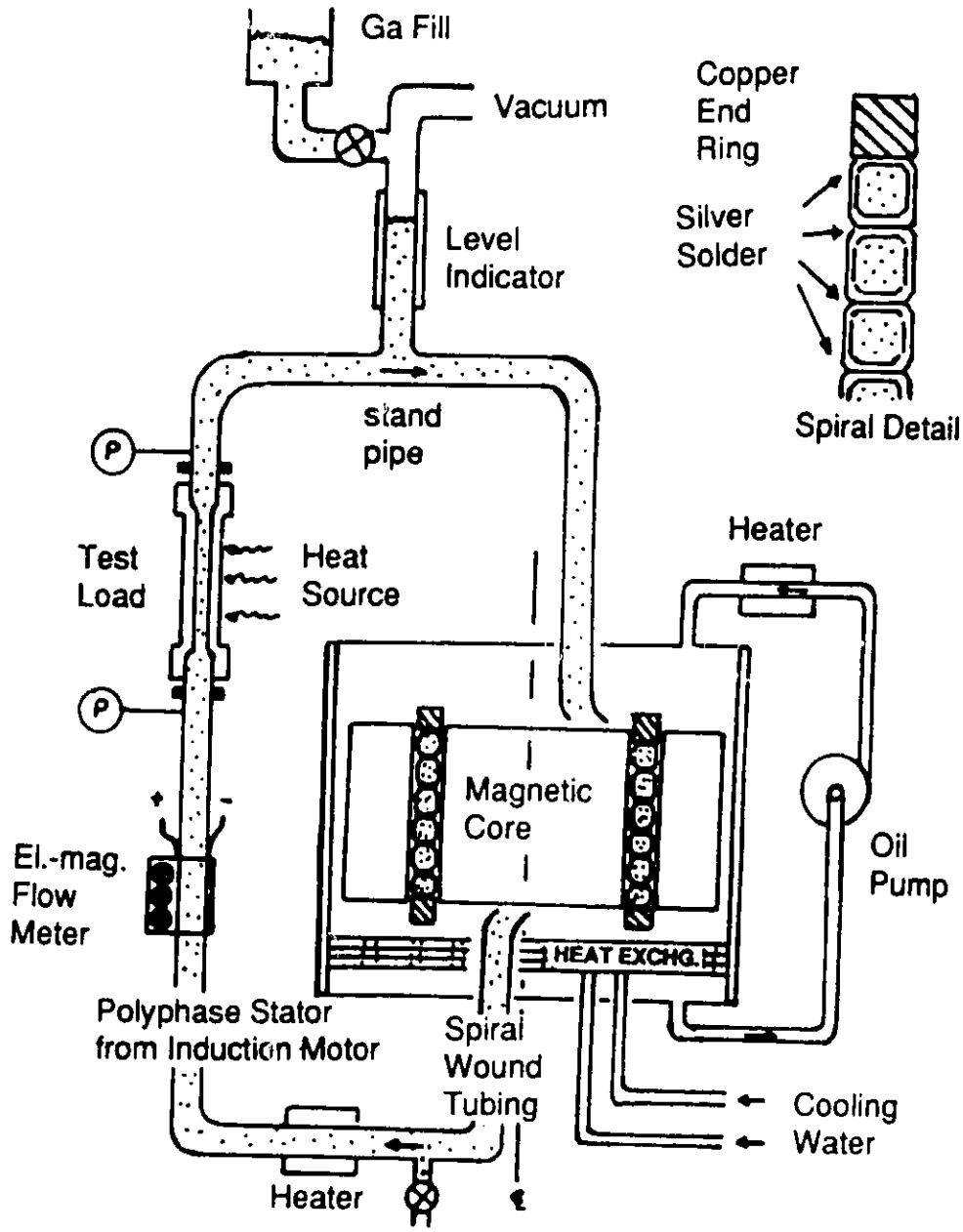

Figure III.2.5-1
Schematic of an electromagnetic induction pump used for circulating liquid Ga.

3.1 Facility-Funded Beam Lines

The initial complement of facility-funded beam lines calls for a total of 15 beam lines based on three different types of radiation sources: seven undulators, five wigglers, and three BMs. In many of the undulator beam lines, there will be either device A or B (see Sections II.9.4 and II.9.5). These tunable devices will cover the energy ranges of interest through gap variation.

Five of the 15 beam lines (i.e., two wigglers, one undulator, and two BM beam lines) are dedicated to perform general sample characterization for users needing a quick answer to their scientific or technical problems. Many users in industry, in academia, and elsewhere have expressed a strong need for such "quick-response" beam lines. As an example, researchers dealing with unstable samples that have very limited lifetimes would find such a facility invaluable. Users of the quick-response beam lines would not be required to go through the usual proposal-referee procedure.

A possible set of "quick-response" beam lines is listed below. Final plans for these beam lines will be made after consultation with the APS Program Advisory Committee.

- Q1 - general-purpose elastic x-ray scattering (wiggler B).
- Q2 - optical metrology (undulator A).
- Q3 - anomalous scattering (wiggler B).
- Q4 - variable-focus white beam using BM radiation.
- Q5 - variable-energy monochromatic beam using BM radiation.

The remaining 10 beam lines in the initial complement will be developed by Argonne to accommodate a variety of investigations in solid-state physics, materials science, materials technology, and chemical technology. The designs for these beam lines will employ state-of-the-art x-ray optics and hardware.

The present plan for the types of investigations and the nature of the radiation sources to be accommodated by these 10 beam lines are given below:

- F1 - topography and radiography/tomography (wiggler A).
- F2 - ultrahigh-resolution inelastic scattering (undulator B).
- F3 - inelastic Compton scattering (wiggler A).

- F4 - nuclear Bragg scattering (undulator B).
- F5 - intermediate-energy-resolution inelastic scattering (undulator, 6-cm period).
- F6 - small-angle scattering (undulator A).
- F7 - advanced x-ray photoelectron spectroscopy (undulator, 13.6-cm period).
- F8 - surface x-ray scattering with vertical polarization axis (wiggler B).
- F9 - time- and space-resolved x-ray spectroscopy (BM).
- F10 - magnetic scattering (undulator A).

The final choices of beam capabilities will be based on the advice of the APS Program Advisory Committee.

3.2 Insertion Devices for the Beam Lines

The characteristics of the radiation sources for the 15 beam lines are given in Table III.3.2-1. The sources include seven undulators, five wigglers, and three BMs. The choice of an undulator or a wiggler for a specific research program should not be considered definitive at this point. The IDs are based on either a Nd-Fe-B hybrid magnet or electromagnet technology, and their designs are within the framework presented in Sections II.9.4, II.9.5, and II.9.8.

The total power radiated by each of the IDs with the storage ring at 7 GeV and 100 mA (see Table III.3.2-1) ranges from 1.0 kW to 10.3 kW, and the average maximum power for the group is approximately 4.5 kW. If this average power is assumed to be typical, the total of 34 IDs would radiate roughly 150 kW. Provision for this power has been made in the rf design (see Section II.3). The general nature of the energy spectra of such IDs is discussed in Sections II.9.4, II.9.5, and II.9.8.

3.3 Beam Line Concepts

In this section, possible designs for some of the above-mentioned beam lines are briefly presented. Additional details of these conceptual designs are found in Ref. 1.

Beam line F1 is designed to perform topography and radiography/tomography experiments with a white beam and monochromatic beam; a wiggler is used as the ID. This state-of-the-art design provides very high geometric resolution, wide area coverage, and the capability to perform real-time characterization of materials with a CCD detector offering high spatial resolution. The layout (Fig. III.3.3-1) includes two experimental stations: one is located at about 80 m and the other at 350 m from the

Table III.3.2-1

Parameters of Radiation Sources Used in the 15 Beam Lines Listed in Section III.3.2.1

Beam Line No.	Device	Peak[a] Magnetic Field (T)	E_c[b] (keV)	Period (cm)	Number of Periods	Peak[a] K	Device Length (m)	Vertical Opening Angle (± μrad)	Horizontal Opening Angle (± μrad)	Total Power[c] (kW)	Peak Power[c] (kW/mrad^2)	Normal-Incidence Surface Peak Power Density (W/mm^2) at 30 m	Normal-Incidence Surface Peak Power Density (W/mm^2) at 50 m
Q2,F6, F10	Undulator A	0.77	3.5	3.3	156	2.5	5.2	73	182	10.3	326	362	130
F2,F4	Undulator B	0.45	13.5	2.3	226	1.0	5.2	73	73	3.5	273	303	109
F5	Undulator	0.24	4.0	6.0	86	1.4	5.2	73	102	1.0	57	63	23
F7	Undulator	0.27	0.5	13.6	38	3.5	5.2	73	255	1.2	27	30	11
F1,F3	Wiggler A	1.0	32.6	15.0	10	14.0	1.5	73	1022	4.6	26	29	10
Q1,Q3, F8	Wiggler B	0.3	9.8	25.0	20	7	5.0	73	511	1.4	16	18	6
Q4,Q5, F9	Bending	0.6	19.5	-	1	-	3.04	73	-	6.7	0.6	0.67	0.24

[a]Value at smallest gap.

[b]Refers to critical energy for the wigglers and first-harmonic energy at smallest gap for the undulators.

[c]Calculated for 7-GeV operation with 100 mA of stored current.

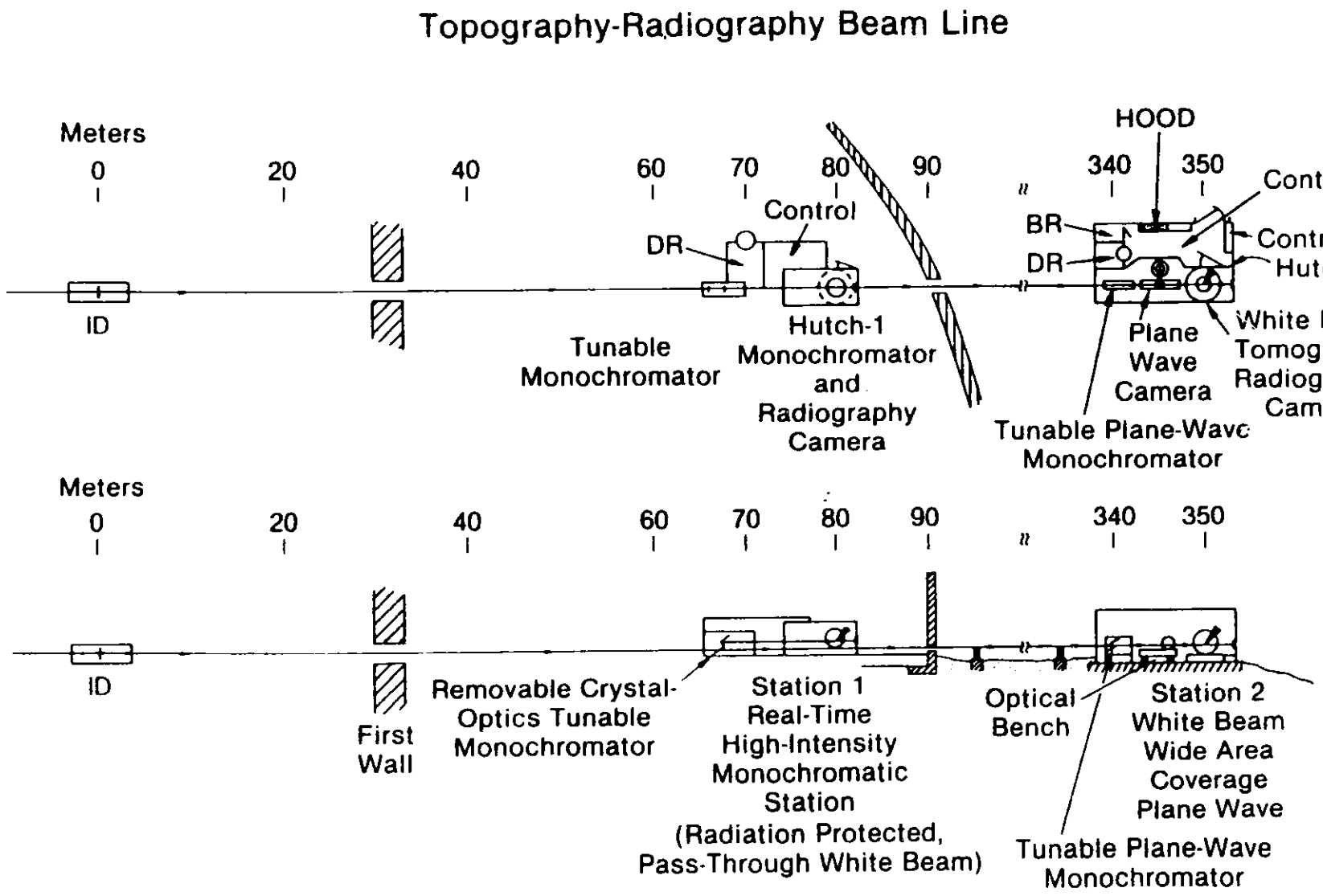

Figure III.3.3-1
Schematic of beam line for topography and radiography/tomography.

wiggler source. The latter experimental station will be placed outside the experimental hall.

The ultrahigh-energy-resolution spectrometer designed for beam line F2 can carry out inelastic scattering of x-rays from collective excitations in condensed matter, such as phonon excitations. The required resolution of about 20 meV at 20 keV is realized in a crystal monochromator using high-order reflections in a nearly back-scattering geometry. The optical acceptance angle for such high-order reflections ideally matches the opening angle of the undulator radiation. The required undulator is described in Section II.9.5.2, and a schematic of the optical design is presented in Fig. III.3.3-2. A similar beam line, F4, will be utilized for performing nuclear Bragg diffraction studies.

On beam line F8, the high-brilliance, vertical orientation of the polarization vector and tunability of radiation from a high-brightness/low-critical-field wiggler are exploited for various bulk and surface investigations that demand high-momentum resolution. Proposed studies include detailed three-dimensional mapping of deviations from structural periodicity, surface reconstruction, surface corrugation, segregation, and two-dimensional melting. The beam line optics, shown in Fig. III.3.3-3, provide photons in the energy range from 4 keV to more than 20 keV with a momentum resolution of greater than 5×10^{-4} Å^{-1}.

Inelastic scattering with an intermediate energy resolution of $\Delta E/E \sim 10^{-4}$ provides information on electron and spin excitations in solids. Beam line F5 requires an undulator with a 6-cm period. The conceptual layout of the optics is shown in Fig. III.3.3-4. The beam line uses an optional mirror. The optics for the Compton-scattering beam line, F3, are similar to those needed for the low-energy inelastic scattering from electrons. However, the analyzer for the Compton-scattering studies is more complex. To perform Compton scattering from magnetic spins, one needs circularly polarized x-rays, which are produced by using the polarizing monochromator described by Golovchenko.[5]

Beam line F7 provides a facility for advanced x-ray photoelectron spectroscopy studies with high-energy, spatial, and/or spin resolution. A high-brilliance, low-energy undulator source produces photons with energies ranging from about 250 eV to 1600 eV. Energy tuning is achieved both by varying the magnet gap and by moving an aperture away from the undulator axis. The variable-aperture and grating optics are shown in Fig. III.3.3-5. The optics are operated in the plane-grating monochromator mode, the high-K-resolution mode, or the double-grating mode.

Small-angle scattering is a unique method used in polymer science, chemistry, geology, materials science, and physics to study variations in scattering density over distances spanning 10 Å to 1000 Å. Beam line F6 fully utilizes the potential of a high-brilliance tunable undulator for such studies. The characteristics of the source considerably simplify both the optics and the data-reduction procedures. The layout shown in Fig. III.3.3-6 features a CCD-based area detector with annular recording capability.

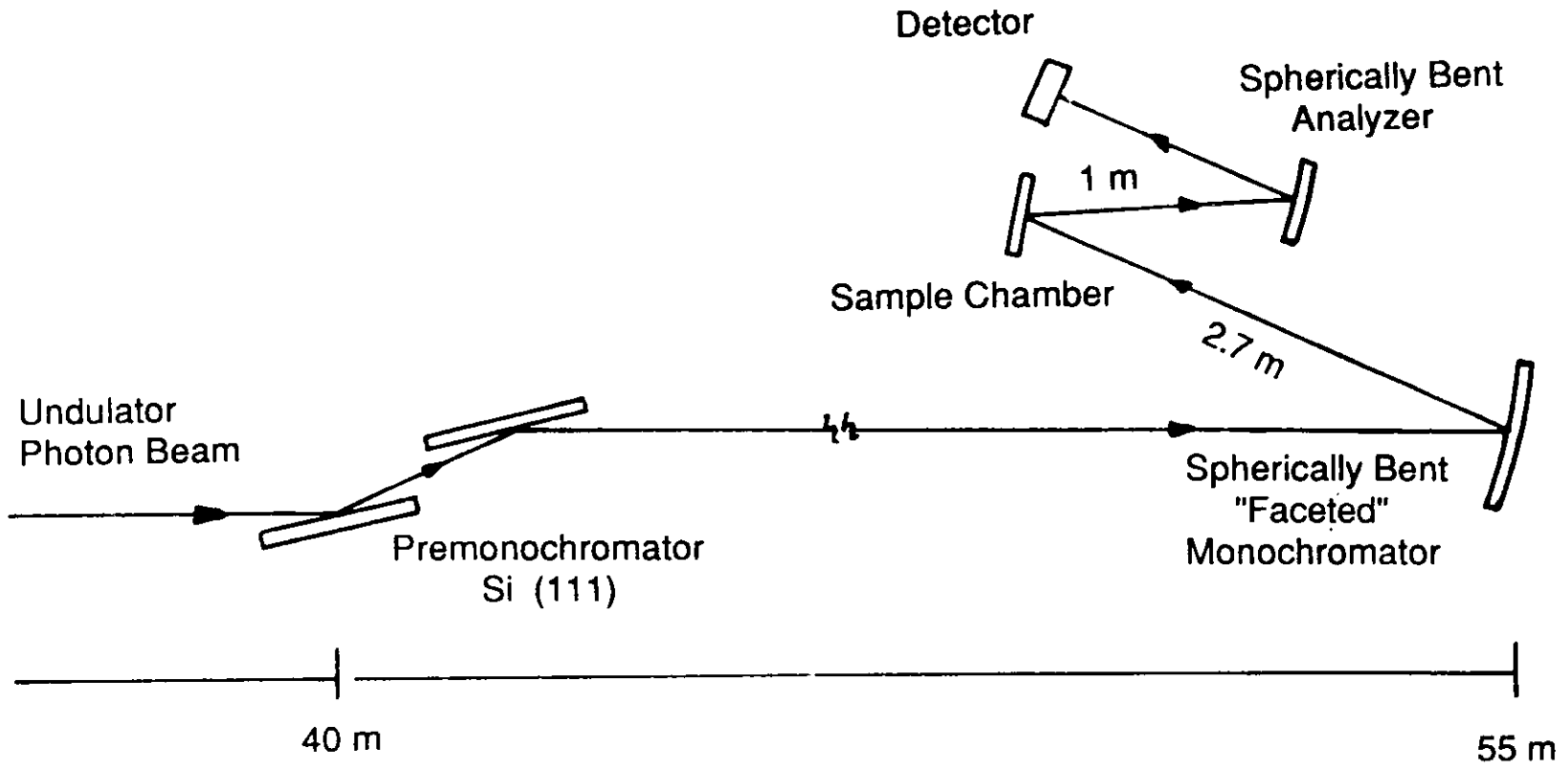

Figure III.3.3-2
Schematic drawing of the optical elements for inelastic scattering with the ultrahigh-energy-resolution beam line, F2.

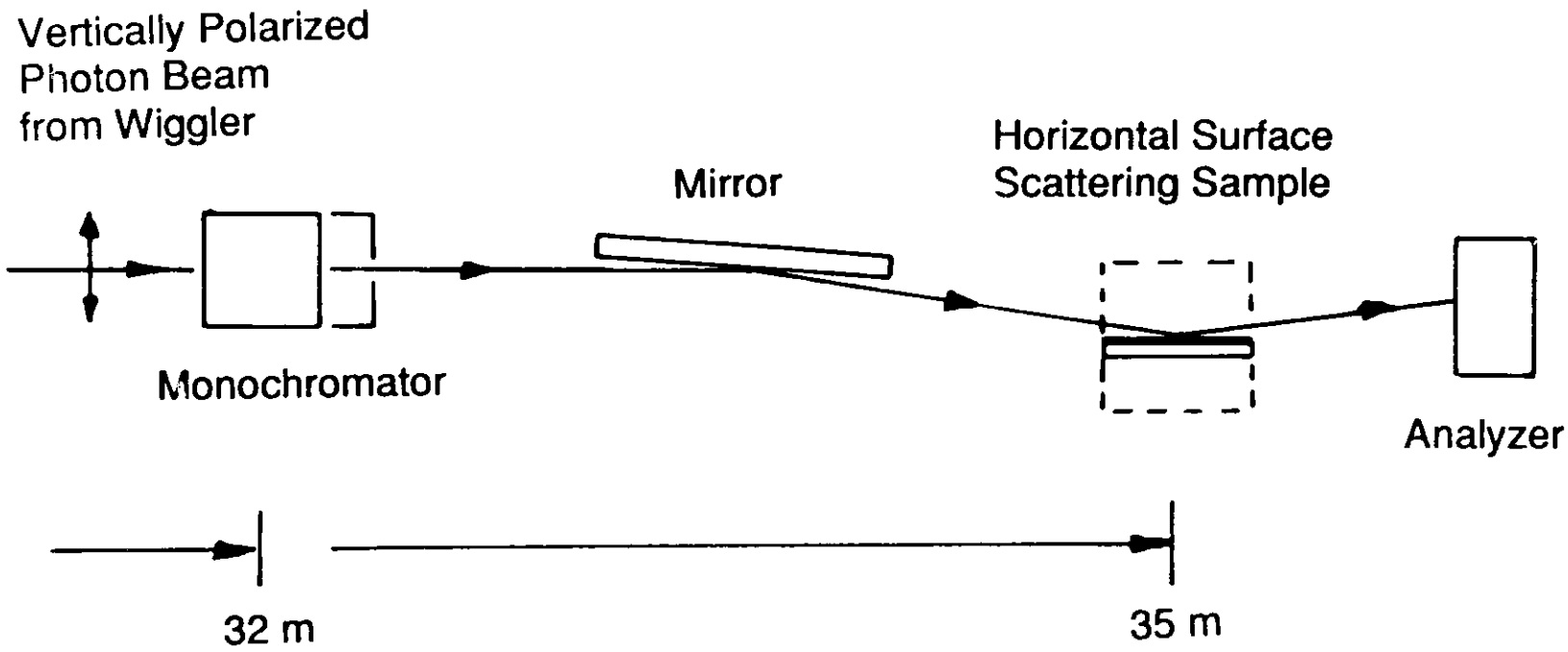

Figure III.3.3-3
Schematic drawing of the high-momentum-resolution beam line, F8.

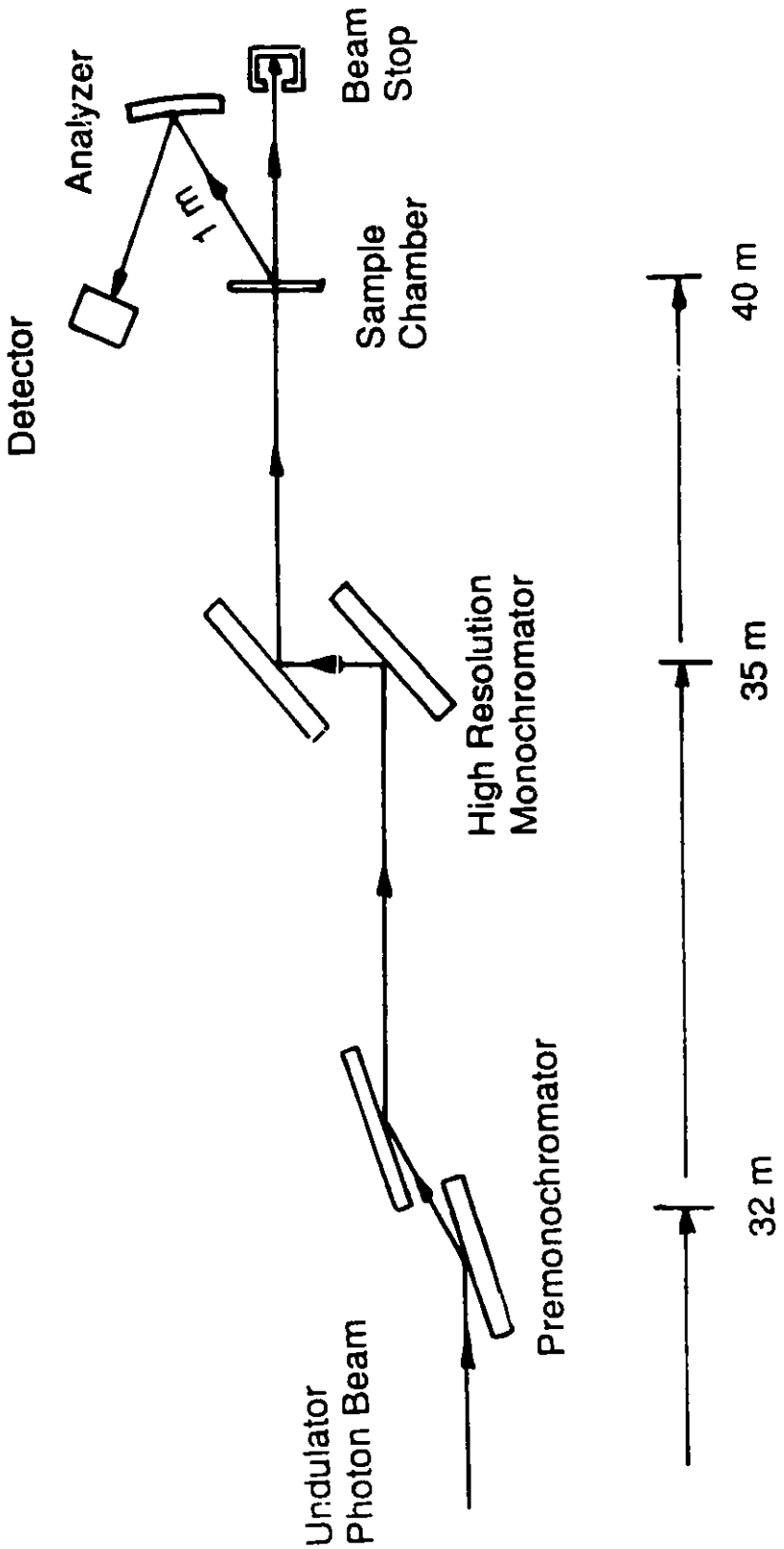

Figure III.3.3-4
Schematic drawing of the low-energy inelastic scattering beam line, F5.

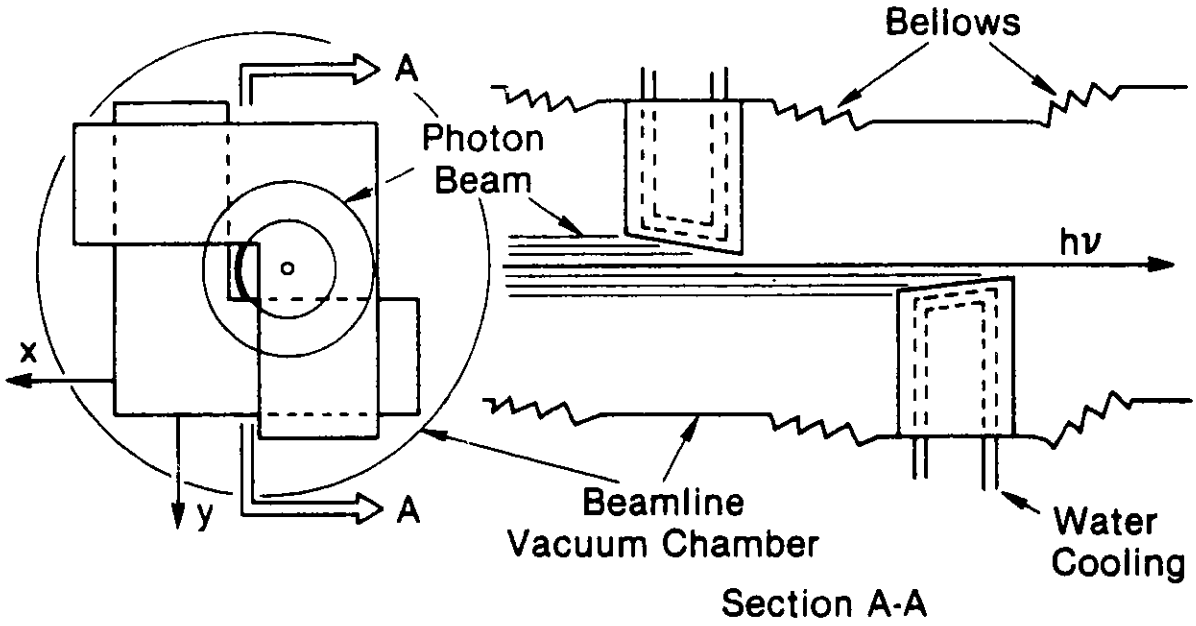

Variable Aperture

(a)

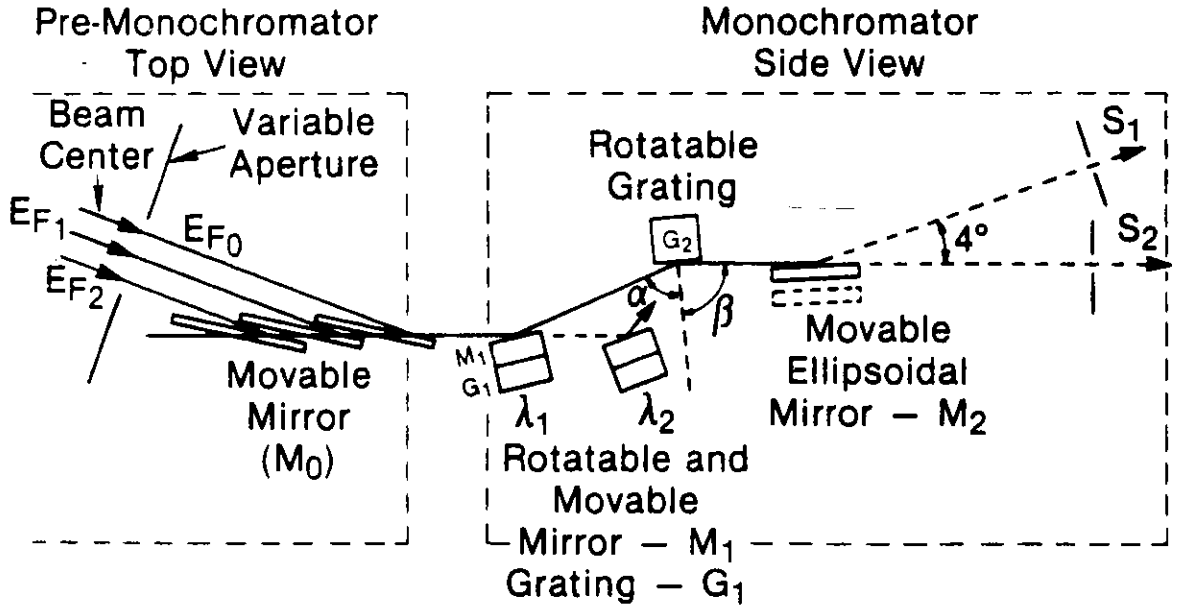

(b)

Figure III.3.3-5

Beam line, F7, for advanced x-ray photoelectron spectroscopy. (a) Schematic of the variable aperture. (b) Schematic of the premonochromator-monochromator layout.

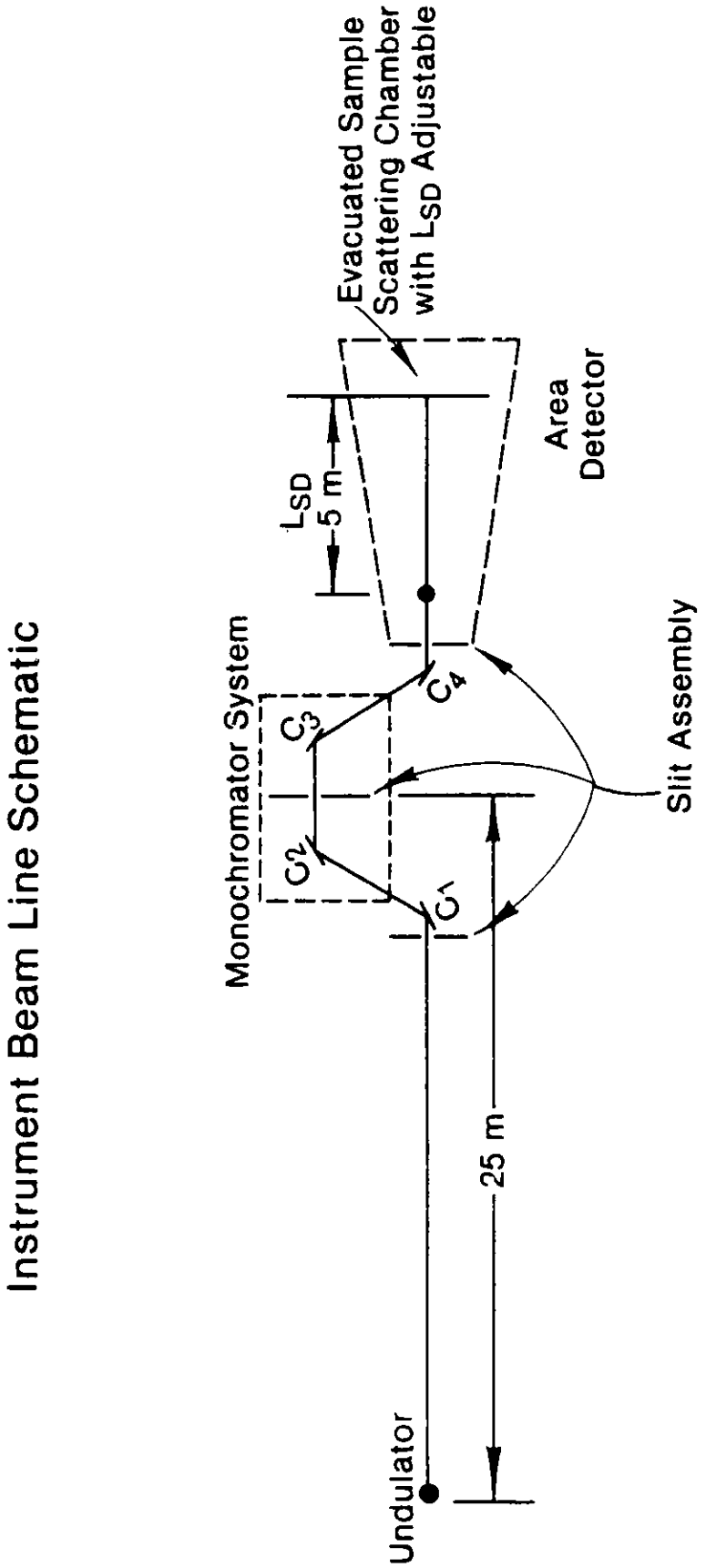
Instrument Beam Line Schematic
Evacuated Sample Scattering Chamber with L_{SD} Adjustable
Area Detector
L_{SD} 5 m
Monochromator System
C_4
C_3
C_2
C_1
Slit Assembly
25 m
Undulator

In materials science, one often needs beam lines that can be used as workhorses for characterization. To meet this demand, beam line Q1 has been designed with high-throughput optics to provide photon energies ranging from about 4 keV to 30 keV with 0.1% resolution. The ID is a high-brightness wiggler. The versatile diffractometer design accommodates a variety of techniques, including diffuse scattering, high-resolution powder diffraction at high temperatures and pressures, and anomalous scattering.

One of the unique capabilities of the APS is the high intensity of undulator sources, which permits measurement of small-scattering cross sections. This capability is exploited in magnetic scattering beam line F10.

The above beam lines use the radiation from 7-GeV APS IDs. The technique of space- and time-resolved x-ray spectroscopy exploits the unique characteristics of the 7-GeV APS BM radiation. In Fig. III.3.3-7, a design concept is presented for this beam line, F9, in which a BM source, a dispersive monochromator, and a position-sensitive detector are used to perform such studies. The expected spatial resolution is about 50 μm, and a time resolution of about 140 μs is feasible. The mirrors in this design provide harmonic rejection and focusing.

3.4 Detector Development

It is clear from Section III.3.3 that detectors will play a major role in the research conducted at the APS facility. At the same time, it is well recognized that x-ray detector technology has not kept up with the needs of synchrotron-based investigations. This technology has to be developed during the next few years so that the radiation from the APS facility can be effectively used. Scientists and engineers at Argonne are involved in developing CCD-based detectors to meet the general needs in this important area. The research and development plans are presented in Appendix B.

3.5 References

1. "Conceptual Design of Proposed Beam Lines for the 6 GeV Light Source," ANL Report, Light Source Note, LS-51 (March 1986).

2. R. K. Smither, G. A. Forster, C. A. Kot, and T. M. Kuzay, "Liquid Ga Cooling for Optical Elements with High Heat Loads," Synchrotron Radiation Instrumentation Conf., Madison, Wis. (June 22-25, 1987).

3. G. K. Shenoy and P. J. Viccaro, "An Overview of the Characteristics of the 6-GeV Synchrotron Radiation: A Preliminary Guide for Users," ANL Report ANL-85-69 (October 1985).

4. "Characteristics of the Insertion Devices for the 6 GeV Synchrotron Source," ANL Report, Light Source Note, LS-52 (March 1986).

5. J. A. Golovchenko, in SSRL 83/102, K. Cantwell and C. Mitchell, eds., p. 147 (1983).

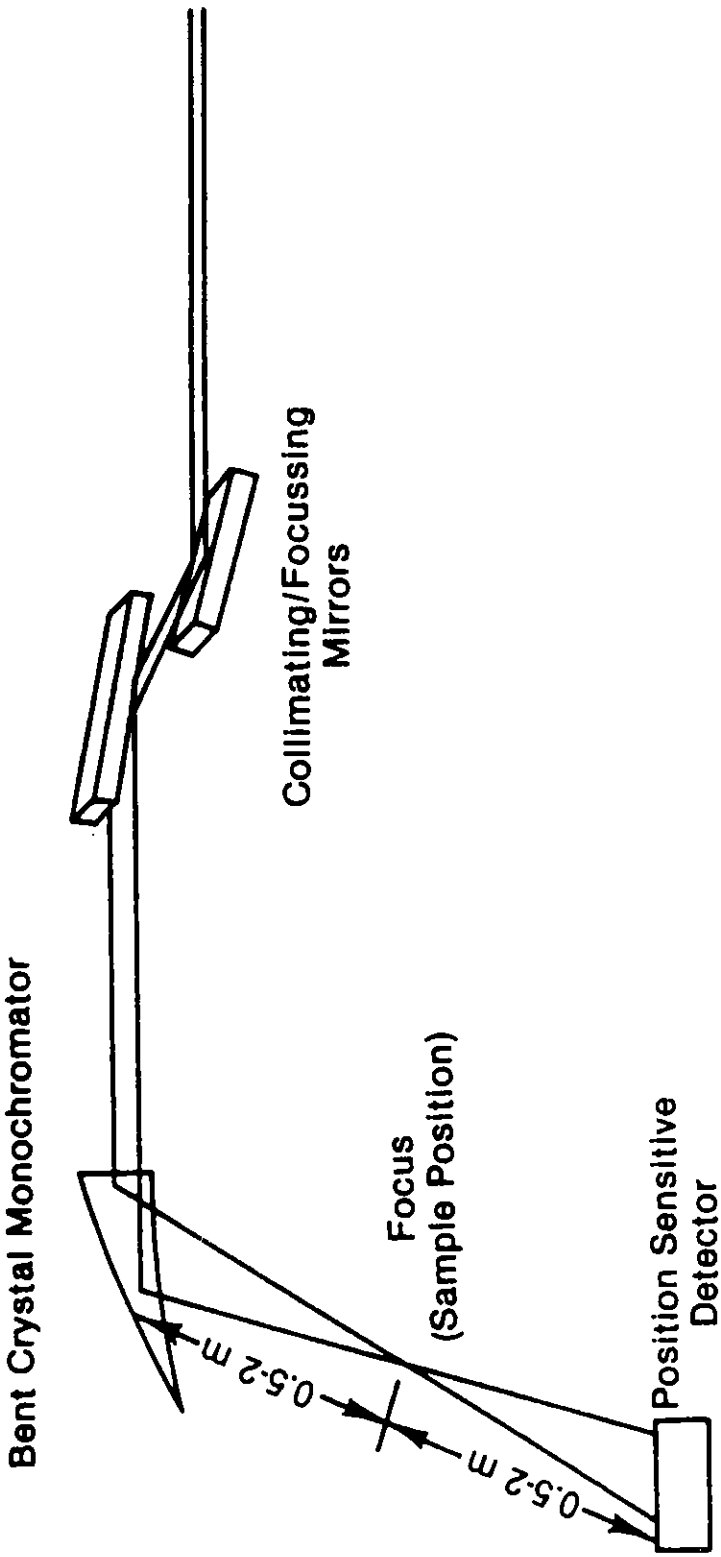

Figure III.3.3-7
Conceptual layout of the energy-dispersive beam line, F9.

4.1 Introduction

The data analysis computer facility consists of a cluster of high-performance processors and peripherals, connected through a network to a complement of workstations for use by the scientists to analyze experimental data. The facility does not include the beam line data-collection computers, but it does provide network connection support, database and software management, and data-archiving services for these systems.

The data analysis computers are linked to the beam line computers in a high-speed Local Area Network (LAN), and data preprocessing is done on the beam line computers to avoid overloading the network. Terminal servers and multiport repeaters are used to connect individual workstations to the network, so that users log on to the data analysis computers and/or their own beam line computer from the same workstation. The data analysis computers and the beam line computers are able to run the same operating system and networking software and have compatible file formats.

The data analysis computer facility provides disk backup, data migration, and archival storage and retrieval of data. High-density tapes will be used for disk backup and data export. Optical disks will be used for mig ated data sets. Consultants and operations personnel will be available for assisting users.

The data analysis computer facility is sized to satisfy the computational needs of an initial complement of 15 beam lines, but the size of the computer room is planned to allow expansion to support up to 60 beam lines.

In the hardware and software descriptions that follow, we describe plans based on systems that are now in wide scientific use or are expected to be in wide use soon. We will update these plans in terms of the corresponding systems of 1990-1992, when many of the APS computing systems will actually be produced.

4.2 Computer Hardware

4.2.1 Host Processor

The data analysis computer system consists of a cluster of computers, each capable of performing two million floating-point operations per second (MFLOPS). The cluster contains two processors, with space provided for the addition of at least four more processors of the same size as future growth dictates. The cluster has the advantages of file and resource sharing and simple addition of computing power and storage capacity. Users are able to use the system without knowledge of the actual

processor involved. The processors run the VMS operating system, and one of the machines also runs a UNIX shell. The provision of these two operating systems makes it possible for most university users to work in a familiar programming environment. The processors are connected to disks and tapes through disk/tape servers using a high-speed (70-MB/s) computer interconnect bus, as shown in Fig. III.4.2-1. User workstations connect to the host processors through terminal servers or repeaters connected to the LAN through transceivers. Other peripherals are connected through the terminal servers or through direct connections to one of the data analysis computers. The data analysis computers are also linked to the Argonne computer network for electronic mail and for access off-site, which allows file transfer to and from the users' home institutions over BITNET, HEPNET, and other networks.

4.2.2 Cluster Hardware

Clustering of the processors is accomplished through the use of a dual-path computer-interconnect assembly with initial provision for eight nodes, including host processors and file storage servers. The cluster hardware is a passive connector assembly designed for coupling processors and is expandable to 16 nodes.

4.2.3 Disk/Tape Server

Disk drives and tape drives are controlled by an intelligent server, allowing all processors in the cluster to access common disk or tape drives. The server allows (a) host-independent sharing of common data, (b) reading and writing of shared files by multiple processors, and (c) use of a common operating system for all processors in the cluster to enhance transparency. Dual disk/tape servers are provided to prevent system shutdown due to the failure of a single server unit. These intelligent input-output (I/O) servers also provide off-line volume backups. The design of the system allows maintenance operations to be done without shutting down the cluster, so it can be operational 100% of the time. The disks are dual-ported to the I/O servers for high availability. Each disk/tape server includes data channel interfaces for up to eight disk drives and four tape drives. Each server is expandable to handle twice this capacity. Private disks can be connected directly to the computer bus for storing sensitive or proprietary data.

4.2.4 Disk Drive

A large disk-storage capacity is provided because of the large volume of data produced. These data reside on the disks as long as they are being actively analyzed. This analysis extends over several months in some cases. In other cases, the user's data are sent to the home institution over the network or carried on tapes. Files that are not used for a period of time are migrated to minimize the disk space needed. Each disk drive stores 456 MB of data, and nine such drives are provided. The considerable effort

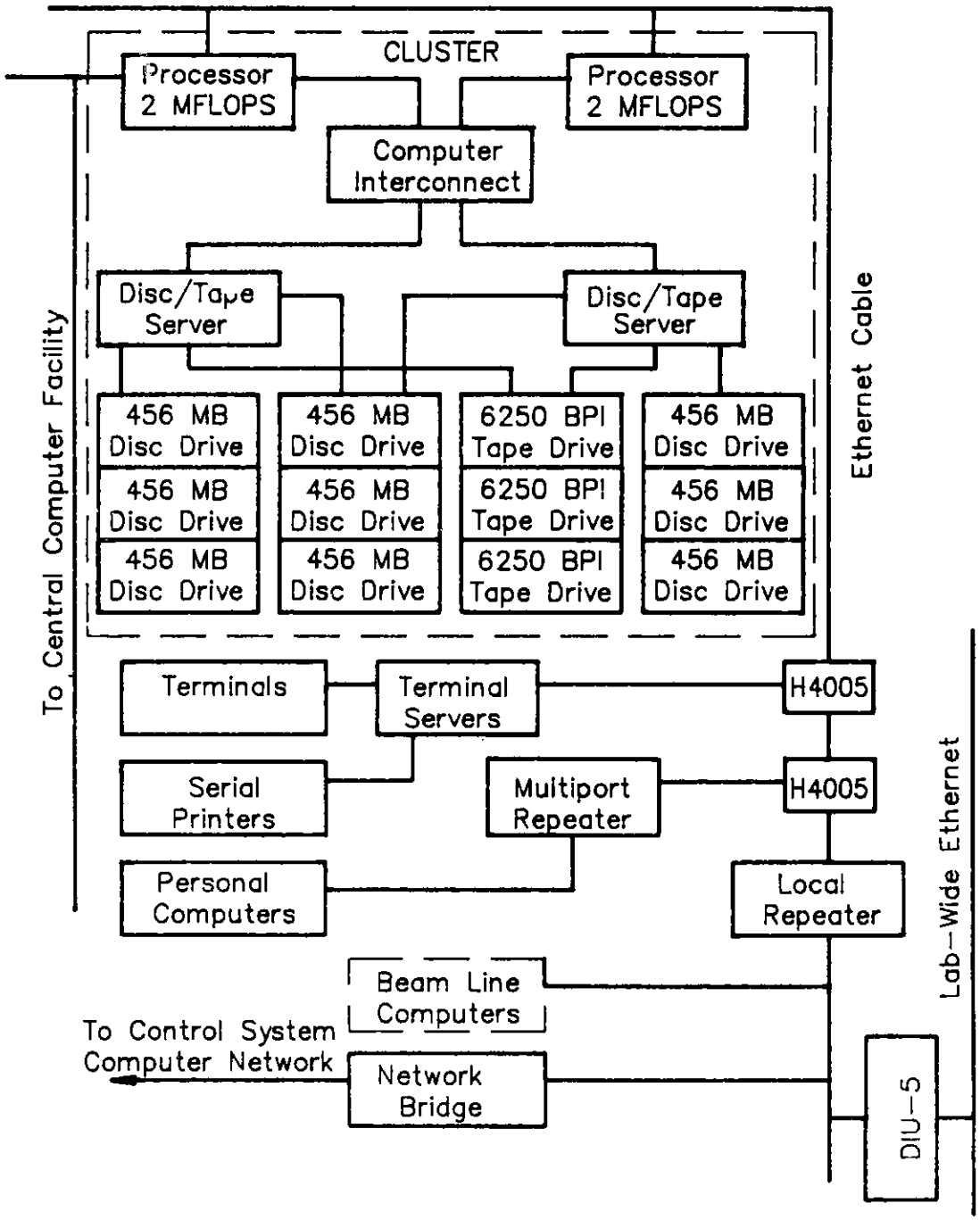

Figure III.4.2-1
Diagram of the data analysis computer facility network.

required to keep the disks backed up on tape and to migrate old files is made easier by the use of data migration software and disk servers that can handle backups offline.

4.2.5 Tape Drive

Tape drives for the data analysis computer system are capable of operating at 1600 or 6250 bpi and can be controlled directly by the disk/tape server; thus, it is not necessary to shut down the processor for backup. Incremental backup of each disk in the system is done daily, with full backup of each disk on a monthly basis. The data-archiving system keeps track of all migrated and archived data and makes it easy to recover these data in a short time. Data are transferred to the data analysis computer from the beam line computers over the network. Transfer of enough data to fill a 2400-ft reel of 6250-bpi tape over the network takes about 20 min. The limiting factors are the front-end computer processing speed and the tape drive speed.

4.2.6 Optical Disk

An optical disk system that allows writing once and reading many times (WORM) is provided for data migration of inactive files. It is also used to store libraries of less frequently accessed information. This optical disk handling system allows rapid restoration of migrated files without operator intervention. A jukebox-type arrangement automatically inserts these disks into the drive. The WORM optical disk system stores 2.0 GB per disk, and the changer holds 32 such disks.

4.2.7 Printers

Two 600-line-per-minute dot-matrix printers are provided for the data analysis computer systems. They are capable of compressed print, so that 132 columns of printout fits on an 11-in.-wide sheet.

4.2.8 Plotting Equipment

The primary graphics activity is the production of black and white plots on paper, using two high-volume laser printer/plotters. Color-plot capability is provided by a pen plotter with automatic paper feed. Publication-quality color output and slides for presentations can be obtained by sending graphics metafiles to the Argonne Central Computing Facility. Graphic displays for previewing plots are provided by the user workstations and by the beam line computers. Medium-speed laser printers are located in each of the lab/office modules for convenient plotting of output.

4.2.9 Local Network Interface

The data analysis computers are linked to the beam line computers through a base-band ETHERNET LAN. One local network interconnect (LNI) connects all the data analysis computers to the trunk cable through a transceiver. Other LNIs are used to link printer, plotter, and terminal servers to the ETHERNET. The data analysis computer LAN is connected to the APS control computer network through a LAN bridge that stores and forwards network access requests (see Section II.8.2.7, Host and System Networks). The central lab/office building housing the data analysis computers forms one segment of the LAN, and two other segments are formed by the beam line computers around the ring. A local repeater and a pair of transceivers are used between each segment of the network. Each office has access to the ETHERNET via a terminal server connection and a coaxial cable connection.

4.2.10 Interface to Central Computing Facility

The data analysis computer link to the Argonne Central Computing Facility (CCF) provides access to special graphics devices, higher-performance computers, and other computer networks. Argonne Computing Services provides an NJE (network job entry) network, which links VAX and IBM computers throughout the laboratory for electronic mail and access to the CCF computers. This network is currently operational at 19.2 K-baud. The CCF is connected to BITNET over a 9.6 K-baud link that gives access to other networks, such as ARPANET, CCNET, CSNET, VNET, MAILNET, MFENET, etc. This allows the sending of text files to the user's institution. Binary files may be transmitted over HEPNET or carried on magnetic tape.

4.2.11 Terminal Server

Terminals are connected to the data analysis computers and to the beam line computers through terminal servers directly connected to the ETHERNET. This allows each terminal to have concurrent sessions on several computers and reduces the cabling requirements. A total of 80 lines are provided, some of which are used to connect serial printer/plotters so that they can be accessed easily from any computer on the network. Sixteen of the terminal server lines are provided for connection to the digital public branch exchange (PBX) for dial-up access to the data analysis computer network.

4.2.12 User Workstation

User workstations consist of video terminals, graphics terminals, and/or personal computers with graphics capability. Terminals connect to the network through an RS-423 connection to a terminal server. Personal computers connect to the network through an ETHERNET station adapter and ThinWire ETHERNET cable going to a

multiport repeater. An initial complement of 50 graphics workstations is provided. Most of the workstations are in private offices, but some are in a common user area.

4.2.13 Phone Lines/Modems

Dial-up access to the APS data analysis computer system network is provided through the Argonne modem pool. Sixteen phone lines from the Argonne digital PBX connect to terminal server lines for remote access to the computers. These modems are capable of 2400-baud operation, with a 1200-baud fall-back speed, and automatically determine the required baud rate. One additional phone line is provided for each processor in the cluster, for remote diagnostics. As an added security measure, modem lines require a system password before prompting for user name and password.

4.2.14 Cabling

The coaxial cable for the ETHERNET network and twisted-pair cabling for the terminals are installed during building construction. The ETHERNET trunk cables are in sections of 100-125 m for ease of handling and replacement. Up to four cable sections are joined to form segments of trunk cable up to 500 m long. Separate segments of the network are connected by local network repeaters. The ETHERNET trunk cable is placed in a cable tray on the outside wall in the experiment hall and runs through each wiring closet in the central lab/office building. A transceiver and LNI are installed for each eight nodes connected to the network. Offices have outlets wired with twisted-pair wires going to a terminal server and RG-58 coaxial cable going to a multiport repeater for connection of a terminal or personal computer. Wiring closets are placed strategically to reduce the amount and concentration of cabling. Wiring closets serve each floor of the central lab/office building and each of the five lab/office modules. They are used to connect the twisted-pair wiring for phones and terminals to the terminal servers and the coaxial cable for personal computers to the multiport repeaters.

4.3 Computer Software

4.3.1 Operating System

The operating system software is DEC's VMS for both the data analysis computers and the beam line computers, except where special needs dictate. A large number of UNIX users are found at universities, so a UNIX-like shell operating under VMS is provided. A host license for VAXELN is provided to support development of software for the beam line computers using this operating system.

4.3.2 Languages

Most scientific programming is done in FORTRAN, and this language is provided on all computer systems. The FORTRAN compilers include all features of the FORTRAN 77 standard, as well as some enhancements, but are capable of flagging nonstandard statements to assist in preparing code for export to other systems. PASCAL and C language compilers are also provided. PASCAL and C are used for development of software to run under VAXELN, which is used on some beam line computers.

4.3.3 Graphics

The data analysis computers and the beam line computers use graphics software based on the Graphics Kernel Standard (GKS). ISSCO's TELLAGRAF and DISSPLA are available on the CCF VAX 8700. Graphics packages for export to users' institutions are based on GKS or public-domain software packages. Software is provided to simplify conversion of DISSPLA graphics software to GKS or the public-domain package for export.

4.3.4 Communications

Communications software allows file transfer between the data analysis and beam line computers and provides terminal emulation using either system as the host. The networking software allows file transfer and electronic mail between the APS computers and nodes on major international computer networks through BITNET. This software also provides dial-out capability to allow reaching nodes not on a directly connected network.

4.3.5 Data Management

Data are backed up on tape or removable optical disks at periodic intervals. Software is provided that makes it easy to find and recover data sets with a minimum of human intervention. Database management software is also used to keep track of users, experiments, proposals, and publications and to assist in report production.

4.3.6 Code Management

To minimize duplication of effort, subroutine libraries are maintained that contain code useful to many users. A software package that keeps track of subroutine modules and codes using them is also provided. This makes it possible to automatically rebuild all codes using a given subroutine when the subroutine is modified. Standard procedures ensure proper testing of all software before it is released for general use. The operating system software provides a uniform calling standard so that codes written in any language can call subroutines written in any other language.

4.3.7 User Interface

At a national user facility, it is important to make the software easy to use, because some users are typically on site for only one or two days. Software is provided to present an easily understandable interface to outside users. Comprehensive documentation and online help are provided as part of all data analysis software.

4.3.8 Data Analysis

Special data analysis software is used for each type of experiment. A team of scientists knowledgeable about software will set standards and specify software needs. Data collection standards are imposed for the data files to be created, which facilitates development of special data-handling software provided on a facility-wide basis.

4.3.9 Performance Monitoring

Software for monitoring computer performance is provided in order to use the available processing power in the most efficient manner. Software is also provided for tuning individual computer codes to eliminate inefficiency in the data analysis.

4.3.10 Office Automation

The data analysis computers are used for administrative data processing as well as for scientific data analysis, so an office automation (OA) software package is provided. This aids the APS staff in its work and is useful to the scientists and outside users as well. Scientific papers and reports are prepared using the scientific word processor provided in the OA package. The OA package also assists in keeping track of calendars, setting up meetings, and using electronic mail.

IV.

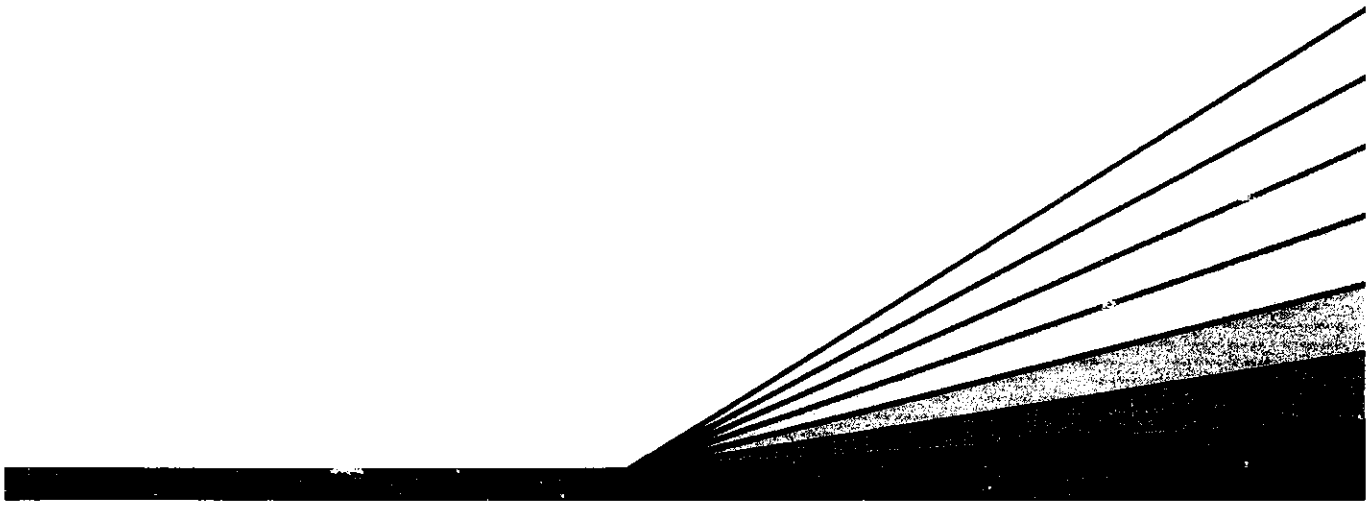

Conventional Facilities

IV. 1. OVERVIEW

1.1 Objective of the Facilities' Construction

The APS conventional facilities are designed to accommodate a 7-GeV positron storage ring, a full energy synchrotron, a positron linear accelerator, and an electron linear accelerator. The storage ring is housed in an annular building, which also provides space for external photon beam lines and for the set-up of experiments utilizing the beam lines. Laboratories, clean rooms, and offices for the use of the experimenters are located adjacent to this experiment hall. Site access roads, parking facilities, and miscellaneous site amenities are included.

The layout of the components and spaces and the construction systems selected provide precise geometric relationships, specific environmental conditions, isolation from outside vibration, and appropriate safety and shielding measures. The design of the conventional facilities addresses the usability and operational efficiency of the overall project. Engineering design provisions follow the U.S. Department of Energy (DOE) Order 6430.1, entitled "General Design Criteria Manual."

The design of the conventional facilities considers the following significant criteria in arriving at the siting, configuration, and building system selections:

- The geometry of the technical component dictates the scale and organization of the conventional facilities. In general, the forms and dimensions of the buildings follow the functional organization of the linear accelerator, synchrotron, positron storage ring, and photon beam lines, as illustrated by Fig. IV.1.1-1, the Project Site Isometric.

- The 1060-m-circumference storage ring, being the largest technical component, is the primary element in organizing the conventional facilities. Requirements for housing the ring dictate the design dimensions for the arrangement of the conventional facilities.

- Safety of personnel during facility operations requires that the storage ring, linear accelerators, and synchrotron be shielded. Shielding calculations indicate the need for 3 to 6 ft of concrete, supplemented, where appropriate, by lead bricks, steel plate, or earth cover to safely contain radiation. (See Section IV.2.3.)

- Reliable operation of the beam lines and related technical components requires their installation on a vibration-free structure and their containment in a controlled, stable environment.

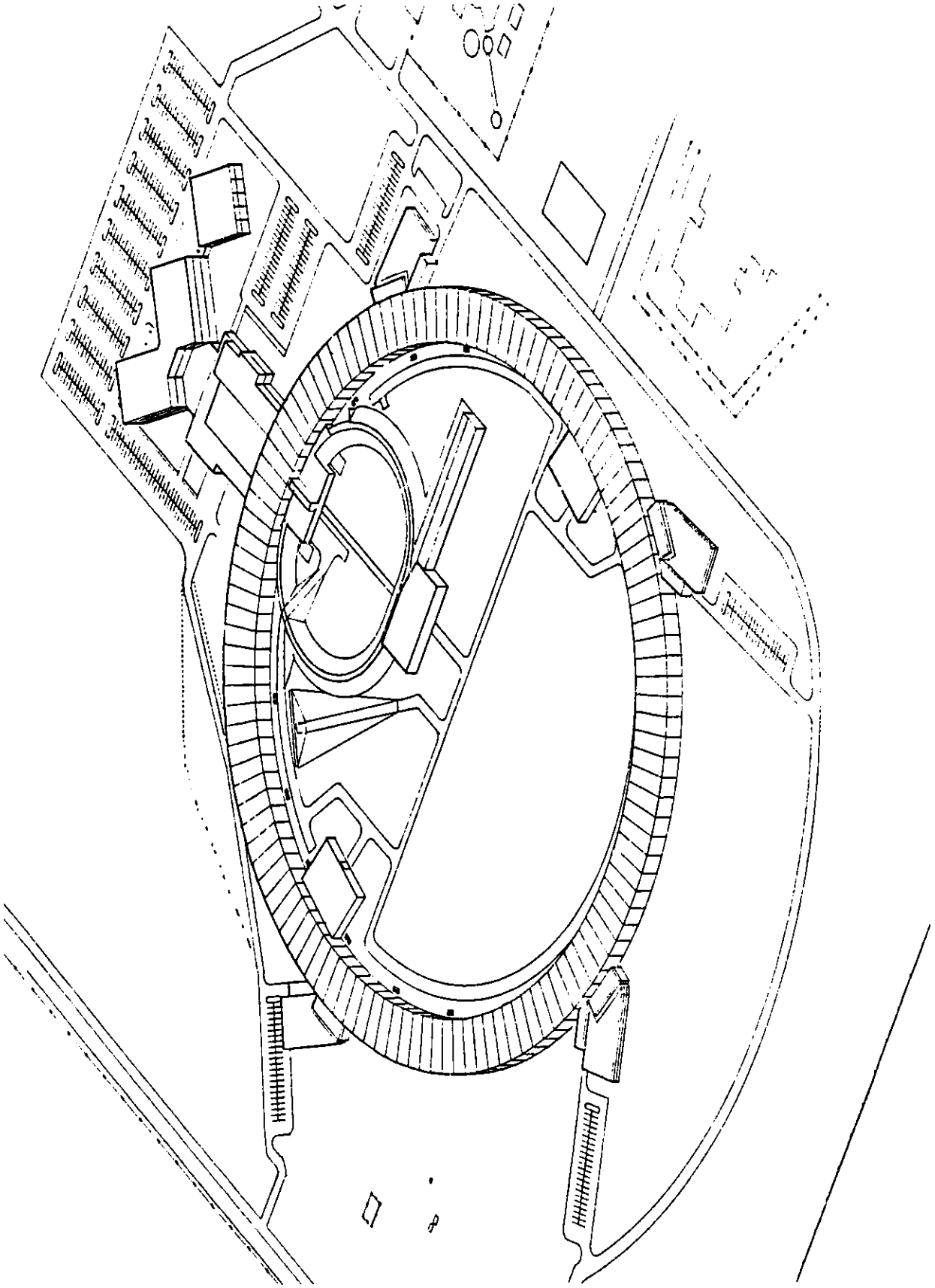

Figure IV.1.1-1
Project site isometric.

- Ease of installation, operation, and maintenance of the technical components requires safe, convenient access into the areas containing the technical components.

- Optimum use of stored beams by researchers requires the flexibility for photon beams to exit at tangents to the storage ring approximately every 4.5°. The photon beam lines range up to 80 m long in the 83-ft-wide, environmentally stable, vibration-free, column-free experiment floor, which completely surrounds the positron storage ring.

- Projected experiment installation criteria and operating conditions require the hall to have stable, level floors, a controlled heated and air-conditioned environment, clear heights up to 21 ft, and accessibility to utility services. The provision of these services is sufficiently flexible to anticipate varied operating routines and to accommodate an evolving technology.

- The research areas must have convenient access to laboratory, office, service and delivery, and related support spaces to maximize and enhance the experimenters' use of the facility.

- Operation of the total facility is accommodated in the central laboratory/office building that contains offices, shops, laboratories, assembly areas, and the main control and computer rooms. The central laboratory/office building is a distinctive but functional structure that serves as the identifying "front door" for the total facility.

- The materials and character of the facility are consistent with Argonne plant standards, recognizing the long-term maintenance and operating requirements of such a large-scale facility. Utility distribution systems are designed to meet the anticipated demand loads of a fully operating research facility. Operating equipment is provided to meet initial demand levels, with provisions for planned additions as the facility usage increases. The systems are expected to maintain a high degree of reliability in their operation, without the need for installation of excessive standby components or redundancy.

Building placement and orientation were influenced by the following considerations:

- Technical component configuration

- Functional relationships

- Existing structures

- Existing utilities

- Radiation protection
- Subsurface conditions
- Topography
- Vibration sources
- Site access
- Environmental impact
- Archeological locations
- Possible extended beam-line projections
- Expansion potential

Figure IV.1.1-2 shows the proposed location for the APS, in the southwestern section of the Argonne site, centered on Bluff Road east of Kearney Road. The buildings are sited on a large land area away from possible adverse consequences of traffic-generated vibration, as shown on Fig. IV.1.1-3, the Project Area Plan. The site accommodates both the proposed initial and future growth expectations for the project.

1.2 Organization and Layout of Facility Components

The conventional facilities comprise thirteen buildings, illustrated on Fig. IV.1.2-1, the Project Site Plan. The predominant structure is the experiment hall, which encloses the storage ring; the other buildings are either located within the infield of the experiment hall or appended to the outer perimeter of the experiment hall.

The machine-support structures -- structures housing the accelerator facilities -- are located in the infield of the storage ring. They house the concrete-shielded beam enclosures and technical components for acceleration and containment of the beam. They consist of the linac building, the synchrotron injection building, the synchrotron building, the synchrotron extraction building, and the storage ring enclosure (located within the experiment hall). These structures are connected to each other in series and linked directly to the storage ring. The two rf/power buildings that house the rf power supplies for the storage ring also connect directly to the storage ring enclosure and the experiment hall.

The experiment-support buildings -- buildings housing people -- are extensions off the outer perimeter of the storage ring enclosure. The experiment hall is a ring-shaped, long-span structure that contains the concrete-shielded storage ring enclosure along the inner perimeter, with an unobstructed, continuous, column-free hall to contain the

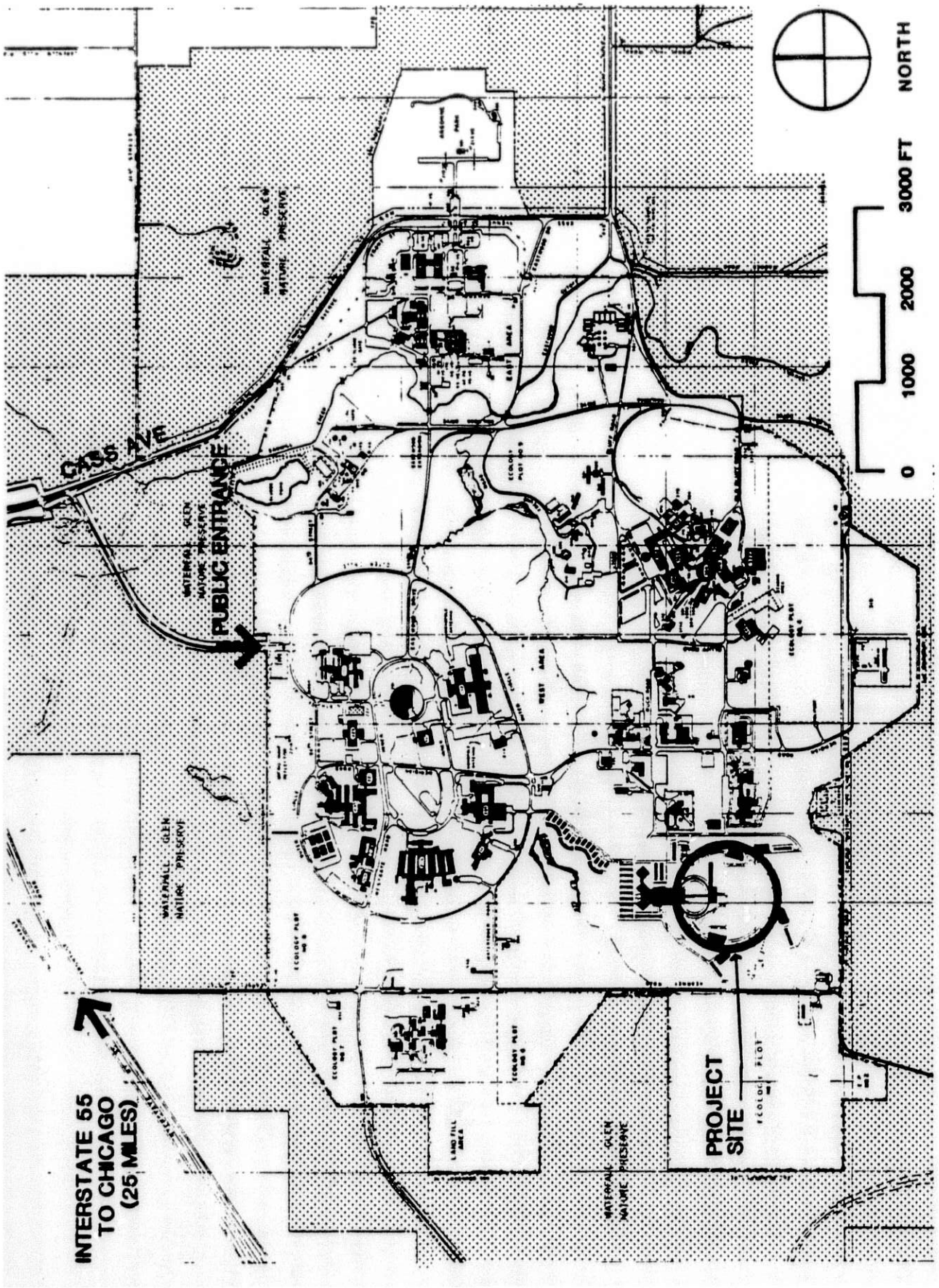

Figure IV.1.1-2
Argonne campus plan.

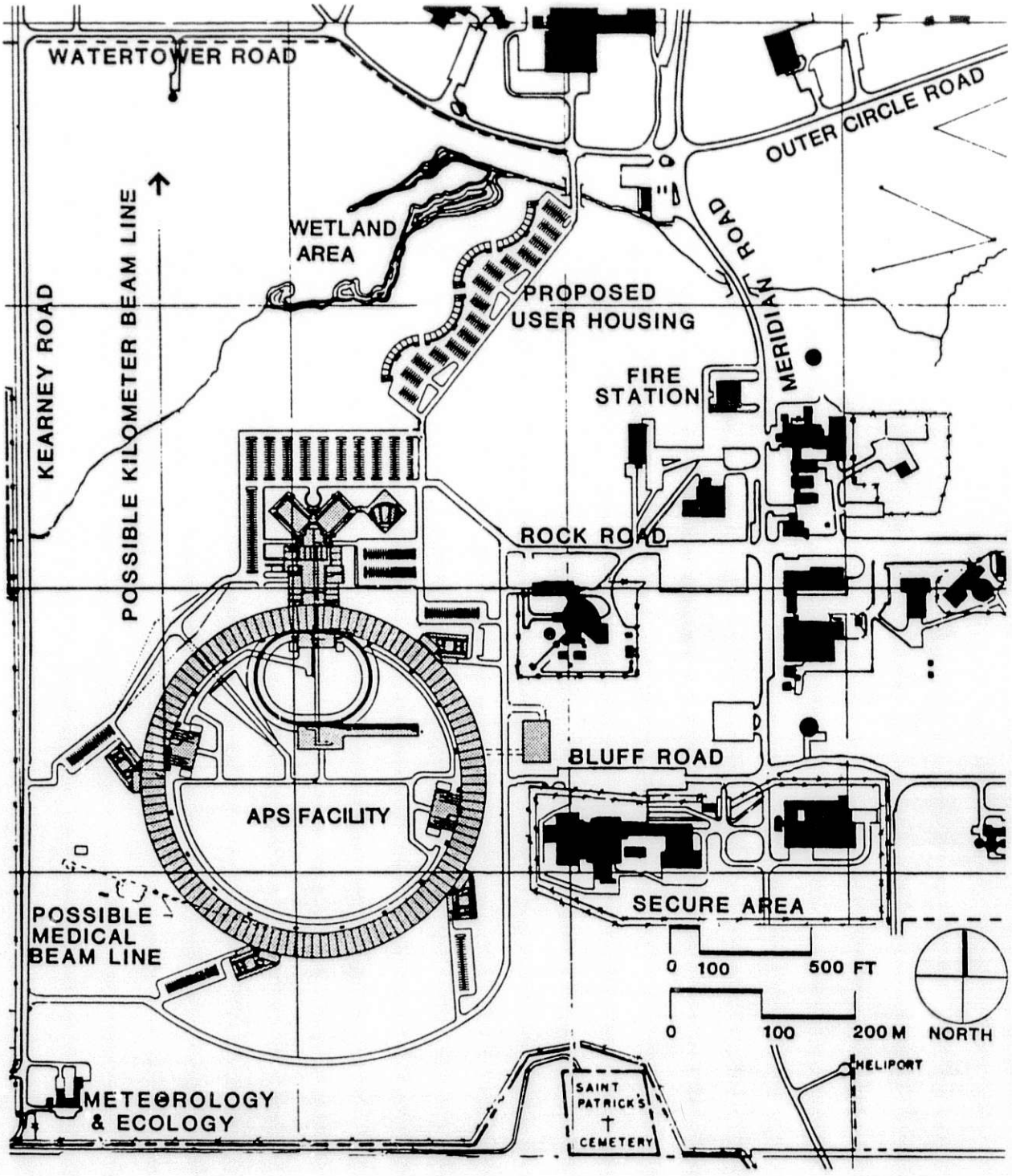

Figure IV.1.1-3
Project area plan.

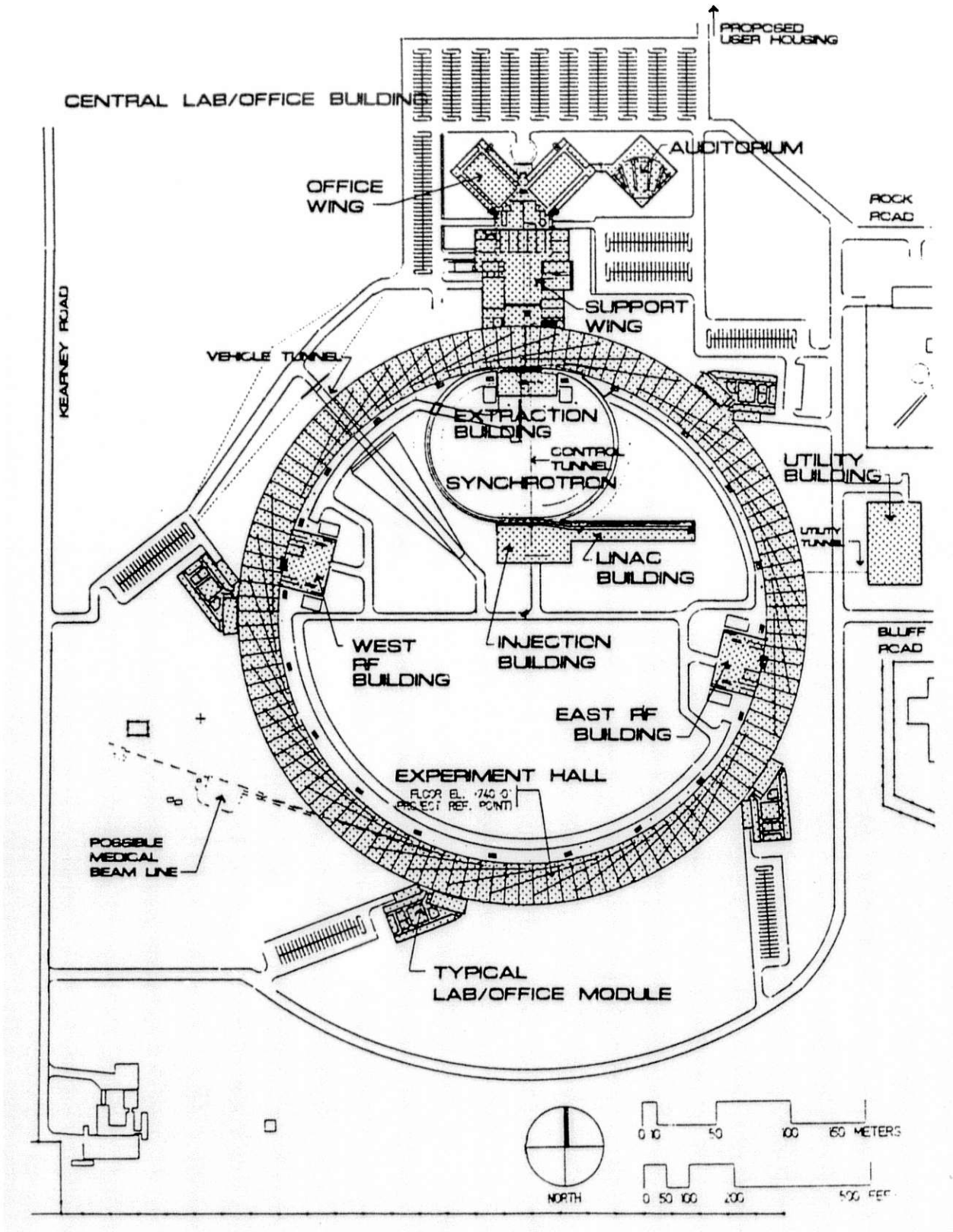

Figure IV.1.2-1
Project site plan.

experiments between the storage ring and the outer perimeter. The central laboratory/office building contains the administrative offices and support spaces for the permanent staff assigned to manage the APS. The office wing of this building contains conference facilities, laboratories, and the main computer and control rooms for the entire facility, and an adjacent auditorium. The support wing contains specialized labs, clean rooms, receiving areas, shops, stock room, and toilet/locker rooms. In addition, there are four laboratory/office modules - four similar, single-story buildings of 13,600 ft^2 each, located around the outer perimeter of the experiment hall. Each is composed of five laboratories that connect directly to the experiment hall, 20 offices for the experimenters, conference and support spaces, and a truck air lock to facilitate delivery of components to the experiment hall.

Chillers, compressors, and pumps for the facility are contained in a 21,600-ft^2 utility building located at a distance from the experiment hall. The primary electrical distribution switchgear is also located in this structure. The utility tunnel carries piping and conduit for mechanical and electrical services from the utility building at the eastern edge of the site, under the ring road to the outer perimeter of the experiment hall. The utility loop in the experiment hall provides utility service to the rest of the site.

Two tunnels provide access directly to the infield areas from outside the experiment hall. The largest tunnel, entering the infield from the northwest corner of the site, is sized to accommodate emergency and maintenance vehicles. A smaller control tunnel provides access for utilities and pedestrians from the lower service level of the central laboratory/office building beneath the control room; under the support wing, experiment hall, and synchrotron buildings; to a stairway and elevator in both the synchrotron extraction and synchrotron injection buildings. Building footprint, areas, and dimensions for all structures of the conventional facilities are shown in Table IV.1.2-1.

Table IV.1.2-1

Building Dimensions

Building	Clear Height (ft)	Overall Size		Footprint		Gross Floor Area (ft^2)
		Width (ft)	Length (ft)	Part (ft^2)	Bldg. (ft^2)	
Linac Building					10,554	10,554
Linac Enclosure	9.0	18.8	272	5,114		
Klystron Gallery	17.5	20.0	272	5,440		
Synchrotron Injection Building	20.0	82.0	164	13,138	13,138	14,751
Synchrotron Enclosure	9.0	11.5	1210	13,915	13,915	13,915
Synchrotron Extraction Building	14.0	49.0	132	6,470	6,470	7,060
RF/Power Buildings					21,600	21,600
East RF/Power Building	14.0	90.0	120	10,800		
West RF/Power Building	14.0	90.0	120	10,800		
Experiment Hall	24.5	91.3	3,665		334,836	334,836
Utility Corridor	11.5	7.0	2,743	19,200		
Storage Ring Enclosure	9.0	20.7	3,478	72,000		
Experiment Floor	24.5	63.3	3,849	243,636		
Lab/Office Modules					54,400	54,400
East Lab/Office Module	9.0	83.0	149	13,600		
Southeast Lab/Office Module	9.0	83.0	149	13,600		
Southwest Lab/Office Module	9.0	83.0	149	13,600		
West Lab/Office Module	9.0	83.0	149	13,600		
Central Lab/Office Building					88,875	199,878*
Office Wing	9.0	100.0	353	35,320		
Support Wing	27.0	201.0	206	41,455		
Auditorium Wing	17.0	110.0	110	12,100		
Utility Building	30.0	120.0	180	21,600	21,600	21,600
Subtotal					565,388	678,594
Tunnels					16,100	16,100
Utility Tunnel	15.0	15.0	153.0	2,300		
Control Tunnel	15.0	15.0	720.0	10,800		
Vehicle Tunnel	20.0	20.0	150.0	3,000		
Total					581,488	694,694

*Includes 35,320 ft^2 service level and 11,272 ft^2 fan room.

2.1 Siting Constraints

The configuration of the technical components, especially the machine itself, was the primary determinant of the site layout. Ring shapes for the storage ring and synchrotron and relationships in the beam transfer area are a critical part of the machine design. The locations of the conventional facilities housing the machine are fixed by the chosen configuration of the machine. The rf power supply connections to the storage ring must be located directly opposite one another, requiring compatible locations for the rf/power buildings. The shape, location, and width of the experiment hall are all determined by the number, length, and tangent locations of the photon beam lines.

Beyond the configuration requirements of the machine itself, certain functional relationships are critical to the layout of the APS facility. The central laboratory/office building houses the control room and the operating staff for the machine. Because of the need to interface with the injection facilities, a close relationship between the central laboratory/office building and the infield buildings was required.

The 720-ft-long control tunnel that connects these buildings provides direct access for both pedestrians and cabling, as well as other utilities. The support wing of the central laboratory/office building is located between the office wing and the experiment hall because of the constant need for direct passage between these two areas. The laboratory/office modules are spaced around the outer perimeter of the experiment hall to minimize the distances that experimenters must traverse between their labs and offices and their beam lines.

In order to meet federal guidelines, a buffer zone between the radiation sources and the Argonne property line is provided. The skyshine radiation calculations help to establish how far the facility must be located from the west and south boundaries of the site. (See Section IV.2.3, Shielding Requirements.) Topography and subsurface conditions, although relatively uniform over the entire site, are less suitable in the northern portions of the site. In order to provide the firmest foundations for the critical machine supports, the complex was positioned as far to the south as possible and oriented to allow the storage ring foundations to benefit from the most consistent conditions.

Sources of vibration outside the boundaries of this facility could cause unacceptable levels of vibration in the experiment areas. Vehicular traffic, particularly that of heavy trucks, is to be avoided in the vicinity of the APS. The proposed site is located at a remote corner of the Argonne campus, away from the major traffic arteries and truck delivery routes. Adjacent non-Argonne land is not expected to contribute vibration because of its use as a nature preserve and recreation area.

To facilitate access, the central laboratory/office building (the primary population area of the facility) is located closest to Rock Road, which provides the primary

vehicular access from Meridian Road and Argonne's main entrance off Cass Avenue. The roadways encircling the facility have direct connections to Bluff and Kearney Roads. The cooling towers and utility building housing mechanical equipment are positioned at the eastern edge of the site closest to Bluff Road and all connections to the main Argonne site utility distribution systems.

The environmental impact of the facility is expected to be slight. This minimal impact is in part due to the siting of the facility so as to avoid encroachment on wetland areas at the northern edge of the site.

Although several areas of some archeological interest are included in the site, it was possible to avoid disturbing a number of them by close coordination with the archeological investigators.

The facility may need to accommodate beam lines up to one kilometer in length. For this reason, the location of present and potential roadways, parking lots, and building sites was taken into account to provide the greatest flexibility in locating possible future additions to the facility.

The need for expansion of selected portions of the facility has been anticipated, and space to allow future expansion has been provided in the required locations. The central laboratory/office building is laid out to allow independent expansion of the office wing, the clean rooms, support labs, and shop areas. The utility building is designed to accommodate a full complement of experimental facilities and is organized to allow the addition of mechanical equipment if the demand on the facility increases beyond this level.

Beam lines up to 200 m in length can be contained within the southern perimeter road. Laboratory/office modules are oriented along tangents to the storage ring to minimize their obstruction of potential beam lines that may be extended beyond the present building line. Each module may be expanded to provide additional work spaces without infringing on any additional beam line exterior areas, or new modules may be built along the experiment hall with the loss of only two or three extended beam line positions for each new module.

The topographic and geologic characteristics of the site are typical of much of the Laboratory. The site is well suited for this development, including both the building construction phase and the intended operation of the APS. The specific characteristics of the site that support its selection include the relatively level terrain, an adequate stay-clear area, space for extended beam lines, and close proximity to a security area for classified work.

Several alternative sites were considered. One of these is an area just east of Building 362, near the former 12-GeV Zero Gradient Synchrotron complex. Although at that location the adjacent existing buildings with their associated services and utilities offer some conveniences, the essential stay-clear areas necessary for reducing vibrational effects and for future extensions of beam lines are limited.

A level-terrain site on the eastern boundary of the Laboratory is limited by the lack of a similar stay-clear area on the east, adjacent to heavily traveled Cass Avenue. Studies showed that the rerouting of Cass Avenue was not a viable solution. The "800" area on the far western boundary has terrain limitations, as well as size and location limitations.

2.2 Geotechnical Evaluation

2.2.1 Geology

The geology of the site consists of approximately 30-m-thick deposit of glacial drift on top of the Niagaran and Alexandrian dolomite bedrock of Silurian age (about 400 million years old). These formations are underlain by Maquoketa shale of Ordovician age and older dolomites and sandstones of Ordovician and Cambrian age. Precambrian crystalline bedrock lies at a depth over 1000 m beneath the site. The beds are nearly horizontal.

The Niagaran and Alexandrian dolomite is about 60 m thick in the Argonne area; it is widely quarried in northeastern Illinois and is important as a source of ground water. The Maquoketa shale separates the upper dolomite aquifer from the underlying sandstone and dolomite aquifers; the lower aquifer has a much lower piezometric level and does not appear to be affected by pumpage from the overlying Silurian bedrock.

During the Pleistocene epoch, glaciers deposited drift over most of Illinois. Arcuate-shaped moraines, roughly parallel to the shoreline of Lake Michigan, were formed in the Chicago area during the last glacial stage (the "Wisconsinean" stage). The younger moraines are generally closer to Lake Michigan. Argonne is on the "Keeneyville Moraine," which is part of the Valparaiso morainic system.

Detailed geological and geotechnical measurements have been undertaken at the site to identify any variations in the physical properties of the glacial drift that might affect the design, construction, or exact location. In particular, a geotechnical investigation has been initiated for the purpose of determining general subsurface soil types, ground water conditions, and various soil characteristics. Twelve borings, six of which were to bedrock, have been made at the site. Soil profiles were determined in the field, and soil samples were tested in the laboratory to determine moisture content, dry unit weight, and unconfined compressive strength.

Test results have shown that the surface soils are glacial tills composed predominantly of clay-silt mixtures with lesser portions of sand and gravel. At the deeper elevations, rock debris is frequently present. The underlying bedrock consists of a thin- to medium-grained grayish-white dolomite. The site soils are preconsolidated and are usually high in density and strength. The site is well suited for construction of the APS facility.

Additional field tests are planned to determine dynamic properties of the soil, in particular the compression, shear, and Rayleigh wave speeds. Further borings will be required to obtain these data. Wave speeds will be measured by using in situ seismic testing techniques such as the crosshole test method. Among other things, the shear wave speeds will be used to calculate the shear modulus for the soil, which, in turn, is required as input for dynamic analyses of the experiment hall foundation and floor slab (see Section IV.2.5.3.4). Data relative to the general subsurface soil types and static soil characteristics will also be obtained from the new borings to supplement the data from the original twelve borings.

2.2.2 Seismology

There are only four faulted areas in Illinois that are relevant to any discussion of earthquake-induced motion at the Argonne site: the Sandwich Fault zone; the Des Plaines disturbance; minor tunnel faults in Chicago; and an ancient (older than Cambrian) fault. These are all located within about 75 km of Argonne.

In addition to the four local faulted areas, there are several areas of considerable seismic activity at moderate distances from Argonne, e.g., near the southern tip of Illinois (New Madrid, Missouri) and along the Wabash River. Other historical earthquakes having magnitudes less than approximately 4.5 are randomly located throughout the midcontinent, with frequency of occurrence increasing from exposed shield areas toward the flanks of the continent. Since the ground acceleration varies essentially inversely as the square of the distance from the epicenter, any resulting ground acceleration at Argonne due to distant earthquakes would be minor compared with that arising from nearby fault zones.

Based on an evaluation of both local and more distant fault areas, the maximum ground acceleration predicted for the Argonne site would most likely occur as a result of activity of the Sandwich Fault. The Sandwich Fault is the only significant fault known to exist in the Argonne vicinity. It is about 120 km long and extends N60°W-S60°E. Argonne lies about 31 km distant (N30°E) from it, near its southeastern end. Fault age is post-Silurian and pre-Pleistocene. Some reactivation may have occurred during glacial advance and retreat.

The building complex is structurally designed to accommodate a Uniform Building Code (UBC) Zone 1 lateral force (per DOE Order 6430.1). No earthquake of magnitude 4.5 or greater is likely, and, accordingly, a UBC Zone 1 design criterion is an acceptable limit.

Exploratory measurements of ground surface vibrations have been made at the site under "quiet" and "normal" site noise conditions. Most vibration energy seems to be associated with frequencies less than 20 Hz. Preliminary analysis of the vibration measurements suggest that "natural" ground vibrations may be less than those due to "cultural" noise in large experimental facilities. As discussed in Section IV.2.5.3.1, additional ground motion measurements are planned.

2.3 Shielding Requirements

2.3.1 Introduction

The shielding approach limits the radiation doses to DOE guidelines for both on-site and off-site exposure. The approach also addresses access to particular areas during certain operations. The shielding is designed for the radiation resulting from several types of operations that involve normal beam loss mechanisms, as well as for certain abnormal beam loss scenarios. The shielding design is based on experimental data obtained from existing accelerator and synchrotron light source facilities, used in conjunction with theoretical formulations based upon well-known attenuation characteristics. Details of the calculations and the parameters used for the specified shielding requirements are given in Refs. 1, 2, and 3.

2.3.2 Shielding Design Objectives

The basic occupational exposure limit for DOE contractors is 5 rem per year for whole body exposure.[4] However, in its guidance for ALARA (As Low As Reasonably Achievable) contained in the same DOE Order, the design objective for new facilities is to limit exposures to 1/5 of the basic limit. In addition, DOE has proposed as an ALARA guide that the predicted exposure to individual members of the public should not exceed 25 mrem per year.[5] These guidelines for on-site and off-site locations are used as the basis for shielding for normal operation of the facility.

Considering only normal loss conditions, the wall shielding provided for the storage ring (0.8 m of concrete) limits the on-site dose rate from continuous loss of the beam around the ring circumference for a 10-h mean lifetime to ~ 0.04 mrem/h,[1] well within the guidelines. This assumes a circulating current of 300 mA of positrons at 7 GeV. The computation is based on semi-empirical formulas suggested by Swanson et al.[6] that assume a uniform loss around the ring.

For the case of off-site doses, the skyshine component contribution, in relation to the low permissible level (25 mrem/yr), becomes an important consideration. Since the distance to the boundary is 220 m, a prudent approach to estimating the potential yearly dose from this component was taken.[1] The results of several calculations indicated that 1 m of concrete roof shielding is required to limit the off-site contribution to 8.3 mrem/yr, for an assumed 8000 h of operation. The calculation that predicts this dose rate of 8.3 mrem/yr contains a safety factor of three due to formulation uncertainties that are borne out by field measurements.[7]

An accidental loss of the entire beam at a single point is an extremely unlikely event. However, sufficient shielding is provided to ensure that the potential dose to an individual on the outside of the shield in the vicinity of the incident is not dangerous. With respect to such a rare accidental occurrence, the objective is to supply sufficient

shielding to limit the dose per occurrence to less than 500 mrem. Assuming a circulating current of 300 mA of 7-GeV positrons and a shield thickness of 0.8 m of concrete, an accidental loss of the beam at a point would result in a dose of < 100 mrem, if this event occurred at a location where the distance from the positron orbit to the outside of the shield is minimal.

In the case of the radiation dose rate outside the storage ring shield but in the vicinity of the injection area during beam transfer from the synchrotron, a conservative assumption of 50% loss at a point was assumed for 5×10^{9} e^{+}/s at 7 GeV.[1] The computed dose rate for this condition is above the guideline, but the addition of sufficient lead and dense polyethylene at high-loss points in the injection region reduces the dose rate during the injection phase to within the guidelines (< 0.5 mrem/h).

2.3.3 Access Objectives

The shielding allows unrestricted access to the experimental area and all laboratories and offices, both during injection and while the stored beam is circulating. Access to areas on the infield side of the storage ring tunnel is unrestricted. No access into the storage ring tunnel is allowed while the beam is injected or stored.

For the synchrotron, the shielding is adequate to allow unrestricted access to the outside of the building and its infield region, but no access is permitted into the synchrotron tunnel while the synchrotron is operating. Work in the storage ring tunnel is permitted while the synchrotron is operating and in the synchrotron tunnel while the storage ring is operating.

The shielding for the electron linac, positron converter, and positron linac allows unrestricted access to the regions outside the linac radiation enclosure. Additional lead, dense polyethylene, and steel shielding around the converter target ensure unrestricted access to the area outside the shield in the vicinity of the converter.

2.3.4 Shielding Approach

The shielding achieves the design goal of ≤0.5 mrem/h at accessible points on the outside of the shield during normal operations. At certain locations this requires additional lead and dense polyethylene.

The shielding requirements are satisfied by using sufficient concrete as a bulk shield to ensure adequate attenuation of the bremsstrahlung, giant resonance neutrons, and the high-energy component produced in the positron-photon showers. The concrete is supplemented by earth berms in some places, and steel, lead, and dense polyethylene are used to reinforce the shielding at localized regions of high-radiation fields. Points of localized loss during injection include septum magnets and other bending and focusing magnets in the injection system and downstream of the injection straight sections.

Localized shielding of such loss points has been used successfully at Aladdin and NSLS.[6,8]

2.3.5 Recommended Shielding

2.3.5.1 Linac System

The linac system (~75 m long) features an electron linac (~20 m) to accelerate e^- pulses (3.0 A peak current, 16.5 ns pulse width) to 200 MeV at a repetition rate of eight pulses per second (8 pps). The electrons impinge on a tungsten target (with a thickness of two radiation lengths) to produce positrons, with an assumed conversion efficiency e^+/e^- of 0.008. The positrons, which are accepted by the second linac, are accelerated to an energy of 450 MeV and injected into the synchrotron. The entire linac system is housed in a concrete tunnel of inner dimensions 9 ft × 9 ft with the beam located 5 ft above the floor. Linac shielding is adequate for continuous operation.

The shielding consists of a concrete enclosure (or concrete-earth equivalent) 2 m thick on the sides and roof of both the electron and positron linacs. For the positron converter section, which is located in a 5-m-long section between the electron and positron linacs, the shielding consists of 0.3 m of steel and 1.7 m of concrete (or concrete equivalent) on the sides and top. Localized high-beam loss points are shielded with additional lead and dense polyethylene.

2.3.5.2 Injector Synchrotron

The injector synchrotron (367 m in circumference) accelerates e^+ from 450 MeV to 7.0 GeV. Eight bunches of e^+ are injected into the synchrotron each second during the storage ring filling operation. The particle bunches are accelerated to full energy and extracted one at a time, producing ~10^{10} e^+ per cycle. The shielding is adequate for operation at 7.7 GeV with the same charge. The synchrotron is housed in a 9 ft × 9 ft cross-section concrete tunnel with earth coverage. Entry to the synchrotron tunnel to perform maintenance or repairs is permitted when a beam is circulating in the storage ring. In both beam transfer areas, where the linac shielding merges with the synchrotron shielding and the synchrotron shielding merges with the storage ring shielding, sufficient shielding is provided to isolate radiation fields produced in the operating machine from the synchrotron tunnel. Additional lead and dense polyethylene shielding is provided at localized beam loss points.

Except in the injection and extraction areas, where the concrete wall is 0.8 m thick, the shielding for the synchrotron consists of 0.3 m of concrete on the sides and roof of the tunnel, supplemented by earth berms to achieve an equivalent of 0.8 m of concrete shielding.

2.3.5.3 Storage Ring

The storage ring shielding is adequate at 7.7 GeV and 300 mA. The circulating beam produces synchrotron radiation, which is directed down beam lines to the experiment area. The storage ring is housed in a concrete tunnel whose outside wall is in the form of a ratchet wheel or sawtooth configuration (see Fig. III.1.2-1). The tunnel cross-section dimensions are 9 ft x 9 ft in regions where the outside wall runs parallel to the storage ring circumference, but wider in the regions of the ratchets to provide space for beam lines. The inside wall of the concrete tunnel is parallel to the storage ring.

Both tunnel side walls are 0.8 m concrete due to single-point beam loss considerations. For a ratchet section, where the shield extends in the radial direction, the shielding consists of 0.8 m concrete, except for a 2-ft x 2-ft square opening centered on a photon beam line. The shielding in these openings consists of 25 cm of lead followed by 55 cm of concrete. The tunnel roof is 1.0 m of concrete due to off-site skyshine considerations. Additional provision has been made for lead and dense polyethylene shielding for use as needed.

2.3.5.4 Photon Beam Line Safety Consideration for Injection

It is necessary to guard against an accidental positron beam loss during injection that could result in high-energy bremsstrahlung radiation being directed down a photon beam line. To prevent such an occurrence, a lead shutter 30-cm thick in the beam direction and 10-cm thick transversely is inserted in the front-end of the photon beam line before injection commences. The shutter is located within the shield tunnel to allow the concrete shield to adequately attenuate the neutrons produced.

Lead collars are installed to ensure that any scattered bremsstrahlung radiation is adequately intercepted. The lead collars are placed around the beam tube so as to block all optical paths except the beam tube aperture. A complete description of the front-end components for the front-end of the photon beam line are presented in Section III.2.4.

2.4 Alignment

2.4.1 Introduction

The 7-GeV storage ring has a circumference of 1060 m. The injection ring has a circumference of 367 m. The facility can support in excess of 75 beam lines. Together there are over 1200 components that are to be positioned to a great accuracy. In order to accomplish this task in an efficient and economical manner, it is necessary to utilize techniques that employ distance measurements only during the final positioning of the components. This technology is available today and is used successfully in accelerator alignment around the world.

2.4.2 Geodetic Reference

The absolute position of the APS components is dependent on the accuracy obtained in establishing the geodetic control points. Twelve monuments are used to establish geodetic control for the project (see Fig. IV.2.4-1). These points are located to an accuracy of 1.0 mm by using a combination of electronic distance measuring (EDM) systems, global positioning system (GPS) satellite receivers, and optical theodolites.

2.4.3 Alignment Tolerances

The radial and vertical displacements from the ideal geometry of one quadrupole to the next must be minimized. The relative alignment tolerances required for the synchrotron magnets are as follows:

$x = \pm 0.1$ mm,
$y = \pm 0.1$ mm, and
$z = \pm 0.1$ mm.

Rotation or tilt is kept within 0.2 mrad.

2.4.4 Storage Ring Alignment

The storage ring has 40 primary control points, of which four are geodetic. It also has 40 secondary points that expedite the rough positioning of machine components (see Fig. IV.2.4-2). The geodetic points enable alignment on a quarter of the ring at a time. The primary control point reference system is 1.0 m radially out from the machine centerline. The control points are established by means of a laser interferometer system with a self-aligning reflector to determine distance and a laser alignment system with a tracking receiver to determine the straight-line offset between three adjacent control points.

The magnets between each dipole and insertion device are prealigned on a rigid frame and installed in the ring as a unit. Magnet sets, dipoles, and insertion devices have precision reference sockets located on their ends. As each unit is brought into the ring enclosure, it is rough-positioned by using the location marks that were positioned by using the control points. Then it is leveled by using a Wild N-3 optical level. Tilt is controlled with an electronic clinometer.

Final positioning of the magnets in the radial direction and magnet smoothing are accomplished by the accepted methods of Distinvar wire measurements and nylon wire offsets.

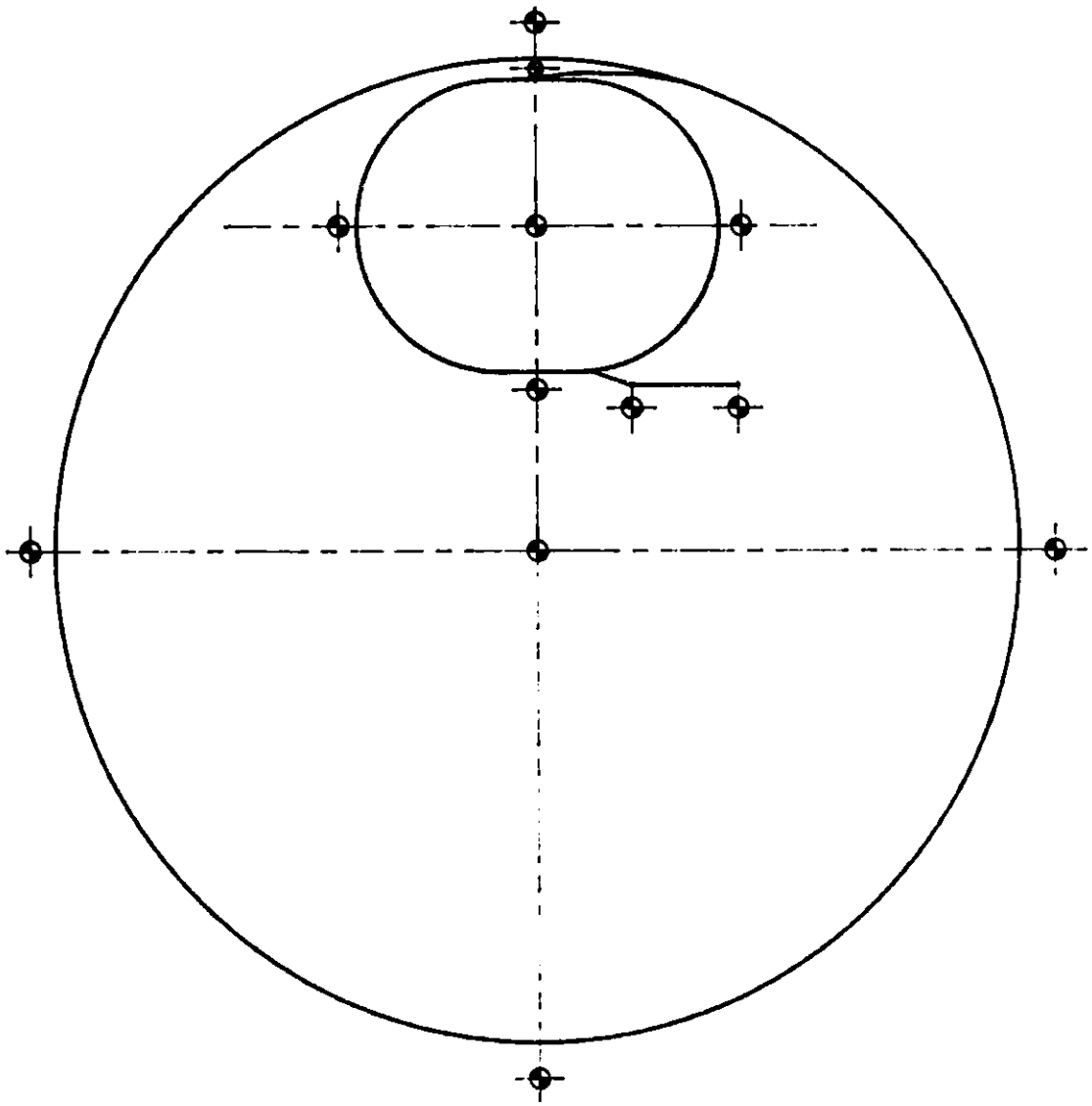

Figure IV.2.4-1
Position of geodetic control points.

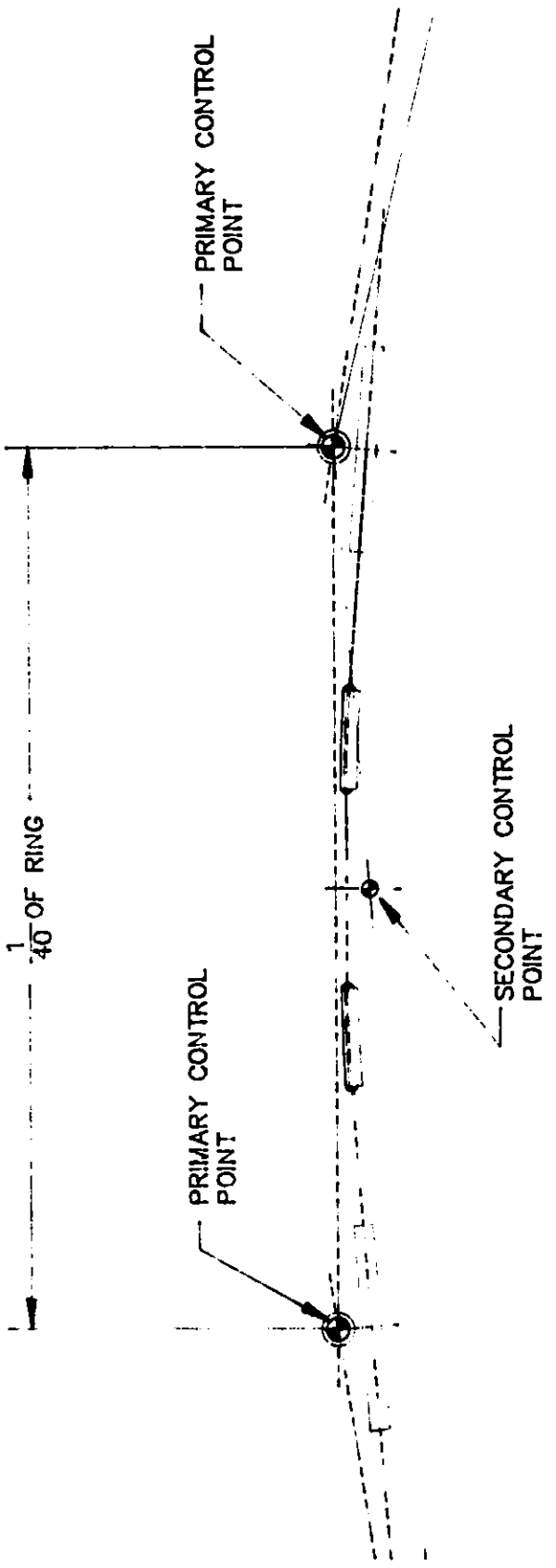

Figure IV.2.4-2
Position of control points in one cell of storage ring lattice.

2.4.5 Injector Synchrotron Alignment

The injector synchrotron is aligned in a manner similar to that for the storage ring. There are 40 control points for the synchrotron, of which four are geodetic. The control points are located with an invar tape for distance and a theodolite for radial position. From these points the magnet stand positions are marked on the floor. The same procedure as that used for the storage ring magnets is used for leveling and radially positioning the magnets.

2.4.6 Beam Line Layout

The beam lines exiting the storage ring are laid out by using the control points established in the ring. Standard optical methods are used to locate the lines.

2.4.7 Alignment Facilities and Equipment

A calibration bench with a length of 50 m is used to calibrate the distance-measuring equipment. The standard calibrating tool is the Hewlett-Packard Interferometer. The invar wires used with Distinvar and other alignment equipment are calibrated on the calibration bench. An instrument calibration system is used to maintain the optical alignment instruments.

2.5 Vibration Control

2.5.1 Introduction

Successful operation of the storage ring as a source of synchrotron radiation requires a beam with very low natural emittance. As discussed in Section II.1.8, mechanical vibrations of the magnet lattice of the storage ring represent a perturbation that contributes to an increase in effective emittance that, at low frequencies, can be viewed as beam steering and thereby can adversely affect the characteristics of the synchrotron light source. Consequently, successful design of the storage ring requires that vibrations of the magnet lattice be effectively eliminated or controlled to restrict emittance growth to an acceptable level.

Vibration criteria, based on allowable emittance growth, are presented in Section II.1.8. As discussed, these criteria must be met for vibration frequencies greater than 20 Hz.

2.5.2 Excitation Sources

Potential vibration excitation sources can be classified as "external" or "internal." External sources are defined as sources whose origin is external to the experiment hall. These sources include ground motion associated with microseismic activity, nearby road and rail traffic, rotating and/or reciprocating equipment (pumps and compressors) operating in the utility building, linac and synchrotron operation, and wind loading on the experiment hall. Internal sources, on the other hand, are those whose origin is internal to the experiment hall. These would include coolant water flow through the magnets, vacuum pumps, and related equipment operating in the storage ring tunnel and on the beam lines; the operation of HVAC equipment; operation of the overhead crane; and the like.

In the case of the external sources, energy transmission, for the most part, is through the ground, propagated in the form of body (compression and shear) waves and Rayleigh (surface) waves to the experiment hall floor slab. Floor motion, in turn, is transmitted to the magnets via the magnet support structure (girder on jack screws as shown in Fig. II.4.10-2). The soil-slab-support-magnet system represents a dynamic system that can either amplify or attenuate the ground motion associated with the various external sources.

Energy transmission from internal sources can be direct, as in the case of excitation induced by coolant flow. In other cases the energy may be transmitted via the magnet support structure or via the floor coupling to the magnet support structure. Once again we have a dynamic system that can act to amplify or attenuate the motion associated with the excitation source.

2.5.3 Vibration Study

A vibration study has been planned and is being performed to (1) identify and characterize the excitation sources, in particular the source level, frequency content, and energy transmission; and (2) analytically model the pertinent dynamic systems (e.g., soil-slab-support-magnet system) in order to design the APS storage ring to meet the vibration criteria given in Section II.1.8. As described below, the vibration study includes a measurement program, model development and analysis, and vibration isolation.

2.5.3.1 Measurement Program

The vibration measurement program consists of three measurement tasks: (1) Argonne site buildings/facilities, (2) ground motion in the vicinity of the storage ring site, and (3) wave propagation velocities in soil.

For the purpose of obtaining data and insights to support the vibration study, a vibration survey of an existing accelerator facility, the Intense Pulsed Neutron Source

(IPNS) at Argonne, was performed.[9] Various vibration excitation sources associated with the design and operation of the IPNS facility were selected for study as being representative of the type of sources and energy transmission paths to consider in the design of the light source facility. These sources include the following: coolant (water) flow through the beam line magnets; energizing the magnets; and, in the experiment hall, operating a large water pump, ventilating fans, and overhead crane. A preliminary analysis of results indicates that, with one or two exceptions, the rms vibration levels are below 0.1 μm, with the energy predominantly in the low frequency range (< 20 Hz). These amplitudes are well below the required level.

While it is expected that internal excitation sources will dominate, consideration is also being given to external sources. To this end, ground motion measurements are being made in the vicinity of the storage ring site. The results of these measurements will allow for assessment of the level and frequency content of the ground motion and the effect of microseismic activity, road and rail traffic, Argonne site facilities operation, and the like. Additionally, the attenuation characteristics of the ground will be measured and characterized.

Exploratory measurements of ground surface vibrations have been made at the site under "quiet" and "normal" site noise conditions.[10] Most vibration energy seems to be associated with frequencies less than 20 Hz. Preliminary analysis of the vibration measurements suggests that "natural" ground vibrations may be less than those due to "cultural" noise in large experimental facilities. As discussed in Section IV.2.5.3.4, additional ground motion measurements are planned.

As discussed above, energy associated with external excitation sources will be transmitted to the experiment hall and storage ring via body (compression and shear) and surface (Rayleigh) waves. Also, the vibration analysis methods require knowledge of the shear modulus that can be determined from the shear wave speed. For these reasons, it is important to measure the various wave speeds. In general, the wave speed will be a function of the type of soil and soil substructure and will vary as a function of depth. Wave speed measurements are being made at the storage ring site with in-situ seismic refraction testing methods.

2.5.3.2 Modeling/Analysis Program

The vibration study modeling/analysis program includes the development of models that, among other things, account for soil structure interaction. Because of the complexities and uncertainties associated with modeling soil structure interaction, simplified models will be used to obtain insights into the dynamic behavior of the experiment hall floor slab in response to ground motion and operating equipment mounted on the floor. Initially we will model the experiment hall as a flexible slab resting on an elastic foundation. Results of elastic-half-space theory with a knowledge of shear modulus and Poisson's ratio allow us to calculate equivalent springs and dashpots for the soil for use in mass-spring-dashpot models. Results from the scoping models and ground

motion measurement will dictate whether more detailed (for example, finite-element models) are required.

The magnet support system, on the other hand, represents a much better defined structural system. For this system, detailed models are being developed and studied to obtain the dynamic characteristics (natural frequencies and mode shapes) of the system and the transfer functions between floor motion and magnet response.[11] Among other things, the models and analysis results will be used to optimize the design of the support systems (e.g., location of supports relative to bending vibration modes of the magnet-supporting girder) to minimize the transmission of vibration energy from the floor to the magnets.

2.5.3.3 Flow-Induced Vibration of Magnets

The vibration survey of the IPNS indicates that coolant flow through the magnets is not a significant vibration excitation source. Nonetheless, the potential for vibration excitation due to coolant flows will be considered, and flow-induced vibration evaluation of the magnet design will be undertaken.

2.5.3.4 Vibration Isolation

The experiment hall floor slab is poured independently of the experiment hall building structure with an air gap between the floor slab and building structure foundation to minimize the transfer of vibrational energy from the building structure to the floor slab. Further isolation is provided by elastomeric bearing pads installed beneath the base plates of the columns that support the building and the overhead crane to damp vibrations generated by operation of the crane and heating, ventilating, and air-conditioning equipment. Based on the results of the vibration measurement and analysis programs described above, additional vibration isolation techniques will be applied as possible and appropriate to isolate the experiment hall floor slab from external as well as internal vibration sources and to isolate the magnets from motion of the experiment hall floor slab. For example, maintaining sufficient distance from the source is known to be the most effective means of isolating a structure from vibrations transmitted through the ground. Attenuation characteristics, obtained from site ground motion measurements, will contribute to the siting of the utility building. In the utility building itself, rotating rather than reciprocating equipment will be specified to eliminate the need to contend with unbalanced forces inherent in reciprocating machinery, and vibration isolation methods will be applied.

2.6 Life Safety Provisions

Because of the unique organization, construction, and functions of the APS facility, several kinds of life safety provisions have been implemented in the design of

the conventional facilities. The storage ring enclosure is essentially a shield around the storage ring. Door openings through this enclosure would by definition be weak points in the shielding. Such openings are therefore not acceptable for constructing exits. Although this is normally an uninhabited space, a peak population of twenty persons in a section of the enclosure during a technical component "emergency" has been postulated. Emergency exits from this enclosure are limited to four mazes from the infield side of the ring and three mazes opening to the experiment floor side from the enclosure. Maximum travel distances are about 400 ft, which is allowable for this type of structure.[12]

On the experiment floor of the experimental hall, a 3-ft-wide "stay clear" path has been defined near alternate beam lines from the ratchet wall to the outer perimeter wall. No utility lines or equipment are allowed on these paths, which constitute an assured clear exiting lane through the otherwise congested area.

Experiment hutches and office cubicles requiring internal sprinklered fire protection will be tied to the experiment hall sprinkler system. Additional fire protection such as Halon or hand-operated extinguishers are provided where needed as part of the hutch or cubicle construction.

Roadways are provided around both the inner and outer perimeters of the experiment hall and over the synchrotron building to the infield of the synchrotron to provide emergency vehicle access to all parts of the facility.

2.7 Other Special Requirements

Construction of the conventional facilities is phased to coincide with the construction of the technical components: the linac building is constructed first, followed by the synchrotron structures, followed by the storage ring and segments of the experiment hall. The support wing of the central laboratory/office building is crucial to early phases of the project because it houses the high-bay assembly area, clean rooms, and specialized labs, where portions of the technical components are fabricated.

Differential movement of the experimental hall floor and storage ring enclosure foundations (other than the deflections described under Section IV.2.5, Vibration Control) is addressed in the following sections along with planned methods and procedures to eliminate or minimize such movements.

2.7.1 Temperature Differential

The experiment hall has a temperature-controlled environment that will preclude seasonal variations. Heat loss or gain at the edges of the floor slab due to outside ground temperature changes will be effectively eliminated by a thermal barrier between the floor slab and the concrete grade beams.

2.7.2 Soil Volume Change

The soil volume change due to seasonal freeze/thaw cycles will be eliminated by the same environmental control and thermal barrier as above. The construction-period freeze/thaw cycle will be avoided by pouring over unfrozen ground.

2.7.3 Concrete Shrinkage

The floor will be cast in segments to minimize cracks due to curing and drying shrinkage. The long-term dimensional changes due to curing and drying will be completed by the time final alignment and operation of the storage ring is begun.

2.7.4 Variations in Load on the Storage Ring Tunnel Roof

The largest load variation will be due to the movement of the tunnel roof hatch cover blocks (limited in weight to 10 tons each by the overhead crane rating). The concrete and soil creep associated with this load variation can cause a vertical movement of as much as 81 microns, according to preliminary calculations. This movement will take days, but can be eliminated by operational procedures that counterbalance the weight. The blocks are stored nearby on the tunnel roof or replaced with pairs of 5-ton steel weights. Final alignment of the ring will be made with all blocks (or substitute weights) in place. Actual tests with 10-ton masses, bedrock-based survey monuments, and existing floor systems will be conducted at Argonne.

2.8 Applicable Codes and Standards

All systems are designed to meet the latest edition (as of beginning date of design) of the applicable codes, standards, and guides published by the organizations listed below:

Architectural/Structural

- United States Department of Energy, "General Design Criteria Manual - DOE 6430.1."
- International Conference of Building Officials, "Uniform Building Code (UBC)."
- American Concrete Institute, "Building Code Requirements for Reinforced Concrete (ACI 318)."
- ANSI/ACI 302, "Practice for Concrete Floor and Slab Construction."

- ANSI/ACI 531, "Building Code Requirements for Concrete Masonry Structures."
- Prestressed Concrete Institute Standards.
- ANSI/NBS 211, "Building Code Requirements for Masonry."
- ANSI/NBS Handbook H74, "Building Code Requirements for Reinforced Masonry."
- Structural Clay Products Institute, "Recommended Building Code Requirements for Engineered Brick Masonry."
- National Concrete Masonry Association, "Specifications for the Design and Construction of Load Bearing Concrete Masonry."
- American Institute of Steel Construction, "Specification for Design, Fabrication, and Erection of Structural Steel for Buildings."
- Steel Joist Institute, "Standard Specifications, Load Tables and Weight Tables for Steel Joists and Joist Girders."
- Steel Deck Institute, "Steel Deck Design Manual for Composite Decks, Form Decks and Roof Decks."
- Steel Deck Institute, "Steel Deck Institute Diaphragm Design Manual."
- American Iron and Steel Institute, "Specifications for the Design of Light Gauge Cold-Formed Steel Structural Members."
- American Welding Society," Structural Welding Code (AWS D1.1)."
- ANSI A58.1, "Building Code Requirements for Minimum Design Loads in Buildings and Other Structures."
- Metal Building Manufacturers Association, "Metal Building Systems Manual."
- TM 5-809-10, U.S. Department of the Army, "Seismic Design for Buildings," (Lateral force design methodologies in this technical manual can be used effectively for wind design as well as seismic design.)

Heating, Ventilation, and Air-Conditioning

- U.S. Department of Energy, USDOE 6430.1, "General Design Criteria Manual," Chapter 5.
- American National Standards Institute (ANSI), "Code Requirements."
- American Society of Mechanical Engineers (ASME), "Boiler and Pressure Vessel Code Requirements."
- National Fire Protection Association (NFPA), "National Fire Codes."
- International Association of Plumbing and Mechanical Officials, "Uniform Mechanical Code."
- Associated Air Balance Council (AABC).
- Air Moving and Conditioning Association (AMCA).
- American National Standards Institute (ANSI).
- Air-Conditioning and Refrigeration Institute (ARI).
- ASHRAE Standard 90A, "Energy Conservation in New Building Design."
- Construction Specifications Institute (CSI).
- Cooling Tower Institute (CTI).
- Hydronics Institute (HI).
- National Environmental Balancing Bureau (NEBB).
- National Electric Manufacturers Association (NEMA).
- National Fire Protection Association (NFPA) Standard 90A, "Air Conditioning and Ventilation Systems."
- Sheetmetal and Air Conditioning Contractors National Association, Inc., (SMACNA).
- Underwriters' Laboratories, Inc. (UL).
- American Conference of Government Industrial Hygienists, "Industrial Ventilation Manual."

- General Services Administration/Public Buildings Service (GSA/PBS) Publication, "Energy Conservation Design Guidelines for New Office Buildings."

- Federal Construction Council (FCC), "Federal Construction Guide Specifications."

- ASHRAE "Handbook of Fundamentals".

Plumbing

- U.S. Department of Energy, USDOE 6430.1 "General Design Criteria Manual."

- U.S. Department of Energy, USDOE 5480.4 "Environmental Protection, Safety, and Health Protection Standards."

- "National Standard Plumbing Code", 1983 Edition.

Fire Protection

- U.S. Department of Energy, USDOE 6430.1, "General Design Criteria Manual."

- U.S. Department of Energy USDOE 5480.4, "Environmental Protection, Safety and Health Protection Standards."

- National Fire Protection Association, NFPA 10 "Portable Fire Extinguishers."

- National Fire Protection Association, NFPA 12A "Halon 1301 Fire Extinguishing Systems."

- National Fire Protection Association, NFPA 12B "Halon 1211 Fire Extinguishing Systems."

- National Fire Protection Association, NFPA 13 "Installation of Sprinkler Systems."

- National Fire Protection Association, NFPA 24 "Installation of Private Fire Service Mains and their Appurtenances."

- National Fire Protection Association, NFPA 101 "Safety to Life from Fire in Buildings and Structures."

Electrical

- American National Standards Institute (ANSI).
- American Society for Testing Materials (ASTM).
- Certified Ballast Manufacturer (CBM).
- Electrical Testing Laboratories (ETL).
- Institute of Electrical and Electronic Engineer (IEEE).
- Insulated Power Cable Engineers Association (IPCEA).
- National Electric Code (NEC).
- National Electrical Manufacturers Association (NEMA).
- National Electrical Safety Code (NESC).
- National Fire Protection Associations (NFPA).
- Occupational Safety and Health Act (OSHA).
- Underwriters Laboratories, Inc. (UL).
- Joint Industrial Council (JIC).

2.9 Environmental Compliance

2.9.1 Approach to Environmental Compliance

In accordance with the National Environmental Policy Act (NEPA) and to meet the Department of Energy Guidelines for compliance with NEPA (see DOE Order 5440.1B), the procedures in DOE's Environmental Compliance Guide (Rept. DOE/EV-0 132 Vol. 1, February 1981) are followed. Based on information on the expected impact on the environment of the construction and operation of the facility provided to DOE in an action description memorandum, permission was received from the DOE Assistant Secretary for Environment, Safety, and Health to prepare an environmental assessment (EA). The preparation of an EA for this project is being carried out by Oak Ridge National Laboratory and will be completed shortly. The early identification of potential environmental effects will help ensure proper compliance with minimum impact on

schedule by allowing coordination and integration of the NEPA process during the design-development phase.

The preparation of the EA entails a comprehensive review of the action with regard to federal, state, and local environmental statutes and regulations. In addition, surveys for cultural resource sites of historic and prehistoric periods have been undertaken and coordinated with the State Historic Preservation Officer.

2.9.2 Preliminary Environmental Evaluation

A preliminary evaluation of environmental issues has been made on the basis of the conceptual design of the facility. The evaluation has had value in consideration of siting and design matters as well as in consideration of mitigating strategies. The Argonne site EA (DOE/EA-0181, August 1982) and federal environmental statutes were reviewed to provide the basis for the preliminary evaluation.

Potential environmental effects during the construction stage include debris, litter, gaseous exhausts from construction machinery and equipment, construction equipment noise, disposal of sanitary waste generated by construction personnel, dust, habitat destruction, soil erosion, and stormwater run-off.

The operation of the proposed facility has environmental effects such as physical-plant mechanical fan and cooling tower noises, normal plant/vehicular heat radiation, and stormwater run-off. Contamination from experimental sources is contained with fume hoods and HEPA filters. The quantities of radioactive material generated are expected to be minute; they will be monitored and controlled in strict adherence to established Argonne procedures.

The preliminary evaluation of the federal environmental statutes yields the following conclusions regarding their applicability to this project:

- Clean Air Act - Air pollutants may be emitted from the proposed facility; accordingly, this issue is being examined in the EA. Fugitive emissions (dust etc.) will probably arise during construction activities. Mitigation efforts will be investigated and corrective measures undertaken to assure compliance.

- Clean Water Act - Discharges are anticipated to be limited to storm water runoff, cooling tower blowdown, and sanitary wastes. This statute may only apply to this project in terms of runoff, but it will be addressed in the EA.

- Corps of Engineers Permits - This facility has no interface connections to a navigable waterway, and this statute is not applicable.

- Floodplains/Wetlands - This statute may be applicable since the project is located near a wetland environment and will be addressed either in the EA or

in a Floodplain/Wetland Assessment document. No construction footprint will occur in a floodplain or wetland area.

- Coastal Zone - Not applicable to this project.

- Endangered Species - An investigation by the Laboratory will be required to determine the applicability of this statute. If this statute is applicable, appropriate measures will be undertaken to assure compliance.

- Fish and Wildlife - Not applicable to this project.

- Wild and Scenic Rivers - Not applicable to this project.

- Historic Preservation - The proposed construction site is located near an area where historic and prehistoric cultural relics have been recovered. This statute is applicable, and appropriate measures will be undertaken to assure compliance.

- Water Resources Council - Not applicable for this project.

- Resource Conservation and Recovery Act (Hazardous Wastes) - This statute is probably not directly applicable since the predicted quantities of any hazardous material appear to be less than threshold limits. An investigation by the Laboratory should determine applicability in the EA.

- Safe Drinking Water - No underground injection of any substance is anticipated, but to assure compliance, the Laboratory will review the relevancy during EA preparation.

Preliminary consideration has been given to means for mitigating some environmental effects. Potentially adverse environmental effects will be controlled by the following methods:

- Debris is removed from the construction site in accordance with established Laboratory procedures stipulated in all construction contracts. Excess soil will be transported to Argonne's on-site approved landfill area.

- Gaseous exhausts from construction equipment, based upon an average 8-hour workday, are diluted into the atmosphere without need of special control measures.

- Noise levels associated with anticipated construction activity do not exceed 85 dB. The noise levels of existing occupied facilities are below 35 dB due to their distance from the construction site.

- Commercial sanitary-waste disposal stations and the existing waste treatment system dispose of all sanitary waste.

- Soil erosion is controlled by temporary construction berms and/or a drainage swale to specified collection ponds for surface water run-off. Concrete delivery truck and masonry wash-off facilities are provided to contain cement waste products for subsequent removal.

The operational environmental impacts are expected to be categorized as minimal. The following control measures are included:

- Building mechanical systems are placed within industry-standard noise-attenuating enclosures or provided with sound-insulating material.

- The cooling tower is located at a distance from occupied facilities to reduce adverse environmental effects.

2.10 References

1. H.J. Moe and V.R. Veluri, "Shielding Estimates for the ANL Advanced Photon Source," ANL Report, Light Source Note LS-90 (1987).

2. H.J. Moe, "Radiological Impacts from Operation of Argonne Synchrotron X-ray Source," ANL Report, Light Source Note LS-84 (March 1987).

3. H.J. Moe and V.R. Veluri, "Shielding Estimates for the ANL 6-GeV Synchrotron Light Source," ANL Report, Light Source Note LS-55 - Revised (March 1987).

4. U.S. Department of Energy, "Requirements for Radiation Protection," DOE Order 5480.1, Chg. 6, Chap. IX-3 (1981).

5. U.S. Department of Energy, "Proposed Revision of DOE Order 5480.1A, Radiation Standards for Protection of the Public," memorandum dated Sept. 17, 1984, Ref. PE-243 (1984).

6. W.P. Swanson, P.M. DeLuca, R.A. Otte, and S.W. Schilthelm, "Aladdin Upgrade Design Study: Shielding," University of Wisconsin (1985).

7. A. Rindi and R.H. Thomas, "Skyshine-A Paper Tiger?," Particle Accelerators, Vol. 7, 23-39 (1975).

8. K. Batchelor, ed., "National Synchrotron Light Source Safety Analysis Report," Brookhaven National Laboratory (July 1982).

9. J.A. Jendrzejczyk, R.K. Smith, and M.W. Wambsganss, "Vibration Survey of IPNS Beam Line Magnets and Experiment Hall," ANL Report, Light Source Note LS-89 (1987).

10. D.L. McCowen and R. Brown, "Ground Vibration Measurements Near the Site of the Proposed ANL Light Synchrotron Radiation Facility," ANL Report, Light Source Note LS-49 (January 1986).

11. W. Chou, "Emittance Growth due to Ground Motions, ANL Report, Light Source Note LS-88 (1987).

12. M.J. Knott, "Entrance Maze Locations for the Storage Ring Tunnel," ANL Report, Light Source Note LS-83 (February 1987).

3.1 Machine Support

3.1.1 Introduction

This section describes the buildings and facilities that support the various accelerator and storage ring systems. All of these buildings are located in the infield region of the experiment hall in order to provide 360-degree utilization of the storage ring for experimental facilities. The structures are basically defined by the dimensional and functional requirements of the accelerators (see Fig. IV.3.1-1). The final dimensions have been determined by actual equipment sizes and placement.[1]

The building designs are purely functional and amenities are minimal. Air-conditioning is provided only in essential areas such as accelerator containment structures, small electronics interfacing and control rooms, and in the few laboratories and offices in the synchrotron injection building.

A control tunnel connects the accelerator buildings (linac, synchrotron injection, and synchrotron extraction) with the control room area in the central laboratory and office building. This minimum length "spinal column" tunnel carries computer network and control signals, communication wiring, utilities, and personnel traffic between the various buildings. The same tunnel is used to house waveguides carrying rf power to the north side cavities of the synchrotron. From the synchrotron extraction building, passage can be made to the storage ring control area located atop the ring roof.

Control system, vacuum, and diagnostic equipment and multipole power supplies for the storage ring are located atop the ring tunnel roof, with their communication and utilities distributed along the inner wall of the experiment hall. Periodic slots through the ring inner shield wall at the ceiling level and an internal tray system carry wiring to the storage ring itself.

The two rf/power buildings contain the rf klystrons and waveguides for the storage ring. The third-harmonic rf system and the storage ring magnet power supply are each contained in one of these two buildings. A small air-conditioned room is provided in each of these buildings to accommodate the critical electronics and control system components. The remainder of the buildings are provided with heating and ventilation only.

Nearly all buildings have been designed with some provision for future expansion. The linac gun-end shielding is made up with removable concrete blocks to allow expansion of the linac system. The positron linac beam is shielded with concrete blocks to allow future test beam activities on the floor of the synchrotron injection building. The full-energy positron beam dump area has been provided with full concrete wall

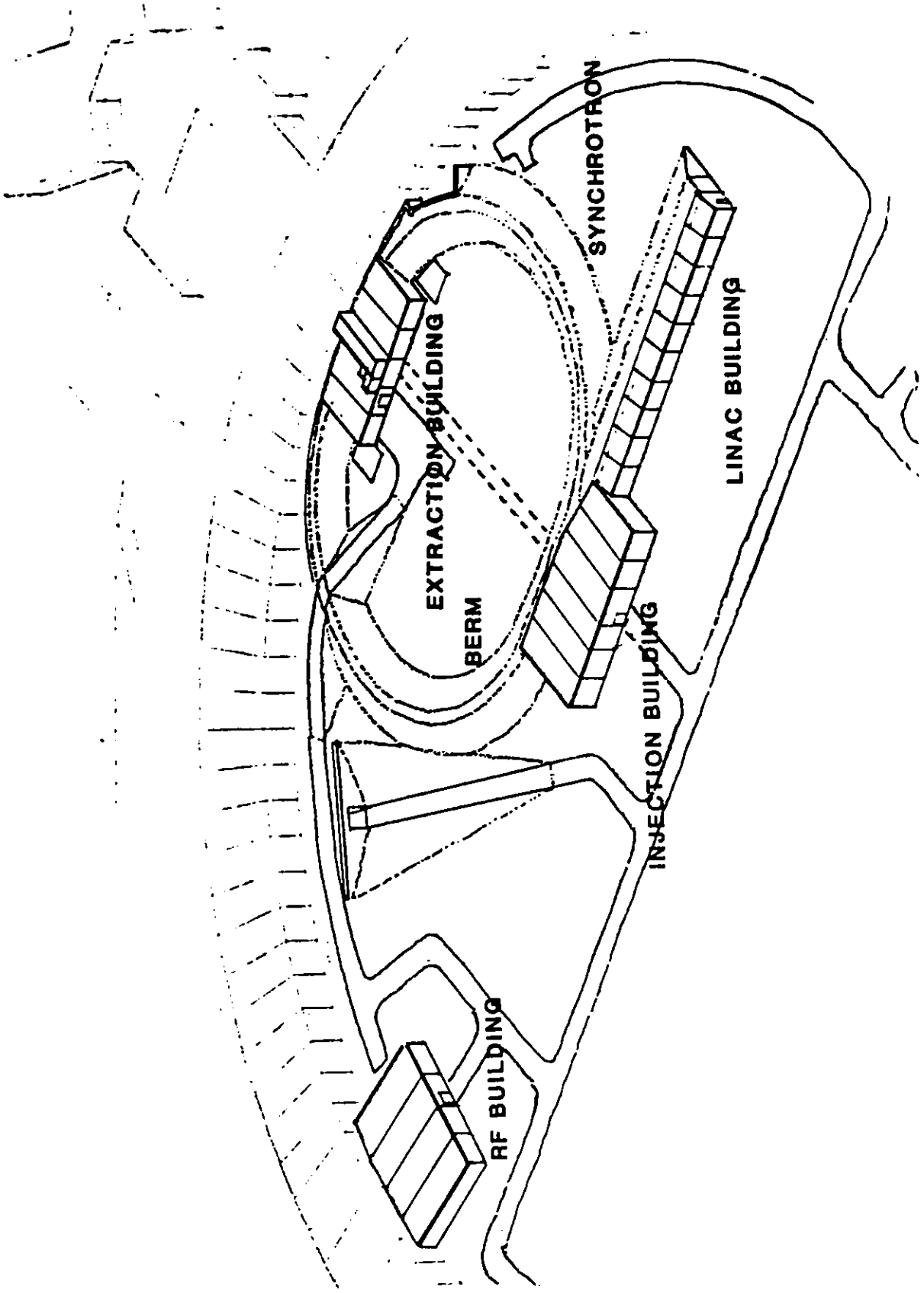

Figure IV.3.1-1
Infield isometric projection.

shielding instead of an earth berm to allow future use of this beam. Finally, the two rf/power buildings have identical dimensions to allow the installation of a fourth rf power system.

A shield wall configuration is provided to allow occupation of the synchrotron during storage ring operation and vice versa. Initial operation may require temporary stay-clear barriers because of possible beam losses.

Radiation-safe entrances to the linac are provided by a maze in the linac gun area and a moving block door at the high-energy end. Access to the synchrotron is by moving block doors from the synchrotron injection and extraction buildings and by maze to the storage ring tunnel in the beam transfer area. Infield-side entrances to the storage ring are by maze from each of the rf/power buildings, a maze in the beam transfer area, and a maze in the south portion of the ring. Access to the storage ring from the experiment hall side are by mazes near the injection and rf straight sections. These placements of access/egress points for the storage ring results in maximum travel distances of about 400 ft, which is a fire safety requirement for this type of structure. The moving block doors giving access to the photon beam front-ends are not considered fire safety exits.

Construction staging for the linac and synchrotron technical components occurs in the synchrotron injection building. Equipment is moved through the removable-block-shielded areas. The control tunnel is used to transport equipment from this staging area or from the central laboratory/office building to the synchrotron extraction building. Construction staging for the storage ring occurs in the experiment hall with equipment passed through the roof hatches in the straight-section regions.

3.1.2 Linac Building

At its west end, the linac building is connected to the synchrotron injection building. The one-story linac building is composed of two parts: the linac enclosure and the klystron gallery, which are parallel to each other and share a common wall along their entire length. The linac enclosure houses the electron and positron linear accelerators, while the klystron gallery encloses the associated klystrons and other equipment.

The rectangular klystron gallery is 272 ft long by 20 ft wide and 19 ft high, with a gross area of 5440 ft^2. The interior of the 272-ft-long linac enclosure is 9 ft wide by 9 ft high. This space is surrounded by radiation protection material -- 6.5 ft (2 m) of concrete on the klystron gallery side and 3.25-ft-thick (1-m-thick) concrete roof and wall, with earth berm on the roof and opposite side, respectively. Refer to Fig. IV.3.1-2 for plan and section views of this building. The low-energy (east) end shielding enclosure is made up from 2 m of removable concrete blocks.

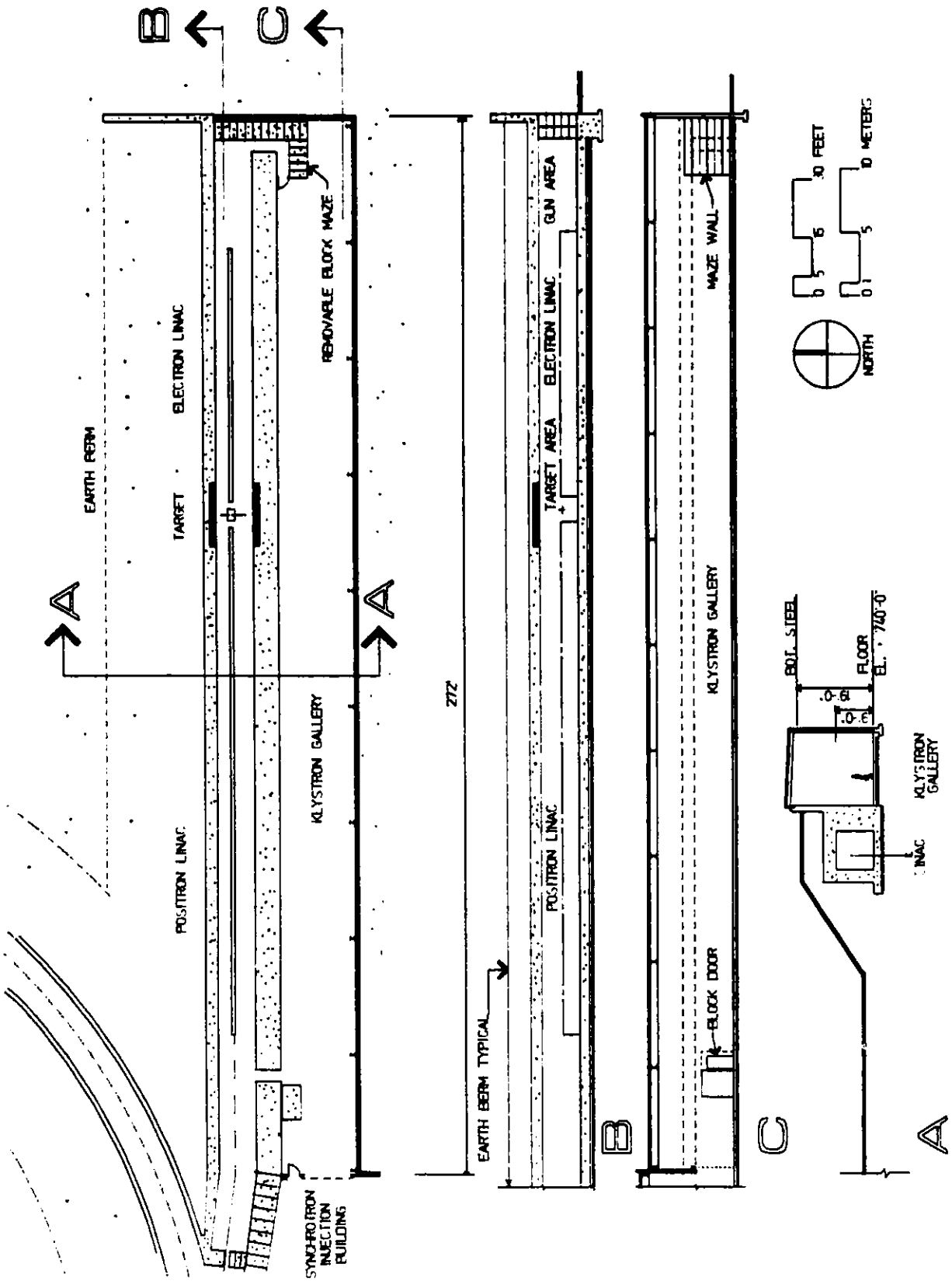

Figure IV.3.1-2
Linac building.

3.1.2.1 Architecture

The interior of the klystron gallery is open to accommodate technical component equipment along the length of the linac enclosure. The klystron gallery is entered from the synchrotron injection building and has an emergency exit at the opposite end.

There are no interior partitions or doors in the linac building except for those forming the linac enclosure itself. The radiation protection afforded by the 6.5-ft-thick (2-m-thick) concrete shielding is augmented by 1-ft-thick steel plates in the walls and roof that extend for 16 ft (5 m) in the positron target area near the middle of the building.

Conduit, piping, and ductwork in the enclosure are exposed and unpainted. Floors are exposed, surface-hardened concrete. No furnishings are provided for this building.

The windowless exterior of the klystron gallery is clad with 4-in. insulated metal panels supported on horizontal girts. The roof of the klystron gallery is protected by a single-ply roofing membrane, board insulation, and ballast in an inverted roof membrane assembly (IRMA) system conforming to Argonne's current standard. The outer wall and roof of the linac enclosure shielding is covered with a waterproofing membrane and an earth berm.

Unistrut channels are cast into all usable linac enclosure walls and ceilings and the klystron side of the shielding wall. The channel (1-5/8 in.) is embedded in the concrete on 6-ft centers, vertically on the walls and across the width of the enclosure on the ceilings, to form a rack for mounting equipment.

3.1.2.2 Structure

The structural system for the klystron gallery consists of a beam and girder roof system supporting a welded metal deck with wide flange columns with spread footings. A 9-in.-thick reinforced concrete floor slab rests on 6-in.-thick compacted granular backfill.

A shielding wall separates the linear accelerator from the adjacent klystron gallery and is constructed of reinforced concrete, 6.5 ft thick. The opposite wall and the roof of the linac, also of reinforced concrete construction, are 3.25 ft thick. Compacted backfill placed on top of the roof and against the outer wall provides additional shielding. This shielding berm has a slope of approximately 1 vertical in 1.5 horizontal, and is protected against erosion. The slab on grade for the linac consists of a 2-ft-thick reinforced concrete slab over 6 in. of compacted granular backfill.

3.1.2.3 Heating, Ventilation, and Air-Conditioning (HVAC)

The klystron gallery of the linac building, although not air conditioned, is ventilated with outside air to limit the maximum space temperature to 10°F above the outside ambient temperature during the summer. For this purpose, three 4000-ft^3/min supply fans with steam coils and exhaust fans are provided. In winter, six unit heaters with steam coils and integral thermostats operate to maintain the space temperature above 60° F when process equipment is not operating. No space humidification is provided.

The linac enclosure is air-conditioned to maintain a space temperature of 75°F ± 2°F year-round. Two 100% outside air units at 1300 ft^3/min each with steam and chilled water coils supply conditioned air to each end of the enclosure. Two fans exhaust air from the middle of the enclosure, and three fan coil units with integral thermostats located along the inside of the enclosure provide cooling, heating, and dehumidification. No space humidification is provided. Chilled water and steam are supplied from a connection through the control tunnel to the utility loop above the storage ring. A direct digital controller (DDC) in this building controls the HVAC equipment.

3.1.2.4 Plumbing/Process Piping/Fire Protection

Plumbing systems for the linac building consist of floor drains, domestic cold water, and sanitary waste and vent systems. Process piping systems supply compressed air and process water (90°F) as required for specific equipment and functions. Fire protection consists of a wet-pipe automatic sprinkler system. Hand-operated fire extinguishers are located as required near electronic components.

3.1.2.5 Electrical Power

Electrical power is distributed to the linac building at 480Y/277 V from a substation located in the synchrotron injection building.

The klystron gallery is lighted with high-bay, high-pressure sodium fixtures to an average of 30 footcandles of illumination. Lighting in the linac enclosure consists of two-lamp, wall-mounted fluorescent fixtures mounted on 8-ft centers, switched from lighting panels.

An equipment grounding system is provided from connections on each piece of equipment to grounding conductors running with all power feeders. Lightning protection is provided by copper rods mounted around the perimeter of the roof. These rods are connected by copper cables Cadwelded to the building structural steel. A building ground system uses bare copper cable Cadwelded to the building structural steel, which is connected to ground rods spaced around the building. In addition, all computer and related equipment is provided with a separate quiet grounding system that is isolated

from the other grounding systems and is connected to a separate counterpoise and ground rod system.

The fire alarm system consists of manual pull stations located at the building exits and flow and tamper switches in the sprinkler system. Smoke detectors are installed throughout the building and in the HVAC system. The alarm system is annunciated at the Argonne fire station and at the APS security point in the main control room.

Telephone communications are a branch from the private branch exchange (PBX) in the central laboratory/office building, with a telephone terminal cabinet in the klystron gallery.

3.1.3 Synchrotron Injection Building

The synchrotron injection building is located between the linac building and the synchrotron enclosure. The building houses the beam transfer area where the beam of positrons (generated by the linac) is injected into the synchrotron. Included within the building are the synchrotron power supplies, linac test beam areas, and injection facility control room. The synchrotron injection building also serves as the southern terminus of the control tunnel.

The building incorporates portions of the synchrotron and linac enclosures, in addition to the concrete enclosure for the beam transfer area, as shown on Fig. IV.3.1-3. Removable blocks in the sidewall of the beam transfer enclosure allow redirection of the linac beam to targets in the building for test purposes.

This one-story rectangular building is 82 ft by 164 ft with a footprint of 13,138 ft^2 and a gross floor area of 14,751 ft^2, including a 1613 ft^2 mezzanine. The beam transfer area occupies 470 ft^2, and 2900 ft^2 is used for enclosed laboratory, electronic, office, control, and toilet areas. Refer to Fig. IV.3.1-3 for plan and section views of this building.

3.1.3.1 Architecture

The interior of the building is open except for several small rooms in the southeast corner. The building may be entered from four directions: from grade along the south wall; on the east, through a block door from the synchrotron enclosure and from the klystron gallery; and from the control tunnel to the synchrotron extraction building and central laboratory/office building. Access to the control tunnel from the main floor level is provided by a stairway and an elevator located at the southeast corner. Emergency exits are provided at several locations along the exterior building walls.

Interior partitions are of gypsum drywall construction with a painted finish. In the open areas, the roof structure is left exposed and unpainted; conduit, piping, and ductwork are also exposed and unpainted. In the small rooms in the southeast corner of

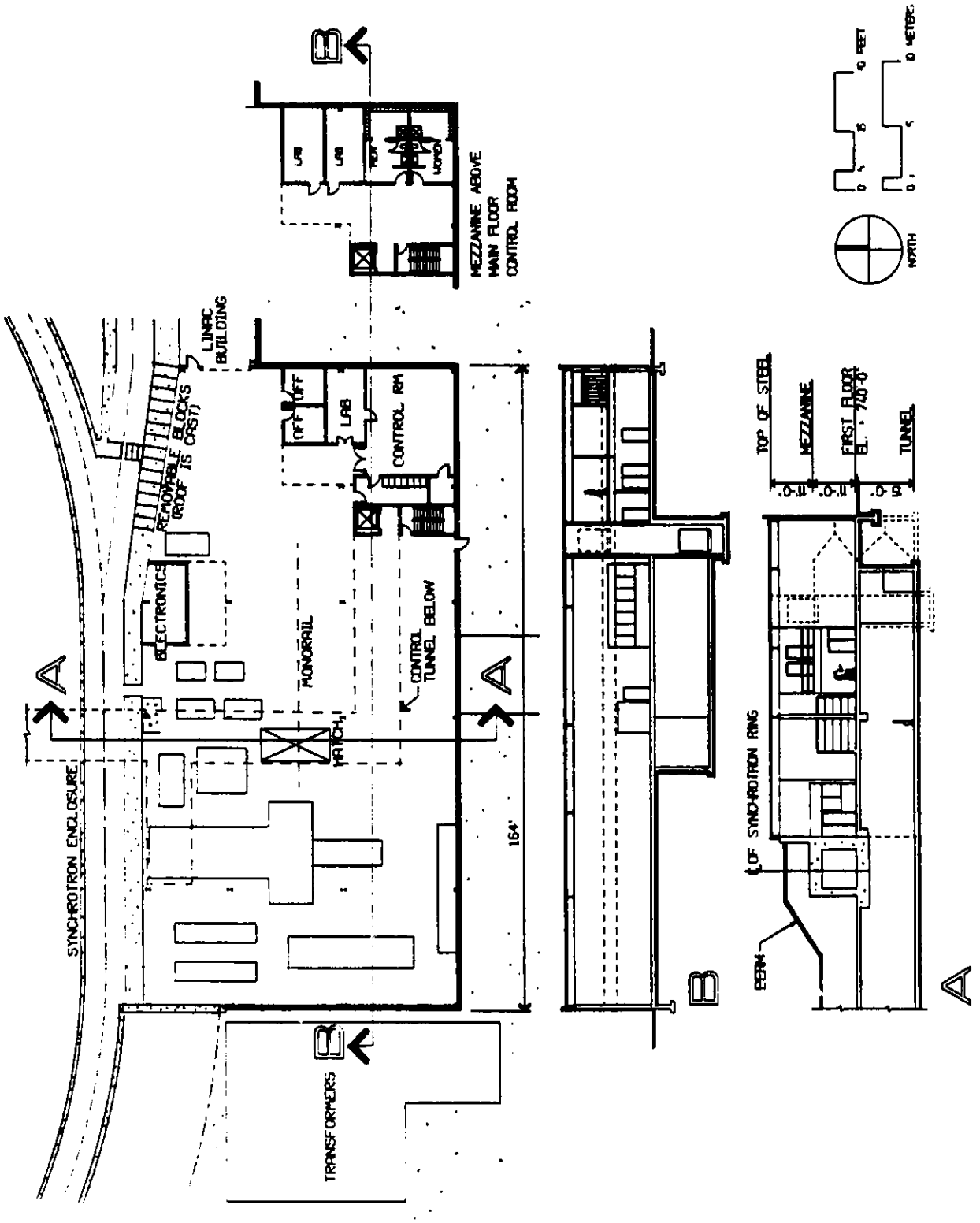

Figure IV.3.1-3
Synchrotron injection building.

the building, acoustical tile ceilings with recessed lighting and HVAC diffusers are suspended from the structure, with the electrical and mechanical distribution systems concealed in the ceiling space. The floors in the open area are exposed, surface-hardened concrete. In the small rooms, floors are covered with vinyl tile.

The windowless exterior of the building is clad with 4-in.-thick insulated metal panels supported on horizontal girts. A 14-ft rolling steel door accessible from the roadway on the south provides drive-in access for equipment deliveries. The roof of the building is protected by a single-ply roofing membrane, board insulation, and ballast in an inverted (IRMA) system conforming to Argonne's current standard.

Furnishings to be provided include desks, chairs, bookcases, and filing cabinets in the offices, and cabinets and counters along the long walls of the laboratories.

Unistrut channels are cast into the exposed wall of the beam transfer area and synchrotron enclosures. The channels (1-5/8 in.) are embedded vertically, 6 ft on center, to form a rack for the mounting of equipment.

3.1.3.2 Structure

The synchrotron injection building structure consists of a beam, girder, and column system supporting a welded metal deck roof, with structural steel bracing in the exterior wall for resistance against lateral loads. Foundations are conventional spread footings. The floor is a 6-in. reinforced concrete slab on grade over 6 in. of compacted granular material.

A monorail-type crane/hoist enables heavy equipment transfer from the control tunnel via a floor hatch.

3.1.3.3 Heating, Ventilation, and Air-Conditioning

This building is ventilated with outside air to limit the maximum space temperature to 20°F above the outside ambient temperature during the summer in areas containing high-heat-generating equipment, and 10°F above the ambient elsewhere. Three supply fans at 27,000 ft^3/min with steam coils and six exhaust fans are provided. In winter, five unit heaters with steam coils and integral thermostats operate to maintain the space temperature above 60°F when process equipment is not operating. No space humidification is provided.

The offices, laboratories, and control room of the synchrotron injection building are air-conditioned to maintain a space temperature of 75°F ± 2°F year-round. A 20-ton constant air volume packaged air-conditioning unit with chilled water coil and steam coil, located on the mezzanine of the building, provides the heating and air-conditioning. Reheat coils temper the supply air to each room to maintain space temperature. No humidification is provided.

The electronics room of the injector building is air-conditioned by a 20-ton packaged unit located above this room to maintain a space temperature of 75°F ± 2°F and space humidity of 45% ± 10% relative humidity (RH) year-round.

Chilled water and steam are supplied from a connection through the control tunnel to the utility loop above the storage ring. A DDC in this building controls the HVAC equipment.

3.1.3.4 Plumbing/Process Piping/Fire Protection

Plumbing systems for the synchrotron injection building consist of sanitary facilities with plumbing fixtures, domestic hot and cold water, and sanitary waste and vent systems. Process piping systems supply natural gas for the laboratories and compressed air and process water (90°F) as required for specific equipment and functions. A drainage system, for maintenance of specific equipment, is connected to the sanitary sewer or the laboratory waste sewer as required. Fire protection consists of a wet-pipe automatic sprinkler system. Hand-operated fire extinguishers are located as required.

3.1.3.5 Electrical Power

Electric power is delivered to the synchrotron injection building from the 13.2-kV switchboard in the utility building via a 15-kV loop feeder to a 3750-kVA, 13.2-kV to 2400V, pad-mounted power transformer and a 2000 kVA, 13.2-kV to 480Y/277 V pad-mounted distribution transformer located adjacent to the building. The 480Y/277 V power is then distributed to the linac building, the synchrotron enclosure, and the synchrotron extraction building from the substation in the synchrotron injection building.

An equipment grounding system is provided from connections on each piece of equipment to grounding conductors running with all power feeders. Lightning protection is provided by copper rods mounted around the perimeter of the roof. These rods are connected by copper cables Cadwelded to the building structural steel. A building ground system uses bare copper cable Cadwelded to the building structural steel, which is connected to ground rods spaced around the building. In addition, all computer and related equipment is provided with a separate quiet grounding system that is isolated from the other grounding systems and is connected to a separate counterpoise and ground rod system.

The building is lighted by high-bay, high-pressure sodium fixtures for an average illumination of 30 footcandles. Lighting in the control room, laboratory, electronics room, and offices is provided by 2-ft by 4-ft lay-in fluorescent fixtures, wall-switched in two levels.

The fire alarm system consists of manual pull stations located at the building exits, and flow and tamper switches in the sprinkler system. Smoke detectors are installed throughout the building and in the HVAC system. The alarm system is annunciated at the Argonne fire station and at the APS security point in the main control room.

Telephone communications are a branch from the PBX in the central laboratory/office building, with a telephone terminal cabinet in this building. Telephone outlets are provided in the electronics room, control room, and offices.

3.1.4 Synchrotron Enclosure

The synchrotron building is located between the synchrotron injection and synchrotron extraction buildings. The building houses the annular synchrotron in a rectangular concrete tube, which is partially buried and partially bermed with earth to provide radiation shielding.

The interior of the enclosure is 9 ft wide by 9 ft high, with curved concrete walls and ceiling 12 in. thick. Walls adjacent to the extraction and injection buildings are straight sections 2.6 ft thick. The enclosure forms an oval, 1210 ft in circumference, measuring 420 ft in the east/west direction and 330 ft in the north/south direction at the beam centerlines.

3.1.4.1 Architecture

The interior of the building is completely open. Entry to the usually uninhabited enclosure is through radiation-proof block doors in the synchrotron injection and synchrotron extraction buildings, and through a maze from the storage ring enclosure. Because strict operational procedures prevent access during operational periods when the doors are closed, no additional emergency exits are provided. The building is clad with membrane waterproofing and completely earth-covered.

To provide a mounting rack for technical equipment, Unistrut channels are cast into the walls and ceilings of the enclosure, as well as the surface on the outside of the enclosure adjacent to usable spaces. The channels (1-5/8 in.) are embedded every 6 ft on center, vertically on the walls and across the width of the enclosure on the ceilings. Conduit, piping, and ductwork in the enclosure are exposed and unpainted. The floors are surface-hardened concrete.

3.1.4.2 Structure

The synchrotron building is constructed of reinforced concrete walls and roof covered by earth berms built up with backfill material, which contributes additional

shielding characteristics. Perimeter drains and membrane waterproofing of the walls and roof are provided to ensure that groundwater does not penetrate the enclosure.

3.1.4.3 Heating, Ventilation, and Air-Conditioning

The synchrotron building is air-conditioned to maintain 75°F ± 2°F year-round as required by the synchrotron equipment. Two 5000 ft^3/min air-conditioning units suspended from the roof truss of the synchrotron injection building supply tempered 100% outside air into the enclosure. Two exhaust fans located at the roof level of the synchrotron extraction building exhaust the air from the enclosure. Twenty fan coil units located throughout the enclosure provide heating, cooling, and dehumidification. No humidification is provided.

Chilled water and steam are supplied from a connection through the control tunnel to the utility loop above the storage ring. A DDC in this building controls the HVAC equipment.

3.1.4.4 Process Piping/Fire Protection

A process piping system supplies compressed air and process water (90° F) as required for specific equipment and functions. A wet-pipe automatic sprinkler system is installed throughout for fire protection. Hand-operated fire extinguishers are located at intervals around the ring as required. The alarm system is annunciated at the Argonne fire station and at the APS security point in the main control room.

3.1.4.5 Electrical Power

Electrical power is distributed to the synchrotron building at 480Y/277 V from a substation located in the synchrotron injection building.

An equipment grounding system is provided from connections on each piece of equipment to ground conductors running with all power feeders. From the main building switchboard ground bus, a copper cable is connected to the building water main. In addition, all computer and related equipment is provided with a separate quiet grounding system that is isolated from the other grounding systems and is connected to a separate counterpoise and ground rod system.

The synchrotron building is lighted by 2-lamp, 4-ft, wall-mounted, fluorescent fixtures mounted on 8-ft centers on both sides of the enclosure, and is switched from the lighting panels.

Duplex receptacles are mounted on 50-ft centers, 3 ft above the finished floor on both walls of the enclosure. A series of 480-V, 60-A welding outlets are provided on the outer perimeter wall at 100-ft centers. Smoke detectors are installed throughout the

building and in the HVAC system. The alarm system is annunciated at the Argonne fire station and at the APS security point in the main control room.

3.1.5 Synchrotron Extraction Building

The synchrotron extraction building connects the synchrotron building to the storage ring within the experiment hall, housing the beam transfer area where a positron beam is extracted from the synchrotron for injection into the storage ring. The building also houses the synchrotron connections for rf power, which is supplied through the control tunnel from the klystron in the synchrotron injection building.

The building is constructed as an adjoining structure against the inner perimeter of the Experiment Hall. A plan and sections of the synchrotron extraction building are shown on Fig. IV.3.1-4. This building is 49 ft by 132 ft, for a footprint of 6470 ft^2. The gross floor area of 7060 ft^2 includes 590 ft^2 at the bridge level, which connects the control tunnel to the top of the storage ring enclosure.

3.1.5.1 Architecture

The interior of the building is open except for the portion of the synchrotron enclosure that passes through the building, the shielded beam transfer area, and the stairway, elevator, toilet, and electronics room at the center of the south wall.

The building is entered from the control tunnel, through a block door from the synchrotron enclosure, or from the top of the storage ring enclosure. Emergency exits are provided along the exterior wall. Access between the three floor levels is provided by a stairway and an elevator located at the southern edge of the building. Partitions are of concrete masonry construction with a painted finish.

Conduit, piping, ductwork, and the exposed underside of roof deck in the open areas are unpainted. In the electronics room, acoustical tile ceilings with recessed lighting and HVAC diffusers are suspended from the structure, concealing electrical and mechanical distribution systems in the ceiling space. The floors are generally exposed, surface-hardened concrete, except the floors in the electronics room, which are covered with vinyl tile. No furnishings are provided for this building.

The windowless exterior of the building is clad with 4-in.-thick insulated metal panels supported on horizontal girts. The roof of the building is protected by a single-ply roofing membrane, board insulation, and ballast in an inverted (IRMA) system conforming to Argonne's current standard.

Unistrut channels are cast into the exposed walls of the beam transfer area and synchrotron enclosures. The channels (1-5/8 in.) are embedded vertically 6 ft on center to form a mounting rack for technical equipment.

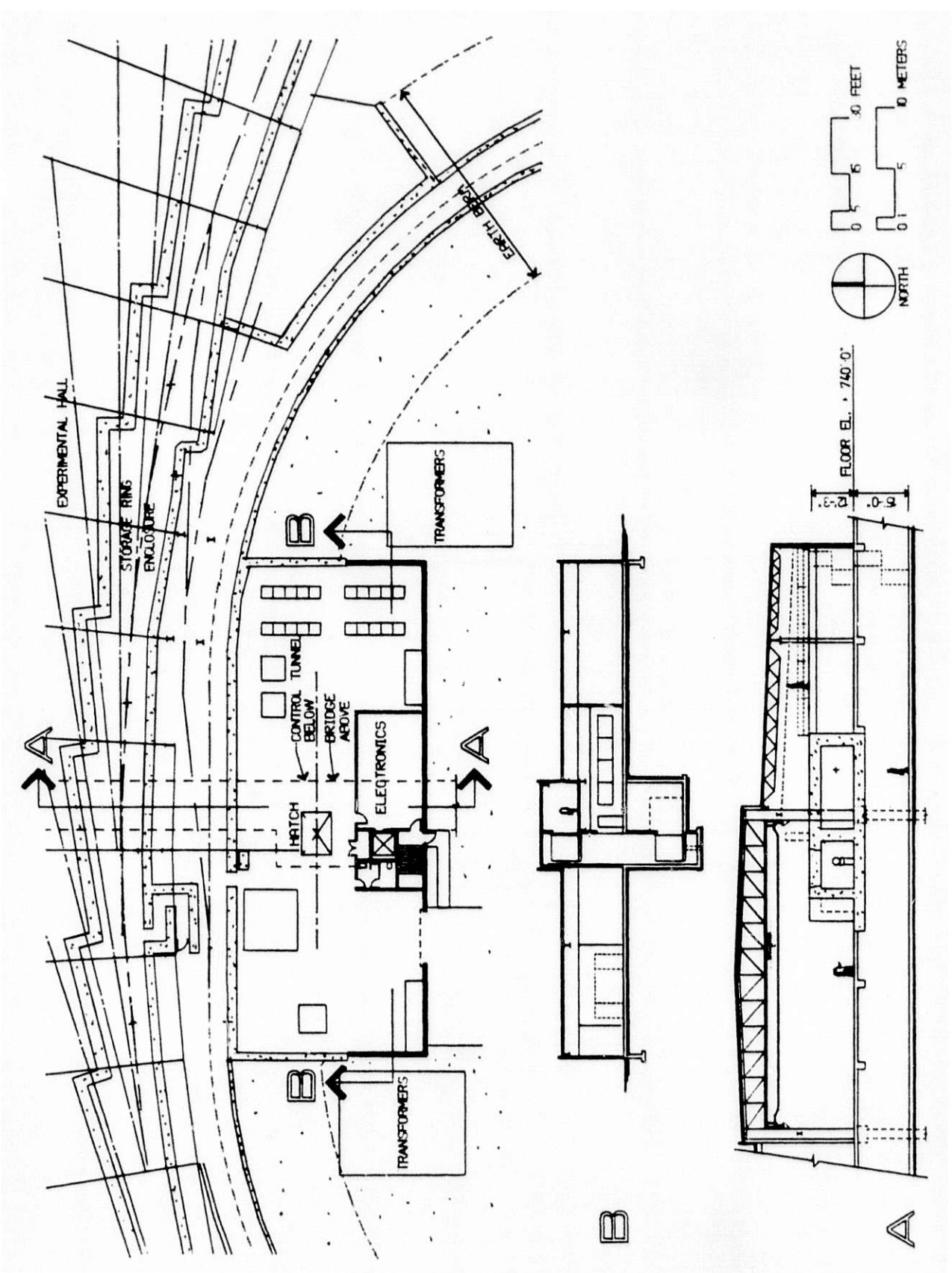

Figure IV.3.1-4
Synchrotron extraction building.

3.1.5.2 Structure

The synchrotron extraction building structure consists of a long span joist, girder, and column system supporting a welded metal deck roof. The north side of the building is directly supported by the experiment hall column system. Structural steel bracing in the exterior walls provides lateral resistance. Foundations under the extraction building columns are on spread footings. A 6-in. slab on grade of reinforced concrete construction is placed over 6 in. of compacted granular backfill. A monorail-type crane/hoist enables heavy equipment transfer from the control tunnel via a floor hatch.

3.1.5.3 Heating, Ventilation, and Air-Conditioning

This building, although not generally air-conditioned, is ventilated with outside air to limit the maximum space temperature to 10°F above the outside ambient temperature in summer, using two 10,000-ft^3/min supply fans with steam coils and four exhaust fans. In winter, four unit heaters with steam coils operate to maintain the space temperature above 60°F when process equipment is not operating. No space humidification is provided.

The electronics room is air-conditioned by a 10-ton packaged unit located above this room to maintain a space temperature of 75° F ± 2° F and space humidity of 45% ± 10% RH year-round. Chilled water and steam are supplied from a connection through the control tunnel to the utility loop above the storage ring. A DDC in this building controls the HVAC equipment.

3.1.5.4 Plumbing/Process Piping/Fire Protection

Plumbing systems for the synchrotron extraction building consist of sanitary facilities with plumbing fixtures, domestic hot and cold water, and sanitary waste and vent systems. Process piping supplies compressed air and process water (90° F) as required for specific equipment and functions. A drainage system, for maintenance of specific equipment, is connected to the sanitary sewer or the laboratory waste sewer as required. A wet-pipe automatic sprinkler system is provided throughout, and hand-operated fire extinguishers are located as required.

3.1.5.5 Electrical Power

Electrical power is distributed to the synchrotron extraction building at 480Y/277 V from a substation located in the synchrotron injection building. An equipment grounding system is provided from connections on each piece of equipment to grounding conductors running with all power feeders. Lightning protection is provided by copper rods mounted around the perimeter of the roof. These rods are connected by copper cables Cadwelded to the building structural steel. A building ground system uses

bare copper cable Cadwelded to the building structural steel, which is connected to ground rods spaced around the building. In addition, all computer and related equipment is provided with a separate quiet grounding system that is isolated from the other grounding systems and is connected to a separate counterpoise and ground rod system.

The building is lighted by high-bay, high-pressure sodium fixtures for an average of 30 footcandles of illumination, switched from the lighting panel. Two-ft by four-ft lay-in fluorescent fixtures, wall-switched in two levels, light the electronics room.

The fire alarm system consists of manual pull stations located at the building exits, and flow and tamper switches in the sprinkler system. Smoke detectors are installed throughout the building and in the HVAC system. The alarm system is annunciated at the Argonne fire station and at the APS security point in the main control room.

Cabling from the PBX in the central laboratory/office building is run to a telephone terminal cabinet in this building, and telephone outlets are provided in the electronics room.

3.1.6 Storage Ring Enclosure

The normally uninhabited storage ring enclosure is located inside the inner perimeter wall of the experiment hall. The concrete tunnel-like enclosure, which is 3478 ft (1060 m) long, houses the storage ring technical components. The primary purpose of the enclosure is to provide radiation shielding with its use of 2.6-ft-thick (0.8-m-thick) walls and a 3.25-ft-thick (1.0-m-thick) roof. The enclosure is basically circular in plan, although the outer perimeter wall is composed of numerous "L"-shaped sections resulting in a ratchet-like configuration, as illustrated on Fig. IV.3.1-5. The size and spacing of the sections are determined by the exit points of the photon beam lines. The resulting interior cross section of the enclosure varies from 11.6 ft to 18.9 ft wide, at a constant ceiling height of 9 ft clear inside. A detailed cross section through the enclosure is shown in Figure IV.3.1-6.

3.1.6.1 Architecture

The interior of the storage ring enclosure is open, with no intervening partitions. Entry from the experiment floor side is provided by any one of three concrete mazes located near the injection and two rf regions, and by any one of 32 6.5-ft-long by 6.5-ft-high movable concrete doors that are located adjacent to each bending magnet beam line enclosure exit point. Entry from the infield side is provided by any one of four concrete mazes located, one each, in the two rf/power buildings, the synchrotron injection building, and at the south end of the ring. Electronic and procedural controls ensure that alternate exit routes are available when the enclosure is open, and that no personnel are inside when the enclosure is sealed for normal operation.

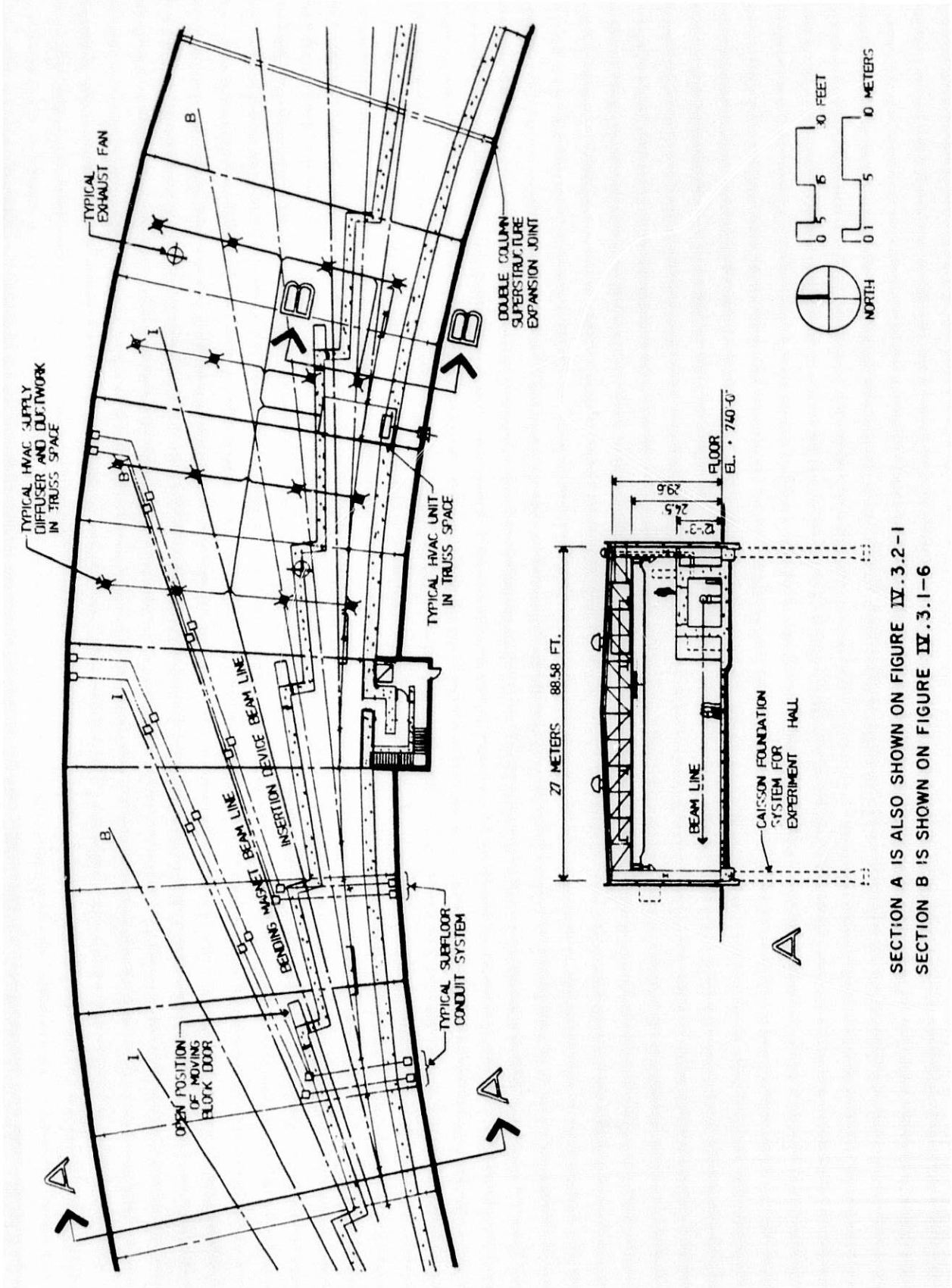

Figure IV.3.1-5
Experiment hall segment.

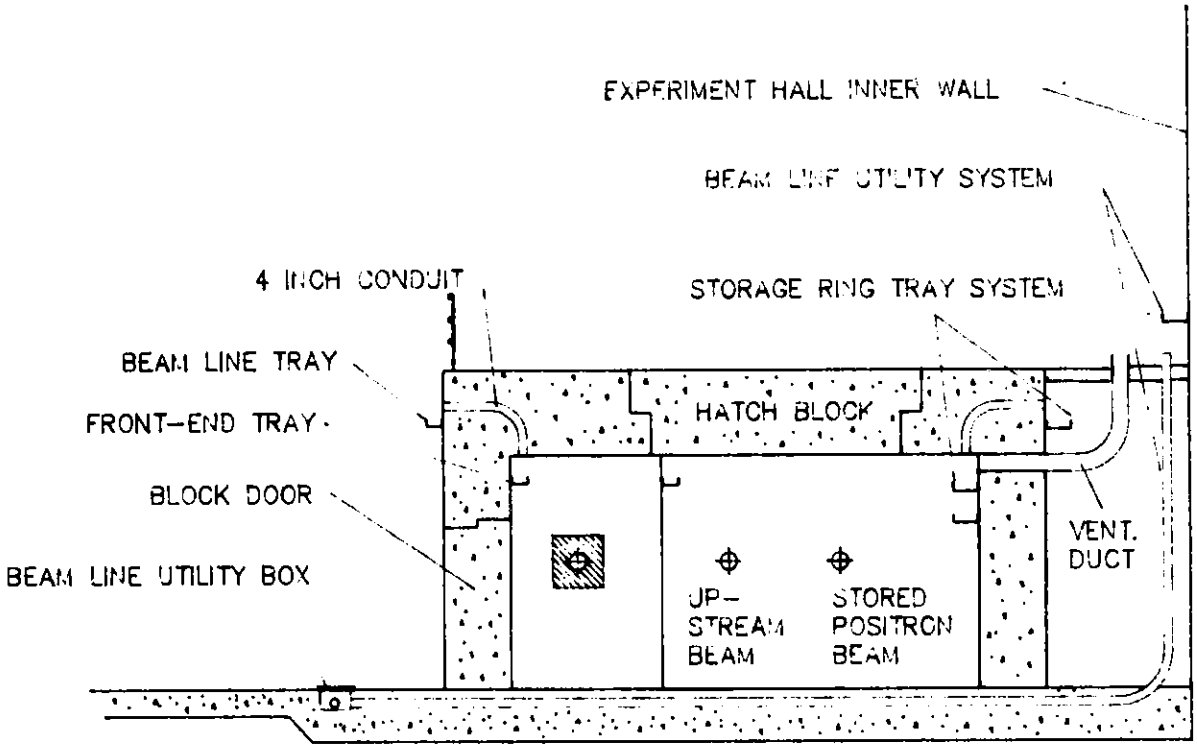

(SECTION B FROM FIGURE IV.3.1-5)

Figure IV.3.1-6
Cross section through storage ring enclosure.

Access between the roof of the enclosure and the main experiment floor level is provided by permanent stairways to the experiment floor near the rf/power and synchrotron injection buildings and to the infield area at the maze locations. In addition, an equipment lift is provided at each of the infield mazes, except in the synchrotron injection building, where an elevator to the main floor and control tunnel is available.

The storage ring technical component may be accessed by 40 large openings in the roof of the enclosure, one above each straight section. During beam operation, these openings are sealed by 3.25-ft-thick (1-m-thick) shielding cover blocks, which are removed and replaced as required using the experiment hall radial bridge crane.

Conduit, piping, and ductwork within the enclosure are exposed and unpainted. Unistrut channels are embedded into the concrete walls and ceiling at 6-ft intervals to provide support for the extensive utility loops that are needed. The same channel spacing is used on the outside of the outer perimeter wall of the enclosure, where it forms the ratchet wall of the experiment floor area. The interior floor and the technical equipment area atop the shield both have a surface-hardened finish.

3.1.6.2 Structure

The storage ring enclosure is constructed of walls 2.6 ft thick and a roof 3.25 ft thick, both of reinforced concrete construction. A 2-ft-thick reinforced concrete slab is set on 6 in. of compacted granular backfill. The base slab of the beam enclosure is separated from the experiment hall structure by expansion joints. Reinforced concrete cover blocks that provide roof access openings of the beam enclosure are 3.25 ft thick, 8.2 ft wide, and 32.8 ft long. Steel framing along the block edges maintain true linear alignment, and inserts on top of the blocks facilitate removal and placement of the blocks by the overhead crane.

3.1.6.3 Heating, Ventilation, and Air-Conditioning

The storage ring enclosure is air-conditioned to maintain a space temperature of $75^{\circ}F \pm 2^{\circ}F$ year-round. Twenty fan coil units located throughout the enclosure provide cooling to maintain the space temperature. Slots in the wall near the roof of the enclosure allow ventilation air to flow from the experiment hall into the enclosure, and thirty 3,600-ft^3/min exhaust fans located on the roof of the experiment hall exhaust air from various points in the storage ring enclosure. These units operate continuously on low speed, but are switched to high-speed operation to function as smoke-purge units if smoke is detected in the enclosure. No space humidification is provided. Chilled water and steam are supplied from a connection to the utility loop above the storage ring. A DDC in this building controls the HVAC equipment.

3.1.6.4 Process Piping/Fire Protection

A process piping system supplies compressed air as required for specific equipment and functions. A wet-pipe automatic sprinkler system is installed throughout for fire protection. Hand-operated extinguishers are located as required. The alarm system is annunciated at the Argonne fire station and at the APS security point in the main control room.

3.1.6.5 Electrical Power

An equipment grounding system is provided from connections on each piece of equipment to ground conductors running with all power feeders. From the main building switchboard ground bus, a copper cable is connected to the building water main. In addition, all computer and related equipment is provided with a separate quiet grounding system that is isolated from the other grounding systems and is connected to a separate counterpoise and ground rod system.

The storage ring is lighted by 2-lamp, 4-ft, wall-mounted, fluorescent fixtures mounted on 8-ft centers on both sides of the enclosure, and is switched from the lighting panels.

Duplex receptacles are mounted on 50-ft centers, 3 ft above the finished floor on both perimeter walls of the ring. Smoke detectors are installed throughout the enclosure and in the HVAC system. The alarm system is annunciated at the Argonne fire station and at the APS security point in the main control room.

Telephone outlets are provided at 20 locations within the storage ring enclosure and at 20 locations atop the enclosure, all distributed uniformly around the ring.

3.1.7 RF/Power Buildings (East and West)

The two rf/power buildings are each connected to the inner perimeter walls of both the storage ring enclosure and the experiment hall, directly across the infield from each other at the "four o'clock" and "ten o'clock" positions, "twelve o'clock" being due north. These buildings house the rf klystrons for the storage ring and emergency power generators for the entire facility. In addition, one of the rf/power buildings houses the dipole magnet power supply for the storage ring. Each provides a maze access point into the storage ring enclosure from the inner perimeter side.

Each one-story rectangular building is 90 ft by 120 ft with a footprint and gross floor area of 10,800 ft^2, of which 600 ft^2 is devoted to the enclosed electronics area and sanitary facilities. A plan and a section through a typical rf/power building are illustrated on Fig. IV.3.1-7.

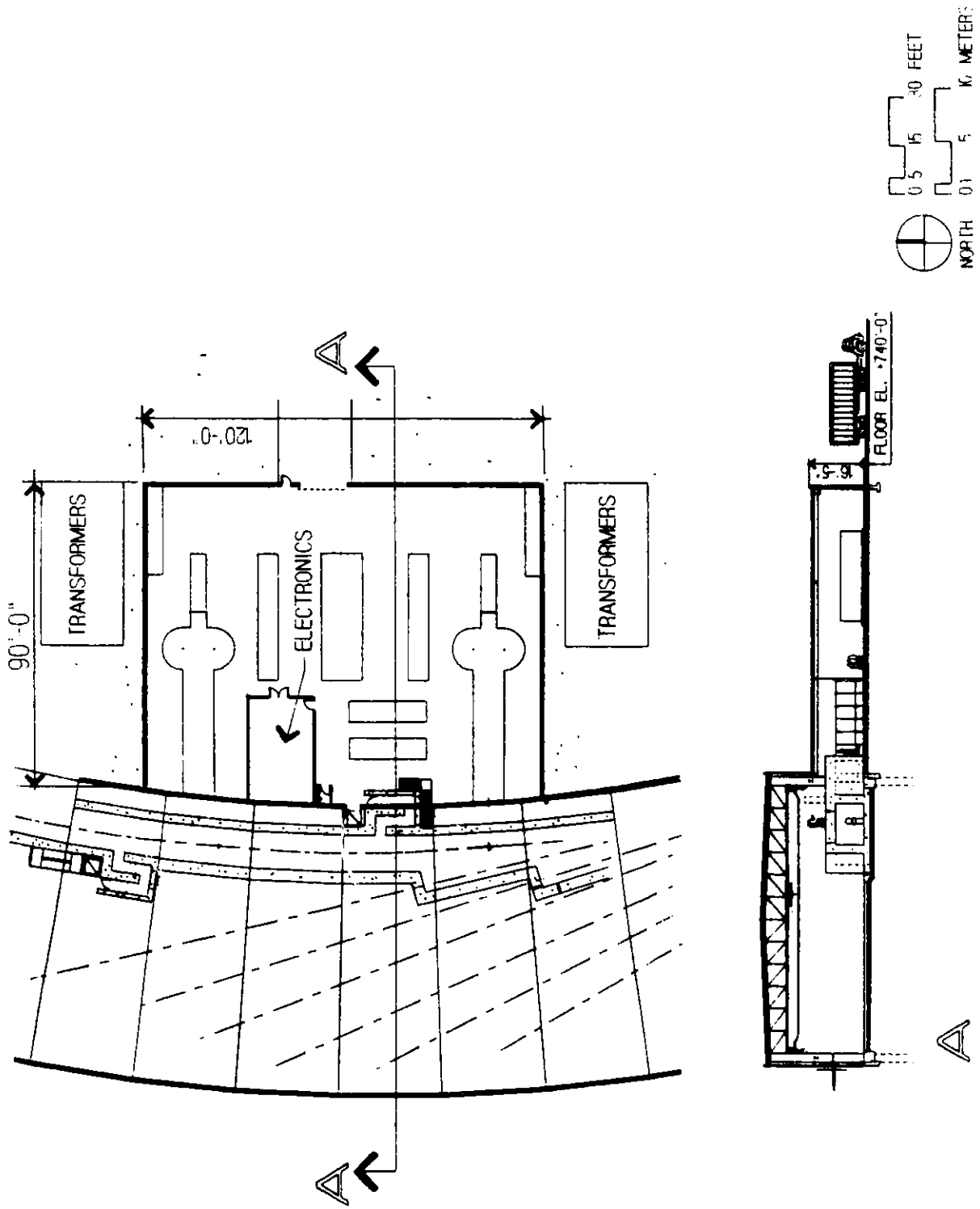

Figure IV.3.1-7
Typical rf building.

3.1.7.1 Architecture

The interior of each building is open, with the exception of an enclosed, air-conditioned electronics room and a toilet room located near the center of the building against the wall of the experiment hall. Entry to each building is through an exterior door from the infield area, through a maze from the storage ring enclosure, or from the top of the storage ring enclosure via a stairway and an equipment lift adjacent to the storage ring maze access point.

All partitions are of metal stud and gypsum board construction with a painted finish. In the electronics room, conduit, piping, ductwork, and the exposed underside of roof deck are unpainted. In the control room, acoustical tile ceilings with recessed lighting and HVAC diffusers are suspended from the structure, concealing the electrical and mechanical distribution systems in the ceiling space. The floors are generally exposed, surface-hardened concrete, except the floors in the electronics room, which are covered with vinyl tile. No furnishings are provided for this building.

Except for the wall shared with the experiment hall, the windowless exterior of the building is clad with 4-in. insulated metal panels hung on horizontal girts. The roof of the building is protected by a single-ply roofing membrane, board insulation, and ballast in an inverted (IRMA) system conforming to Argonne's current site standard.

Furnishings provided include desks, chairs, bookcases, and filing cabinets in the electronics room.

3.1.7.2 Structure

Each building has a long span joist, girder, and column system supporting a welded metal deck roof. One side of each building is directly supported on the experiment hall columns, and structural steel bracing in the exterior walls provides resistance against lateral forces. Foundations under the building columns are on spread footings. A 6-in. slab-on-grade of reinforced concrete construction is set over 6 in. of compacted granular backfill.

3.1.7.3 Heating, Ventilation, and Air Conditioning

Each of these buildings is ventilated with outside air in summer to limit the maximum space temperature to 20°F above the ambient in high-heat-generating areas, and to 10°F above the ambient in low-heat-generating areas. Two 15,000-ft^3/min supply fans with steam coils and four 7,500-ft^3/min exhaust fans are provided. In winter, six unit heaters with steam coils operate to maintain the space temperature above 60°F when process equipment is not operating. No space humidification is provided.

The electronics room in each rf/power building is air-conditioned by a 10-ton packaged unit located above this room to maintain a space temperature of 75°F ± 2°F

and space humidity of 45% year-round. Chilled water and steam are supplied from a connection to the utility loop above the storage ring. A DDC in this building controls the HVAC equipment.

3.1.7.4 Plumbing/Process Piping/Fire Protection

Plumbing systems for the rf/power buildings consist of sanitary facilities with plumbing fixtures, domestic hot and cold water, and sanitary waste and vent systems. Process piping supplies compressed air and process water (90°F) as required for specific equipment and functions. A drainage system is provided for maintenance of specific equipment and is connected to the sanitary sewer or the laboratory waste sewer, as required. Fire protection consists of wet-pipe automatic sprinkler systems for each building and hand-operated fire extinguishers located as required.

3.1.7.5 Electrical Power

Electrical power is delivered to the rf/power buildings from the 13.2-kV switchboard in the utility building via a 15-kV loop feeder to two 13.2-kV to 2400V pad-mounted power transformers at each building. In the rf/power building containing the power supply for the storage ring dipole magnets, one of the transformers is rated at 3750 kVA, and one is 2500 kVA. The other building houses two 2500-kVA transformers. Power at 480Y/277 V is furnished from a dry-type transformer fed from one of the 2400V transformers. A 400-kVA diesel-driven standby generator is located in each building to run selected equipment in the event of the loss of electric power.

An equipment grounding system is provided from connections on each piece of equipment to grounding conductors running with all power feeders. Lightning protection is provided by copper rods mounted around the perimeter of the roof. These rods are connected by copper cables Cadwelded to the building structural steel. A building ground system uses bare copper cable Cadwelded to the building structural steel, which is connected to ground rods spaced around the building. In addition, all computer and related equipment is provided with a separate quiet grounding system that is isolated from the other grounding systems and is connected to a separate counterpoise and ground rod system.

Both buildings are lighted by high-bay, high-pressure sodium fixtures for an average of 30 footcandles of illumination, switched from the lighting panel. Lighting for the electronics and toilet rooms is provided by 2-ft by 4-ft lay-in fluorescent fixtures.

The fire alarm system consists of manual pull stations located at the building exits, flow and tamper switches in the sprinkler system, and smoke detectors in the HVAC system. Smoke detectors are installed throughout the building and in the HVAC system. The alarm system is annunciated at the Argonne fire station and at the APS security point in the main control room. The telephone system is a branch of the PBX

from the central laboratory/office building, with a telephone terminal cabinet provided in each building. A telephone outlet is installed in the electronics room.

3.2 Experiment Support

3.2.1 Introduction

This section describes the buildings and facilities which support the experimental program and the general administration of the Advanced Photon Source. The most prominent feature is the experiment hall and this structure determines the geometry and placement of most other buildings. Because of the large size of this building and the fact that it has a controlled environment, its size was the subject of much optimization effort. The radial width is determined by the storage ring cross section and shield wall thickness plus the floor area needed for photon beam lines. The maximum beam line length accommodated within the building is 80 m measured from the radiation source point. The addition of a 3-m equipment circle and a 1.5-m outer aisle space results in a building width of 27 m. The height of the building is determined by the necessary roof truss depth, crane depths, and the hook clearance of 21 ft (6.4 m). The hook clearance will allow 10-foot-high structures to be moved over each other. The crane clearance over the storage ring roof is 8.75 ft and is sufficient for equipment racks and the removal of the 1-m thick roof access-hatch blocks. The resulting building height is 32 ft (9.75 m).

Hatches with overlapping concrete cover blocks are provided in the storage ring tunnel roof at each insertion device location (including the injection and rf areas) to facilitate the installation of machine, insertion device (ID), and beam line front-end components. The clear opening provided is 10 m by 2.5 m.

The length of beam line occurring outside the shield wall is determined by the lattice geometry, the shield wall thickness, and the beam-centerline-to-wall clearances. For a front-end-to-wall clearance of 0.8 m, a shield wall thickness of 0.8 m, and an exit clearance of 0.2 m, the resulting ID beam line length inside the shield is 29 m. For a bending-magnet beam line, this length is 27 m. The resulting beam line length available outside the shield is 50 m for the ID beam and 52 m for the bending-magnet beam (see Fig. III.1.2-1).

Access to the beam line front-ends is provided by three maze entrances located near the injection and rf straight sections and by 32 movable block doors located at each bending magnet front-end. Stairway access to the ring roof is provided at each maze and ladder access at each block door.

Utility distribution to the beam line front-end within the ring shield is from distribution centers located above the ring shield along the inner wall of the experiment hall. Utility distribution to the floor portion of the beam line is from these same distribution centers via an underfloor conduit system parallel to each beam line. Cooling

water is routed through a dedicated conduit for use along the beam line. All conduits extend to the building outer wall, to provide the capability of distributing computer network, communication, and special purpose wiring.

The four laboratory/office modules provide clean rooms, laboratories, offices, and meeting rooms in close proximity to the experimental stations. A floor-level truck air lock and entrance is provided at each module, to facilitate delivery and crane access for large equipment, while maintaining the building temperature and cleanliness.

The central laboratory/office building houses the administrative staff of the APS, operations and control staff, user liaison staff, Argonne-based research and development staff, central clean room, and shop facilities. It will also act as the central interaction point for all research activities. As such, this building has been given considerable design effort and some amenities and appearance features which will help define its role as the "front door" of the project. At the same time, construction efficiency and expandablity have been built in, to allow nearly all of the building functions to be expanded in the future.

The support wing of this building, comprising the high-bay area, shops, stockroom, clean rooms, and large assembly laboratories, will be constructed initially, and will be used during technical component construction and assembly. The office wing, comprising the control and computer rooms, the lab and office sections, and the auditorium will be constructed later. The office wing contains space for a library and conference rooms for project activities. The clean room facilities can accommodate the long vacuum chamber sections common to the storage ring and insertion devices. Both Class 100 and Class 1000 clean rooms are provided. These are connected with air locks.

The control room and the data analysis computer facilities are located in this building. High-performance computer networks link the data analysis computer system to the laboratory/office modules and beam lines. The data network can be extended to the proposed user housing facility, allowing high-performance terminal or workstation interaction with experimental equipment.

3.2.2 Experiment Hall

The single-story experiment hall is an annular structure housing both the storage ring enclosure and the experiment floor, where the experiments are conducted.

The building is 91 ft wide by 3472 ft (1060 m) in circumference at the storage ring centerline, for a gross area of 334,836 ft^2. Of that total, 72,000 ft^2 is occupied by the storage ring enclosure, 19,200 ft^2 is reserved for the utility corridor between the inner perimeter wall and the storage ring enclosure, and 243,636 ft^2 is available for experiments. The clear height from the experiment floor to the underside of the trusses is 24.5 feet. Refer to Fig. VI.3.1-4, Experiment Hall Segment and Fig. IV.3.2-1, the Experiment Hall Cross Section.

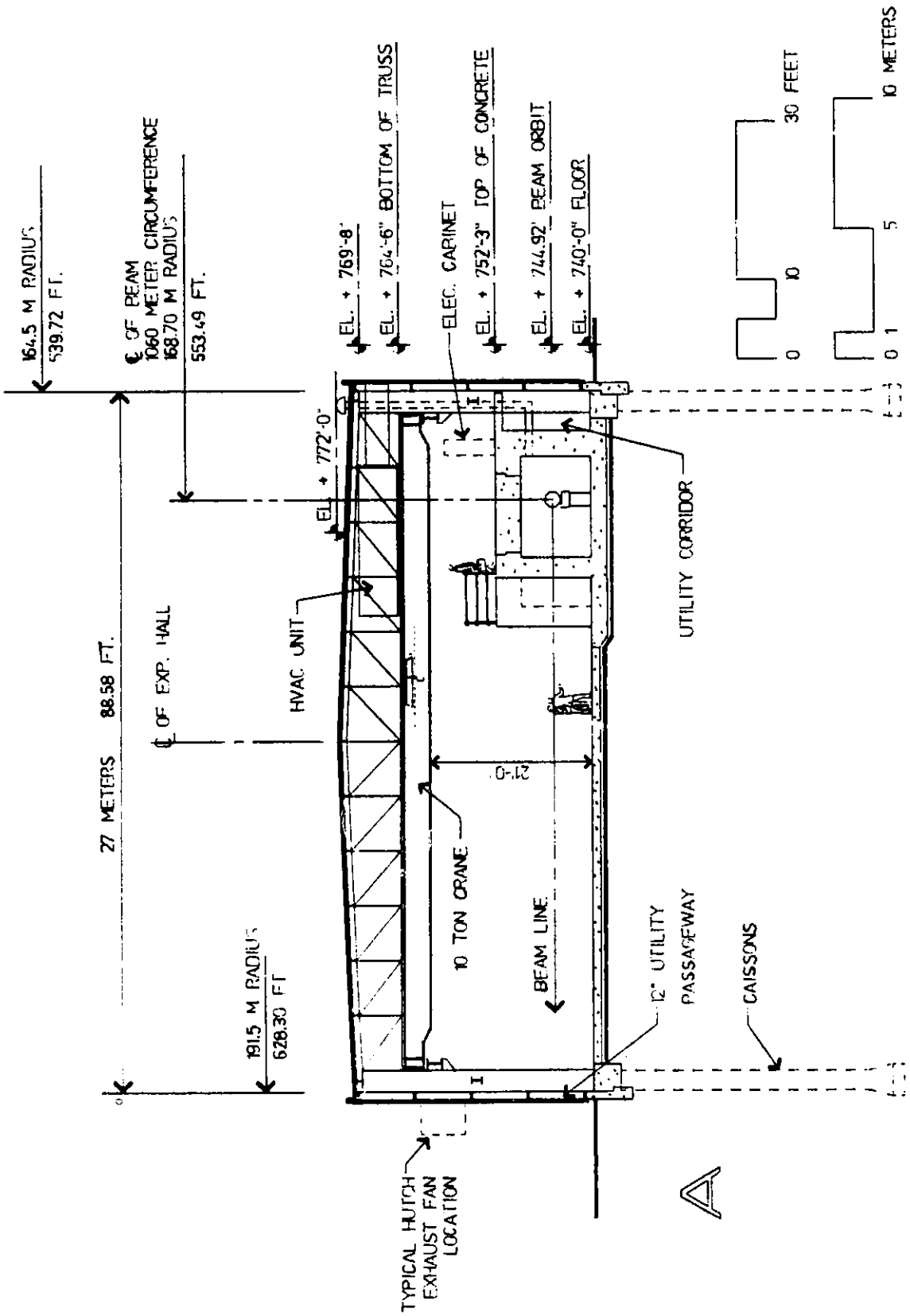
164.5 M RADIUS
539.72 FT.
℄ OF BEAM
1060 METER CIRCUMFERENCE
168.70 M RADIUS
553.49 FT.
EL. + 769'-8"
EL. + 764'-6" BOTTOM OF TRUSS
ELEC. CABINET
EL. + 752'-3" TOP OF CONCRETE
EL. + 744.92' BEAM ORBIT
EL. + 740'-0" FLOOR
30 FEET
10 METERS
0
10
5
0 1
EL. + 772'-0"
UTILITY CORRIDOR
℄ OF EXP. HALL
HVAC UNIT
27 METERS 88.58 FT.
21'-0"
10 TON CRANE
BEAM LINE
12" UTILITY
PASSAGEWAY
CAISSONS
191.5 M RADIUS
628.30 FT
TYPICAL HUTCH
EXHAUST FAN
LOCATION

A system of underfloor conduits with access boxes on 33-ft centers provides a means of supplying process or chilled water, electrical power, telephone, and computer services to the beam line experiments. These conduits parallel every experiment beam line tangentially across the experiment hall.

3.2.2.1 Architecture

Except for the enclosed areas around the storage ring and the utility corridor at the inner perimeter, the experiment floor is a continuous open space.

Primary entry to the building is from the laboratory/office modules and the central laboratory/office building. Secondary entries are from the rf/power buildings, the synchrotron extraction building, and the maze entry at the south end of the infield. Emergency exits are provided at the outer perimeter end of every insertion device beam line position. Passage between the experiment floor and the top of the storage ring enclosure is provided by permanent stairways near the rf/power and synchrotron extraction buildings. Access to the interior of the storage ring enclosure is provided by hydraulically-movable block doors, 6.5 ft high, 6.5 ft wide, and 2.6 ft thick, adjacent to each bending magnet beam line front-end.

Conduit, piping, ductwork and the exposed underside of the roof deck are unpainted. The floors are exposed, surface-hardened concrete. Two radial 10-ton bridge cranes run on concentric tracks around the building to provide full crane coverage for the placement of experiment equipment and for the moving of shielding blocks on top of the storage ring enclosure. No furnishings are provided in the experiment hall.

The windowless exterior of the building is clad with 4-in. insulated metal panels supported on 12-in.-wide horizontal girts. The roof of the building is protected by a single-ply roofing membrane, board insulation, and ballast in an IRMA system conforming to Argonne's current standard.

3.2.2.2 Structure

Trusses spanning 83 ft carry purlins and a welded metal deck. The trusses are spaced 30.5 ft on centers at the building center line, and frame into 33-in.-deep, wide-flange perimeter columns, to create a column-free interior in this annular building. A steel beam track directly below the truss system supports two 10-ton cranes, which span the experiment hall area. The trusses are arrayed in a radial configuration; purlins, girts, truss bracings, crane support beams, and bracing members located in the exterior walls are installed on chords. The building is divided into ten segments, with expansion joints between them. A double set of trusses and columns, supported on single

sets of caissons, occurs at each expansion joint. Reinforced concrete foundation members have the following dimensions:

Component	Dimensions
Caissons	2 ft, 6 in. diameter
Caisson bells	4 ft, 0 in. diameter, 40 ft below finished grade
Caisson caps	4 ft, 6 in. wide x 4 ft, 6 in. high x 2 ft, 6 in. deep
Grade beams	1 ft, 6 in. wide x 4 ft, 0 in. deep
Exp. hall slab	1 ft, 0 in. thick, on 6 in. compacted granular backfill
Storage ring slab	2 ft, 0 in. thick, on 6 in. compacted granular backfill

In both the injector facilities and the storage ring, the guiding and focusing magnets around the beam tube are mounted on pedestals that are approximately four feet high and rest on reinforced concrete slabs. The magnets have adjustment capabilities at the pedestals to correct for vertical and lateral movements due to creep and soil settlements.

In order to minimize vibration transfer by isolating the source from the receiving system, the following provisions are included:

- Expansion joints are provided at the outer edges of the slab-on-grade of the experiment hall and storage ring, separating them from the other foundation members, to minimize vibration transfer from the structure to the machine foundation and experiment hall slab.

- Elastomeric bearing pads are provided beneath the base plates of the columns, to dampen vibrations generated by wind loads on the building exterior, by mechanical equipment supported from the trusses, and by movement of the two column-supported 10-ton cranes.

In order to minimize the vibration induced into the accelerators and storage ring, machinery with moving parts are centrifugal rather than reciprocating, and these machines are installed with proper base isolation devices. To limit the creation of additional cultural vibration, the moving of heavy loads across the building floor during beam line operation is to be avoided.

3.2.2.3 Heating, Ventilation, and Air-Conditioning

The experiment hall is air-conditioned, to maintain the space temperature to 75°F ± 2°F year-round. Relative humidity is 50% maximum in summer and 25% minimum in winter.

Thirty air-conditioning units at 18,000 ft^3/min with chilled water coils, steam coils, and humidifiers are suspended within the roof truss. Air is distributed through

diffusers and ductwork in the truss space. Sixty roof-mounted exhaust fans, each at 9000 ft^3/min, operate when the air-conditioning units are in outside-air mode, and are also used for smoke purge operation when required.

The smoke purge system for the experiment hall has the overall capability of exhausting 1-1/2 cfm/ft^2, and supplying an equivalent amount of outside air. Upon the detection of smoke in a given fire zone, the roof exhaust fans in that fire zone will operate, and the supply air unit will stop. In the adjacent zones, the exhaust fans will not operate, and the supply air units will introduce outside air. Fire department fan override/control panels located at designated entry points control this system.

Provision is made for wall-mounted exhaust fans to serve for experimental-hutch air removal. This provision is made on the outside wall as shown in Fig. IV.3.2-1 (left side) and the fans are installed as needed.

One-megohm deionized chilled water supply and return mains located around the inner perimeter supply cooling to all air-conditioning units. High-pressure steam is reduced in pressure for each air-handling unit, and provides the required heating and steam humidification for winter operation for all air-handling units. Individual direct digital controllers are provided for each air-handling unit in the experiment hall to control the above equipment.

3.2.2.4 Plumbing/Process Piping/Fire Protection

Plumbing systems in the experiment hall are limited to system loops of 4-in. domestic water, 3-in. laboratory service water, and process system loops of 3-in. compressed air and 3-in. natural gas. These loops are routed around the inside of the utility corridor concentric with the storage ring enclosure, with valved service adjacent to the starting point of the underfloor conduit system. Drainage systems include the sanitary waste system with a floor drain located near the center of the building between alternate beam lines.

The 90°F equipment process water cooling loop (one megohm deionized) is located around the inner perimeter above the storage ring. Both the 40°F loop and the 90°F loop contain one valve per bay, at approximately 30-ft intervals around the inner perimeter of the ring. These valves are 2-in. connections to link to the technical component cooling equipment located in the storage ring.

A wet-pipe automatic sprinkler system is provided for fire protection. The experiment hall is divided into ten equal segments, with each segment a complete fire zone with individual water supply, control and drain valves, and alarm functions. Experiment hutches requiring internal fire protection are linked to the experiment hall sprinkler system. Automatic sprinkler systems are based on the requirements of NFPA 13, "Ordinary Hazard - Group 1," with protection provided by 1/2-in.-orifice sprinkler

heads as approved by Factory Mutual for this occupancy. Hand-operated fire extinguishers are distributed in accordance with FM and NFPA requirements.

3.2.2.5 Electrical Power

Electric power is delivered to the experiment hall from the 13.2-kV switchboard in the utility building via 15-kV loop feeders to a total of forty 13.2 kV to 480Y/277 V distribution transformers. Thirty-six of the transformers are rated at 500 kVA, and four are rated at 1000 kVA. The four 1000-kVA units supply power to the laboratory/office modules as well as the experiment hall. The distribution transformers feed motor control centers located on the top of the storage ring enclosure.

An equipment grounding system is provided from connections on each piece of equipment to grounding conductors running with all power feeders. Lightning protection is provided by copper rods mounted around the perimeter of the roof, which are connected by copper cables Cadwelded to the building structural steel. A building ground system uses bare copper cable Cadwelded to the building structural steel, which is connected to ground rods spaced around the building. In addition, all computer and related equipment is provided with a separate quiet grounding system, which is isolated from the other grounding systems and is connected to a separate counterpoise and ground rod system.

The experiment hall is lighted by high-bay, high-pressure sodium fixtures, for an average of 50 footcandles of illumination, switched from the 480Y/277 volt lighting panel. Duplex receptacles are mounted on 50-ft centers, three feet above the finished floor on both perimeter walls. A series of 480-V, 60-A welding outlets are located on 100-ft centers on the inner perimeter.

The fire alarm system consists of manual-pull stations located at the building exits, flow and tamper switches in the sprinkler system. Smoke detectors are installed throughout the building and in the HVAC system. The alarm system is annunciated at the Argonne fire station and at the APS security point in the main control room.

Telephone cabling is run from the PBX in the central laboratory/office building, and ten telephone terminal cabinets are provided along the outer perimeter wall. Two telephone outlets are provided for each beam line.

3.2.3 Laboratory/Office Modules

The four identical laboratory/office module buildings are connected to the outer perimeter wall of the experiment hall, oriented on tangents extended from the storage ring. The modules provide office and lab space for researchers working with beam lines in the experiment hall.

There are twenty offices around the exterior walls, and five laboratories adjacent to the experiment hall in each module. Four of the five laboratories have direct access into the experiment hall. The remaining laboratory is configured as a Class 1000 clean room. Additional facilities in each module include a lounge, toilet and locker areas, corridors and mechanical space, and a truck air lock to facilitate deliveries to the experiment hall. Each of the one-story buildings has a floor area of 13,600 ft^2. A plan and section through a typical module is shown on Fig. IV.3.2-2.

3.2.3.1 Architecture

The interior of each module is organized by an inner service core surrounded by a corridor loop which provides access to laboratories, offices, and entry points. Entry to the building is from the adjacent parking areas or from the interior of the experiment hall. Emergency exits are provided at several locations around the building.

Partitions are of gypsum drywall construction with a painted finish, except in the clean room laboratory, where special wall finishes are required. Acoustical tile ceilings with recessed lighting and HVAC diffusers are suspended from the structure, concealing the electrical and mechanical distribution systems in the ceiling space. A sloped skylight over the corridor outside the windowless labs provides outside awareness in interior spaces. Floors are covered with vinyl tile, except in the mechanical areas and in the truck air lock where the floors are exposed, surface-hardened concrete.

The exterior of the building is clad with 4-in.-thick insulated metal panels. Energy-efficient thermal-break aluminum window frames with one-inch insulating glass form a continuous band around the building exterior, except in the windowless truck dock area, as shown on Fig. IV.3.2-3. The roof of the building is protected by a single-ply roofing membrane, board insulation, and ballast in an IRMA system conforming to the current Argonne site standard.

Furnishings to be provided include desks, chairs, bookcases, and filing cabinets in the offices, and cabinets and counters along the long walls of the laboratories.

3.2.3.2 Structure

Each laboratory/office module consists of a beam, girder, and column system supporting a welded-metal deck roof, with structural steel bracing in the exterior wall for resistance against lateral loads. Foundations are conventional spread footings. The floor is a 6-in. reinforced concrete slab on grade over six inches of compacted granular backfill.

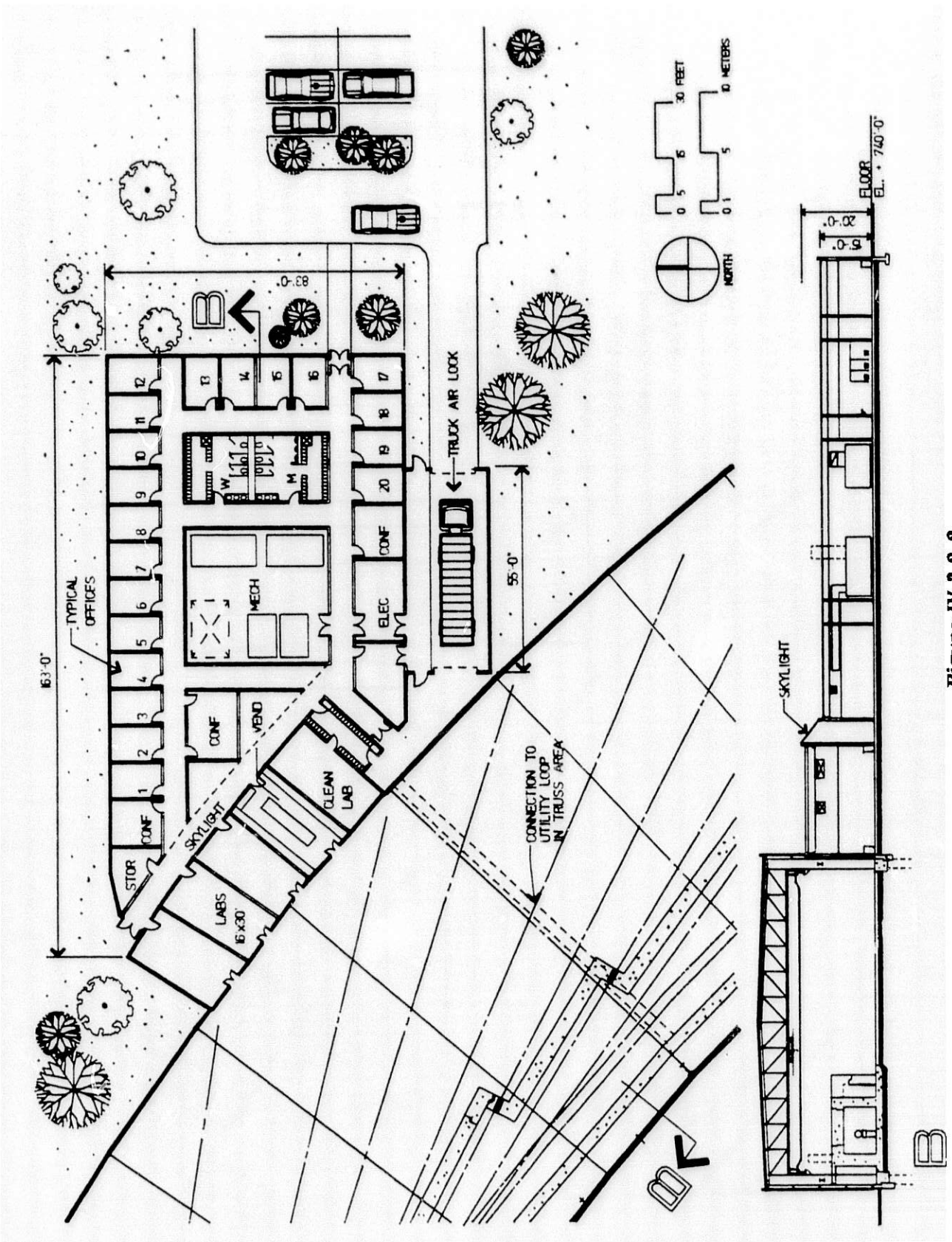

Figure IV.3.2-2
Typical laboratory/office module.

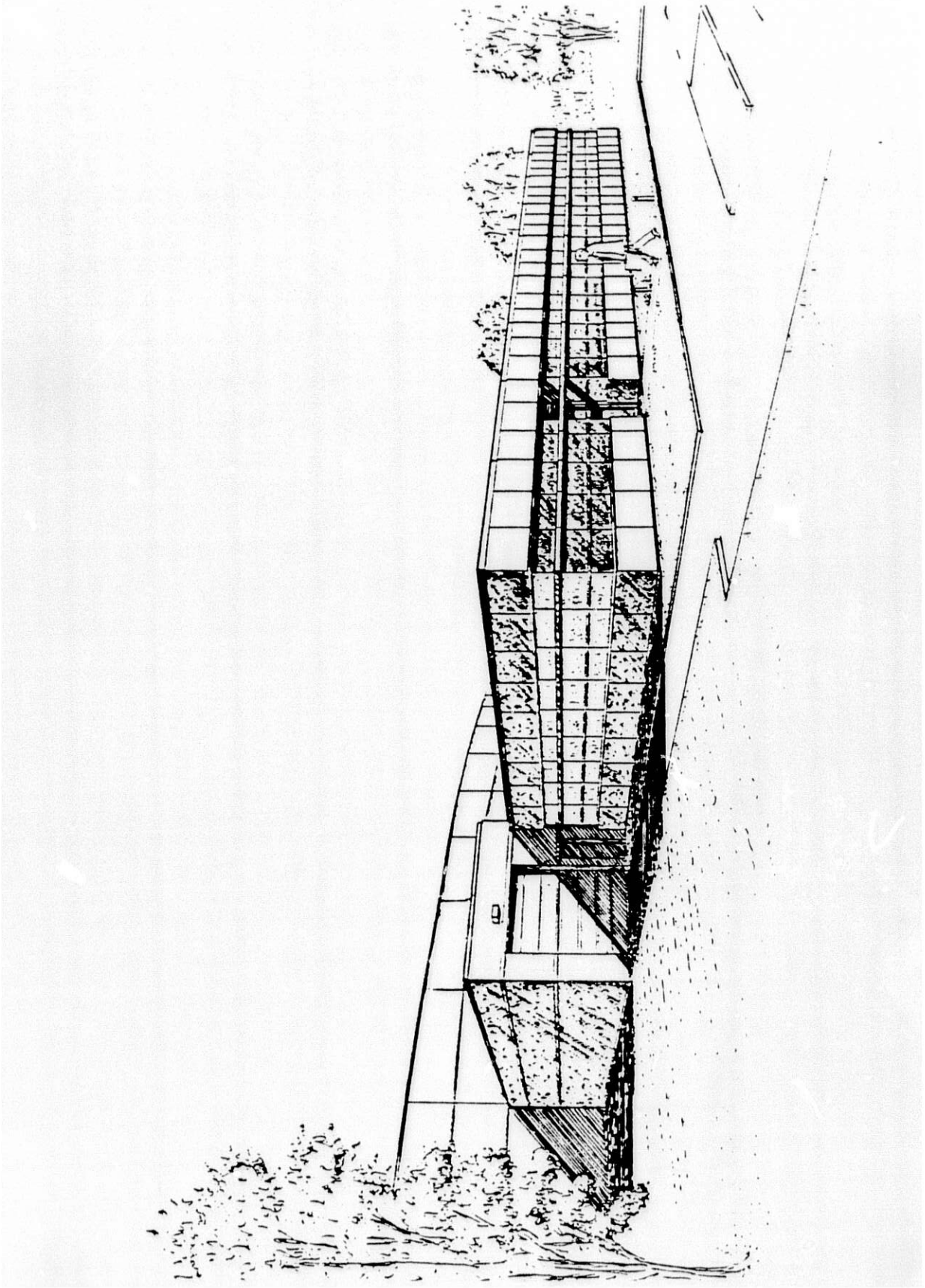

Figure IV.3.2-3
Laboratory/office module eye level perspective.

3.2.3.3 Heating, Ventilation, and Air-Conditioning

The office area of each module will be maintained at a space temperature of 75°F ± 2°F year-round and a relative humidity of 50% maximum in summer and 25% minimum in winter. A variable-volume air-conditioning unit sized at 25 tons, with a return fan, is located in the mechanical equipment room of each module, and each office has a variable-volume terminal box to adjust space temperature to local conditions. A hot-water-baseboard heating system is provided in perimeter offices.

The laboratory area of each module is kept at a space temperature of 75°F ± 2°F year-round and relative humidity of 50% maximum in summer and 25% minimum in winter. A constant-volume ten-ton air-conditioning unit with a return fan located in the mechanical equipment room is provided for air circulation. The temperature in each laboratory is individually controlled with a reheat coil at the supply air duct.

The clean room of each module is designed to meet Class 1000 standards. Equipment for this space maintains a temperature of 72°F ± 1°F and relative humidity of 40% ± 5% year-round. One 6000-cfm air-handling unit (and one standby unit) supply air at a rate of 15 cfm/ft^2 of floor area. Air is returned through an underfloor plenum and vertical air shaft. Makeup air to this air-handling unit is supplied from the laboratory air-conditioning unit, to provide space dehumidification and pressurization.

Hot water is converted from steam in the mechanical room. Chilled water and steam are supplied from a connection to the utility loop above the storage ring. A direct digital controller in this building controls the HVAC equipment.

3.2.3.4 Plumbing/Process Piping/Fire Protection

Complete independent plumbing systems provided for the laboratory/office modules consist of plumbing fixtures, water-heating equipment, domestic cold and hot water distribution, sanitary and laboratory waste collection, and vent piping systems in accordance with Argonne standards. Laboratory/office modules receive individually valved domestic cold water and laboratory service water from the distribution loops in the experiment hall. Process piping systems for the laboratory/office modules distribute natural gas and compressed air to each laboratory space.

A wet-pipe automatic sprinkler system is installed throughout. Hand-operated fire extinguishers are located in accordance with FM and NFPA requirements.

3.2.3.5 Electrical Power

Electric power is furnished to the laboratory/office modules from the experiment hall load centers, located atop the storage ring enclosure, at 480Y/277 volts.

An equipment grounding system is provided from connections with each piece of equipment to grounding conductors running with all power feeders. Lightning protection is provided by copper rods mounted around the perimeter of the roof, which are connected by copper cables Cadwelded to the building structural steel. A building ground system uses bare copper cable Cadwelded to the building structural steel, which is connected to ground rods spaced around the building. In addition, all computer and computer-related equipment is provided with a separate quiet-grounding system, which is isolated from the other grounding systems and is connected to a separate counterpoise and ground-rod system.

Lighting fixtures for offices, laboratories, and other finished areas are 2-ft by 4-ft lay-in troffers with parabolic lenses and two, three, or four fluorescent lamps as required to obtain the desired illumination levels. Three- and four-lamp fixtures are wired for two-level switching. In mechanical equipment rooms and other nonfinished areas, two-lamp fluorescent fixtures are panel-switched.

The fire alarm system consists of manual pull stations located at the building exits, flow and tamper switches in the sprinkler system, and smoke detectors installed throughout the building and in the HVAC system. The alarm system is annunciated at the Argonne fire station and at the APS security point in the main control room.

Telephone cabling is run from the PBX room in the central laboratory/office building to a telephone terminal cabinet in each laboratory/office module. Telephone outlets are provided in all offices, laboratories, conference rooms, and other finished areas.

3.2.4 Central Laboratory/Office Building — Support Wing

As shown in a perspective view from the southeast on Fig. IV.3.2-4, the support wing of the central laboratory/office building is located between the office wing of the same building and the north end of the experiment hall. The support wing houses the large-equipment assembly areas, oversize laboratories, clean rooms, and machine shops. It is of special importance during the machine assembly period as the technical components are prepared for installation.

As shown in the floor plan on Fig. IV.3.2-5, the building includes an 80-ft by 156-ft high-bay assembly area with full bridge-crane coverage, delivery truck air lock, Class-100 and Class-1000 clean rooms, eleven oversize laboratories, machine shops, offices, employee break areas, and an observation area for visitors.

The basically rectangular one-story support wing has a footprint of 41,455 ft^2 and a gross floor area of 52,727 ft^2, including a 11,272 ft^2 mechanical room above the clean room and lab areas along the east side of the building. The high-bay assembly area has a clear height of 27 ft.

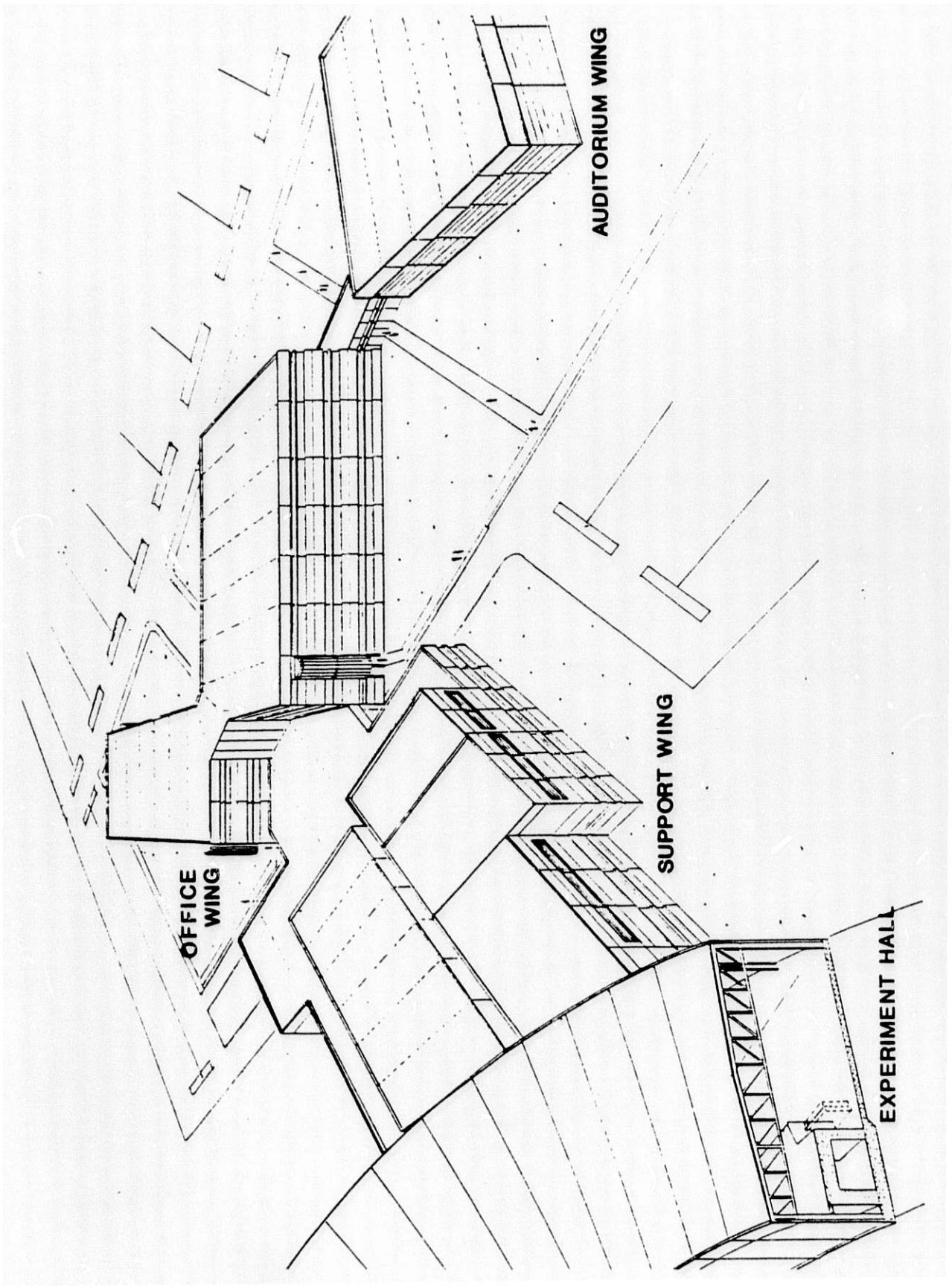

Figure IV.3.2-4
Central laboratory/office building bird's-eye perspective

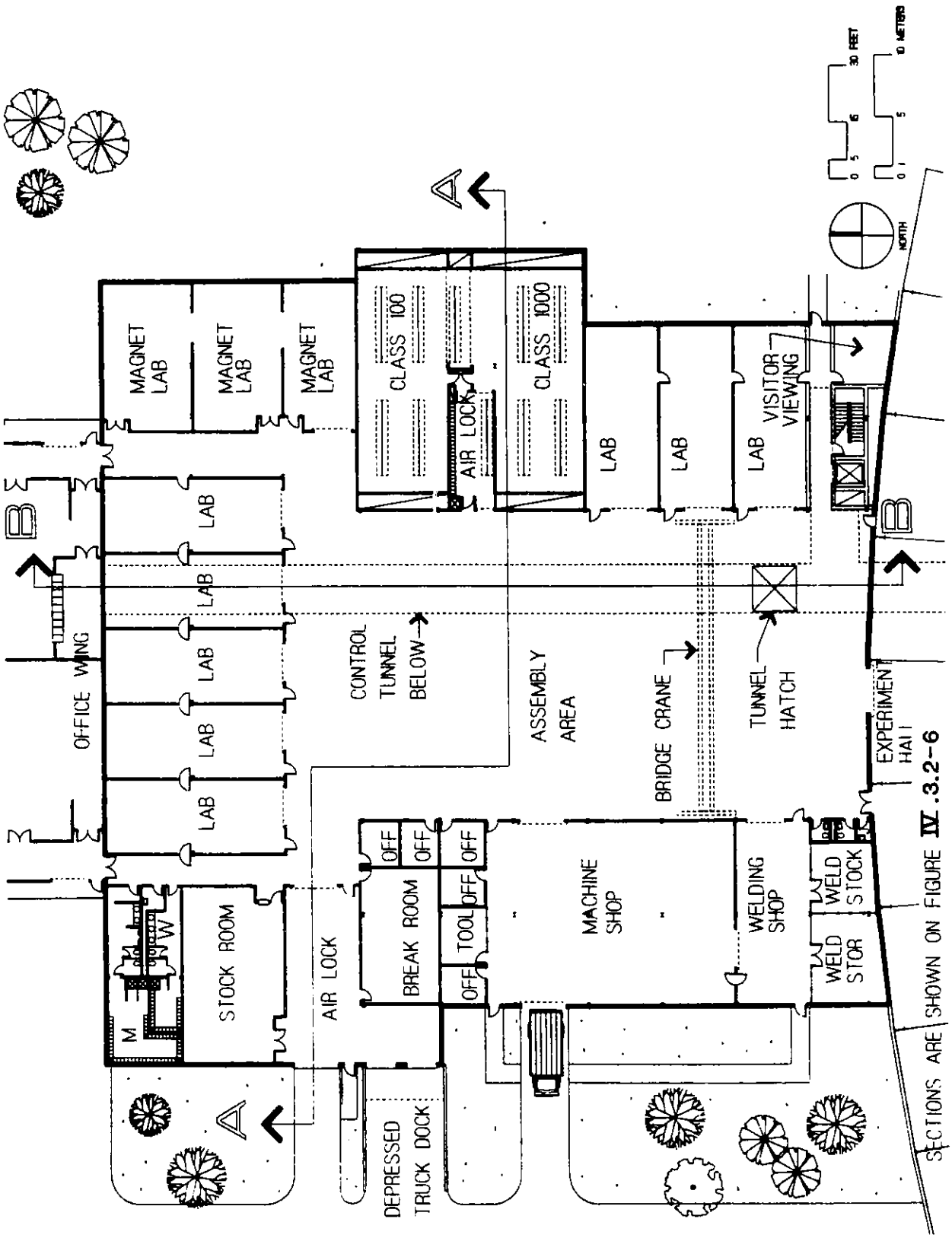

Figure IV.3.2-5
Support wing, central laboratory/office building ground floor plan.

3.2.4.1 Architecture

The interior of the building is organized around the central high-bay assembly area, with all shops and labs having direct access to it, as illustrated by the cross sections on Fig. IV.3.2-6. The support wing is entered through two corridors from the office wing, through doors from the experiment hall, and through a truck air lock in the northwest corner. A stairway and elevator located in the southeast corner of the building provide movement between the main floor, the control tunnel that runs beneath the assembly bay, and the upper-level mechanical room. A floor hatch allows direct crane access from the high-bay assembly area to the control tunnel.

Partitions are concrete masonry construction with a paint finish, except in the clean rooms, where special wall finishes are required. Steel overhead roll-up doors provide access between the high-bay area and the laboratories and shop areas. In the high-bay assembly and mechanical areas, conduit, piping, ductwork and the exposed structure are unpainted. In the laboratories, offices, toilets, locker, and break areas, acoustical tile ceilings with recessed lighting and HVAC diffusers are suspended from the structure. Electrical and mechanical distribution systems are concealed in the ceiling space. The clean rooms use special HEPA filter (high-efficiency particulate air filter) integrated ceiling systems.

Floors are covered with vinyl tile in the labs, offices, and lounge areas. Toilet rooms have ceramic tile floors and walls. In all other areas, the floors are exposed, surface-hardened concrete.

The exterior of the building is clad with 4-in.-thick insulated metal panels supported on horizontal girts. Energy-efficient thermal-break aluminum window frames with 1-in. solar insulating glass are provided in the shop and break areas. The roof of the building is protected by a single-ply roofing membrane, board insulation, and ballast in an IRMA system conforming to Argonne standards. Skylights provide natural light to the high-bay and shop areas.

Furnishings to be provided include desks, chairs, bookcases, and filing cabinets in the offices, and cabinets and counters along the long walls of the laboratories.

3.2.4.2 Structure

The support wing consists of a beam, girder, and column system supporting a welded metal deck roof, with rigid frames for resistance against lateral loads, and a roof truss spanning the high-bay assembly area. Foundations are conventional spread footings. The floor is a 6-in. reinforced concrete slab on grade over 6 in. of compacted granular backfill.

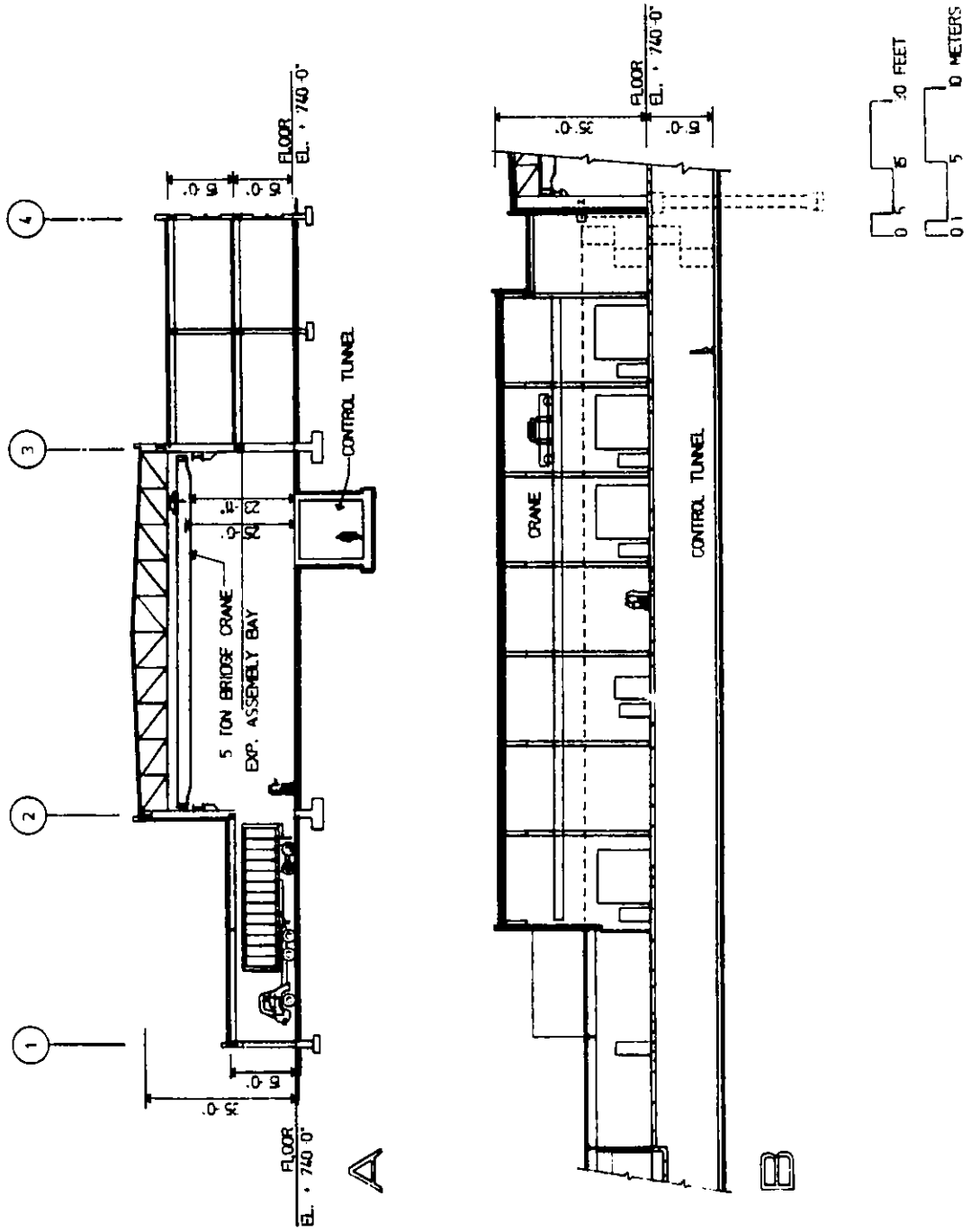

Figure IV.3.2-6
Support wing, central laboratory/office building sections.

3.2.4.3 Heating, Ventilation, and Air-Conditioning

The laboratories are maintained at a space temperature of 75°F ± 2°F year-round, with relative humidity of 50% maximum in summer and 25% minimum in winter. Three constant-volume air-conditioning units with three return fans are located in the upper level mechanical equipment room, a plan of which is shown on Fig. IV.3.2-7. Each laboratory is provided with a reheat coil at the supply air duct for space temperature control.

The two clean rooms have different ventilation requirements. The Class 100 clean room has a 90-cfm/ft^2 air supply. The Class 1000 clean room is supplied with air at 15 cfm/ft^2. The clean rooms are served by three air-handling units (with one additional for standby). Air is returned through an underfloor plenum and a vertical air shaft. A make-up air-handling unit supplies conditioned outside air to the three air-conditioning units for dehumidification and pressurization of the clean rooms.

The upper level mechanical equipment room is ventilated in summer and heated in winter to maintain a space temperature of 60°F. Hot water is converted from steam in the mechanical room. Chilled water and steam are supplied from a connection to the utility loop above the storage ring. A direct digital controller in this building controls the HVAC equipment.

3.2.4.4 Plumbing/Process Piping/Fire Protection

The plumbing systems consist of plumbing fixtures, water heating equipment, domestic cold- and hot-water distribution, sanitary waste collection, and vent piping systems in accordance with Argonne standards. The central laboratory/office building is supplied with individually valved domestic cold water from the loops on site, and laboratory service water, natural gas, and compressed air from the distribution loops in the experiment hall.

Process piping systems for the central lab and office building distribute natural gas and compressed air throughout the building, including all laboratories and work areas, from the service loops in the experiment hall.

Fire protection for the central laboratory/office building is provided by a wet-pipe automatic sprinkler system throughout. Hand-operated fire extinguishers are located as required.

3.2.4.5 Electrical Power

Electric power is delivered to the central laboratory/office building from the 13.2-kV switchboard in the utility building via a 15-kV loop feeder to one load center of 13.2-kV to 480Y 277-V, 1000-kVA, and one double-ended 13.2-kV to 120/208 V, 1000-kVA load center.

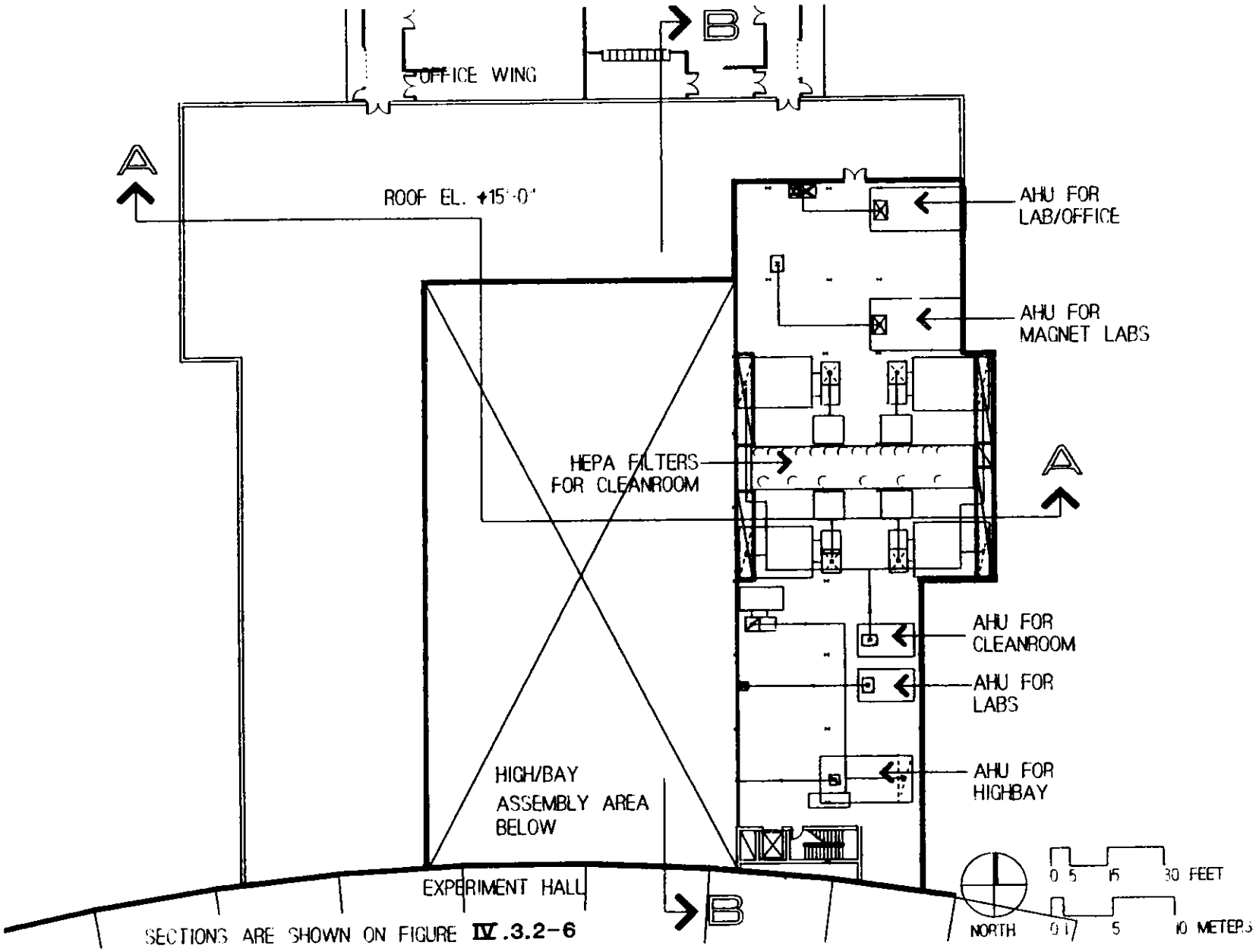

Figure IV.3.2-7
Support wing, central laboratory/office building mechanical penthouse plan.

An equipment grounding system is provided from connections on each piece of equipment to grounding conductors running with all power feeders. Lightning protection is provided by copper rods mounted around the perimeter of the roof, which are connected by copper cables Cadwelded to the building structural steel. A building ground system uses bare copper cable Cadwelded to the building structural steel, which is connected to ground rods spaced around the building. In addition, all computer and computer-related equipment is provided with a separate quiet-grounding system, which is isolated from the other grounding systems and is connected to a separate counterpoise and ground rod system.

The fire alarm system consists of manual-pull stations located at the building exits, flow and tamper switches in the sprinkler system, and smoke detectors throughout the building and in the HVAC system. The office wing and support wing are separately alarmed and controlled fire zones. The alarm system is annunciated at the Argonne fire station and at the security point in the APS control room.

3.2.5 Central Laboratory/Office Building - Office Wing

The office wing of the central laboratory/office building is connected to the support wing of the same building by a common wall, penetrated by two corridors and the control tunnel. The office wing houses the APS main reception area, laboratories, and offices for the APS operating staff, as well as the main computer and control rooms. A short corridor on the east side links the office wing to the auditorium and the exhibition/lounge area.

The building includes 44 laboratories, 2 laboratory-size shops, 132 offices, 10 conference rooms, a 3-laboratory space for a library, and various associated support spaces. Entry, reception, and display spaces provide a front door for the facility. The large computer and control rooms serve as the APS nerve center.

The "Y"-shaped, three-story building has a footprint of 35,320 ft^2. The gross floor area of 128,267 ft^2 includes a lower service level, in addition to the main floor level and the two upper floors of lab and office space. The ground floor plan is shown on Fig. IV.3.2-8. Figure IV.3.2-9 shows the layout of mechanical-equipment spaces on the service level.

3.2.5.1 Architecture

The main entry to the building is from the north, into a skylighted single-story section that provides space for the public entry and reception areas and the main computer and control rooms. From there, two corridors on the right and left loop around two cores of windowless laboratories and other building support areas in multistoried sections. Offices ring the outer perimeters of each loop. Alternative entry points are near the ends of each office block and through corridors from the support wing to the south.

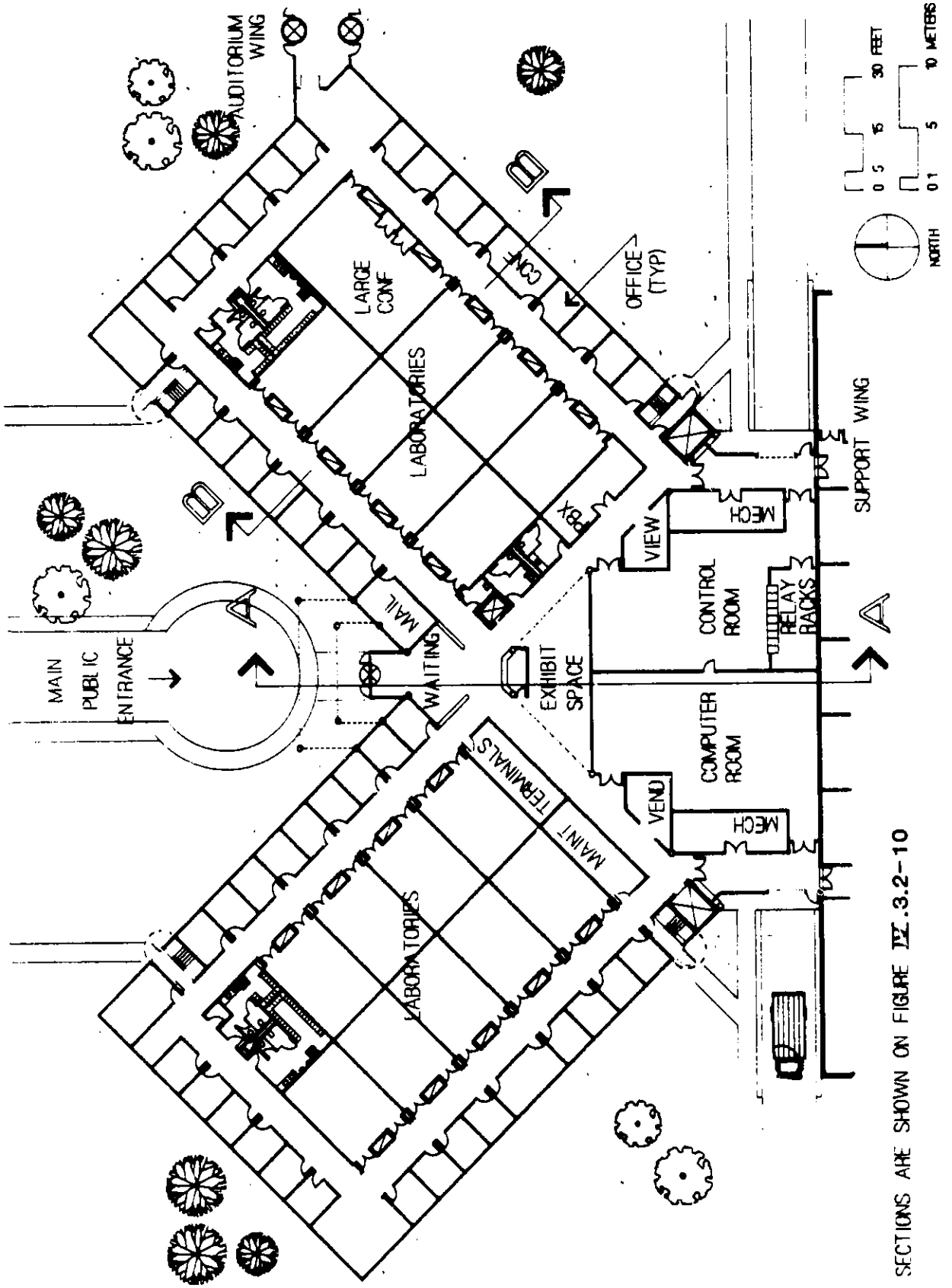

Figure IV.3.2-8
Office wing, central laboratory/office building ground floor plan.

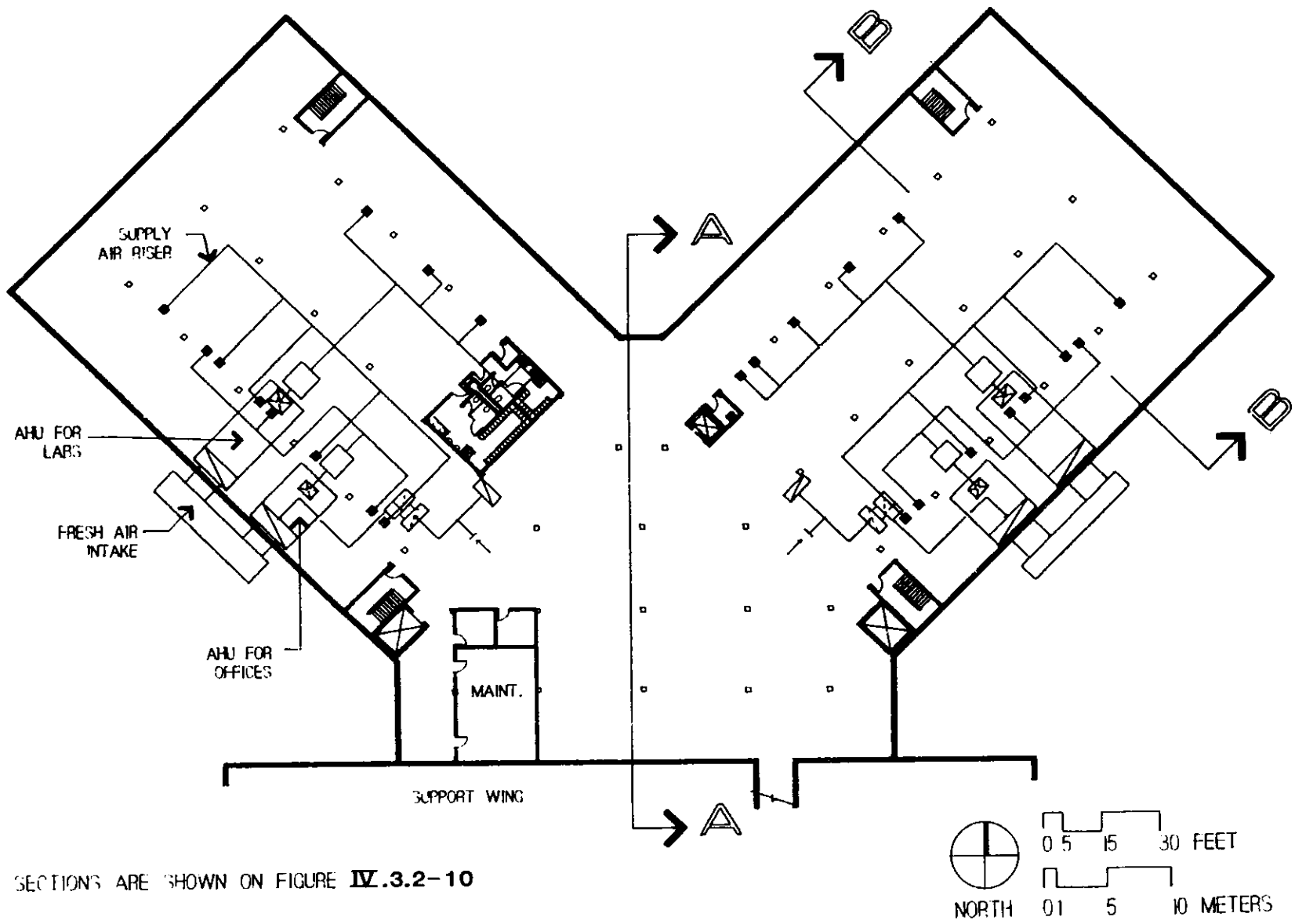

Figure IV.3.2-9
Office wing, central laboratory/office building service level plan.

The computer and control rooms each have raised-floor cable-way and air-plenum systems.

Personnel movement between the four floor levels is provided by stairways at each exit location, by a passenger elevator located next to the main building entry and reception area, and by two freight elevators located at the south end of each loop corridor. The central laboratory/office building sections are shown in Fig. IV.3.2-10.

Wall partitions are of gypsum drywall construction with painted finish. Hollow metal doors and frames are 8 ft high for all lab spaces. Acoustical tile ceilings with recessed lighting and HVAC diffusers are suspended from the structure, concealing the electrical and mechanical distribution systems in the ceiling space. Vinyl tile is the typical floor finish, except in the mechanical areas, where the floors are exposed, surface-hardened concrete.

The exterior of the building is clad with an aluminum panel and glass curtain wall system. Energy-efficient thermal-break aluminum framing, insulated panels, and 1-in. solar insulating glass are provided to minimize energy loss through the building skin. A light shelf is incorporated into the exterior wall design, to reflect daylight farther into the office areas, thereby reducing the need for artificial lighting and, thus, conserving energy. The roof of the building is protected by a single-ply roofing membrane, board insulation, and ballast in an IRMA system conforming to Argonne standards.

Furnishings to be provided include a reception desk and seats in the reception area; tables and chairs in conference rooms; desks, chairs, bookcases, and filing cabinets in the offices, and cabinets and counters along the long walls of the laboratories.

3.2.5.2 Structure

The office wing consists of a beam, girder, and column system supporting a welded metal deck roof, with structural steel bracing in the exterior wall for resistance against lateral loads. Foundations are conventional spread footings. The floor is a 6-in. reinforced concrete slab on grade over 6 in. of compacted granular backfill.

3.2.5.3 Heating, Ventilation, and Air-Conditioning

The office area is maintained at an ambient temperature of $75^{\circ}F \pm 2^{\circ}F$ year-round, with relative humidity of 50% maximum in summer and 25% minimum in winter, using two variable-volume air-conditioning units with two return fans located in the lower level mechanical equipment room. Each office has a variable-volume terminal box to control the space temperature. In addition, a hot-water baseboard heating system is provided in all perimeter offices.

The laboratory area is maintained at a space temperature of $75^{\circ}F \pm 2^{\circ}F$ year-round and relative humidity of 50% maximum in summer and 25% minimum in

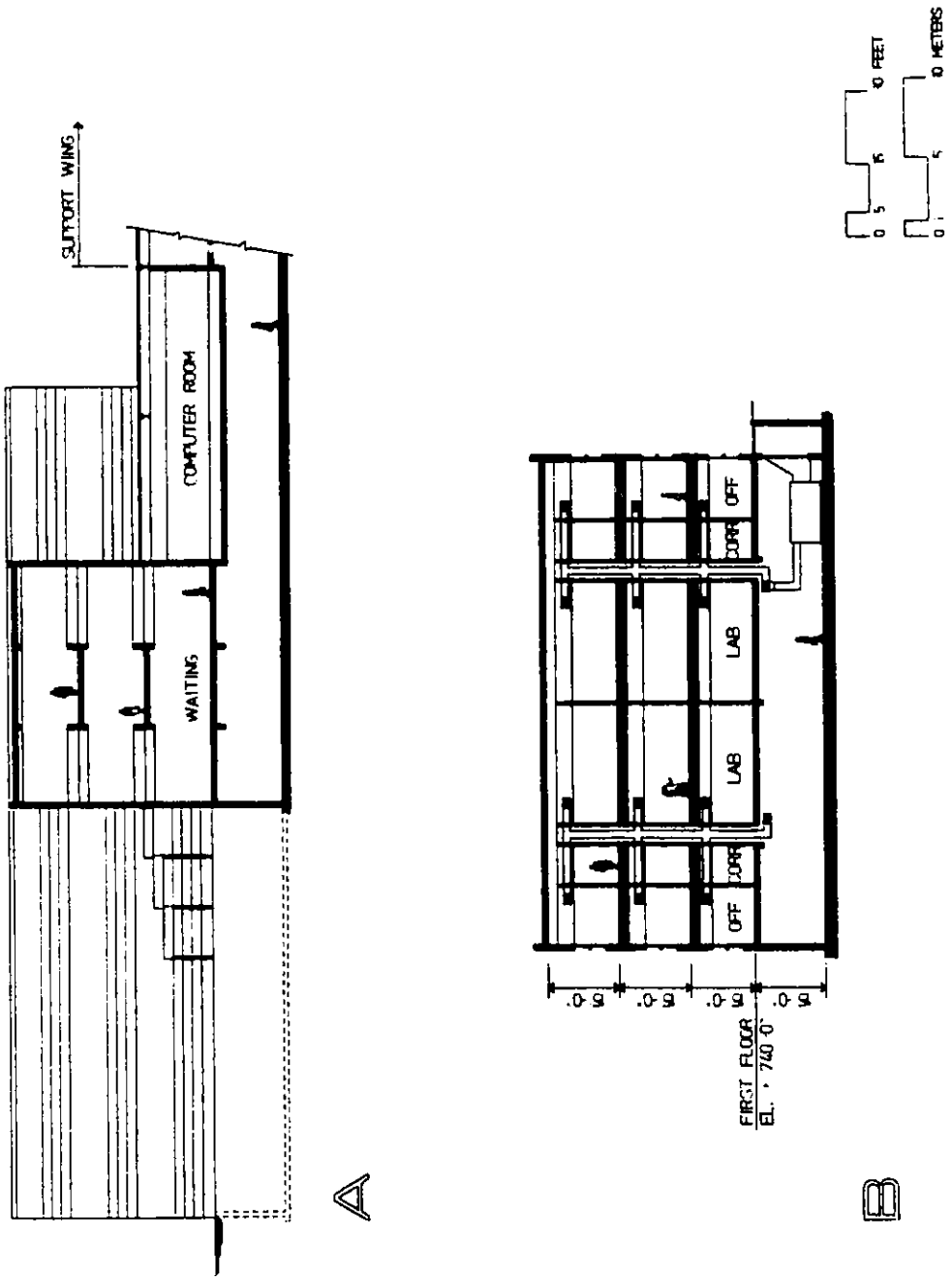
SUPPORT WING
COMPUTER ROOM
WAITING
A
LAB
LAB
OFF
CORR
OFF
CORR
FIRST FLOOR
EL. + 740 0"
B
0 5 10 FEET
0 1 3 METERS

winter. Two constant-volume air-conditioning units with two return fans located in the equipment room are provided for air circulation. The temperature is controlled in each laboratory with a reheat coil at the supply-air duct.

The main control room and computer room each have two packaged air-conditioning units located in adjoining rooms to maintain a 72°F ± 2°F space temperature and 45% ±10% relative humidity year-round. Conditioned air is supplied to equipment via a raised-floor plenum system. Make-up air is supplied from the laboratory air-conditioning units.

3.2.5.4 Plumbing/Process Piping/Fire Protection

The plumbing systems consist of plumbing fixtures, water-heating equipment, domestic cold and hot water distribution, sanitary waste collection, and vent piping systems in accordance with Argonne standards. The central laboratory/office building is supplied with individually valved domestic cold water from the loops on-site, and laboratory service water, natural gas, and compressed air from the distribution loops in the experiment hall.

Process piping systems for the central laboratory/office building distribute natural gas and compressed air throughout the building, including all laboratories and work areas, from the service loops in the experiment hall.

Fire protection for the central laboratory/office building is provided by a wet-pipe automatic sprinkler system throughout, with the addition of Halon 1301 systems in the main computer and control rooms. Hand-operated fire extinguishers are located as required.

3.2.5.5 Electrical Power

Electric power is delivered to the central laboratory/office building from the 13.2-kV switchboard in the utility building via a 15-kV loop feeder to one load center of 13.2 kV to 480Y 277-V, 1000 kVA, and one double-ended 13.2-kV-to-120/208 V. 1000-kVA load center.

An equipment grounding system is provided from connections on each piece of equipment to grounding conductors running with all power feeders. Lightning protection is provided by copper rods mounted around the perimeter of the roof, which are connected by copper cables Cadwelded to the building structural steel. A building ground system uses bare copper cable Cadwelded to the building structural steel, which is connected to ground rods spaced around the building. In addition, all computer and computer-related equipment is provided with a separate quiet-grounding system, which is isolated from the other grounding systems and is connected to a separate counterpoise and ground rod system.

The building lighting utilizes 4-ft-long fluorescent fixtures. The fixtures for offices, laboratories, and other finished areas are 2-ft by 4-ft lay-in lighting troffers with parabolic lenses and two, three, or four lamps, as required to obtain the desired illumination levels. Three- and four-lamp fixtures are wired for two-level switching.

The fire alarm system in both wings consists of manual-pull stations located at the building exits, flow and tamper switches in the sprinkler system, and smoke detectors throughout the building and in the HVAC system.

The office wing and support wing are separately alarmed and controlled fire zones. All alarm and annunciation signals annunciate in the Argonne fire station and at the security point in the APS control room.

The telephone system consists of cabling from the PBX room to telephone terminal cabinets on each floor. There are telephone outlets in all offices, laboratories, conference rooms, and other finished areas.

3.2.6 Central Laboratory/Office Building - Auditorium Wing

The auditorium wing is located just east of the office wing. The building houses a 600-seat auditorium designed for lectures, with associated lobby and display spaces. The auditorium is attached to the office wing by an enclosed entry corridor. It is adjacent to the APS main parking area and is separated from the central laboratory/office building, so that visitors may enter the auditorium without disturbing the operations of the central laboratory/office or the experiment hall. The square building is 110 ft on each side, with a footprint of 12,100 ft^2. Figure IV.3.2-11 shows plans and cross sections of the auditorium wing.

3.2.6.1 Architecture

The auditorium is laid out within the square structure with the podium at the south corner of the square, and rows of fixed seating radiating out so that the rows are approximately on a diagonal of the square. This column-free lecture hall uses continental seating to maximize user legroom and the number of prime seat locations. The lobby and display area fills the north corner of the square, and support spaces run along the east and west sides of the auditorium.

Inside the building, the wall partitions are of gypsum drywall construction with painted finish. Ceilings with recessed lighting and HVAC diffusers are suspended from the structure, concealing electrical and mechanical distribution systems in the ceiling space. Acoustical tile is used on all ceilings except in the auditorium itself. Special finishes are used on the auditorium walls and ceilings for acoustical control. Floors in all areas are finished with vinyl tile.

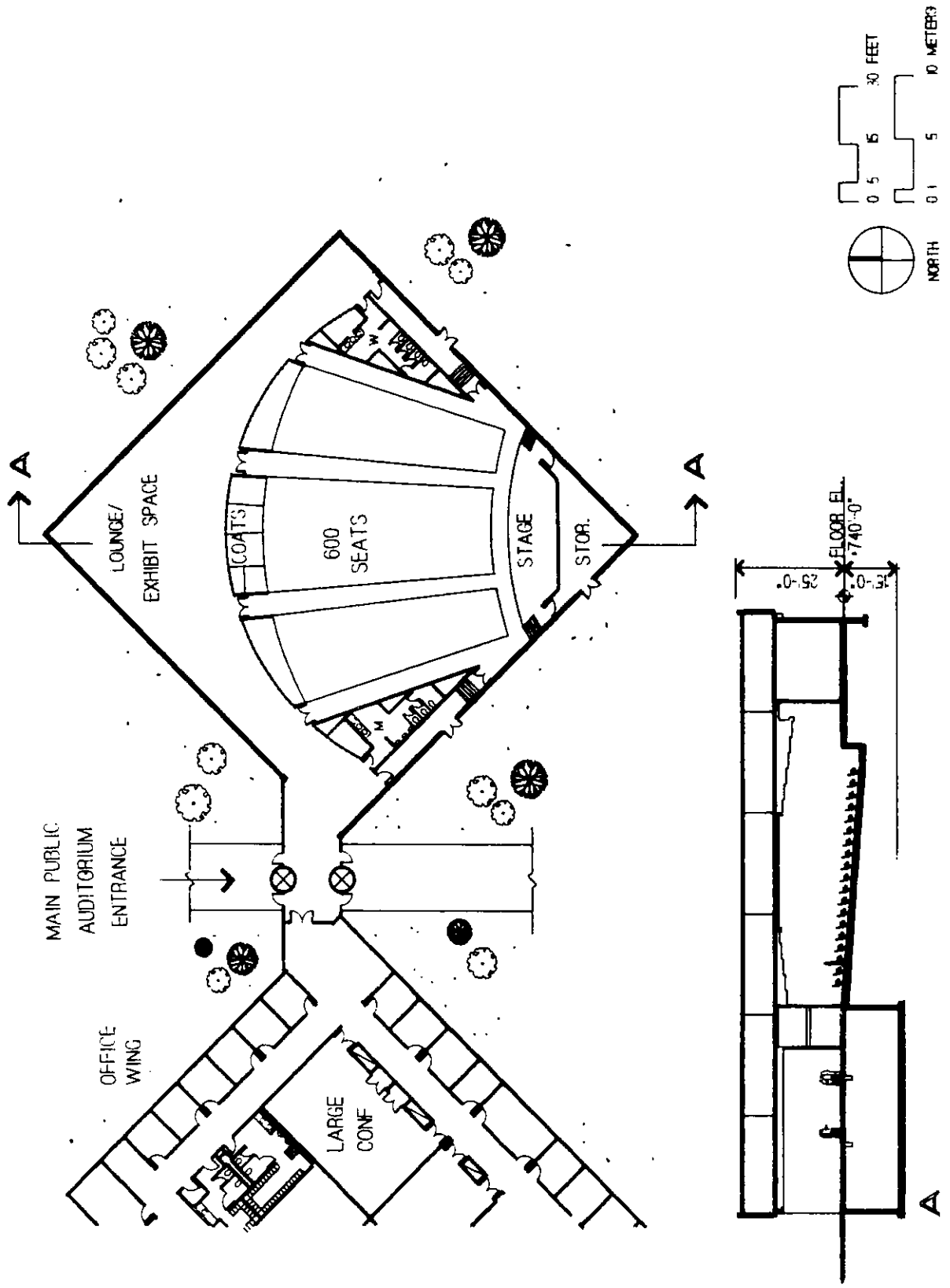

Figure IV.3.2-11
Auditorium wing, central laboratory/office building.

The exterior of the building is clad with an aluminum panel and glass curtainwall system matching that used for the office wing. Energy-efficient thermal-break aluminum framing, insulated panels, and 1-in. solar insulating glass are provided, to minimize energy loss through the building skin. The roof of the building is protected by a single-ply roofing membrane, board insulation, and ballast in an IRMA system conforming to Argonne standards.

Furnishings include fixed seating in the auditorium, coat racks, and counters.

3.2.6.2 Structure

The auditorium consists of deep long-span steel joists, girders and columns supporting a welded metal deck roof, with structural steel bracing in the exterior wall for resistance against lateral loads. Foundations are conventional spread footings. The floor is a 6-in. reinforced concrete slab on grade over six inches of compacted granular backfill.

3.2.6.3 Heating, Ventilation, and Air-Conditioning

Two variable-volume air-handling units located in the mechanical-equipment room in the basement maintain a space temperature of 75°F ± 2°F year-round, with 45% maximum relative humidity in summer and 25% minimum in winter in the auditorium and the exhibit/lounge space. The unit serving the auditorium is sized at 50 tons; a 40-ton unit serves the exhibit area. Hot-water baseboard and fin-tube radiators at the perimeter walls maintain the space temperature in winter. Units are on local direct-digital control.

3.2.6.4 Plumbing/Fire Protection

The plumbing systems consist of plumbing fixtures, water heating equipment, domestic cold- and hot-water distribution, sanitary waste collection and vent piping systems. The auditorium is supplied with individually valved domestic cold water from the site utility loop.

Fire protection includes a wet-pipe automatic sprinkler system separately alarmed and interlocked with the Argonne central fire alarm and security system.

3.2.6.5 Electrical Power

Electrical power is distributed to the auditorium at 480Y/277 V from the central laboratory/office building.

An equipment grounding system is provided from connections on each piece of equipment to grounding conductors running with all power feeders. Lightning protection is provided by copper rods mounted around the perimeter of the roof, which are connected by copper cables Cadwelded to the building structural steel. A building ground system uses bare copper cable Cadwelded to the building structural steel, which is connected to ground rods spaced around the building.

General illumination for the auditorium is provided by metal halide downlights, arranged in a uniform pattern and controlled from a master dimming system, with local controls in the projection room and provisions for remote control from the stage. Speakers, amplifiers, and input jacks located on the stage and in the projection room make up the auditorium sound system.

Three lighting systems: fluorescent fixtures, track lighting, and downlights, serve the lighting needs of the exhibit/lounge area. Each lighting system is switched separately. Floor receptacles are installed in a grid pattern throughout the exhibit/lounge space to accommodate various display configurations.

The fire alarm system, a separate zone of the central laboratory/office building, consists of manual stations at the exits, flow and tamper switches in the sprinkler system, and smoke detectors throughout the building and in the HVAC system.

3.3 Utilities and Sitework

3.3.1 Utility Services to the Site

The APS area utility plan, Fig. IV.3.3-1, shows the locations of utility feeders to the APS site.

3.3.1.1 Electrical Power

The two existing overhead 13-kV feeders, ZR-1 and ZR-2, extend on a common pole line along Bluff Road to a pole adjacent to the utility building. From this point, they run underground to the distribution switchgear in the buildings.

3.3.1.2 Steam System

The energy source for all heating systems for the facility is the site steam distribution network. An 8-in.-diameter high-pressure steam main and 4-in.-diameter condensate return main extend above ground to the utility building from the existing overhead piping located adjacent to Bluff Road.

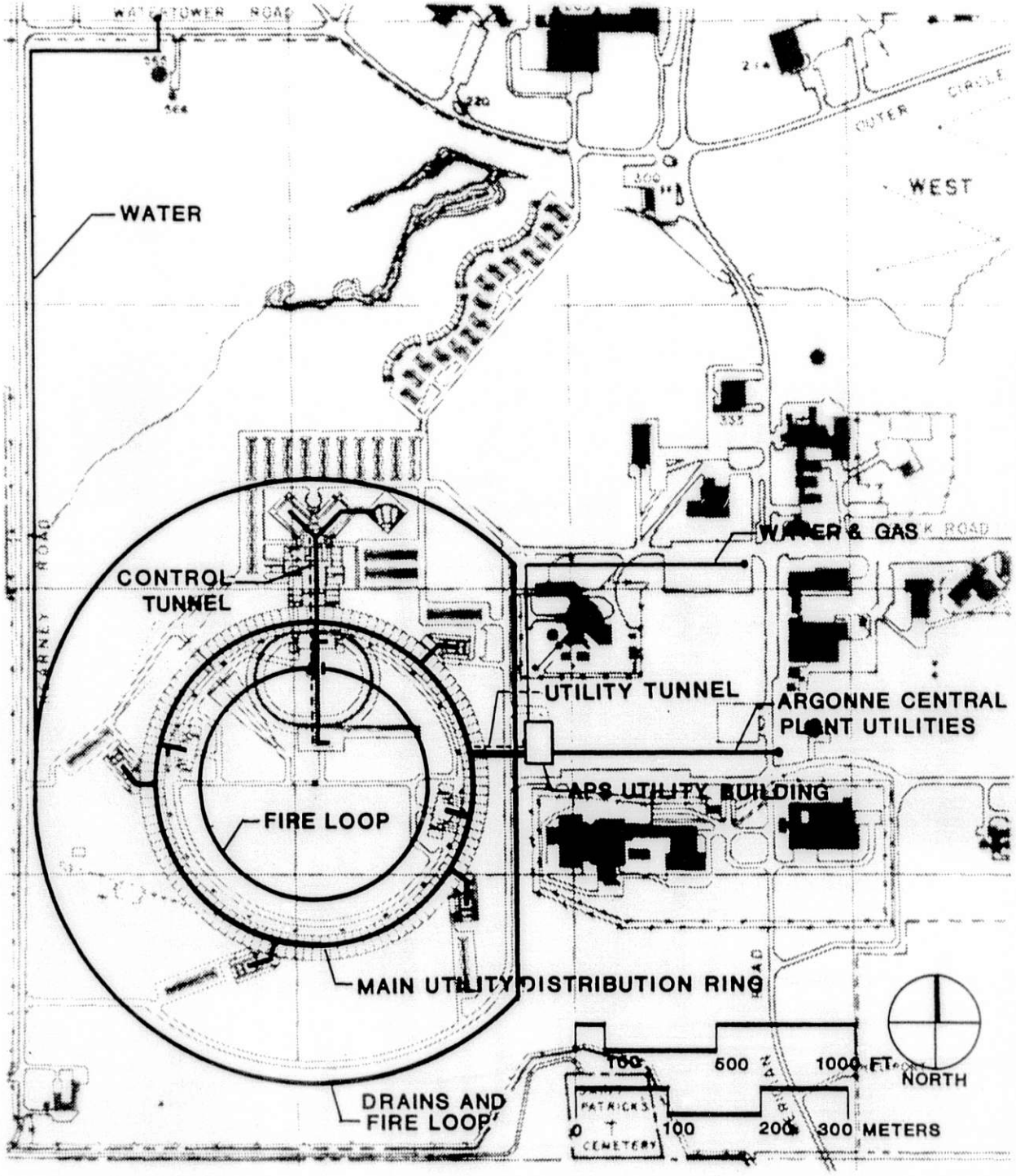

Figure IV.3.3-1
Utility area plan.

3.3.1.3 Cooling Tower Makeup Water

Makeup water for the cooling towers is provided by the canal cooling water distribution system. A 6-in.-diameter main runs underground along Bluff Road to the existing underground 10-in. main located adjacent to Bluff Road and west of Meridian Road.

3.3.1.4 Domestic Water and Fire Protection Water Supply

The existing domestic and fire protection water network is interconnected to make a loop by extending a 10-in. water main from a connection on Bluff Road near Meridian Road, around the south perimeter of the facility and along Kearney Road to the water tower on Water Tower Road, thereby ensuring uniform pressure and flow for the project's domestic water and fire protection demands.

UL/FM-approved fire hydrants, of traffic-type barrel design, are spaced at a maximum of 300 ft in accordance with the FM requirement for fire hose connections.

Individual zones of fire protection within each of the APS buildings are supplied by an individual feed main from the loop, equipped with a UL/FM-approved post indicator valve, complete with electrical supervisory devices. An additional 8-in. subloop is provided in the infield area of the APS, with fire hydrants for protection of the infield buildings and equipment. Individual zones of domestic water demand are supplied by an individual feed main from the loop and are equipped with a post-indicating shut-off valve.

3.3.1.5 Laboratory Service Water Supply

The laboratory service water supply extends along Bluff Road as a 4-in.-diameter water main from the existing network east of the project site. Laboratory service water is routed to the utility building for metering before being routed through the utility tunnel into the experiment hall.

3.3.1.6 Natural Gas Supply

Natural gas supply lines extend as a 3-in. underground main from the existing network east of the project site near the intersection of Bluff and Meridian Roads. Gas is routed to the area adjacent to the utility building, for pressure regulation, before being routed through the utility tunnel into the experiment hall.

3.3.1.7 Drainage Systems

Eight-in.-diameter laboratory waste and sanitary sewers encircle the project site, but are not complete loops. Each APS sewer system connects into its corresponding existing network east of the project site in two locations along both Rock Road and Bluff Road. Each sewer system uses lift stations along its route to provide necessary elevation to interface with the existing networks.

3.3.2 Utility Building

The utility building is located at the eastern edge of the APS site along Bluff Road, and is separated from the rest of the APS facility by a portion of the perimeter road. The utility building is connected to the outer wall of the experiment hall by a utility tunnel.

The one-story rectangular building is 120 ft by 180 ft with a footprint of 21,600 ft^2, as shown on Fig. IV.3.3-2. The steel structure is composed of steel joists and metal roof deck supported on 30-ft-square column bays with 30-ft clear heights.

The utility building serves as the sole source for all utilities and heating and cooling requirements for the facility. The structure is located at a sufficient distance from the main facility to preclude vibration transfer problems. Most utility lines are run between the utility building and the experiment hall via the underground utility tunnel. The following services are provided to the APS:

- Chilled water loop (40°F)
- High-temperature equipment cooling water loop (90°F)
- High-pressure steam main and condensate return for heating requirements
- Natural gas line
- Domestic water main
- Laboratory service water
- Compressed air for general services
- Electrical power at 13.2 kV.

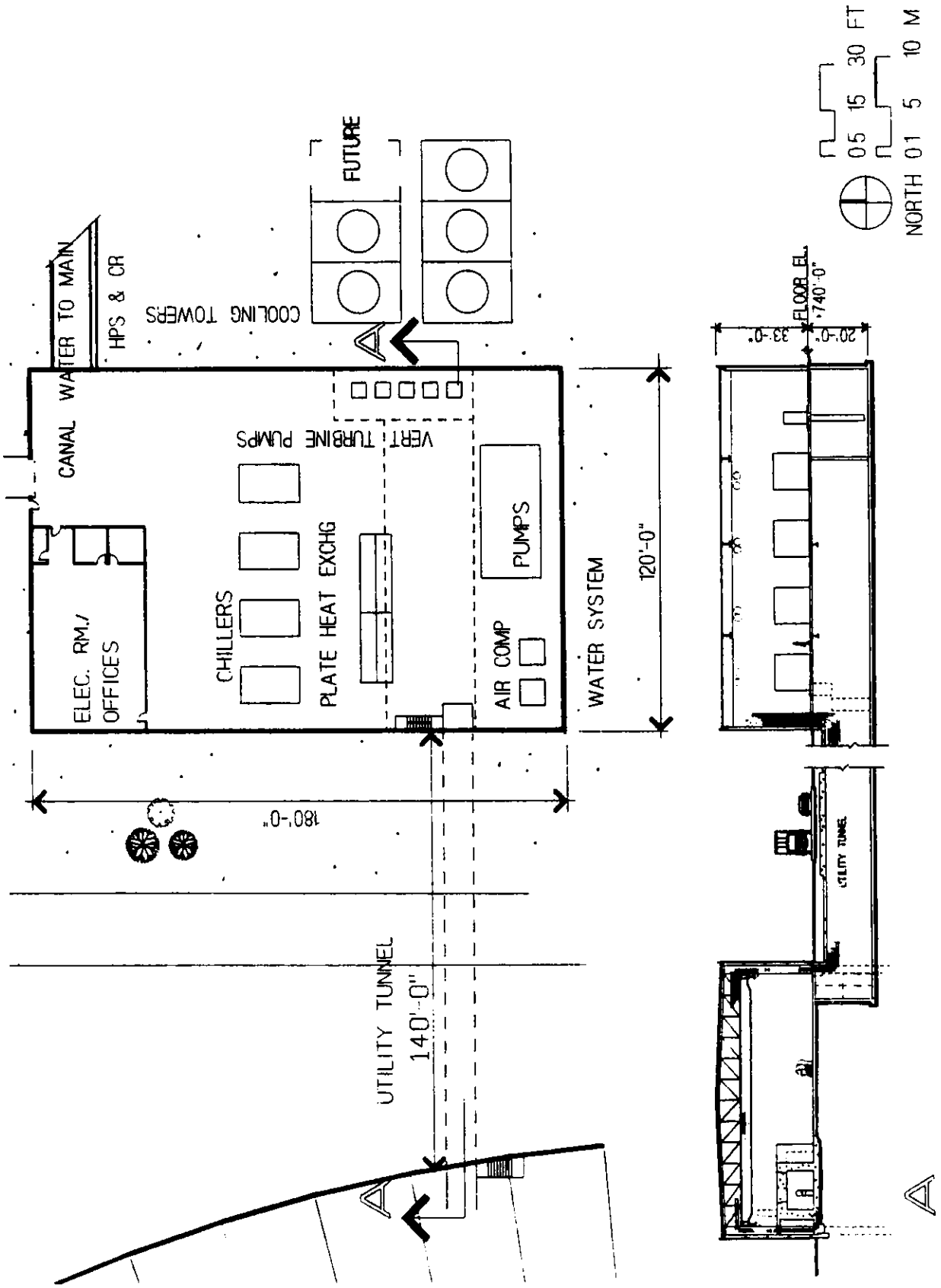

Figure IV.3.3-2
Utility building.

3.3.2.1 Architecture

The interior of the building is open, except for the enclosed control area. Entry to the building is directly from grade. Movement between the main level and the utility tunnel is provided by a stairway and a large floor hatch adjacent to the tunnel access point.

The wall partitions are of concrete masonry construction with a painted finish. Conduit, piping, ductwork, and the exposed structure in the ceiling areas are unpainted. In the control room, acoustical tile ceilings with recessed lighting and HVAC fixtures are suspended from the structure.

The windowless exterior of the building is clad with four-inch insulated metal panels supported on horizontal girts. The roof of the building is protected by a single-ply roofing membrane, board insulation, and ballast in an IRMA system conforming to Argonne standards. Furnishings include desks, chairs, bookcases, and filing cabinets in the control room.

3.3.2.2 Structure

The utility building structural system consists of a beam, girder and column system supporting a welded metal deck roof, with structural steel bracing in the exterior wall for resistance against lateral loads. Foundations are conventional spread footings. The floor is a 6-in. reinforced concrete slab on grade over six inches of compacted granular backfill.

3.3.2.3 Heating, Ventilation, and Air-Conditioning

Cooling water systems are interconnected in an arrangement to maximize energy conservation and allow for equipment flexibility. Both the 40°F chilled water system and the 90°F equipment cooling system utilize deionized water. The 40°F chilled water system serves the facility air conditioning and low-temperature equipment cooling systems. The 40°F chilled water system capacity is estimated at 4700 tons of refrigeration: the facility air-conditioning has a 3800-ton load and the low-temperature equipment cooling has a 900-ton load.

Four 1500-ton chillers are provided (one on standby, except during the peak summer load period, when all units are used). The chillers are electric-drive centrifugal refrigeration units, either hermetic or open motors. Chilled water is pumped through the chillers and out to the air-conditioning load throughout the facility. These refrigeration units are cooled by adjacent banks of induced-draft cooling towers, located immediately outside the utility building. Six cells and six vertical-turbine-type pumps (one future) are provided.

The 90°F equipment cooling system is estimated at 6000 tons. This cooling is provided directly from the above cooling towers through stainless steel plate-and-frame heat exchangers.

Each pair of heat exchangers has 100% capacity, and is equipped with stand-by circulating pumps. Both the 40°F chilled water system and 90° F equipment cooling system are of the constant-temperature variable-flow type.

A deionized water-producing facility, located in the utility building, continuously maintains the cooling water systems at a one-megohm level. This unit is of the packaged dual-bed resin type. All piping is fiberglass-reinforced epoxy resin; pumps are of stainless steel.

Adequate space has been allocated in the utility building for maintenance and service for of HVAC equipment for the entire APS facility.

From the steam main in the utility building (supplied from the Argonne central system), high-pressure steam is distributed to each building of the APS, where it is converted to low-pressure steam for space heating and humidification through pressure-reduction stations. At the central laboratory/office building, the synchrotron injection building, and each laboratory/office module, the low-pressure steam is converted to hot water for space temperature control.

3.3.2.4 Plumbing/Process Piping/Fire Protection

The plumbing system is complete with plumbing fixtures, domestic cold and hot-water piping, domestic-water-heating equipment, sanitary waste and vent piping systems as required for toilet rooms, locker rooms with showers, and for support, supply, and drainage of mechanical equipment.

Compressed air is provided to the APS from the utility building. The process-air-compressing system utilizes two 150-horsepower electric-driven rotary screw air compressors (with provision for a future third unit), with a 600-gallon air receiver and a refrigerated air drier/filter assembly. Compressed air is distributed to the buildings at approximately 125 psi.

The utility building is protected with a wet-pipe sprinkler system and 17-pound-capacity Halon 1211 portable extinguishers.

A process water (90°F) producing facility is located in the utility building, to provide make-up water to the cooling loop. This unit is of the packaged dual-bed resin type. All piping is Schedule 80 PVC, and pumps are of stainless steel. Water is maintained at a one-megohm level. There is no distribution of process water to the laboratories.

Adequate space has been allocated in the utility plant for maintenance and service for all process-water equipment and for the entire APS facility.

3.3.2.5 Electrical Power

Electrical power is delivered from the Argonne site electrical distribution by two 15-kV underground feeders, originating at a pole adjacent to Bluff Road. The feeders supply a double-ended, secondary-selective, 15-kV fused load interrupter switchgear. Distribution from this switchgear to the substations serving the APS is via three-conductor armored cable in cable tray in tunnels and buildings, and single-conductor 15-kV cable in underground ductwork in the infield. A single-line diagram, the electrical site distribution system, is Fig. IV.3.3-3. A typical building electrical system is diagrammed on Fig. IV.3.3-4.

The electric service for the utility building consists of two 13.2-kV-to-2400-V, 5000 kVA substations and a 13.2-kV-to-480Y/277 V, 500-kVA unit substation. The building distribution voltages will be 2400 V for motor loads of 250 hp and larger, 480 V for motor loads from 1/3 hp to 200 hp, and 277 V for lightning.

One 400-kVA diesel-driven standby generator will run selected cooling water pumps in the event of the loss of electric power.

An equipment-grounding system is provided from connections on each piece of equipment to grounding conductors running with all power feeders. Lightning protection is provided by copper rods mounted around the perimeter of the roof, which are connected by copper cables Cadwelded to the building structural steel. A building ground system uses bare copper cable Cadwelded to the building structural steel, which is connected to ground rods spaced around the building.

The utility building is lighted by high-bay, high-pressure sodium fixtures for an average of 30 footcandles of illumination, switched from the 480Y/277-V lighting panel.

The fire alarm system consists of manual pull stations located at the building exits, flow and tamper switches in the sprinkler system, and smoke detectors throughout the building and in the HVAC system. The alarm system is annunciated at the Argonne fire station and at the APS security point in the main control room. The telephone system is a branch of the private branch exchange (PBX) from the central laboratory/office building.

3.3.3 Site Preparation and Excavation

The existing ground contours in the project area are undulating, with elevations ranging from 755.00 to 735.00. Trees cover approximately 11 acres of the site's 78 acres. The site is cleared and stripped of topsoil before major excavation begins.

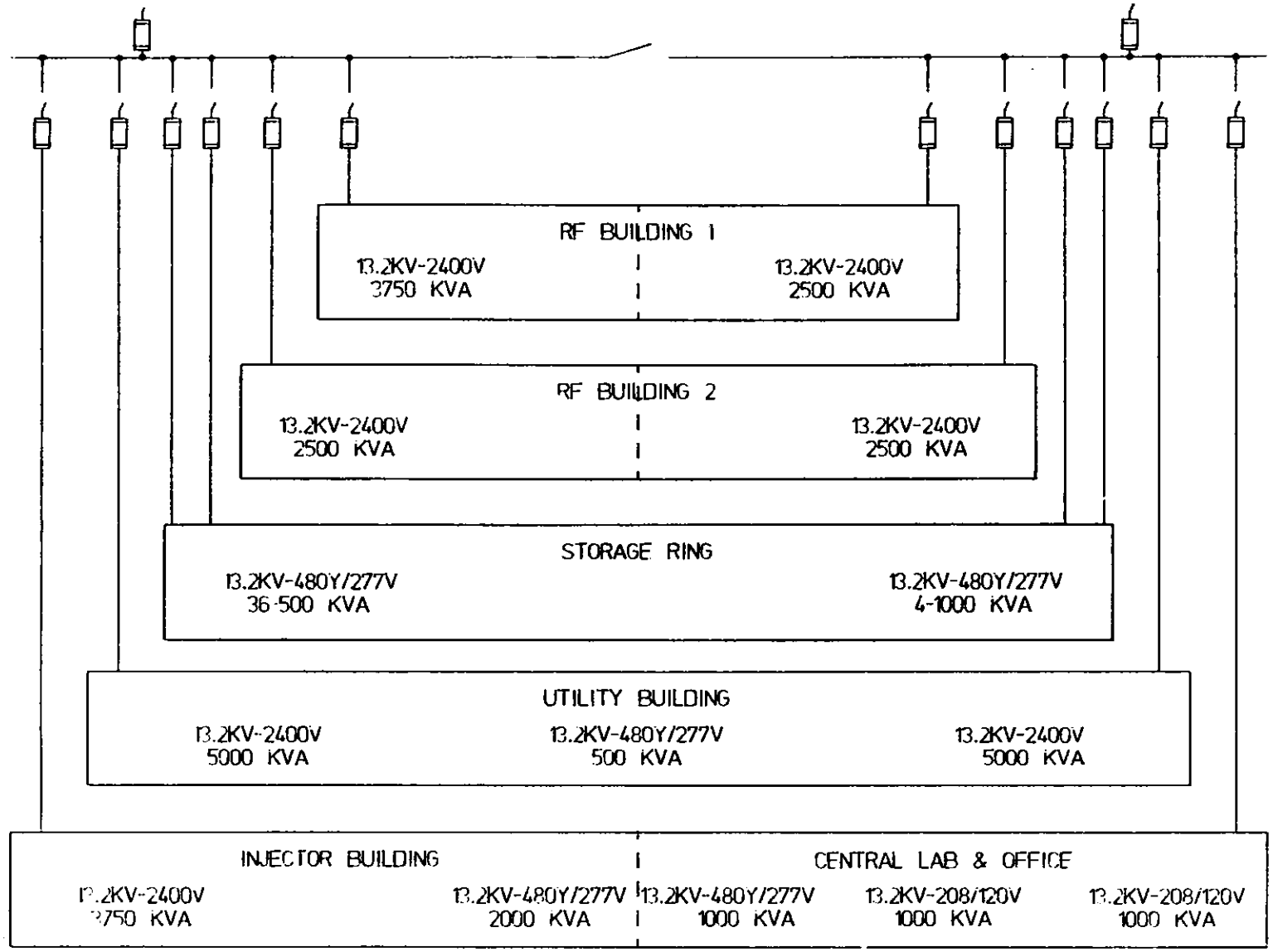

Figure IV.3.3-3
Electrical site distribution system.

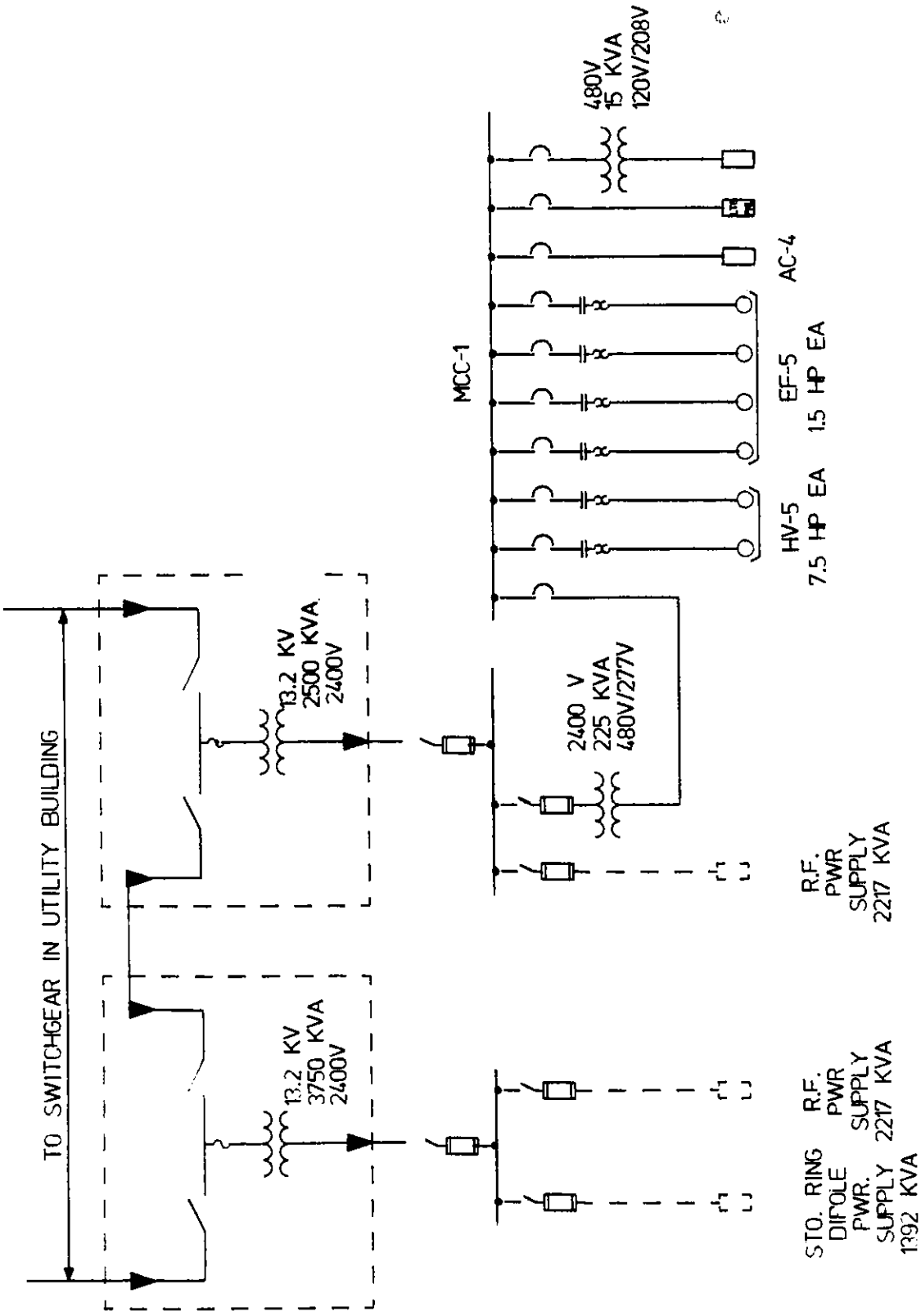
TO SWITCHGEAR IN UTILITY BUILDING
13.2 KV
2500 KVA
2400V
13.2 KV
3750 KVA
2400V
MCC-1
2400 V
225 KVA
480V/277V
480V
15 KVA
120V/208V
HV-5
7.5 HP EA
EF-5
1.5 HP EA
AC-4
R.F.
PWR
SUPPLY
2217 KVA
STO. RING
DIPOLE
PWR.
SUPPLY
1392 KVA
R.F.
PWR
SUPPLY
2217 KVA

Topsoil is stockpiled for respreading after building and roadway construction is completed. Excess spoils are moved to disposal sites on Argonne property.

This facility has a ring-type building that houses sensitive experimental equipment, making it essential that its concrete foundation slab be set level, with only minimal settlement. To meet this requirement, the floor slab is set into the undisturbed natural soil. The lowest finished slab elevation considered for this report is 740.00. Any existing unstable areas under the ring building are backfilled with engineered structural fill to prevent settlement. Where fill is required, the existing ground is removed to a minimum depth of two feet and replaced by cohesionless, well-compacted backfill.

Because of the difference in ground elevations across the site, there is an excess of excavated material (approximately 308,000 yd^3, which includes 70,000 yd^3 of topsoil) for a finished slab elevation of 740.00. This excess material is moved to designated areas on Argonne property. Locating the slab at elevation 740.00 requires that approximately 11,500 yd^3 of structural backfill be placed under the storage ring/experiment hall. Cut-and-fill ratios were investigated for other proposed top-of-slab elevations, evaluating potential cost savings from reducing the amount of excess material versus the advantages of placing the storage ring on undisturbed soil. Elevations above 740.000 were rejected, to provide the firmest possible foundation.

All of the construction associated with earthwork uses methods that minimize soil erosion.

3.3.4 Grading and Drainage

Storm water detention provisions have been incorporated to meet the local ordinance. Under the terms of this ordinance, approximately 17.4 acre-ft of storage for the site are provided. The total allowable release rate from the site is approximately 7.8 ft^3/s, based on a calculation of 0.1 ft^3/s per acre for 78.3 acres.

The site is split into two sections by a major drainage divide, with approximately 42.8 acres falling north of the divide and 35.5 acres located south of the divide. Existing storm drainage flows from the north side of the site to Sawmill Creek on its way to the Des Plaines River; the south side drains in natural drainageways directly to the Des Plaines River. Because of the divide, normally dry detention basins are located in several places around the perimeter of the APS site to slow the run-off to downstream areas. Eleven acre-ft of storage is provided on the north side of the site, and 6.4 acre-ft is provided on the south side. Restrictor pipes control the release flow rate from these areas.

Storm water collecting on the APS site is conveyed to the detention basins in properly sized storm sewers or ditches. Storm water runoff from the buildings, roadways, parking areas, and the infield area are conveyed to the outlet sewers via

ditches or small storm sewers. A drain system around building foundations also drains to the outlet sewers.

3.3.5 Access Tunnels

Access to the APS facility is enhanced by three tunnels. The utility tunnel carries utility piping and cables under the east perimeter road, between the utility building and the experiment hall. The vehicle tunnel allows emergency and service vehicles to drive under the experiment hall into the infield. The control tunnel connects the central laboratory/office building and the infield injection facilities with direct pedestrian, utility, and control access.

3.3.5.1 Vehicle Tunnel

From the northwest, the vehicle tunnel passes under the experiment hall, with approaches descending to the tunnel from outside the experiment hall and from the infield. The tunnel is constructed with reinforced concrete with a waterproof exterior. Descending and ascending grades for the tunnel are approximately 5.0%.

The vehicle tunnel requires a storm water lift station to drain the low area of the tunnel. The lift station is a submersible-type, with dual pumps (1500-2000 gpm), a concrete-type wet-well with necessary controls and emergency generator.

The tunnel is illuminated by wall-mounted high-pressure sodium lighting fixtures, arranged to meet the IES-recommended lighting levels. Lighting is controlled from a master timing system, in two stages (night and day).

3.3.5.2 Control Tunnel

The control tunnel runs from the lower level of the office wing of the central laboratory/office building beneath the main control room, beneath the support wing and experiment hall to the synchrotron extraction and synchrotron injection buildings. The tunnel carries control wiring, utilities, and rf waveguides, in addition to providing direct, all-weather access for APS operations staff and equipment to the primary technical components. The tunnel interior is 13 ft wide and 13 ft high, but only a 9-ft by 9-ft cross section is available for pedestrians; the rest is reserved for wiring, piping, and ductwork.

Access to the tunnel is provided by a stairway and an elevator at the southeast corner of the office wing, at the southwest corner of the support wing, and in the synchrotron extraction and synchrotron injection buildings. In addition, floor hatches provide crane access to the tunnel from the high-bay assembly area and the synchrotron injection and extraction buildings.

The tunnel is constructed of reinforced concrete, protected from water penetration by membrane waterproofing and perimeter drains.

The conduit, cable trays, piping, and ductwork are exposed and unpainted. Unistrut channels are cast into the walls and ceilings. The 1-5/8-in. channel is embedded on 6-ft centers, vertically on the walls, and across the width of the tunnel on the ceilings.

Packaged air-handling units with chilled-water coils provide the necessary air changes and dehumidification.

A wet-pipe automatic sprinkler system provides fire protection. Hand-operated Halon 1211 fire extinguishers are located at intervals along the tunnel.

The tunnel is lighted by two-lamp, four-foot long, wall-mounted fluorescent fixtures mounted on 8-ft centers on one side of the tunnel. They are switched from lighting panels. Duplex receptacles are mounted on 50-ft centers, 3 ft above the floor on one wall.

The fire alarm system consists of manual-pull stations located at the tunnel exits, flow and tamper switches in the sprinkler system, and smoke detectors throughout the tunnel and in the HVAC system.

3.3.5.3 Utility Tunnel

The utility tunnel runs from below the utility building at the east edge of the site, under the east perimeter road, to beneath the outer perimeter wall of the experiment hall. The tunnel carries building systems control wiring and utilities between the utility building and the rest of the APS facilities, in addition to providing direct, all-weather access for building maintenance staff. The interior of the 153-ft-long tunnel is 13 ft across and 13 ft high, but only a 5-ft by 9-ft cross section is available for pedestrians, because the rest is reserved for conduit, cable trays, and piping. Access to the tunnel is provided by a stairway at each end, in the utility building and in the experiment hall.

The tunnel is constructed of reinforced concrete, protected from water penetration by membrane waterproofing and perimeter drains.

The conduit, cable trays, piping and ductwork are exposed and unpainted. Unistrut channels are cast into the walls and ceilings. The 1-5/8-in. channel is embedded on 6-ft centers, vertically on the walls, and across the width of the tunnel on the ceilings.

Packaged air-handling units with chilled-water coils provide the necessary air changes and dehumidification.

A wet-pipe automatic sprinkler system provides fire protection. Hand-operated Halon 1211 fire extinguishers are located at intervals along the tunnel.

The tunnel is lighted by two-lamp, 4-ft long, wall-mounted fluorescent fixtures mounted on 8-ft centers on one side of the tunnel. They are switched from lighting panels. Duplex receptacles are mounted on 50-ft centers, 3 ft above the floor on one wall.

The fire alarm system consists of manual pull stations located at the tunnel exits, flow and tamper switches in the sprinkler system, and smoke detectors throughout the tunnel and in the HVAC system.

3.3.6 Roadways and Parking

Access roads and parking areas serve all areas of the APS facility, including the central laboratory/office building, electrical substation, utility building and cooling tower. The roadways are 24 ft wide, with 3-ft wide aggregate shoulders. Roadways are sloped to drain to ditches or storm sewer inlets. Curbs and gutters are provided at parking areas.

Paving consists of a 1.5-in. surface course and a 1.5-in. binder course of bituminous concrete over an 8-in. portland cement base course. The aggregate shoulders are 6 in. thick. The pavement structure is constructed on a well-compacted subgrade.

Roadway and parking lots are lighted by pole-mounted high-pressure sodium fixtures.

3.3.7 Landscaping

Stored topsoil is respread over exposed areas of the new site to a depth of at least 6 in., to promote groundcover growth. Topsoil areas are seeded and trees and shrubbery are planted, in accordance with an approved landscape plan.

3.4 References

1. M.J. Knott, "General Specifications of the Infield Buildings of the Advanced Photon Source," ANL Report, Light Source Note LS-78 (January 1987).

V.

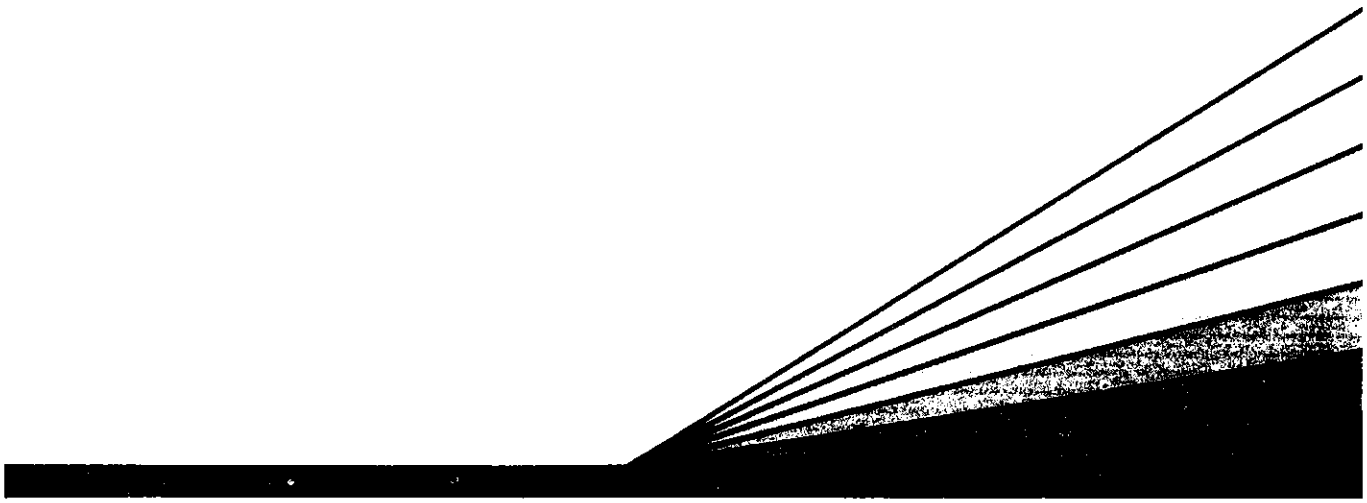

Cost & Schedule

V. 1. INTRODUCTION

All costs for the project are developed from the Work Breakdown Structure (WBS). The WBS encompasses all elements of the construction phase from design to end of construction. The accelerator facility technical components and the initial set of beam lines were designed and cost estimated by ANL personnel. The conventional facility designs were developed by ANL staff and the architect/engineering firm of Lester B. Knight and Associates, and cost estimated by the construction consulting firm of Hanscomb Associates, Inc.

The WBS in Table V.1-1 shows the project at Level 1. Level 2, the responsibility and functional level, groups functionally identifiable items of the project. Also included in this level are project management, contingency, and miscellaneous costs such as Laboratory overhead and the materials and service expenses of the Laboratory staff. Level 3 in the WBS identifies major components of the facility, such as the linac, storage ring technical components, photon beam line, etc. The Engineering, Design, and Inspection (ED&I) costs for each Level 2 item are shown in Level 3.

The cost estimates include all costs incurred after project approval. The project scope includes the accelerator facility, an initial complement of 15 beam lines, 12 insertion device systems, conventional facilities, and associated engineering, design and inspection, and project management. The preconstruction R&D and the preoperational activities required for commissioning the facility and/or readying the scientific research program are not included in the estimate.

The time estimates for the conventional facilities engineering, design, and construction and the beneficial occupancy date of each building were generated by the A/E firm of Lester B. Knight and Associates. The beneficial occupancy dates are used to set schedules for activities related to the technical components. The schedule assumes availability of FY 1988 preconstruction R&D funds.

Table V.1-1

Complete Work Breakdown Structure

WBS Code	Element Description
1	ANL 7-GeV Advanced Photon Source
1.1	Project Management
1.1.1	Project Direction
1.1.1.1	Project Administration
1.1.1.2	Manpower Management
1.1.1.3	Cost Control
1.1.1.4	Schedule Control
1.1.1.5	Procurement Coordination
1.1.1.6	Lab. Support Services Coordination
1.1.2	Technical
1.1.2.1	Project Coordination
1.1.2.2	QA Coordination
1.1.2.3	Safety
1.1.2.4	Environmental Assurance
1.1.2.5	Construction Management
1.2	Injector
1.2.1	Linac
1.2.1.1	Linac Injector
1.2.1.1.1	Gun Assembly
1.2.1.1.1.1	Gun Enclosure
1.2.1.1.1.2	Electron Gun
1.2.1.1.1.3	Pulser
1.2.1.1.1.4	Current Transformer (Pulse)
1.2.1.1.1.5	150-kV Power Supply
1.2.1.1.1.6	Gun Filament Power Supply
1.2.1.1.1.7	Vacuum Valve
1.2.1.1.2	Lens and Power Supply
1.2.1.1.3	Prebuncher
1.2.1.1.3.1	Prebuncher I
1.2.1.1.3.2	Prebuncher II
1.2.1.1.3.3	Phase Shifter
1.2.1.1.4	Main Buncher
1.2.1.1.4.1	Tapered Waveguide
1.2.1.1.4.2	Tapered Waveguide Cooling System
1.2.1.2	Accelerator Cavities
1.2.1.2.1	Waveguides
1.2.1.2.2	RF Windows
1.2.1.2.3	Waveguide Cooling
1.2.1.3	RF Power System
1.2.1.3.1	Modulators and Power Supplies

Table V.1-1

(Cont'd)

WBS Code	Element Description
1.2.1.3.2	Klystron Assembly
1.2.1.3.3	RF Power Transmission
1.2.1.3.3.1	Power Splitter
1.2.1.3.3.2	Magic T
1.2.1.3.3.3	High-Power Phase Shifter
1.2.1.3.3.4	RF Power Water Load
1.2.1.3.3.5	Transmission Waveguide
1.2.1.3.3.6	RF Phase Measurement Equipment
1.2.1.3.3.7	SLED Cavities
1.2.1.3.3.8	SLED Electronics
1.2.1.3.3.9	Flexible Sections
1.2.1.3.3.10	Recirculator
1.2.1.3.3.11	Bidirectional Couplers
1.2.1.3.3.12	Power Meters
1.2.1.4	RF Control-Triggering Systems
1.2.1.4.1	Ultrastable Oscillator
1.2.1.4.2	Trigger Generator
1.2.1.4.3	RF Amplifier
1.2.1.4.3.1	Modulator and Power Supplies
1.2.1.4.3.2	Klystron Assembly
1.2.1.4.4	Low Power Phase Shifters
1.2.1.4.5	Phase Control System
1.2.1.5	Positron Convertor
1.2.1.5.1	Retractable Target
1.2.1.5.2	High Field Focusing Coil
1.2.1.6	Vacuum
1.2.1.6.1	Vacuum Ion Pumps
1.2.1.6.2	Turbo Pumps
1.2.1.6.3	Vacuum Valves
1.2.1.6.4	Vacuum Lines
1.2.1.6.5	Gauges and Controls
1.2.1.7	Monitoring and Control
1.2.1.7.1	Network Infrastructure
1.2.1.7.2	Linac Klystron Nodes
1.2.1.7.3	Linac Diagnostic Node
1.2.1.7.4	Linac Timing System Driver
1.2.1.7.5	Cable X-Bar Plant
1.2.1.7.6	Local Control Consoles
1.2.1.8	Beam Diagnostics
1.2.1.8.1	Current Monitor
1.2.1.8.2	Beam Position and Phase

Table V.1-1

(Cont'd)

WBS Code	Element Description
1.2.1.8.3	Fluorescent Screens
1.2.1.8.4	Loss Monitors
1.2.1.9	Safety - Interlocks
1.2.1.9.1	Controlled Access Zone
1.2.1.9.2	Area Radiation Monitor
1.2.1.9.3	Miscellaneous Interlocks
1.2.1.10	Beam Line
1.2.1.10.1	Vacuum Chambers
1.2.1.10.2	Beam Windows
1.2.1.11	Helmholtz Coils
1.2.1.11.1	Supports
1.2.1.11.2	Power Supply
1.2.1.11.3	Shunts
1.2.1.11.4	Helmholtz Coils
1.2.1.12	Earth Field Coils
1.2.1.12.1	Coils
1.2.1.12.2	Power Supply
1.2.1.13	Steering Coils
1.2.1.13.1	Coils
1.2.1.13.2	Power Supply
1.2.1.14	Quadrupole Magnets and Power Supplies
1.2.1.14.1	1.5-Inch Quadrupole Magnet
1.2.1.14.2	Power Supply
1.2.1.14.3	6-Inch Quadrupole Magnets
1.2.1.14.4	6-Inch Power Supply
1.2.1.15	Solenoid
1.2.1.15.1	Solenoid Coil
1.2.1.15.2	Power Supply
1.2.1.16	Support and Alignment
1.2.1.16.1	Equipment
1.2.1.17	Supplemental Shielding
1.2.1.17.1	Positron Convertor Shielding
1.2.2	Injector Synchrotron
1.2.2.1	Magnets
1.2.2.1.1	Dipoles
1.2.2.1.2	Quadrupole
1.2.2.1.3	Sextupole
1.2.2.1.4	Injection Septum
1.2.2.1.5	Injection Kicker
1.2.2.1.6	Extraction Septum (ac)
1.2.2.1.7	Extraction Septum (dc)

Table V.1-1

(Cont'd)

WBS Code	Element Description
1.2.2.1.8	Extraction Kicker
1.2.2.1.9	Supports
1.2.2.1.10	Correction Magnet
1.2.2.1.11	Magnet Interlocks
1.2.2.1.12	Magnet Wiring & Installation
1.2.2.1.13	Magnet Cooling Installation
1.2.2.1.14	Magnet Measurements
1.2.2.1.15	Magnet ED&I
1.2.2.2	Power Supplies
1.2.2.2.1	Dipole Power Supply
1.2.2.2.2	Quadrupole Power Supply
1.2.2.2.3	Sextupole Power Supply
1.2.2.2.4	Injection Septum Power Supply
1.2.2.2.5	Injection Kicker Power Supply
1.2.2.2.6	Extraction Septum (ac) Power Supplies
1.2.2.2.7	Extraction Septum (dc) Power Supplies
1.2.2.2.8	Extraction Kicker
1.2.2.2.9	Correction Magnets
1.2.2.2.10	Installation and Wiring
1.2.2.2.11	Power Supply ED&I
1.2.2.3	Vacuum
1.2.2.3.1	Vacuum Chamber
1.2.2.3.1.1	Stainless Steel Chamber
1.2.2.3.1.2	Extraction Vacuum Chamber
1.2.2.3.2	Pumping
1.2.2.3.2.1	Ion Pumps
1.2.2.3.2.2	Turbo Pumping Stations
1.2.2.3.3	Baking System
1.2.2.3.4	Vacuum Isolation Valves
1.2.2.3.4.1	Ring Isolation Valves
1.2.2.3.4.2	Diagnostic Isolation
1.2.2.3.5	Bellows
1.2.2.3.6	Vacuum Monitoring
1.2.2.3.6.1	Ion Gauges
1.2.2.3.6.2	Thermocouple Gauges
1.2.2.3.6.3	Penning Gauges
1.2.2.3.6.4	Gas Analyzer
1.2.2.3.6.5	Leak Detectors
1.2.2.3.7	Miscellaneous Hardware
1.2.2.3.7.1	Feedthroughs
1.2.2.3.7.2	Nuts and Bolts

Table V.1-1

(Cont'd)

WBS Code	Element Description
1.2.2.3.7.3	Seals
1.2.2.3.7.4	Flanges, etc.
1.2.2.4	RF System
1.2.2.4.1	39-MHz RF System
1.2.2.4.1.1	Cavity
1.2.2.4.1.1.1	Cavity-Coaxial Assembly
1.2.2.4.1.1.2	Cavity-Tuning Plate
1.2.2.4.1.1.3	Cavity-Coupling Loop
1.2.2.4.1.1.4	Cavity-Probes & Antennas
1.2.2.4.1.1.5	Cavity-Stand
1.2.2.4.1.1.6	Vacuum
1.2.2.4.1.2	Power Amplifier
1.2.2.4.1.3	Low-Level Controls
1.2.2.4.2	353-MHz System
1.2.2.4.2.1	Cavity
1.2.2.4.2.1.1	Cavity (353-MHz 7-cell)
1.2.2.4.2.1.2	Vacuum
1.2.2.4.2.2	RF Power System
1.2.2.4.2.2.1	Klystron and Magnet
1.2.2.4.2.2.2	Klystron Power Supplies
1.2.2.4.2.2.3	Computer Interface
1.2.2.4.2.3	Waveguide System
1.2.2.4.2.4	Low-Level RF Systems
1.2.2.4.3	RF System ED&I and Support
1.2.2.4.3.1	Engineering support
1.2.2.4.3.2	RF ED&I
1.2.2.5	Beam Diagnostics
1.2.2.5.1	Current Monitors
1.2.2.5.2	Position Monitors
1.2.2.5.3	Photon Monitor
1.2.2.5.4	Tune Measuring System
1.2.2.5.4.1	High-Frequency Pickup
1.2.2.5.4.2	Beam Excitation System
1.2.2.5.5	Beam Loss System
1.2.2.5.6	Injection Diagnostics
1.2.2.5.6.1	Fluorescent Screens
1.2.2.5.6.2	Beam Scraper System
1.2.2.6	Control and Monitoring
1.2.2.6.1	Network Infrastructure
1.2.2.6.2	High-Frequency RF Node
1.2.2.6.3	Low-Frequency RF Node

Table V.1-1

(Cont'd)

WBS Code	Element Description
1.2.2.6.4	Synchrotron (vacuum, power supplies, diag.) Node
1.2.2.6.5	Injector Front-End Computer
1.2.2.6.6	Synchrotron Timing System Driver
1.2.2.6.7	Cable X-Bar Plant
1.2.2.6.8	Local Consoles
1.2.2.7	Security - Interlocks
1.2.2.7.1	Controlled Access Zone
1.2.2.7.2	Radiation Monitors
1.2.2.7.3	Miscellaneous Interlocks
1.2.2.8	Supplemental Shielding
1.2.2.8.1	Extraction Region Shielding
1.2.3	Low-Energy Transport Line
1.2.3.1	Magnets
1.2.3.1.1	Dipole
1.2.3.1.2	Quadrupole
1.2.3.1.3	Magnet Interlocks
1.2.3.1.4	Supports
1.2.3.1.5	Magnet Wiring & Installation
1.2.3.1.6	Magnet Cooling Installation
1.2.3.2	Power Supplies
1.2.3.2.1	Dipole
1.2.3.2.2	Quadrupole
1.2.3.2.3	Installation and Wiring
1.2.3.3	Vacuum
1.2.3.3.1	Vacuum Chambers
1.2.3.3.2	Supports
1.2.3.3.3.	Valves
1.2.3.3.3.1	Valves
1.2.3.3.3.2	Fast-Acting Valve
1.2.3.3.4	Pumps
1.2.3.3.5	Gauges
1.2.3.3.6	Miscellaneous Hardware
1.2.3.4	Beam Diagnostics
1.2.3.4.1	Current Monitors
1.2.3.4.2	Position Monitors
1.2.3.4.3	Wire Scanners
1.2.3.4.4	Fluorescent Screens
1.2.3.4.5	Loss Monitors
1.2.3.5	Control and Monitoring
1.2.3.5.1	Linac > Synchrotron Beam Transport Node
1.2.3.5.2	Cable Plant

Table V.1-1

(Cont'd)

WBS Code	Element Description
1.2.3.5.3	Local Console
1.2.3.6	Security - Interlocks
1.2.3.6.1	Area Radiation Monitor
1.2.3.6.2	Safety Shutters
1.2.3.6.3	Miscellaneous Interlocks
1.2.3.7	Supplemental Shielding
1.2.3.7.1	Bending-Magnet Shielding
1.2.4	High-Energy Transport Line
1.2.4.1	Magnets
1.2.4.1.1	Dipoles
1.2.4.1.2	Quadrupole
1.2.4.1.3	Magnet Interlocks
1.2.4.1.4	Supports
1.2.4.1.5	Magnet Wiring & Installation
1.2.4.1.6	Magnet Cooling Installation
1.2.4.2	Power Supplies
1.2.4.2.1	Dipoles
1.2.4.2.2	Quadrupole (0.6 m)
1.2.4.2.3	Installation and Wiring
1.2.4.3	Vacuum
1.2.4.3.1	Vacuum Chambers
1.2.4.3.2	Supports
1.2.4.3.3	Valves
1.2.4.3.3.1	Valves
1.2.4.3.3.2	Fast-Acting Valve
1.2.4.3.4	Pumps
1.2.4.3.5	Gauges
1.2.4.3.6	Miscellaneous Hardware
1.2.4.4	Beam Diagnostics
1.2.4.4.1	Current Monitors
1.2.4.4.2	Position Monitors
1.2.4.4.3	Wire Scanners
1.2.4.4.4	Fluorescent Screens
1.2.4.4.5	Loss Monitors
1.2.4.5	Control and Monitoring
1.2.4.5.1	Synchrotron > Storage Ring Beam Transport Node
1.2.4.5.2	Cable Plant
1.2.4.5.3	Local Console
1.2.4.6	Security - Interlocks
1.2.4.6.1	Area Radiation Monitor

Table V.1-1

(Cont'd)

WBS Code	Element Description
1.2.4.6.2	Safety Shutters
1.2.4.6.3	Miscellaneous Interlocks
1.2.4.7	Supplemental Shielding
1.2.4.7.1	Bending Magnet Shielding
1.2.5	Injector ED&I
1.3	Storage Ring
1.3.1	Storage Ring Tech Component
1.3.1.1	Magnets
1.3.1.1.1	Dipoles
1.3.1.1.1.1	Dipoles
1.3.1.1.1.2	Trim Coil Windings
1.3.1.1.2	Quadrupoles
1.3.1.1.2.1	Quadrupole 0.8-m Long
1.3.1.1.2.2	Quadrupole 0.6-m Long
1.3.1.1.2.3	Quadrupole 0.5-m Long
1.3.1.1.3	Sextupoles
1.3.1.1.3.1	Sextupole
1.3.1.1.3.2	Vertical Correction Windings
1.3.1.1.4	Correction Dipoles
1.3.1.1.4.1	Horizontal Correction Dipole
1.3.1.1.4.2	Horizontal-Vertical Correction Dipole
1.3.1.1.5	Injection Magnets
1.3.1.1.5.1	Septum (ac)
1.3.1.1.5.2	Septum (dc)
1.3.1.1.5.3	Beam Bump
1.3.1.1.6	Beam Abort Magnets
1.3.1.1.6.1	Abort Kicker
1.3.1.1.6.2	Abort Septum (Permanent Magnet)
1.3.1.1.7	Magnet Interlocks
1.3.1.1.8	Magnet Supports
1.3.1.1.8.1	Section 1
1.3.1.1.8.2	Section 2
1.3.1.1.8.3	Section 3
1.3.1.1.8.4	Section 4
1.3.1.1.8.5	Section 5
1.3.1.1.9	Magnet Wiring & Installation
1.3.1.1.10	Magnet Cooling Installation
1.3.1.1.11	Magnet Measurements
1.3.1.1.12	Magnet ED&I
1.3.1.2	Power Supplies
1.3.1.2.1	Dipoles

Table V.1-1

(Cont'd)

WBS Code	Element Description
1.3.1.2.1.1	Dipole
1.3.1.2.1.2	Trim Coil
1.3.1.2.2	Quadrupoles
1.3.1.2.2.1	Quadrupole (0.8 m)
1.3.1.2.2.2	Quadrupole (0.6 m)
1.3.1.2.2.3	Quadrupole (0.5 m)
1.3.1.2.3	Sextupoles
1.3.1.2.3.1	Sextupole
1.3.1.2.3.2	Vertical Correction Windings
1.3.1.2.4	Correction Dipoles
1.3.1.2.4.1	Horizontal Correction Dipole
1.3.1.2.4.2	Horizontal-Vertical Correction Dipole
1.3.1.2.5	Injection Magnets
1.3.1.2.5.1	Septum (ac) Power Supply
1.3.1.2.5.2	Septum (dc) Power Supply
1.3.1.2.5.3	Beam Bump
1.3.1.2.6	Abort Kicker
1.3.1.2.7	Choppers
1.3.1.2.7.1	Chopper dc Power Supply (No. 1)
1.3.1.2.7.2	Chopper dc Power Supply (No. 2)
1.3.1.2.7.3	Chopper dc Power Supply (No. 3)
1.3.1.2.8	Installation and Wiring
1.3.1.2.9	Power Supply ED&I
1.3.1.3	Vacuum
1.3.1.3.1	Vacuum Chambers
1.3.1.3.1.1	Section 1
1.3.1.3.1.2	Section 2
1.3.1.3.1.3	Section 3
1.3.1.3.1.4	Section 4
1.3.1.3.1.5	Section 5
1.3.1.3.1.6	Section 6
1.3.1.3.1.7	Injection Vacuum Chamber
1.3.1.3.1.8	Abort Chamber
1.3.1.3.2	Pumping System
1.3.1.3.2.1	Primary System (NeG Strip)
1.3.1.3.2.1.1	Integrated
1.3.1.3.2.1.2	Lumped NeG Pumps
1.3.1.3.2.2	Holding and Intermediate System
1.3.1.3.2.2.1	Lumped Ion
1.3.1.3.2.2.2	Ion Pump
1.3.1.3.2.3	Roughing System

Table V.1-1

(Cont'd)

WBS Code	Element Description
1.3.1.3.2.3.1	Turbomolecular Pumps
1.3.1.3.2.3.2	Sorption Pumps
1.3.1.3.2.4	Beam Absorbers
1.3.1.3.2.4.1	Crotch
1.3.1.3.2.4.2	Distributed Absorbers
1.3.1.3.3	Bakeout System
1.3.1.3.4	Valves
1.3.1.3.4.1	Ring Isolation Valves
1.3.1.3.4.2	Beam Line Isolation Valves
1.3.1.3.4.3	Turbopump Isolation Valves
1.3.1.3.4.4	Diagnostic Isolation Valves
1.3.1.3.4.5	Interlock Gauge Isolation Valve
1.3.1.3.5	Bellows
1.3.1.3.5.1	Ring Bellows
1.3.1.3.5.2	Beam Exit Bellows
1.3.1.3.6	Vacuum Monitoring
1.3.1.3.6.1	Vacuum Gauges
1.3.1.3.6.2	Gas Analyzer
1.3.1.3.6.3	Leak Detector
1.3.1.3.7	Miscellaneous Hardware
1.3.1.3.7.1	Vacuum Seals
1.3.1.3.7.2	Feedthroughs
1.3.1.3.7.3	Nuts & Bolts
1.3.1.3.7.4	Flanges
1.3.1.4	RF System
1.3.1.4.1	353-MHz System
1.3.1.4.1.1.	Cavity
1.3.1.4.1.1.1	Shell (353-MHz Single Cell)
1.3.1.4.1.1.2	Vacuum
1.3.1.4.1.2	RF Power System
1.3.1.4.1.2.1	Klystron and Magnet
1.3.1.4.1.2.2	Klystron Power Supplies
1.3.1.4.1.2.3	Computer Interface
1.3.1.4.1.3	Waveguides
1.3.1.4.1.4	Low-Level RF Systems
1.3.1.4.2	Harmonic RF System
1.3.1.4.2.1	Shell (Harmonic Cavity)
1.3.1.4.2.2	RF Amplifier System
1.3.1.4.2.3	Waveguides
1.3.1.4.2.4	Amplitude & Phase Computer Control
1.3.1.4.3	RF ED&I and Support

Table V.1-1

(Cont'd)

WBS Code	Element Description
1.3.1.4.3.1	RF Engineering Support
1.3.1.4.3.2	ED&I
1.3.1.5	Beam Diagnostics
1.3.1.5.1	Beam Position
1.3.1.5.2	Current Monitor
1.3.1.5.3	Photon Monitor
1.3.1.5.3.1	Bending Magnet Photon Monitoring Station
1.3.1.5.3.2	ID Photon Monitoring Station
1.3.1.5.4	Special Beam Studies
1.3.1.5.5	Beam Loss System
1.3.1.5.6	Transverse Damper
1.3.1.5.7	Beam Scraper System
1.3.1.5.8	Fluorescent Screens
1.3.1.6	Control and Monitoring
1.3.1.6.1	Network Infrastructure
1.3.1.6.2	RF Nodes
1.3.1.6.3	Power Supply Node
1.3.1.6.4	Diagnostic Nodes
1.3.1.6.5	Storage Ring Nodes
1.3.1.6.6	Storage Ring Front-End Computer
1.3.1.6.7	Storage Ring Timing System Driver
1.3.1.6.8	Cable X-Bar Plant
1.3.1.6.9	Loop Processors
1.3.1.6.10	Local Consoles
1.3.1.7	Security - Interlocks
1.3.1.7.1	Controlled Access Zone
1.3.1.7.2	Area Radiation Monitor
1.3.1.7.3	Miscellaneous Interlocks
1.3.1.8	Supplemental Shielding
1.3.1.8.1	Injection Region Shielding
1.3.1.8.2	Lead Collar
1.3.1.8.3	Uninstrumented Photon Port
1.3.1.8.4	Photon Beam Exit Ports
1.3.1.8.5	Beam Dump Shielding
1.3.2	Storage Ring ED&I
1.4	Insertion Devices & Beam Lines
1.4.1	VHR Inelastic Scattering
1.4.1.1	20-keV Undulator
1.4.1.2	Undulator Front End
1.4.1.3	Premonochromator Station
1.4.1.4	Monochromator

Table V.1-1

(Cont'd)

WBS Code	Element Description
1.4.1.5	Experimental Station
1.4.1.6	Beam Transport
1.4.1.7	Data Acquisition and Control
1.4.2	Intermediate Resolution Inelastic Scattering
1.4.2.1	8-keV Undulator
1.4.2.2	Undulator Front End
1.4.2.3	Premonochromator Station
1.4.2.4	Mirror
1.4.2.5	Experimental Station
1.4.2.6	Beam Transport
1.4.2.7	Data Acquisition and Control
1.4.3	Small Angle X-ray Scattering
1.4.3.1	14-keV Undulator
1.4.3.2	Undulator Front End
1.4.3.3	Premonochromator Station
1.4.3.4	Monochromator
1.4.3.5	Experimental Station
1.4.3.6	Beam Transport
1.4.3.7	Data Acquisition and Control
1.4.4	Advanced X-ray Photoelectron Spectroscopy
1.4.4.1	1-keV Undulator
1.4.4.2	Undulator Front End
1.4.4.3	Slit Assembly
1.4.4.4	Mirror
1.4.4.5	Monochromator
1.4.4.6	Experimental Station
1.4.4.7	Beam Transport
1.4.4.8	Data Acquisition and Control
1.4.5	Magnetic Elastic Scattering
1.4.5.1	14-keV Undulator
1.4.5.2	Undulator Front End
1.4.5.3	Premonochromator Station
1.4.5.4	Monochromator
1.4.5.5	Experimental Station
1.4.5.6	Beam Transport
1.4.5.7	Data Acquisition and Control
1.4.6	Nuclear Bragg Scattering
1.4.6.1	14-keV Undulator
1.4.6.2	Undulator Front End
1.4.6.3	Premonochromator Station
1.4.6.4	Monochromator

Table V.1-1

(Cont'd)

WBS Code	Element Description
1.4.6.5	Experimental Station
1.4.6.6	Beam Transport
1.4.6.7	Data Acquisition and Control
1.4.7	Quick Response Metrology
1.4.7.1	14-keV Undulator
1.4.7.2	Undulator Front End
1.4.7.3	Premonochromator Station
1.4.7.4	Experimental Station
1.4.7.5	Beam Transport
1.4.7.6	Data Acquisition and Control
1.4.8	Topography/Tomography
1.4.8.1	32.5-keV Wiggler
1.4.8.2	Wiggler Front End
1.4.8.3	Premonochromator Station
1.4.8.4	Experimental Station 1
1.4.8.5	Experimental Station 2
1.4.8.6	Beam Transport
1.4.8.7	Data Acquisition and Control
1.4.9	Compton Scattering
1.4.9.1	32.5-keV Wiggler
1.4.9.2	Wiggler Front End
1.4.9.3	Premonochromator Station
1.4.9.4	Monochromator
1.4.9.5	Experimental Station
1.4.9.6	Beam Transport
1.4.9.7	Data Acquisition and Control
1.4.10	Surface X-ray Scattering
1.4.10.1	9.8-keV Wiggler
1.4.10.2	Wiggler Front End
1.4.10.3	Premonochromator Station
1.4.10.4	Mirror
1.4.10.5	Experimental Station
1.4.10.6	Beam Transport
1.4.10.7	Data Acquisition and Control
1.4.11	General Purpose Elastic X-ray Scattering
1.4.11.1	9.8-keV Wiggler
1.4.11.2	Wiggler Front End
1.4.11.3	Premonochromator Station
1.4.11.4	Mirror Assembly
1.4.11.5	Experimental Station
1.4.11.6	Beam Transport

Table V.1-1

(Cont'd)

WBS Code	Element Description
1.4.11.7	Data Acquisition and Control
1.4.12	Anomalous X-ray Scattering
1.4.12.1	9.8-keV Wiggler
1.4.12.2	Wiggler Front End
1.4.12.3	Premonochromator Station
1.4.12.4	Monochromator
1.4.12.5	Mirror Assembly
1.4.12.6	Experimental Station
1.4.12.7	Beam Transport
1.4.12.8	Data Acquisition and Control
1.4.13	Time & Space Resolved Spectroscopy
1.4.13.1	Bending Magnet Front End
1.4.13.2	Double Mirror Assembly
1.4.13.	Beam Conditioning
1.4.13.4	Experimental Station
1.4.13.5	Beam Transport
1.4.13.6	Data Acquisition and Control
1.4.14	Quick Response Variable Energy
1.4.14.1	Bending Magnet Front End
1.4.14.2	Double Mirror Assembly
1.4.14.3	Monochromator Assembly
1.4.14.4	Focusing Mirror
1.4.14.5	Experimental Station
1.4.14.6	Beam Transport
1.4.14.7	Data Acquisition and Control
1.4.15	Quick Response Variable Focus White Beam
1.4.15.1	Bending Magnet Front End
1.4.15.2	Beam Conditioning
1.4.15.3	Experimental Station
1.4.15.6	Beam Transport
1.4.15.7	Data Acquisition and Control
1.4.16	Insertion Device & Beam Line ED&I
1.5	Computer Systems
1.5.1	Central Control & Monitoring
1.5.1.1	Central Control Computer System
1.5.1.1.1	Main Frame
1.5.1.1.2	Disk Drives
1.5.1.1.3	Printers
1.5.1.1.4	Tape Drives
1.5.1.1.5	Host Terminal
1.5.1.1.6	Network Equipment

Table V.1-1

(Cont'd)

WBS Code	Element Description
1.5.1.1.7	Terminal Server Interface
1.5.1.1.8	Software Licenses
1.5.1.1.9	Software Development Terminals
1.5.1.2	Central Consoles
1.5.1.2.1	Console Computers
1.5.1.2.2	Network Equipment
1.5.1.2.3	Engineering Development Console
1.5.1.2.4	Software Licenses
1.5.1.2.5	Video Processors
1.5.1.2.6	Video Displays
1.5.1.2.7	Consoles
1.5.1.2.8	Signal Display Systems
1.5.1.2.9	Cable Plant
1.5.1.3	Ancillary Control & Monitoring Equipment
1.5.1.3.1	Signal Analysis Instrument.
1.5.1.3.2	Signal Oscilloscopes
1.5.1.3.3	Machine Access Control Consoles
1.5.1.3.3.1	Access Video Displays
1.5.1.3.3.2	Video Support Equipment
1.5.1.4	Networks
1.5.1.4.1	Network Infrastructure
1.5.1.4.2	Network Analysis Instrument.
1.5.1.5	Control System Software
1.5.2	Data Analysis Computer System
1.5.2.1	Computer Hardware
1.5.2.1.1	Host Computer System
1.5.2.1.2	Storage Devices
1.5.2.1.3	I/O Devices
1.5.2.1.4	Plotting Equipment
1.5.2.1.5	Interfacing
1.5.2.2	Host Computer Software
1.5.2.2.1	Operating System
1.5.2.2.2	Languages
1.5.2.2.3	Graphics
1.5.2.2.4	Word Processing
1.5.2.2.5	Data Management
1.5.2.2.6	Code Management
1.5.3	Computer Systems, Control & Monitoring ED&I
1.6	Technical Component Support Facilities
1.6.1	Magnet Measuring Facility
1.6.2	Survey & Alignment

Table V.1-1

(Cont'd)

WBS Code	Element Description
1.6.2.1	Optical Level
1.6.2.2	Electronic Theodolite System
1.6.2.3	Optical Calibration System
1.6.2.4	Distinvar System
1.6.2.5	Laser Interferometer System
1.6.2.6	Laser Alignment System
1.6.2.7	Calibration Bench
1.6.2.8	Tilt Sensing System
1.6.2.9	EDM System
1.6.2.10	Nylon Wire Offset System
1.6.2.11	Data Management System
1.6.2.12	Optical Tooling Equipment
1.6.2.13	Magnet Hardware
1.6.2.14	Miscellaneous Hardware
1.6.2.15	Ring Reference System
1.6.2.16	Injector & Storage Ring Alignment
1.6.3	Technical Component Support Facility ED&I
1.7	Conventional Facilities
1.7.1	Central Lab/Office Building
1.7.1.1	Office Wing
1.7.1.1.1	Foundation
1.7.1.1.2	Substructure
1.7.1.1.3	Superstructure
1.7.1.1.4	Exterior Enclosure
1.7.1.1.5	Roofing
1.7.1.1.6	Partition
1.7.1.1.7	Interior Finishes
1.7.1.1.8	Specialties
1.7.1.1.9	Conveying Systems
1.7.1.1.10	Mechanical
1.7.1.1.11	Electrical
1.7.1.1.12	Equipment
1.7.1.1.13	General Conditions
1.7.1.2	Support Wing
1.7.1.2.1	Foundation
1.7.1.2.2	Substructure
1.7.1.2.3	Superstructure
1.7.1.2.4	Exterior Enclosure
1.7.1.2.5	Roofing
1.7.1.2.6	Partition
1.7.1.2.7	Interior Finishes

Table V.1-1

(Cont'd)

WBS Code	Element Description
1.7.1.2.8	Specialties
1.7.1.2.9	Conveying Systems
1.7.1.2.10	Mechanical
1.7.1.2.11	Electrical
1.7.1.2.12	Equipment
1.7.1.2.13	General Conditions
1.7.1.3	Auditorium
1.7.1.3.1	Foundation
1.7.1.3.2	Substructure
1.7.1.3.3	Superstructure
1.7.1.3.4	Exterior Enclosure
1.7.1.3.5	Roofing
1.7.1.3.6	Partition
1.7.1.3.7	Interior Finishes
1.7.1.3.8	Specialties
1.7.1.3.9	Mechanical
1.7.1.3.10	Electrical
1.7.1.3.11	Equipment
1.7.1.3.12	General Conditions
1.7.2	Linac Building
1.7.2.1	Linac Enclosure
1.7.2.1.1	Mechanical
1.7.2.1.2	Electrical
1.7.2.1.3	Beam Enclosure
1.7.2.1.4	General Conditions
1.7.2.2	Klystron Gallery
1.7.2.2.1	Foundation
1.7.2.2.2	Substructure
1.7.2.2.3	Superstructure
1.7.2.2.4	Exterior Enclosure
1.7.2.2.5	Roofing
1.7.2.2.6	Partitions
1.7.2.2.7	Interior Finishes
1.7.2.2.8	Specialties
1.7.2.2.9	Mechanical
1.7.2.2.10	Electrical
1.7.2.2.11	Equipment
1.7.2.2.12	General Conditions
1.7.3	Synchrotron Injection Building
1.7.3.1	Foundation
1.7.3.2	Substructure

Table V.1-1

(Cont'd)

WBS Code	Element Description
1.7.3.3	Superstructure
1.7.3.4	Exterior Enclosure
1.7.3.5	Roofing
1.7.3.6	Partition
1.7.3.7	Interior Finishes
1.7.3.8	Specialties
1.7.3.9	Conveying Systems
1.7.3.10	Mechanical
1.7.3.11	Electrical
1.7.3.12	Equipment
1.7.3.13	General Conditions
1.7.4	Synchrotron Enclosure
1.7.4.1	Within Synchrotron Injection Building
1.7.4.1.1	Mechanical
1.7.4.1.2	Electrical
1.7.4.1.3	Beam Enclosure
1.7.4.1.4	General Conditions
1.7.4.2	Within Synchrotron Extraction Building
1.7.4.2.1	Mechanical
1.7.4.2.2	Electrical
1.7.4.2.3	Beam Enclosure
1.7.4.2.4	General Conditions
1.7.4.3	Exterior Synchrotron Enclosure
1.7.4.3.1	Mechanical
1.7.4.3.2	Electrical
1.7.4.3.3	Beam Enclosure
1.7.4.3.4	General Conditions
1.7.5	Synchrotron Extraction Building
1.7.5.1	Foundation
1.7.5.2	Substructure
1.7.5.3	Superstructure
1.7.5.4	Exterior Enclosure
1.7.5.5	Roofing
1.7.5.6	Partition
1.7.5.7	Interior Finishes
1.7.5.8	Specialties
1.7.5.9	Conveying Systems
1.7.5.10	Mechanical
1.7.5.11	Electrical
1.7.5.12	Equipment
1.7.5.13	General Conditions

Table V.1-1

(Cont'd)

WBS Code	Element Description
1.7.6	RF Buildings
1.7.6.1	East RF Building
1.7.6.1.1	Foundation
1.7.6.1.2	Substructure
1.7.6.1.3	Superstructure
1.7.6.1.4	Exterior Enclosure
1.7.6.1.5	Roofing
1.7.6.1.6	Partition
1.7.6.1.7	Interior Finishes
1.7.6.1.8	Specialties
1.7.6.1.9	Mechanical
1.7.6.1.10	Electrical
1.7.6.1.11	Equipment
1.7.6.1.12	General Conditions
1.7.6.2	West RF Building
1.7.6.2.1	Foundation
1.7.6.2.2	Substructure
1.7.6.2.3	Superstructure
1.7.6.2.4	Exterior Enclosure
1.7.6.2.5	Roofing
1.7.6.2.6	Partition
1.7.6.2.7	Interior Finishes
1.7.6.2.8	Specialties
1.7.6.2.9	Mechanical
1.7.6.2.10	Electrical
1.7.6.2.11	Equipment
1.7.6.2.12	General Conditions
1.7.7	Experiment Hall
1.7.7.1	Foundation
1.7.7.2	Substructure
1.7.7.3	Superstructure
1.7.7.4	Exterior Enclosure
1.7.7.5	Roofing
1.7.7.6	Interior Construction
1.7.7.7	Mechanical
1.7.7.8	Electrical
1.7.7.9	Equipment
1.7.7.10	Storage Ring Enclosure
1.7.7.11	General Conditions
1.7.8	Lab/Office Modules
1.7.8.1	East Lab/Office Module

Table V.1-1

(Cont'd)

WBS Code	Element Description
1.7.8.1.1	Foundation
1.7.8.1.2	Substructure
1.7.8.1.3	Superstructure
1.7.8.1.4	Exterior Enclosure
1.7.8.1.5	Roofing
1.7.8.1.6	Partition
1.7.8.1.7	Interior Finishes
1.7.8.1.8	Specialties
1.7.8.1.9	Mechanical
1.7.8.1.10	Electrical
1.7.8.1.11	Equipment
1.7.8.1.12	General Conditions
1.7.8.2	Southeast Lab/Office Module
1.7.8.2.1	Foundation
1.7.8.2.2	Substructure
1.7.8.2.3	Superstructure
1.7.8.2.4	Exterior Enclosure
1.7.8.2.5	Roofing
1.7.8.2.6	Partition
1.7.8.2.7	Interior Finishes
1.7.8.2.8	Specialties
1.7.8.2.9	Mechanical
1.7.8.2.10	Electrical
1.7.8.2.11	Equipment
1.7.8.2.12	General Conditions
1.7.8.3	Southwest Lab/Office Module
1.7.8.3.1	Foundation
1.7.8.3.2	Substructure
1.7.8.3.3	Superstructure
1.7.8.3.4	Exterior Enclosure
1.7.8.3.5	Roofing
1.7.8.3.6	Partition
1.7.8.3.7	Interior Finishes
1.7.8.3.8	Specialties
1.7.8.3.9	Mechanical
1.7.8.3.10	Electrical
1.7.8.3.11	Equipment
1.7.8.3.12	General Conditions
1.7.8.4	West Lab/Office Module
1.7.8.4.1	Foundation
1.7.8.4.2	Substructure

Table V.1-1

(Cont'd)

WBS Code	Element Description
1.7.8.4.3	Superstructure
1.7.8.4.4	Exterior Enclosure
1.7.8.4.5	Roofing
1.7.8.4.6	Partition
1.7.8.4.7	Interior Finishes
1.7.8.4.8	Specialties
1.7.8.4.9	Mechanical
1.7.8.4.10	Electrical
1.7.8.4.11	Equipment
1.7.8.4.12	General Conditions
1.7.9	Utility Support Building
1.7.9.1	Foundation
1.7.9.2	Substructure
1.7.9.3	Superstructure
1.7.9.4	Exterior Enclosure
1.7.9.5	Roofing
1.7.9.6	Partition
1.7.9.7	Interior Finishes
1.7.9.8	Specialties
1.7.9.9	Mechanical
1.7.9.10	Electrical
1.7.9.11	Equipment
1.7.9.12	General Conditions
1.7.10	Tunnels
1.7.10.1	Utility Tunnel
1.7.10.1.1	Mechanical
1.7.10.1.2	Electrical
1.7.10.1.3	Civil
1.7.10.1.4	General Conditions
1.7.10.2	Control Tunnel
1.7.10.2.1	Mechanical
1.7.10.2.2	Electrical
1.7.10.2.3	Civil
1.7.10.2.4	General Conditions
1.7.10.3	Vehicle Tunnel
1.7.10.3.1	Mechanical
1.7.10.3.2	Electrical
1.7.10.3.3	Civil
1.7.10.3.4	General Conditions
1.7.11	Site Development
1.7.11.1	Mechanical

Table V.1-1

(Cont'd)

WBS Code	Element Description
1.7.11.2	Electrical
1.7.11.3	Civil
1.7.11.4	General Conditions
1.7.12	Conventional Facilities EDI&A
1.8	Miscellaneous Costs
1.8.1	Lab ED&I Labor Overhead
1.8.2	Lab ED&I Labor M&S
1.9	Contingency
1.9.1	Project Management
1.9.2	Injector
1.9.3	Storage Ring
1.9.4	Insertion Device & Beam Lines
1.9.5	Computer Systems
1.9.6	Technical Component Support Facilities
1.9.7	Conventional Facilities
1.9.8	Miscellaneous Costs
1.9.9	ED&I

All cost estimates include ED&I and hardware deliverables. Fiscal Year 1987 dollars are used throughout. Crafts needed for the construction are grouped into three categories, and details of the crafts used and their rates are shown in Table V.2-1. Contingency is addressed at the estimating stage and is discussed later in this section. Escalation is added after the budget profile is applied. The rates used for this purpose come from DOE-HEP 1981, "Analysis of Cost and Price Changes," HEP 81402 and subsequent updates, and from a letter to A. Schriesheim from D. T. Goldman, "Escalation Rates for Preliminary FY 1989 Construction Project Data Sheets," dated August 11, 1986, and are shown in Table V.2-2.

The project cost detail is shown in Table V.2-3 in FY 1987 dollars. The costs are broken down into three major categories: (A) ED&I Cost, (B) Construction Cost, and (C) Contingency. Each category is further subdivided to provide detail corresponding to Level 3 of the WBS. The costs for technical components are rolled up from detailed WBS sheets generated by the ANL staff, showing all hardware and effort costs for each item from design through installation and checkout. The costs for conventional facilities are estimates generated by the construction consulting firm of Hanscomb Associates, Inc. (see Supplement B) and are based on designs by ANL staff and the A/E firm of Lester B. Knight and Associates. With regard to the costs associated with B.1.c., Insertion Devices and Beam Lines, we have designed 15 specific sample beam lines for future scientific programs. It is anticipated that in the future, as the initial scientific research program of the facility becomes firmed-up, the costs of the insertion devices and beam lines may vary. For this reason, the estimate contains about 30% contingency.

The project management costs shown in Table V.2-3 consist of three parts:

1. Project management staff effort costs.

   These are the costs of personnel involved in project direction and coordination.

2. Laboratory overhead.

   The Laboratory recovers its indirect expenses, the costs associated with administration (functions such as personnel, accounting, and procurement) and maintenance of physical facilities, by means of charges against the funds received for operations -- commonly known as operating funds -- as contrasted to (1) capital equipment funds, which are used for equipment fabrication or purchase, and (2) plant funds, which are used for construction projects. Essentially, indirect costs of the Laboratory are recovered through

Table V.2-1

Craft Code and Rate Table

	Craft Code	Rate ($/h)
Manufacturing/Fabrication/Assembly/Test:*		
Technician (Assy,tst,etc.), relatively unskilled	T1	22.89
Technician (Assy,tst,etc.), experienced/skilled	T2	34.86
Shops (Average capability machinists,fab.,etc.)	S1	40.32
Shops (Specialized,precision,high tech,etc.)	S2	45.78
Factory Support (Parts handling,inspectors,QA,etc.)	F1	34.86
Factory Support (Superv,mangrs,prod.engr.,etc)	F2	45.78
Installation: (Assumes "Davis-Bacon")*		
Plumber, Steam Fitter, Sheet Metal	IP	40.32
Electrician	IE	37.06
Carpenter, Painter, Rigger, Crane Operator	IC	38.32
Laborer	IL	28.35
Technician	IT	28.35
Technical Engineering/Design/Inspection:**		
Physicist	PH	34.86
Engineer (Mechanical and Electrical)	EN	34.86
Computer Designer (Software)	SW	34.86
Designer/Coordinator	DC	22.89
Drafter	DR	17.43

*Includes hourly base pay, employee benefits, and overhead & profit for "outside" vendor or contractor.

**Includes effective hourly base pay and benefits, but does not include laboratory overhead (which is included in a separate WBS category).

Table V.2-2

Escalation Rates

Fiscal Year	Inflation (%)	Scaling Factor
1987	-	1.000
1988	4.0	1.040
1989	4.8	1.090
1990	5.3	1.148
1991	5.6	1.212
1992	6.1	1.286
1993	6.1	1.364

a charge of 22%* applied to all in-house direct operating costs. Construction projects, which usually add only incrementally to indirect expenses, contribute a smaller amount to cover indirect expenses. Under Laboratory policy, this is achieved by a charge of 22%, the in-house rate, applied only to the effort costs of Laboratory project management and ED&I personnel.

Therefore, the indirect charge to be borne by this construction project is tentatively calculated as 22% of the effort cost of Laboratory project management and ED&I personnel.

3. Materials and services costs.

   These are the M&S costs of the Laboratory direct personnel in the project and are estimated to be 20% of the effort costs of those personnel.

It should be noted that inclusion of the last two items is necessitated by the fact that the craft code and craft rate shown in Table V.2-1 for EDI&A (Engineering, Design, Inspection, and Administration) personnel take into account only the hourly base pay and benefits.

Contingency costs are applied to the rates shown in Table V.2-3. The rates shown for ED&I and Technical Components are averages of the rates for the individual components and reflect the completeness of the design, uncertainties, and the variability

*Rounded from the 1987 Laboratory indirect rate of 21.65%.

of market conditions. The rate for conventional facilities is based on estimates by Hanscomb Associates, Inc.

The contents of Table V.2-3 can be rearranged to show the project cost profile by the major cost components. This is shown in Table V.2-4.

The cost schedule that takes into account escalation and budget time profile is discussed in Section V.4.

Table V.2-3

Project Cost Breakdown by Major Categories (FY 1987 M$)

A.	Engineering, Design, & Inspection			36.910
	1. Technical Components		21.419	
	a. Injector	4.726		
	b. Storage Ring	5.344		
	c. Insertion Devices & Beam Lines	5.935		
	d. Computer Systems, Control & Monitoring	4.510		
	e. Technical Component Support Facilities	0.904		
	2. Conventional Facilities EDI&A (17%)		15.491	
B.	Construction Costs			224.916
	1. Technical Components		115.426	
	a. Injector	20.185		
	b. Storage Ring	51.804		
	c. Insertion Devices & Beam Lines	35.131		
	d. Computer Systems, Control & Monitoring	4.202		
	e. Technical Component Support Facilities	4.104		
	2. Conventional Facilities		91.125	
	a. Central Lab/Office Building	20.630		
	b. Linac Building	1.235		
	c. Synchrotron Injection Building	1.900		
	d. Synchrotron Enclosure	2.040		
	e. Synchrotron Extraction Building	0.790		
	f. RF Buildings	2.150		
	g. Experimental Hall	36.065		
	h. Lab/Office Modules	7.860		
	i. Utility Support Building	6.820		
	j. Tunnels	2.165		
	k. Site Development	9.470		
	3. Project Management		18.366	
	a. Management Staff Cost	6.599		
	b. Laboratory ED&I Overhead Cost	6.164		
	c. ANL ED&I Material and Service (M&S) Cost	5.603		
C.	Contingency			57.885
	1. ED&I (25%)		9.227	
	2. Technical Components (23%)		26.759	
	3. Conventional Facilities (20%)		18.225	
	4. Project Management (20%)		3.673	
TOTAL PROJECT CONSTRUCTION COST (FY 1987 M$)				319.711

Table V.2-4

Project Cost Breakdown by WBS Code

WBS Code	Description	Cost in FY87 M$		
1	ANL 7-GeV APS Project			319.711
1.1	Project Management		6.599	
1.1.1	Project Direction	3.570		
1.1.2	Technical	3.029		
1.2	Injector		24.911	
1.2.1	Linac	6.504		
1.2.2	Injector Synchrotron	12.008		
1.2.3	Low Energy Beam Transport	0.597		
1.2.4	High Energy Beam Transport	1.076		
1.2.5	Injector ED&I	4.726		
1.3	Storage Ring		57.148	
1.3.1	Technical Components	51.804		
1.3.2	Storage Ring ED&I	5.344		
1.4	Insertion Devices & Beam Lines		41.066	
1.4.1	VHR Inelastic Scattering	2.698		
1.4.2	Intermediate Resolution Inelastic Scattering	2.674		
1.4.3	Small Angle X-ray Scattering	2.959		
1.4.4	Advanced X-ray Photoelectron Spectroscopy	2.991		
1.4.5	Magnetic Elastic Scattering	2.729		
1.4.6	Nuclear Bragg Scattering	2.834		
1.4.7	Quick Response Metrology	2.537		
1.4.8	Topography/Tomography	3.938		
1.4.9	Compton Scattering	2.197		
1.4.10	Surface X-ray Scattering	2.001		
1.4.11	General Purpose Elastic X-ray Scattering	1.951		
1.4.12	Anomalous X-ray Scattering	2.294		
1.4.13	Time & Space Resolved Spectroscopy	1.195		
1.4.14	Quick Response Variable Energy	1.300		
1.4.15	Quick Response Variable Focus White Beam	0.833		
1.4.16	Insertion Device & Beam Line ED&I	5.935		
1.5	Computer Systems, Controls & Monitoring		8.712	
1.5.1	Central Control & Monitoring	1.746		
1.5.2	Data Analysis Computer System	2.456		
1.5.3	Computer Systems, Controls & Mon. ED&I	4.510		

Table V.2-4

(Cont'd)

1.6	Technical Component Support Facilities		5.007
1.6.1	Magnet Measuring Facility	1.073	
1.6.2	Survey & Alignment Facility	3.030	
1.6.3	Tech. Component Support Facility ED&I	0.904	
1.7	Conventional Facilities		106.616
1.7.1	Central Lab/Office Building	20.630	
1.7.2	Linac Building	1.235	
1.7.3	Synchrotron Injection Building	1.900	
1.7.4	Synchrotron Enclosure	2.040	
1.7.5	Synchrotron Extraction Building	0.790	
1.7.6	RF Buildings	2.150	
1.7.7	Experiment Hall	36.065	
1.7.8	Lab/Office Modules	7.860	
1.7.9	Utility Support Building	6.820	
1.7.10	Tunnels	2.165	
1.7.11	Site Development	9.470	
1.7.12	Conventional Facilities EDI&A	15.491	
1.8	Miscellaneous Costs		11.767
1.8.1	ANL ED&I Labor Overhead Cost	6.164	
1.8.2	ANL ED&I M&S Cost	5.603	
1.9	Contingency		57.885
1.9.1	Project Management	1.320	
1.9.2	Injector	3.626	
1.9.3	Storage Ring	11.053	
1.9.4	Insertion Devices & Beam Lines	10.207	
1.9.5	Computer Systems	0.848	
1.9.6	Technical Component Support Facilities	1.026	
1.9.7	Conventional Facilities	18.225	
1.9.8	Miscellaneous Costs	2.353	
1.9.9	ED&I	9.227	

The schedule is based on the assumptions that the construction project starts in FY 1989, and that there are sufficient funds to carry out preconstruction R&D and construction planning, including environmental assessment and site development design, in FY 1986 to FY 1988. The preconstruction R&D activities are described in Appendix B. In addition, the following concepts have been incorporated in scheduling of the construction:

- For optimum project efficiency, front loading of the project is exercised wherever possible.
- In order to make the best possible foundations for the machines, all of the building floor slabs are constructed in nonwinter months.
- Design, construction, and installation periods for technical components used in the scheduling are based on experiences of accelerator personnel in this Laboratory as well as those at other laboratories, together with vendor quotations.
- All technical components of a subsystem to be installed in a building will be assembled and tested beforehand in order to maintain an optimum installation schedule with a relatively uniform level of effort.
- Accelerator system construction is determined by using the A/E firm-supplied conventional construction schedule of beneficial occupancy.
- Sequential commissioning of three major accelerators is planned. The first accelerator to be commissioned is the linac system. Six months after the linac is commissioned, the injector synchrotron is scheduled to be commissioned. Another six months after the injector synchrotron is commissioned, the storage ring is scheduled to be commissioned.

Figure V.3-1 shows the conventional facilities schedule and Figs. V.3-2(a) and V.3-2(b) show the technical components schedule. Figure V.3-3 is the project critical path diagram for the major components of the project at Level 3 of the WBS. As the project design progresses, a more-detailed critical path analysis at Level 4 and below will be established and will be used to monitor the progress of the project. As shown in Fig. V.3-3, the commissioning of the storage ring begins at the start of FY 1993, with beam lines in "routine" operation beginning in the third quarter of FY 1993.

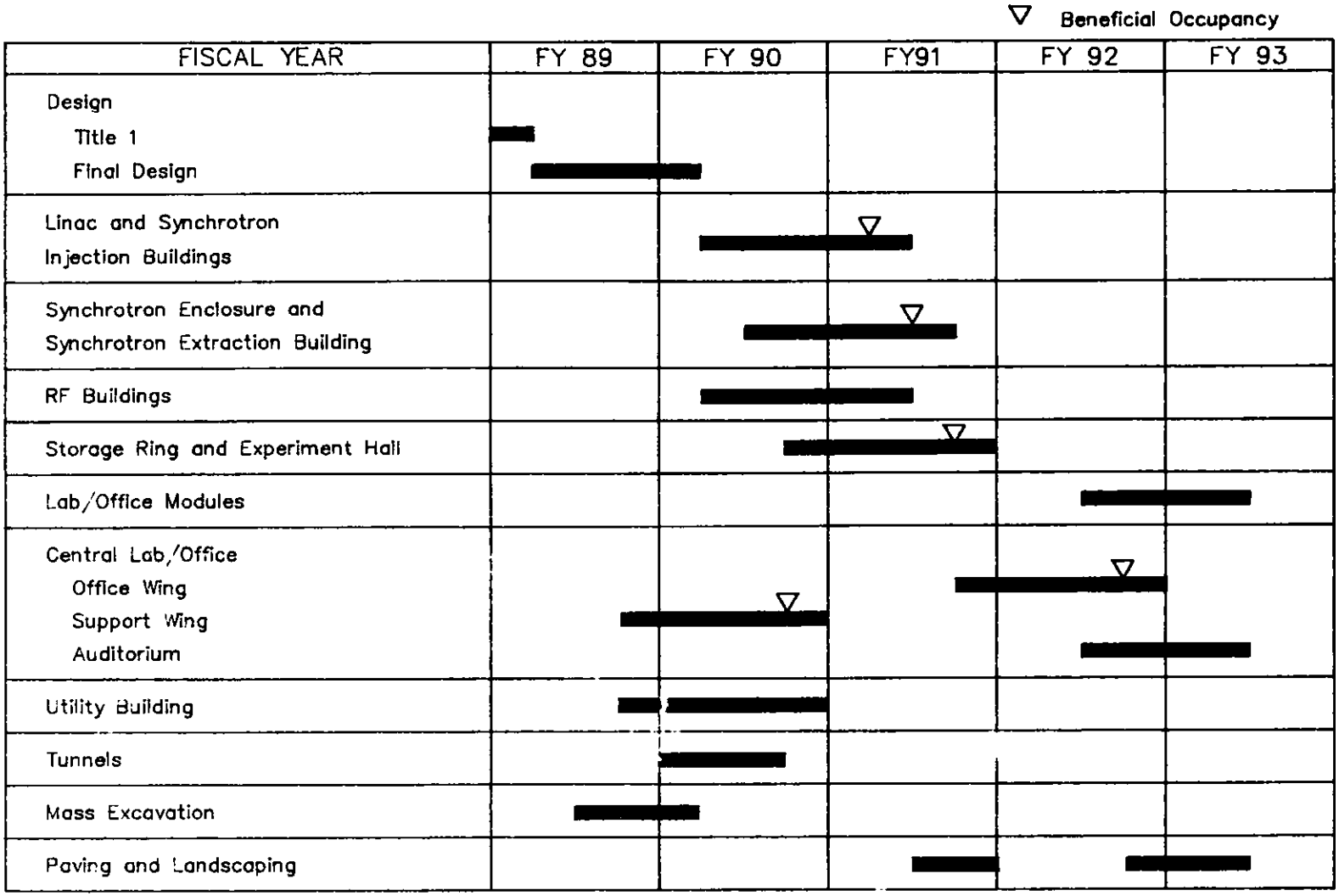

Figure V.3-1
Conventional facilities schedule.

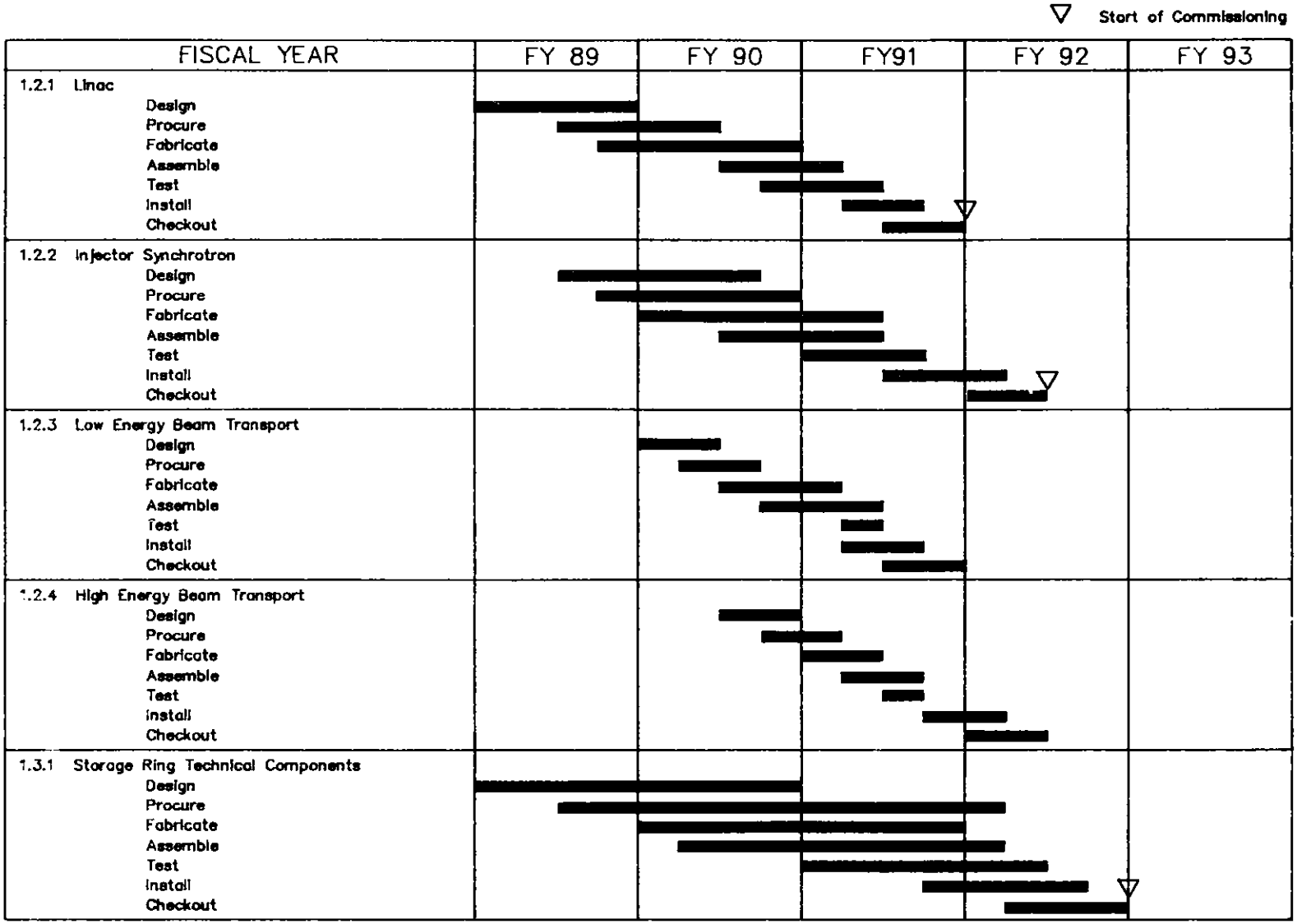

Figure V.3-2(a)
Technical components schedule.

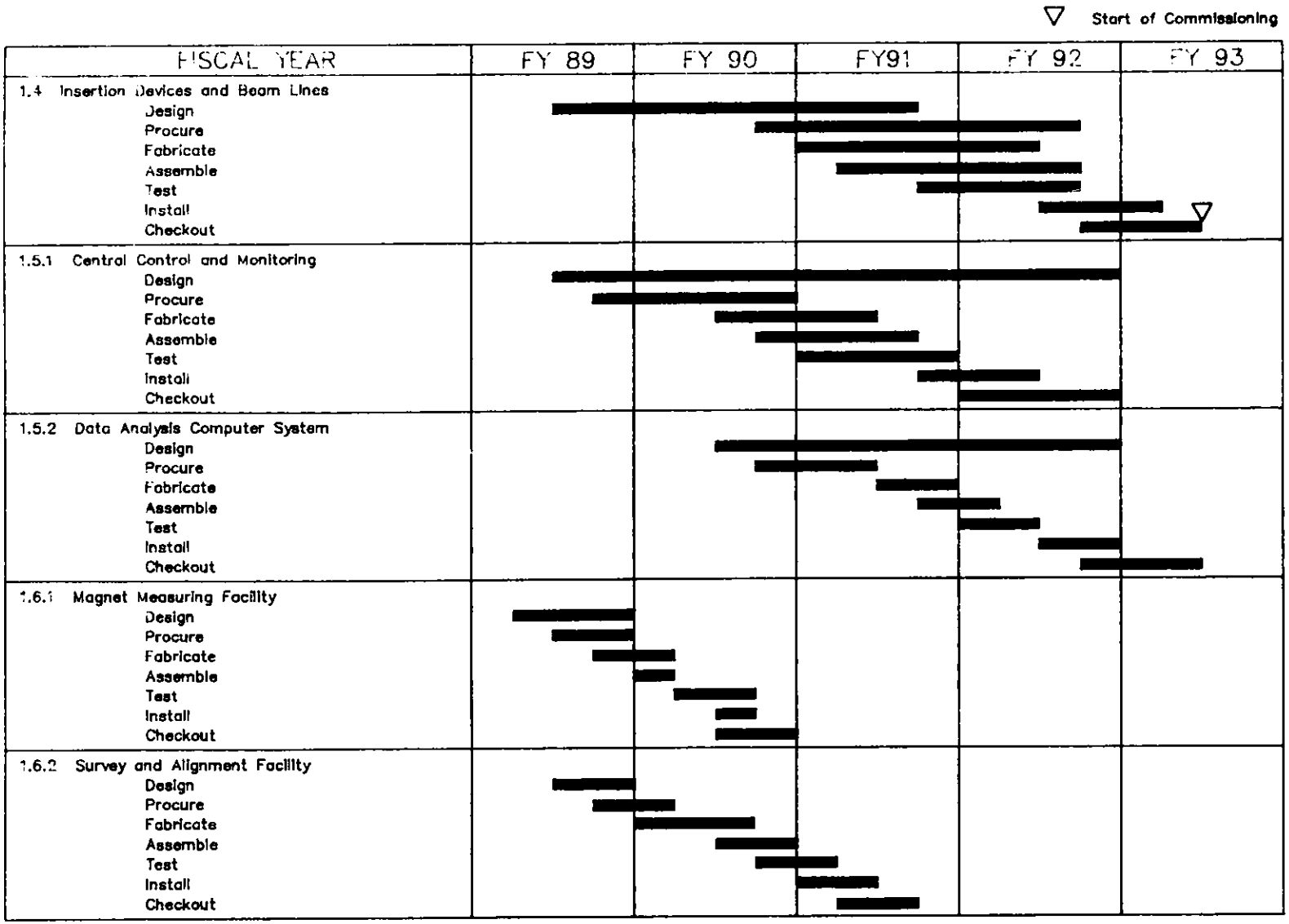

Figure V.3-2(b)
Technical components schedule.

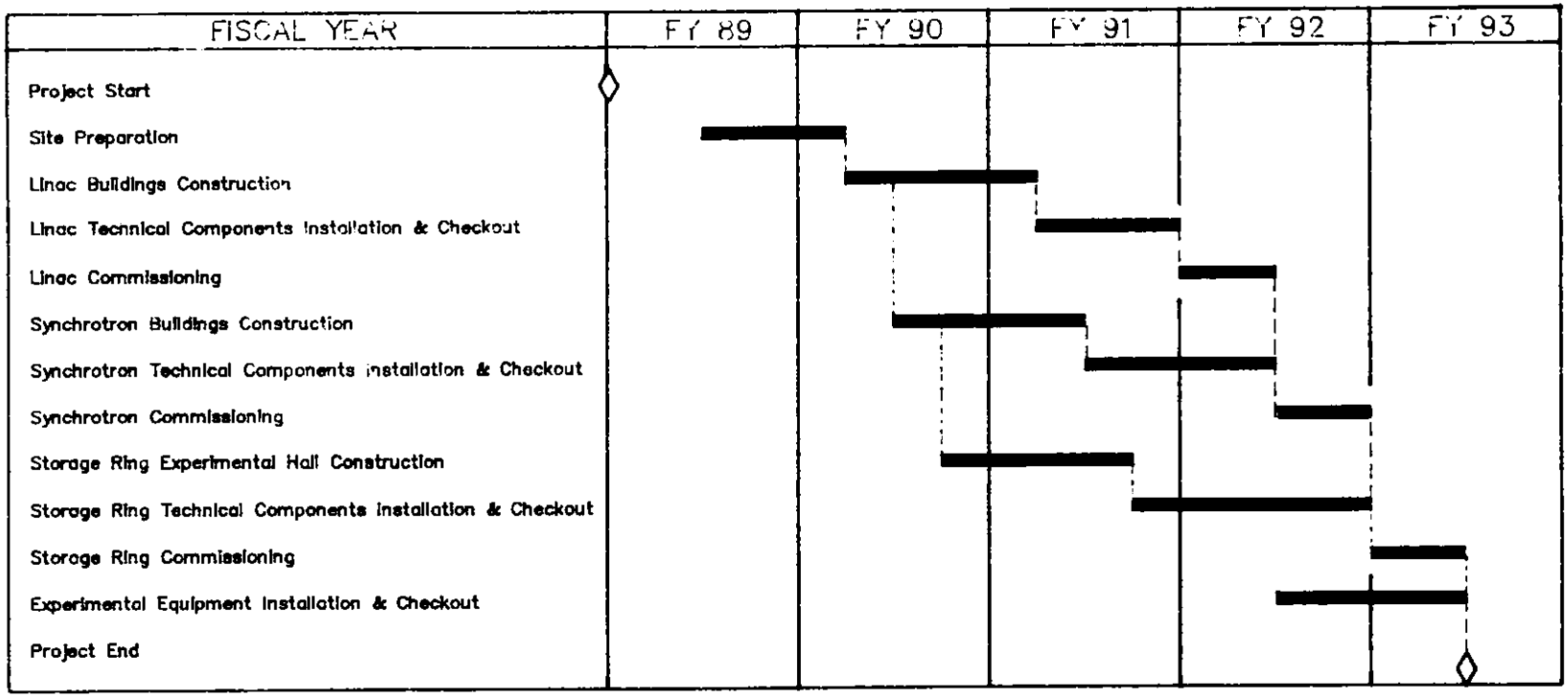

Figure V.3-3
Project critical path.

Using the detailed WBS cost estimates, which contain the costs of materials and labor of various crafts for each of the components together with the technical components construction schedule described in the previous section, technical component manpower needs per quarter year have been estimated as a function of time. These are shown in Fig. V.4-1. Material costs based on the procurement schedule and conventional facility construction costs based on the A/E schedule are similarly projected for each quarter year.

The budget profile of the project is obtained from

- the manpower distribution (Fig. V.4-1),
- materials costs distribution,
- adding contingency proportional to the part of the task or activity not completed, and
- incorporating the escalation shown in Table V.2-2.

This profile is shown in Fig. V.4-2 and Table V.4-1. Figure V.4-3 shows the cumulative budget distribution for the construction project, taken to extend from FY 1989 to FY 1993. The contents of Table V.4-1 are broken down into (1) Plant and Capital Equipment (PACE) -- construction and (2) PACE -- ED&I costs. The breakdown follows the DOE guidelines established by the Engineering, Design and Inspection Steering Committee of the Department of Energy Committee for Cost Methods Development and described in a report dated August 23, 1985.

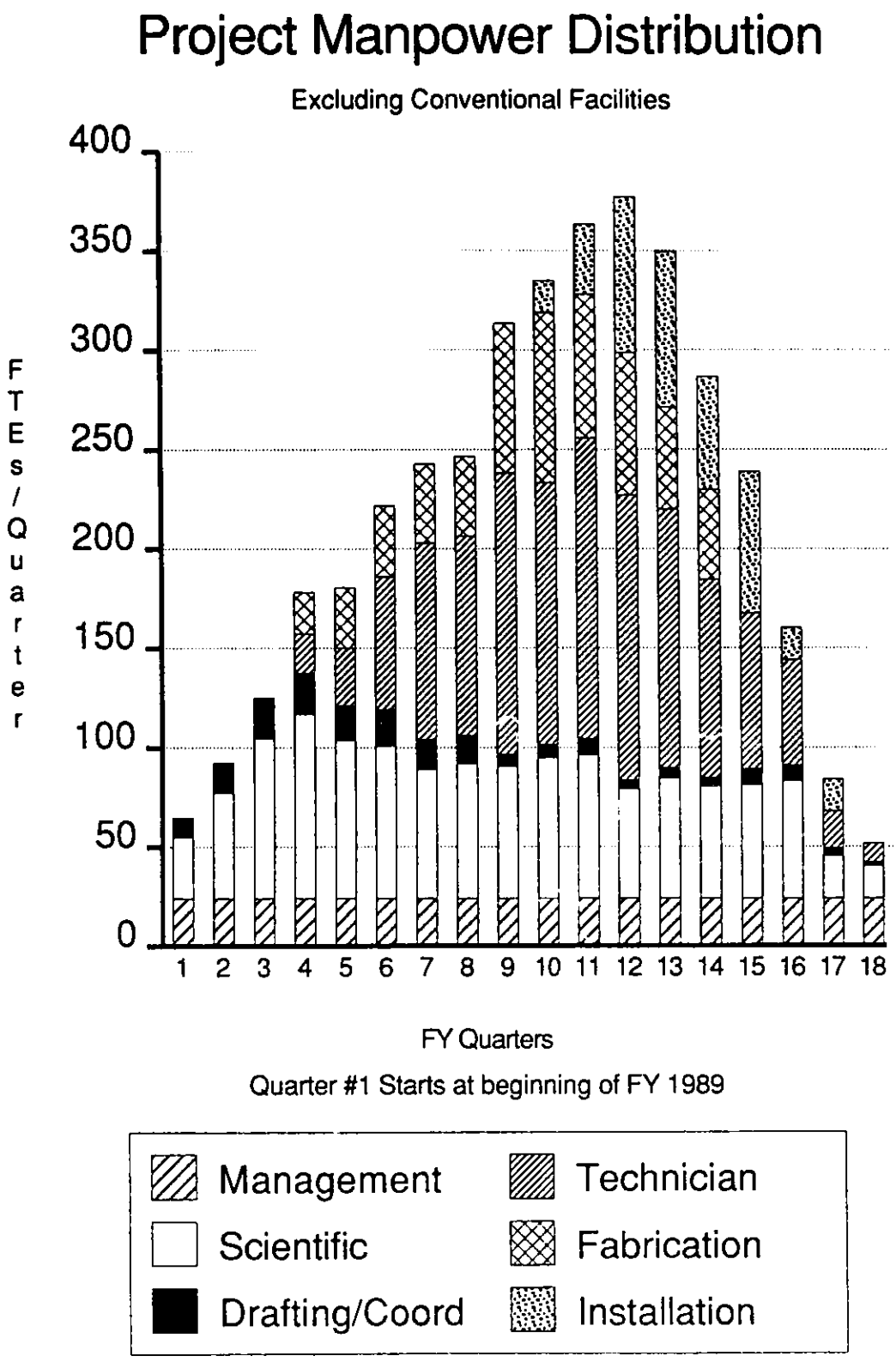

Figure V.4-1
Effort distribution.

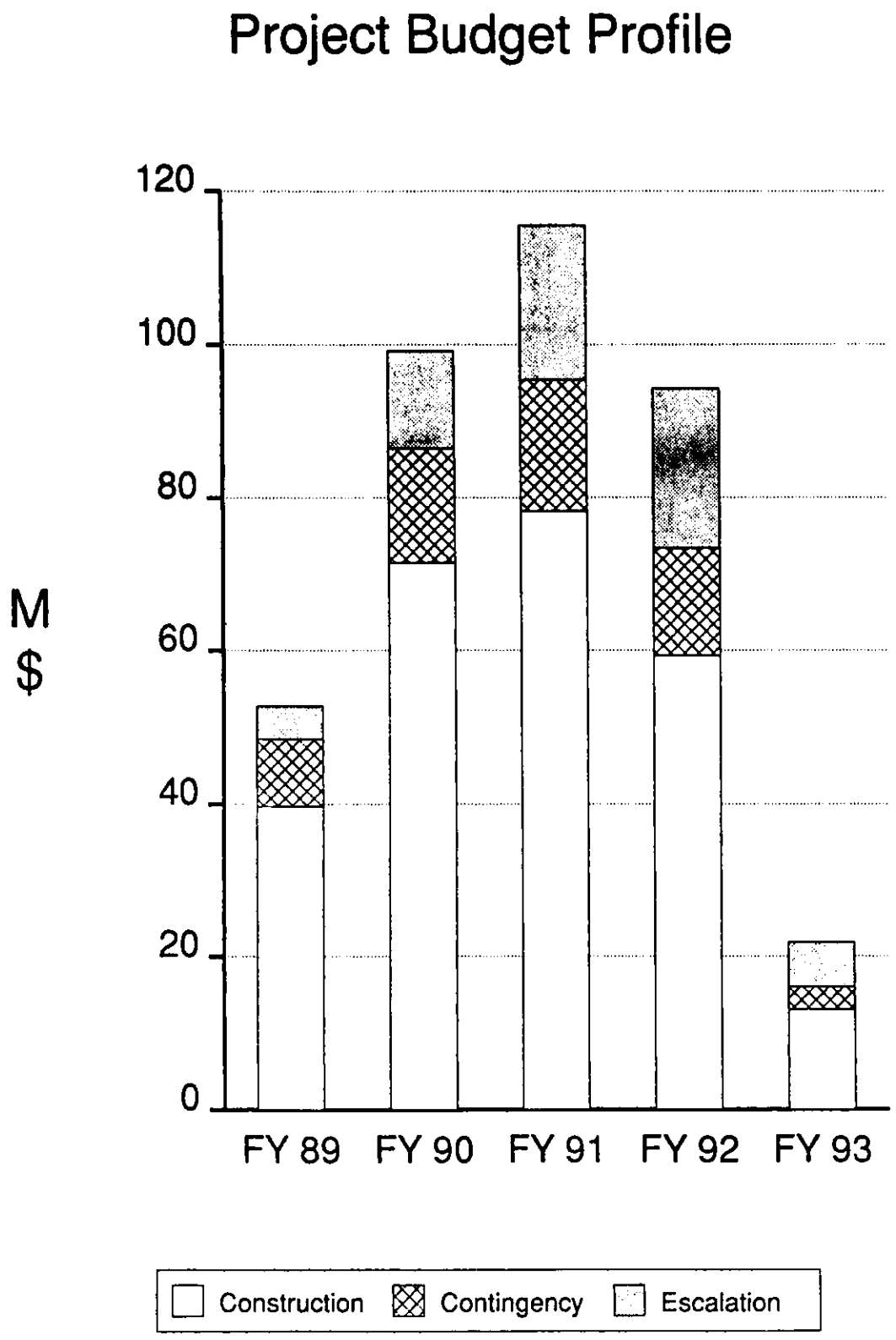

Figure V.4-2
Project budget profile.

Table V.4-1

Project Cost Breakdown by FY (M$)

	FY89	FY90	FY91	FY92	FY93	Total
PACE - ED&I	13.48	9.19	7.41	5.58	1.26	36.91
PACE - Construction	26.22	62.29	70.84	53.74	11.82	224.92
Subtotal	39.70	71.48	78.25	59.32	13.07	261.83
Contingency	8.73	14.99	17.17	14.04	2.96	57.88
Subtotal	48.43	86.47	95.41	73.36	16.03	319.71
Escalation	4.35	12.77	20.23	20.97	5.84	64.17
TOTAL	52.79	99.24	115.64	94.34	21.87	383.88

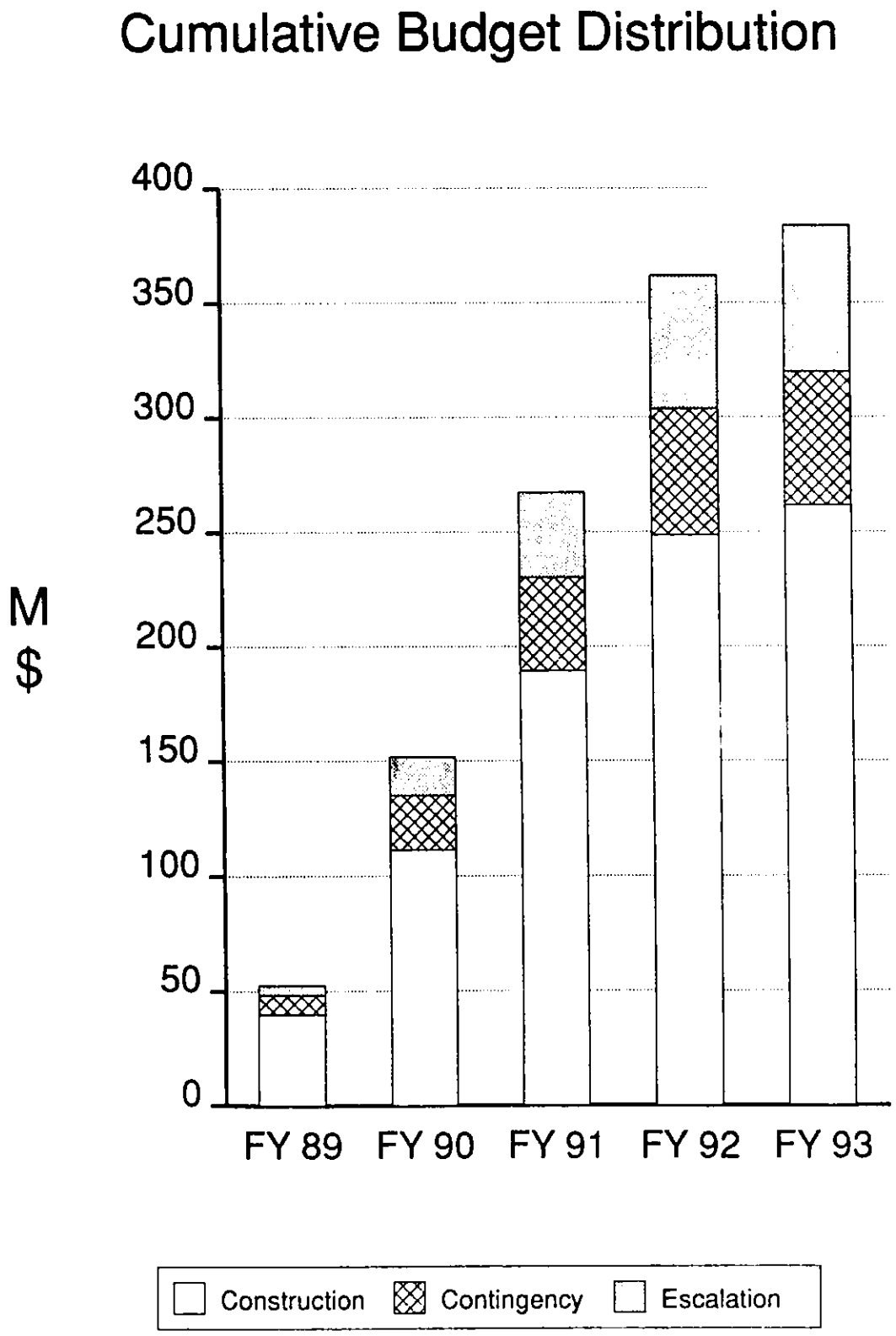

Figure V.4-3
Cumulative budget distribution.

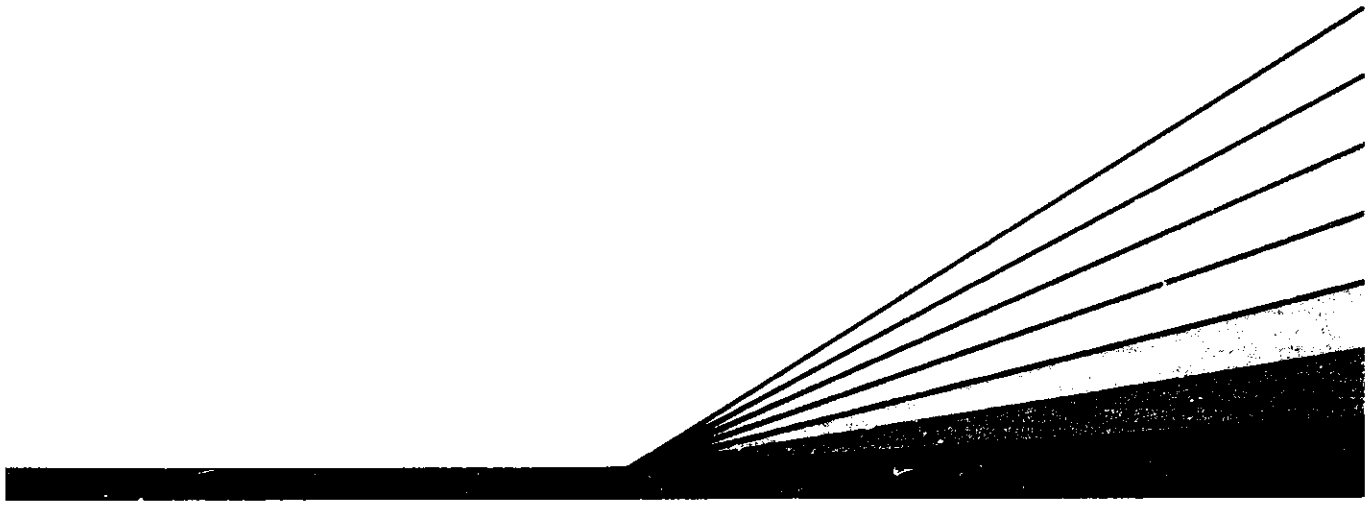

Appendices

APPENDIX A

PARAMETER LIST

All parameters are at nominal operating conditions unless otherwise noted.

---

1. Storage Ring Performance Parameters

Nominal energy (GeV)	7.0
Nominal circulating current, multibunch (mA)	100
Nominal number of stored positrons, multibunch	2.21×10^{12}
Maximum circulating current, multibunch (mA)	300
Maximum number of stored positrons, multibunch	6.62×10^{12}
Maximum circulating current, single bunch (mA)	5
Number of stored positrons, single bunch	1.10×10^{11}
Number of bunches	1-60
Natural emittance (m-rad)	8×10^{-9}
Natural energy spread, rms	9.6×10^{-4}
Energy spread, rms, at max. bunch current	2.9×10^{-3}
Bunch length, rms, natural (mm)	5.8
Bunch length, 2×rms, natural (ps)	38.7
Bunch length, 2×rms, maximum bunch current (ps)	116
Peak energy (GeV)	7.7
Beam lifetime, mean-life (hr)	
Gas scat., 8-mm vert. gap, 1 nTorr 75% H_2 & 25% CO	76
Touschek, maximum bunch current	190
Filling rate (no. e^+/s)	1×10^{10}
Filling time	
Multibunch, to 100 mA (min)	3.7
Single bunch, per 5 mA bunch (s)	11

2. Storage Ring Lattice and Orbit Parameters

Circumference (m)	1060
Revolution time (μs)	3.5358
Revolution frequency (MHz)	0.2828
Harmonic number	1248
Radio frequency (MHz)	352.96
Number of periods	40
Insertion straight section length (m)	6.2
Length available for insertion device (m)	5.2
Mean radius (m)	168.7
Bending field (T)	0.599
Bending radius (m)	38.9611
Maximum quadrupole strength (T/m)	18.9
Injection energy	Full energy
Injection field (T)	0.599

Number of dipoles per period	2
Number of quadrupoles per period	10
Number of chromatic sextupoles per period	3
Number of harmonic sextupoles per period	4
Magnetic lengths in 1/2 period (m)	
L=drift, M=bend, Q=quad, S=sext.	
L	3.10
Q1	0.50
L1	0.66
Q2	0.80
L21	0.13
S1	0.24
L22	0.13
Q3	0.50
L31	0.73
S2	0.24
L32	0.20
M	3.06
L41	0.20
SD	0.24
L42	0.70
Q4	0.50
L5	0.37
Q5	0.60
L6	0.23
SF	0.12
Betatron tunes	
Horizontal	35.22
Vertical	14.30
Synchrotron tune	0.0066
Synchrotron frequency (kHz)	1.88
Natural chromaticities	
Horizontal	-63.7
Vertical	-26.0
Maximum beta functions (m)	
Horizontal	22.3
Vertical	19.8
Average beta functions (m)	
Horizontal	10
Vertical	13
Beta functions at insertion symmetry points (m)	
Horizontal	13.0
Vertical	10.0
Maximum dispersion (m)	0.39
Ring acceptance (m)	
Horizontal	32.7×10^{-6}
Vertical	17.1×10^{-6}
Vertical acceptance with undulators	1.45×10^{-6}
Beam size at insertion symmetry point, rms (μm)	
Horizontal	320
Vertical, 10% emittance ratio	90

Momentum compaction	2.374×10^{-4}
Transition Gamma	64.91
Damping time (ms)	
Horizontal	9.08
Vertical	9.08
Longitudinal	4.54
Radiation loss per turn, dipoles (MeV)	5.45
Bending magnet critical energy (keV)	19.5
Radiation loss per turn, insertion devices, max. (MeV)	1.25
Number of sextupole families	
Chromatic	2
Harmonic	2
Beam elevation above floor (m)	1.5

3. Storage Ring Tolerances, rms

Quadrupole placement (m)	10^{-4}
Sextupole placement (m)	10^{-4}
Random dipole field error, $\Delta B\ell/B\ell$	10^{-4}
Random quadrupole strength error, $\Delta B'\ell/B'\ell$	10^{-4}
Random sextupole strength error, $\Delta B''\ell/B''\ell$	10^{-3}
Random dipole roll angle error (rad)	10^{-4}
Correcting-dipole current	10^{-3}

4. Storage Ring Hardware

a. Magnets and power supplies

Dipoles	
Number	80+1
No. of independent power supplies	1
Magnetic length (m)	3.06
Bending radius (m)	38.9611
Field (T)	0.6
Beam stay clear (mm)	
Horizontal	±35.0
Vertical	±20.0
Dipole trim coils	
Number	80+1
No. of independent power supplies	80
Magnetic length (m)	3.06
Field (T)	0.04
Quadrupoles, type A	
Number	80
No. of independent power supplies	80
Magnetic length (m)	0.8
Max. gradient (T/m)	19.1
Beam stay clear (mm)	
Horizontal	±35.0
Vertical	±20.0

Quadrupoles, type B	
Number	80
No. of independent power supplies	80
Magnetic length (m)	0.6
Max. gradient (T/m)	19.1
Beam stay clear (mm)	
Horizontal	±35.0
Vertical	±20.0
Quadrupoles, type C	
Number	240
No. of independent power supplies	240
Magnetic length (m)	0.5
Max. gradient (T/m)	19.1
Beam stay clear (mm)	
Horizontal	±35.0
Vertical	±20.0
Sextupoles	
Number	280
No. of independent power supplies	280
No. of chromatic families, SF, SD	2
No. in family SF	40
No. in family SD	80
No. of harmonic families, S1, S2	2
No. in family S1	80
No. in family S2	80
Magnetic length (m)	0.24
Max. strength (T/m^2)	490
Beam stay clear (mm)	
Horizontal	±35.0
Vertical	±20.0
Sextupole, dipole coils	
Number	280
No. of independent power supplies	280
Magnetic lengths (m)	0.28
Horizontal peak field (T)	0.11
Beam stay clear (mm)	
Horizontal	±35.0
Vertical	±20.0
Skew quadrupoles	
Number	20
Magnetic length (m)	0.15
Max. gradient (T/m)	2
Beam stay clear (mm)	
Horizontal	±35.0
Vertical	±20.0
Correction dipoles, horizontal correctors	
Number	240
No. of independent power supplies	240
Magnetic length (m)	0.14
Vertical peak field (T)	0.24

Beam stay clear (mm)	
Horizontal	±35.0
Vertical	±20.0
Correction dipoles, horiz. & vert. correctors	
Number	78
No. of independent power supplies	156
Magnetic length (m)	0.2
Peak field (T)	0.16
Beam stay clear (mm)	
Horizontal	±35.0
Vertical	±20.0

b. RF system

Number of cavities	15
Frequency (MHz)	352.96
Harmonic number	1248
Peak effective voltage (MV)	9.5
Transit time factor, T	0.717
Quality factor, unloaded Q	48,600
Effective shunt impedance, V_T^2/P (MΩ)	168
Fundamental-mode cavity dissipation (MW)	0.582
Synchrotron radiation loss, dipoles (MeV)	5.45
Synchrotron radiation loss, full complement (MeV)	1.25
Parasitic mode losses (MV)	0.2
Waveguide and other power losses, 10% (kW)	127
Total transmitter power available (kW)	3000
Total power in storage ring (kW)	1272
Total available accelerating voltage (MV)	12.0

c. Injection hardware

Injection septa	
DC septum, thin	
Number	1
Minimum septum thickness (mm)	14
Physical length (m)	1.15
Effective length (m)	1.1
Bending angle (deg)	3.08
Field at 7 GeV (T)	1.14
Gap height (mm)	25
Gap width (mm)	40
DC septum, thick	
Number	1
Minimum septum thickness (mm)	30
Physical length (m)	1.25
Effective length (m)	1.2
Bending angle (deg)	3.36
Field at 7 GeV (T)	1.14
Gap height (mm)	30
Gap width (mm)	40

Pulsed septum	
Number	1
Minimum septum thickness (mm)	2
Physical length (m)	0.85
Effective length (m)	0.8
Bending angle (deg)	1.57
Field at 7 GeV (T)	0.8
Gap height (mm)	20
Gap width (mm)	40
Bumper magnets	
Magnet type B1	
Number	2
Magnetic length (m)	0.4
Bending angle (mrad)	7.9
Field (T)	0.460
Gap (mm)	45.4
Magnet type B2	
Number	2
Magnetic length (m)	0.4
Bending angle (mrad)	8.9
Field (T)	0.522
Gap (mm)	40.0

d. Abort system

Kicker magnets	
Number	2
No. of independent power supplies (one PFN and two transmission lines)	1
Magnetic length (m)	0.55
Field (T)	0.0485
Gap height (mm)	40
Gap width (mm)	57.5
Septum magnet	
Number	1
Minimum septum thickness (mm)	2.0
Lambertson type with permanent magnets	
Magnetic length (m)	3.0
Field (T)	0.7
Gap height (mm)	20
Gap width (mm)	30

e. Beam diagnostics (no. of each type)

4-Button pickups	360
Accuracy (μm)	30
Sensitivity (μm)	25
Current transformers	2
Photon monitoring stations	2
Including: Photomultipliers	
Photodiodes	
TV Cameras	
Streak Camera	

RF-drive electrodes and amplifiers	2
Stripline pickups	2
Horizontal and vertical pingers	2
Loss monitors	80
X and Y beam scrapers	2
Fluorescent screens	40

f. Vacuum chamber

Material	Aluminum
Horizontal aperture (mm)	70
Vertical aperture (mm)	40
Minimum vertical aperture in undulator (mm)	8
Vacuum pressure (nTorr)	1

5. Injector Synchrotron Performance Parameters

Nominal energy (GeV)	7.0
Peak energy (GeV)	7.7
Injection energy (MeV)	450
Cycle rate (Hz)	1
Maximum circulating current, multibunch (mA)	1.62
Number of stored positrons, multibunch	1.24×10^{10}
Injected beam emittance at 450 MeV (m·rad)	1.1×10^{-6}
Longitudinal bunch area at 450 MeV (eV-s)	0.082
Natural emittance at 7 GeV (m·rad)	1.32×10^{-7}
Energy spread, rms at 7 GeV	1×10^{-3}
Bunch length, rms, natural at 7 GeV (mm)	18.3

6. Injector Synchrotron Lattice and Orbit Parameters

Circumference (m)	366.92
Revolution time (μs)	1.224
Harmonic number	
System I	48
System II	432
Radio frequency (MHz)	
System I	39.218
System II	352.96
Lattice structure: 10 FODO cells per quadrant	
Number of superperiods	2
Normal FODO cells per quadrant	8
Missing magnet FODO cells per quadrant	1
Empty FODO cells per quadrant	1
Mean radius (m)	58.40
Bending field (T)	0.696
Bending radius (m)	33.548
Magnetic lengths in a normal FODO cell (m)	
L=drift, M=bend, Q=quad, S=sext.	
QD	0.6
L1	0.1217
SD	0.2

L1	0.1217
M	3.1
L	0.4433
QF	0.6
L1	0.1217
SF	0.2
L1	0.1217
M	3.1
L	0.4433
Betatron tunes	
Horizontal	11.714
Vertical	9.760
Synchrotron frequency (kHz)	
At 2.73 GeV	1.81
At 7 GeV	25.34
Natural chromaticities	
Horizontal	-15.3
Vertical	-13.01
Beta functions (m)	
Maximum horizontal	15.9
Minimum horizontal	2.08
Maximum vertical	16.1
Minimum vertical	2.73
Maximum dispersion (m)	0.91
Momentum compaction	9.78×10^{-3}
Transition Gamma	10.112
Damping time (ms)	
Horizontal	2.7
Vertical	2.7
Longitudinal	1.35
Number of sextupole families	2
Beam elevation above floor (m)	1.5

7. Injector Synchrotron Tolerances, rms

Quadrupole placement (m)	10^{-4}
Sextupole placement (m)	10^{-4}
Random dipole roll angle error (rad)	10^{-4}
Dipole tracking error	5×10^{-4}
Quadrupole tracking error	5×10^{-4}
Sextupole tracking error	5×10^{-4}
Correcting-dipole tracking error	4×10^{-3}

8. Injector Synchrotron Hardware

a. Magnets and power supplies

Dipoles	
Number	68
No. of independent power supplies	2
Magnetic length (m)	3.1
Bending radius (m)	33.548

Dipole field 7 GeV (T)	0.696
Beam stay clear (mm)	
Horizontal	±30.0
Vertical	±18.5
Quadrupoles	
Number	80
No. of independent power supplies, QF, QD	2
No. in family QF	40
No. in family QD	40
Magnetic length (m)	0.6
Max. gradient (T/m)	13.9
Beam stay clear (mm)	
Horizontal	±30.0
Vertical	±18.5
Sextupoles	
Number	68
No. of independent power supplies, SF, SD	2
No. in family SF	34
No. in family SD	34
Magnetic length (m)	0.2
Max. strength (T/m^2)	130
Beam stay clear (mm)	
Horizontal	±30.0
Vertical	±18.5
Correction dipoles	
Horizontal correctors	
Number	40
No. of independent power supplies	40
Magnetic length (m)	0.15
Peak field (T)	0.12
Beam stay clear (mm)	
Horizontal	±30.0
Vertical	±18.5
Vertical correctors	
Number	40
No. of independent power supplies	40
Magnetic length	0.12
Peak field (T)	0.15
Beam stay clear (mm)	
Horizontal	±30.0
Vertical	±18.5

b. RF system

System I, 0.45 to 2.73 GeV	
Frequency (MHz)	39.22
Number of cavities	1
Harmonic number	48
Peak voltage (kV)	250
Cavity power (kW)	26.1
Cavity Q	25900
Cavity shunt impedance (MΩ)	2.4

System II, 2.73 to 7 GeV	
Frequency (MHz)	352.96
Number of cavities	4
Number of cells per cavity	7
Harmonic number	432
Peak effective voltage (MV)	12
Shunt impedance (MΩ/m)	26.1
Active length per cavity (m)	2.97
Effective shunt impedance (MΩ)	310
Fundamental mode cavity dissipation (kW)	466.4
Synchrotron radiation loss per turn (MeV)	6.33
Synchrotron radiation power at 1.6 mA (kW)	10
Waveguide and other losses, 10% (kW)	47
Total transmitter power available (kW)	1000

c. Injection equipment

AC Septum, pulsed	
Number	1
Min. septum thickness (mm)	2.0
Physical length (m)	0.9
Effective length (m)	0.8
Bending angle (deg)	15
Peak field at 450 MeV (T)	0.49
Gap height (mm)	30
Kicker	
Number	1
Magnetic length (m)	0.25
Deflection angle (mrad)	5.1
Field at 450 MeV (T)	0.0308
Gap (mm)	27
Fall time (ns)	72

d. Extraction equipment

DC septum, thin	
Number	1
Min. septum thickness (mm)	14.0
Physical length (m)	1.15
Effective length (m)	1.1
Bending angle (deg)	2.34
Peak field at 7 GeV (T)	0.87
Gap height (mm)	25
DC septum, thick	
Number	1
Min. septum thickness (mm)	30
Physical length (m)	1.25
Effective length (m)	1.2
Bending angle (deg)	2.56
Peak field at 7 GeV (T)	0.87
Gap height (mm)	30

AC septum, pulsed	
Number	1
Min. septum thickness (mm)	2
Physical length (m)	0.85
Effective length (m)	0.8
Bending angle (deg)	1.6
Peak field at 7 GeV (T)	0.8
Gap height (mm)	20
Kicker	
Number	1
Length (m)	1.8
Deflection angle (mrad)	2.35
Field (T)	0.031
Gap height (mm)	27

e. Beam diagnostics (no. of each type)

Current transformer	1
4-Button pickups	80
Photon Monitors	1
RF electrodes and driver	2
Loss monitors	40
Fluorescent screens	8
X and Y Beam scrapers	2

f. Vacuum chamber

Material	Stainless steel
Horizontal aperture (mm)	60
Vertical aperture (mm)	37
Vacuum pressure (nTorr)	10

9. Linacs

a. General

Linac e^- (MeV)	200
Linac e^+ (MeV)	450
Frequency (GHz)	2.856
Total number of TW accelerating sections	13
Total number of SW accelerating sections	1
Number of klystrons with SLEDS	3
Number of klystrons without SLEDS	1

b. Linac e^-

Gun voltage (kV)	130
Pulse Current (A)	5
Prebuncher I, type SW, single-gap	
Prebuncher II, type TW, $\lambda/2$ long	
Buncher, TW, tapered, 0.6 β to β, λ long	
1st accelerating section, SW	
Number of TW accelerating sections	3
Pulse repetition rate (Hz)	60
Beam pulse length (ns)	16.5

Pulse current (A)	3
Number of pulse	8
Average current (μA)	0.4
Emittance (mm-mrad)	1.2
Bunch length (RF)	25°
Energy spread	0.05

c. Linac e^+

Target material	Tungsten
Target thickness, ($2x_o$) (mm)	7
e^- beam diameter on target (mm)	< 3
Average incident power (W)	100
Pulsed solenoidal field (T)	1.5
Conversion efficiency e^+/e^-	0.0083
Mean energy of positrons (MeV)	8
Input current (mA)	25
Output energy (MeV)	450
Output current (mA)	15
Emittance, 95th percentile (mm-mrad)	6.6
Energy spread, 95th percentile	0.01
Transmission efficiency	60%
Number of TW sections	10

10. Transport Line between Linac and Injector Synchrotron

a. Magnets

Dipoles

Number	1
No. of independent power supplies	1
Magnetic length (m)	1.0
Field at 450 MeV (T)	0.27
Bending angle (deg)	10
Gap (mm)	40

Quadrupoles

Number	12
No. of independent power supplies	12
Magnetic length (m)	0.3
Pole tip inscribed radius (mm)	35
Max. gradient (T/m)	3.8

b. Beam diagnostics (no. of each type)

Current transformers	2
Wall current	4
Fluorescent screens	3
Wire scanners	4
Loss monitors	6

11. Transport Line between Injector Synchrotron and Storage Ring/Beam Dump

a. Magnets	
Dipoles	
Number	6
No. of independent power supplies	3
Magnetic length (m)	1.36
Field at 7 GeV (T)	1.24
Bending angle (deg)	4.125
Gap (mm)	20
Quadrupoles	
Number	19
No. of independent power supplies	19
Magnetic length (m)	0.6
Pole tip inscribed radius (mm)	25
Max. gradient (T/m)	20
b. Beam diagnostics (no. of each type)	
Current transformers	3
Wall current	4
Fluorescent screens	6
Wire scanners	4
Loss monitors	6

12. Insertion Devices (IDs)

Number of IDs, maximum possible	34
Number of undulators, initial construction	7
Number of wigglers, initial construction	5
Vacuum chamber full vertical aperture (cm)	
APS initial operation phase	1.2
APS mature operation phase	0.8
Magnet gap, minimum (cm)	
APS initial operation phase	1.4
APS mature operation phase	1.0
Straight section length, maximum (m)	
Standard section	6.2
Extra-long section	8.5
Insertion device length, maximum (m)	
Standard straight section	5.2
Extra-long straight section	7.5

APPENDIX B

PRECONSTRUCTION RESEARCH AND DEVELOPMENT PROGRAM

B.1 Introduction

Our research and development work during Fiscal Years 1986-1987 consists mainly of conceptual design of the facility, re-optimizing the storage ring parameters to increase the tunability of the insertion devices, hardware research associated with the storage ring vacuum system, and undulator and beam line research and development (R&D). It has been particularly useful to review the designs of all accelerator components during the course of the ring energy change described in this report.

Assuming that the construction of the facility will start in FY 1989, we plan to continue and broaden the scope of R&D to include prototyping of hardware in order to provide the best possible performance of the facility, to optimize conceptual engineering designs, and to devise quality assurance plans by which all hardware deliverables are to be tested. One of the primary goals of this work will be to establish fabrication procedures and testing methods such that both industry and in-house personnel will be able to produce hardware components that meet performance specifications on a timely schedule.

Our R&D plan includes:

- Accelerator physics - theoretical.
- Accelerator physics - experimental.
- Component prototyping and testing.
- Optimization of the designs for the conventional facilities.
- Design of insertion devices.
- Design of beam line components.
- Detector development.

With regard to the conventional facilities, it is worthwhile to note that the experimental hall and the central office/laboratory building are the most expensive items in the construction project. The size of the experimental hall is determined by the lengths of the photon beam lines, and the size of the central office/laboratory building is determined by the combination of the facility operations and the scientific program supports needs. Therefore it is essential to carefully optimize the designs of both buildings to achieve the required program capability at the lowest cost.

The preconstruction R&D is scheduled so that it blends smoothly with the initiation of the construction phase in FY 1989. Key R&D items are scheduled with decision-making milestones that are phased appropriately with the construction schedule.

B.2 Accelerator Physics

B.2.1 Theoretical - Lattice and Beam Dynamics

The emphasis of our beam dynamics studies during FY 1986 and FY 1987 has been on refinement and optimization of the storage ring lattice. This work includes tracking of particles with nonlinear elements and with reasonable tolerances on the element parameters. Effects of the nonlinear elements or other imperfections can best be estimated by the use of numerical simulations, although we have also obtained valuable analytical results. There are several computer codes available for the tracking. The first step in our work has been to study the effect of one imperfection at a time, using several computer codes, in order to assure that there are no code-dependent anomalies. The next step in tracking includes more than one source of the imperfections. Our work to date includes such sources of field error as insertion devices, higher-order multipole field components of the ring magnets, and magnet placement errors.

A preliminary study of tracking with the synchrotron oscillation included has been performed using the computer code RACETRACK, and the result is that the inclusion of the synchrotron oscillation does not change the tracking result of the dynamic apertures within the simulation accuracy. However, it should be noted that tracking with simulations such as synchrotron oscillation and synchrotron damping requires tracking of particles through many-thousand turns because the synchrotron oscillation period and the energy damping time are on the order of 0.5 to 4 ms.

Our plan for the coming years is, then, to further refine the tracking study to include all relevant physical phenomena in the simulation one at a time as well as all phenomena at once. Once such a detailed study for the APS lattice has been performed, particle tracking for an existing ring will be performed with equal thoroughness, thus enabling us to experimentally check the calculations with an actual machine. Our expectation is that, although it may be difficult to check some absolute predictions of the numerical simulations, a number of very useful comparisons between the predictions and measurements can be made.

B.2.2 Experimental - Measurements at Existing Storage Rings

As discussed in above sections, our R&D plan includes experimental verifications of theoretical predictions whenever possible. We have discussed with other laboratories some possibilities for performing machine experiments with existing rings. One such possibility is to set up a collaborative experimental program with accelerator physicists

at the 1-GeV ring at the Synchrotron Radiation Center (SRC), the University of Wisconsin-Madison. The experimental program under discussion includes:

- Dynamic aperture and phase space smearing for large amplitude oscillations as functions of nonlinear components in the ring. This is a series of experiments using known amounts of nonlinearity in the lattice to compare the predictions and measurements. The SRC ring is particularly suitable for this kind of experiment because it has straight sections available at this time.

- Impedance measurements in a circulating beam. This is a delicate problem because installing a "foreign" vacuum chamber to an existing ring is not an easy task to perform.

- Photon-stimulated desorption of adsorbed gas from the vacuum chamber surface. A piece of our extruded aluminum chamber material is already under study by the Surface Physics Group of Argonne Chemistry Division. This group is measuring the degassing rate under electron-stimulated conditions. The plan is to measure the degassing rates under various conditions that include not only electron bombardments, but also laser beam and surface treatments of different kinds. The group has built a scattering chamber that can be moved to other laboratories to perform measurements. The plan is to take this set-up to SRC or National Synchrotron Light Source (NSLS). Further details of this work are described below in connection with the vacuum chamber prototyping.

- Photon beam steering. A photon beam steering and position feedback system will be built and tested at a storage ring with an insertion device.

- Beam position measuring (BPM) system. This work includes developing and testing both kinds of systems for charged particles and photons.

B.2.3 Coupling Impedance - Vacuum Chamber

Since the coupling impedance of the circulating beam to its surroundings limits the beam current of the storage ring, it is essential to understand and to budget the impedance contributions from various elements of the ring hardware placed along the circulation path. Much of the equipment to be used is standard hardware employed in existing storage rings. Experience from these rings is used in the impedance budget. An exception is our storage ring vacuum chamber system, which uses a new type of distributed pumping within an antechamber to the beam chamber. Therefore, it is necessary to understand the behavior of electromagnetic waves in the chamber-antechamber system.

Modeling studies performed to date indicate that there will be a negligible contribution to the impedance coming from the antechamber. In addition, in the past

year we have performed measurements of the impedance using a wire and a network analyzer. Our results confirm predictions made by modeling studies. Methods used for this purpose and the experimental results are explained in Section II.2.

Future R&D on this topic includes continuation of the present work on the loss parameter measurement into a higher-frequency domain using a single-pass beam measurement, and measurement of the impedance using the circulating beam at an existing ring. The planned single-pass measurement involves the transmission of the 1-kA, 30-ps electron beam pulse through the beam chamber to generate the wake field throughout the chamber. Then the frequency spectrum of the generated wake will be measured using a thin wire in the antechamber. The 1-kA, 30 ps electron beam pulse is available at the 22-MeV Argonne Chemistry Division linac.

In addition to the impedance study of the chamber itself, careful consideration will be given to the effect on the impedance of having a relatively large number of beam port, bellows, and insertion devices in the chamber system. Implications of impedance are also discussed below in connection with rf R&D.

B.2.4 Accelerator Physics R&D Milestones

Both theoretical and experimental accelerator physics studies will continue throughout the project. However, the following milestones are set to assure timely decisions for the construction of the facility. These milestones are shown in Fig. B.2.4-1.

- Major lattice review: May 1987
- Joint vacuum chamber review with ESRF: June 1987
- Decision on the final chamber geometry: September 1987
- Decision on the final lattice: March 1988
- Further refinements: Throughout project

Vacuum chamber impedance measurements using wire and a network analyzer have been completed in early FY 1987. In order to make comparisons, the measurements involved several chamber geometries. The linac (single-pass) impedance measurements will be completed in FY 1987. The decision as to the final chamber geometry will be made at the end of this summer after a joint review meeting between Argonne and ESRF personnel. A bar chart for this activity is shown in Fig. B.2.4-1.

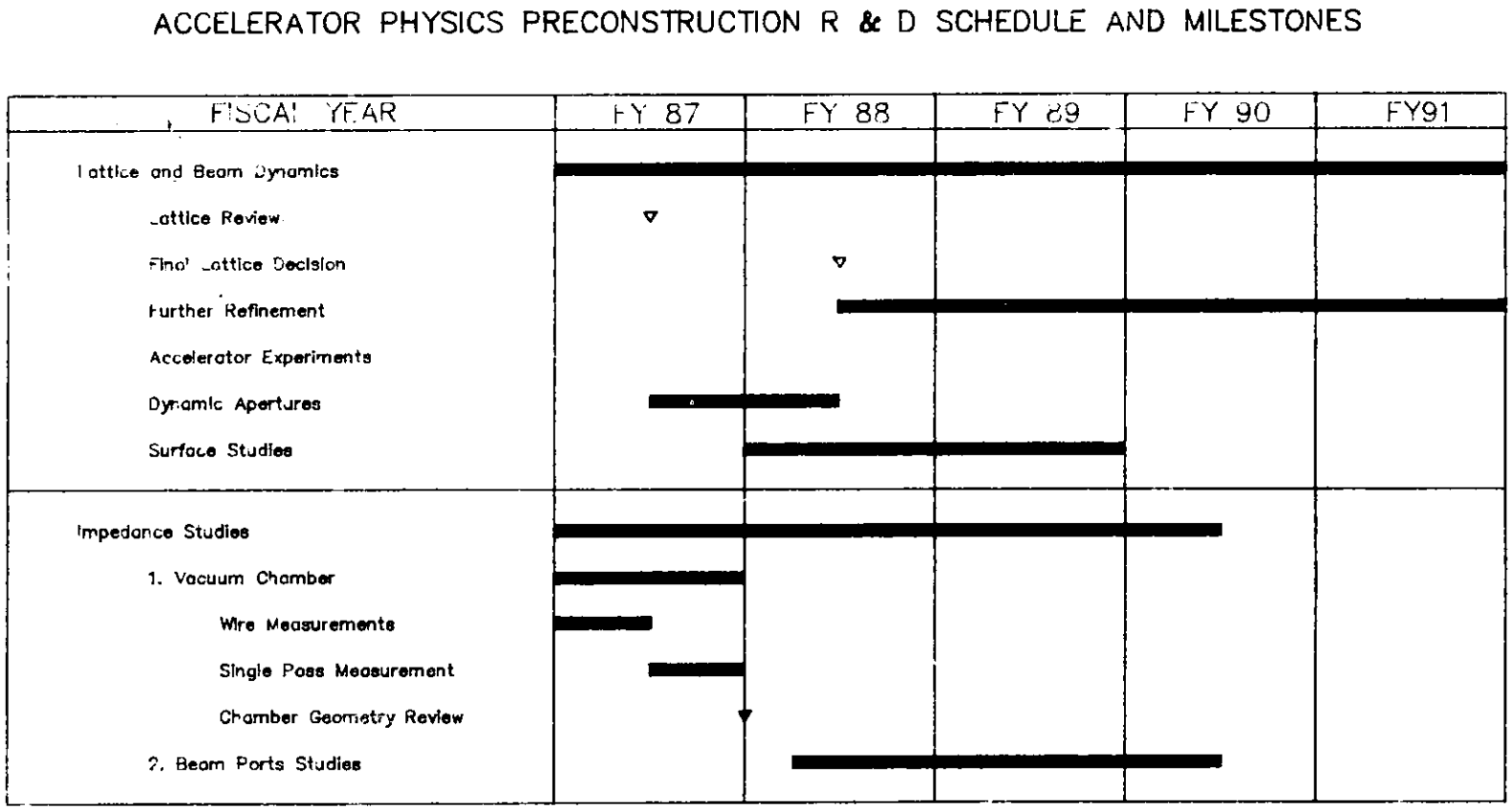

Figure B.2.4-1
Accelerator physics preconstruction R&D schedule and milestones.

B.3 Accelerator Components Prototyping and Testing

B.3.1 Vacuum Chamber

During FY 1985, a prototype vacuum chamber, using aluminum plate bent to form the beam chamber and antechamber geometry, was constructed to test the pumping effectiveness of nonevaporating-getter (NeG) strips. The chamber reached a pressure of 0.1 nTorr. During FY 1986-87, several lengths of vacuum chamber with geometry specified in this report were extruded in order to test the constructibility of such a design.

The prototyping of the vacuum chamber system to date includes: extrusion of about 100 m of the ring vacuum chamber, bending of segments of the chamber to fit into the bending magnets of the ring, and another extrusion of 6 pieces of 6-m-long insertion device vacuum chamber. Demonstration of the constructibility of the insertion device vacuum chamber is very important because its geometry, 8-mm vacuum chamber aperture with a wall thickness of 1-mm, dictates the design of the insertion devices.

A sector vacuum chamber mock-up is planned for late FY 1987. Using the prototype chambers that we now have and wooden models of the ring components (magnets and other hardware), a full-scale mock-up of a sector is now being built. The vacuum system installed in the mock-up is a real system to determine the serviceability of the vacuum system. For this purpose, we have acquired all vacuum components necessary for a sector. Also planned in this set-up are mock-ups of the ring shielding and the photon beam line front-end in order to check that the spatial arrangement of the ring is matched to the requirements of the experimental program.

One of the most important engineering issues associated with the vacuum chamber system is the welding of aluminum to aluminum. Extreme care must be taken in the welding in order to achieve the desired vacuum pressure. For this reason, we have started a welding program. The first part of the program was to weld various geometries and shapes of the chamber materials manually. Because human factors are involved in manual welding, the reproducibility of weldments from one piece to another was found to be less than desirable. Therefore, we have started an "automatic welding" program with an outside vendor. The word "automatic" implies use of either robotics or any other computer-driven system to control the welding process.

Due to photon-stimulated desorption of adsorbed gas from the chamber surface, newly installed chambers usually degas substantially during the initial period of operation. This effect, in turn, limits the stored current until the surface area of the chamber is cleaned by the photodesorption process. This so-called "beam scrubbing" of the chamber surface may take a long time; 1000 hr or more is not unusual. To minimize this conditioning period, it is customary to prepare the chamber by using chemical cleaning and glow discharge before installation.

Preconstruction R&D includes investigations of surface treatments of various kinds and measurements of degassing rates under photon- or electron-stimulated conditions in the laboratory, using lasers or electron guns. These investigations will be repeated under actual machine conditions at an existing storage ring. This work is being carried out by surface scientists from Argonne in collaboration with accelerator personnel. The goal is to study various chamber surface treatment procedures and to produce a check list for chamber construction, treatment, and installation.

B.3.2 Storage Ring Magnets and Power Supplies

Prototyping of the ring magnets is planned to devise and document construction methods and to generate detailed check lists for the specifications required to construct 80 dipoles, 400 quadrupoles, and 280 sextupoles.

The prototyping will start with construction of a quadrupole, which is the magnet most sensitive to construction errors, and then will proceed to the construction of a dipole and a sextupole.

A magnet-measuring laboratory tailored to the special needs of this facility is essential. This measuring facility will be expanded eventually to a "measuring factory" to handle hundreds of magnets. Also planned is a data reduction system to process and store the magnet measurement data.

Since the proposed storage ring has 400 independent quadrupole power supplies and 280 independent sextupole power supplies using pulse modulation techniques, it is important to detail performance specifications, and then to develop specific designs and test procedures suitable for quantity industrial production.

B.3.3 Radio-Frequency System

The proposed rf system uses existing technology and requires no major development work. Goals of the R&D are to:

- Obtain refined construction specifications and cavity testing procedures.
- To search for improvements in cavity performance, especially with respect to higher-order-mode losses. Minimizing these losses can increase the stored current substantially. This work is to be done in a low-power testing program.
- To incorporate additional reliability.

B.3.4 Diagnostic Equipment

As discussed in Section II.7, accurate and reproducible positioning of the circulating beam in the storage ring and the external photon beams is essential for the scientific program. R&D on the circulating beam position monitors addresses improvement of measuring accuracy to below 30 μm, which is roughly the current limit. With respect to external photon beam position measurement, measuring accuracy has been improving substantially during the past years. About a year or so ago, the nominal measuring accuracy was about 100 μm, where the presently achievable accuracy is about 1 μm. The new generation of machines, such as the one proposed here and the Stanford Linear Collider (SLC), requires such accurate position measurements. The plan is to pursue this research throughout the project duration and to test prototypes constructed during the course of the study at existing facilities. We anticipate substantial worldwide effort in this area and will watch closely for developments that complement ours.

B.3.5 Milestones for Accelerator Component Prototyping and Testing

Figure B.3.5-1 shows the bar chart for this activity along with decision-making milestones where applicable.

B.4 Preconstruction R&D on Architecture and Engineering

The goal of this R&D effort is further optimization to decrease the cost of the construction and/or to increase the functionality of the buildings included in the project. This effort is to be pursued by Argonne personnel along with an architectural/engineering firm, as we have done in the past. As noted in Section V.3, some preconstruction design work is planned in FY 1988 to expedite the construction schedule.

B.5 Detector Development

B.5.1 Introduction

Two-dimensional distributions of x-rays are currently recorded with pulse-counting detectors or with integrating media such as photographic films. Counting detectors, such as the commonly used gas-filled proportional counters, are inherently count-rate limited at about 10^5 ph/s. Thus, these detectors are useful only in synchrotron experiments where the samples are weakly scattering or very small. In most of the experiments being contemplated for the APS, the counting rates will be significantly higher and, therefore, counting-type detectors will not be usable. This proposal focuses on the development of a new generation of integrating detectors, or imaging detectors, for synchrotron radiation research, which are based on charge-coupled

ACCELERATOR COMPONENTS PRECONSTRUCTION R & D SCHEDULE AND MILESTONES

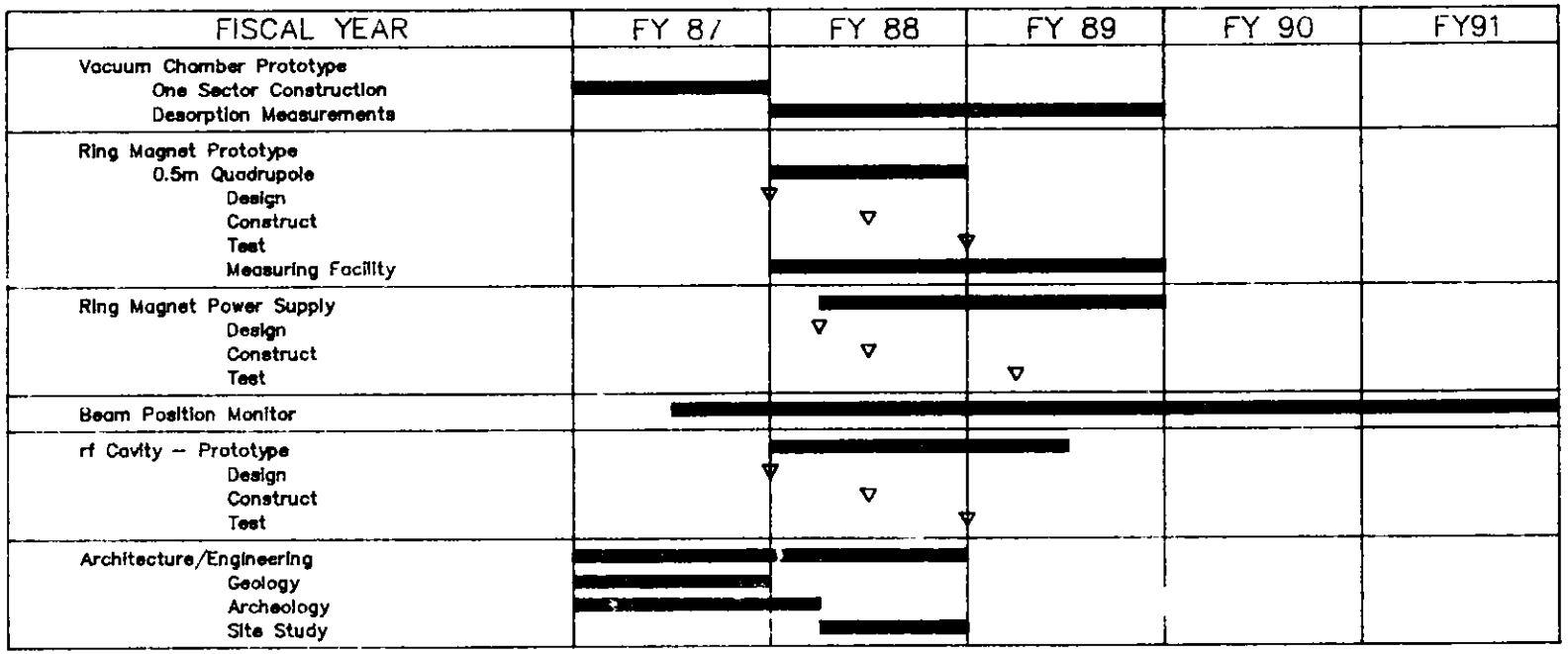

Figure B.3.5-1
Accelerator components preconstruction R&D schedule and milestones.

devices (CCDs). These detectors have essentially no count-rate limitations and, therefore, are expected to meet most of the future experimental requirements.

To take full advantage of the high flux and pulsed nature of the APS, one would like to perform the experiments on time-dependent phenomena. The major objectives are:

1. Capability for real-time studies of physical and chemical processes.

2. Capability for kinetic experiments with excited samples (time-resolved diffraction, extended x-ray absorption fine structure (EXAFS), topography, etc.).

The detectors needed for the synchrotron studies have differing requirements. Some experiments may require a two-dimensional detector with high spatial resolution, and others may require a one-dimensional detector with high statistical precision. The range of detector requirements expected for the APS-based research is given in Table B.5-1.

B.5.2 Detector Design

Adapting the detector system for specific experiments requires the assembly of several components. These include a phosphor or a scintillator, a lens optics, a fiber-optic taper, an image intensifier, a charge-coupled device (CCD), an analog-to-digital converter (ADC) and a computer for fast mass storage.

Table B.5-1

Detector Requirements for Synchrotron Radiation Studies

Photon Energy (keV)	5-100
Detector Flux (ph/s)	10^{5}-10^{16}
Resolving Time (s)	10^{-7}-1
Gate Actuation (ns)	100
Sensitive Area (mm^2)	25x1-500x250
Frame Size (pixels)	250x1-2000x2000
Dynamic Range	10^{2}-10^{4}
Statistical Precision	10^{-2}-10^{-4}

The design of a detector system requires the selection of components to meet specific performance requirements. As shown above, this often involves conflicting characteristics, but in many cases these can be compensated for with other components. Thus, for example, high light output from a phosphor is desirable for signal-to-noise ratio considerations. For time-resolved experiments, the phosphor should also have a fast decay. However, fast phosphors have reduced light output and hence may require an image intensifier for light amplification. The image intensifier will enhance the signal-to-noise ratio but will also cause the CCD well to fill faster. Therefore, more frequent readouts will be required and the resolving time will be degraded. To mitigate this effect, fast readout from the CCD, fast ADC, and fast data storage are desirable. Thus, a detector design involves a comprehensive systems approach whereby components with complementary performance are combined and electronics and software with compatible characteristics are developed to meet the requirements specific to a given experiment. Detectors for dispersive EXAFS and protein crystallography are now being developed at Argonne.

B.5.3 Detector Development

A detector development program must proceed in parallel with the design and construction of the APS in order to have suitable detectors available when the facility becomes operational. The need for such a program is explained below:

1. A number of different detectors are required for the various experimental programs that are being planned. Only two prototype detectors are now under active development at Argonne: one for dispersive EXAFS and the other for protein crystallography. Detectors for the other applications have yet to be developed. Each detector usually has some unique requirements. In topography, for example, ultrahigh spatial resolution may be required, whereas in angiography a large sensitive area is of primary importance. Thus, the development of each detector must be addressed separately.

2. Several of the components being used in prototype imaging detectors were originally developed for use with low light levels, such as in night vision and astronomy, and have serious limitations for use with bright beams such as those from a synchrotron. The high data rates, volume of information, response time, and spatial resolution encountered in synchrotron radiation experiments often exceed the capability of existing devices.

The R&D program in detector technology will focus on the following areas:

Fast CCD Readout

1. New parallel architectures.

2. Fast analog signal processing.

3. Fast CCD controllers.

Phosphors/Scintillators

1. Thin and uniform phosphor deposition techniques.

2. Investigations of fast, high-light-output phosphors and scintillators.

3. Evaluation of linearity of phosphors/scintillators (input vs. output intensity response) at high input fluxes.

Image Intensifiers

1. Input rate limitations.

2. Fast gating.

3. Large, uniform photocathodes.

Computers

1. Fast storage of large data arrays.

2. On-line data reduction.

B.6 Insertion Devices on APS Storage Ring

B.6.1 Insertion Device Technology

The permanent-magnet technology for insertion devices (IDs) is advancing very rapidly, and new undulator magnet materials and design concepts are currently being developed. While the Nd-Fe-B hybrid magnet configuration presently used will definitely meet the ID requirements of the proposed APS, new materials and concepts will provide considerable flexibility in the ID design and improved performance of the radiation sources.

We propose to begin R&D work on several ID-related projects in close collaboration with scientists and engineers from other laboratories who have similar

goals. It is also essential to involve industry in such an endeavor. For example, Spectra Technology (Bellevue, Washington) has developed long undulators for the Defense Department and Field Effects (Boston, Massachusetts) has built a transverse optical klystron (TOK) for AT&T Lab., and are eager to participate in the development of IDs for the APS.

The preconstruction R&D plans include the following:

- Prototype hybrid devices with small periods will be fabricated from Nd-Fe-B or similar new materials. Their field profiles and homogeneity will be measured and compared with field profiles calculated by two- and three-dimensional modeling.

- Rigid-wall extruded aluminum ID chambers, 5 m in length, with 8- and 12-mm apertures (as described in Section II.9) will be constructed. Various mechanical tolerances on such a chamber will be measured. The vacuum performance of Zr/Al strips installed in the chamber will be determined. The results of this work, which is to be completed by the end of FY 1989, will determine the type of ID chambers to be constructed for the APS.

- Electromagnetic IDs assisted by active permanent-magnet materials[1] are likely to provide superior tunability and performance in a wide variety of applications at the APS. A prototype device will be developed for use on the APS storage ring during FYs 1989-92.

- It is important to explore every means of enhancing the field strength and field quality in an undulator configuration. This has many implications on the performance of APS undulators and its utility. A new concept of using wedged-poles has recently been proposed.[2] The benefits of this new type of hybrid configuration will be evaluated and a mock-up of one section of such an undulator will be built. Various tests of magnetic homogenity, strengths, and multipole character will be completed during FYs 1988-89. The results will be compared to those predicted by the model calculations.

- Computer codes for ID spectral calculations will be expanded to incorporate actual magnetic field profiles and magnet placement errors. These codes will be coupled to a ray-tracing routine that will enable a more realistic design and performance evaluation of the optical elements. The work will be carried out during FYs 1988-89.

- Various possible concepts and methods to obtain polarized hard x-rays with variable ellipticity will be evaluated. Such radiation is useful for many types of chemical, biological, and materials investigations. The design work on specific devices will follow in FY 1990.

- There are many new experimental areas that demand specialized spectral characteristics from IDs. An example is a broad-band undulator for spectroscopic applications. Concepts for such new devices will be developed and design work will be carried out to meet various user requirements. This work will begin in FY 1989.

B.6.2 Undulator Tuning and Positron Beam Stability

Variable magnet gaps in the undulator on the 7-GeV APS storage ring permit tuning of the peaked harmonic spectra to the desired energy. However, the gap variation at one undulator must not be allowed to influence the phase-space stability of the positrons in the rest of the storage ring. Otherwise, the photon beams that are delivered to other users will not be stable. Positional stabilities of ± 10 μm are what have been tentatively specified for the positron beam. At present, positron beam monitors with this level of accuracy are not available. Therefore, photon beam monitors will be used for high-precision measurement. Each beam line will have two sets of such monitors, separated by about 5 m; each set will monitor both the vertical and the horizontal movement of the beam. This arrangement will provide both positional and angular monitoring of the photon beam. The signals generated from these monitors will be sent to correction magnets located downstream on either side of the ID.[3] The photon beam monitors will be designed and tested during FYs 1989-90 on an existing storage ring.

B.7 Beam Line Components

B.7.1 Introduction

The high brightness of the radiation from the undulators and wigglers on the APS storage ring will produce very large power densities and power density gradients on the first optical element. It is necessary to develop procedures to deal with such power loads without sacrificing the performance of the first optical element. An initial study of this problem, involving finite element analysis on the first optical component, has already suggested directions for a fruitful R&D program in this area. However, further computational work is needed in order to model real components and power profiles generated by specific IDs. In addition, the performance of newer designs for first optical elements should be tested in a situation that matches the expected radiation from the APS IDs.

The first optical element in a beam line could be a crystal, a mirror, or a metallic superlattice. The choice will depend on the nature of the radiation from the source and the application. In the following, we present R&D plans for the development of various types of first optical elements.

An equally important developmental issue for beam line design relates to the choice of advanced optics suitable for specific ID sources and applications. These

choices require the kind of detailed ray-tracing analyses mentioned earlier. Such analyses will include accurately modeled ID sources and realistic optical elements.

B.7.2 Power Density Reduction

All the power radiated by an ID need not impinge on the first optical element. The power density on the first optical element can be reduced, and the energy and spatial distributions of the power density profile can be modified, by using absorbers and filters. Toward this goal, the following work will be initiated:

- Numerical computations of the power density distributions from model IDs to be constructed on the APS storage ring for various applications.

- Accurate calculations of the energy and spatial distributions of power densities and gradients in the above cases after transmission through various absorbers and filters.

This work, to be completed in FY 1988, will provide the refined design of the first optical element.

B.7.3 First Optical Element

In many beam line configurations, the maximum photon flux available at the experimental sample is determined by the maximum power that can be absorbed by the first optical component without causing serious distortions of its surface or changes in its internal structure (lattice spacing). An effective way to increase the flux at the experimental sample is to improve the cooling and/or the control of the surface temperature of the first crystal. The following is an example of a configuration that could improve the cooling of a first optical component that is kept at shallow angles with respect to the beam. A relatively thick crystal is used, and liquid Ga is pumped through holes drilled parallel to the incident surface. This cooling reduces the heat load and thereby decreases bowing. When the back surface of the crystal is heated in a fashion that mimics the heat profile due to the photon beam on the front surface, the heat stresses cancel, leaving the crystal undistorted.

The power density also has a large gradient over the beam footprint on the first optical element. This gradient results in a variation in the temperature across the footprint. The net effect is to change the lattice spacing. It is, in principle, possible to make the temperature of the surface relatively constant over the area of the footprint.[4]

Following is the R&D plan for handling power density and its gradient on the first crystal optics:

- Finite element analysis of the thermal and mechanical stress profiles in a representative set of optical elements, with realistic power loads, different radiation footprints, and a variety of coolants and geometries.

- Construction of liquid metal pumps and testing of their performance on heat-loaded optical components. Simultaneous evaluation of the performance of the optical components subjected to simulated heat loads and cooled with liquid metal using different cooling geometries with a high-power electron source.

- Development of an infrared detector system to measure the heat profile on the optical component exposed to ID radiation.

- Construction and testing of optical components that make use of the new "variable metric" approach to focusing,[4] i.e., crystals in which the lattice spacing varies with position in the crystal.

- Evaluation of the long-term stability of optical components repeatedly subjected to large power loads.

- Construction of a short-period undulator on CHESS, which provides a radiation source that will mimic various aspects of the APS ID radiation sources. This source will be used for power loading tests on Si cooled with liquid Ga.

- Construction of beam lines on the above-mentioned sources to test the ultrahigh-energy-resolution ($\Delta E/E \sim 10^{-7}$) performance of optical elements that will be used on the APS beam lines.

The work described in this subsection will begin immediately. Various subtasks are coordinated with the R&D effort on IDs during FYs 1988-91.

B.7.4 Superlattice Optical Elements

The most obvious advantages of certain metallic superlattices for APS applications are their high reflectivity and large adjustable bandpass in the 4-30 keV energy range.[5] Another important advantage is that the layers themselves can be deposited on high-thermal-conductivity substrates for power load applications and the possibility of producing optics with special figures.

Although these novel optical elements show great promise for APS applications, several aspects of these systems require further study:

- The factors affecting the reflectivity and bandpass behavior, such as degree of registry roughness and interface composition, are poorly understood and not adequately modeled. Extensive characterization of superlattices produced

under well-controlled and reproducible conditions is needed to fully understand these factors.

- The ability of superlattices to handle large power loads from the APS ID sources needs to be evaluated. The superlattices must maintain their integrity at peak power loads of up to 1000 W/cm^2 if they are to be used effectively as power filters. Our preliminary results on the behavior of carbon/tungsten superlattices under conventional heat loads are very encouraging.[6]

Additional investigations are needed with more realistic power loading, such as that from ID sources at existing synchrotrons. The R&D effort described in this subsection will be carried out during FYs 1987-90.

B.7.5 Optical Ray-Tracing Analysis

The performance of a beam line can be reliably computed only by means of a detailed ray-tracing analysis. Computer programs to be developed for this purpose will include accurately modeled ID sources and optical elements that are exposed to large power loads. This computational effort will lead to a precise evaluation of the performance of beam line designs and consequent optimization of the designs for the best use of the high-brilliance source.

This effort has begun in FY 1987 in collaboration with F. Cerrina of SRC, Stoughton, and will be completed in FY 1990.

B.8 Costs for Preconstruction Research and Development Program

The funds needed to accomplish the preconstruction R&D work are based on the R&D items identified in this appendix. The budget profile for this work takes into account the construction schedule described in Chapter V of this report. One of the most important considerations in developing the schedule is the need for a smooth transition from the R&D phase to the construction phase while maintaining the schedule of the key milestones of the project.

It should be noted that adequate operating funds (not listed here) will be needed to support the precommissioning activities that are necessary to make the transition to the commissioning phase as the various subsystems of the facility are ready for trial operation. These precommissioning activities are scheduled to start in the FY 1991-1992 period. Their costs are described in the APS Project Management Plan document.

Costs for preconstruction R&D effort, materials and services, and equipment are shown in Table B.8-1. The dollars shown are cost escalated in each fiscal year, using the rates in Table V.2-2.

Table B.8-1

Effort and Costs for Preconstruction R&D

Activity	FY87	FY88	FY89	FY90	FY91	FY92
			Start Construction in FY 1989			
Effort (FTE)						
Accelerator Physics	7	10	10	10	10**	10**
Vacuum Chamber Prototype	3	5	5	*		
Ring Magnet Prototype	2	5	5	*		
Ring Magnet Power Supplies Prototypes	1	3	4	*		
Diagnostics	2	4	4	4	4	4
rf Cavity/Linac Prototype	4	5	5	*		
Controls	2	4	*			
Conventional Facility	3	4	*			
Vibration/Geoscience	2	2	2			
Other General Accelerator Designs	4	10	*			
Detector Development	2	2	3	3	2	2
Insertion Device Development	3	4	6	8	7	5
Beam Line Development	4	5	7	10	9	7
X-ray Optics	-	1	3	4	4	4
Instrument Development	-	-	2	2	3	3
Program Coordination	3	4	3	2	2	2
Effort Total (FTE)	42	68	59	43	29	27
Effort (Cost escalated $000)	3800	6400	5800	4500	3200	3100
Materials and Services (Cost escalated $000)	1300	3600	2200	2200	1500	1500
Equipment (Cost escalated $000)	1000	1000	1500	800	800	800
Total (Cost escalated $000)	6100[A]	11000[B]	9500[C]	7500	5500[D]	5400[D]

[A]Includes approximately 50% Argonne discretionary funds.

[B]Revised FY-1988 budget request; the FY-1988 President's Budget is $5.5 M.

[C]This corresponds to the $11 M FY 1988 level. If actual FY-1988 funding is at the President's Budget level, the Fiscal Year 1989 requirement will be $11.5 M.

[D]Precommissioning operating costs must be added to these R&D costs to obtain FY 1991 and FY 1992 operating budgets as described in the Management Plan.

*Personnel involved in this activity are, during and beyond this point, supported by the construction project.

**Supported by precommissioning operating funds -- not included in totals.

B.9 References

1. K. Halbach, Nucl. Instr. Method. A246, 77 (1986).

2. K.-J. Kim, Nucl. Instr. Meth. 222, 11 (1984).

3. J. Norem et al., IEEE Trans. Nucl. Sci. NS-32, 1883 (1985).

4. R.K. Smither, Rev. Sci. Instr. 63, 131 (1983); G.S. Knapp and R.K. Smither, Nucl. Instr. Method. A246, 365 (1986).

5. D.H. Bilderback et al., Nucl. Instr. Meth. 208, 251 (1983).

6. E. Ziegler et al., Appl. Phys. Lett. 48, 1354 (1986).

APPENDIX C

USER POLICIES AND PROCEDURES

C.1 Introduction

The 7-GeV Advanced Photon Source (APS) will attract a great many users, and a number of modes of usage will be represented. Since several of these modes will involve users in the planning and construction of the beam lines, it is necessary that procedures and policies addressing user involvement be in place early. In this Appendix, we describe a number of mechanisms for user participation in the APS program. It should, of course, be expected that these mechanisms will evolve with technological developments and as a result of our ongoing interactions with the user community.

A tentative beam line plan is given in Section C.2. Our present thinking regarding user access arrangements and policies for Participating Research Teams (PRTs) is described in Section C.3.

C.2 Overall Beam Line Plan

The storage ring can accommodate 34 insertion device (ID) and 35 bending magnet ports. We will assume, here, that each port provides only one beam line, even though it may be possible, and even desirable, to split wiggler and bending magnet ports into two beam lines in the future. We also assume that, at full utilization of the APS, there will be 22 undulators (U) and 12 wigglers (W) to meet the objectives of the experimental program. It need hardly be stated that this distribution is subject to change. Indeed, one of the objectives of our accelerator physics research and development work is to provide as much flexibility as possible in setting the ratio of U to W straight sections.

Assuming that the source is user-ready at the beginning of FY 1993, our tentative plan for the completion of beam lines is as given in Table C-1. This plan includes 30 beam lines operating in FY 1993, 15 as part of the APS construction project and 15 provided through PRTs. The distribution of the construction project beam lines (7 undulators, 5 wigglers, and 3 bending magnets) was discussed in Section III.3.1, where it was emphasized that this distribution is subject to revision through interactions with the user community and, more specifically, with a yet-to-be-established Program Advisory Committee.

Table C-1

Projected Distribution of Beam Lines between Argonne and PRTs

	U			W			BM			Total Beam
Year	ANL	PRT	Total	ANL	PRT	Total	ANL	PRT	Total	Lines
1993	7	5	12	5	2	7	3	8	11	30
1994	8	6	14	5	4	9	7	11	18	41
1995	9	8	17	5	5	10	10	14	24	51
1996	10	10	20	5	7	12	12	18	30	62
1997	10	12	22	5	7	12	13	22	35	69

C.3 User Access

C.3.1 Introduction

User access will take a number of forms but, in each case, will involve the use of either an Argonne beam line or a PRT beam line. The policies and procedures which we now envision for access to these beam lines are described below. We will aim to make firm decisions on such policies in 1988, based on advice from the Program Advisory Committee mentioned above. Of course, we must also expect to make modifications of these policies as the project proceeds.

C.3.2 Argonne Beam Lines

The so-called Argonne beam lines will be of three types:

- Lines built by Argonne scientists primarily for Argonne research;
- "Quick Response Lines" constructed by and maintained by Argonne for users;
- Lines built by users with funding subcontracted from Argonne.

It is our judgment that the user-dominated research program at the APS source will be far more effective if there is a substantial amount of in-house work conducted by scientists who have research as well as user-liaison responsibilities. Accordingly, we have included in the construction project an initial complement of 15 beam lines, to be constructed by Argonne, of which perhaps two-thirds will be used primarily for Argonne research programs, and the remaining one-third designated "Quick Response Lines" and used primarily for user research.

Those lines primarily for Argonne research will include an extensive array of collaborative programs with non-Argonne scientists. In addition, the qualified general user will have access to these lines. Consistent with current policy at the National Synchrotron Light Source (NSLS), we anticipate a minimum of 25% of the time on these lines will be available to the community at large via a proposal mechanism after the beam lines are fully commissioned.

The "Quick Response Lines" will be operated in a different fashion. These lines, though built and maintained by Argonne staff members, will be reserved for outside users. Access to these lines will involve a proposal review process, but we also intend to provide a "quick response" capability much desired by many industrial users and by some others. One way to accomplish this would be to reserve one or more beam lines for short experiments. Details must be worked out, but this quick response capability is something that we see as of substantial importance.

We would also like to emphasize that all of the "Argonne beam lines," even those specified as part of the construction project, need not be constructed by Argonne. We will establish a mechanism through which a university or laboratory user group can construct a beam line which is funded as a subcontract from Argonne. In return, the "subcontractor" shall have time preference on the line. Although specifics remain to be defined, we anticipate that a complete beam line construction might translate into 75% use time for three years, with the remaining 25% available to the general user community, as for the remainder of the "Argonne" lines.

C.3.3 Participating Research Teams

Given the generally positive response to the PRT concept at NSLS, we anticipate that the Department of Energy (as well as other funding agencies) will encourage and fund proposals for the construction of PRT beam lines, and will also encourage industry to construct beam lines within PRT guidelines similar to those used at NSLS. Indeed, we see these PRT beam lines as a vital component of the overall beam line plan, as is indicated clearly in Table C-1.

At this point, the current PRT policy, whereby 75% of the time on the PRT line is provided to the PRT with 25% of the time available to the general user community through a proposal process, appears reasonable, as does agreeing to such an arrangement for three years with the possibility of renewal.

C.3.4 University/Argonne Synchrotron Radiation Professorships

We commented above that the Argonne beam lines are expected to support a substantial measure of collaborative research with non-Argonne users. We have devised a novel plan that will assist in enhancing these collaborative efforts, will expedite the assembly of a committed user group, will enhance the educational impact of the source, and will bring additional people into the process of constructing beam lines. This plan is the University/Argonne Synchrotron Radiation (UASR, pronounced "user") Professorship program that we will propose to the Department of Energy.

Assuming that the source will be user-ready in 1993, we propose making a number of appointments in 1990 to these UASR Professorships. (By starting in 1990, these people will have an opportunity to prepare themselves for operation in 1993.)

We propose that the UASR Professorships be handled as follows. Participating universities will announce the availability of these positions, with selection to be made by joint university/Argonne committees. For each such position, Argonne will agree to pay half of the salary and benefits for three years, with multiple renewals possible if agreed to by both the university and Argonne. Further, each such position will receive from Argonne a specified sum ($50,000 per year?) of either capital equipment or operating funds, with, to the extent possible, the choice to be that of the UASR Professor. The capital equipment funds could be used to build specialized equipment; the operating funds could be used, for example, for supporting a postdoctoral appointee or students whose work is primarily associated with the source. At the conclusion of each three-year appointment, a review of the efficacy of the appointment will be carried out, and a renewal decision made.

In view of the enthusiasm with which the UASR concept has been received - some 18 research universities have already expressed an intention to participate - we propose to make approximately 20 initial UASR appointments in 1990. The total number of UASR appointments could then increase gradually to approximately 30 in 1995. It should be emphasized that we are proposing the UASR Professorship program as a new program to accompany the Advanced Photon Source, not as a program to supplant the spectrum of sabbatical and summer appointments for university faculty members and the several kinds of student appointments that Argonne already makes.

APPENDIX D

TBA LATTICE STUDIES

In order to more realistically compare the performance for an alternative three-bend achromatic (TBA) lattice to that of the chosen Chasman-Green (CG) lattice, a certain number of properties or design goals were fixed. These properties were:

- Horizontal natural emittance ≈ 7 nm.
- Number of 6-m straight sections ≥ 32.
- Bending radius ≈ 39 m.
- Circumference ≈ 1060 m.
- Insertion region β_x and $\beta_y \approx 10$ m.

The lattice function of the TBA lattice designed to meet these goals is shown in Fig. D-1, for a half-cell with reflective symmetry. This lattice has had preliminary adjustments (magnet size and spacing, etc.) in its design in order to facilitate its construction. Additional refinements, such as moving the defocusing sextupoles closer to the dipole magnets (a change that increases their strength) to facilitate photon beam extraction and moving or reducing magnet lengths to allow placement of vacuum components, have not been performed. In fact, the reduced bend angle and the angular requirement for beam line placement make photon beam extraction quite difficult from the central bend magnet. Despite these technological difficulties with this TBA lattice, the comparison of lattice performance should be quite realistic. Table D-1 lists the parameters for this TBA lattice.

The TBA lattice, which has a central bending magnet that also contributes to the natural emittance, requires that the dispersion function be kept small in this magnet. Symmetry requirements demand that the slope of the dispersion be zero at the center of this magnet. This requires focusing quadrupoles between the dipole magnets. Control of the vertical beam size in the dispersion section requires vertical focusing. At lower energies[1], where the dipole bend radius can be small, this vertical focusing can be provided by gradient fields in the dipole magnets themselves. For a 7-GeV ring, the bending magnets are longer and would require larger gradients. The placement tolerance required for 2.6-m-long focusing dipoles makes gradient focusing unattractive. For ease of construction and greater flexibility (reduced dependence of the tune on the natural emittance), the vertical focusing has been removed from the dipoles (zero gradient) and separate quadrupoles provided. Although a single, vertically focusing quadrupole would be sufficient for very small emittance tunes, adequate solutions for the desired emittance were not found. Therefore, a quadrupole triplet is used. By separating the

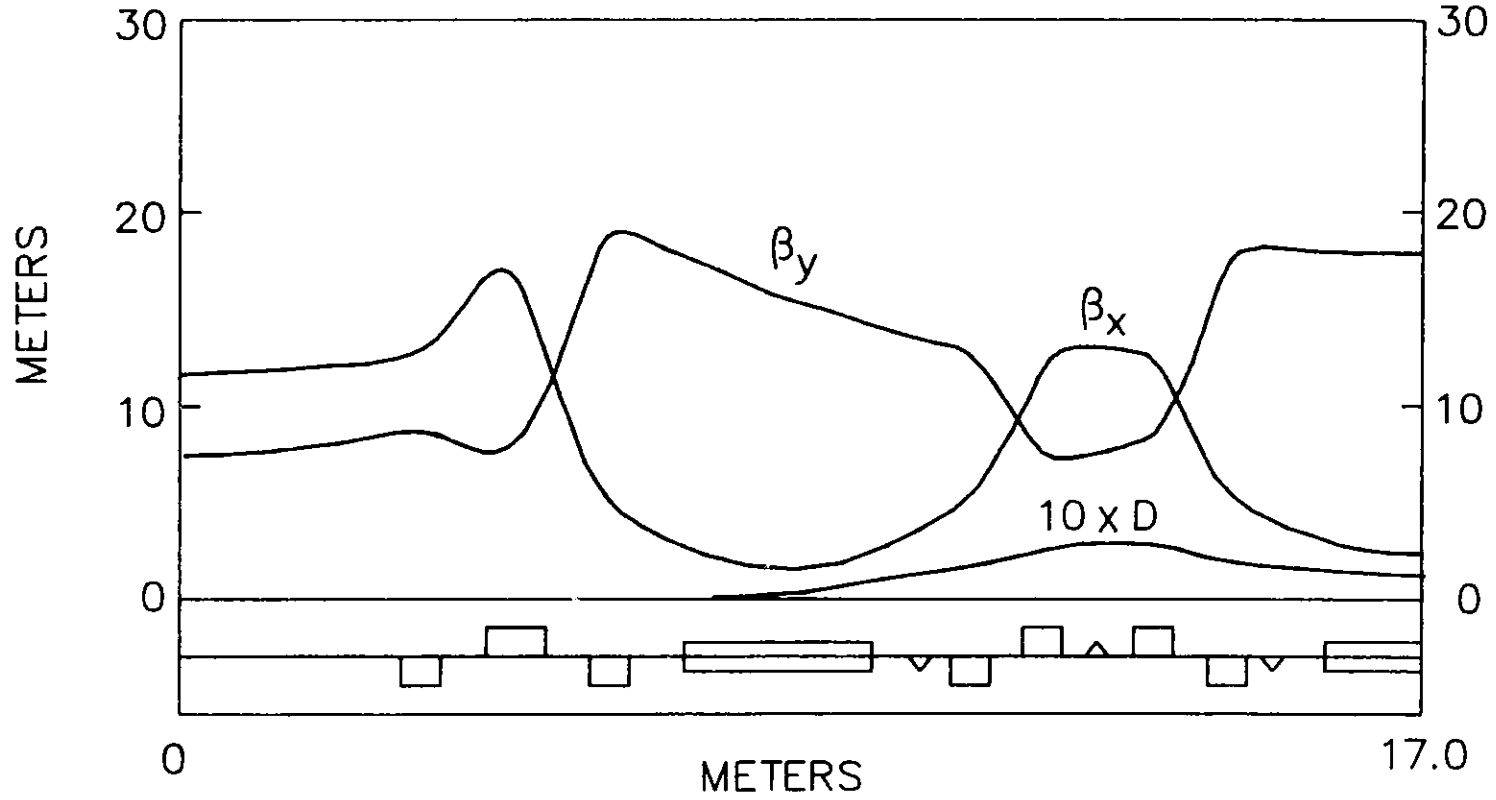

Figure D-1

Lattice functions (β_x and β_y) and dispersion function (D) for one half-cell of the TBA lattice. The parameters shown are mirror symmetric about the midpoint of the cell.

TABLE D-1

Three-Bend Achromat Lattice Parameters

Circumference, C	1088 m
Revolution Time, T_o	3.629 μs
Energy, E	7 GeV
No. of Insertion Regions	32
Length of Insertion Region	6.0 m
Dipole Length	2.6 m
Dipole Field	0.587 T
Bend Radius, ρ	39.73 m
Maximum Quadrupole Strength	17.34 T/m
No. of Dipoles	96
No. of Quadrupoles	448
Tunes, ν_x and ν_y	37.22, 15.30
Transition Gamma, γ_T	52.5
Momentum Compaction, α_p	3.627×10^{-4}
Chromaticities, ξ_x, ξ_y	-54.4, -29.8
Chrom. Corr. Sextupoles	2.99, $-3.88/m^2$
Number of Chromatic Sextupoles	192
Maximum β_x and β_y	16.7, 19.2
Maximum Dispersion	0.28 m
Natural Emittance, ε_n	7.0×10^{-9} m
Transverse Damping Time, $\tau_x=\tau_y$	9.5 ms
Synchrotron Damping Time, τ_E	4.7 ms
Bending Magnet Critical Energy, ε_c	19.2 keV
Energy Loss per Turn, V_o	5.35 MeV
Radio Frequency, f_{rf}	352.7 MHz
Harmonic Number, h	1280
Natural Energy Spread, σ_E/E	0.095%
Horizontal Beam Size in Undulator, (zero coupling), σ_x	0.29 mm
Vertical Beam Size in Undulator, (100% coupling), σ_y	0.16 mm

central quadrupole (strong horizontal focusing quadrupole) into two shorter quads, an improved location for the focusing sextupole (facilitating reduced sextupole strength) is provided.

The insertion straight section has been provided with a quadrupole triplet to provide similar undulator beam size tuning to that provided by the CG lattice. The tunes for the TBA lattice have been set to $\nu_x = 1.1667$ and $\nu_y = 0.48$ per cell. These are midway between the $\nu_x = 1$ and $3\nu_x = 4$ resonances and avoiding the $\nu_x + 2\nu_y = 1$ or 2 sextupole resonances. The total tunes have the same noninteger value as the CG lattice but differ by two units in the horizontal and one unit in the vertical. Since the total length is approximately the same, the higher tune means that the average beta functions are smaller and, therefore, the closed-orbit amplification factors will be slightly smaller.

The chromaticity for this lattice is larger per cell due to the higher tune values, but requires less sextupole strength due to the larger number of sextupoles per cell available for chromaticity correction. Figure D-2 shows the residual chromaticity after correcting the natural chromaticity with two families of sextupoles. The residual chromaticity, although less than for the chromaticity-corrected CG lattice (Fig. II.1.4-2), is greater than for the harmonically corrected CG lattice (Fig. II.1.4-5).

The amplitude-dependent tune shifts are shown in Figs. D-3 and D-4. First-order perturbation theory calculates these tune shifts to be

$$\Delta\nu_x = -8.38\times10^{-5}\ N_x^2 - 3.7\times10^{-5}\ N_y^2 \quad ,$$

and

$$\Delta\nu_y = -7.40\times10^{-5}\ N_x^2 - 2.76\times10^{-5}\ N_y^2 \quad .$$

These coefficients are 1.6 to 3.7 times smaller than the chromaticity-corrected CG lattice (see Section II.1.4.2), while 3 to 10 times greater than the harmonically corrected CG lattice. This tune shift with amplitude contributes to an increased sensitivity for imperfection of this lattice compared to an harmonically corrected CG lattice.

The dynamic aperture for this lattice, without errors, is shown in Fig. D-5. Although quite symmetric in shape, unlike the CG lattice, the dynamic aperture for TBA lattice cannot be predicted by a low-order resonance condition (i.e., $\nu_x = P$, $3\nu_x = P$). Consequently, all attempts at adding harmonic sextupole correction have yielded little improvement in either expanding the dynamic aperture or in reducing the tune shift with amplitude. Although the dynamic aperture is quite large, the rapid tune shift with amplitude will reduce the dynamic aperture when imperfections are included. This effect is shown in the working point diagram, Fig. D-6. With lattice imperfections, the $\nu_x = 37$ resonance will limit the horizontal aperture to $N_x \lesssim 55$ and the vertical aperture to $N_x \leq 85$. With a 10^{-5} tolerance level, these limits on the dynamic aperture are reached, but at a 5×10^{-5} tolerance level, the dynamic aperture has been reduced a factor of 2 below this level, as shown in Fig. D-7.

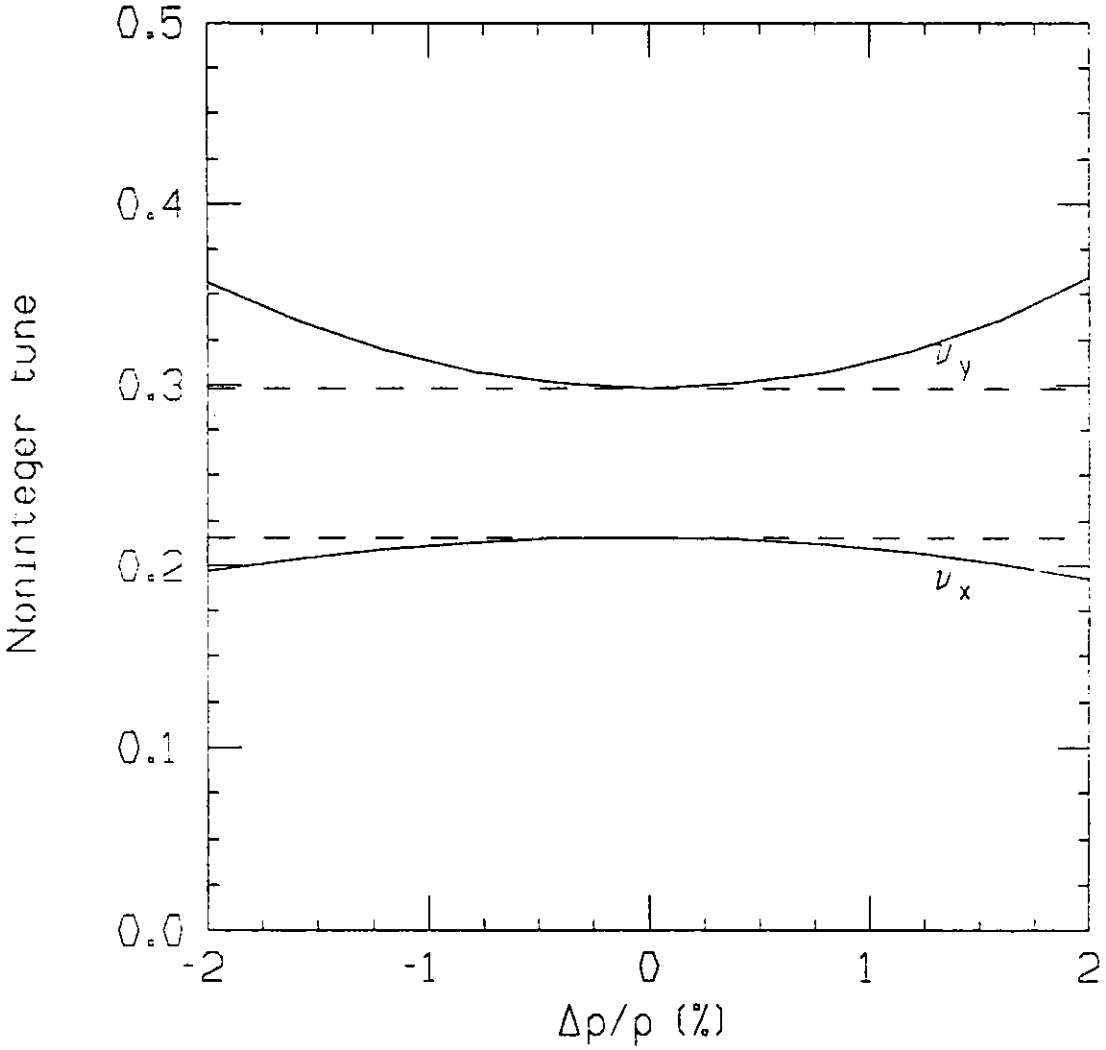

Figure D-2
The noninteger tune dependence on momentum for the TBA lattice, with the natural chromaticity tuned to zero using two sextupole families.

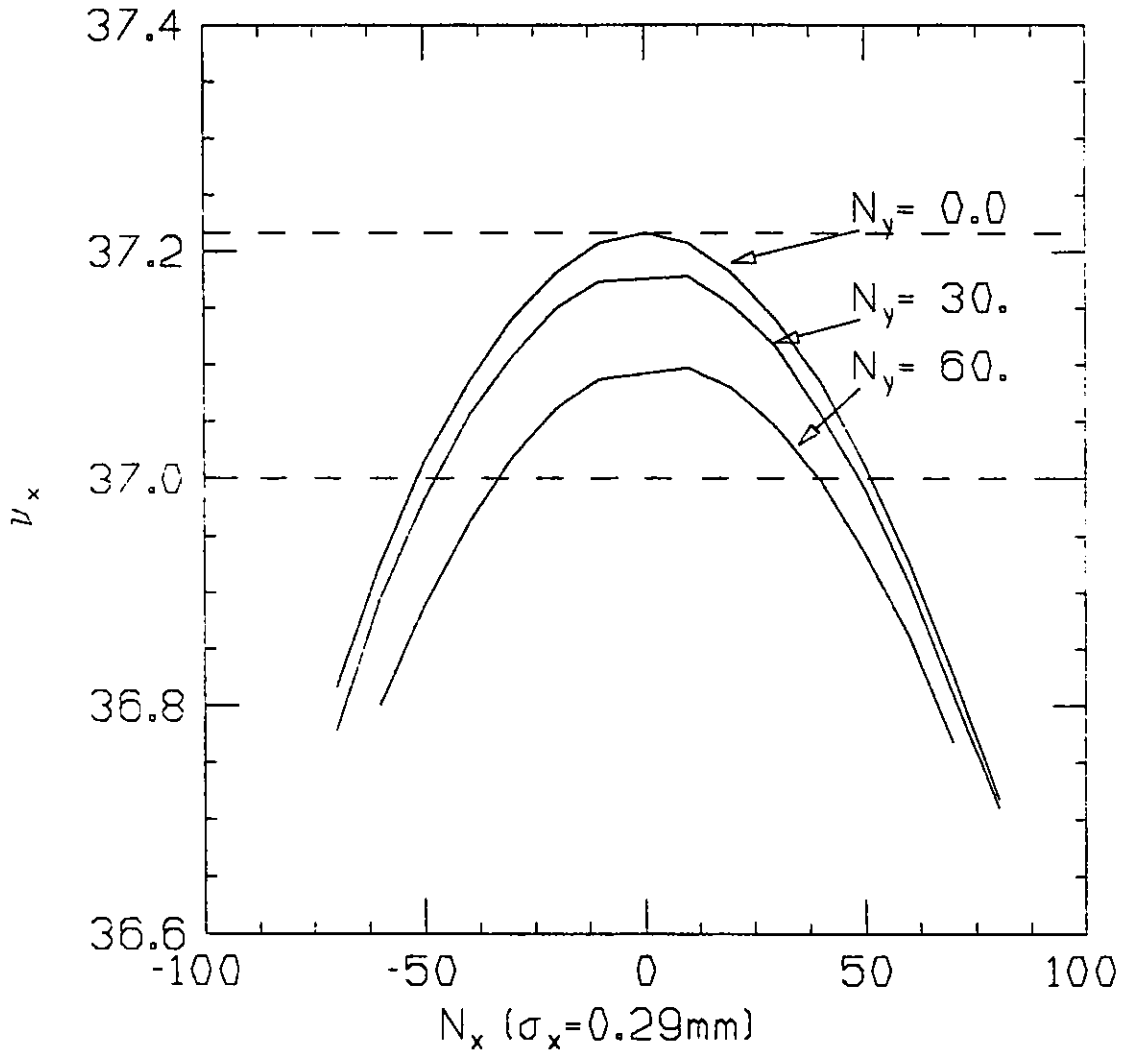

Figure D-3

The horizontal tune dependence on the horizontal betatron amplitude, $N_x = \Delta x/\sigma_x$ for fixed values of the vertical betatron amplitude $N_y = \Delta y/\sigma_y = 0$, 30, and 60. These results were obtained by Fourier analysis of particle trajectories obtained with PATRICIA.

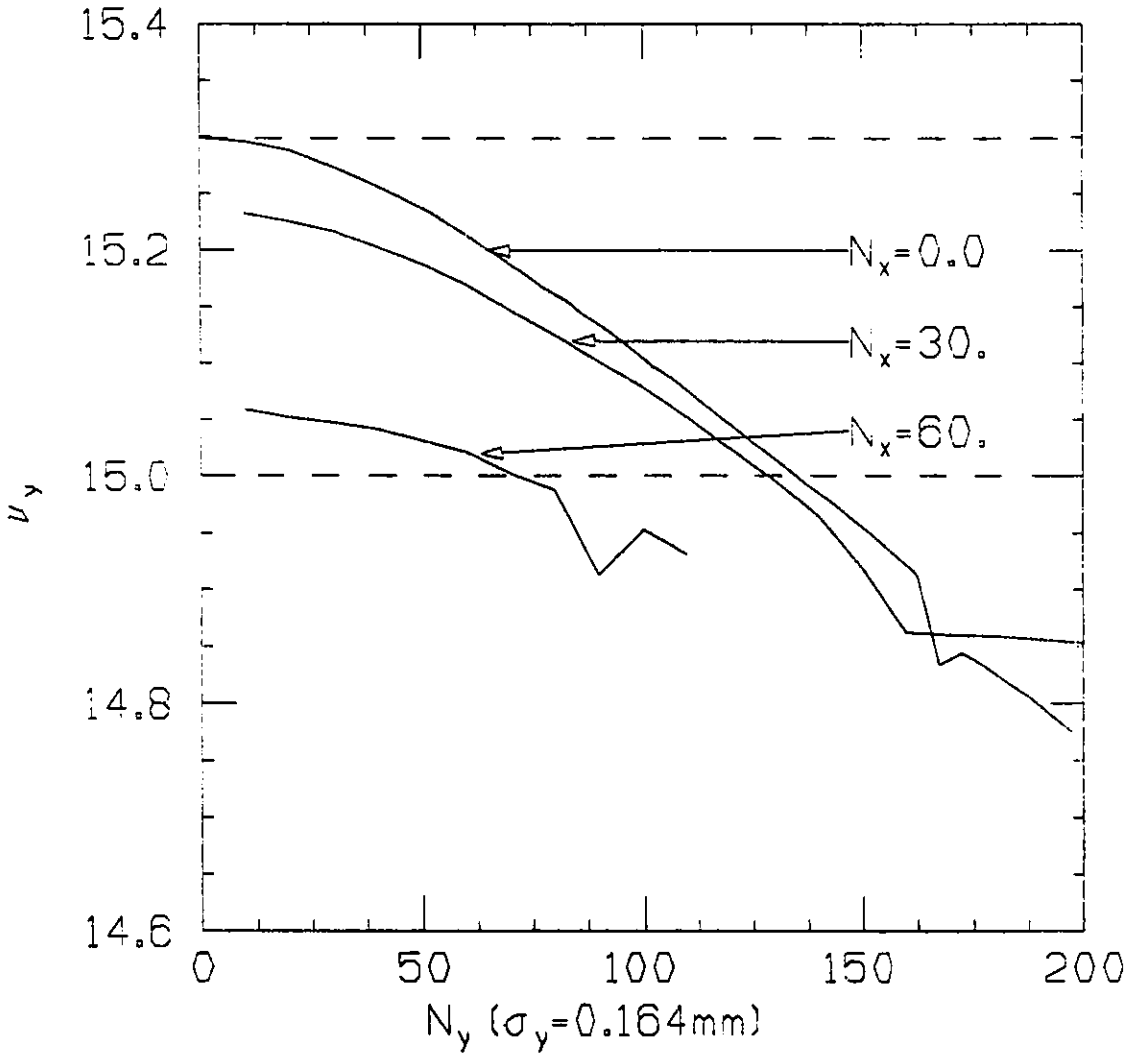

Figure D-4
The vertical tune dependence on the vertical betatron amplitude, N_y for fixed N_x = 0, 30, and 60.

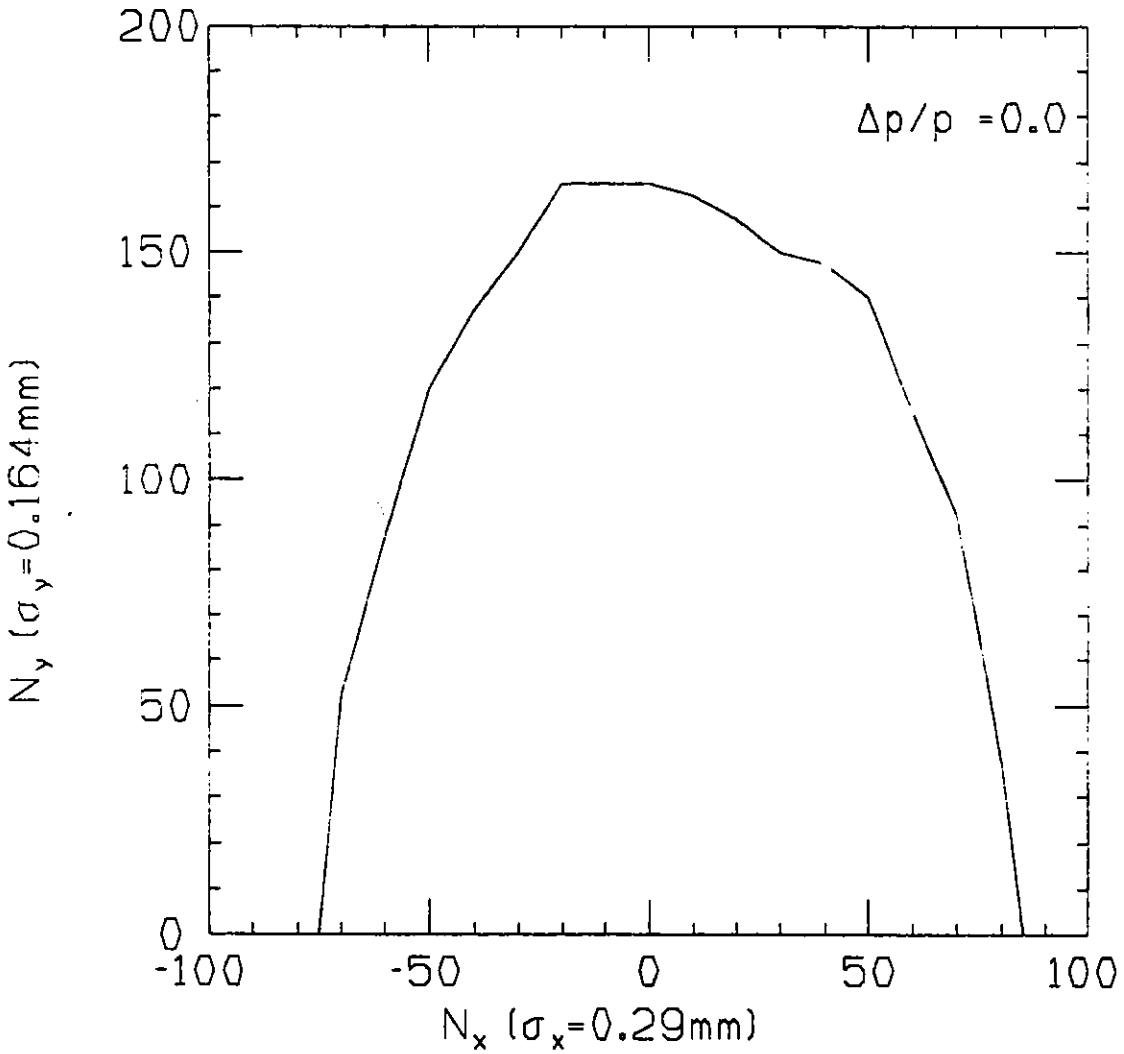

Figure D-5
The dynamic aperture for the TBA lattice obtained by tracking particles for 1000 turns using PATRICIA.

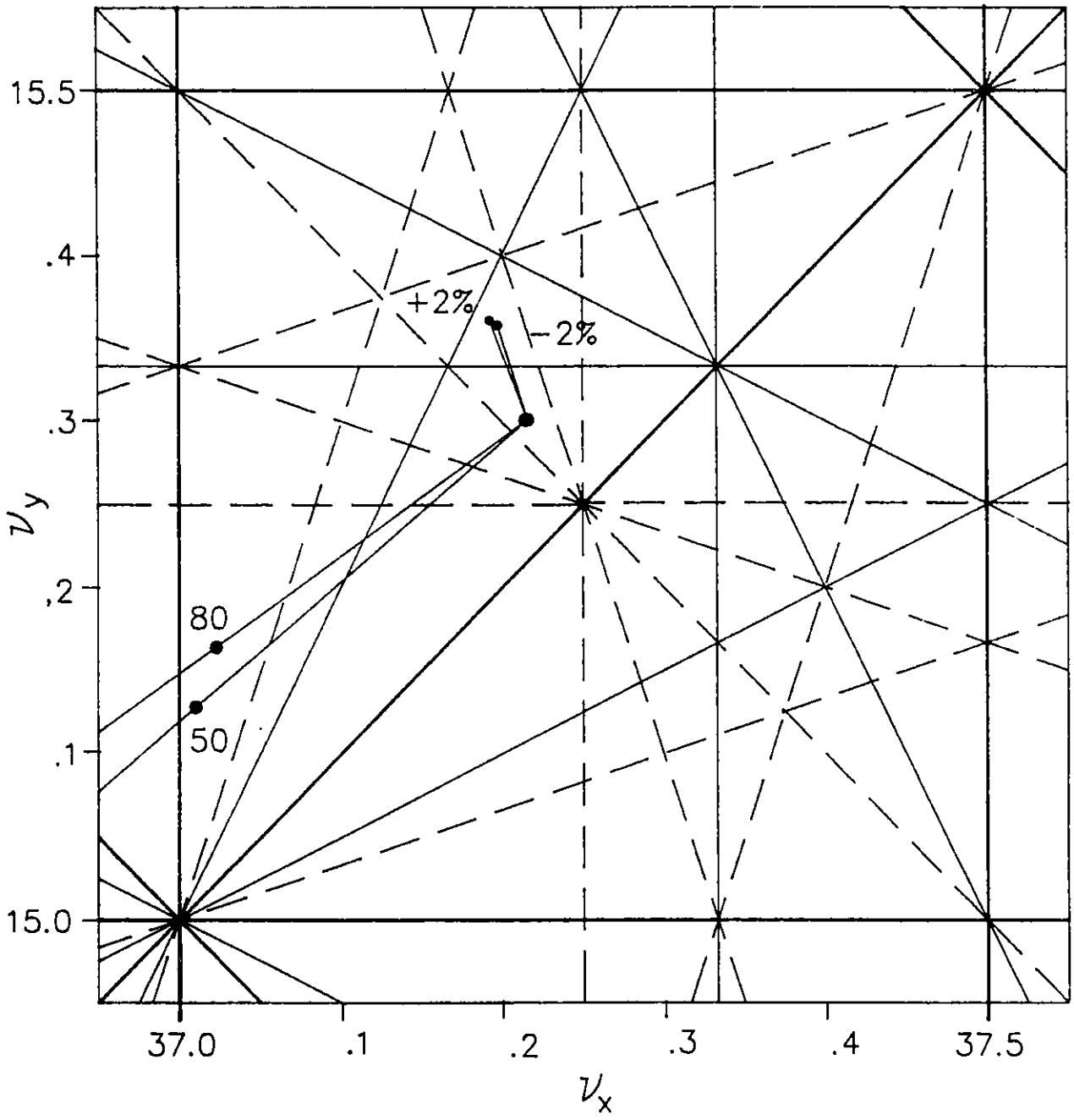

Figure D-6

Working point diagram for the TBA lattice solid point, with chromatic tune shifts for $\Delta p/p = \pm 2\%$ and amplitude-dependent tune shifts for $N_y = 0$ to 80 (for $N_x = 10$), and $N_x = 0$ to 50 (for $N_y = 10$). Heavy straight lines are 1st- and 2nd-order resonances, light lines are the 3rd-order resonances and dashed lines are for 4th-order resonances.

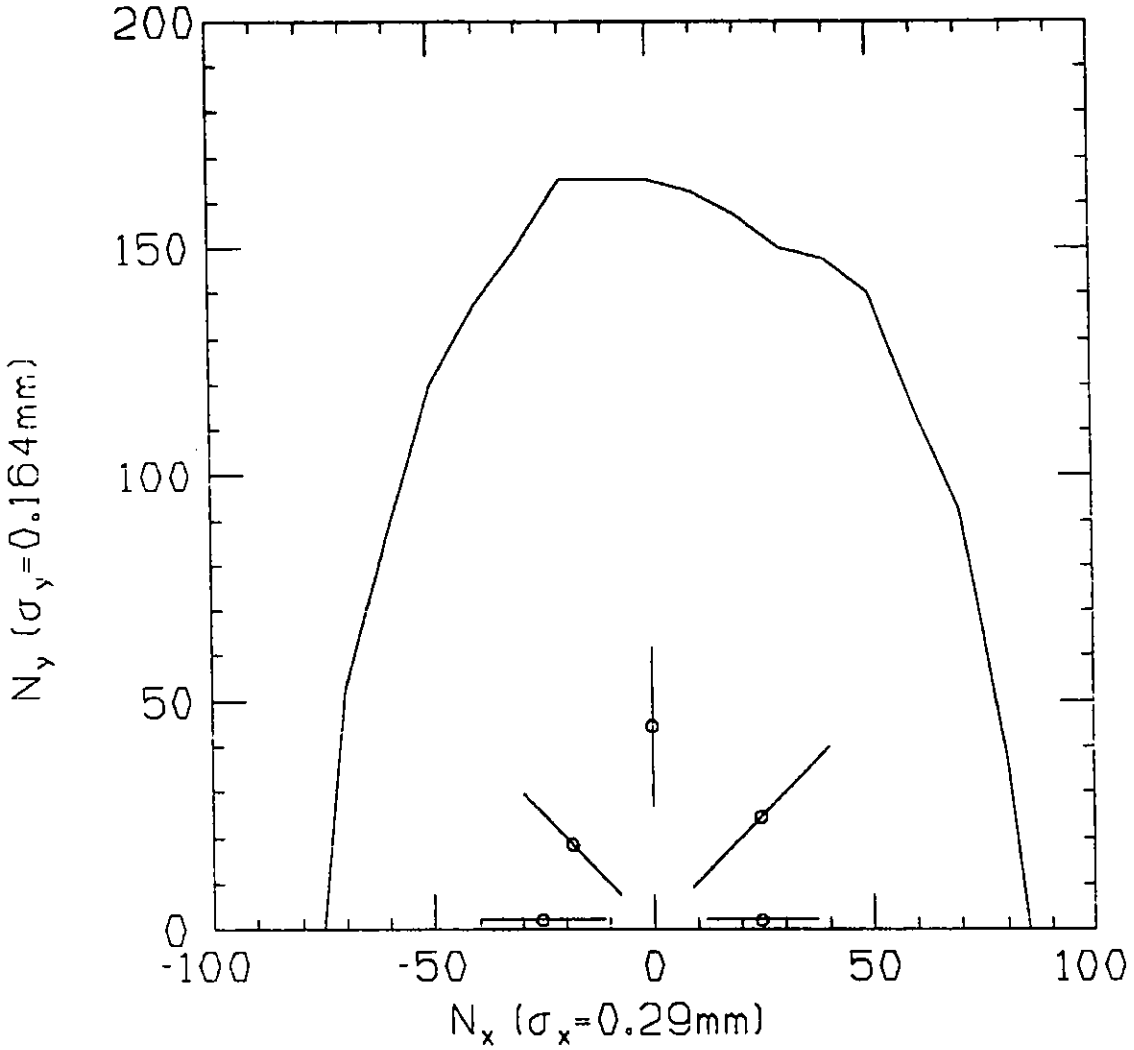

Figure D-7

The average value and rms spread (circles and error bars, respectively) for the dynamic aperture obtained by tracking for 10 TBA machines with a tolerance level of 5×10^{-5}. The solid curve is the zero-tolerance-level dynamic aperture.

Figure D-8 shows the dynamic aperture variation with tolerance level, to be compared with Fig. II.1.4.3-3 for the CG lattice. Although the TBA lattice has a finite aperture at a 10^{-4} error level, it is not adequate for efficient injection and is comparable with the CG lattice at a 2×10^{-4} tolerance level.

Correction of the amplitude-dependent tune shifts by adding harmonic-correcting sextupoles in the dispersion-free straight sections has been considered. For the CG lattice, these tune shifts are readily identified as being caused by the nearby first-order resonance and can be corrected by tuning the harmonic sextupoles to reduce the amplitude of the fundamental harmonic. The amplitude-dependent tune shifts for the TBA lattice are not caused by first-order resonances. Therefore, their reduction by tuning harmonic-correcting sextupoles is less straightforward. The use of these sextupoles will continue to be studied as a possibility for reducing the sensitivity with tolerance level for the TBA lattice.

In summary, the TBA lattice studied here has the relative disadvantages of

- greater number of dipole and quadrupole magnets,
- fewer straight sections for given machine circumference,
- greater difficulty of photon beam extraction,
- greater sensitivity to quadrupole placement errors.

However, the advantages of the TBA lattice are

- a lower possible natural emittance,
- greater dynamic aperture and reduced momentum dependence with only chromatic sextupoles,
- fewer sextupoles to achieve dynamic aperture. (The TBA lattice normally requires 6 sextupoles per cell compared to 7 per cell for the CG lattice. To reduce the amplitude-dependent tune shifts, the TBA lattices require 8 or 10 sextupoles per cell.)
- reduced dependence of the natural emittance on the horizontal tune.

Reference

1. A. Jackson, "Comparison of the Chasman-Green and Triple Bend Achromat Lattice," LBL-21279 (1986).

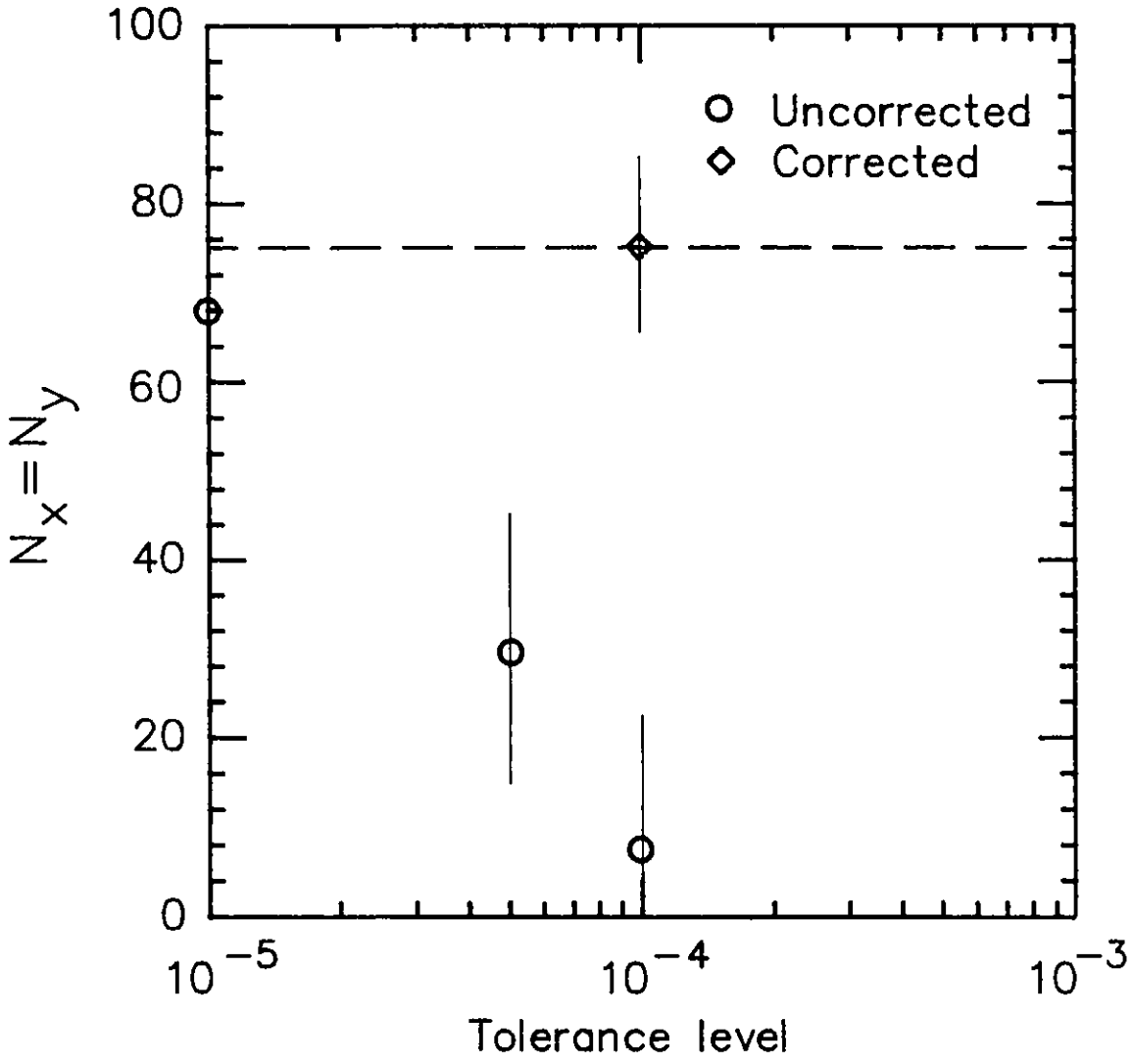

Figure D-8

The circles with error bars represent the average and rms dynamic aperture for ten machines, as a function of tolerance level for the point $N_x = N_y$. The diamond represents the dynamic aperture for two machines at a 10^{-4} tolerance level, with closed-orbit correction.

Distribution for ANL-87-15

Internal:

Associate Laboratory Director for the
Advanced Photon Source (ALD/APS) (661)
ANL Patent Dept.
ANL Contract File
ANL Libraries
TIS Files (3)

External:

DOE-TIC, for distribution per UC-400 (25)
DOE Chicago Operations Office:
Manager
University of Chicago Board of Governors for Argonne National Laboratory, Committee to Advise the Laboratory Director on APS Construction (7)